THE ATMOSPHERES OF THE SUN AND STARS

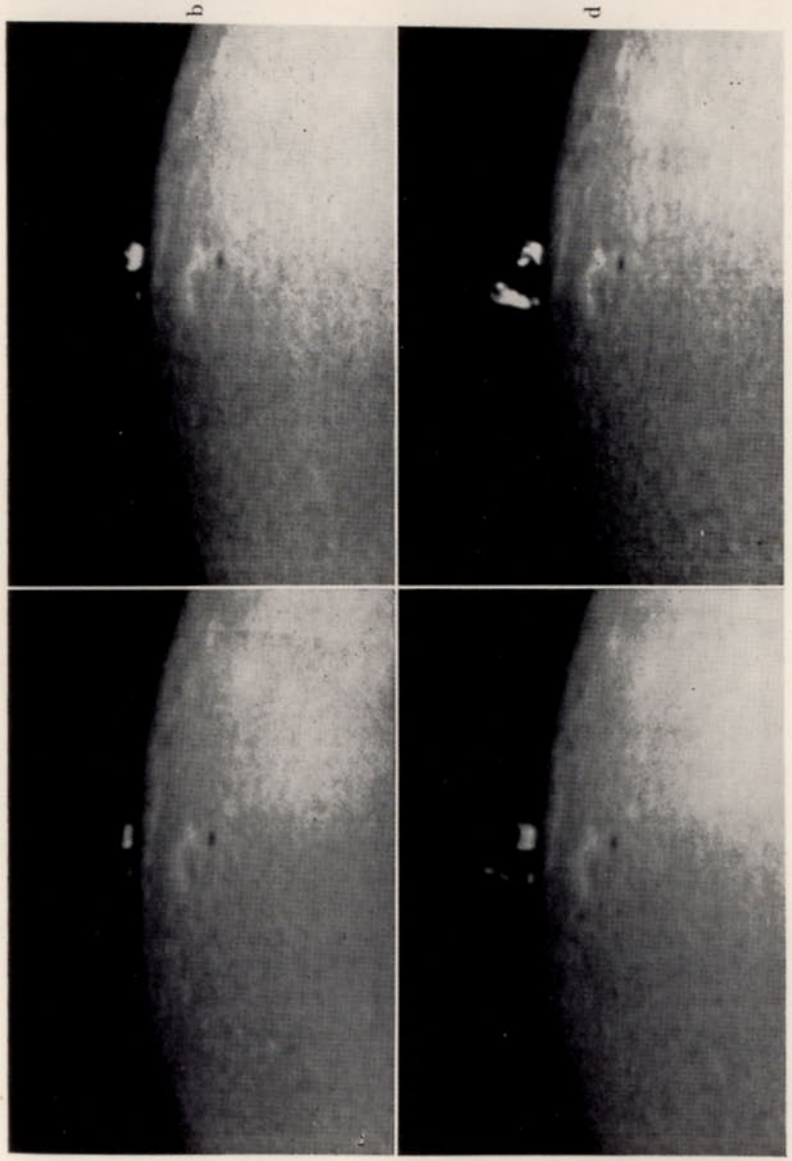

Hα Spectroheliograms Showing Development of Limb Flare, May 8, 1951

(a) 15ʰ05ᵐ.2 U.T. (b) 15ʰ05ᵐ.7 U.T. (c) 15ʰ06ᵐ.3 U.T. (d) 15ʰ07ᵐ.4 U.T.

A sudden ionospheric disturbance and a burst of 200 mc/s solar radio noise occurred simultaneously with the development of this flare-prominence. On the disk can be seen a small sunspot with its accompanying *plage* or bright hydrogen flocculus. To the left of the flare there is a large prominence of average intensity. (Photographed by Helen Dodson at the McMath-Hulbert Observatory of the University of Michigan.)

ASTROPHYSICS

The Atmospheres of the Sun and Stars

By

LAWRENCE H. ALLER

ASSOCIATE PROFESSOR OF ASTRONOMY
UNIVERSITY OF MICHIGAN

THE RONALD PRESS COMPANY ✦ NEW YORK

Library of Congress Catalog Card Number: 53-5711

PRINTED IN THE UNITED STATES OF AMERICA

TO MY STUDENTS AND COLLEAGUES
HERE AND ABROAD, WHOSE HELP
AND ENCOURAGEMENT HAVE MADE THIS
BOOK POSSIBLE

PREFACE

Despite a number of excellent monographs and reviews covering specialized branches of astrophysics, teachers and research workers in astronomy and physics have long felt the need for a work covering not only the fundamentals necessary for an understanding of the field but also the major modern developments. This volume is intended for those who wish to learn something of the methods employed and the results obtained in the study of the atmospheres of the sun and stars and solar-terrestrial relationships. A companion volume will treat of nuclear transformations and stellar interiors, variable stars, and the interstellar medium.

After a brief astronomical introduction the background of physics necessary for a study of stellar atmospheres and other branches of astrophysics is carefully given. The subjects treated include atomic structure and spectra, gas laws and velocity distribution, ionization, excitation, dissociation of atoms and molecules, and selected aspects of radiation theory. In following chapters of the book, these principles are applied to the radiation of the sun and stars, to their continuous and dark-line spectra, to solar phenomena, and solar-terrestrial relationships.

Throughout this book I have stressed not merely the results but also the methods by which they are obtained. The reader is shown how each principle or important formula is applied to some definite numerical problem concerned with the interpretation of the stars and nebulae. For example, I have shown in detail how the energy flux of the sun and stars may be calculated and compared with the observations, how the abundance of calcium may be determined from the profile of the "K" line in the solar spectrum, and how the cosmic abundances of elements not observable in the sun are inferred from studies of the hot stars. The chemical composition of a "normal" star is critically discussed, followed by an account of composition differences between stars. In the largely descriptive chapter on solar phenomena use is made of numerous excellent photographs obtained in France and the United States. Considerable original material is included.

It would have been impossible to produce a book of this scope without the enthusiastic cooperation of many astronomers and students who have offered helpful comments and suggestions. Particular thanks are due to Daniel Barbier, S. Chandrasekhar, Helen W. Dodson, Leo Gold-

berg, Jesse L. Greenstein, Gerhard Herzberg, V. Kourganoff, Jean McDonald, D. B. McLaughlin, D. H. Menzel, Paul W. Merrill, M. Minnaert, Orren Mohler, Seth B. Nicholson, R. M. Petrie, A. Keith Pierce, Evry Schatzman, Otto Struve, and K. O. Wright. Original photographs and illustrations have been provided by the Mount Wilson and Lick Observatories, by Andrew McKellar, Jason Nassau, R. M. Petrie, and by my colleagues at Michigan, particularly Robert R. McMath and Helen Dodson. Special mention must be made of the beautiful photographs of solar phenomena supplied by Lucien and Marguerite d'Azambuja and the late Bernard Lyot. Finally, it is a pleasure to acknowledge that this book was written at the suggestion of Henry Norris Russell.

LAWRENCE H. ALLER

Ann Arbor
January, 1953

CONTENTS

LIST OF PHYSICAL CONSTANTS

Velocity of light	$c = 2.99776 \times 10^{10}$ cm sec^{-1}
Planck's constant	$h = 6.6234 \times 10^{-27}$ erg sec
Electron mass	$m = 9.1055 \times 10^{-28}$ grams
Electronic charge	$\varepsilon = 4.8024 \times 10^{-10}$ e.s.u.
Boltzmann's constant	$k = 1.38032 \times 10^{-16}$ erg deg^{-1}
Volume of a mole	22.4146×10^{3} cm^3
Gas constant per mole	$R_0 = 8.31436 \times 10^{7}$ erg mol^{-1} deg^{-1}
Avogadro's number (number of atoms or molecules per mole)	$N_0 = 6.0251 \times 10^{23}$
Loschmidt's number	$n_0 = 2.68731 \times 10^{19}$ cm^{-3}
Density of oxygen gas (0°C)	1.429×10^{-3} grams/cm^3
Radius of first Bohr orbit	$a_0 = 0.529161 \times 10^{-8}$ cm
Stefan-Boltzmann constant	$\sigma = 5.6724 \times 10^{-5}$ erg cm^{-2} deg^{-4} sec^{-1}
Second radiation constant	$hc/k = 1.43847$ cm deg
Wien displacement law constant	$\lambda_m T = 0.289715$ cm deg
Bohr magneton	$\mu_1 = \dfrac{\epsilon h}{4\pi mc} = 0.92731 \times 10^{-20}$ erg gausses^{-1}
Ratio: mass proton/mass electron	$M_p/m = 1836.57$
Mass of proton	$M_p = 1.67248 \times 10^{-24}$ grams
Mass of hydrogen atom	$M_H = 1.6734 \times 10^{-24}$ grams
Wave length associated with 1 ev (electron volt)	$\lambda_0 = 12394.2 \times 10^{-8}$ cm
Frequency associated with 1 ev	$= 2.41867 \times 10^{14}$ sec^{-1}
Energy associated with 1 ev	$= 1.60199 \times 10^{-12}$ erg
Conversion factor atomic mass units to Mev	1 a.m.u. = 931.04 Mev
Energy equivalent of electron mass	$mc^2 = 0.51079$ Mev
Constant of gravitation	$G = 6.670 \times 10^{-8}$ dynes cm^2/gram^2
Standard atmosphere (pressure)	1,013,246 dynes/cm^2/atmosphere
Melting point of ice	273.16°K
Mechanical equivalent of heat	4.185 joules/calorie
Acceleration of gravity	$g_0 = 980.665$ cm/sec/sec

The numerical values are taken from the data of R. T. Birge (1941), and from J. W. M. DuMond and E. R. Cohen, *Rev. Mod. Phys.* **20,** 82, 1948.

ASTROPHYSICS

CHAPTER 1

Survey of the Basic Data

1. Scope of Astrophysical Problems

Astronomy differs from its sister physical sciences in that the phenomena with which it deals cannot be handled by the experimental method. Stars, planets, and nebulae are known only through the radiation they emit, absorb, or reflect. Much of this radiation cannot be observed. For example, the earth's atmosphere cuts out all light of wave length shorter than 2.9×10^{-5} cm (2900 angstrom units, written as $\lambda 2900$). In the infrared much radiation is obstructed by water vapor. Furthermore, we can observe only the outermost layers of a star. The interior lies concealed from view; conditions there may be inferred only with the aid of universal physical laws. The stars tell us what they please; skilled interpretation of more or less slender clues leads to further knowledge. The problem is to apply known physical laws to the interpretation of the observational data. Thus we may learn the structure, temperature, and composition of stellar atmospheres, the state of stellar interiors, and the conditions prevailing in the gaseous nebulae and in the interstellar medium.

Let us first review the observational data: The positions of the stars and nebulae may be measured upon the celestial sphere with a high order of precision.

The apparent brightnesses of stars and nebulae can be measured with various light-detecting devices such as the eye, photographic plate, or photoelectric cell. To be able to convert apparent luminosity to true luminosity, one must know the distance of the star or the nebula. Visual double stars of established distances and orbital periods are the source of most of our knowledge of stellar masses. Radii and densities may be found for the components of eclipsing binaries.

The physical nature and chemical compositions of stellar atmospheres may be deduced from their continuous and dark-line spectra.

Much more detailed information may be obtained for the sun. Direct photographs show granules, spots, and faculae. Spectroheliograms show flocculi, flares, and prominences. (See Fig. 1.) The structure of the inner corona may be studied with the coronagraph.

The gaseous and diffuse nebulae present special problems of observation and interpretation. Here the significant data are often the surface

brightnesses and the angular dimensions. It is possible to measure the size and luminosity of the planetary nebula in each of its characteristic emissions; while slit-spectrographic observations give the internal motions.

The presence of unorganized material in the galaxy is revealed by its effect on the light of distant stars; "stationary" lines often appear in the spectra of these stars and their light is often reddened.

Radio-frequency static from the sun and Milky Way has recently been observed. This new technique has already given important data on the outer envelope of the sun, and on the physical state of the interstellar medium.

Among the questions which astrophysics seeks to answer are: What are the densities, temperatures, and compositions of stellar atmospheres? How are they constructed? Are the atmospheric strata in balance with gravity like those of the earth, or do such atmospheres consist of jets and filaments hurled from the depths of the star, the whole atmosphere resembling a vast fountain of heated gases?

The sun poses many additional problems, such as that of the origin of the sunspots. How are we to explain the shapes and motions of prominences? What causes the high excitation of the corona? What is the origin of the solar cycle of 11.5 years?

The gaseous nebulae derive their luminosities from enclosed or nearby stars. What are their densities, temperatures, compositions, and total masses?

Are the interstellar obscuring clouds composed of dust, droplets, or large chunks of matter—of ice, metals, or silicates? Was the débris scattered between the stars originally expelled from them or is it the stuff from which the stars are made?

These are but a few of the questions that might be asked. We shall see that some of them can be answered in a fairly satisfactory manner—to others we can supply but the crudest conjectures. The interpretation of the observational data of modern astrophysics requires knowledge of almost all branches of physics, from aerodynamics to nuclear transformations. At the top of our list we place the theory of the absorption and emission of radiation. We must become familiar with definitions of flux, intensity, and energy density as well as such topics as Kirchhoff's, Planck's, Wien's, and the Stefan-Boltzmann law. Furthermore, since we are dealing with heated gases we need to apply the kinetic theory of gases.

In some respects stellar atmospheres are close to thermal equilibrium —the state of affairs that would prevail in a box whose walls were kept at constant temperature. This situation may be studied with the aid of the ionization and dissociation equations that are derived from statistical mechanics. These relations should be labeled *handle with care*, since a stellar atmosphere is not strictly in thermal equilibrium; we must be prepared to recognize and allow for the differences that do occur.

Since we study the behavior of atoms and molecules by means of their spectra, an understanding of atomic and molecular structure is necessary. The arrangement of the energy levels in the atom determines the character of the spectrum. The intensity of a spectral line will depend on (among other factors) the number of atoms capable of absorbing it, and the probability coefficient for the transition. Except at very high temperatures, most of the atoms in any stage of ionization are in the ground level and thus can absorb lines arising from this level (resonance lines). Thus the calcium H and K lines attain great strengths in the sun. On the other hand, the lines of the more abundant oxygen and carbon are weak in the sun, simply because the observable lines arise from high energy levels; at the relatively low temperature of the sun, only a few of these atoms are in these levels. The role of transition probabilities is exhibited by the $\lambda 3302$ and the D pairs of sodium; both are resonance lines but the former are inconspicuous whereas the latter are strong. This happens because the absorption probability is much larger for the D pair.

For other problems, e.g., the interpretation of faint lines of carbon and oxygen in the gaseous nebulae, we must know the probabilities for the recombination of ions and electrons.

The production of the so-called forbidden lines in the spectra of novae and nebulae, however, depends on the cross-section for collisional excitation of certain metastable levels, whence the atom can return to the ground level with the emission of the forbidden lines. Usually the determination of these basic physical parameters requires either difficult quantum mechanical calculations or experimental techniques.

Electromagnetic phenomena are involved in the sunspots, in the peculiar stars which have strong general magnetic fields that sometimes reverse themselves periodically, and probably also in the motions of prominences and in the behavior of coronal streamers.

Shock waves, presumably arising from acoustical disturbances moving through gases of varying density, may account for the high temperature of the corona and the peculiarities of the atmospheres of supergiant stars. Aerodynamics has been employed to study the interaction of clouds in the interstellar medium.

In recent years the theory of the solid state has become important to the astrophysicist in connection with the accretion of gas molecules by small crystals in interstellar space, in the analysis of comets and of the structure of the solid cores of planets.

The energy output of the sun and stars cannot be accounted for by chemical or gravitational processes. Actual transformations of the elements occur by thermal reactions involving the nuclei of light atoms and protons. The basic quantities here are the cross-sections for the capture of protons by protons and by nitrogen and carbon nuclei and the dependence of these cross-sections on the speeds of the colliding particles. These quantities must be determined experimentally. A reaction of interest in connection with the red dwarf stars (objects that are fainter and smaller than the sun) is the encounter between two protons to form a deuteron. This process cannot be observed in the laboratory and its reality depends on the validity of theories of nuclear forces and β-ray emission. A further understanding of the basic phenomena in nuclear physics will be helpful to astrophysics.

2. Distances of the Stars

Much of the work of the astronomer is devoted to the measurement of the masses, radii, and luminosities of the stars. For these measurements it is usually necessary to know the distance.

For the nearer stars we may measure the distance by the trigonometric method. The distance of a star is related to its *parallax* (the angular radius of the earth's orbit about the sun as seen from the star) by

$$r = 1/p \qquad (1)$$

If p is measured in seconds of arc, r is the distance in *parsecs*. (One parsec is 206,265 times the distance of the earth from the sun, i.e., 206,265 *astronomical units*.)

The distances of more remote stars are found by statistical methods, some of which depend on motions relative to the sun and the rotation of the galaxy. The fact that the spectrum of a star is related to its intrinsic luminosity permits the determination of "spectroscopic" parallaxes which must be calibrated, however, by trigonometric and statistical determinations of distances. The distances of faint dwarf stars less luminous than the sun are usually well known. The distances of the very luminous stars are less accurately known, while data on the distances of such objects as the planetary nebulae are very meager.

3. Luminosities of the Stars

We express the brightness of a star in terms of its magnitude.* The magnitude scale is logarithmic, a difference of five magnitudes corre-

* Because of the physiological character of the eye, its response to light is logarithmic. A series of lamps arranged by brightness in a geometrical progression will be appreciated by the eye as an arithmetical progression of luminosity.

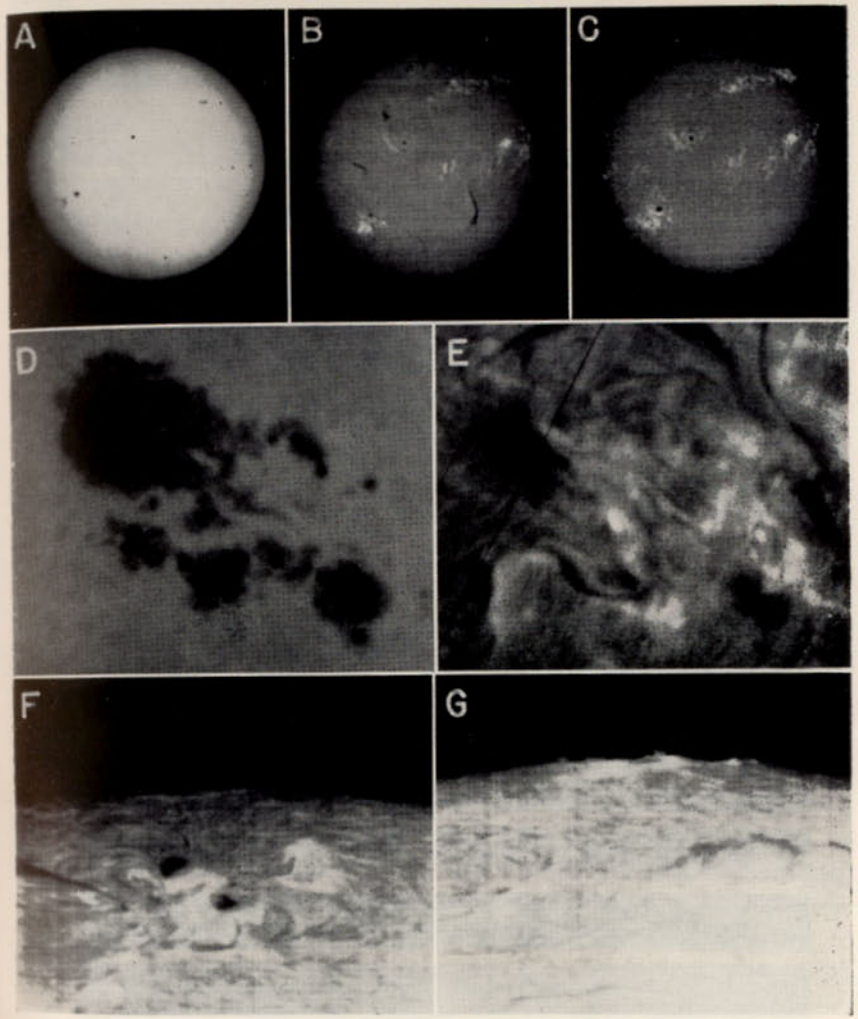

FIG. 1.—PHOTOGRAPHS OF SOLAR DISK PHENOMENA

A. Direct or white light photograph of solar disk (August 18, 1939).

B. Photograph of disk in the light of the red line of hydrogen. (Hα spectroheliogram).

C. Photograph of disk in the light of ionized calcium (λ3933 of Ca II). (Ca II or "*K*" line spectroheliogram)

Notice the dark filaments upon the disk in the Hα image and the bright areas (plages) in the vicinity of spots on both the Hα and the Ca II photographs.

D. Direct photograph of sunspot group of September 1, 1939.

E. Hα spectroheliogram of the same sunspot group.

F. Hα spectroheliograms of a sunspot group approaching the limb of the sun, September 14, 1939.

G. The same sunspot group observed on September 16, 1939.

(McMath-Hulbert Observatory, University of Michigan.)

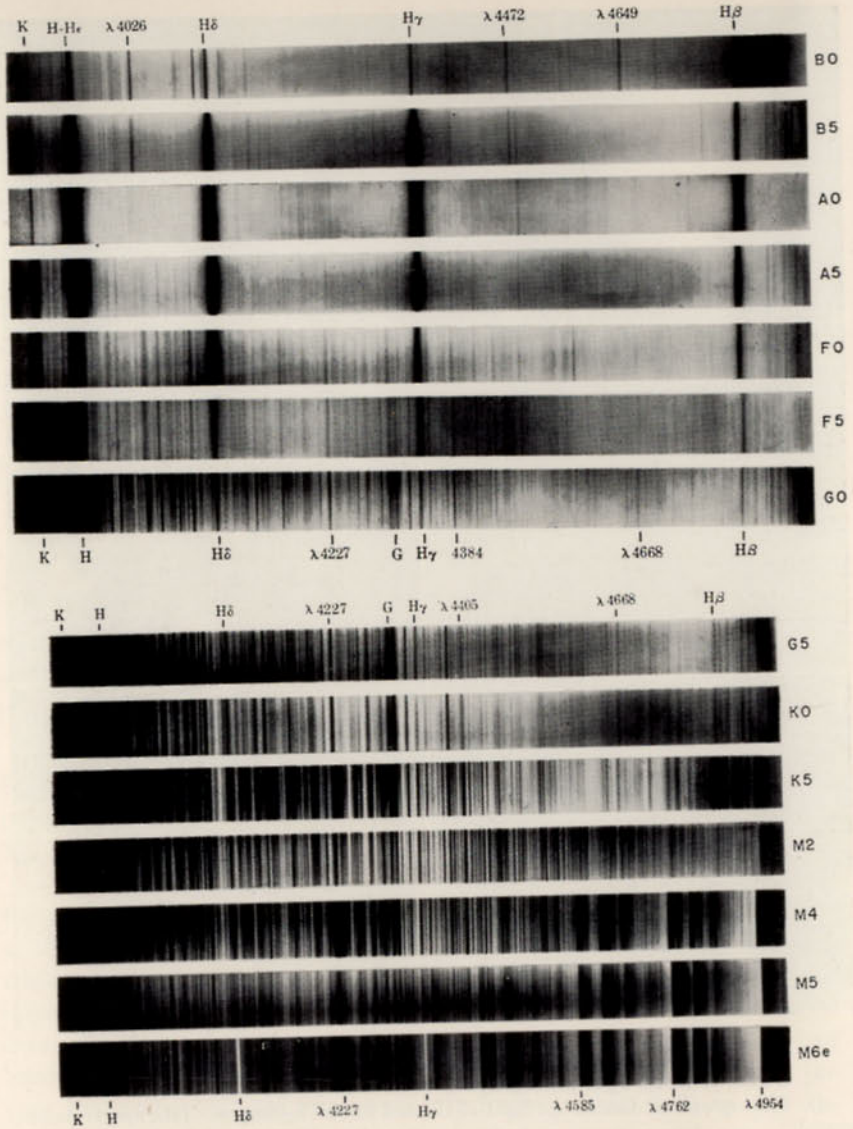

FIG. 2.—THE SPECTRAL SEQUENCE FROM *B*0 TO *M*6

Notice the decline in the intensity of the He I, λ4472 and λ4026 lines from *B*0 to *A*0, the great increase in the strength of the hydrogen lines to a maximum at *A*0 and subsequent decline, and the steady increase in the intensities of the metallic lines: *H* and *K* of ionized calcium (Ca II), λ4227 of neutral calcium (Ca I), and λ4384, λ4668, and λ4405 of neutral iron (Fe I), toward the lower temperatures. The bands of compounds become increasingly conspicuous toward the lower temperatures. The bands of titanium-oxide, whose heads (see Chapter 2) fall at λ4585, λ4762, and λ4954, are strong in the *M*-type stars. The last strip, *M*6e, is the spectrum of Mira Ceti. (Photographed by R. H. Curtiss and W. C. Rufus at the University of Michigan Observatory.)

sponding to an apparent luminosity ratio of 100. A first magnitude star* is the fifth root of 100 or 2.512 times brighter than one of the second magnitude which in turn is 2.512 times brighter than a third magnitude star. The magnitude difference between two stars is related to their relative apparent luminosities l_1 and l_2 by

$$\frac{l_1}{l_2} = (2.512)^{m_2 - m_1} \tag{2}$$

or

$$m_2 - m_1 = 2.5 \log (l_1/l_2) \tag{3}$$

The magnitude of a star depends on its color and the wave length sensitivity of the device used to observe it.† The various light-measuring devices employed by astronomers differ in their response to light of different colors. The eye is most sensitive to the green and relatively insensitive to the violet and deep red. Ordinary photographic emulsions which are most sensitive from the blue down to the ultraviolet limit of transmission of the atmosphere are used to determine *photographic* magnitudes. Orthochromatic plates used in conjunction with yellow filters have a color sensitivity roughly similar to that of the eye. Magnitudes determined with such a combination are designated as *photovisual* (*pv*) magnitudes. Red- or infrared-sensitive plates can be employed with appropriate filters to determine red and infrared magnitudes.

Among the most sensitive photoelectric cells is the RCA type 1P21 multiplier phototube that employs an antimony-caesium surface. The sensitivity falls off to the red side of λ4000 and approaches zero around λ6200. Photocells using a "caesium-oxide on silver" surface are employed for photoelectric photometry in the red and infrared.

In the infrared where photographic plates are insensitive or unusable, the thermocouple and lead-sulfide cells are employed. The former is sensitive to all parts of the spectrum. In the region of 1 to 3 microns, however, the lead-sulfide photoconductive cell is about one hundred times as sensitive as the best thermocouple.

Both photographic and visual magnitude systems are widely used. The zero-point of the two systems is so adjusted by convention that the mean photographic magnitudes of certain white stars of spectral class *A*0 (see Sec. 4) between 5.5 and 6.5 shall equal the mean Harvard

* The zero-point of the magnitude scale has been set by general agreement among astronomers.

† For example, Edmondson's red variable, BN Monocerotis, has a photographic magnitude of 14, a photovisual magnitude of around 9, and a photored magnitude of about 7.5.

visual magnitudes for these stars. The procedure is not free from objections.*

We define the difference between the photographic and visual magnitude of a star as the *color index*, viz.:

$$\text{C.I.} = m_{\text{ptg}} - m_{\text{vis}}$$

Red stars are fainter photographically than visually. Thus BN Monocerotis has a color index of about 5 magnitudes. The color indices of blue stars are negative but never by more than a few tenths of a magnitude.

For many problems we need a number which characterizes the total amount of energy received from the star, at a point just outside the earth's atmosphere. We call this quantity the apparent *bolometric magnitude*. The magnitude measured by the eye, photographic plate, photoelectric cell, or thermocouple must be corrected for the fact that the detector may not be sensitive to all wave lengths, and for the absorption in the earth's atmosphere. These corrections are called *bolometric corrections*. (See Chapter 6.)

The apparent brightness of the star as measured by the observer can be converted to its intrinsic luminosity only when the distance of the star is known. We define as its absolute magnitude, M, the magnitude the star would have if placed at a distance of 10 parsecs. Let m be the apparent, M the absolute magnitude, and r the distance of the star in parsecs. Let l refer to the amount of light received from the star at its true distance, and L to that which would be received at the standard distance r_o of 10 parsecs. Then

$$\frac{l}{L} = \left(\frac{r_o}{r}\right)^2$$

and

$$M - m = 2.5 \log l - 2.5 \log L = 5 \log r_o - 5 \log r \qquad (4)$$

Since $\log r_o = 1$, we have

$$M = m + 5 - 5 \log r \qquad (5)$$

The apparent magnitudes of distant stars are often affected by the absorption of light in the interstellar medium. If this absorption amounts to A magnitudes then the star is actually brighter than would be judged from its apparent magnitude and distance. Therefore,

$$M = m + 5 - 5 \log r - A \qquad (6)$$

The absolute visual magnitude of the sun is +4.7, which means it would be nicely visible to the eye on a clear night at a distance of 10 parsecs. The intrinsically faintest known star, the companion to BD + 4° 4048, discovered by van Biesbroeck, has an absolute magnitude of +19; it is a million times fainter than the sun. The brightest star, S Doradus, is of the order of 500,000 times as brilliant as the sun. Most of the stars in a volume of space in our part of the galaxy are fainter than the sun, while most of those visible to the eye are actually brighter, since brighter stars are visible at greater distances than fainter ones.

* The choice of $A0$ stars is unfortunate because the energy distribution in their spectra deviates appreciably from that of a black body. They include many intrinsically bright stars which are situated at great distances and are often reddened by space absorption. Also the Harvard visual magnitudes are inhomogeneous. It would have been better to have used the Potsdam Generalkatalog, probably the best catalog of visual magnitudes that has been made. Today such measures can best be made with the photocell.

4. Spectra of the Stars

Surface temperatures of the stars, their chemical compositions, and their velocities in the line of sight may be deduced from a study of their spectra. The majority of stars show a continuous spectrum upon which are superposed the dark Fraunhofer absorption lines.

Despite the vast range in the luminosities of the stars, the spectra of all but a few may be grouped into a small number of spectral classes, which form a continuous sequence. The order of the Harvard spectral sequence is

$$\begin{array}{c} \qquad\qquad R\text{—}N \\ O\text{—}B\text{—}A\text{—}F\text{—}G\text{—}K\text{—}M \\ \qquad\qquad S \end{array}$$

The spectral sequence O to M is continuous whereas the R and N stars form one side branch and the S stars another. Decimal subdivisions are also employed. Thus $F5$ denotes a spectrum about half-way between F and G in appearance, whereas $B8$ indicates a spectrum closer to $A0$ than to $B0$. On this system the sun is near $G2$ or $G3$ (subdivisions not employed in the Henry Draper Catalogue but required for refined work).

In classes O and B both emission-line and absorption-line objects are observed. Prominent in class O are the lines of hydrogen, H I; neutral helium, He I; ionized helium, He II, as well as doubly ionized oxygen, nitrogen, and carbon, O III, N III, and C III. In class B, the helium, He I, and hydrogen lines strengthen, while ionized helium disappears. Singly ionized carbon, nitrogen, and oxygen are important and the lines of doubly ionized iron, Fe III, and ionized magnesium, Mg II, put in their appearance. The hydrogen lines attain their greatest strength near $A2$, the lines of He I disappear, and the metals gain in prominence. Throughout classes A and F the hydrogen lines weaken and the metals

strengthen until at *G*0 the most prominent lines are the *H* and *K* lines of ionized calcium (Ca II), the "*G-band*" which is a mixture of atomic lines and molecular bands, and the lines of common metals, Fe, Ti, Mg, Cr, etc. In class *K* the low temperature lines of the metals strengthen and finally in class *M* the titanium-oxide bands dominate the spectrum. The *R* and *N* branch comprise stars with strong bands of the carbon compounds, whereas class *S* shows bands of ZrO rather than bands of TiO.

An important fact about the spectral sequence is that it is also a color sequence. The *O* and *B* stars are intrinsically blue, the *A* and *F* stars are white, the *K* stars orange, and the *M* stars red. In other words, the *O* and *B* stars must be the hottest and the *M* stars the coolest in the spectral sequence. As Saha pointed out in 1922 the spectral sequence is essentially a temperature sequence and spectral variations arise from differences in temperature rather than from differences in composition. The late *O* stars have temperatures near 30,000°K, the early *B*'s near 21,000°K, an *A* star like Sirius has a temperature of 10,000°K, *G* stars have temperatures in the 4900°K–5800°K range, and the *M*'s have temperatures in the 2500°K–3200°K range.

5. The Spectrum-Luminosity Relation

If the absolute magnitudes of the stars are plotted against their spectral classes the points do not scatter all over the diagram as one might expect, but fall in a definite pattern. The resultant plot is called the *Russell diagram* or the *Russell-Hertzsprung diagram*. Most of the

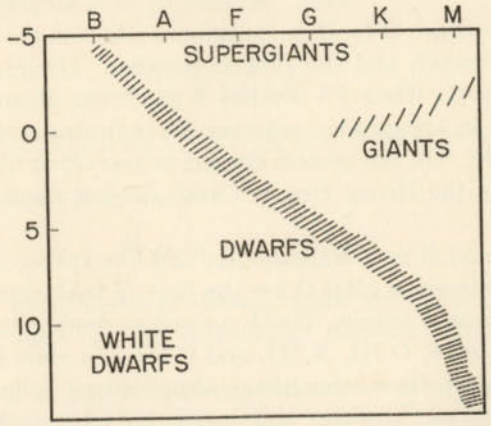

FIG. 3.—THE SPECTRUM-LUMINOSITY RELATIONSHIP

When the absolute visual magnitudes of the stars are plotted against their spectral types most of the points fall in groups which define the dwarf or main sequence, the giants, the supergiants, and the white dwarfs. A diagram of this type was first prepared by H. N. Russell about 1913.

stars cluster along a curve running diagonally from highly luminous blue stars at one corner to dim red ones at the other, color and luminosity changing progressively. This group of stars is called the **main sequence** (or **dwarf sequence**). The sun is a main-sequence star. Its absolute magnitude is about 5 and its spectral class is *G*2.

The rest of the diagram is more sparsely populated. The *giants* form a group around absolute magnitude 0 to +1.0 extending from about *G*0 to the later (i.e., redder) spectral classes. At the top of the diagram is a thin sprinkling of the highly luminous *supergiants* ($M = -3$ to -7) in which all spectral classes are represented. These stars are rare; their enormous candlepower enables them to be seen at great distances with the result that among naked-eye stars there is a large proportion of supergiants.

Beneath the giants and above the dwarfs is the group of *subgiants*, whereas just below the main sequence are occasional representatives of the *subdwarfs*. The lower left-hand side of the diagram includes certain intrinsically faint stars—the famous "*white dwarfs*" whose sizes are comparable with those of planets but whose masses are similar to that of the sun. Hence their densities exceed that of the sun by many thousands of times. Yet in spite of this fact, or more accurately because of it, these stars are better understood than the giants or supergiants.

The terms giant, supergiant, and dwarf, originally invoked to express the relative luminosities of the stars, apply to their sizes as well. The emissivity of matter per cm² depends primarily on its temperature. Hence a supergiant ten thousand times as luminous as the sun but of the same surface temperature must have very closely ten thousand times the surface area or a radius a hundred times as great. The giant, Capella, has a radius 16 times that of the sun while the red supergiant, α Herculis, which has ten thousand times the sun's luminosity but a much lower surface temperature, has a diameter 800 times that of the sun. Even this star is outdone by VV Cephei whose vast atmosphere would envelop Saturn if its center were placed in the position of the sun.

On the other hand, the most luminous main-sequence stars of whose sizes we have any precise knowledge, the components of the eclipsing system Y Cygni, which are ten thousand times as bright as the sun, have radii only six times that of the sun. Krueger 60A, a typical red dwarf, has a radius about half that of the sun, while its luminosity is 0.017 that of the sun.

The usual Russell diagram applies to the Milky Way in the neighborhood of the sun. Globular star clusters, however, give a somewhat different picture. Many years ago, Shapley plotted the colors of stars in globular clusters against their magnitudes. (See Fig. 4.) Since colors

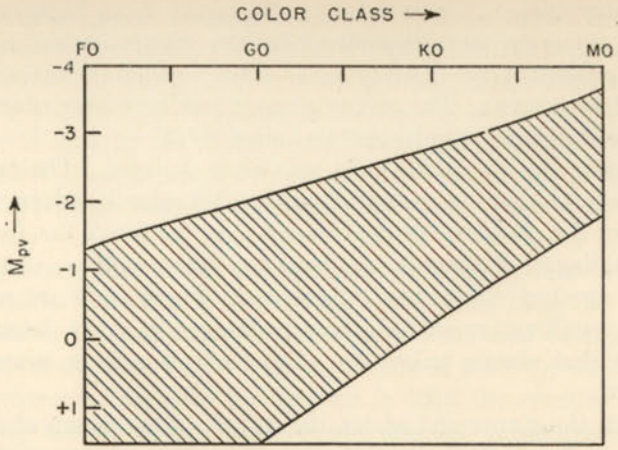

FIG. 4.—COMPOSITE COLOR-MAGNITUDE ARRAY FOR THE GLOBULAR CLUSTERS, *M3*, *M13*, AND *M22*

The color class, expressed in terms of the corresponding spectral class, is plotted against the absolute photovisual magnitude. The majority of the stars fall in the cross-hatched area; the individual points are not shown. (After Harlow Shapley.)

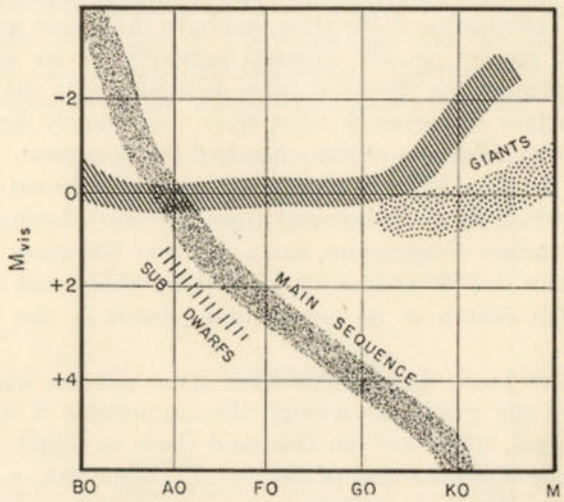

FIG. 5.—TYPE I AND TYPE II STELLAR POPULATIONS

The Type I distribution is indicated by the shaded areas. The Type II distribution of the most luminous stars, to which we have added the subdwarfs, is indicated by the cross-hatching. Compare this schematic diagram with Fig. 6 where an observed color-magnitude array for a globular cluster is given with a similar plot for a Type I population. (Adapted from a diagram by Walter Baade, *Astrophysical Journal*, University of Chicago Press, **100,** 143, 1944.)

are correlated with spectral types and since all objects in a cluster are at practically the same distance from the sun, his color-magnitude array is equivalent to a spectrum-luminosity plot. There are no blue main-sequence stars in globular clusters. The dwarf sequence appears to start near *A*0 and continue to the fainter stars. The giant stars are distributed along a curve such that, the redder a star, the higher its luminosity. In particular, the gap at absolute magnitude 0, between the main sequence and the giants (the Hertzsprung gap) now appears to be populated and includes the cluster-type Cepheid variables. More recently, W. Baade has emphasized the existence of two types of stellar distribution, one characterizing the majority of stars found in our part of the galaxy, Type I, and the other, Type II, characterizing the globular clusters, the elliptical nebulae, and the center of our own Milky Way. (See Fig. 5.) Galactic clusters represent pure Type I distribu-

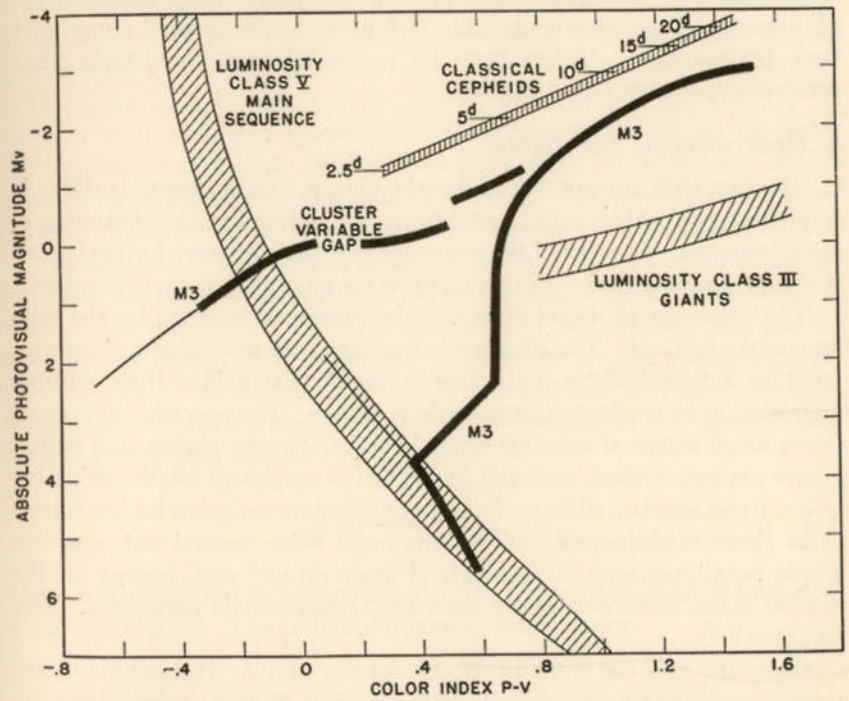

FIG. 6.—COLOR MAGNITUDE ARRAY FOR THE GLOBULAR CLUSTER MESSIER 3

In this diagram, based on the work of Allan Sandage, absolute photovisual magnitudes are plotted against color indices for stars of the globular cluster, Messier 3. This Type II population is compared with the giant and main sequences of a Type I population (cross-hatched area). The cluster variables fall in the gap indicated. Notice the extension of the cluster stars to the left (blue stars) and that the main sequence does not extend to the hotter, more luminous, stars. The position of the classical Cepheid variable stars at medium light is indicated.

tions as apparently do the outer regions of the Magellanic clouds. The globular clusters exhibit a pure Type II population. Near the sun, representatives of both types are found. Stars moving about the galactic center in nearly circular orbits, e.g., the *B* stars, belong to Type I. Bona fide Type II objects, such as the cluster-type variables, tend to move in highly elliptical orbits; evidently they are invaders from distant regions of our galaxy. Below *A*0 both types seem to follow the main sequence.

When absolute magnitude is plotted against spectral type for stars whose trigonometric parallaxes, apparent magnitudes, and spectra are determined, the main sequence shows an appreciable scatter. The sun does not fall at the center of the distribution. Some of this scatter may be real but most of it probably arises from observational error. It is to be noted that when accurate colors and magnitudes of stars in galactic clusters such as the Pleiades or Hyades are determined (by photoelectric photometry), the color-magnitude plot gives a well-defined curve with very little scatter. Colors may be measured more accurately than spectral types may be estimated.

6. Spectroscopic Parallaxes

The fact that the spectra of dwarfs, giants, and supergiants differ in small but noticeable details enables us to determine the distances of stars from the character of their spectra and their apparent magnitudes. A stellar parallax derived in this way is called a *spectroscopic parallax.*

The distances of dwarf stars may be measured directly by the trigonometric method. The distances of giants and supergiants, however, must be established by statistical methods that utilize their motion, membership in clusters, and galactic rotation. The spectral differences (for a small range of spectral type) between dwarfs, giants, and supergiants are established, and the quantitative empirical relationships between these spectral differences and the absolute magnitudes are found. Once these fundamental calibrations have been worked out, spectroscopic parallaxes may be determined more rapidly and, except for the nearest stars, more accurately than the trigonometric parallaxes. (See Chapter 8.)

Since the pioneer work of W. S. Adams and A. Kohlschütter, extensive work has been carried out at Mount Wilson, particularly by A. H. Joy, culminating in a catalog of spectroscopic parallaxes. Mention must be made of the investigations of Lindblad and his colleagues in Sweden and the *Atlas of Stellar Spectra* due to Morgan and Keenan. The Yerkes system of classification assigns luminosity classes as well as Henry Draper classes. Thus I, II, III, IV, and V refer respectively to supergiants, bright giants, giants, subgiants, and dwarfs. Keenan has

carried out a calibration of these luminosity classes in terms of absolute magnitudes. The reader is referred to his paper for an account of this problem.

7. Eclipsing Binaries

Our considerations about the sizes of stars are fortunately substantiated by data of quite an independent sort. Little exact information may be obtained from single stars, but double stars that occur as eclipsing binary systems provide a wealth of facts. Two stars move about each other in elliptical orbits whose orientation with respect to the observer is such that an eclipse will occur when one passes in front of the other. The inclination of the orbit and the radii of the stars determine whether the eclipse will be partial, annular, or total.

The observational data are a light-curve which shows the variation of the brightness of the system as a function of time, and occasionally measurements of the velocity of one or both of the components in the line of sight. From the light-curve it is possible to derive the relative radii of the stars in terms of the size of the orbit. If the velocity of the star is known from spectroscopic measurements of radial velocity, the circumference follows at once from the period. With the size of the orbit given in kilometers, the radii of the stars can be computed immediately. Thus Stebbins determined the diameter of β Aurigae in 1911.

The analysis of the light-curve gives the inclination i of the plane of the orbit to the line of sight. The spectroscopic measurements give $a_1 \sin i$, the semi-major axis a_1 of the orbit of the brighter star multiplied by the sine of the inclination. If both spectra are visible we find $(a_1 + a_2) \sin i$. A combination of the photometric and spectroscopic data therefore yields a and the period P. The sum of the masses then may be found from Kepler's third law

$$m_1 + m_2 = \frac{a^3}{P^2} \tag{7}$$

where a is measured in astronomical units, P in years, and m in terms of the sun's mass. The individual masses follow from

$$\frac{m_1}{m_2} = \frac{a_2}{a_1}$$

The relative depths of eclipses give the ratio of the surface brightnesses of the two stars. If the parallax of the system is known and the sizes of both components are calculated with the aid of spectroscopic observations, one can compute the absolute surface brightnesses of the stars in ergs radiated per cm^2 per second. Fortunately, it is possible to

obtain such detailed information for a $B3$ and for a $K6$ system (μ' Scorpii and YY Geminorum). Thus we have an independent check on the system of stellar temperatures, since the relation between emissivity/cm^2 and temperature is known (Stefan-Boltzmann law—Chapter 5).

In addition to radii and masses, much other useful information can be found from eclipsing binary systems. Often the stars tidally perturb each other; the amount of distortion depends on their separation and the concentration of mass towards the center. Because of these distortions the stars do not attract each other as point masses and as a consequence the whole elliptical orbit slowly rotates in space, a phenomenon we refer to as the motion of the line of apsides. From the rate of this motion much has been learned concerning density distributions in the interiors of stars. Theoretically, the deformation of the figure of the star by tidal action can be determined from the shape of the light-curve. However, the interpretation of the latter outside of eclipse is complicated by the reflection of the light of one star from the surface of the other and by the phenomenon of gravity darkening. Usually the rotations of eclipsing stars are synchronized exactly with the orbital revolution. The stars keep the same sides pointed toward each other just as the moon keeps the same face pointed toward the earth. In a few systems, the smaller, heavier component of the pair spins more rapidly than it revolves, but in all instances the direction of rotation is in the same sense as the orbital revolution.

The darkening to the limb, a phenomenon observed in the sun, depends on the wave length, surface temperature, gradient, and source of opacity in the stellar atmosphere. Its dependence on wave length can be inferred from good light-curves in different colors but its absolute value may be established only with difficulty.

The most abundant eclipsing stars are the W Ursae Majoris variables—dwarf stars closely comparable to the sun. They revolve around each other almost in contact and are highly distorted.

Further information on stellar diameters comes from certain red supergiants whose angular diameters have been measured directly with the interferometer. If the parallax of the star is known, the true diameter can be found immediately from the angular diameter.

8. The Mass-Luminosity Law

Visual binaries are the most important source of data on stellar masses. The orbit gives the period P and semi-major axis, a'', in seconds of arc. If the parallax p is known, we may find $a = a''/p''$, the semi-major axis in astronomical units. Then from Kepler's third law, eqn. (7), it is possible to solve for the sum of the masses. Hence a good

mass determination requires an accurate parallax. The individual masses, m_1 and m_2, of a visual double can be found only if the orbit of each component can be measured in relation to the center of gravity of the pair. That is, the absolute motions of the stars upon the background of the sky must be determined.

A comparison of stellar masses and intrinsic luminosities leads to the important mass-luminosity law, which played so significant a role in the development of the theory of stellar interiors.

According to the discussion by Russell and Miss Moore, the absolute bolometric magnitude M is related to the mass $\mathfrak{M}$ by

$$\log \mathfrak{M} = -0.1048(M - 5.23) \tag{8}$$

If both the intrinsic luminosity L and the mass $\mathfrak{M}$ are measured in units of the sun's luminosity and mass,

$$\log L = 3.82 \log \mathfrak{M} - 0.24 \tag{9}$$

The significance of the constant 0.24 is that the sun is 1.7 times as bright as it should be for its mass. That is, an average main-sequence star of solar mass would be fainter by 0.60 magnitude. It would also be smaller and denser than the sun. An "average" star of the same intrinsic luminosity as the sun would be 15 per cent more massive and would be slightly cooler and redder than the sun.

Both giants and dwarfs appear to fit the mass-luminosity relation reasonably well, but our data concerning the supergiants are less certain. The brighter components of eclipsing binaries usually agree with the normal mass-luminosity relationship although the faint components are often discordant. If two members of an eclipsing system are main-sequence stars, the fainter star will be smaller, cooler, and less massive than the brighter one. Therefore it cannot totally eclipse the more luminous one. Observational selection tends to favor the deeper eclipses, that is, to pick objects in which a normal main-sequence star is accompanied by a larger, less dense, cooler companion. This latter star tends to be a subgiant, whose mass, luminosity, and radius may be abnormal. The masses of the tenuous companions turn out to be smaller than one would estimate from their luminosities. Russell and Miss Moore have found that the more tenuous the companion, the greater the deviation.

The abnormalities of the objects found in eclipsing systems is in one sense disappointing, but in another useful, for they may cast some light on problems of stellar structure.

The white dwarfs are much too faint for their masses. Their internal structures and energy sources appear to differ fundamentally from those of normal stars.

The surface gravity, g, of a star depends on its mass and radius. If $\mathfrak{M}$ and R are measured in terms of the solar mass and radius

$$g = g_0 \mathfrak{M}/R^2 = 2.74 \times 10^4 \, \mathfrak{M}/R^2 \quad \text{cm/sec}^2 \tag{10}$$

From the data of eclipsing variables, Russell has found that the surface gravities of main-sequence stars can be well represented by the empirical formula

$$\log g = 3.79 + 0.64\theta \tag{11}$$

while for the giant stars, a rough approximation is given by

$$\log g = 5.20 - 2.24\theta \tag{12}$$

where $\theta = 5040/T$. The surface gravity g and temperature T, together, determine the spectrum of a star of normal composition. When we distinguish giants and dwarfs by spectroscopic criteria we separate them in terms of their surface gravities.

It must be remarked that the effective surface gravities of supergiant stars are often smaller than the values computed from their radii and masses. Perhaps the atmospheres of such stars are not in ordinary mechanical equilibrium. (See Chapters 7 and 8.)

9. The Plan of Attack

With this brief sketch of some of the basic astronomical data we turn next to an account of the physical background required for an interpretation of stellar atmospheres and interiors. Chapter 2 summarizes salient facts on spectroscopic nomenclature, and atomic and molecular structure. Chapter 3 treats of the gas laws and the distribution of molecular velocities, whereas Chapter 4 gives an account of basic thermodynamic relationships we shall need. The important subject of the interaction of radiation with matter occupies the bulk of Chapter 5.

In the following chapters we proceed with the study of the continuous and dark-line spectra of the sun and stars, the gaseous nebulae, and the interstellar medium as well as with the problems of stellar interiors and of energy generation. We shall pay special attention to the sun, whose interpretation is one of the most fundamental tasks of astrophysics. Most of our discussion is concerned directly with solar or closely allied problems.

REFERENCES

The basic material of this chapter is covered very well in

Russell, H. N., R. S. Dugan, and J. Q. Stewart. *Astronomy*, II, Boston: Ginn & Co., 1927.

For a general discussion of stellar magnitudes and photometry see:

Weaver, H. F. *Pop. Astr.* **54**, 211, 287, 339, 451, 504, 1946.

Spectral classification is discussed in the introduction to the Henry Draper Catalogue, Harvard College, Observatory. The modern system is given in:

Morgan, W. W., P. C. Keenan, and E. Kellman. *An Atlas of Stellar Spectra*. Chicago: University of Chicago Press, 1943.

The fundamental paper on the two types of stellar distribution is:

Baade, W. *Ap. J.* **100**, 137, 1944.

The mass-luminosity relationship is discussed by:

Kuiper, G. P. *Ap. J.* **88**, 472, 1938.
Russell, H. N., and C. E. Moore. *The Masses of the Stars*. Chicago: University of Chicago Press, 1940.

The classical papers on eclipsing binaries are:

Russell, H. N. *Ap. J.* **35**, 315, 1912; **36**, 54, 1912.
Russell, H. N., and H. Shapley. *Ap. J.* **36**, 239, 385, 1912.
Shapley, H. *Princeton Contr.* **3**, 1915.

The last paper gives the orbits of 90 systems computed by Russell's methods.

A bibliography of important modern papers may be found in Newton Pierce's article in:

Hynek, J. A. (ed.). *Astrophysics, A Topical Symposium*. New York: McGraw-Hill Book Co., Inc., 1951.

CHAPTER 2

Atomic and Molecular Spectra

1. Introduction

Before the modern quantum theory was developed, the interpretation of spectra had progressed scarcely beyond the rudimentary level. The chemical origin of most of the lines in the spectra of the sun and similar stars had been established. Kirchhoff's three laws of spectral analysis gave the relation between the general nature of the source and the kind of spectrum emitted, viz., (1) an incandescent solid, liquid, or a gas under sufficient pressure gives a continuous spectrum, (2) an incandescent gas under low pressure emits a spectrum of discrete bright lines, and (3) a gas placed in front of a hotter source of continuous radiation will produce a dark-line or absorption spectrum superposed upon the continuous background. These absorption lines will fall at precisely the same wave lengths that the gas regularly emits. In addition to the bright- and dark-lined atomic spectra, the complicated "band" spectra of molecules were also recognized and studied.

Thus the Orion nebula, which emits a bright-line spectrum, was correctly interpreted as an incandescent gas whereas the dark-line spectra of the sun and stars could be explained in terms of the Kirchhoff third law. It was generally believed that the bright surface or "photosphere" of the sun emitted a continuous spectrum and relatively cooler gas in the overlying atmosphere, then called the "*reversing layer*," absorbed certain wave lengths characteristic of the elements present. In 1874, Young obtained a striking demonstration of the second and third laws by observing an eclipse with the spectroscope. Before totality, the dark-line or *Fraunhofer spectrum* was evident; the instant the photosphere of the sun was covered by the moon, the dark lines disappeared and were replaced by bright lines in exactly the same positions. Before totality, the light reaching the observer passed through the cooler gases of the sun's atmosphere and produced a dark-line spectrum in the usual way. When the photosphere is blocked from view, the observer receives radiation from only the upper atmosphere and thus obtains the characteristic bright-line spectrum of an incandescent gas. We now know this picture to be somewhat oversimplified. The Fraunhofer and the continuous spectra of the sun and stars are both produced in the same layers. Only the tiniest fraction of the atoms in the solar atmosphere, namely those

in the attenuated chromosphere, produce the bright lines of the flash spectrum observed by Young.

The source of the continuous spectrum of the sun was a puzzle for many years. Kirchhoff's first law would suggest that it was produced by a hot gas under pressure (since the temperature of the solar atmosphere is too high to permit solids or even liquids to exist). Later studies by J. Q. Stewart and others showed that the pressure at the bottom of the solar atmosphere was much too low to admit this explanation. Atoms and molecules are known to emit and absorb continuous as well as discrete line spectra, but the continuous absorption in the solar atmosphere is produced primarily by the negative hydrogen ion.

The astronomers and physicists of the late nineteenth century could make a qualitative chemical analysis of the stars and nebulae. Kirchhoff, who pioneered in these investigations, was able to identify most of the lines in the solar spectrum with such familiar elements as hydrogen, iron, nickel, calcium, chromium, titanium, sodium, magnesium, etc. Similar studies of stellar spectra by Huggins, Lockyer, and others established the essential identity of the chemical composition of the stars and the earth. Elements abundant in the earth were usually well represented in the sun and stars, and rare elements on the earth were often missing. The recognition of the sameness of the matter throughout the universe was the first great discovery of astrophysics. Nevertheless, some abundant elements are poorly represented in the spectra of stars like the sun.

Atomic carbon and oxygen—very abundant constituents of the earth—are represented in the sun by moderately conspicuous lines in the infrared. The strongest lines of these and many other elements lie in the astronomically inaccessible ultraviolet below $\lambda 2900$. No lines of abundant neon appear in the observable solar spectrum at all! The appearance of molecules of carbon and nitrogen, CN, oxygen and hydrogen, OH, etc., show these elements to be abundant in the sun.

The gaseous nebulae presented real difficulties. Their spectra showed the familiar emissions of hydrogen and helium but the strongest nebular radiations had never been produced on the earth. For many years astronomers spoke of a hypothetical and mysterious nebulium until the advance of physics showed there was no room in the periodic table for such an element. Ultimately, these radiations were assigned to such familiar constituents of the earth's atmosphere as oxygen, nitrogen, neon, and argon.

Any quantitative analysis of the sun and stars presented formidable difficulties. How is the intensity of a spectral line related to the abundance of the relevant element? Can the temperature of the atmosphere of a star be determined from its spectrum? These questions could be

answered only when the structure of the atom was understood and when the processes of the emission and absorption of energy could be expressed in quantitative terms.

Thus the relationship between the structure of atoms and their spectra proves of crucial importance to astrophysics and our survey of basic principles can well begin with a brief excursion into this problem.

The fundamental building block of all the complicated substances of nature, the *atom*, consists of a positively charged core or *nucleus* which contains nearly all the mass, surrounded by one or more negatively charged, constantly moving *electrons*. Each electron carries a negative charge of 1.6×10^{-19} coulombs or 4.80×10^{-10} e.s.u. In the complete atom the positive charge on the nucleus equals the sum of the negative charges on the electrons. For example, eight electrons surround the nucleus of the oxygen atom which carries a positive charge of $8 \times 4.80 \times 10^{-10} = 3.84 \times 10^{-9}$ e.s.u.

The simplest of all atoms is hydrogen, which consists of a positively charged particle called a *proton* and a single negatively charged electron. The charge on the proton is the same as that on the electron, but the mass of the proton, 1.67248×10^{-24} grams, exceeds that of the electron, 9.1055×10^{-28} grams, by a factor of 1836.57.

The hydrogen nucleus or proton is a fundamental particle of nature like the electron. All other atomic nuclei are more complicated, containing both protons and particles of about the same mass but no charge, called *neutrons*. Thus ordinary carbon of atomic number six (determined by the number of protons) and atomic weight 12 has 6 protons and 6 neutrons. The carbon *isotope* of atomic weight 13 has 7 neutrons and 6 protons.

2. Spectral Series

The outer or electronic structure of the atom determines the spectral lines that will be radiated. A basic postulate of the quantum theory is that an atom can exist in certain definite energy states and when it jumps from one of energy W_2 to another of lesser energy W_1 it emits radiation in accordance with the law

$$W_2 - W_1 = h\nu \tag{1}$$

or if $W_2 - W_1$ be denoted as E,

$$E = h\nu \tag{2}$$

represents the basic relation between energy and frequency ν. Here h is a basic quantity of nature called *Planck's constant;* $h = 6.6234 \times 10^{-27}$ erg sec.

Hydrogen, the simplest of all atoms, shows the simplest of all spectra. In 1885 Balmer showed that the wave numbers $\bar{\nu}$ of the visible hydrogen lines could be expressed by

$$\bar{\nu} = R\left(\frac{1}{2^2} - \frac{1}{n^2}\right) \tag{3}$$

where $n = 3, 4, 5$, etc., and R is a constant the same for all values of n, i.e., for all lines of the series. Subsequently series in the ultraviolet and infrared were found that could be represented by the formulae

$$\text{Lyman series} \quad \bar{\nu} = R\left(\frac{1}{1^2} - \frac{1}{n^2}\right) \quad n = 2, 3, 4, \text{ etc.} \tag{4}$$

$$\text{Paschen series} \quad \bar{\nu} = R\left(\frac{1}{3^2} - \frac{1}{n^2}\right) \quad n = 4, 5, 6, \text{ etc.} \tag{5}$$

Subsequently, Brackett and Pfund found other series yet farther in the infrared. The same constant R was involved in all of these formulae.

Alkali metals show somewhat similar series that may be represented by formulae of the type

$$\nu = T' - R/(n + \delta)^2 \tag{6}$$

where T' corresponds to the wave number of the series limit and δ is nearly constant for a given series.

Quite generally the wave numbers of spectral lines can be written as

$$\nu = T' - T'' \tag{7}$$

where T' and T'' are *term values* which are usually expressed in wave number units and correspond to the energy levels of the atom.

3. The Bohr Atom

In order to explain the hydrogen spectrum Bohr postulated that the electron traveled in a circular orbit around the positively charged proton. During this time it does not radiate; it emits energy only when it jumps from one orbit to another.

The orbits permitted to the electron have radii given by

$$a = \frac{h^2}{4\pi^2 m\varepsilon^2 Z} n^2 = 0.52916 \times 10^{-8} n^2 \text{ cm} \tag{8}$$

where m and ε denote the mass and charge on the electron respectively, Z is the atomic number (1 for hydrogen) and the integer n is called the principal quantum number. The energy in the nth orbit is

$$W_n = -\frac{2\pi^2 m Z^2 \varepsilon^4}{h^2} \frac{1}{n^2} \tag{9}$$

where $W = 0$ corresponds to the complete detachment of the electron from the atom. The ionization energy from the lowest level is

$$|W_1| = \frac{2\pi^2 m Z^2 e^4}{h^2} \tag{10}$$

and the energy radiated in the transition $(n–n')$ is:

$$W_n - W_{n'} = \frac{2\pi^2 m Z^2 e^4}{h^2}\left(\frac{1}{n'^2} - \frac{1}{n^2}\right) \tag{11}$$

The Bohr theory correctly predicted the frequencies of the lines of the hydrogen spectrum. We may represent the energies of the Bohr orbits in the hydrogen atom by means of an energy-level diagram. In accordance with eqn. (9) the zero of energy corresponds to complete detachment of the electron from the atom. The energy of the lowest level is $-W_1$, that of the second level is $-W_1/4$, etc. If we depict the transitions as vertical lines connecting the possible energy states we get Fig. 2. Thus lines ending on the first level represent radiation of the Lyman series, those ending on the second level radiation of the Balmer series, etc.

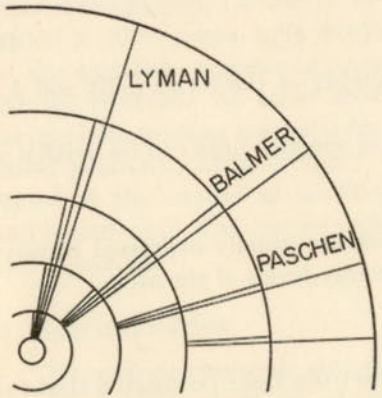

FIG. 1.—THE BOHR MODEL OF THE HYDROGEN ATOM

Transitions corresponding to the Lyman, Balmer, and Paschen series are depicted.

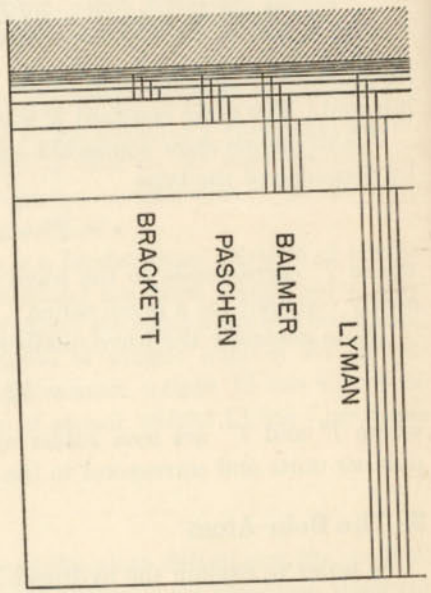

FIG. 2.—ENERGY LEVEL DIAGRAM FOR HYDROGEN

The energy levels (each of which corresponds to a Bohr orbit) are depicted as horizontal lines. The transitions are shown as vertical lines. If the lowest level is taken as 0 ev, the first excited level lies at 10.15 ev and the ionization potential (the highest horizontal line) lies at 13.54 ev. The cross-hatched area represents the continuum which corresponds to a complete detachment of the electron from the atom.

Downward transitions represent emission of energy by the atom; upward transitions represent absorption of energy.

Although eqn. (9) gives the energy in ergs, term diagrams are often plotted with wave-number units or electron volts (ev). The *excitation potential* of a level in ev is the potential through which a bombarding electron must drop in order to acquire sufficient energy to excite an atom from the ground level to the level in question. Energies expressed in electron volts are related to energies expressed in wave-number units by

$$V = 1.234 \times 10^{-4}\bar{\nu} \tag{12}$$

The energy-level diagram illustrates why the lines of the various spectral series crowd together and ultimately coalesce into a continuous spectrum. The larger the orbit the weaker the proton-electron attraction until the addition of a small amount of energy suffices to detach the electron completely, i.e., ionize the atom.

Whereas in the transition between two discrete levels the atom absorbs or emits precisely the correct amount of energy so that a spectral line is emitted or absorbed, in order to eject an electron the atom may absorb any amount of energy equal to or greater than that required to go from its initial state to the one represented by $W = 0$. The excess energy imparts a velocity, v, to the free electron, viz.,

$$h\nu - W_n = \tfrac{1}{2}mv^2 \tag{13}$$

In hot stars a strong continuous absorption is observed beyond the limit of the Balmer series. This continuum corresponds to the photoionization of hydrogen atoms from the second level. Conversely, the capture of free electrons of various velocities by protons in the second energy level gives the bright continuous spectrum observed beyond the Balmer limit in the planetary nebulae.

Ionized helium (denoted as He II) displays a hydrogen-like spectrum. Its ionization potential, however, is four times greater than that of hydrogen, 54.17 ev instead of 13.54 ev. Since $Z = 2$, eqn. (11) shows that the wave numbers of the He II lines will be given by

$$\bar{\nu} = 4R\left(\frac{1}{n'^2} - \frac{1}{n^2}\right)$$

An interesting result is that alternate lines of the Brackett $(4–n)$ series of He II correspond with the Balmer (hydrogen H I) lines. This series was first discovered in the stars and called the Pickering series. The general structure of the spectrum of any singly ionized atom resembles that of the atom immediately preceding it in the periodic table.

4. The Wave Atom

As we shall soon see, the planetary atom may be modified to produce a useful model for the prediction of lines emitted and absorbed by more complex atoms. The refined Bohr model or *vector model* is valuable for the enumeration of the kinds of levels of complex atoms, but fails to predict the energy levels correctly.

The modern quantum theory does not assign electrons to planetary orbits. Instead it is concerned with a wave amplitude, ψ, whose square expresses the probability of finding an electron at a given point at a given time. Not only the energy levels but the probabilities of transitions between them may be computed by these new techniques. Although the planetary orbits must be discarded, the concept of the energy level diagram (which involves no assumption concerning the atom model) remains intact.

5. Spectra of the Alkali Atoms

The alkali atoms Li, Na, K, etc., display the simplest spectra next to that of hydrogen. In depicting the Bohr model of an alkali atom we find it useful to refer to Sommerfeld's generalization of the Bohr theory to elliptical orbits. He showed that the allowed orbits were of such a

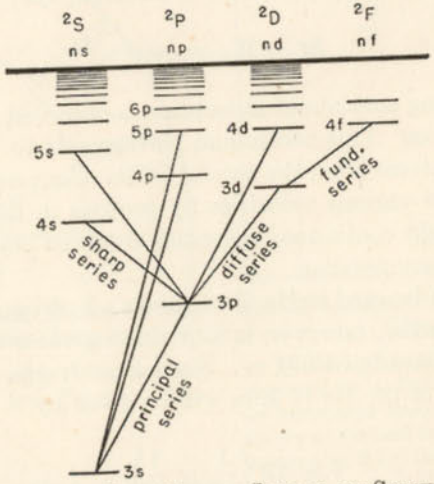

FIG. 3.—THE ENERGY LEVELS OF SODIUM

shape that the ratio of minor to major axis was k/n where k and n are integers. Here k is an integer subject to the rule $1 \leq k \leq n$ and n determines the major axis. Circular orbits require $k = n$.

In the quantum picture, the electron retains an angular momentum even though the concept of an orbit is discarded. We define an orbital

angular momentum quantum number $l = k - 1$ such that the angular momentum is $l\frac{h}{2\pi}$. Atomic states with $l = 0$ are called s states; $l = 1$ corresponds to a p state, $l = 2$ to a d state, and $l = 3$ to an f state. Now s states correspond to orbits of increasingly greater ellipticity as n increases. In hydrogen the energy depends on n and hardly at all on l, but in other atoms the energy depends on both n and l. Notice that the $3s$ level in sodium falls far below the corresponding hydrogenic $n = 3$ level, the $3p$ level falls closer, and the $3d$ only slightly below the hydrogenic level.

The ten inner electrons of sodium are held in tightly bound shells whereas the eleventh electron which is responsible for the optical spectrum is held only loosely. In the highly elliptical $3s$ orbit this electron spends much of its time close to the nucleus where the screening by the core electrons is less and the attraction of the nuclear charge is greater. Hence the electron is more tightly held in this orbit than in the $3p$ or $3d$ configurations which correspond to more nearly circular orbits for which the shielding by the ten core electrons is more nearly complete.

The observed spectral lines in sodium belong to the following series:

Sharp series	$= 3p - ns$	$n = 4, 5, 6$, etc.
Principal series	$= 3s - np$	$n = 3, 4, 5$, etc.
Diffuse series	$= 3p - nd$	$n = 3, 4, 5$, etc.
"Fundamental" series	$= 3d - nf$	$n = 4, 5, 6$, etc.

Transitions always take place between levels in adjacent columns in the energy level diagram, i.e., between levels whose l-values differ by unity. In the alkalis different l-values correspond to substantially different energies. The strongest lines in sodium correspond to the $3s - 3p$ transition, the first line of the *principal series*. This is also called a *"resonance line"* since it involves the ground level. Transitions between higher levels give what are called *subordinate lines*.

A conspicuous characteristic of alkali levels is their doubling which Uhlenbeck and Goudsmit suggested to be a consequence of the interaction between the magnetic moment of the orbital motion and that of the spin of the optical electron. All the p, d, f, etc., energy levels are doubled. The s-levels are not doubled because $l = 0$, and the orbital angular momentum and magnetic moment vanish.

6. Orbital and Spin Angular Moments

The angular momentum associated with electron spin is always numerically $\frac{1}{2}\left(\frac{h}{2\pi}\right)$. It and the orbital angular momentum $l\left(\frac{h}{2\pi}\right)$ have the important property they may be added and subtracted like ordinary

vectors.* The total angular moment j of an alkali atom in which only the outermost electron plays a role in the production of the optical spectrum is the vector sum of the orbital and spin angular momenta, thus

$$j = l + s \tag{14}$$

Numerically $j = l + s$ or $l - s$, the spin is lined up parallel or antiparallel to the orbital motion vector. For an s-level $j = \frac{1}{2}$, for a p-level $j = \frac{1}{2}$ and $\frac{3}{2}$, etc.

We designate a level by the notation

$$n^2(L)_J$$

where n is the total quantum number, L, which only for one electron spectra (hydrogen and the alkalis) is equal to l, is the azimuthal quantum number. The superscript 2 indicates that the levels are doubled and the subscript J (here equal to j) denotes the angular momentum quantum number. The L-value symbol is chosen according to the scheme

L-value	0	1	2	3	4	5
Symbol	S	P	D	F	G	H

The sodium ground level for which $l = L = 0$ and $j = l + \frac{1}{2} = 0 + \frac{1}{2}$ is written $3s^2S_{1/2}$. Likewise $3p^2P_{1/2}$ and $3p^2P_{3/2}$ refer to the two lowest p-levels with $J = 1/2$ or $3/2$. The sodium "D" lines are represented by the transitions:

$$3s^2S_{1/2} - 3p^2P_{3/2}\ \lambda 5889.953 \quad 3s^2S_{1/2} - 3p^2P_{1/2}\ \lambda 5895.923$$

7. The Vector Model for Complex Atoms

For atoms with several electrons responsible for the optical spectrum, the positions, numbers, and kinds of energy levels can be computed by quantum mechanics. The vector model, nevertheless, predicts the kind and number of energy levels in complex atoms; hence it is a useful device for remembering the results of quantum mechanical calculations.

We suppose that to each electron we can assign n, l, and s values appropriate to the size and shape of the corresponding Bohr orbit and electron spin. The vector l's and s's of the individual electrons are added to get the total angular momentum J of the whole atom in the particular energy level. For light atoms the appropriate mode of vector combination is to add the s's of the individual electrons to form the total spin vector S and the individual l's to form the resultant angular momentum L, viz.,

$$L = \Sigma l_i \qquad S = \Sigma s_i \tag{15}$$

* Quantum mechanics shows the angular momentum actually to be $\sqrt{l(l+1)}\,\frac{h}{2\pi}$ but the approximation $l\,\frac{h}{2\pi}$ suffices to give the number and kind of energy levels.

The sum of these vectors

$$J = L + S$$

tells the total angular momentum in the energy state; this mode of vector coupling is called LS coupling.*

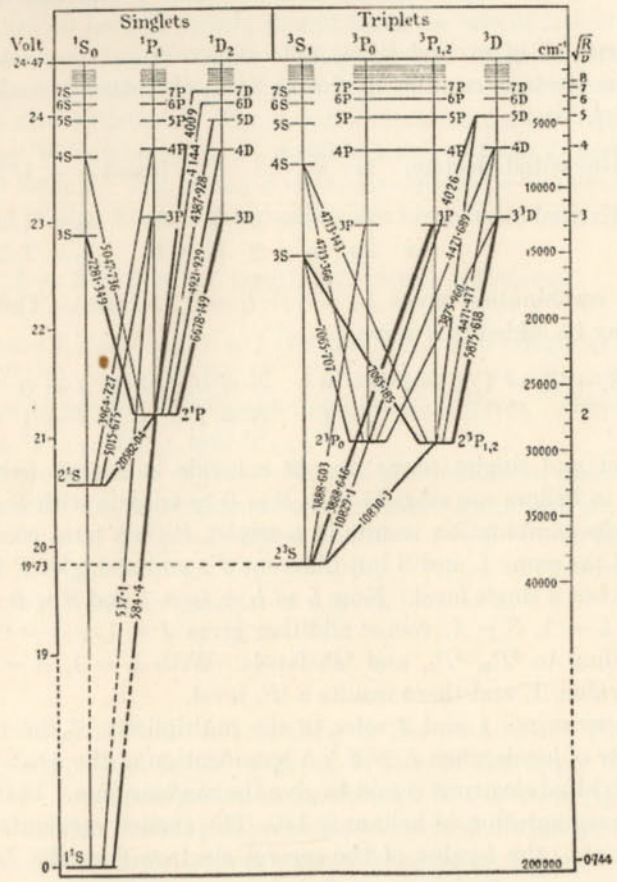

FIG. 4.—TERM DIAGRAM FOR HELIUM

(Courtesy, O. Struve and K. Wurm, *Astrophysical Journal*, University of Chicago Press, **88**, 87, 1938.)

Helium will serve as the simplest example of a 2-electron spectrum (see Fig. 4). The lowest level is represented by two 1s electrons, viz.:

$$1s^2 \quad l_1 = 0 \quad l_2 = 0 \quad L = l_1 + l_2 = 0$$

* The use of the letter S to denote both the term with $L = 0$ and the total spin vector is unfortunate. It arises from the fact that the notation S for the term $L = 0$ was firmly established before the S-vector was invented.

The Pauli Exclusion Principle (section 9) requires that the two s-electrons in the $n = 1$ have oppositely directed spins, i.e., $S = s_1 + s_2 = 1/2 - 1/2 = 0$. Also $J = 0$. Levels for which $S = 0$ are called singlet levels (denoted by the superscript 1). The ground level of helium is denoted as $^1S_0$, where the subscript 0 means $J = 0$ and the "S" means $L = 0$.

The first set of excited levels falls about 20 ev above the ground level. One electron remains in the 1s level; the other is excited to an $n = 2$ level, viz.:

Unexcited electron	$1s$	$n_1 = 1$	$l_1 = 0$ and	$s_1 = 1/2$	
Excited electron	$2s$	$n_2 = 2$	$l_2 = 0$		$s_2 = 1/2$
or	$2p$	$n_2 = 2$	$l_2 = 1$		$s_2 = 1/2$

The 1s2s combination gives $L_1 = l_1 + l_2 = 0$ (S term). The spins S_1 and S_2 may be added in 2 ways

$$S = S_1 + S_2 = 1/2 + 1/2 = 0 \qquad S = 0, L = 0, J = 0 \qquad {}^1S_0$$
$$= 1 \qquad S = 1, L = 0, J = 1 \qquad {}^3S_1$$

The triplet and singlet terms do not coincide in energy (see Fig. 4). All terms in helium are singlets with $S = 0$ or triplets with $S = 1$.

The 1s2p combination results in a triplet P (^3P) term consisting of 3 levels of the same L and S but different J's and a singlet P (^1P) term which has but a single level. Now $L = l_1 + l_2 = 1$ and $S = 0$ or $S = 1$. Choosing $L = 1$, $S = 1$, vector addition gives $J = 1 + 1 = 0$, 1, or 2, corresponding to $^3P_0$, $^3P_1$, and $^3P_2$ levels. With $L = 1$, $S = 0$, J has only one value, 1, and there results a $^1P_1$ level.

The superscripts 1 and 3 refer to the multiplicity of the term, i.e., the number of levels when $L > S$. A specification of the n- and l-values of the individual electrons is said to give the *configuration*. In its ground state the configuration of helium is $1s^2$. The excited configurations are ss, sp, sd, etc., the l-value of the second electron fixes the L-value of the terms.

The observed transitions in helium consist of jumps between triplet terms or between singlet terms, but not between singlet and triplet terms, i.e., there are $^1S - {}^1P$, $^3S - {}^3P$ jumps but not $^1S - {}^3P$ transitions. The totality of transitions between 2 terms comprises a multiplet. In Fig. 4 notice that the ^1S term in helium lies lower than the ^1P term. The $1s2s\,{}^1S - 1s^2\,{}^1S$ transition is strictly forbidden; the $2s\,{}^1S$ level is called a *metastable* level. In helium, which is in pure LS coupling, the ^3S level is also metastable and atoms may escape from such levels only by going to a higher level or by giving up their energy to a passing electron (*superelastic collision*).

Now consider the problem of more complex atoms. Two electrons that have the same n and l values are called equivalent electrons. The normal state of carbon or doubly ionized oxygen is $1s^22s^22p^2$ which means there are 2 electrons in a closed shell with $n = 1$, $l = 0$, two in a shell with $n = 2$, $l = 0$, and two in a shell with $n = 2$, $l = 2$. The s-electrons are all held in tightly bound shells for which $L = 0$, $S = 0$, $J = 0$. There are 3 sets of equivalent electrons. Suppose now one of the $2p$ electrons becomes excited to a $3d$ orbit so the configuration of the atom is now $1s^22s^22p3d$. The p and d electrons are not equivalent; their l's may be combined in all possible ways to form L and the s's similarly to form S. The p and d electrons determine the entire L, S, and J of the excited atom. The possible L's are

$$L = 1 + 2 = 3(F \text{ term}), 2(D \text{ term}), 1(P \text{ term})$$

Since there are 2 electrons, $S = 1$ (triplets) or $S = 0$ (singlets) and the terms are ^3P, ^3D, ^3F, or ^1P, ^1D, ^1F. For each term we must add the L and S values to get the J values of the individual levels. There results $^1P_1$, $^1D_2$, $^1F_3$, $^3P_{2,1,0}$, $^3D_{3,2,1}$, and $^3F_{4,3,2}$.

The arithmetical sum of the l-values of the individual electrons defines the "*parity*" of the configuration. If the l-sum is odd, we use the superscript "0". In the pd configuration $\Sigma l = 1 + 2 = 3$ so the levels are denoted as $^1P_1{}^0$, $^1D_2{}^0$, $^1F_3{}^0$, $^3P_2{}^0{}_{,1,0}$; $^3D_3{}^0{}_{,2,1}$; $^3F_4{}^0{}_{,3,2}$. In modern spectroscopic notation the designation of a given level is

$$^{(2S+1)}(L)_J{}^{0(\text{when odd})}$$

First write the symbol for L according to the notation S, P, D, etc. The multiplicity, equal to $(2S + 1)$, is written in the upper left-hand corner and the J-value is added in a subscript in the lower right-hand corner. If the term is odd, a superscript ^{0} is placed in the upper right-hand corner. The complete spectroscopic designation of a level involves also the (nl) values of the electrons. For example, the ground level of carbon is $1s^22s^22p^2\,{}^3P_0$, that of nitrogen is $1s^22s^22p^3\,{}^4S_{3/2}{}^0$. We denote the spectrum of a neutral atom by a I following the chemical symbol; II, III, IV, etc., denote successive stages of ionization. Thus O I means neutral oxygen, O II singly ionized oxygen, and O III doubly ionized oxygen.

Quantum mechanical calculations show that the separation of the terms of a given configuration arises from the electrostatic repulsion between the individual electrons. The fine structure of a term, e.g., the splitting of a ^3P term into $^3P_0$, $^3P_1$, and $^3P_2$ levels arises from the magnetic effects of spin-orbit interaction. (See Fig. 5.)

A comparison of the term separations with the distances between the individual levels composing the term will indicate how close the atom comes to LS coupling. If, as in helium, the separation of the terms of a given configuration much exceeds the distance between levels, the LS coupling approximation is a good one. Otherwise, the l's of the individual electrons no longer combine strictly with one another to form

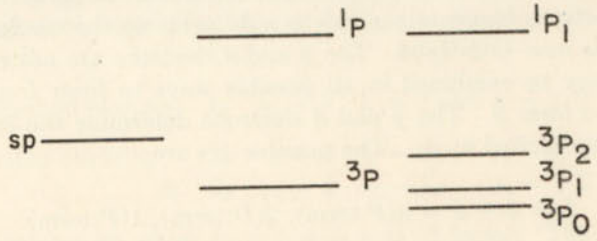

Fig. 5.—Origin of Terms and Levels

L, nor do the s's combine to form S. Instead the l-vector of a given electron may interact with its own spin as well as with the l-vectors of other electrons. This is the condition of *intermediate coupling*. The extreme condition is that of *jj coupling* wherein the l and s vectors of each electron combine to form individual j's and these in turn combine to form a resultant J. Departures from LS coupling become important in the heavier elements and noble gases. Sometimes, as in carbon, a single atom displays a transition from LS to jj coupling; the lowest level is in good LS coupling, whereas the higher levels show pronounced departures. (See Fig. 6.)

8. Alternation Law of Multiplicities

The value of the spin vector S and hence the multiplicity, $2S + 1$, depends on the number of electrons engaged in the production of the outer spectrum. Two electrons give singlets and triplets. With 3 electrons we see that since the s-vectors must be added parallel or antiparallel, $S = 3/2$ or $1/2$. Four electrons will give $S = 2$, 1, or 0, i.e., quintets, triplets, and singlets. Oxygen supplies a useful illustration. The O I ground level is $1s^2 2s^2 2p^4\ ^3P_2$, but the excitation of one of the $2p$ electrons may yield $2p^3 3d$, etc., configurations. We omit the closed $1s^2 2s^2$ shells which contribute nothing. Four electrons are now involved and there occur quintets, triplets, and singlets. Singly ionized oxygen contains 3 optical electrons and there occur quartets and doublets, whereas doubly ionized oxygen with 2 optical electrons has only triplets and singlets. If 3 electrons are removed there will be doublets only as the $2p$ electron is excited. As the number of electrons active in the

production of the optical spectrum changes, the multiplicity is alternately even (quartets, doublets, etc.) and odd (triplets, singlets, etc.).

The spectra of ions with the same number of outer electrons resemble one another in term structure except that with increasing atomic number the corresponding spectral lines become shifted to higher and higher

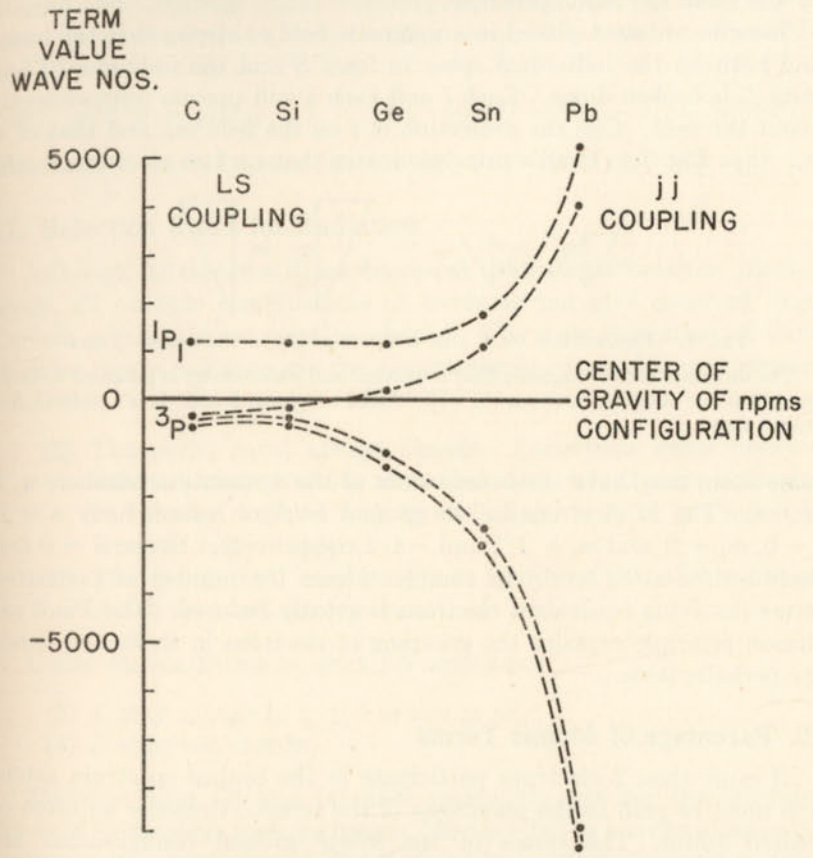

Fig. 6.—Departures from LS Coupling

The level separations of the first excited ^1P and ^3P terms in C, Si, Ge, Sn, and Pb, whose configurations are $2p3s$, $3p4s$, $4p5s$, $5p6s$, and $6p7s$, respectively, exhibit a transition from fair LS coupling to almost complete jj coupling. Notice that in carbon the triplet-singlet separation is much greater than is the splitting of the ^3P term, but that in the heavier atoms, $^3P_0$ and $^3P_1$ deviate in one direction and $^3P_2$ and $^3P_1$ in the other. The horizontal line represents the average energy of the configuration. Energies are plotted in wave number units.

frequencies. A series of ions with the same number of outer electrons is said to form an *iso-electronic sequence*. Thus the $1s^2 2s^2 2p^2$ iso-electronic sequence contains C I, N II, O III, F IV, and Ne V.

9. The Pauli Exclusion Principle

Our vector coupling model permits the calculation of terms for non-equivalent electrons. Thus a $2p3p$ configuration would give the terms ^1S, ^1P, ^1D, and ^3S, ^3P, ^3D. For a p^2 configuration, however, the only observed terms are ^1S, ^1D, ^3P. The number of allowed terms is restricted by the Pauli Exclusion principle.

Imagine an atom placed in a magnetic field so strong that the coupling between the individual spins to form S and the individual l's to form L is broken down. Each l and each s will precess independently about the field. Call the projection of l on the field m_l, and that of s, m_s. (See Fig. 7.) Pauli's principle states that no two electrons in the

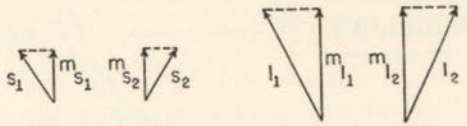

FIG. 7.—PROJECTION OF l AND s VECTORS ON A MAGNETIC FIELD

The direction of the magnetic field is vertical and its intensity is assumed to be so great that the coupling between the individual l's to form L and the s's to form S is broken down.

same atom may have the same values of the 4 quantum numbers n, l, m_l, m_s. The $1s$ electrons in the ground level of helium have $n = 1$, $l = 0$, $m_l = 0$, and $m_s = 1/2$ and $-1/2$ respectively. Hence $S = 0$ and there results a $^1S_0$ level. In complex atoms the number of permitted terms involving equivalent electrons is greatly reduced. The Pauli exclusion principle explains the grouping of electrons in shells and hence the periodic table.

10. Parentage of Atomic Terms

If more than 2 electrons participate in the optical spectrum attention must be paid to the *parentages* of the terms. Consider an atom of ionized sulfur. The terms of the $3s^23p^3$ ground configuration are $^4S(L = 0, S = 3/2)$, $^2D(L = 2, S = 1/2)$ $^2P(L = 1, S = 1/2)$. Let us add a $4p$ electron ($l = 1, s = 1/2$) and compute the terms of $3s^23p^34p$ of S I. We add the l and s vectors of the $4p$ electron to the L and S values of the original terms. There results

S II	$3p^3$	^4S	^2D	^2P
	$+p$			
S I	$3p^34p$	^5P ^3P	$^3P^3D^3F$ $^1P^1D^1F$	$^3S^3P^3D$ $^1S^1P^1D$

We denote the parentages as $(^4S)^5P$, $(^2D)^3F$, etc. Notice there are 3 distinct ^3P terms and 2 distinct ^3D's, ^1P's, and ^1D's based on different parents and possessing different energies.

Suppose, however, that the added p electron is equivalent to the others and a p^4 configuration results. We have an example of what Menzel and Goldberg called fractional parentage: the ^3P term of p^4 is based on all the terms of the p^3 configuration, ^1D is based on ^2P and ^2D, and ^1S is based only on ^2P, thus

$$^3P\text{:}\quad p^3(\tfrac{4}{3}\,^4S + \tfrac{5}{3}\,^2D + {}^2P), \qquad ^1D\text{:}\quad p^3(3^2D - {}^2P), \qquad ^1S\text{:}\quad p^3(4^2P).$$

The factor 4 enters because there are 4 equivalent p electrons.

11. Selection Rules for Radiation

Although all spectral lines represent transitions between distinct levels, all possible combinations of levels do not give observed lines. Certain selection rules must be obeyed. The most important of these rules for dipole radiation are the *Laporte parity rule* and the restrictions on J, viz.,

(1) The parity must always change. Transitions occur between different configurations such that $\Delta l = \pm 1$. Levels belonging to $2p^3$ may combine with levels in $2p3d$ or $2p3s$, but not with levels in $2p3f$ or $2p3p$.
(2) The change in J may be ± 1 or 0, except that the transition $J = 0$ to $J = 0$ never occurs.

Under the conditions of strict LS coupling:

(3) L may change to $L \pm 1$ or not at all.
(4) S must not change.

Selection rules (3) and (4) hold reasonably well for the low-lying levels of light atoms such as oxygen, but they fail in heavier atoms such as iron or titanium, where L and S are no longer "good" quantum numbers. When violations of rules (1) and (2) occur, the radiation is spoken of as "forbidden" (Sec. 13).

12. Identifications of Spectral Lines; Term Diagrams

The analysis of the spectrum with assignment of energy levels is often difficult. Various clues are employed: the changing appearance of the spectrum with temperature is helpful since at low temperatures only lines associated with the lower levels are strong. The splitting of the lines in a magnetic field (*Zeeman effect*) enables the kind of term to be identified since the Zeeman pattern depends in a known fashion on

the L, S, and J values of the terms involved. *Intercombination lines* which arise from transitions between terms of different S values serve to locate terms of differing multiplicity, e.g., the positions of singlets and triplets.

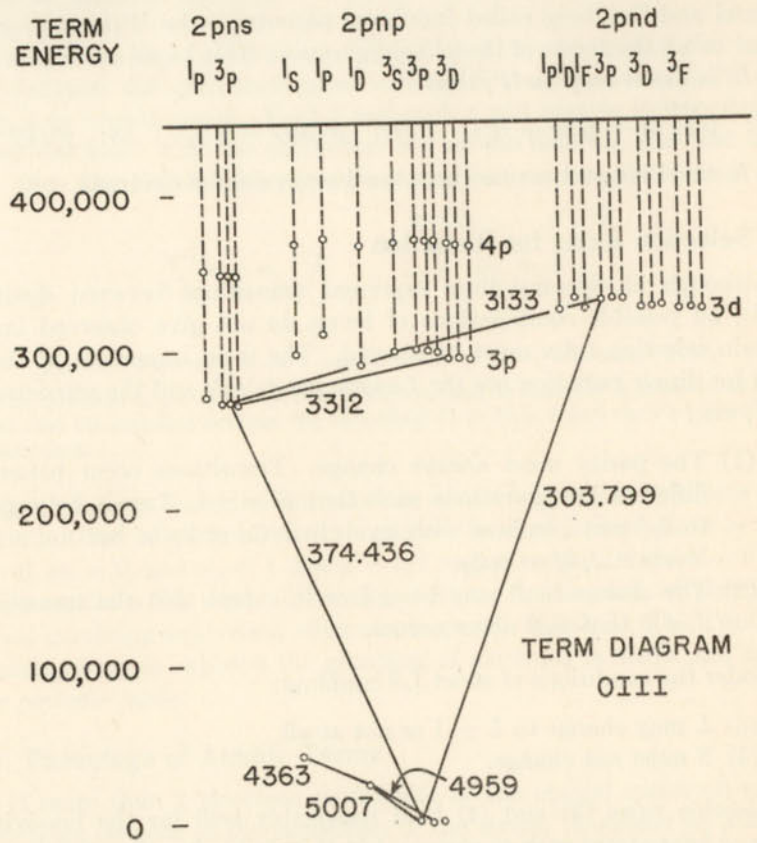

FIG. 8.—TERM DIAGRAM FOR O III

The levels are plotted on a wave number scale. Notice that the ^3P, ^1D, and ^1S terms of the ground $2p^2$ configuration lie very much lower than the first excited levels. As with the alkalis, although less strikingly, the $3s$ term lies below the $3p$ and $3d$ terms. Ordinary (dipole-radiation) transitions can take place only between terms in adjacent configurations. The "forbidden" λ5007, λ4959, and λ4363 lines are strong in the spectra of the gaseous nebula.

Analyses have been carried out for the spectra of all important elements in their neutral and first ionized stages, although the higher level lines of some metallic ions have not been assigned. Few permitted lines of elements heavier than silicon and in ionization stages higher than the second are observed in absorption in stellar spectra.

The indispensable aid for identification work is Charlotte Moore's "Multiplet Table of Astrophysical Interest."* The lines are grouped according to ion and multiplet, with laboratory intensities, excitation potentials, and J-values in successive columns. For the more abundant elements such as iron, the table lists the predicted as well as the observed lines. It also gives the predicted positions of many forbidden lines.

Energy level diagrams often help us visualize excitation mechanisms in stars and nebulae. To construct such a diagram we employ a term table, e.g., Miss Moore's "Atomic Energy Levels," which gives for each energy level the configuration, the term, the J-value, and the height of the level above the ground term expressed in wave number units.

Fig. 8 gives a portion of such a diagram for O III. The top horizontal line represents the ionization potential of 54.71 ev. Transitions from $3d$ to $3p$ and $3s$ to $3p$ represent lines observable in O stars where the temperature is high enough to excite the O III lines.

13. Forbidden Lines

Notice that the ground configuration ($2p^2$) which contains ^3P, ^1D, and ^1S terms lies far below the first excited levels of $2p3s$ or $2p3p$.† Transitions from ^1S to ^1D or from ^1D to ^3P in the $2p^2$ configuration violate the Laporte rule, $\Delta l = \pm 1$, and are called *forbidden lines*. The ^1D and ^1S levels, which in O III lie 2.48 and 5.3 volts respectively above the ground level, are called metastable levels. An atom in one of the ordinary high levels like $2p3s^3P$ will cascade downwards in a time of the order of 10^{-8} seconds. If it finds itself in one of the low-lying metastable levels, it may remain there for a time of the order of a second before it escapes to the lower level with the emission of radiation.

Menzel, Payne, and Boyce proposed the following terminology for the forbidden lines: In a p^2 or p^4 configuration, jumps between ^1S and ^1D are called *auroral transitions*, since the strong λ5577 line of the permanent aurora of the night sky is of this type. The strongest lines in the gaseous nebulae arise from $^1D - {}^3P$ transitions; hence they are called *nebular transitions*. A *transauroral* line denotes one of the type $^1S - {}^3P$ and is usually weak. In a p^3 configuration, e.g., O II, the auroral, nebular, and transauroral transitions are analogously $^2P - {}^2D$, $^2D - {}^4S$,

* Princeton Observatory Contribution No. 20, 1945.

† *Hund's rule* states that in the ground configuration the term of highest multiplicity will lie lowest. If there are several terms of the same multiplicity, the term with the highest L value will be lowest. If the shell is less than half-filled, e.g., p or p^2, d, d^2, d^3, or d^4, the level of smallest J value will be lowest; otherwise the term will be inverted. Thus in O III, the $^3P_0$ level of the ground $2p^2$ configuration lies lowest, while in O I, F II, or Ne III ($2p^4$) the $^3P_2$ level is lowest and the term is inverted, cf. Fig. 9.

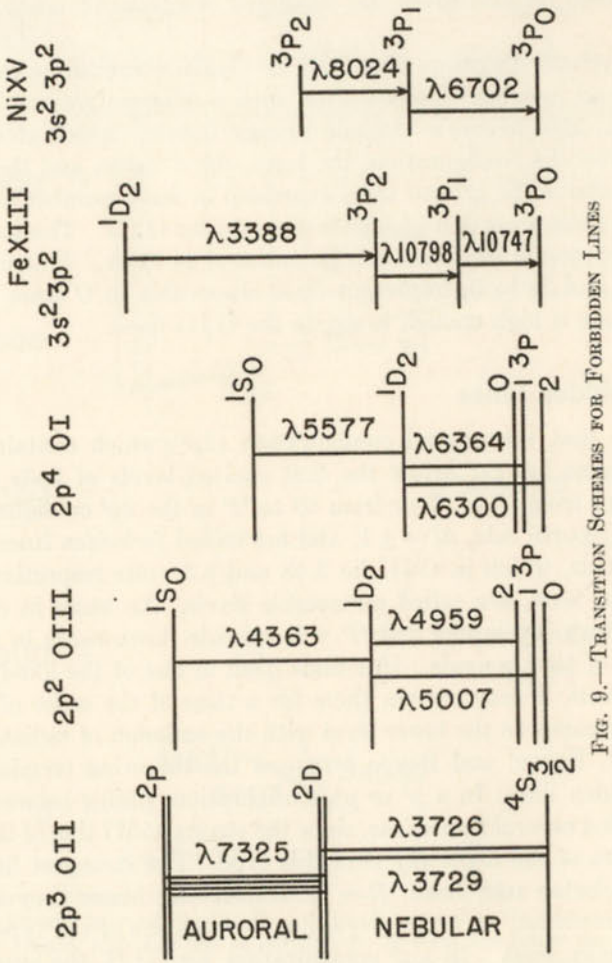

FIG. 9.—TRANSITION SCHEMES FOR FORBIDDEN LINES

and $^2P - {}^4S$. The lines identified by Edlén in the solar corona mostly represent transitions between levels of the ground terms. (See Fig. 9.) The symbol [ ] is used to denote forbidden lines.

Although forbidden lines usually appear in emission, I. S. Bowen has utilized the faint [O I] λ5577, 6300, and λ6363 absorption lines which appear in the solar spectrum to estimate the abundance of oxygen in the sun. One of the coronal lines of iron has been suspected as a diffuse absorption feature upon the solar spectrum.

Relatively few forbidden lines can be produced experimentally. In general they can be predicted only after an analysis of the spectrum has located the low-lying metastable levels. If the analysis is not sufficiently complete to locate the metastable levels, the extrapolation of the energy levels in an isoelectronic sequence may be employed. (See Ch. 9, Sec. 14.)

Lack of space prevents our discussion here of the topics of X-ray spectra and *hyperfine structure*. The latter refers to the very minute splitting of certain spectral lines because of a coupling between the spin of the nucleus and the total angular momentum J of the surrounding electrons. Arthur Abt finds that hyperfine structure can contribute appreciably to the widths of certain lines in the solar spectrum.

The Zeeman and Paschen-Back effects are important in the analysis of spectra. The number and positions of the components of a line depend in a characteristic way on the L, S, and J values of the upper and lower levels. Furthermore, these components show distinctive polarization and intensity relationships.* Astrophysical applications of the Zeeman effect lie in the interpretation of sunspot spectra and those of peculiar A stars. (See Ch. 8, Sec. 19.)

Spectral lines may be broadened or even split by electric as well as by magnetic fields. No large-scale electric fields appear to exist in stellar atmospheres, but rapid motions of charged particles may produce intense ephemeral microscopic electric fields near a radiating atom. Hydrogen and helium lines are widened by these fields (Ch. 8, Secs. 16 and 17).

14. Structure of Diatomic Molecules

The predominant molecules in stars like the sun are diatomic such as OH, CH, and CN. Despite their seemingly simple structure they show complicated spectra consisting of extensive bands composed of numerous closely packed lines.

We may think of a molecule AB, e.g., CN, as composed of two ions A^+ and B^+, surrounded by a cloud of electrons and held together by

* For an account of the physical theory the reader is referred to the texts of White and Herzberg.

electrostatic forces. The potential energy curve of the system (Fig. 10) shows that there exists a distance r_0 that corresponds to the minimum potential energy. At greater distances the potential curve gradually rises and approaches the horizontal dotted line which corresponds to the dissociation energy of the molecule. At distances smaller than r_0, the repulsive forces of the two atomic nuclei become increasingly important and prevent a close approach of the two nuclei. The horizontal solid lines represent the quantized vibrational energy states of the molecule. Notice that they fall closer together with increasing energy. Energies above the dotted line represent states wherein the molecule is dissociated and the free atoms are flying about. These states are unquantized.

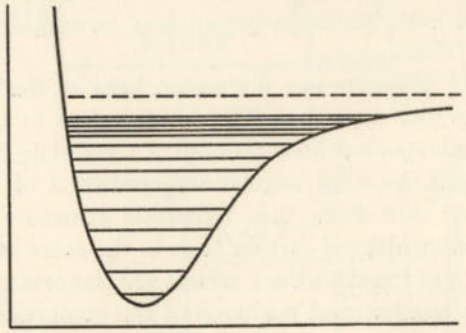

FIG. 10.—VIBRATIONAL ENERGY LEVELS OF A DIATOMIC MOLECULE

The potential energy curve is indicated by the heavy solid curve. The thin solid horizontal lines indicate the vibrational levels and the dotted line the energy corresponding to dissociation. The abscissa is the distance r between the component atoms. The minimum of the potential curve lies at the equilibrium distance r_0. The ordinate is the energy.

Such a molecule may take up energy in several ways. First, it may rotate about an axis perpendicular to the line joining the two atoms. Second, the two component atoms may vibrate back and forth along the line joining them. Third, the molecule may be excited to definite electronic energy states analogous to atomic energy levels.

The rotational modes (not shown in Fig. 10) involve the smallest amounts of energy. Radiations corresponding to transitions from one rotational level to another are in the far infrared. The vibrational energies are greater and transitions between the corresponding levels produce bands in the relatively near infrared. The excitation of electronic states requires frequencies falling in the visible and ultraviolet part of the spectrum. Each type of energy, rotational, vibrational, and electronic is quantized according to definite rules. The total energy of the molecule is:

$$E = E_{\text{rotational}} + E_{\text{vibrational}} + E_{\text{electronic}} \tag{16}$$

15. Rotational Energies of Diatomic Molecules

Quantum mechanics shows that in the first approximation the rotational energy of the molecule is

$$E_r = K(K+1)\frac{h^2}{8\pi^2 I} \tag{17}$$

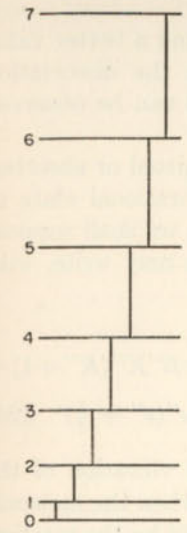

FIG. 11.—PURE ROTATIONAL TRANSITIONS IN A DIATOMIC MOLECULE

Transitions are restricted to $\Delta K = 1$.

Here

$$I = \frac{m_A m_B}{(m_A + m_B)} r^2 = \mu r^2 \tag{18}$$

is the moment of inertia of the molecule, μ is called the reduced mass, and the integer K, called the rotational quantum number, follows the rule

$$\Delta K = \pm 1 \tag{19}$$

in transitions from one rotational level to another. The wave number of the transition between rotational levels K' and K'' is

$$\tilde{\nu} = \frac{1}{hc}(E_{r'} - E_{r''}) = 2BK' \tag{20}$$

where

$$B = \frac{h}{8\pi^2 Ic} \tag{21}$$

A pure rotation spectrum would consist of a series of equidistant lines were it not for an increase in the size of the molecule due to the centrifugal force of rotation. This effect leads to a small correction term of the form $CK^2(K+1)^2$ in eqn. (17). Pure rotation bands do not exist if the two atoms are identical.

16. Rotation and Vibration Bands

If the component atoms are displaced slightly from their equilibrium separation, r_0, the restoring force is proportional to $(r - r_0)$. If the displacements are large, this is no longer true as the potential energy curve is asymmetrical. Consequently, the energy levels, E_{vib}, do not show an even spacing. They fall closer and closer together, in accordance with the empirical formula.

$$E_{\text{vib}} = hc\omega(v + \tfrac{1}{2}) - hc\omega x_e (v + \tfrac{1}{2})^2 + \text{etc.} \tag{22}$$

Here ω (expressed in wave number units) and x_e are found from the analysis of the band spectrum. If higher terms can be neglected, the energy necessary to raise the molecule from the lowest vibrational level

to the point of dissociation (heat of dissociation D_0) can be shown to be related to x_e and ω by

$$D_0 = \frac{\omega^2}{4\omega x_e}(1 - x_e)^2 \tag{23}$$

Other spectroscopic methods are often capable of giving a better value of D_0. Sometimes the absorption continuum above the dissociation limit (analogous to the ionization continua of atoms) can be observed and yields a good value of D_0.

We now consider the character of the spectrum emitted or absorbed when a molecule jumps from one rotational and vibrational state to another rotation-vibration state. For the time being, we shall suppose that there is no change in the electronic energy. We may write, with the aid of eqns. (17) and (22):

$$\tilde{\nu} = \tilde{\nu}_r + \tilde{\nu}_v = \frac{1}{hc}[E_{r'} + E_{v'} - E_{r''} - E_{v''}] = B'K'(K'+1) - B''K''(K''+1) + \omega'(v' + \tfrac{1}{2}) - x_e'\omega(v' + \tfrac{1}{2})^2 - \omega''(v'' + \tfrac{1}{2}) + x_e''\omega''(v'' + \tfrac{1}{2})^2 \tag{24}$$

Here the vibrational energy E_v is the energy of the vibration of the component atoms about their equilibrium separation when the molecule does not rotate. The rotational energy, E_r, is that added by the rotation of the molecule. It usually includes the small energy interaction between rotation and vibration and the effect of the expansion of the molecule by the centrifugal force.

The totality of transitions from one vibrational state of the molecule v' to another vibrational state v'' constitutes a band. A transition from a particular $v'K'$ state to another $v''K''$ state corresponds to a single line of the $v'v''$ band.

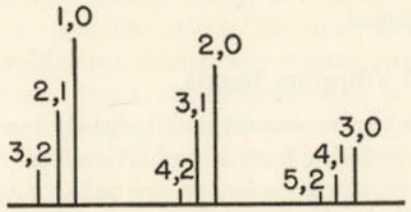

FIG. 12.—VIBRATION BANDS FOR $\Delta v = 1, 2, 3$ (SCHEMATIC)

If the molecular potential curve (Fig. 10) were a parabola, the molecule would constitute a harmonic oscillator and the selection rule for the transitions would be $v' - v'' = 1$. To the extent that the potential curve approximates a parabola we would expect transitions of the type $v' = 0$ to $v'' = 1$, $v' = 1$ to $v'' = 2$, etc., to be the strongest. The curve is most nearly parabolic at low energies. For the lowest levels, the bands

corresponding to $\Delta v = 1$ are indeed the most intense, but among the higher vibrational levels, transitions in which $\Delta v = 2$, 3, etc., can become important. A pure vibrational transition is denoted as (v', v''). Thus, (1, 0) means a jump from the vibrational level $v = 1$ to the vibrational level $v = 0$.

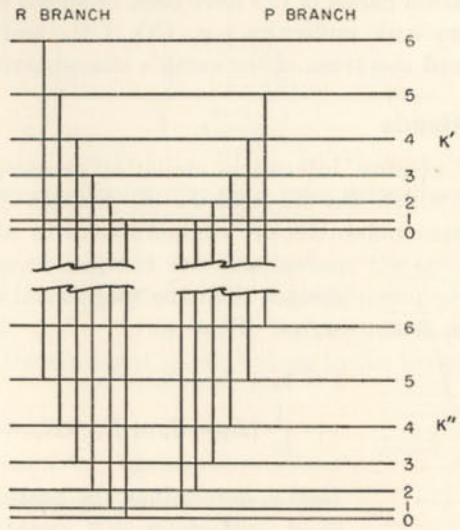

FIG. 13.—R AND P BRANCHES IN PURE VIBRATIONAL TRANSITIONS

Now consider the rotational structure of the pure vibration-rotation bands. The moment of inertia of the molecule will depend upon the state of vibration. Because of the asymmetry of the potential curve, the average separation of the atoms in the molecule and therefore the moment of inertia is greater in the higher vibrational level. Hence $I_{v'} > I_{v''}$ and $B' < B''$. Neglecting the small rotational terms of higher order, the rotational structure of a particular vibration-rotation band will be given by

$$\tilde{\nu} = \tilde{\nu}_v + \tilde{\nu}_r = \tilde{\nu}_v + B'K'(K'+1) - B''K''(K''+1) \tag{25}$$

where $\tilde{\nu}_v$ is the wave number of the band. For a given change in v, $\tilde{\nu}_v$ is fixed, and since K can change by ± 1, there are two branches of lines depending on whether

$$K' = K'' + 1 \ (R\text{-branch}), \quad \text{or} \quad K' = K'' - 1 \ (P\text{-branch}) \tag{26}$$

Then

$$\begin{aligned} \tilde{\nu} &= \tilde{\nu}_v + (B' + B'')(K+1) + (B' - B'')(K+1)^2 && R\text{-branch} \\ \tilde{\nu} &= \tilde{\nu}_v - (B' + B'')K + (B' - B'')K^2 && P\text{-branch} \end{aligned} \tag{27}$$

Since $B' - B''$ is negative, the lines of the R-branch tend to crowd together; those of the P-branch to spread apart. Since the change in K cannot be zero, the line corresponding to the band origin does not appear. Homonuclear molecules such as C_2 or N_2 show no vibration-rotation bands.

Vibration-rotation bands of CO have been observed in the sun. Similar bands of polyatomic molecules, e.g., CO_2, CH_4, and N_2O are prominent in the infrared spectrum of the earth's atmosphere.*

17. Electronic Bands

The bands of greatest interest in stellar spectroscopy are the electronic bands in which E_e, E_v, and E_r all change. Since molecular electronic excitation potentials are comparable with atomic excitation potentials, the energies involved are much greater than the vibrational or rotational energies. That is,

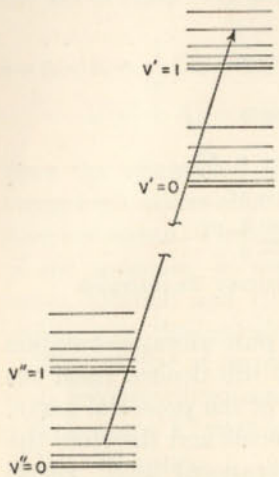

FIG. 14.—ELECTRONIC TRANSITIONS

The particular transition illustrated herewith takes place from the 4th rotational state of the lowest vibrational level ($v'' = 0$) of the lower electronic state to the 5th rotational state of the vibrational level ($v' = 1$) of the upper electronic state. This transition corresponds to one molecular line of the entire band system.

$$\tilde{\nu} = \tilde{\nu}_e + \tilde{\nu}_v + \tilde{\nu}_r$$
$$= \frac{1}{hc}\{E_{e'} - E_{e''} + E_{v'} - E_{v''} + E_{r'} - E_{r''}\} \quad (28)$$

Here $\tilde{\nu}_e$ determines the position of the entire band system, $\tilde{\nu}_v + \tilde{\nu}_e$ locates the position of a particular band in the system, and $\tilde{\nu}_r + \tilde{\nu}_v + \tilde{\nu}_e$ fixes the position of a single line in the entire set of bands. Since the potential curve of an excited level usually differs from that of the ground level, I and therefore B will be different and $B' - B''$ may be positive, negative, or zero. Let

$$\tilde{\nu}_o = \tilde{\nu}_e + \tilde{\nu}_v = \tilde{\nu}_e + \omega'(v' + \tfrac{1}{2})[1 - x'(v' + \tfrac{1}{2})] - \omega''(v'' + \tfrac{1}{2})[1 - x''(v'' + \tfrac{1}{2})] \quad (29)$$

denote the position of a band origin. In electronic transitions all values of Δv are permitted. All bands which have a common lower or a common upper level are said to form a progression or a series. Bands for which the change in v is constant are said to form a sequence.

* The relative intensities of the bands, either in absorption or emission, will depend upon the temperature of the gas. At low temperatures most of the molecules are in the lowest vibrational level and the 0–1 band tends to be the strongest.

The relative intensities of the bands within a given band system depend on the potential curves of the molecules in the two electronic states and may be estimated with the aid of quantum mechanics in accordance with the Franck-Condon principle. If the bands are arranged

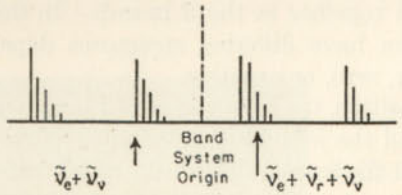

FIG. 15.—SCHEMATIC RESOLUTION OF A BAND SYSTEM INTO INDIVIDUAL LINES AND BANDS

in a (v', v'') array, it is found that the locus of the strongest bands is a parabola. If r_0' is nearly equal to r_0'', the strongest bands fall near the diagonal, $\Delta v = 0$, $\Delta v = -1$, $\Delta v = +1$, i.e., sequences are strongest. If r_0' and r_0'' differ, the strongest bands belong to the progression, $v'' = 0, 1$ and $v' = 0, 1$.

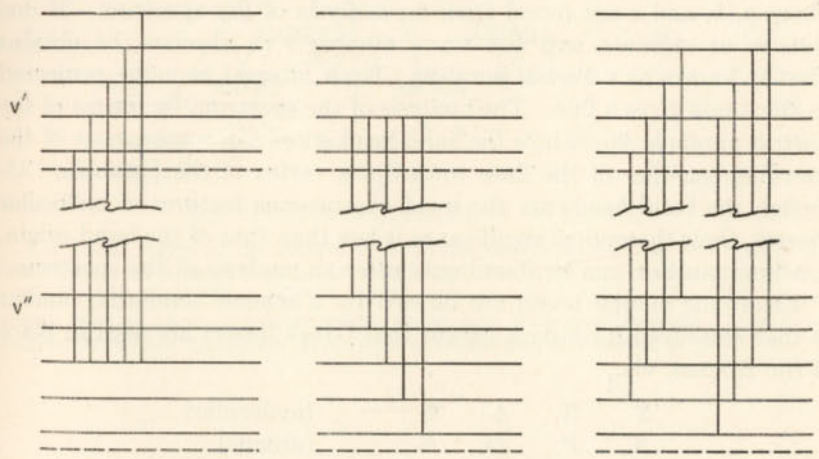

FIG. 16.—PROGRESSIONS AND SEQUENCES

The bands at the left have a common lower vibrational level and are said to form a v' progression. The middle sketch depicts a v'' progression, while a sequence is shown at the right.

The wave number of a particular line of an electronic band is

$$\tilde{\nu} = \tilde{\nu}_o + B'K'(K' + 1) - B''K''(K'' + 1) \quad (30)$$

As before, a change in K of ± 1 is possible, but $\Delta K = 0$ can also occur in some transitions. Hence in addition to the P- and R-branches, a Q-branch sometimes appears.

$$\begin{aligned}
\tilde{\nu} &= \tilde{\nu}_o + 2B' + (3B' - B'')K + (B' - B'')K^2 = R(K) \quad K' = K'' + 1 \\
\tilde{\nu} &= \tilde{\nu}_o \quad + (B' - B'')K + (B' - B'')K^2 = Q(K) \quad K' = K'' \qquad (31) \\
\tilde{\nu} &= \tilde{\nu}_o \quad - (B' + B'')K + (B' - B'')K^2 = P(K) \quad K' = K'' - 1
\end{aligned}$$

For the vibration-rotation bands, $B' - B''$ is always negative and the lines tend to crowd together in the R branch. In the electronic transitions the bands can have differing structures depending on whether $B' - B''$ is positive, zero, or negative.

If $B' - B''$ is positive, the lines will crowd together, i.e., form a head, in the P-branch and the individual lines will tend to spread out in the violet. We say that the band is degraded toward the violet. If $B' = B''$ the bands form no head at all, while if B' is less than B'', the head will be formed on the violet side of the band origin and the bands are degraded toward the red. Notice that we may represent the lines of the P- and R-branches by the same formula if we replace K by $(m - 1)$ in the P-branch and by m in the R-branch and suppose that the P-branch corresponds to negative m values. That is,

$$\tilde{\nu} = a + bm + cm^2$$

where a, b, and c are found from an analysis of the spectrum. If one plots m as ordinate and the wave number $\tilde{\nu}$ as abscissa, he obtains what is known as a *Fortrat parabola*. Each integral m value projected on the $\tilde{\nu}$ axis gives a line. The analysis of the spectrum by means of the Fortrat parabola shows how the band head arises as a consequence of the crowding together of the lines toward the vertex of the parabola. Although the band heads are the most conspicuous features of molecular spectra, their theoretical significance is less than that of the band origin, $\tilde{\nu}_o$, whose position can be found only after an analysis of the spectrum.

Electronic energy levels are labeled by a scheme somewhat similar to that employed for atoms, except that Greek letters are used in place of the Roman, viz.,

Σ	Π	Δ	Φ	(molecular)
S	P	D	F	(atomic)

The significant quantities are the projections of the orbital and spin angular moments, L and S, upon the line joining the nuclei of the two atoms, Λ and Σ. The sum of these projections is $\Omega = |\Lambda + \Sigma|$. As we would write $^3P_2$ for the atomic term for which $S = 1$, $L = 1$, and $J = 2$, we write $^3\Pi_2$ for the molecular term for which $S = 1$, $\Lambda = 1$, and $\Omega = 2$. In general we use the symbolism

$$^{2S+1}\Lambda_\Omega$$

The multiplicity is $2S + 1$, the kind of term is Λ, and the subscript denotes the value Ω may take. Multiplicity is indicated as in atomic

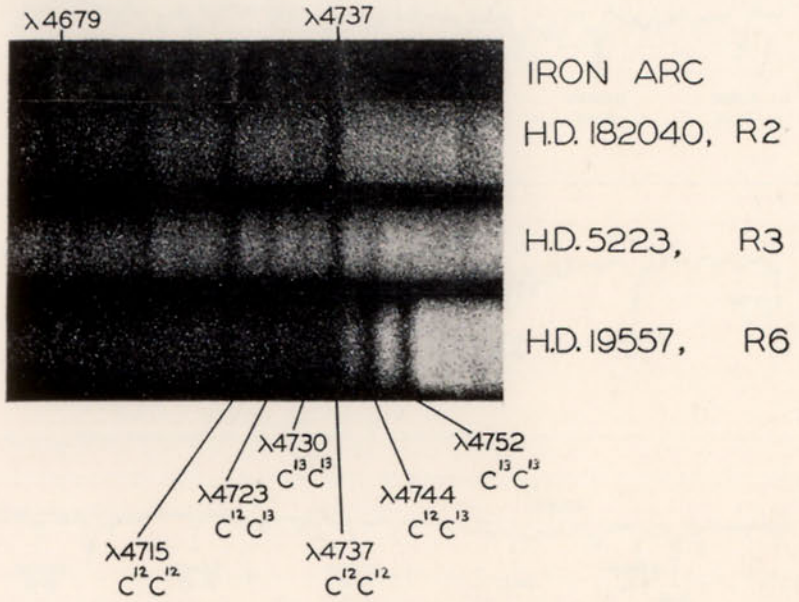

FIG. 17.—THE ISOTOPIC BANDS OF CARBON

The λ4737 region of the spectra of 3 *R*-type stars is shown. In *HD* 182040 the $C^{12}C^{12}$ bands are present with moderate strength but no isotopic bands are seen with certainty. In *HD* 5223 the $C^{12}C^{13}$ bands are prominent, while in *HD* 19557, bands arising from all three molecular species are present with great strength. (Courtesy, Andrew McKellar, Dominion Astrophysical Observatory, Victoria, B. C.)

spectra, e.g., $^1\Sigma$ $^1\Pi$ $^3\Sigma$ $^3\Pi$ $^2\Delta$, etc. A $^1\Sigma$ is analogous to a $^1S_0$ state, i.e., the resultant angular and spin momentum of the molecule is zero. The parity of a molecular configuration is fixed by whether the sum of the l values of the individual electrons is even or odd, and is denoted by the letters g and u (*gerade* and *ungerade*).*

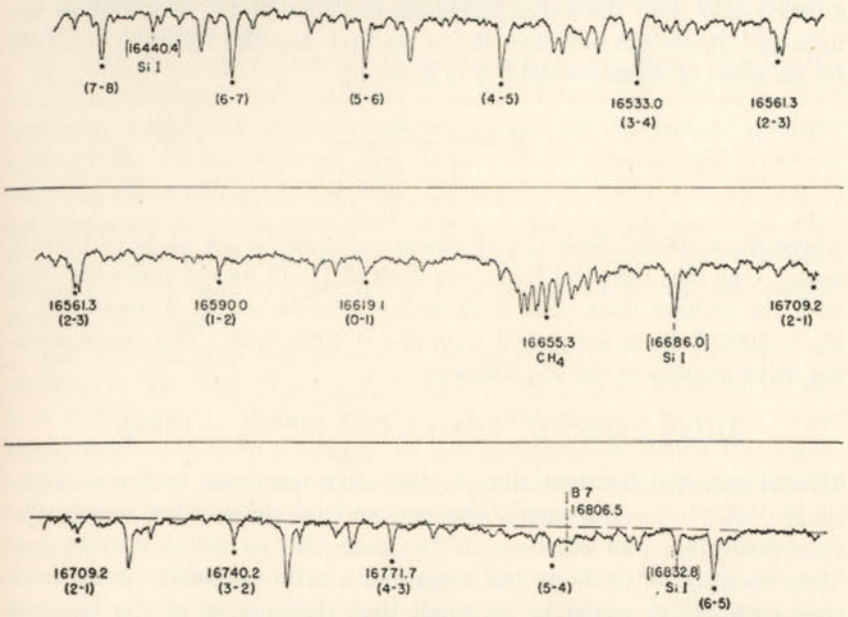

FIG. 18.—A PORTION OF THE INFRARED SOLAR SPECTRUM AS OBSERVED WITH THE LEAD-SULFIDE CELL

The tracing shows the diffuse λ16806.5 line of the Brackett series of hydrogen, whose computed position is indicated by the vertical broken line, and certain silicon lines. The [ ] indicate that the wave lengths were computed for a vacuum. The positive (0–1), (1–2), etc., and negative (3–2), (2–1), etc., branches of the band system of atmospheric methane CH_4 are indicated. The wave lengths are given for air and are indicated on the trace by dots. Most of the other lines on the trace are of atmospheric origin. (McMath-Hulbert Observatory, University of Michigan.)

A few permitted band systems of astrophysical interest are:

$$^2\Sigma - {}^2\Pi,\ CH;\quad {}^3\Pi - {}^3\Pi,\ C_2,\ N_2,\ TiO,\ ZrO;\quad {}^2\Delta - {}^2\Pi,\ OH$$

Among forbidden electronic bands, the best known is the telluric† band

* Symbols (+) and (−) are also used to denote spatial symmetry properties of the molecular electronic wave functions. See G. Herzberg, *Molecular Spectra and Molecular Structure* (New York: D. Van Nostrand Co., Inc., 1950), p. 238.

† Telluric lines in the solar spectrum are lines which arise from absorption by molecules in the earth's atmosphere such as O_2, H_2O, etc. They can be identified by their marked increase in intensity as the sun gets lower in the sky and by the fact that they do not partake of the Doppler shift of solar rotation.

of atmospheric oxygen. Even in spite of a low transition probability this absorption band is strong because of the long air path.

18. Isotope Effects in Atomic and Molecular Spectra

Except for the lightest elements different isotopes may be distinguished only with the aid of hyperfine structure data. For ionized helium and deuterium one may utilize the fact that the Rydberg constant for an atom of atomic weight A is given by

$$R = \frac{R_o}{1 + \frac{1}{1837A}}$$

where $R_o = 109737.30$ is the Rydberg constant for an atom of infinite mass. One sees that the Pickering lines of He II do not quite coincide with the Balmer lines. For hydrogen of atomic weight 2 (deuterium), $R_D = 109707.42$ as compared with $R_H = 109677.68$. The corresponding wave lengths of the Hα line are:

$$\lambda(\mathrm{H}\alpha) = 6562.817 \quad \lambda(\mathrm{D}\alpha) = 6561.032 \quad \delta\lambda = 1.785\mathrm{A}$$

Menzel searched for deuterium in the solar spectrum, in the chromosphere, and in several stellar spectra, and concluded that within the stars deuterium was less than 10^{-5} as abundant as ordinary hydrogen. More recently C. de Jager has suggested a ratio of 0.0001. In heavier atoms the shifts would be so small that the spectra of the isotopes would not be separated from one another by detectable amounts.

Isotope effects can be important in band spectra, since molecules composed of different isotopes will have different vibration frequencies. The binding forces are nearly the same in a $C_{12}C_{12}$ molecule as in a $C_{12}C_{13}$ molecule, for example, but the masses are different. Since the vibration frequency parameter ω (cf. eqn. 22) depends on the mass in the sense that the greater the mass the slower the vibration, the band origin or head of $C_{12}C_{12}$ will be shifted with respect to that of $C_{12}C_{13}$. Furthermore, the moment of inertia will be changed so that B will differ for molecules of different isotopes. The positions of corresponding lines will differ.

Diatomic molecules with two identical nuclei show alternating intensities of the lines in their band systems. The amount of the variation depends on the nuclear spin. When the two nuclei are isotopes of different mass, the alternation disappears.

The isotopic bands of carbon appear in the R and N type stars where strong $C_{12}C_{12}$ bands are flanked by weaker bands of $C_{12}C_{13}$ and $C_{13}C_{13}$. Although the C_{12} isotope is 90 times as abundant as the C_{13} isotope on the earth, McKellar finds certain carbon stars in which the ratio is more nearly of the order of 3. The C_{13} isotope is responsible for some weak telluric lines of CO_2 in the infrared.

19. Some Polyatomic Molecules of Astrophysical Interest

Polyatomic molecules abound in comets, in the coolest stars, and in planetary atmospheres.

As with diatomic molecules, there exist electronic states like $^1\Sigma$, $^1\Pi$, etc., and the vibrational states are split into rotational substates. The type and complexity of the spectrum depend on the spatial arrangement of the atoms. Carbon dioxide is a linear symmetrical molecule with the three atoms arranged in a straight line, O—C—O. Water is neither linear nor symmetrical; it gives a complicated spectrum with overlapping rotational structure. In methane, CH_4, the four hydrogen atoms are arranged symmetrically in a tetrahedron with the carbon atom at the center.

The fundamental frequencies of vibration of the CO_2 molecule according to Ta You Wu are $\tilde{\nu}_1 = 1321.7$ cm^{-1}, $\tilde{\nu}_2 = 667.9$ cm^{-1}, and $\tilde{\nu}_3 = 2362.8$ cm^{-1}. These correspond to excitations of first one vibrational mode and then another. In the spectrum of Venus the higher overtones, $5\tilde{\nu}_3$, $5\tilde{\nu}_3 + \tilde{\nu}_1$, and $5\tilde{\nu}_3 + \tilde{\nu}_2$ are observed in appreciable strength. Methane has four fundamental frequencies: $\tilde{\nu}_1 = 2915$ cm^{-1}, $\tilde{\nu}_2 = 1520$ cm^{-1}, $\tilde{\nu}_3 = 3020$ cm^{-1}, and $\tilde{\nu}_4 = 1306$ cm^{-1}. Overtones of these bands are observed in the earth's atmosphere, but they are particularly strong in the spectra of the outer planets. In Neptune harmonics as high as $16\tilde{\nu}_4$ are observed. Since these high harmonics have never been observed in the laboratory, the amount of vapor in the light path must be considerable. There also appear bands in which the difference of two modes of excitation occur, e.g., $5\tilde{\nu}_3 - \tilde{\nu}_2$, which means that the lower state of vibration is excited. Ammonia bands appear in the spectra of Jupiter and Saturn although they are missing in the spectra of Uranus and Neptune where the substance must be frozen out.

Actual estimates of the amount of material in the line of sight are difficult because the band structures are sensitive to temperature, pathlength, and density. Eventually, with the aid of appropriate laboratory studies, we may be able to interpret the strengths and structures of these bands in terms of the temperature and density of the planet's atmosphere.

REFERENCES

General references on spectra:

Herzberg, G. *Atomic Spectra and Atomic Structure, Molecular Structure and Molecular Spectra.* I, "Diatomic Molecules." New York: D. Van Nostrand Co., Inc., 1950.

MOORE, CHARLOTTE. "A Multiplet Table of Astrophysical Interest," *Princeton Observatory Contribution No. 20,* 1945.
———. "Atomic Energy Levels," Bureau of Standards Circular 467, 1948, 1952.
WHITE, H. E. *Introduction to Atomic Spectra.* New York: McGraw-Hill Book Co., Inc., 1934.

The present status of the identification of lines in astronomical sources is discussed by:

SWINGS, P. *J. Opt. Soc. Am.* **41,** 153, 1951.

A summarizing account of fundamental molecular spectra research is given by:

PEARSE, R. W. B. *J. Opt. Soc. Am.* **41,** 148, 1951.

Forbidden lines are discussed by:

BOWEN, I. S. *Rev. Mod. Phys.* **8,** 55, 1936.
MROZOWSKI, S. *Rev. Mod. Phys.* **16,** 153, 1944.

CHAPTER 3

THE GAS LAWS AND THE EQUATIONS OF STATE, TURBULENCE

1. The Gaseous Phase of Matter

The astrophysicist enjoys but few advantages over the chemist or physicist; one of them is that most of the objects he studies, the stars and nebulae, are gaseous throughout. To be sure, the planets appear solid enough, comets seem to contain small particles, and the interstellar medium contains many small solid grains, but these objects require rather special techniques for their study. The spectroscope is the astrophysicist's most faithful and useful tool, and the spectroscope is primarily a means for studying matter in its gaseous condition.

2. The Equation of State for a Perfect Gas

The fundamental equation of state for a perfect gas is

$$PV = RT \tag{1}$$

where P is the pressure, V is the volume, and T is the temperature in absolute degrees (°K). The constant R depends on the mass of gas involved. As our standard of quantity we usually take one gram-molecule or mole, which amounts to a volume of 22.4 liters at 0°C (273°K) and one atmosphere pressure. Then

$$PV = \mathfrak{R}T \tag{2}$$

where $\mathfrak{R} = 8.314 \times 10^7$ ergs/deg/mole if the pressure P is measured in dynes/cm^2. If P is measured in atmospheres (one atmosphere equals 1.013×10^6 dynes/cm^2) and the volume V is expressed in cm^3, $\mathfrak{R}$ is 82.05 atmospheres/deg/mole. The number of molecules in a mole (Avogadro's number) must be established empirically; it is $N_0 = 6.025 \times 10^{23}$ molecules/mole. The Loschmidt number, the number of molecules per cm^3 under standard conditions, is 2.687×10^{19}.

It is sometimes convenient to define the gas constant per atom or molecule, instead of per mole. Thus, Boltzmann's constant is $k = \mathfrak{R}/N_0 = 1.38032 \times 10^{-16}$ ergs/deg. The gas law then becomes

$$P = NkT \tag{3}$$

where N is the number of molecules per unit volume.

There is a third useful form of the perfect gas law. If the N_0 atoms or molecules in a mole, each of mass m, have a total mass of μ, the actual density in grams per cm³ will be $\rho = Nm$, and since $N_0 k = \mathcal{R}$,

$$P = \frac{\rho \mathcal{R} T}{\mu} = \rho \left(\frac{k}{\mu H}\right) T \tag{4}$$

where H is the mass of a particle of unit atomic weight.

3. The Law of Partial Pressures

An important corollary of the equation of state is Dalton's law of partial pressure. If a gas contains a number of non-reacting constituents each of which exerts a pressure of its own, the gas pressure is the sum of the pressures exerted by each constituent. Each kind of particle contributes its own partial pressure, $p_i = n_i kT$, so that the total gas pressure is

$$P_g = \Sigma p_i = kT \Sigma n_i = NkT \tag{5}$$

For example, a mixture of hydrogen and nitrogen exerting partial pressures p_H and p_N will exert a total pressure $P = p_H + p_N$.

The high temperatures that exist in the atmospheres of certain stars and in the interiors of all of them serve to break down the molecules into their constituent atoms and finally the atoms themselves become stripped of their electrons. Let us illustrate by the history of a mass of hydrogen gas whose temperature is raised. Under normal conditions of temperature and pressure, hydrogen exists in a molecular form, each molecule consisting of two hydrogen atoms. If the temperature is raised to the order of that of the solar atmosphere, H_2 becomes dissociated into separate hydrogen atoms, and whereas formerly two grams contributed 6.03×10^{23} particles (hydrogen molecules), only one gram of the dissociated hydrogen gas now suffices to contribute the same number of particles (hydrogen atoms). At still higher temperatures the hydrogen atom itself becomes broken down into its constituent electron and proton, so that only a half gram of the completely ionized hydrogen contains 6.03×10^{23} particles (protons plus electrons), each as capable of contributing to the pressure as the other. The molecular weight of H_2 is 2, that of atomic hydrogen is 1, and completely ionized hydrogen is 1/2. Thus in the perfect gas law, eqn. (4), μ is itself a function of the temperature, and also of the pressure, since a high pressure tends to jam the electrons back into the atoms again.

With a view to later applications to stellar interiors, let us show how the molecular weight μ may be computed when the material is highly ionized. Let one gram of the gas contain w_E grams of element E, and suppose that the stage of ionization is such that each gram of atoms of

the kind E provides $\alpha_E N_0$ particles (ions, bare nuclei, and electrons), where N_0 is Avogadro's number. In other words, α_E is the number of free particles per $1/N_0$ grams of material of type E. The number of particles per gram of the mixture comprising the star is:

$$n' = N_0 \Sigma w_E \alpha_E$$

Hence each cm³ contains

$$n = \rho N_0 \Sigma w_E \alpha_E$$

particles and the corresponding gas pressure is

$$P_g = \Sigma n_i kT = \rho N_0 kT \Sigma w_E \alpha_E = \rho \mathcal{R} T \Sigma w_E \alpha_E \tag{6}$$

Comparison with eqn. (4) reveals

$$\mu = \frac{1}{\sum_E w_E \alpha_E} \tag{7}$$

Once the chemical composition has been chosen (w_E fixed), α_E (which depends on the ionization) will be determined by ρ and T.

Strömgren adopted the relative cosmic abundances of the heavier elements as determined by Russell, the so-called Russell mixture, and calculated a mean value, $\bar{\alpha}$ for these constituents as a function of temperature and electron density. We shall not make too large an error if we assume complete ionization throughout most of the stellar interior. Then each atom will contribute one nucleus plus Z electrons or $Z + 1$ particles in all. The number of atoms per gram of the substance in question will be N_0/A where A is the atomic weight, and each gram will contribute $(Z + 1)N_0/A$ particles of which ZN_0/A will be electrons. Hence $\alpha_E = (Z_E + 1)/A$ for complete ionization as compared with $\alpha_E = 1/A_E$ for the neutral material. For iron, $Z = 26$, $A = 56$, and $\alpha = 27/56 = 0.483$; for oxygen $Z = 8$, $A = 16$, and $\alpha = 9/16 = 0.562$. For helium, $Z = 2$, $A = 4$, and $\alpha = 0.750$, whereas for hydrogen, $A = 1$, $Z = 1$, and $\alpha = 2$. Quite generally, α is of the order of 0.50 for the heavier elements.

Let each gram of the stellar material contain X grams of hydrogen, Y grams of helium, and therefore $(1 - X - Y)$ grams of heavier constituents as oxygen, nitrogen, iron, etc. Then,

$$\mu = \frac{1}{2X + 0.75Y + \bar{\alpha}(1 - X - Y)} \sim \frac{1}{0.5 + 1.5X + \frac{1}{4}Y} \tag{8}$$

since $\bar{\alpha}$ is approximately 1/2. The electron density in the stellar interior will be

$$\begin{aligned} N_e &= \rho N_0 \Sigma (Z_E/A) w_E \\ &= \rho N_0 [X + \tfrac{1}{2}Y + \tfrac{1}{2}(1 - X - Y)] = \tfrac{1}{2}\rho N_0 (1 + X) \end{aligned} \tag{9}$$

Strömgren computed useful tables of $\bar{\alpha}(\rho, T)$. For a completely ionized Russell mixture he finds $\bar{\alpha} = 0.54$, but in view of the great preponderance of oxygen it is probably better to use $\bar{\alpha} = 0.56$. Later R. E. Marshak, P. M. Morse, and H. York discussed the equation of state for the Russell mixture at high temperatures and pressures and took into account certain quantum mechanical refinements. More recently, G. Keller and R. E. Meyerott greatly improved the theory of ionization of gas mixtures in stellar interiors.

4. The Adiabatic Gas Law

Our gas law, eqn. (1), represents a relation between three variables, P, V, and T. If we keep the temperature constant, and vary the pressure or volume, we obtain Boyle's law. On the other hand, if the volume is maintained constant and the temperature is changed, the pressure will be proportional to the temperature, and we have Charles's law. If both P and T are changed, one cannot, in general, say anything about V. One special type of change merits our attention. Suppose a mass of gas is allowed to expand or contract and no heat is permitted to enter or leave it during the change. Such a change is called an adiabatic process and may be of importance in those regions of a star where the chief transport of energy is by convection currents rather than by radiation.

In a mass of a gas undergoing an adiabatic change, the pressure and volume are related by

$$PV^{\gamma} = \text{constant} \tag{10}$$

where $\gamma = c_p/c_v$. Here c_p denotes the specific heat of a gas under conditions of constant pressure and c_v is the specific heat when the volume is kept constant. Now γ is always larger than 1, but approaches unity for complex atoms. It depends on the number of degrees of freedom of the atom or molecule, i.e., the minimum number of separate data we must have to describe the motion, e.g., (1) a point mass has three degrees of freedom, (2) a rigidly connected rotator has two degrees of rotation and three degrees of translation.* A complicated molecule may possess modes of vibration as well as rotation. For a monatomic gas $\gamma = 5/3$. Furthermore, the specific heats, c_p and c_v, will depend upon modes in which the energy may be stored internally within the gas, by dissociation of molecules, and by ionization of atoms, for example. A gas which is undergoing ionization at the temperature and density in question may have an effective γ different from that of a monatomic gas which is either wholly neutral or wholly ionized. This

* The motion of a dumbbell whose center of gravity is fixed can be represented as the resultant of motion about two axes.

fact is of considerable interest in connection with the origin of the solar granules.

5. The Law of Distribution of Velocities

If we could look at the individual molecules of a gas we would witness a hurly-burly of rapidly rushing particles, running hither and yon, colliding with one another and with the walls of the container. The impact of these particles with the walls and upon one another produces the pressure of the gas. Were we able to tag one of these molecules and follow it through the vicissitudes of its wanderings we would find it moving now fast, now slow, first in one direction and then, after a collision, in quite another. Or, if we took a couple of snapshots of the gas and measured the magnitude and direction of the motion of the molecules, we would find them to be moving in random directions and with different speeds. A few would be going with speeds considerably greater than the average, while others would be scarcely moving at all, but the majority would have speeds differing from the average by less than a factor of two.

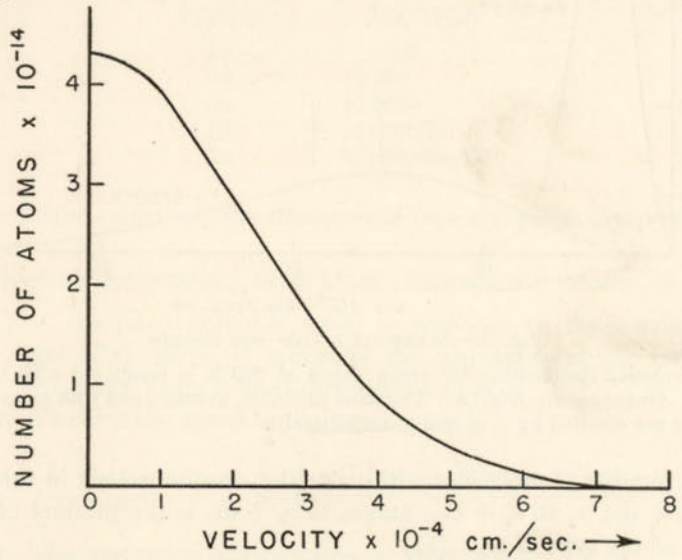

FIG. 1.—MAXWELLIAN DISTRIBUTION OF VELOCITIES IN THE x-DIRECTION

We plot the number of argon atoms/cm³ with x-velocities between v and $v + dv$ for N.T.P. (273°K and 760 mm or one atmosphere pressure).

The exact law of the distribution of velocities follows from the kinetic theory of gases or statistical mechanics. The result may be stated briefly. Denote the three components of velocity v, by v_x, v_y, and v_z. The Maxwell law of distribution of velocity states that the number of

molecules moving in the x-direction with velocities between v_x and $v_x + dv_x$ is

$$dN(v_x) = \frac{N}{\alpha\sqrt{\pi}} e^{-v_x^2/\alpha^2}\, dv_x \tag{11}$$

where α, the most probable speed, is given by

$$\tfrac{1}{2}M\alpha^2 = kT \tag{12}$$

and N is the number of molecules/cm^3. M is the mass of the molecule. That is, the velocities of the molecules in any specified direction follow a curve of the Gaussian error type, whose dispersion is determined by the most likely speed of the molecule which in turn depends on the temperature.

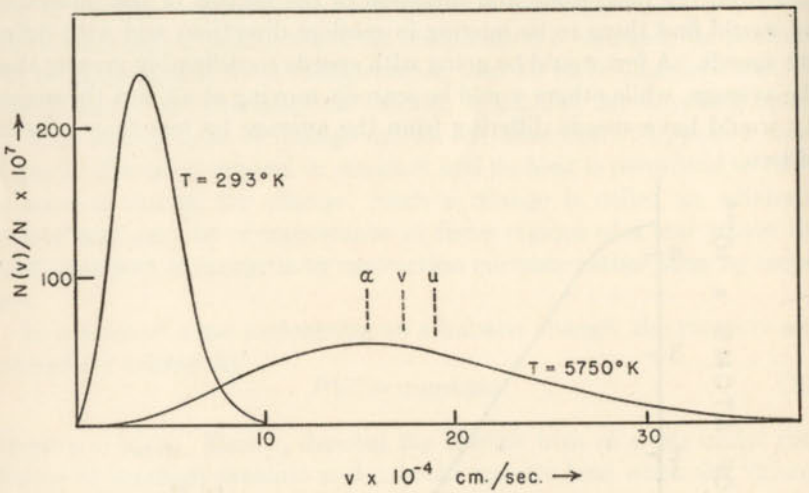

FIG. 2.—MAXWELL'S LAW FOR SPEEDS

The velocity distribution for argon atoms at 293°K is compared with that for 5750°K. Ordinates are $N(v)/N$. The most probable, average, and root mean square velocities are denoted by α, v, and u, respectively.

The number of molecules with velocities simultaneously in the range v_x to $v_x + dv_x$, v_y to $v_y + dv_y$, and v_z to $v_z + dv_z$ is the product of three factors of the type of eqn. (11)

$$dN(v_x v_y v_z) = \frac{N}{\alpha^3\pi^{3/2}} e^{-v^2/\alpha^2}\, dv_x\, dv_y\, dv_z \tag{13}$$

where

$$v^2 = v_x^2 + v_y^2 + v_z^2 \tag{14}$$

Often we are less interested in the actual velocities in the x, y, z directions than in the total speeds of the molecules themselves. Maxwell's law for speeds rather than velocities is:

$$Nf(v)\, dv = N(v)\, dv = 4\pi N \left(\frac{M}{2\pi kT}\right)^{3/2} v^2 e^{-Mv^2/2kT}\, dv \tag{15}$$

which gives the numbers of atoms $N(v)$ with velocities between v and $v + dv$ per unit volume. A plot of $N(v)$ against v shows a skewshaped curve which rises rapidly from the origin to a maximum and then falls off less abruptly on the high energy side. The shape of the curve depends on the temperature. For low temperatures, the curve is steep and narrow, but as the temperature rises the curves flatten out in accordance with the fact that the molecules have a greater range of velocities.

We find that few atoms have speeds greatly exceeding the mean. If we compute the relative numbers of atoms with speeds α, 2α, 3α, 4α, 5α from eqn. (15), viz.,

$$\frac{N(v)}{N(\alpha)} = \frac{v^2}{\alpha^2} e^{(\alpha^2 - v^2)/\alpha^2}$$

we obtain the following results:

Velocity	$N(v)/N(\alpha)$
1α	1.0000
2α	0.199
3α	0.0030
4α	0.000005
5α	0.0000000009

At the larger velocities, the exponential factor rapidly overpowers the v^2 factor.

At a given temperature, three kinds of speeds will interest us:

(1) α: the most probable speed corresponds to the maximum of the $N(v)$ curve; it measures the dispersion of the molecular velocities along a fixed direction, e.g., x.

(2) The average speed in the usual sense is

$$\bar{v} = \frac{1}{N}\int N(v) v\, dv = \frac{2\alpha}{\sqrt{\pi}} \tag{16}$$

(3) The root mean square speed, u, given by

$$\tfrac{1}{2}mu^2 = \tfrac{3}{2}kT \tag{17}$$

is the "average velocity of the molecules" computed in elementary physics texts. In our calculations we shall be primarily interested in α or u; $\bar{v}$ has few practical applications.

As an example, let us compute the values of α, $\bar{v}$, and u for nitrogen molecules at $T = 0°\text{C} = 273°\text{K}$. The mass of the nitrogen molecule is

$28 \times 1.66 \times 10^{-24}$ grams since the molecular weight of nitrogen is 28 and 1.66×10^{-24} grams is the mass of an atom of unit atomic weight. Then α is computed from eqn. (12), viz.:

$$\alpha = \left[\frac{2 \times 1.380 \times 10^{-16} \times 273}{28 \times 1.66 \times 10^{-24}}\right]^{1/2} = 4.02 \times 10^4 \text{ cm/sec}$$

Similarly, $v = 2\alpha/\sqrt{\pi} = 1.1284\alpha = 4.54 \times 10^4$ cm/sec

$$u = \sqrt{\tfrac{3}{2}}\alpha \quad = 1.2248\alpha = 4.93 \times 10^4 \text{ cm/sec}$$

Let us compare the root mean square speeds of an argon atom at room temperature (20°C), at the temperature of the solar atmosphere (5750°K), and at the temperature of the center of Sirius (20,000,000°K). The atomic weight of argon is 39.94, whence

$$u = \sqrt{\frac{3kT}{M}} = \left[\frac{3 \times 1.380 \times 10^{-16} \times 293}{39.94 \times 1.660 \times 10^{-24}}\right]^{1/2} = 4.277 \times 10^4 \text{ cm/sec}$$

At the temperature of the solar atmosphere, an application of the above formula with $T = 5750$°K instead of 293°K gives

$$u = 18.95 \times 10^4 \text{ cm/sec}$$

while at 20,000,000°K, we find $u = 1.12 \times 10^7$ cm/sec. Notice that the mean velocity increases as the square root of the temperature.

6. Thermal Broadening of Spectral Lines

The broadening of a spectral line, as a consequence of the kinetic motion of the radiating atoms, provides a useful illustration of Maxwell's law for the distribution of velocities. Let us suppose that each individual atom radiates monochromatically.* That is, an atom at rest radiates a sharp line of frequency ν_0 (or wave length λ_0). If it is moving toward the observer with a velocity v_x, the observed frequency and wave length of the emitted radiation will be changed by an amount given by

$$\frac{\Delta\nu}{\nu} = \frac{\Delta\lambda}{\lambda} = \frac{v_x}{c} \tag{18}$$

in accordance with Doppler's principle. Here c denotes the velocity of light. The number of atoms moving at any time with a velocity v_x toward the observer follows from Maxwell's velocity law, eqn. (11). If

* We suppose we can neglect all other effects that would make the atoms radiate split or fuzzy lines, e.g., density effects, disturbances produced by electric and magnetic fields acting upon the atom, and the phenomenon of "natural breadth" described in Chapter 5. If there were no large-scale motions of the gas, the forbidden lines in the spectra of the gaseous nebulae would provide a good example.

the intensity distribution within the spectral line is proportional to the number of atoms radiating at a frequency ν, then

$$I(\nu)\,d\nu = \frac{I_0}{\sqrt{\pi}}\, e^{-\frac{c^2}{\alpha^2}\left(\frac{\nu-\nu_0}{\nu}\right)^2} \frac{c\,d\nu}{\alpha\nu} \tag{19}$$

since

$$\left(\frac{\nu-\nu_0}{\nu}\right)^2 = \frac{v_x^2}{c^2} \quad \text{and} \quad dv_x = \frac{c\,d(\Delta\nu)}{\nu} = \frac{c\,d\nu}{\nu} \tag{20}$$

In wave length units the expression is similarly,

$$I(\lambda)\,d\lambda = \frac{cI_0}{\lambda\alpha\sqrt{\pi}}\, e^{-\frac{c^2(\lambda-\lambda_0)^2}{\alpha^2\lambda_0^2}}\, d\lambda \tag{21}$$

Here I_0 denotes the total intensity of the line, which is related to the central intensity I_c by

$$I_c = \frac{cI_0}{\lambda\alpha\sqrt{\pi}} \tag{22}$$

Notice that the line has a roughly bell-shaped profile; the top is rounded, and the intensity thereafter falls off abruptly with wave length. If we record such a line upon a photographic plate of high contrast, we are likely to get a broadened line of rather definite width. We define the half-width of the line as the width at which I has fallen to one half its maximum value. The wave length at which $I = \frac{1}{2}I_c$ is given by

$$e^{-\frac{Mc^2(\lambda-\lambda_0)^2}{2\lambda_0^2 kT}} = \tfrac{1}{2} \tag{23}$$

Thus the total half-width of the line is

$$\delta\lambda_a = 2\delta\lambda = 2(\lambda - \lambda_0) = 2\sqrt{\frac{2\lambda_0^2 kT}{Mc^2}\log_e 2} \tag{24}$$

whence

$$\delta\lambda_a = 7.16 \times 10^{-7}\lambda\sqrt{T/\mu} \tag{25}$$

where μ is the molecular weight, T is the temperature in absolute degrees, and λ is measured in angstrom units.

Example: What is the half-width of the λ4861 line of hydrogen in a gaseous nebula at a temperature of 10,000°K? Assume that the line is widened only by the Doppler effect.

$$\delta\lambda_a = 7.16 \times 10^{-7} \times 4861 \times \sqrt{\frac{10{,}000}{1}} = 0.35\text{A}$$

For the [O III] lines at λ4960 and λ5007, since $\mu = 16.0$, we find that $\delta\lambda = 0.087$A.

7. The Distribution Law Under Diverse Conditions

The Maxwellian distribution law of velocities is one of the most persistent phenomena of nature. Under diverse conditions, the atoms, ions, or molecules assume a Maxwellian distribution appropriate to some temperature T, which we may call the gas kinetic temperature. For example, experiments by Langmuir and Tonks showed that the electrons in a gas discharge followed a Maxwellian distribution very closely. Even under such extreme conditions as those obtaining in a gaseous nebula the electrons maintain a Maxwellian distribution!

Processes tending to destroy a Maxwellian distribution compete with processes tending to restore it. In a planetary nebula an electron is freed from an atom by photoelectric ejection, wanders about and is finally recaptured. In the course of its life as a free particle it may collide with an oxygen atom, say, and give up its energy in an inelastic collision to excite the atom to a nearby energy level. Such collisional excitations tend to destroy the Maxwellian distribution, but encounters with other electrons and ions tend to restore it. Electron-electron and electron-ion encounters are enormously more frequent than any other type of process. Hence deviations from the Maxwell distribution law are negligible. Each type of particle will set up a velocity distribution and since the different particles tend to interact with one another, the velocity distribution will be appropriate to some unique kinetic temperature T.

8. Breakdown of the Perfect Gas Law

The perfect gas law assumes point molecules that exert no forces upon one another except at actual times of collisions. If the gas is compressed to the point where the intermolecular distances become comparable with the dimensions of the molecules themselves, short range attractive van der Waals forces and the finite sizes of the gas molecules conspire to limit the accuracy of the perfect gas law. Below the so-called critical point the gas will liquefy if the pressure is increased. On the other hand, as the temperature is raised and the pressure decreased, all gases tend to become "perfect." In the atmospheres and throughout the interiors of most stars, the density is sufficiently low or the temperature sufficiently high for the perfect gas law to be nearly exact.

Nevertheless, the interactions between the charged particles of an ionized gas produce some deviations from the perfect gas law. R. E. Williamson finds that the correction $\delta P/P$ will amount to about 0.43 per cent for the sun, and only 2.1 per cent for the dense star σ_2 Eri C whose mass is 0.20 that of the sun. The standard model is assumed.

In the interiors of some stars the density becomes so high that deviations from the perfect gas law do occur. They are not of the type expressible by the van der Waals' equation, but require a whole new equation of state.

Consider what happens as the pressure upon a block of material is increased. Even at experimentally attainable pressures, common substances often show remarkable properties. We mention Bridgman's hot ice, solid water at a temperature above 100°C. Nevertheless, the highest pressures we can produce are small compared with the pressures at the interior of the earth, to say nothing of those within the giant planets.

If the pressure upon a cold body is increased, ultimately the "incompressible" atoms themselves are jammed so tightly together that electrons will become detached. We call this phenomenon pressure ionization. If the density is increased sufficiently, all the electrons will be detached from their respective atoms. The detached electrons are free in the sense that the conduction electrons in a metal are free. That is, they do not belong to particular atoms. They follow, however, a distribution law which is quite different from the classical Maxwellian law. Under these circumstances, the electrons will exert a larger pressure than will an equivalent number of nuclei. The material possesses quite different properties than it does under ordinary conditions, and we say that it is degenerate. Degeneracy can set in even at a high temperature if the pressure is sufficiently great.

9. Equation of State for a Degenerate Gas

In order to explain the phenomenon of degeneracy in a gas we must introduce the concept of "phase space." At any instant a particle in a fluid may be characterized by three space coordinates, usually denoted as q_1, q_2, and q_3 (e.g., x, y, z) and three velocity, or rather momentum coordinates, p_1, p_2, and p_3. All six of these numbers are needed to specify the position and momentum of each particle at any one time. If we know the forces acting upon the particles, classical mechanics asserts that theoretically it should be possible to tell what they will be doing at any later time. To indicate the state of a given particle, we could employ three separate graphs, one for each pair of momentum and space coordinates, or we could adopt a single point in a 6-dimensional space called a "phase space." The latter point of view is the more useful; we imagine this 6-dimensional space divided up into small boxes of volume h^3. If the particles have spin, e.g., electrons, the generalized Pauli principle states that two and only two particles may be found in each cell of dimensions h^3. Under conditions existing in stellar interiors, degeneracy is important only for electrons.

To understand how the Pauli principle puts a limit on the density which matter can attain at a given temperature, let us compare two

dissimilar volumes A and B wherein the same total amount of energy is available. In Fig. 3 each box is divided into cells of volume h^3. In the large box A there is little chance of more than one electron residing in each cell. The electrons then have a Maxwellian distribution. If the gas is compressed to a small volume B and the energy supplied by the work of compression taken away, space becomes precious and electrons

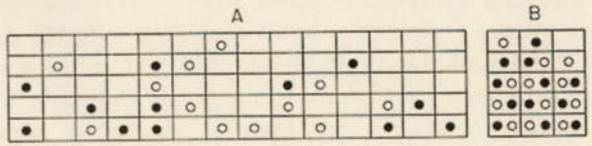

FIG. 3.—APPROACH TO DEGENERACY WITH INCREASING DENSITY

The box A, to the left, represents a condition under which classical theory can be applied. In box B, on the right, the density is so high that degeneracy has set in. Filled circles indicate electrons with spins $+\frac{1}{2}$; open circles indicate electrons with spins $-\frac{1}{2}$.

are forced into the higher cells of momentum space. Under conditions of complete degeneracy, every cell of available phase space is filled and no more energy can be extracted from the gas since particles in the higher cells cannot go to the already occupied cells of lower energy. To compress the gas further additional energy must be supplied.

Such a gas has peculiar properties; one particle cannot move to another cell unless the particle already in that cell moves elsewhere. Hence the individual particles of the gas behave as though they were geared together.

In a first rough approach to the problem, consider a completely degenerate gas which occupies a physical volume of 1 cm^3, wherein every cell of phase space is filled up to a certain value of the momentum p_0 which corresponds to an energy e_0. The particles would be distributed uniformly in momentum from 0 to a maximum momentum p_0, and in Cartesian coordinates the distribution law would have the form,

$$N(v)\,dv_x\,dv_y\,dv_z = \frac{2m^3}{h^3}\,dv_x\,dv_y\,dv_z = \frac{2}{h^3}\,dp_x\,dp_y\,dp_z \tag{26}$$

since $2/h^3$ particles can be crammed into a unit volume of phase space. Thus $N(v) = 5.20 \times 10^{-3}$ per unit velocity interval for all velocities less than v_0 where $p_0 = mv_0$. Here m denotes the mass of the electron.

Suppose we have an electron gas at 0°C = 273°K and one atmosphere pressure. The number of particles/cm^3 is the Loschmidt number, 2.69×10^{19}. If the electrons follow Maxwell's law, eqn. (13),

$$N(v)\,dv_x\,dv_y\,dv_z = N\left(\frac{m}{2\pi kT}\right)^{3/2} e^{-mv^2/2kT}\,dv_x\,dv_y\,dv_z \tag{27}$$

the number per unit velocity interval will be 0.00645 at the origin as compared with 0.0052 from eqn. (26). This means that in the range of small velocities, Maxwell's law requires more electrons per cm^3 than the Pauli principle permits; hence deviations from the classical expression must occur. Degeneracy of an electron gas can set in even at room temperature.* An increase in temperature or a decrease in pressure may remove degeneracy. The temperature is so high in the solar interior that the electrons follow the classical Maxwellian distribution, but in the much denser companion to Sirius, the electron gas is degenerate.

The exact statistical mechanical treatment shows that eqn. (26) does not hold up to the maximum velocity v_0. The distribution has rounded edges in accordance with the Fermi-Dirac law,

$$N\,dv_x\,dv_y\,dv_z = \frac{2m^3}{h^3}\frac{dv_x\,dv_y\,dv_z}{e^{[\frac{1}{2}mv^2-\phi]/kT}+1} \tag{28}$$

where the characteristic energy,

$$\phi = \left(\frac{3N}{8\pi}\right)^{2/3}\frac{h^2}{2m} \tag{29}$$

is determined by the electron concentration and not by the temperature. When $\frac{1}{2}mv^2$ is much less than ϕ, the exponent is negative and $N(v)$ follows eqn. (26). When $\frac{1}{2}mv^2$ is greater than ϕ, the exponent changes sign and increases rapidly as v increases. Since the exponential factor then is much greater than unity, the latter can be neglected and the curve resembles a Maxwellian distribution. The greater the electron density N, the larger will be ϕ and the more pronounced the degeneracy.

Let us now compute v_0, the upper limit to the velocity of the particles in a completely degenerate gas. The volume of phase space $d\tau$ embracing momenta between p and $p + dp$, where

$$p^2 = p_x^2 + p_y^2 + p_z^2$$

is the volume of a shell of radius p and thickness dp, multiplied by the volume V in physical space, viz.,

$$d\tau = 4\pi V p^2\,dp$$

The total number of possible states is obtained by multiplying by the factor $2/h^3$ since h^3 is the volume of each cell which contains two elec-

* The "free" electrons in a metal are free in the sense that they are not attached to any atom but may wander throughout the structure. Their possible energy states are restricted since those of lower energy are all filled. Hence the electrons are squeezed into states of higher energy than would be appropriate for the temperature in question and a Maxwellian distribution. In particular they cannot share their energies with the metallic ions in the lattice.

trons. Without loss of generality V may be taken as 1. Hence the number of electrons with momenta between p and $p + dp$ is

$$N_e(p)\,dp \leq \frac{8\pi p^2\,dp}{h^3} \tag{30}$$

The equality sign obtains for a completely degenerate gas. Let N_e be the total number of electrons in the unit volume under conditions of complete degeneracy. Their momenta must be less than the maximum value p_0 given by

$$N_e = \frac{8\pi}{h^3}\int_0^{p_0} p^2\,dp = \frac{8\pi}{3h^3}\,p_0^3 \tag{31}$$

Now the pressure of a gas is the rate of momentum transfer across a surface of unit area. For simplicity, consider a unit area perpendicular to the x-direction. The number of electrons of momentum p_x crossing this area per second will be $N_e(p_x)v_x$. Each carries a momentum p_x and since the gas is isotropic, one third can be thought of as moving in the x-direction. Hence the total pressure, obtained by integrating over all momenta, will be

$$P_e = \int_0^{p_0} N_e(p_x)v_x p_x\,dp_x = \frac{8\pi}{h^3}\int_0^{p_0} p^2\left(\frac{p^2}{3m}\right)dp = \frac{8\pi}{15h^3m}\,p_0^5 \tag{32}$$

provided the electronic velocities are so low we can neglect the relativity effects. Eliminating p_0 in terms of N_e, by eqn. (31), we obtain:

$$P_e = \frac{1}{20}\left(\frac{3}{\pi}\right)^{2/3}\frac{h^2}{m}\,N_e^{5/3} \tag{33}$$

Notice that the final formula involves the number of electrons per cm^3 and the pressure, but not the temperature. The explanation is that when a gas is completely degenerate, the temperature, which is really only a measure of the energies of the electrons, tells how many of them can be crowded into a given volume, i.e., it determines N_e or the density all by itself. If the gas is degenerate, all cells of phase space are filled and additional energy has to be supplied before more electrons can be crammed into the given volume. We emphasize again that in a volume containing ions and electrons it is only the electrons that are degenerate. The ions continue to obey something resembling the perfect gas law, but their contribution to the total pressure is so small it may be neglected.

We can write eqn. (33) in the form

$$P = K_1\left(\frac{\rho}{\mu'}\right)^{5/3} \tag{34}$$

where

$$K_1 = \frac{1}{20}\left(\frac{3}{\pi}\right)^{2/3}\frac{h^2}{mM_0^{5/3}} = 9.913 \times 10^{12} \tag{35}$$

in c.g.s. units. Here m is the electronic mass, M_0 the mass of the proton, and μ' is the average mass (in atomic weight units) per free electron of the completely ionized gas. In dealing with a degenerate gas we are interested in the mean weight per free electron since the role played by the heavy atoms can be ignored. When completely ionized, neon gives ten electrons and a nucleus, i.e., 11 particles in all. Hence completely ionized neon will have a molecular weight of $20.18/11 = 1.83$. The average mass per electron, however, is $\mu' = 20.18/10 = 2.02$. For hydrogen, the molecular weight, μ, is $1/2$, but $\mu' = 1$. Helium, of atomic weight 4, supplies two electrons; hence $\mu = 4/3$, but $\mu' = 2$. The distinction between μ and μ' is particularly important for the light atoms.

It is necessary to know under what conditions to use the degenerate gas law, eqn. (34), rather than the perfect gas law, eqn. (4). We may regard the gas as degenerate if the gas pressure computed from the degenerate gas law is greater than that given by the perfect gas law, i.e., if

$$9.91 \times 10^{12}\left(\frac{\rho}{\mu'}\right)^{5/3} > \rho\,\frac{\mathcal{R}T}{\mu} \tag{36}$$

which amounts to

$$\frac{\rho\mu^{3/2}}{\mu'^{5/2}T^{3/2}} > 2.43 \times 10^{-8} \tag{37}$$

If we apply this criterion to hydrogen, assuming that it is completely ionized, the electron gas will be degenerate above the following critical densities:

Temperature	Density gm/cm^3
10,000°K	0.07
100,000	2.2
1,000,000	69.
10,000,000	2170.

In metals where the density is of the order of 8 or 10 gm/cm^3 and the temperature is about 20°C, the electrons are strongly degenerate.

10. Relativistic Degeneracy

At very high densities, the electrons must possess such high velocities that the relativistic change of mass with velocity must be taken into account. Under these circumstances eqn. (33) is no longer valid and a new expression must be found. Chandrasekhar* has indicated

* *An Introduction to the Study of Stellar Structure* (Chicago: University of Chicago Press, 1939), p. 359.

the correct procedure and has shown that the pressure and density may be expressed by means of the parametric equations:

$$P = Af(x) \quad \text{and} \quad \rho = Bx^3 \tag{38}$$

where

$$x = p_0/mc, \quad f(x) = x(2x^2 - 3)(x^2 + 1)^{1/2} + 3\sinh^{-1} x \tag{39}$$

$$A = \frac{\pi m^4 c^5}{3h^3} = 5.998 \times 10^{22}; \quad B = \frac{8\pi m^3 c^3 \mu' M_0}{3h^3} = 9.807 \times 10^5 \mu' \tag{40}$$

The parametric expressions (38) together represent the equation of state over the entire range of degeneracy. The electron density,

$$N_e = \frac{8\pi}{3h^3} p_0^3 = \frac{8\pi m^3 c^3}{3h^3} x^3 = 5.87 \times 10^{29} x^3 \tag{41}$$

and the density of the material in gm/cm^3 are related by

$$\rho = N_e \mu' M_0 = Bx^3 \tag{42}$$

When the density is very large, x is large, and the electrons must move with such high velocities that the relativistic effects become important. Then

$$f(x) \to 2x^4 = 2\left(\frac{3h^3}{8\pi m^3 c^3}\right)^{4/3} N_e^{4/3}, \quad P = \frac{1}{8}\left(\frac{3}{\pi}\right)^{1/3} hcN_e^{4/3} \tag{43}$$

or, in terms of the density,

$$P = K_2\left(\frac{\rho}{\mu'}\right)^{4/3} \tag{44}$$

where

$$K_2 = \left(\frac{3}{\pi}\right)^{1/3} \frac{hc}{8M_0^{4/3}} = 1.2311 \times 10^{15} \tag{45}$$

which is the equation of state for relativistic degeneracy. Whenever the pressure computed by the relativistic degenerate gas law is greater than the pressure computed from the perfect gas law, we must use the relativistic equation. Notice that for small values of x, i.e., relatively low densities, we recover the eqn. (34). Thus eqns. (34) and (44) represent asymptotic forms for eqn. (38).

The temperature and density domains where the various equations of state are to be applied are illustrated in Fig. 4. The curve labeled degeneracy criterion locus divides the T, ρ diagram into two areas in one of which the electrons obey the perfect gas law, and in the other of which the degenerate gas law obtains. The equation of state for the latter region is Chandrasekhar's parametric expression which reduces to eqn. (34) for $\rho \ll 2 \times 10^6$, and to eqn. (44) for $\rho \gg 2 \times 10^6$. The

form of the gas law in the region between the domain of pure degeneracy and perfect gas becomes complicated and in applications to stellar interiors rather involved calculations are required. The degenerate gas laws are of considerable importance in connection with the white dwarf stars.

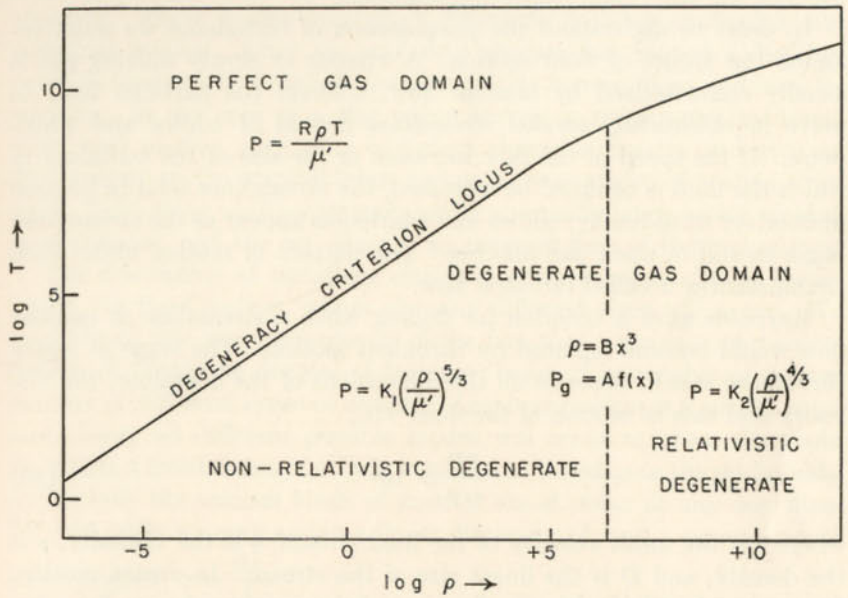

FIG. 4.—THE DOMAINS OF THE GAS LAW

The solid curve, called the degeneracy criterion locus, divides the log ρ—log T diagram into two regions in one of which the perfect gas law holds, while in the other the degenerate gas law must be applied. The latter has two asymptotic forms corresponding to relativistic and nonrelativistic degeneracy. In the neighborhood of the degeneracy criterion locus, the gas laws become extremely complicated. Fortunately, in most applications we are concerned with material that behaves either as a perfect gas or as a degenerate gas. The electrons become degenerate while the heavy particles still follow the classical distribution. (Adapted from a diagram by Gordon Wares, *Astrophysical Journal*, University of Chicago Press, **100**, 159, 1944.)

11. Turbulence

In astrophysics as in other branches of physics we are frequently concerned with large-scale mass motions of gases. Sometimes, orderly stream motion (hydrodynamical flow) may occur. For example, we might expect orderly convection currents to exist in the core of a rapidly spinning star. On the other hand, in the core of a static or slowly rotating star, chaotic, whirlpool-like motions of the gases are likely to carry the energy, since large-scale streams would tend to break down into turbulent eddies.

Turbulence refers to a state of a gas when it is impractical to define its mass motion point by point and minute by minute. For example, one might observe the contortions of cumulus clouds in the earth's atmosphere on a windy day. We would apply a statistical description to the motions of the clouds and not concern ourselves with the vicissitudes of the individual whirls and filaments.

In order to understand the phenomenon of turbulence we must examine the nature of fluid motion. A viscous or slowly moving gas is usually characterized by *laminar* flow, wherein the particles tend to move in *continuous, parallel streamlines* devoid of eddies and whirlpools. If the speed of the flow increases or the size of the container in which the fluid is confined be increased, the streamlines tend to become undulatory until finally, eddies and whirlpools appear as the streamlines begin to roll in upon one another. The pattern of motion under such circumstances is called *turbulent* flow.

Reynolds gave a criterion for finding when a streamline or laminar flow would become replaced by turbulent motion. The stage at which turbulence sets in depends on the dimensions of the container, the viscosity and rate of motion of the fluid, viz.,

$$\frac{\bar{v}D}{\eta/\rho} > 10^3 \tag{46}$$

where $\bar{v}$ is the mean velocity of the fluid stream, η is the viscosity, ρ is the density, and D is the linear size of the stream. In vortex motion, D may be identified with the diameter of the vortex, whereas for other kinds of motion it is of the order of the size of the container. The turbulent viscosity is of the order of a million times greater than the laminar viscosity. The ratio, $\nu = \eta/\rho$, is the *kinematical viscosity*. If the vessel is large, the velocity at which turbulence sets in may become small. Thus turbulence will be set up in an ocean at smaller fluid velocities than in a lake. In a stellar interior, large-scale gas motion would tend to be turbulent. The exact point at which turbulence sets in depends on the factors perturbing the gas. A steep thermal gradient would have a marked effect.

The older discussions of turbulence introduced the concept of a *turbulence element* as follows: Consider two points in a fluid in turbulent flow. If the points lie close together, the motions will be closely correlated, but as we choose them farther and farther apart, we finally find a distance where there is no correlation. Following the definition of Prandtl, we call this critical distance the size of the turbulence element. That is, the turbulence elements are fluid masses in common motion, and different elements may be distinguished from one another. Small eddies tend to be wiped out by viscosity.

The motion of a turbulent fluid is so confused that it is scarcely possible to give it a phenomenological description. Prandtl proposed a rough analogy with the kinetic theory of gases, wherein turbulent elements play the role of molecules. The mean free path of an eddy or turbulent element, l, is of the same order of size as the turbulence element itself, but there seems a certain arbitrariness in choosing this quantity. There is one important difference between molecular and turbulent motion. After the turbulent element has moved a distance equal to its mean free path, it merges with its surroundings and loses its identity. In the core of a star where energy is transported by large-scale mass motion, ascending turbulent elements dissolve and give up their energy to the surroundings, and as a consequence of cooling, contract. Each rising whirlpool is replaced by an equally large, cooler, sinking mass element, and the net effect is an outward flow of thermal energy.

The description of turbulent elements by their mean sizes is inadequate. In fluid motion, whirls of many different sizes will occur. We may regard this as a consequence of the fact that a gas is a mechanical system of numerous degrees of freedom; hence it is capable of a large number of different types of motion. Laminar motion is a special case; more likely all different possible modes will occur at once. It would seem that a fruitful line of attack would be to investigate the probability with which the various kinds of motion would occur at any one time. To each eddy we may assign a linear dimension, l, and a corresponding wave number, $k = \dfrac{2\pi}{l}$.

A quantity of fundamental interest is the energy $\rho F(k)\,dk$ stored in each unit volume in eddies between wave numbers k and $k + dk$. $F(k)$ is said to define the *spectrum* of *turbulence*. Its analytic form has been studied by Kolmogoroff, Heisenberg, Chandrasekhar, and others.

Much as the energy emitted by an incandescent solid, for example, can be analyzed in terms of a continuous spectrum, so can the instantaneous velocity distribution in a turbulent medium (or related quantities such as density and pressure) be analyzed in terms of the turbulence spectrum. In the radiation spectrum we are not interested in the phases of the emitted light waves; we are primarily concerned with the intensity as a function of frequency. Analogously in turbulence, we are not concerned with the details of motions in the individual whirls, but rather with the distribution of energy among them.

Now turbulence must be maintained by some external cause, a steep temperature gradient, mechanical stirring, etc. Otherwise the turbulence will simply decay. Hence we must distinguish between the steady state where energy is continuously being supplied, and the case where turbulence is decaying.

The sizes of the largest eddies $\sim l_0$, say, will depend on the particular mechanism which supplies the energy. The character of the spectrum in this domain will depend on the mechanism involved and may differ from one problem to the next. Among the smaller eddies, for which $k \gg k_0$, we may expect to find some kind of a general law.

The physical nature of a steady state where energy is supplied from an external source is this: The energy goes mostly into the largest eddies at a rate of say ε ergs/cm^3/sec. It is then passed down through a hierarchy of eddies and finally dissipated by viscosity in the smallest eddies where the motion is laminar. The condition of constant flow of energy from the larger to the smaller whirlpools determines the character of the equilibrium spectrum whose exact form has been discussed by Kolmogoroff, Heisenberg, Chandrasekhar, and others.

The significant fact is that, except for the largest eddies, the distribution does not depend on the source of turbulence but only on the rate of energy supply and the viscosity.

A problem of some astrophysical interest is the decay of turbulence when the source of energy is cut off. First the larger eddies will adjust themselves to the disappearance of the energy supply. For some time, the distribution $F(k)$ among the lower eddies will remain as though nothing had happened. During this stage the general character of the spectrum remains unchanged; that is, the form of the spectrum remains the same although the scale changes. Gradually the energy from the larger eddies is used up and the smaller whirls gradually die away.

The total turbulence spectrum, $F(k)$, can be calculated if the mechanism and rate of energy supply as well as the viscosity are known. The distribution function shows a peak corresponding to an eddy of some length, say l_0, but we must remember that energy is lost as heat only from eddies of much smaller linear size.

Turbulence appears to have important astrophysical applications not only to stellar interiors but also to the solar granules, to the atmospheres of giant stars, to the shells of close binaries, to gaseous nebulae, and to the interstellar medium.

The chaotic appearance of extensive emission nebulosities photographed, for example, with the 48-inch Palomar Schmidt strongly suggests turbulence. Since we receive radiation from a considerable range in depth it is difficult to interpret the velocities or intensity variations. From an analysis of the intensity fluctuations, the existence of a turbulence spectrum with a sharp maximum seems compatible with the observations. The large eddies presumably contain a sufficient store of energy to maintain a flow of energy down the hierarchy of eddies to the smaller ones. S. von Hoerner has discussed the evidence for turbulence in the Orion Nebula.

Turbulence in the atmosphere of the sun appears not only in the granules but presumably also in the motions of prominences, where the combined factors of magnetic fields, radiation pressure, mass motion, and turbulence conspire to make an unusually complicated astrophysical problem.

PROBLEMS

1. A mixture of gas in the following proportions H, 0.60; He, 30; C, 0.02; N, 0.02; and O, 0.06 is completely ionized. Calculate the molecular weight.

2. Derive eqn. (15) from eqn. (13).

3. Compute α and u for oxygen at $T = 293°$K, 5700°K, and 1,000,000°K.

4. What is the total Doppler half-width of the sodium "D" lines at 5890 and 5896A at $T = 5700°$K?

5. Assume that each iron atom in a block of the metal contributes one "free" electron. To what temperature must the block be raised in order to remove the degeneracy?

6. At what density would a mass of completely ionized helium become degenerate at a temperature of eight million degrees?

REFERENCES

Maxwell's law of distribution of velocities is derived in a number of physics texts, e.g.:

Loeb, L. B. *Kinetic Theory of Gases.* New York: McGraw-Hill Book Co., Inc., 1935.
Kennard, E. H. *Kinetic Theory of Gases.* New York: McGraw-Hill Book Co., Inc., 1942.

The molecular weight of ionized material has been calculated by:

Marshak, R. E., P. M. Morse, and H. York. *Ap. J.* **111,** 214, 1950.
Keller, G., and R. E. Meyerott. Argonne Nat'l Lab. Report No. 4771, 1952.

The equation of state of a dense ionized gas has been discussed by:

Rosseland, S. *M.N.* **84,** 720, 1924.
Williamson, R. E. *Ap. J.* **103,** 139, 1946.
Jeans, J. H. *The Dynamical Theory of Gases,* (4th ed.). Cambridge: Cambridge University Press, 1925, p. 131.

The equation of state for a degenerate gas is derived by:

Chandrasekhar, S. *An Introduction to the Study of Stellar Structure.* Chicago: University of Chicago Press, 1939, chaps. ix and x.

The transition zone between the domain where the perfect gas law is valid and that in which the degenerate gas law is valid is discussed by:

Wares, G. W. *Ap. J.* **100,** 158, 1944.

The best introductory account of the modern theory of turbulence is given by Chandrasekhar in his Russell Lecture, *Ap. J.* **110,** 329, 1949. Our brief discussion of the turbulence spectrum has been summarized from this paper which gives important references to earlier work. In astrophysical work large eddies are often important. See:

Batchelor, G. K. *Proc. Roy. Soc. A,* **195,** 513, 1949.
Batchelor, G. K., and A. A. Townsend. *Proc. Roy. Soc. A,* **199,** 238, 1949.

Applications of turbulence concepts to stellar atmospheres are made in Chapters 8 and 9. Turbulence in gaseous nebulae and the interstellar medium is discussed in:

"Problems of Cosmical Aerodynamics," Central Air Documents Office, Dayton, Ohio, 1951.
Minnaert, M. *B.A.N.* **10,** 405, 1948.
von Hoerner, S. *Zeits. f. Ap.* **30,** 17, 1951.
Aller, L. H. *Ap. J.* **113,** 120, 1951.

CHAPTER 4

Excitation, Ionization, and Dissociation

Astrophysics is largely concerned with the properties of matter at temperatures ranging from 1500 or 2000 degrees to several million degrees. In the first approximation, interest is centered in steady-state conditions. In the treatment of variable stars, etc., the practice frequently has been to consider the changes in terms of a series of separate stages, each of which can be treated as a steady state.

At the outset it is important to understand that a steady state does not imply thermal equilibrium. Consider radiation passing through a stratum of matter, e.g., the atmosphere of a star. The state may be a steady one, i.e., not change with time but it is certainly not an equilibrium one. The flow of energy from one side of the layer to the other implies a temperature gradient and under equilibrium conditions a temperature difference cannot exist. Nevertheless, the rates of certain atomic processes may be nearly the same as in thermal equilibrium and in the first reconnaissance of the problem, various relationships derived for strict thermodynamic equilibrium will prove useful.

1. Thermodynamic Equilibrium

Let us picture the state of affairs in a gas in thermal equilibrium. Imagine a mass inclosed in a hypothetical box whose walls are maintained at a temperature T of the order of 5 or 10 thousand degrees. The atoms in the box move rapidly about, strike one another in more or less violent collisions, absorb and re-emit energy, and lose and recapture electrons. A condition obtains wherein each process is exactly balanced by its inverse. Every collision in which an electron gives up energy to an atom to excite it to a higher energy level is balanced by an encounter in which an excited atom unloads its excitation energy upon a passing electron (superelastic collision). Every ionization from a particular level is balanced by a recapture upon the same level.

We can express these ideas quantitatively by saying that quite generally the number of absorptions from n to n'' is equal to the number of transitions in which the atoms jump from n'' to n with the emission of radiation. The number of collisional excitations from n to n'' is equal to the number of inverse superelastic collisions, wherein atoms cascade from n'' to n, and a passing particle carries off the excess energy. The number of ionizations from level n is equal to the number of recaptures

on the same level n. An assemblage of particles in which every process is balanced by its inverse, i.e., one in which *detailed balancing* occurs, is said to be in strict thermodynamic equilibrium.

Thermodynamics, which deals with macroscopic properties of matter, gives us much information about material in thermal equilibrium, although pure thermodynamics is of relatively restricted use to the astronomer. An intrinsically easier and more powerful technique is that of statistical mechanics, which makes use of the fact that atoms possess known energy states. The application of the formal procedures of statistical mechanics requires the existence of a thermal equilibrium and assumes that atoms or molecules interact with one another. It does not, however, require any knowledge of the details of how energy passes from one atom to another.

Statistical mechanics enables us to derive important relationships such as the Maxwell law of velocities, Planck's law (Chapter 5), the Boltzmann law, and the ionization and dissociation equations.

2. Boltzmann's Law

The fundamental relationship is Boltzmann's law which states that under conditions of thermal equilibrium the relative numbers of atoms in the two levels A and B is given by

$$\frac{N_B}{N_A} = \frac{g_B}{g_A} e^{-\chi_{AB}/kT} \tag{1}$$

where $\chi_{AB} = E_B - E_A$ is the energy difference between the two levels A and B, g_B is the statistical weight, $2J_B + 1$, for the upper level, $g_A = 2J_A + 1$, that of the lower level,* and T is the absolute temperature.

We shall not attempt to prove this formula but shall adopt it on a postulational basis. If χ is expressed in volts, the Boltzmann formula can be written as

$$\log \frac{N_B}{N_A} = -\frac{5040.4}{T} \chi_{AB} + \log \frac{g_B}{g_A} \tag{2}$$

Sometimes we wish to employ the ratio of the number of atoms in a level r to the total number of atoms in all levels, viz., $N = \Sigma N_r$, where N_r is the number in level r. From eqn. (1) we may express the total number of atoms in terms of the number in the first level, viz.,

* The statistical weight of a level expresses the relative likelihood of an atom being found there, other things being equal. If two states have the same excitation potential, under equilibrium conditions their relative populations will be in proportion to their statistical weights. The statistical weight, $2J + 1$, equals the number of Zeeman states into which a level of inner quantum number J is resolved by a magnetic field.

$$N = \frac{N_1}{g_1} \{g_1 + g_2 e^{-\chi_{12}/kT} + \cdots\} = \frac{N_1}{g_1} B(T) \tag{3}$$

The number in the ground level is

$$N_1 = \frac{g_1}{B(T)} N \tag{4}$$

while for level i,

$$\frac{N_i}{N} = \frac{g_i}{B(T)} e^{-\chi_i/kT} \tag{5}$$

This is the more general form of the Boltzmann equation. Here N refers to the total number of atoms and N_i to the number in the ith excited level. The quantity, $B(T)$, is called the partition function. It tells the way in which the atoms are distributed among the different excited levels. The population of highly excited levels is affected by the perturbations of nearby particles. If p_i denotes the probability that the atom is undisturbed in the excited state, i, the partition function becomes

$$B(T) = \sum_i g_i p_i e^{-\chi_i/kT}$$

where p_i approaches zero as the ionization limit is approached. The convergence of $B(T)$ is thus assured. If the perturbations are produced mainly by ions (as appears to be true for the sun and hotter stars) it turns out that*

$$\ln p_i = -1.33 \times 10^{-22} \frac{P_e}{Z^4 kT} n^6$$

where n is the principal quantum number of the ith level, Z is charge on the atom core of the perturbed particle, and P_e is the electron pressure.

As an example, let us compare the relative populations of the ground and $n = 2$ levels for hydrogen for $T = 6000°K$, $8000°K$, $10{,}000°K$, $15{,}000°K$, and $20{,}000°K$. The statistical weight of the ground level of hydrogen is 2, that of level n is $2n^2$. The excitation potential of the second level is 10.15 ev.

$$\log \frac{N_2}{N_1} = -\frac{5040}{T} \times 10.15 + \log 4 = -\frac{51{,}160}{T} + 0.60$$

Temperature	$\theta = \frac{5040}{T}$	$\frac{N_2}{N_1}$
6,000°K	0.840	0.00000001
8,000	0.630	0.0000016
10,000	0.504	0.000031
15,000	0.336	0.00155
20,000	0.252	0.0110

Notice the rapid increase in the relative number of atoms in the second level with the increase of temperature.

* See, for example, the discussion by Claas, *Utrecht Obs. Researches* **12**, 14, 1951.

3. Deviations from Thermodynamic Equilibrium

The Boltzmann law was derived for thermodynamic equilibrium and is strictly applicable only when these conditions are fulfilled. Many interesting problems arise from the deviations of stellar atmospheres and gaseous nebulae from such an equilibrium.

Consider the state of a stellar atmosphere. On one side are the hot, emitting layers of the star, on the other is the void of empty space. Although possibly in a steady state it cannot be in thermodynamic equilibrium. Just below the layers which we can see, conditions do approach those of thermodynamic equilibrium at some local temperature T and the Boltzmann formula and its corollaries can be employed. Proceeding toward the surface, the assumption of thermodynamic equilibrium begins to break down and it is in this region that the dark-line spectra of the stars are formed. In our first approximation we apply Boltzmann's formula and the ionization equation and compare our predictions with the observations. We find that insofar as the distribution of atoms among various energy states and stages of ionizations is concerned, the simple assumption of thermodynamic equilibrium will be very helpful. The principal task of this chapter will be to show how, with the aid of results derived from statistical mechanics and the concept of thermodynamic equilibrium, we can derive a qualitatively correct interpretation of the spectra of the stars.

The gaseous nebulae provide us with an example wherein thermodynamics and statistical mechanics are of little help. If we attempt to apply them we find ourselves confronted with a host of inconsistencies and contradictions. To interpret the spectra of gaseous nebulae another means of attack must be devised; we must base it on some hypothesis of the physical processes involved, i.e., on detailed mechanisms. We have much evidence to show that the bright lines of hydrogen and helium in the gaseous nebulae are produced by photoionization followed by recombinations, while the forbidden lines are produced by collisions which raise atoms to nearby metastable levels from which they return to the ground level with the radiation of a quantum of energy. Under such conditions we have two types of relationships that must be fulfilled for a steady state: (a) equations of statistical equilibrium which insure that the population of a given level remains the same, and (b) the equation of energy conservation which states that all energy absorbed in a volume element must equal all energy emitted. Even under conditions deviating widely from thermodynamic equilibrium certain processes will go on as though equilibrium still existed. The Boltzmann equation will no longer be applicable and the radiation field may deviate far from that appropriate to an enclosure, but the velocity distribution of the

electrons and ions in an ionized gas will still be Maxwellian appropriate to some temperature T (cf. Ch. 3, Sec. 7).

In problems of stellar atmospheres more and more emphasis is being laid on deviations from thermodynamic equilibrium, and more and more detailed mechanisms are being invoked. The solar chromosphere and corona show many properties that cannot be explained by any appeal to thermodynamic equilibrium. With these limitations in mind, let us return to what can be learned from the equilibrium theory.

4. The Ionization Equation

At any given temperature and density it is important to know not only the relative numbers of atoms in various excited levels but also the relative numbers of neutral and ionized atoms. In thermal equilibrium, atoms will lose electrons at a rate dependent upon the temperature and the ionization potential of the atom. At a given temperature, calcium atoms (ionization potential = 6.09 ev) will lose electrons at a greater rate than will hydrogen atoms whose ionization potential is 13.54 ev. On the other hand, the rate at which ions can recapture electrons will depend on the electron density (or electron pressure since $P_e = N_e kT$).

Saha derived the ionization formula by thermodynamical considerations and in 1922 pointed out its importance for astrophysical problems. We shall follow here, however, a simpler derivation due to Menzel.

Menzel's method is to apply the Boltzmann formula to continuous as well as discrete levels with proper weights chosen for the continuum. In the Bohr model, discrete states were represented by elliptical orbits and continuous states by hyperbolic orbits. From this point of view, the distinction between neutral and ionized atoms is somewhat artificial. That is, we can think of the ionized atom as a neutral atom with the electron in an hyperbolic orbit. Accordingly, the Boltzmann formula should be capable of representing ionization as well as excitation conditions.

Since the ionization energy, χ, must be supplied to liberate an electron, the total energies of the free electrons will be

$$\begin{aligned} E &= \chi_0 + \tfrac{1}{2}m(v_1^2 + v_2^2 + v_3^2) \\ &= \chi_0 + \frac{1}{2m}(p_1^2 + p_2^2 + p_3^2) \end{aligned} \tag{6}$$

Before we can apply the Boltzmann formula to the continuum we must assign "weights" to the continuous energy levels. We saw that the statistical weights for the discrete levels were $2J + 1$ (or for the confluent levels of the hydrogen atom, $2n^2$). In order to keep the system of weighting consistent with that adopted for the discrete levels, it

TABLE 1

IONIZATION POTENTIALS AND PARTITION FUNCTION DATA FOR SOME ATOMS AND IONS OF ASTROPHYSICAL INTEREST*

Element	Symbol	Ionization Potential I	II	III	IV	V	$\log \frac{2g_{s+1,0}}{g_{s,0}}$† $s=0$	$s=1$	$s=2$	$s=3$
Hydrogen	H	13.54					0.00			
Helium	He	24.48	54.17				0.60	0.00		
Lithium	Li	5.37	75.31				−0.13			
Beryllium	Be	9.28	18.13				0.56			
Boron	B		25.02	37.77			−0.48			
Carbon	C	11.20	24.28	47.67	64.22		0.10	−0.48	0.60	0.00
Nitrogen	N	14.49	29.49	47.24	77.09	97.47	0.62	0.13	−0.48	0.60
Oxygen	O	13.56	35.00	54.71	77.08	113.38	−0.05	0.65	0.13	−0.48
Fluorine	F	17.35	34.84	62.39	87.0	114.0	0.48	−0.05	0.65	0.13
Neon	Ne	21.47	40.91	64 ± 1	97	126	1.06	0.48	−0.05	0.65
Sodium	Na	5.12	47.10				−0.16	1.08		
Magnesium	Mg	7.61	14.97	79.9			0.52	−0.01		
Aluminum	Al	5.96	18.75	28.33			−0.50	−0.60		
Silicon	Si	8.11	16.27	33.32	44.95	166	0.06	−0.48	0.60	0.00
Phosphorus	P	10.9	19.57	30.03	51.15	64.74	0.54	0.13	−0.48	0.60
Sulfur	S	10.31	23.3	34.9	47.1		0.01	0.65	0.13	
Chlorine	Cl	12.9	23.70	39.7			0.47	−0.05		
Argon	A	15.69	27.5	40.8	61		1.04	0.48	−0.05	
Potassium	K	4.32	31.7	46			−0.44	1.08	0.48	
Calcium	Ca	6.09	11.82	51.00			0.44	−0.25	1.08	
Scandium	Sc	6.7	12.8	24.65			0.53	−0.27		
Titanium	Ti	6.81	13.6	28.0	43.06		0.50	−0.13	−0.02	
Vanadium	V	6.71	14.1				0.22	0.08		
Chromium	Cr	6.74	16.6				0.12	0.55		
Manganese	Mn	7.40	15.6				0.36	0.23		
Iron	Fe	7.86	16.16	30.48			0.40	0.30		
Cobalt	Co	7.84	17.1				0.25			
Nickel	Ni	7.61	18.4				−0.12			
Copper	Cu	7.69	20.18				−0.15			
Zinc	Zn	9.35	17.89				0.60			
Rubidium	Rb	4.16					−0.52			
Strontium	Sr	5.67	10.98				0.32	−0.30		
Yttrium	Y	6.5	12.3				0.38	−0.11		
Zirconium	Zr	6.92	13.97				0.37	−0.04		
Barium	Ba	5.19	9.96				0.30	−0.57		
Europium	Eu	5.64	11.21							

* See *Princeton Obs. Contr. No. 20*, 1945 for more complete data.

† For some elements, $2g_{s+1}/g_{s,0}$ is not a good approximation to the partition function ratio. Thus, log $2g_{1,0}/g_{0,0}$ is replaced by log $2B_1/B_0$, computed for $T = 6450°K$, $P_e = 58$ dynes from the data by W. J. Claas, *Utrecht Obs. Researches* **12**, 50, 1951. Also log $2g_{2,0}/g_1$ is replaced by log $2B_2/B_1$ for Mg, Si, Ca, Sc, Ti, V, Cr, Fe, Ni, Sr, Y, Zr, and Ba for $T = 10{,}000°K$.

may be shown that for free electrons numbering dN_e with momenta between p_1 and $p_1 + dp_1$, etc., and space coordinates between q_1 and $q_1 + dq_1$, etc., we must adopt weights as follows:

$$g_i = 2g_1' \frac{dp_1\, dp_2\, dp_3\, dq_1\, dq_2\, dq_3}{h^3} \tag{7}$$

where g_1' is the weight of the ground level of the ionized atom, the factor, 2, arises from the two possible orientations of electron spin, and $dp_1 \cdots dq_3$ factor is the volume of phase space expressed in h^3 units. If we now put eqns. (6) and (7) into eqn. (1), we get

$$\frac{dN_e}{N_{01}} = \frac{2g_1'}{g_{01}} \frac{e^{-\chi_0/kT}}{h^3} e^{-p^2/2mkT}\, dp_1 \cdots dq_3 \tag{8}$$

N_{01} is the number of neutral atoms in the ground level and g_{01} is the statistical weight of the ground level. We shall now choose a volume V_0 of such a size that it includes only one ionized atom in its lowest level, and N_e electrons of which dN_e have momenta between p_1 and $p_1 + dp_1$, etc., and coordinates between q_1 and $q_1 + dq_1$, etc. If we make use of the relation

$$\int_0^\infty e^{-a^2x^2}\, dx = \frac{\sqrt{\pi}}{2a}$$

and integrate dN_e with respect to the momenta and over the volume V_0 then

$$\frac{N_e}{N_{01}} = \frac{2g_1'}{g_{01}} \frac{e^{-\chi_0/kT}}{h^3} \int_{-\infty}^{+\infty}\int\int e^{-\frac{p^2}{2mkT}}\, dp_1\, dp_2\, dp_3 \int\int\int dq_1\, dq_2\, dq_3$$

$$= \frac{2(2\pi mkT)^{3/2}}{h^3} \frac{g_1'}{g_{01}} e^{-\chi_0/kT} V_0 \tag{9}$$

Since V_0 is determined by the condition, $N_1' V_0 = 1$, and since $N_{01} = g_{01}N_0/B_0$, $N_1' = N_1 g_1'/B_1(T)$, where N_0 and N_1 are respectively the total number of neutral and ionized atoms/cm³, and N_1' is the number of ionized atoms/cm³ in the ground level, the ionization formula becomes

$$\frac{N_1 N_e}{N_0} = \frac{(2\pi mkT)^{3/2}}{h^3} \frac{2B_1(T)}{B_0(T)} e^{-\chi_0/kT} \tag{10}$$

We may easily show that this type of equation holds for ionization stages higher than the first. Actually under any given conditions only two stages of ionization prevail at any one time, say the qth and $(q+1)$st. Thus we can write,

$$\frac{N_{q+1} N_e}{N_q} = \frac{(2\pi mkT)^{3/2}}{h^3} \frac{2B_{q+1}(T)}{B_q(T)} e^{-\chi_q/kT} \tag{11}$$

where N_q is the number of atoms in the qth stage of ionization, N_{q+1} is the number in the $(q+1)$st stage of ionization, and χ_q is the energy necessary to ionize the atom from the qth stage of ionization to the $(q+1)$st stage.

For many problems, the electron pressure is a convenient parameter to employ in place of the electron density. Substituting $P_e = N_e kT$ in eqn. (10) we obtain

$$\frac{N_1 P_e}{N_0} = \frac{(2\pi m)^{3/2}(kT)^{5/2}}{h^3}\frac{2B_1(T)}{B_0(T)}e^{-\chi_0/kT} \tag{12}$$

For purposes of numerical calculation, the logarithmic form is particularly useful, viz.,

$$\log \frac{N_1}{N_0}P_e = -\frac{5040}{T}I + 2.5\log T - 0.48 + \log 2B_1(T)/B_0(T) \tag{13}$$

where I is the ionization potential in volts, P_e is the electron pressure in dynes/cm^2, N_1 is the number of ionized atoms/cm^3, N_0 is the number of neutral atoms/cm^3, $B_1(T)$ is the partition function of the ionized atoms, and $B_0(T)$ is the partition function of the neutral atoms. The B's can be calculated with the aid of a term table for the atom or ion in question as a function of the temperature. (See Table 1.)

Examples: If the temperature of the solar atmosphere is 5700°K and the electron pressure is 30 dynes, what proportion of aluminum is neutral? The first ionization potential of aluminum is 5.96 ev, and $2B_1(T)/B_0(T) = 0.32$. Let θ denote $5040/T$. Then,

$$\theta I = 5.27, \quad 2.5\log T = 9.39, \quad \log P_e = 1.48$$

Hence $\log N_1/N_0 = 1.68$, whence $N_1/N_0 = 47.7$ or $N_0/(N_1 + N_0) = 1/48.7 = 0.0205$, i.e., 2.1 per cent of all atoms are neutral and the rest are ionized. Since the second ionization potential of aluminum is 18.73 ev a negligible fraction of aluminum atoms have lost a second electron.

What fraction of calcium atoms are in the singly ionized condition in the atmosphere of Sirius if $T = 10{,}000°$ and $P_e = 200$ dynes? For calcium, $I = 6.09$ ev and $\log 2B_1(T)/B_0(T) = 0.44$.

$$\begin{aligned} \theta I &= 3.07 \\ 2.5\log T &= 10.00 \quad \log N_1/N_0 = 4.59, \quad \text{i.e., there is practically} \\ \log P_e &= 2.30 \qquad\qquad\qquad\quad \text{no neutral calcium} \end{aligned}$$

We suspect that the calcium may be doubly ionized. Hence we should apply the ionization formula again. The second ionization potential is 11.82 ev, $\log 2B_1(T)/B_0(T) = -0.25$, $\theta I = 5.95$.

$$\log N_2/N_1 = 1.02 \quad \text{or} \quad N_2/N_1 = 10.5$$

whence $N_1/(N_1 + N_2) = 0.087$, or 9 per cent remain singly ionized and the remainder are doubly ionized.

The strong Mg II doublet at λ4481 arises from transitions from the 3^2D term to the 4^2F term. Calculate for $P_e = 100$ dynes and $T = 7200°$K the fraction of magnesium atoms capable of absorbing λ4481.

The excitation potential of the lower 3^2D term of the transition is 8.83 ev, and the statistical weight of this term is, since $J = 3/2$ and $5/2$, $6 + 4 = 10$. The statistical weight of the ground $^2S_{1/2}$ term is 2. By Boltzmann's formula, the fraction of Mg II atoms in the ^2D term is given by

$$\log N(3^2D)/N(3^2S) = -8.83\theta + \log 5 = -5.47 \text{ at } T = 7200°\text{K } (\theta = 0.7)$$

For magnesium the first ionization potential is 7.61 ev, the second is 14.97 ev. For Mg I, $\log 2B_1/B_0 = +0.52$, whence we find $\log N_1/N_0 = 2.35$, so we conclude that 99.6 per cent of the Mg is at least once ionized.

Is double ionization important? Here $\log 2B_2/B_1 = -0.01$ and we find $\log N_2/N_1 = -3.28$. Of all magnesium atoms, the total fraction in the excited 3^2D level and therefore capable of absorbing λ4481, will be

$$\frac{N(3^2D)}{N(\text{total})} = 0.996 \times 10^{-5.47} = 3.4 \times 10^{-6}$$

5. Combined Boltzmann and Ionization Equations

The lines of the permanent gases observed in the hotter stars and in the solar chromosphere arise from high levels much closer to the ionization limit than to the ground level. It is often useful to combine the Boltzmann and ionization equations in such a way as to refer the number of atoms, $N_{0,r}$, in the rth level of the neutral atom, say, to the total number N_1 of the ionized atoms. If we divide eqn. (12) by the Boltzmann eqn. (5) we obtain

$$\frac{N_1 P_e}{N_{0,r}} = \frac{(2\pi m)^{3/2}(kT)^{5/2}}{h^3}\frac{2B_1(T)}{g_{0,r}}e^{-(I-\chi_r)/kT} \tag{14}$$

which relates the number of atoms in the rth level to the total number of singly ionized atoms. Here we denote the ionization potential by I and the excitation potential of the rth level simply by χ_r. We may generalize this expression for any stage of ionization. Since the numerical value of $(I - \chi_r)$ is much less than I or χ_r for the permanent gases, the Boltzmann correction is much smaller than it would be if we tried to relate the number in level r with the number in the ground level.

Example: In the atmosphere of 10 Lacertae, it is found from the intensities of the Balmer lines that the number of hydrogen atoms in the

second level is antilog (15.80). With $T = 29{,}600°\text{K}$ and $\log P_e = 2.80$, we shall compute the number of hydrogen ions, N_1. We write eqn. (14) in the form:

$$\log \frac{N_1}{N_{0,2}} = -\frac{5040}{T}(I - \chi_2) + 2.5 \log T - 0.48 + \log \frac{2B_1(T)}{g_2} - \log P_e$$

With $I = 13.54$ ev, $\chi_2 = 10.15$ ev, $g_2 = 8$, and $B_1 = 1$, we find

$$\log \frac{N_1}{N_{0,2}} = 6.72, \quad \text{and} \quad \log N_1 = 22.52$$

An application of the ionization equation will show that very few hydrogen atoms are neutral.

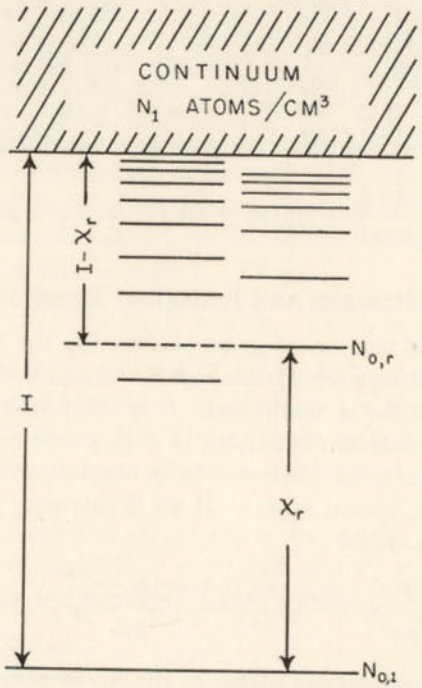

FIG. 1.—SCHEMATIC ENERGY LEVELS

The ionization potential is I. The excitation potential of level r is χ_r. The number of atoms per cm³ in the ground level of the neutral atom is denoted as $N_{0,1}$, the number of atoms in level r is $N_{0,r}$, and the number of ionized atoms is N_1.

6. Tests of the Ionization Theory

At Mount Wilson Observatory, A. S. King carried out qualitative laboratory tests of the ionization theory. Alkaline earth metals such as Ca or Mg have ionization potentials so low that even at temperatures

attainable in an electric furnace an appreciable fraction of their atoms can be ionized. King found that the intensity ratio of λ3933 of ionized calcium to λ4226 of neutral calcium increased as the temperature increased, in harmony with theory. In another experiment the temperature was kept constant and small amounts of caesium (the most readily ionized of all the elements) were added. The ionization of caesium raised the electron pressure and decreased the ionization and hence the intensity of λ3933. King was unable to measure the electron pressure in these experiments; hence a quantitative check on this theory could not be made.

Astrophysical illustrations of the ionization phenomena are numerous. The sunspots, which are refrigerated areas about 1200°K cooler than the surrounding bright surface of the sun (photosphere), provide a good illustration. The alkalis and alkaline earths become almost completely ionized in the region of the photosphere while their neutral lines are greatly strengthened in the cooler spot in accordance with the ionization theory.

7. The Spectral Sequence

The ionization theory's outstanding achievement is its interpretation of the spectral sequence as a temperature sequence. Proceeding from the cooler to the hotter stars, the lines of the neutral elements gradually weaken and become replaced by the lines of ionized elements. Calcium provides a good illustration. In the coolest stars, calcium is mostly neutral and the resonance λ4227 line attains great strength (Fig. 6). In slightly hotter stars ionization begins to be appreciable, λ4227 weakens, and the resonance H and K lines of ionized calcium strengthen until in class G they dominate the spectrum. At still higher temperatures calcium becomes doubly ionized and the H and K lines fade away. When we deal with lines that arise from excited levels, i.e., subordinate lines, we must apply both the ionization and Boltzmann formulae. With rising temperature the subordinate lines grow in intensity as the number of atoms capable of absorbing them increases, but then weaken as the atoms become ionized. Figs. 2 and 3 illustrate the predicted and observed behavior of subordinate iron and magnesium lines along the main sequence.

The behavior of the hydrogen lines is an excellent example. Since the Balmer series arises from transitions from the second to higher levels, a hydrogen atom must first be excited to the second level before it can absorb a Balmer line. Referring to our illustrative calculations in Sec. 2, we notice that at the lower temperatures the number of hydrogen atoms in the second level is negligible, but that it increases rapidly with rising temperature. In harmony with this result, the hydrogen lines

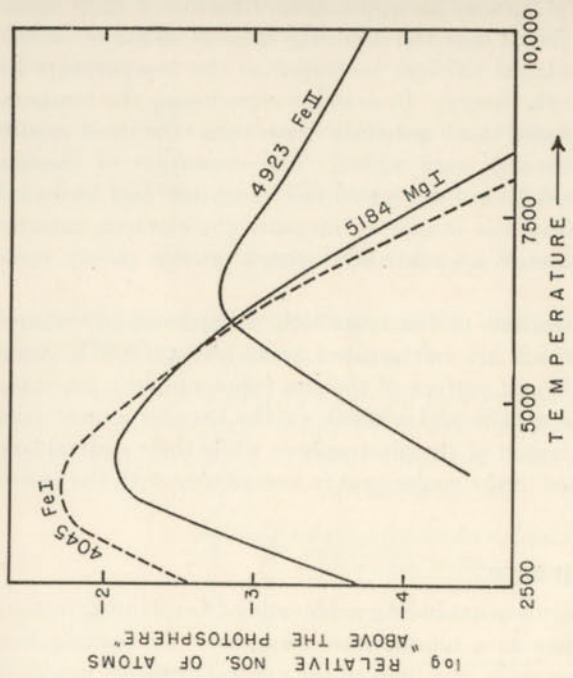

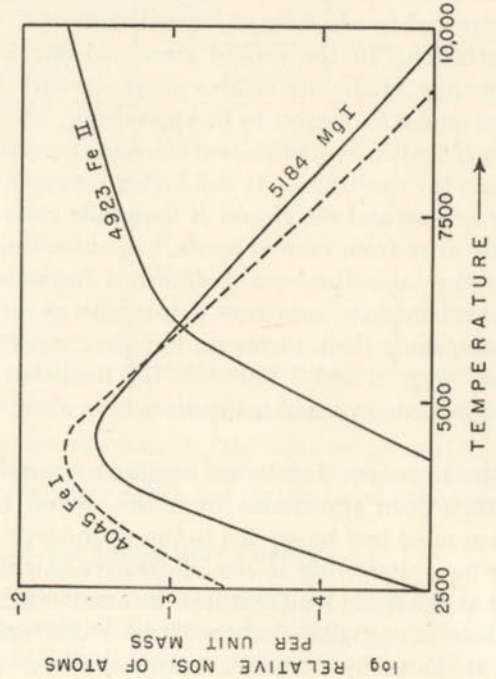

FIG. 2.—VARIATION OF THE NUMBERS OF ABSORBING ATOMS ALONG THE MAIN SEQUENCE

Left: The logarithm of the relative number of atoms per unit mass of element concerned, capable of absorbing the line indicated, is plotted against the temperature for λ4045 Fe I, λ5184 Mg I, and λ4923 Fe II. These are subordinate lines, arising from excited levels. Hence both the Boltzmann and Saha equations must be used. The variation of electron pressure and temperature along the main sequence is taken into account.

Right: Anticipating the results of Chapter 7, we now correct for the effects of the variation of the opacity of the stellar atmosphere with temperature. The hotter the star, the more opaque the atmosphere. Hence the number of atoms in the visible layers of the stellar atmosphere, i.e., "above the photosphere," steadily decreases with rising temperature.

steadily increase in strength from *M* through *K*, *G*, and *F* to *A* where these lines attain their maximum strength. Thereafter, with rising temperature, the intensity of the Balmer lines decreases as ionization makes serious inroads on the number of neutral hydrogen atoms. The Balmer lines are still present in the *O* stars, however, even though about one atom in a hundred thousand remains neutral.

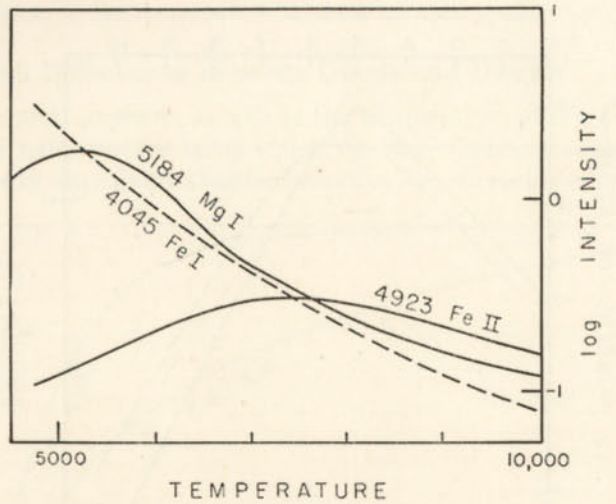

FIG. 3.—OBSERVED VARIATIONS OF LINE INTENSITIES ALONG THE MAIN SEQUENCE

The logarithm of the observed intensities, expressed as equivalent widths (see Chapter 8), is plotted against the temperature. Accurate data for cool dwarf stars are not available. Compare with Fig. 2 of Chapter 4.

In stars hotter than *A*0, the metals become multiply-ionized and their resonance lines fall in the unobservable ultraviolet. The subordinate lines involve very high levels and are very weak. No atom heavier than silicon is observed in absorption beyond the second stage of ionization.

In the *B* stars, the helium lines, together with those of hydrogen, become the most conspicuous features of the spectrum. The *O* stars are so hot that hydrogen is nearly all ionized and even helium is doubly ionized. The light elements O, N, C, and Ne are prominent in various stages of ionization.

Among the *O* and *B* stars, bright lines often appear. Some stars show both bright and dark lines. Generally, the bright lines have been attributed to shells surrounding the star. The very coolest stars also occasionally show bright lines, especially the long period variables in class *M*.

In his original application of the ionization theory to the spectral sequence, Saha attempted to derive a temperature scale for the stars. He

calculated at what point the lines of a given ion would appear or disappear and compared his predictions with the observations. Unfortunately, the method of appearances and disappearances of lines is untrustworthy. It depends on the resolving power of the spectrograph employed, blends, abundances, etc., and also assumes that the atmospheric layers participating in the formation of lines are the same for all

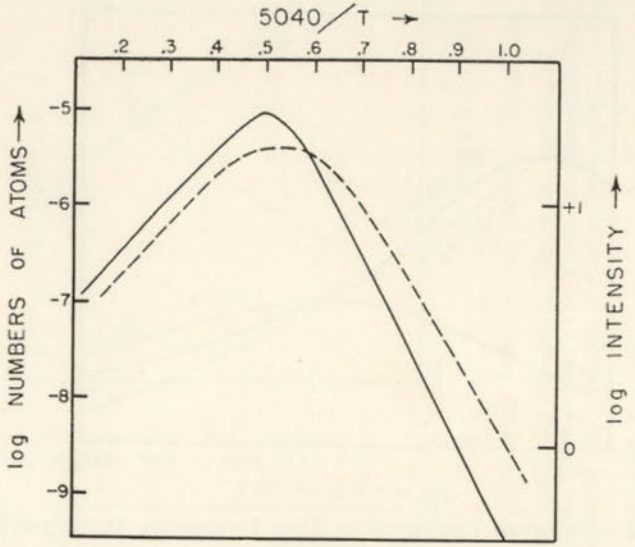

FIG. 4.—THE VARIATIONS OF THE BALMER LINES ALONG THE MAIN SEQUENCE

The solid curve expresses the fraction of all hydrogen atoms in the second level and therefore capable of absorbing the Balmer lines. The dotted curve gives the logarithm of the observed intensity. The vertical scale of the observed curve is adjusted by a factor of 5/2, since theory shows the intensities of strong hydrogen lines to vary roughly as $N^{2/5}$. No correction has been applied for the changing opacity of the atmosphere; such a correction would bring the observed and computed curves more nearly into agreement.

atoms in all stars. Furthermore, Saha assumed too high a pressure. Fowler and Milne calculated the temperatures at which selected lines of certain atoms and ions should reach a maximum, on the assumption that the intensity of a line depended on the number of atoms capable of absorbing it. By a comparison of the predicted positions of the maxima with the observed maxima for stars whose temperatures had been determined from their colors, an estimate of the electron pressure could be obtained. In this way, Fowler and Milne found a mean electron pressure of the order of a hundred dynes. If we can assume that the electron pressure remains about the same for different stars, we can calculate the temperatures of other stars from the ionization equilibrium. For example, if we can find the ratios N II/N III, O II/O III, He I/He II, etc., from the line intensities, we can compute what temperature must exist for these ratios to obtain. Actually the electron pressure does change; it is larger in the hotter stars where the greater ionization supplies greater numbers of electrons. When the electron pressure can be determined for different stars, as is sometimes possible, and when the numbers of atoms in the radiating layers can be found, the ionization equilibrium provides one definition of the temperature of a stellar atmosphere.

8. Spectral Differences Between Giants and Dwarfs

The electron pressure, as well as the temperature, affects the ionization. The temperatures being equal, the star whose atmosphere has a lower density will exhibit a higher ionization, i.e., an earlier spectral class.

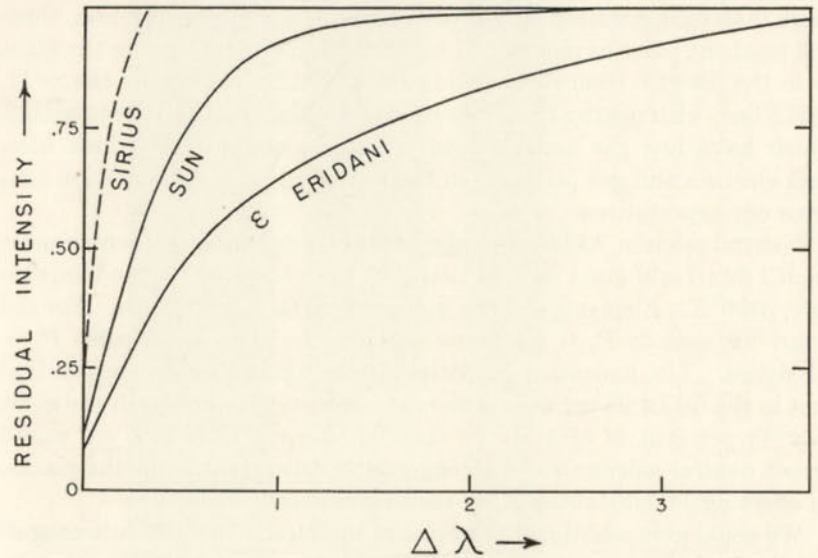

FIG. 5.—THE VARIATION OF THE PROFILE OF λ5889 (SODIUM) ALONG THE MAIN SEQUENCE

The intensity at each point in the line is expressed in units of the continuum. Note the decrease of intensity from ε Eridani (T = 4700°K), through the sun (5700°K) to Sirius (10,000°K), because of the increasing ionization with rising temperature. The profile in Sirius is schematic, so adjusted as to give the correct equivalent width. The profile for the sun is taken from the Minnaert Atlas, whereas the ε Eridani profile is taken from a Mount Wilson coudé plate.

When we differentiate stars according to the densities prevailing in their atmospheres we are really separating them according to their luminosities, since the giant and supergiant stars have much lower densities than dwarfs of the same temperature or spectral class. For example, a giant

star of the same temperature as our dwarf sun would have an earlier spectral type, say *F*8, since the ionization would be greater in the more tenuous atmosphere of the larger star. Usually we compare stars of the same spectral class. Hence giants tend to be cooler than dwarfs of the same spectral class. While the compensation of decreased temperature and electron pressure suffices to give two similar looking spectra, lines of certain ions will not keep in step.

To illustrate, let us compare a giant and a dwarf of the same mean ionization. For the giant we take $5040/T = \theta = 0.97$, and $\log P_e = 0.71$, while for the dwarf we choose $\theta = 0.88$ and $\log P_e = 1.57$. With these combinations of electron density and temperature, iron (7.83 ev ionization potential, I.P.) will have about the same ionization in the two stars. On the other hand, strontium (I.P. = 5.67 ev) will be more strongly ionized in the giant than in the dwarf, the decrease in pressure more than compensating for the decrease in temperature. In fact, there will be about twice as many Sr II ions per gram of strontium in the giant as in the dwarf. Hence we would expect that by comparing the Sr II, λ4215 line, with nearby iron lines we could differentiate between giants, which have low gas and electron pressures, and dwarfs which have high electron and gas pressures in their atmospheres. Observation confirms our expectations.

Neutral calcium, λ4227, provides another illustration. If we compare an *M*2 dwarf and giant we find that they have about the same temperature, 3150°K. Elements such as iron are neutral in both stars. For the dwarf we assume $P_e = 2.5$ dynes and for the giant we assume $P_e = 0.1$ dynes. The ionization potential of calcium is 6.09 ev and we find that in the dwarf 95 per cent of the calcium is neutral, while in the giant only 43 per cent is neutral. In stars of this spectral class, we would expect neutral calcium to be stronger in the dwarfs than in the giants, an effect again substantiated by the observations.

We could give additional examples of luminosity or "absolute magnitude" criteria but these suffice to illustrate the role of ionization theory. We cannot discuss the problem quantitatively because we do not yet know how the transparency and density of the atmosphere and the number of absorbing atoms affect the width and blackness of the lines. Different thicknesses of the radiating layers, differential pressure effects, large-scale motions in stellar atmospheres, etc., all complicate the problem. In practice, all luminosity criteria must be calibrated empirically.

It is clear that a detailed application of the ionization theory requires a knowledge of two things—the electron pressure and the number of atoms acting in the layers producing the lines. If the continuous absorptivity is low we may see to great depths in the star; if it is high we may see only the thinnest portions of the outer layers. Although both line

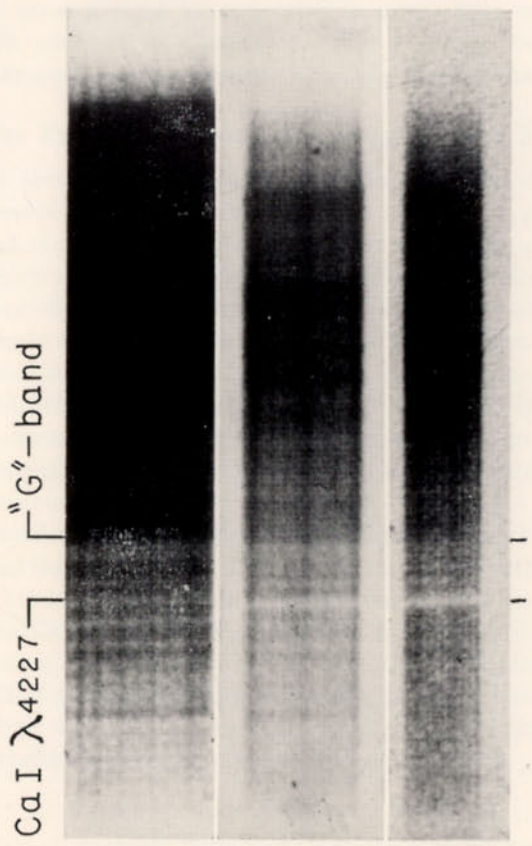

FIG. 6.—COMPARISON OF THE CA I LINE, λ4227, IN DWARFS, GIANTS, AND SUPERGIANTS OF SPECTRAL CLASS *M*2

The symbols Ia, III, and V denote the luminosity class of the star in the classification scheme of the Morgan-Keenan-Kellman *Atlas of Stellar Spectra*. The supergiant μ Cephei is one of the brightest stars known, *HD* 169746 is a giant, and *HD* 199305 is a dwarf. Notice that the Ca I line, λ4227, the most conspicuous feature in the dwarf spectrum, steadily weakens in stars of increasing luminosity, until in μ Cephei it is weaker than the lines on either side. The red edge of the "*G*-band," λ4308, strengthens in the brighter stars. (Courtesy, P. C. Keenan and J. J. Nassau, *Astrophysical Journal*, University of Chicago Press, **104**, 458, 1946.)

and continuous spectrum are produced in the same layers, for many problems it is legitimate to think of the dark-line spectrum as originating in a layer which produces line absorption only, whereas a pure continuous spectrum is supplied by the photosphere. Thus the "number of atoms above the photosphere" will depend on the absorptivity of the outer layers, a quantity which will depend on the electron pressure and temperature. By some means we must estimate the electron pressure. For some of the hotter stars, we can obtain this quantity from the hydrogen line intensities and the continuum at the Balmer limit. For cooler stars it must be estimated in some other way. We shall return to this problem in Chapter 8. Fig. 2 shows the effects of changing opacity and electron pressure upon the lines of the metals.

9. The Relation Between Gas Pressure and Electron Pressure

For theoretical work on stellar atmospheres we shall need to know the relation between the gas pressure and the electron pressure. In the very hottest stars all the atoms are ionized and every atom supplies at least one electron. Since hydrogen is overwhelmingly the most abundant constituent of the atmosphere and since it supplies one electron per atom, the electron pressure is simply half the gas pressure. On the other hand, in a star such as the sun, the bulk of the gas pressure is supplied by hydrogen, whereas the electron pressure comes solely from the ionization of the metals. Hence the gas pressure is related to the electron pressure in a complicated way which depends on the assumed abundance of the various elements.

We calculate the gas pressure P_g as a function of the electron pressure P_e, and the temperature T as follows: Let N_0 denote the number of atoms of all kinds per cm^3, whereas N_e denotes the number of electrons per cm^3. Further, let us sort the N_0 atoms into groups according to their ionization potentials, such that N_j denotes the number of atoms of first ionization potential χ_j, and x_j denotes the fraction that have been once ionized. We shall see that we can neglect the second ionizations because of the overwhelming predominance of hydrogen. Thus,

$$N_0 = N_1 + N_2 + \cdots = \Sigma N_j$$
$$N_e = N_1 x_1 + N_2 x_2 + \cdots = \Sigma N_j x_j$$

and

$$P_g = NkT = (N_0 + N_e)kT, \quad P_e = N_e kT$$

Then

$$\frac{P_g}{P_e} = \frac{N_0 + N_e}{N_e} = \frac{1 + N_e/N_0}{N_e/N_0} \tag{15}$$

Our problem then becomes one of calculating N_e/N_0 as a function of the temperature and electron pressure. We must adopt the relative

abundances of the various elements, group them according to their ionization potentials, and compute the degree of ionization as a function of the electron pressure and temperature. On the basis of the abundance determinations by Goldberg and Menzel for the sun and by Unsöld for τ Scorpii, we adopt the groups shown in Table 2. Oxygen, nitrogen,

TABLE 2

IONIZATION GROUPS OF ELEMENTS

Atom	Group	Ionization Potential	No. of Atoms
Helium	1	24.5	200
Hydrogen	2	13.54	1000
Fe, Si, Mg, Ni	3	7.9	0.43
Al, Ca, Na	4	5.8	0.011

and carbon have ionization potentials near that of hydrogen but their abundances are so very much less, we can neglect their contributions to the total number of electrons. They contribute about three atoms per thousand hydrogen atoms.

For each group and a given temperature and electron pressure, we calculate the percentage ionization x_j and add the $N_j x_j$'s together to get the total number of electrons N_e. The ratio N_e/N_0 is thus known and we can compute P_g/P_e at once. We shall illustrate the procedure as follows:

The total mass in atomic mass units per thousand hydrogen atoms is 1856. The corresponding total number of atoms is 1200 (if we neglect C, N, and O). Hence the mean molecular weight of the un-ionized material is $\mu_0 = 1.54$. From the adopted abundances and eqn. (15) there results:

$$\frac{N_e}{N_0} = \frac{0.011x_4 + 0.431x_3 + 1000x_2 + 200x_1}{1200} \tag{16}$$

At $\theta = 5040/T = 0.4$, $\log P_e = 2$, we find $x_1 = 0.040$, (He), $x_2 = 1.000$ (H) by an application of the ionization equation (12). We can neglect the contribution of the metals which are completely ionized. Then $N_e = 1000 + 8$ and $N_e/N_0 = 0.835$ and $P_g/P_e = 2.2$.

For $\theta = 0.8$, $\log P_e = 2$, $x_2 = 0.00016$ so that the ionization of hydrogen contributes 0.16 electron. For the iron group, $x_3 = 0.835$ and $x_4 = 1.0$ (complete ionization of Al, Ca, Na). Hence the ionization equation gives $N_e = 0.011 + 0.36 + 0.16 = 0.53$ so $\log P_g/P_e = 3.36$, and $\log P_g = 5.36$. It is emphasized that the relation between gas and

TABLE 3

THE RELATION BETWEEN GAS PRESSURE AND ELECTRON PRESSURE AS A FUNCTION OF TEMPERATURE

$\theta =$	Log P_g							
	0.4	0.5	0.6	0.7	0.8	1.0	1.2	1.4
log $P_e = -1$	−0.70	−0.66	−0.66	−0.61	0.00	2.30	2.68	2.92
0	0.30	0.34	0.36	0.67	1.89	3.47	4.31	4.70
1	1.33	1.35	1.47	2.43	3.78	4.78	5.93	6.52
2	2.34	2.38	2.99	4.36	5.36	6.48	7.59	
3	3.35	3.64	4.88	6.15	6.89			

electron pressure depends on our choice of the chemical composition of the stellar atmosphere. As long as the hydrogen/metal ratio is about a thousand, and the relative abundances of the metals are kept about the same, the above table relating electron and gas pressure should remain sufficiently accurate. It is often useful to employ the $P_g(P_e T)$ relationship in the graphic form. (See Ch. 7, Sec. 14.)

10. Dissociation Equilibrium of Chemical Compounds

While the ionization theory gives a rational explanation of the spectral sequence for the hotter stars, it is satisfying that a closely analogous treatment of the formation and dissociation of molecules explains, qualitatively at least, the spectra of the cooler stars.

Suppose 2 atoms, A and B, combine to form the diatomic molecule AB according to the reversible reaction:

$$A + B \rightleftarrows AB \tag{17}$$

The numbers of relevant atoms A and B and molecules AB are related by an expression similar to the ionization equation:

$$\frac{n(A)n(B)}{n(AB)} = K'(AB) \tag{18}$$

where K′(AB) sometimes is called the dissociation "constant." It depends on the temperature and dissociation potential of the molecule. The expression eqn. (18) may be rewritten in a form analogous to the ionization equation:

$$\frac{p_A p_B}{p_{AB}} = \frac{g_A g_B}{g_{AB}} \left[\frac{2\pi MkT}{h^2}\right]^{3/2} \frac{h^2}{8\pi^2 I} (1 - e^{-S}) e^{-D/kT} = K(AB) \tag{19}$$

in terms of the partial pressures, p_A, p_B, p_{AB}. Here g_A, g_B, g_{AB} represent the statistical weights of the ground levels of atoms A and B and the

molecule AB, and M is the "reduced" mass, $M = \frac{M_A M_B}{M_A + M_B}$. There are two additional factors in $K(AB)$ that did not appear in the right-hand side of eqn. (11). These involve the moment of inertia I, and the fundamental vibrational frequency v of the molecule. Here $S = \frac{hv}{kT}$. They occur because of additional modes of motion of the molecule—modes which the atom did not have.

For molecules of astrophysical interest it turns out very nearly that

$$(1 - e^{-S}) = Se^{-0.46S} \tag{20}$$

and if we express the frequency of vibration in wave-number units, cm^{-1}, as w, we have $hv/k = 1.43w$. Further, if r_0 is the equilibrium separation of the atomic nuclei A and B, $I = Mr_0^2$. If the pressures and K are measured in dynes, M in atomic mass units, r_0 in angstrom units, and D in volts (ev), $\log K$ may be written as

$$\log K = -\frac{5040}{T} D + \frac{1}{2}\log T - \frac{0.286w}{T} + \frac{1}{2}\log M - 2\log r_0 + \log w + \log \frac{g_A g_B}{g_{AB}} + 6.24 \tag{21}$$

which is essentially the expression given by H. N. Russell. As an example, consider CH for which $\frac{g_A g_B}{g_{AB}} = 3$, $r_0 = 1.12\text{A}$, $w = 2862\ \text{cm}^{-1}$, $M = 12/13$ (atomic mass units) and $D = 3.47$ ev, approximately. If the partial pressures of C and H in the solar atmosphere are 4 and 8×10^4 dynes, respectively, and if $T = 5700°\text{K}$, we find $\log K = 8.72$, whence the partial pressure of CH $= 61.1 \times 10^{-5}$ dynes.

The most detailed treatment of equilibria of chemical compounds in stellar atmosphere was that by H. N. Russell. He postulated a series of model stellar atmospheres similar in composition to that of the sun but differing in temperature and pressure. Then he investigated the relative proportions of the various kinds of atoms and undissociated molecules.

Now the total number of atoms of any given kind, e.g., carbon, will equal the number of free atoms plus the number tied up in molecules, viz.:

$$n'(\text{C}) = n(\text{C}) + 2n(\text{C}_2) + n(\text{CN}) + n(\text{CO}) + \text{etc.} \tag{22}$$

Nitrogen atoms will satisfy a relation of the form

$$n'(\text{N}) = n(\text{N}) + 2n(\text{N}_2) + n(\text{CN}) + \text{etc.} \tag{23}$$

and analogous expressions may be written for O, H, Ti, etc. From his analysis of the solar spectrum, Russell had derived the relative abundances of the various elements, i.e., $n'(\text{C})$, $n'(\text{N})$, etc. The quantities on the right-hand side of eqns. (22) and (23) are to be computed.

Since the partial pressure is $p = nkT$, one can write a series of simultaneous quadratic equations of the form:

$$p'(\text{C}) = p(\text{C})\left\{1 + \frac{2p(\text{C})}{K(\text{C}_2)} + \frac{p(N)}{K(\text{CN})} + \text{etc.}\right\} \tag{24}$$

in which the p's and K's are known. The solution of these simultaneous equations will give the quantities, $p(\text{C})$, $p(\text{N})$, $p(\text{H})$, etc. The problem

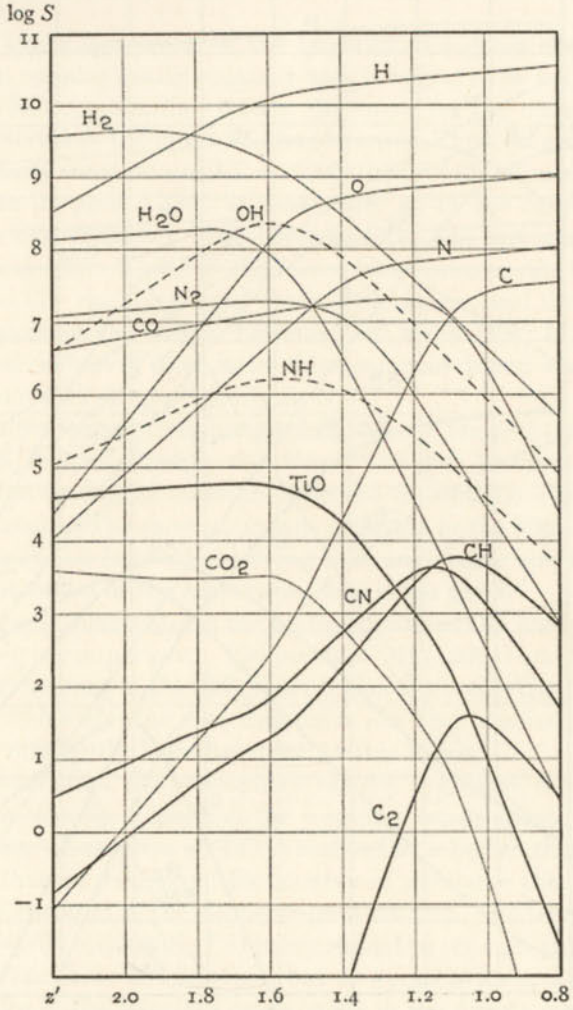

FIG. 7.—THE ABUNDANCES OF MOLECULES AND ATOMS IN GIANT OXYGEN STARS OF SPECTRAL CLASSES K–M

The ordinates are logarithms of the numbers of atoms or molecules per unit area, the abscissae are the values of $\theta = 5040/T$. (Courtesy, H. N. Russell, *Astrophysical Journal*, University of Chicago Press, **79**, 317, 1934.)

is somewhat simplified by the fact that hydrogen is so overwhelmingly abundant and the other elements fall into groups that have little mutual influence and may usually be handled separately. Ionization may deplete the numbers of metals available for molecular formation.

Russell took into account the variation of the electron pressure among

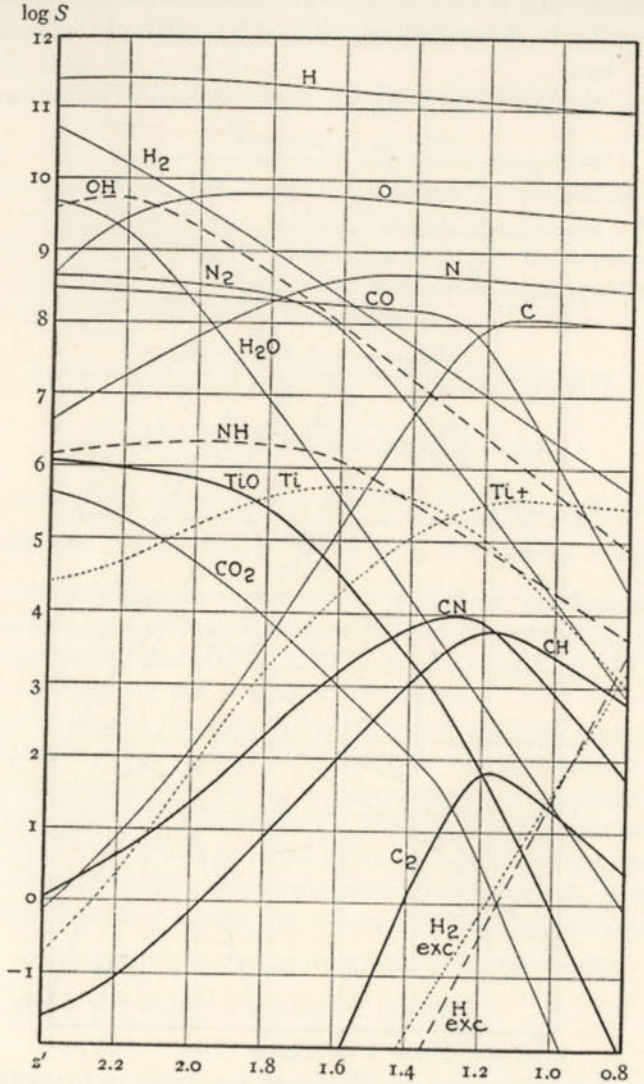

FIG. 8.—THE ABUNDANCES OF MOLECULES AND ATOMS IN DWARF OXYGEN STARS OF SPECTRAL CLASSES *K*–*M*

(Courtesy, H. N. Russell, *Astrophysical Journal*, University of Chicago Press, 79, 317, 1934.)

the giant and dwarf stars, the variation in the thickness of the atmospheric layers responsible for the formation of absorption lines, and introduced other refinements. He made separate calculations for giant and dwarf stars of the same composition as the sun. Although the actual abundance of hydrogen is now known to be greater than Russell supposed, and the molecular constants he used have been superseded by more accurate values, the general qualitative picture he has given seems to be correct.

Toward lower temperatures, the quantity of a given element in the atomic form remains nearly constant until it begins to be tied up in compounds. When combination occurs, the curve for the main compound rises and overtakes the curve of the element. Thus, in giants, atomic carbon is nearly constant until $T = 4200$; then it falls off rapidly and CO rises to take its place. That is, essentially all of the carbon becomes oxidized to CO, relatively little becomes CO_2, and but small amounts form CN and CH. Towards the lower temperatures, the amounts of C_2, CH, and CN rise for a time, reach a maximum, and then fall off as more and more of the carbon becomes tied up in CO. In giants, CN is the most abundant of these latter three compounds and would be more so were N not locked up primarily in N_2.

In the giants ionized titanium predominates to temperatures as low as $T = 3900°$K, neutral titanium rises slowly and then becomes depleted to form titanium oxide, the molecule observed to contribute the strongest molecular bands. The most abundant molecule in the stars is certainly H_2, but there is no hope of observing it in any stellar spectrum as the excitation potential of the observable lines is too great.

At the lowest temperatures the hydroxyl radical OH and water vapor H_2O become very important. The bands of OH (λ3064) and NH (λ3240) should be very strong in the ultraviolet region of the spectra of the coolest stars. Unfortunately, the cool stars have not been studied in sufficient detail with sufficiently high dispersion in this region.

In the dwarf stars, the atmospheric opacity is greater; hence the total number of molecules is less and the resultant bands should be weaker. The maximum abundance of TiO is reached at a higher temperature in the dwarfs than in the giants; the number of molecules then flattens off and remains constant as the temperature is lowered. At temperatures in the range 3000°K to 3500°K, TiO bands should be stronger in dwarfs than in giants of the same temperature, but as we go to lower temperatures, the intensities of the titanium oxide bands in the dwarfs remains about the same whereas the giant bands increase to a much greater maximum intensity. This result explains why no dwarfs are found later (i.e., with more intense bands) than *M*5, although the giants seem to run to *M*9.

The curves give a striking confirmation of Richardson's observation

that C_2 and TiO bands have the same intensity in sunspots, whereas the two bands are not observed simultaneously in any other stellar spectrum.

In the dwarfs, because of the greater pressure, the maximum of the carbon compounds comes at a higher temperature. As predicted, the observed bands of CH and CN attain maxima and then weaken in the cooler stars, and the C_2 bands are weak in the sun. Converting temperatures to spectral classes, Russell finds the following predicted band maxima:

Molecule	Dwarfs		Giants	
	Temp.	Class	Temp.	Class
C_2 max.	4800	*K*1	4300	*G*7
CH max.	4650	*K*2	4350	*G*7
CN max.	4380	*K*4	4000	*K*1
TiO (= CH max.)	3820	*K*8	3500	*K*6
TiO (= CN max.)	3880	*K*8	3350	*K*7
TiO max.	3150	*M*3?	2500	*M*10

Miss Payne found the CH maximum at *K*0 and Lindblad found that of CN at *G*5 to *K*5 in giant stars. For dwarfs, Lindblad found a flat maximum at *K*0 for cyanogen but part of this flatness may arise from blends. The predicted spectral classes where the titanium oxide bands should equal those of CO and CH are in fair agreement with observation.

The cyanogen bands are important criteria for distinguishing between giants and dwarfs. If we compare the abundances of CN in giants and dwarfs at the same spectral class, we find that there are five to six times as many CN molecules in a *G*–*K* giant as in a dwarf. On the other hand, the predicted differences for CH are much smaller so that the *G* band, which arises primarily from this molecule, varies little with absolute magnitude. Both of these predictions are in harmony with the observations. (See Ch. 8, Sec. 20.)

11. Branching of the Spectral Sequence

An important problem is the branching of the spectral sequence in the later types. Classes *R* and *N* branch off between *G* and *K*; class *S* branches off between *K* and *M*. In the later *K* stars, the TiO bands appear and steadily increase in intensity with diminishing temperature through class *M*. Other stars, however, which also merge into the spectral sequence near class *K* show ZrO bands or the bands of the carbon compounds.

The stars with zirconium oxide bands are called *S* stars, those with carbon bands *R* and *N* stars. Many years ago R. H. Curtiss suggested

that the splitting of the spectral sequence was due to differences in the chemical composition. The ordinary *M* stars represent objects in which oxygen exceeds carbon in abundance. Hence the oxides, TiO, CO, OH,

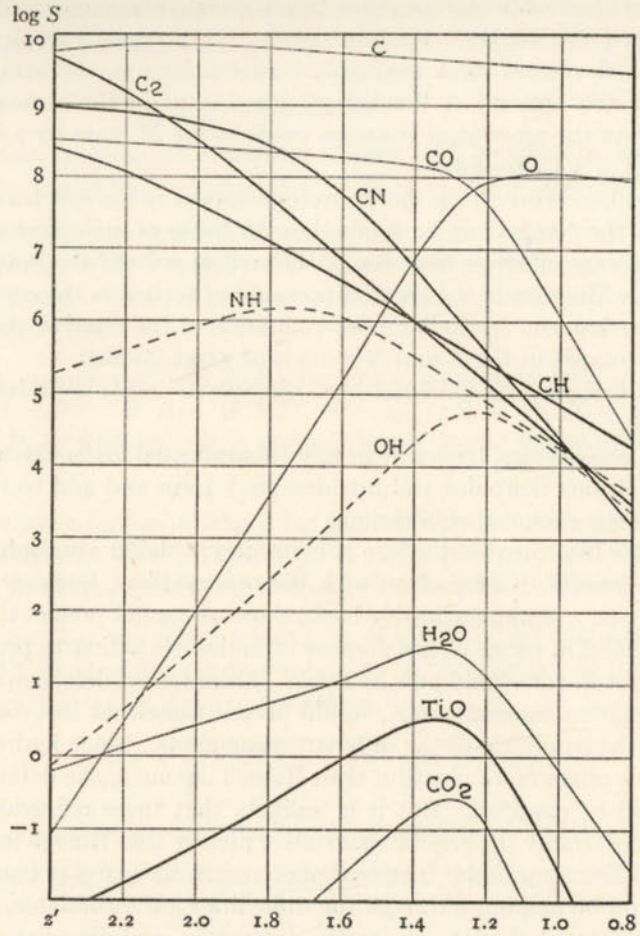

FIG. 9.—THE ABUNDANCES OF MOLECULES AND ATOMS IN GIANT CARBON STARS

In these atmospheres the abundances of carbon and oxygen are interchanged as compared with the normal or "oxygen" sequence. Notice the predominance of C_2, CH, and CN, while O is almost wholly tied up in CO. (Courtesy, H. N. Russell, *Astrophysical Journal*, University of Chicago Press, **79**, 317, 1934.)

etc., play important roles. In the carbon stars, on the other hand, most of the oxygen gets tied up in the unobservable CO and the important bands are those due to carbon and its compounds.

To calculate the properties of the atmospheres of *R* and *N* stars, Russell interchanged the assumed abundances of carbon and oxygen. To-

ward the lower temperatures, CH, CN, and C_2 successively predominate. At temperatures below 2500°K, cyanogen reaches a maximum while C_2 continues to increase. Observations show the carbon bands to gain in the coolest stars while the cyanogen bands remain stationary and CH becomes relatively weaker. Titanium oxide, water vapor, carbon dioxide, and the OH radical form negligible contributions to the atmosphere. The predicted amount of the carbon compounds in the atmosphere is greater than the amount of titanium oxide in the *M* stars by a factor of a hundred or a thousand.

Carbon bands involving the C_{13} isotope appear in the spectra of the *N* stars and the component lines mingle with those of molecules of C_{12} to produce a very effective blocking of the radiation from the lower layers of the star. In view of the great importance of carbon in the energy generation mechanism, McKellar's determination of the relative abundance of these isotopes in the *R* and *N* stars is of great interest.

Dwarf carbon stars have not been discovered and it is probable that none exist.

In the cooler stars, triatomic or more complicated molecules and even solids or liquids (carbides and nitrides) may form and add to the complexity of the chemical equilibrium.

Russell's treatment of the role of molecules in stellar atmospheres was highly successful. Comparison with the observations, however, can be made only on a semiquantitative basis, since we cannot predict the intensity of a band in terms of the number of molecules acting to produce it. Two improvements could now be made. More recent determinations of the dissociation constants, etc., would permit somewhat less rough estimates of the equilibria of the different compounds. Since hydrogen appears to be much more plentiful than Russell assumed, the details of the curves will be modified. But it is unlikely that these refinements will change appreciably the general qualitative picture that Russell has given. On the observational side, improved photometric measures of band intensities would be helpful, although the difficulties are formidable.

It is important that the excitation, ionization, and dissociation equations can account for all of the essential features of the spectral sequence from the very hottest stars to the coolest. Except for the *R*, *N*, and possibly *S* stars, the general features of most stellar spectra can be explained on the hypothesis that the stars have the same composition as the sun and differ only in temperature and atmospheric pressure. For the *R* and *N* stars, however, we must assume a surplus of carbon over oxygen.

We have made comparisons on the basis of the assumption that the intensity of a spectral line depends on the number of atoms capable of absorbing it. The quantitative relations between the number of atoms

and the intensity of a spectral line will be developed in Chapter 8 and we shall see that this relation will involve the temperature, turbulence (if any), pressure, etc., in a not too simple way. Nevertheless, the simple discussion in terms of ionization, excitation, and dissociation must remain as the first approximation in any discussion of stellar spectra.

PROBLEMS

1. What fraction of aluminum atoms will be able to absorb the resonance line, $3^2P_{3/2} - 4^2S_{1/2}$, at $T = 5700°\text{K}$, $P_e = 20$ dynes?

2. Calculate the fraction of all oxygen atoms capable of absorbing $\lambda 4649$, $3s^4P_{5/2} - 3p^4\,D_{7/2}$, of O II. The excitation potential of the lower level is 22.90 ev. The ground term of O II is $^4S_{3/2}$. Assume $T = 25{,}000°\text{K}$ and $\log P_e = 2.80$.

3. The number of N II atoms per gram in the $3p^1P$ level of a certain star is 7×10^{12}. If B_{q+1} is 6.29, $(I - \chi_r) = 9.17$ ev, $T = 20{,}000°\text{K}$, and $\log P_e = 2.80$, calculate the number of atoms in the ground level of N III.

4. If the ionization of iron is the same in a dwarf and a giant *K*0 star of temperatures 4900°K and 4230°K, respectively, what will be the electron pressure in the giant if that in the dwarf is 10 dynes?

5. Show that the relative numbers of atoms in the *n*th energy state in the *q*th stage of ionization are related to the number in the *n'*th energy level in the *q'*th stage of ionization by

$$\frac{N_{nq}}{N_{n'q'}} = \left[\frac{2(2\pi mkT)^{3/2}}{h^3 N_e}\right]^{q-q'} \frac{g_{nq}}{g_{n'q'}}\, e^{-\chi_{nq,n'q'}/kT} \tag{25}$$

where $\chi_{nq,n'q'}$ denotes the total energy separation of the two levels.

6. Show that for hydrogen, the combined Boltzmann and ionization equation is

$$N_n = \frac{N_i N_e}{T^{3/2}} \frac{h^3}{(2\pi mk)^{3/2}}\, n^2 e^{hRZ^2/n^2kT} \tag{26}$$

where N_i is the number of ions, N_n is the number of atoms in level n, and N_e is the number of electrons/cm³. R is the Rydberg constant.

7. If the partial pressure of hydrogen in the sun is 8×10^4 dynes/cm² while that of oxygen is 30 dynes/cm², what will be the relative amounts of OH in the photosphere (5700°K) and in a sunspot (4500°K), assuming the densities of hydrogen and oxygen to remain unchanged from photosphere to sunspot? Take $D = 4.35$ ev, $w = 3735.21$ cm^{-1}, $r_0 = 0.9706$A, and $g_A g_B / g_{AB} = 3$.

REFERENCES

For a derivation of Boltzmann's formula by statistical mechanics see, for example:

KENNARD, E. H. *Kinetic Theory of Gases.* New York: McGraw-Hill Book Co., Inc., 1938, chap. ix.

Our derivation of the ionization formula is taken from:

MENZEL, D. H. *Proc. Nat. Acad. Sci.* **19**, 40, 1933.

A good account of the application of the simple thermal ionization theory to stellar problems may be found in:

PAYNE, C. H. *Stellar Atmospheres.* Harvard Observatory, 1925.

The relation between gas and electron pressure for various hydrogen/metal ratios is given by:

STRÖMGREN, B. *Publ. Copenhagen Obs. No. 138,* 1944.
ROSA, A. *Zeits. f. Ap.* **25**, 1, 1948.

Our discussion of the dissociation equilibrium of molecules in stellar atmospheres is taken from:

RUSSELL, H. N. *Ap. J.* **79**, 317, 1934.

This paper contains references to important earlier work. See also his "The Composition of the Stars," Halley Lecture, Oxford, 1933.

CHAPTER 5

THE EMISSION AND ABSORPTION OF RADIATION

1. Fundamental Definitions

The most important astrophysical property of atoms is that they absorb and emit radiation. The wave lengths of the emitted radiations tell the kind of atoms or ions present in the source. Previous chapters have given a qualitative interpretation of the spectra of the stars and nebulae. To make further progress we must consider the quantity as well as the kind of radiation, and for this purpose it will be necessary to define carefully such concepts as intensity, flux, and energy density.

(*a*) *Specific Intensity*

In a volume of space through which radiation is passing let us consider a surface S which may or may not coincide with an actual physical surface emitting radiation. We fix our attention on an element of area dA, centered at a point O, and on the radiation passing per unit time through this element and confined within the truncated cone defined by dA and the elementary solid angle $d\omega$. (See Fig. 1.) If the amount of this radiation in the frequency range ν to $\nu + d\nu$ be denoted by dE_ν, the specific intensity of the radiation I_ν in the interval $d\nu$ at ν is defined by

$$dE_\nu = I_\nu \cos\theta \, dA \, d\nu \, d\omega \qquad (1)$$

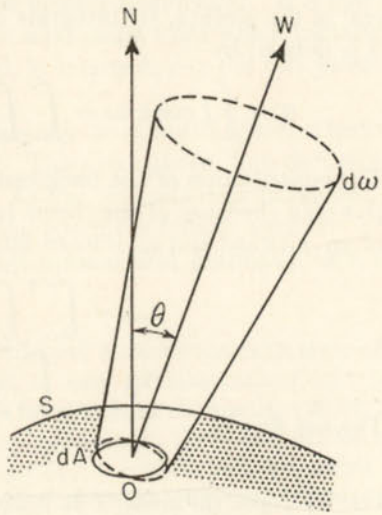

FIG. 1.—DEFINITION OF SPECIFIC INTENSITY

where θ is the angle between the axis of the cone and the outward normal ON. In general, I_ν will depend both on the position of O in space, x, y, z, and on the direction of the pencil of rays OW specified by the co-latitude θ and the azimuthal angle ϕ. Hence $I_\nu = I_\nu(x, y, z, \theta, \phi)$. At any point, the specific intensity of the radiation in the direction θ, ϕ, is defined as the amount of energy which flows per second in unit solid

angle in unit frequency interval through a unit area placed perpendicular to the direction θ, ϕ. In particular the amount of energy flowing per second per cm^2 and in the frequency interval $d\nu$ in the cone $d\omega$ will be $I_\nu(\theta, \phi)\, d\nu\, d\omega$.

Thus, to obtain a quantity in energy units, we must multiply I_ν by $dA\, dt\, d\nu\, d\omega$ where dt is the element of time. Since the element of solid angle is

$$d\omega = \sin\theta\, d\theta\, d\phi$$

the mean value of the intensity averaged over all angles will be

$$J_\nu = \frac{1}{4\pi}\int I_\nu(\theta, \phi)\, d\omega = \frac{1}{4\pi}\int\int I_\nu(\theta, \phi)\sin\theta\, d\theta\, d\phi \qquad (2)$$

We are sometimes interested in the total amount of radiation as integrated over all frequencies, viz.,

$$I = \int_0^\infty I_\nu\, d\nu \qquad (3)$$

(*b*) *Radiation Flux*

A quantity that is often confused with the intensity is the flux of the radiation. To get the total amount of radiation passing through each cm^2 of the surface, we integrate dE over all solid angles. Thus the flux $\mathfrak{F}$ is defined by

$$\mathfrak{F} = \int I\cos\theta\, d\omega = \int_0^\pi\int_0^{2\pi} I(\theta, \phi)\cos\theta\sin\theta\, d\theta\, d\phi = \pi F \qquad (4)$$

The contribution of the backward flowing radiation occurs with a negative sign (because of the cosine factor). Hence it is customary to speak of an outward and an inward flux, viz.

$$\mathfrak{F}_{\text{out}} = \int_0^{\pi/2}\int_{\phi=0}^{2\pi} I\cos\theta\sin\theta\, d\theta\, d\phi;$$

$$\mathfrak{F}_{\text{in}} = -\int_{\pi/2}^{\pi}\int_{\phi=0}^{2\pi} I\cos\theta\sin\theta\, d\theta\, d\phi \qquad (5)$$

The net flux is

$$\mathfrak{F} = \mathfrak{F}_{\text{out}} - \mathfrak{F}_{\text{in}} \qquad (6)$$

For isotropic radiation I is independent of angle; hence eqn. (4) vanishes and F is 0, which means there is no preferential direction of radiation flow. The outward flux of radiation from a surface that emits uniformly in all directions is

$$\mathfrak{F} = 2\pi I\int_0^{\pi/2}\cos\theta\sin\theta\, d\theta = \pi I \qquad (7)$$

Here I is identical with the F introduced in eqn. (4).

The following illustrations may clarify the physical distinction between flux and specific intensity. If we neglect the limb darkening in the sun, the specific intensity of the solar radiation within the solid angle defined by the solar disk is constant as long as the observer is close enough to the sun to see it as a disk. At half the present distance of the sun, its surface brightness and hence the specific intensity of its radiation would remain the same, but its angular area in the sky and the total amount of radiation received from it by each cm^2, i.e., the flux, would be quadrupled. By similar arguments it follows that an extended nebula will have the same surface brightness as long as the eye perceives it as an area.

On the other hand, for an emitter so distant as to appear only as a point, the quantity that counts is the energy actually reaching the observer, i.e., the flux. Thus the apparent brightness of a star, or nebula so distant as to be stellar in appearance, varies as the inverse square of the distance. Along any ray in empty space the specific intensity I is constant, whereas the flux, under such circumstances, falls off according to the inverse square law.

No optical system of lenses or mirrors can increase the specific intensity of the radiation from any object, even though the total amount of energy reaching the receiver may be greatly augmented. If a lens is used to concentrate the sun's rays, the solid angle from which radiation of a given specific intensity is received, is enlarged, i.e., the flux passing through the focus is increased.

In most astrophysical problems amenable to quantitative treatment, I does not depend on ϕ but only on θ. The pronounced limb darkening of the sun is an illustration in point. As Fig. 2 shows, this darkening is a consequence of the dependence of the specific intensity upon θ. The intensity is greatest along the outward normal and gradually falls off as θ increases.

As an illustration of some of these principles, consider the calibration of a surface brightness described as equivalent to sixty tenth-magnitude stars per square degree. The apparent photovisual magnitude of the sun is -26.84; its angular diameter is 32′. Hence its surface brightness in visual magnitudes per square minute of arc is $-26.84 + 2.5\log\pi(16)^2 = -19.58$. Measurements of the radiation received from the sun (Chapter 6) show that this corresponds to an emission rate of 6.25×10^{10} ergs/cm^2/sec (= antilog 10.796) by the solar surface. Sixty tenth-magnitude stars per square degree correspond to one sixtieth of a single tenth-magnitude star per square minute of arc or one star of 14.45 magnitude. Hence the surface brightness will be given by

$$\log S = (-19.58 - 14.45) \times 0.4 + 10.796 = -2.816$$

or

$$S = 0.153 \times 10^{-2}\ \text{ergs/cm}^2\text{/sec}$$

is the surface brightness in c.g.s. units corresponding to 60 tenth-magnitude stars per square degree.

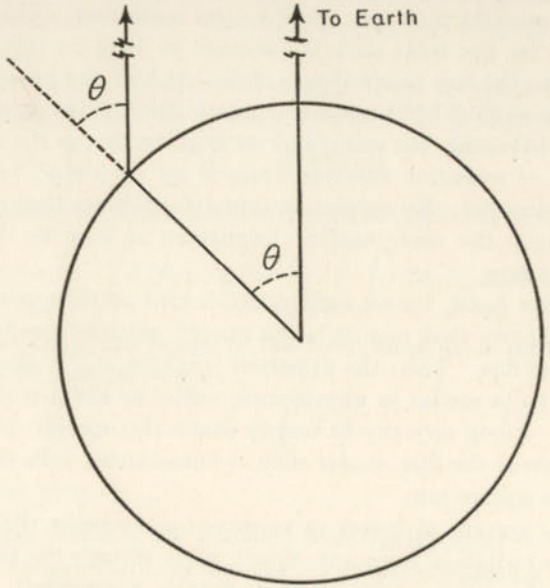

FIG. 2.—EMERGENT RAY FROM THE SUN

(c) *Energy Density*

The energy density of the radiation, u, is the amount of radiant energy per cubic centimeter which at any given instant happens to be passing through space at the point considered. It is related to the specific intensity I by the expression,

$$u = \frac{1}{c}\int I\, d\omega \tag{8}$$

For example, consider an enclosure with heated walls. Radiation will be flying about from one wall to the other and we can speak of the energy density as the amount of energy in ergs/cm³ in the enclosure. An elementary volume will be exposed to radiation from all directions and the amount passing in each second is obtained by summing over all angles, viz., $4\pi I$, i.e., it is simply the constant specific intensity multiplied by the number of solid radians in a sphere. The velocity with which the radiation travels is c; hence the amount of energy residing in a volume at any one time will be $4\pi I/c$ times the volume of the element. Thus the energy density of *isotropic* radiation is related to the intensity by

$$u = \frac{4\pi}{c} I \tag{9}$$

Since the directly observed quantities are intensities or fluxes, it seems better to use I or F rather than u in theoretical discussions of stellar atmospheres or gaseous nebulae. As for stellar interiors where no direct observations can be made, there are some advantages in using u rather than I.

2. Black Body Radiation

Often we are concerned, not with the total radiation but with the emission in certain frequencies. The precise character of the relation between emitted intensity and frequency is known for a perfect radiator or black body. If the radiation is in equilibrium with its surroundings, as for example in an enclosure whose walls are maintained at a fixed temperature T, each cm² of the surface will emit just as much radiation as it absorbs in every wave length, and the condition of a "black" body is fulfilled. Then the intensity is given as a function of frequency and temperature by Planck's law,

$$B_\nu(T) = \frac{2h\nu^3}{c^2}\frac{1}{e^{h\nu/kT} - 1} \tag{10}$$

where $h = 6.62 \times 10^{-27}$ erg sec (Planck's constant), c is 3×10^{10} cm/sec (velocity of light), and k is 1.382×10^{-16} (Boltzmann constant). The derivation of Planck's law, which we omit here, may be found in a number of physics texts.* An important feature of its derivation is the postulate that atoms radiate pulses or quanta wherein energy and frequency are related by $E = h\nu$.

This relationship was subsequently applied by Bohr in his theory of the hydrogen atom. We plot $B_\nu(T)$ for different temperatures in Fig. 3. Notice how the energy distribution changes as the temperature increases, the frequency of maximum energy shifts violetward and the total amount of energy radiated rises rapidly. The energy density of the radiation in the frequency range ν to $\nu + d\nu$ in ergs/cm³ is obtained by multiplying the intensity by $4\pi/c$, thus,

$$u(\nu, T)\, d\nu = \frac{8\pi h}{c^3}\frac{\nu^3}{e^{h\nu/kT} - 1}\, d\nu \tag{11}$$

We find the total energy density by integrating over all frequencies†

$$u(T) = \int_0^\infty u(\nu, T)\, d\nu = aT^4 \tag{12}$$

* E.g., F. K. Richtmyer and E. H. Kennard, *Introduction to Modern Physics* (New York: McGraw-Hill Book Co., Inc., 1942), p. 197.

† See, e.g., Richtmyer and Kennard, *op. cit.*, p. 204.

where the radiation constant $a = 7.569 \times 10^{-15}$ ergs/cm^3/deg^4. That is, the energy density of the black body radiation depends on the fourth power of the temperature. This is the Stefan-Boltzmann law for the energy density of the total radiation. It also may be derived by thermodynamics. Let us compute the rate of emission of energy E by a

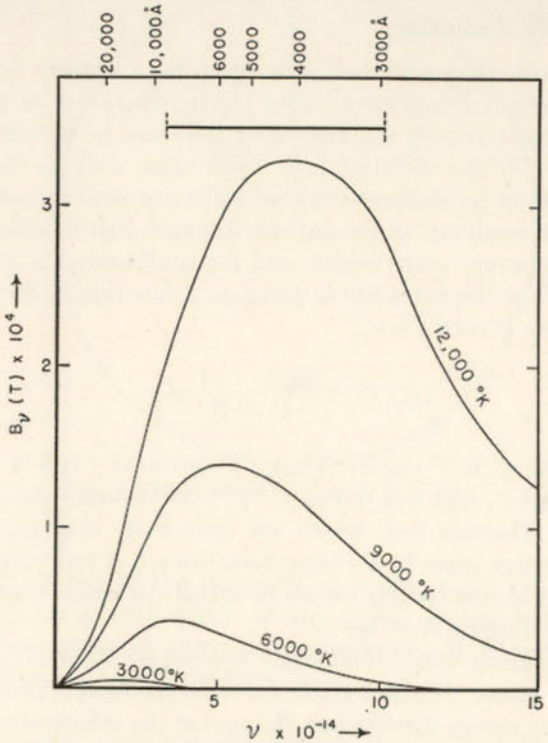

FIG. 3.—THE ENERGY DISTRIBUTION FROM A BLACK BODY

The ordinates are expressed in terms of ergs per unit frequency. The dotted lines indicate the limits reached by photographic plates ordinarily employed in astronomical work. Beyond λ2900 the earth's atmosphere is opaque.

surface that radiates as a black body. If I does not depend on angle for all outward-flowing radiation, the outward flux by eqn. (7) is $\mathfrak{F} = \pi I = \pi B$. Since $u = 4\pi B/c$ by eqn. (9), the amount of energy crossing each cm^2/sec is $cu/4$ or

$$E = \sigma T^4 \tag{13}$$

where $\sigma = 5.6724 \times 10^{-5}$ ergs/cm^2/deg^4/sec.

Example: What is the amount of energy radiated per square centimeter by a star whose surface temperature is 5700°K? From $E = \sigma T^4$, we get

$$E = 5.672 \times 10^{-5}(5700)^4 = 5.99 \times 10^{10} \text{ ergs/cm}^2\text{/sec}$$

or about 6 kilowatts/cm^2.

We often speak of the black sphere temperature of interstellar space. This is the temperature that would be assumed by a perfect black body, or hypothetical black bulb thermometer that absorbed and emitted equally well in all frequencies. It is measured by the energy density u of the radiation field. A black sphere of radius r will intercept and absorb $\pi r^2 uc$ ergs/sec, and will emit $4\pi r^2 \sigma T^4$ ergs/sec. Since the absorbed and emitted energies must be equal, $u = \frac{4\sigma}{c} T^4 = aT^4$, which defines the effective temperature of interstellar space. It does not necessarily correspond to the temperature of any real particle.

From the known distribution and luminosities of the stars, Eddington estimated the energy density at a typical point in interstellar space to be $u = 7.7 \times 10^{-13}$ ergs/cm^3. From $u = aT^4$ we find $T = 3.18$°K.

It is sometimes convenient to express Planck's law in wave length rather than in frequency units. Since $\nu = c/\lambda$,

$$|d\nu| = c\frac{d\lambda}{\lambda^2}$$

and

$$I_\lambda \, d\lambda = \frac{2hc^2}{\lambda^5} \frac{1}{e^{hc/\lambda kT} - 1} d\lambda \tag{14}$$

The wave length at which the intensity of the emitted radiation is a maximum is found by differentiating I_λ with respect to λ and setting the derivative equal to zero. This calculation gives the *Wien Displacement Law*

$$\lambda_{max} \, T = 0.289715 \tag{15}$$

As an example, let us compute the wave length at which the radiation intensity is a maximum for a star the temperature of which is 5000°K. From eqn. (15), we find λ_{max} to be 5.794×10^{-5} cm or λ5794. We emphasize that λ_{max} is the wave length of maximum intensity when I is plotted on a wave length scale. If we plot the intensity I on a frequency scale, so that I_ν represents the amount of energy per unit frequency interval at ν, the wave length corresponding to the frequency at which I_ν is a maximum will be very different from λ_{max}.

The fundamental law of radiation is the Planck law which gives the rate of emission of energy in ergs/cm^2/sec from a surface which radiates like a black body at a temperature T. If we determine the distribution of energy in the spectrum of the sun or a star, we can get an estimate of its temperature from a comparison of the observed energy curve with the Planckian curve. Examples of this procedure will be found in Chapter 6.

The Stefan-Boltzmann law eqn. (13) expresses the total rate of energy emission in terms of the temperature but says nothing about the quality, i.e., the frequency or wave length distribution of the radiation. As we have seen, one can derive this law from Planck's law by integrating over all frequencies, but it can also be derived by thermodynamic reasoning. Astrophysical applications of the Stefan law can be made to the sun and a few other stars whose dimensions and total radiation output are known. For example, Abbot has measured the total amount of energy radiated by the sun. Since the solar surface area is known, the energy output per square centimeter can be found and the temperature computed.

Wien's displacement law tells us how the color of the radiation changes. As the temperature is increased, the wave length at which the maximum output of energy occurs decreases, and the light becomes progressively bluer in quality.

In astronomical applications, certain asymptotic forms of Planck's law are often useful. If λ or T are so small that $hc/\lambda kT \gg 1$ (as in the ultraviolet), the exp $(hc/\lambda kT)$ term will be much larger than unity and we can write

$$B_\lambda(T) = \frac{2hc^2}{\lambda^5} e^{-ch/\lambda kT} \tag{16}$$

the so-called *Wien approximation* to Planck's law. In the red and infrared spectral regions of hot stars, λT becomes large and $ch/\lambda kT$ is much less than 1. The Planck law reduces to

$$I_\lambda = 2kcT\lambda^{-4} \tag{17}$$

This is the *Rayleigh-Jeans formula.*

3. The Coefficients of Absorption and Emission

The flow of energy through the atmosphere of a star and the formation of absorption lines in stellar spectra or of emission lines in the spectra of gaseous nebulae all involve the interaction of matter with radiation—absorption followed by subsequent re-emission. Consequently it is important to have a clear understanding of what is meant by such terms as emissivity, absorption coefficient, etc.

Consider a small volume element dv of density ρ in a heated gas. The total amount of energy emitted by this elementary volume over all directions in the range ν to $\nu + d\nu$ will be

$$dE_\nu = j_\nu \rho \, dv \, d\nu$$

where j_ν, the mass emission coefficient of the material, is the total amount of energy emitted per second (per unit frequency interval) per gram of the radiating substance in all directions.

The absorption coefficient can be defined in the following manner. Consider radiation of intensity I_ν^0 falling perpendicularly upon a slab of thickness x. (See Fig. 4.) Some of the impinging energy will be absorbed and some will pass on through the layer. At any point within

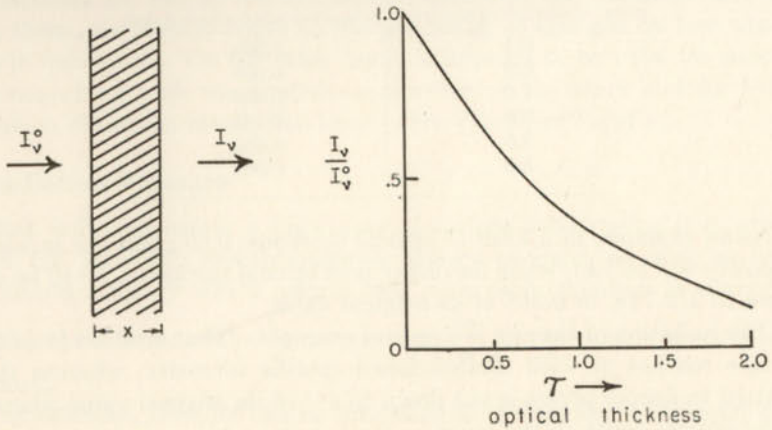

FIG. 4.—THE EXTINCTION OF A BEAM IN A SLAB OF MATERIAL

the slab, the loss of energy will be proportional to the density of the material and to the intensity of the radiation. That is, in a distance dx, the intensity of the beam will be cut down by an amount,

$$dI_\nu = -k_\nu I_\nu \rho \, dx \tag{18}$$

where k_ν is defined as the mass absorption coefficient for radiation of frequency ν. For strongly absorbing substances k will be large; for nearly transparent substances k will be small. We divide eqn. (18) by I_ν and integrate to obtain:

$$\ln I_\nu = -k_\nu \rho x + \text{const, whence } I = I_\nu^0 e^{-k_\nu \rho x}$$

where I_ν^0 is the intensity of the incident beam. This means that when a beam of light passes through a slab of material the intensity falls off exponentially at a rate that depends upon the thickness of the slab, on the density, and on the mass absorption coefficient.

In general k_ν will depend on ρ and x. Hence

$$I_\nu = I_\nu^0 e^{-\tau_\nu} \tag{19}$$

where the quantity

$$\tau_\nu = \int_0^x k_\nu \rho \, dx \tag{20}$$

is called the optical depth or thickness of the slab. The larger the value of τ_ν, the greater will be the extinction in the slab. (See Fig. 4.)

Optical Thickness of the Slab	Ratio of Emergent to Incident Intensity
0.1	0.905
0.5	0.606
1.0	0.368
2.0	0.135
3.0	0.050
5.0	0.007

As an example, in a filter of optical thickness 0.695 half the incident intensity will be lost, while for one of unit optical thickness, I will be cut down to 1/2.718, or 0.368 of its original value.

The radiation of the sun is a second example. That emitted from the surface reaches us with undiminished specific intensity, whereas that emitted in deeper layers is cut down to $e^{-\tau}$ of its original value where τ is the optical depth of the layer.

Sometimes we are concerned with the absorption by small solid particles such as the grains in interstellar space or in a comet. A small mass m exposed to radiation will absorb an amount

$$k_\nu m\, d\nu \int I_\nu(\theta, \phi)\, d\omega = 4\pi k_\nu m J_\nu\, d\nu \tag{21}$$

of radiation between ν and $\nu + d\nu$. The total radiation absorbed follows from an integration over all frequencies, viz.,

$$4\pi m \int k_\nu J_\nu\, d\nu$$

4. Kirchhoff's Law

Kirchhoff showed that if matter is in thermal equilibrium with its surroundings, an important relation exists between the coefficients of emission and absorption; the ratio j_ν/k_ν depends on the temperature only and not on the color, shape, or composition of the body, i.e.,

$$\frac{j_\nu}{k_\nu} = 4\pi B_\nu(T) \tag{22}$$

where $B_\nu(T)$ is the intensity of black body radiation as given by Planck's law. Kirchhoff's law expresses quantitatively the well-known fact that good absorbers are also good emitters, and that a heated substance emits more strongly at those frequencies where the absorption coefficient is high

than at frequencies where the absorption is low. In this connection we may recall the third law of spectrum analysis.

This relationship can be applied only for thermal emission. It is not valid, for example, for the scattering of sunlight by air molecules where the particles are not in thermal equilibrium with the radiation falling upon them, nor does it apply to the scattering of sunlight by free electrons in the corona. On the other hand, it appears to be valid for processes concerned with the continuous spectra of the stars and for the formation of certain absorption lines. (See Chapters 7 and 8.)

5. Radiation Pressure

That radiation exerts a force upon a surface intercepting it is predicted by Maxwell's electromagnetic theory of light, as well as by the quantum theory which asserts that with each quantum of energy, $E = h\nu$, there is associated a momentum, $\frac{h\nu}{c}$, in the same direction as the beam.

The radiation pressure can be computed as the net rate of transfer of momentum through a unit area of arbitrary orientation at the point considered. A similar definition holds for the gas pressure, except that in this more familiar example the momentum is carried by the gas molecules themselves.

The amount of radiation passing per second through our arbitrarily chosen unit area at an angle θ with the normal and in the solid angle $d\omega$ will be $I \cos\theta\, d\omega$. The corresponding amount of momentum transported is $I \cos\theta\, d\omega/c$. Since the ray strikes the surface at an angle θ, the component of momentum normal to the surface will be $\frac{I \cos\theta\, d\omega}{c} \cos\theta$. Hence the total force will be

$$P_R = \frac{1}{c} \int I \cos^2\theta\, d\omega \tag{23}$$

Under the special circumstance where a beam of intensity I falls perpendicularly upon a totally absorbing surface, $\cos\theta = 1$, and $P_R = I/c$ but I/c in this example is simply the radiation density itself!

When the radiation is isotropic,

$$P_R = \frac{4\pi I}{3c} = \frac{u}{3} \tag{24}$$

i.e., the radiation pressure is numerically equal to one third the radiation density. If the radiation is compared with a gas, we may imagine the light quanta divided into three groups traveling in three mutually perpendicular directions. Thus at any one time, one third of the photons or

light quanta may be thought of as exerting a pressure in a given direction.

As an example, let us calculate the radiation pressure at a point in the solar atmosphere where the energy density corresponds to a temperature of 5700°K. From eqns. (12) and (24) we find

$$P_R = 7.569 \times 10^{-15} \times \tfrac{1}{3}(5700)^4 = 2.66 \text{ dynes/cm}^2$$

as compared with a gas pressure (cf. Chapter 7) of about 80,000 dynes/cm²! At the center of the sun, the temperature is about sixteen million degrees. At this point the radiation pressure is 1.66×10^{14} dynes/cm² as compared with a total pressure of 3.2×10^{17} dynes/cm². Thus the radiation pressure is still only a small fraction of the total pressure. In a sufficiently luminous star, radiation pressure may contribute an appreciable fraction of the total pressure.

6. The Mechanical Force Exerted by Radiation

We must be careful to distinguish between the radiation pressure as just described and the net mechanical force exerted by radiation upon a mass of material.

A vane in quiet air is bombarded by molecules on both sides, but it remains motionless because the force on each side is the same. If there is a gust of wind there will be a net mean motion of the air molecules. The resultant mechanical force upon the vane will cause it to turn.

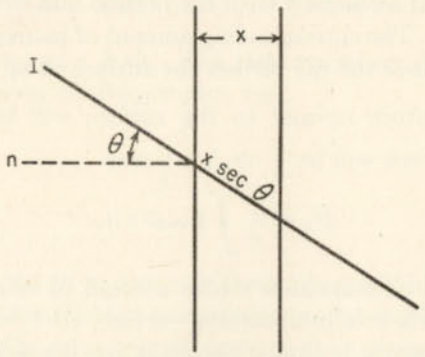

FIG. 5.—THE OBLIQUE PASSAGE OF A RAY THROUGH A SLAB

Let a thin plane slab of thickness dx be illuminated by radiation of intensity $I_\nu(\theta)$. The amount of energy falling upon the slab/cm²/sec in the elementary cone $d\omega$ at an angle θ with the normal will be $I_\nu \cos\theta \, d\omega \, d\nu$. Since the path length of this ray through the slab is $dx \sec\theta$, the amount of energy absorbed/cm²/sec will be

$$de_\nu = I_\nu \cos\theta \, k_\nu\rho \sec\theta \, dx \, d\nu \, d\omega$$

As this radiation is absorbed, its momentum is conveyed to the material. The thrust supplied by de_ν normal to each unit area of the slab is $\frac{\cos\theta \, de_\nu}{c}$.

The resultant mechanical force exerted by radiation of frequency between ν and $\nu + d\nu$ acting upon each cm² is obtained by integrating $\frac{\cos\theta \, de_\nu}{c}$ over all angles of the incoming radiation.

$$\frac{1}{c}\int \cos\theta \, de_\nu = \frac{k_\nu\rho \, dx \, d\nu}{c}\int I_\nu \cos\theta \, d\omega$$

Thus

$$= \frac{k_\nu\rho \, dx \, d\nu}{c}\pi F_\nu \tag{25}$$

where πF_ν is the net flux in ergs/cm²/sec/unit frequency interval.

The total mechanical force/cm² will be obtained finally by an integration over all frequencies.* Thus the total amount of momentum abstracted from the radiation field by the slab will be

$$dp = \bar{k}\rho \frac{\pi F}{c} dx \tag{26}$$

per cm², where

$$\bar{k} = \frac{1}{F}\int k_\nu F_\nu \, d\nu$$

and πF is the total flux.

As an example, let us compute the mechanical force f_R exerted by radiation upon a unit volume of gas in the atmosphere of Sirius. With $T = 10{,}000°\text{K}$, $\pi F = \sigma T^4$, and $\bar{k} = 27$ (see Chapter 7) we get

$$f_R = 27\rho \times \frac{5.75 \times 10^{-5} \times 10^{16}}{3 \times 10^{10}} = 5.17 \times 10^2\rho \text{ dynes}$$

as compared with a force of gravity upon the same volume element of $f_g = 2 \times 10^4\rho$ dynes. In the atmosphere of 10 Lacertae, $k = 3.0$, $T = 29{,}600°\text{K}$, and we find $f_R = 4.4 \times 10^3\rho$ dynes, as compared with a force of gravity of $2.8 \times 10^4\rho$ dynes.

7. The Classical Picture of Radiation

We now seek quantitative information on the absorptivities and emissivities of the atoms and molecules. For example, how may we obtain k_ν for the "D" lines of sodium? Within the scope of this book it will not be possible to give a complete discussion of this problem, but we shall cover the developments essential to a quantitative interpretation of stellar and nebular spectra.

* The k employed here must be corrected for the effects of negative absorption. (See Sec. 11.)

With the aid of the classical theory of the absorption and emission of radiation it is possible to develop, with relative ease, certain expressions that can be transformed easily into the correct relationships, thus avoiding the complexities of the rigorous quantum mechanical treatment.

Nearly a century ago, Maxwell, from a thorough analysis of electrical and magnetic phenomena, showed that a system of electrical charges in motion would produce electric and magnetic waves in space. The velocity of these waves, 299,776 km/sec, which was computed from electrical data alone, is precisely the velocity of light—a fundamental constant of nature. That is, waves of light are waves, not a material substance, but waves of electric and magnetic fields.

Light is but one form of electromagnetic radiation—akin to radio waves, heat radiation, X rays, and γ rays. These radiations differ chiefly by their wave lengths and exhibit similar phenomena of diffraction and polarization. A coarse wire grating produces interference with radio microwaves, a diffraction grating produces a spectrum with visible light, while crystals are used to examine X-ray spectra.

Electromagnetic waves can be polarized, proving that the displacements occur perpendicular to the direction of propagation. In Fig. 6 we imagine that the wave comes perpendicularly out of the plane of the paper. The direction of vibration is then in the plane of the paper. Although the direction of vibration of ordinary light changes in a random fashion many times a second, it always remains in a plane perpendicular to the direction of propagation. If a piece of polaroid be placed in the beam, all vibrations save those in a single direction will be extinguished.

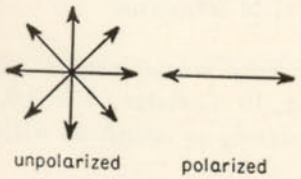

FIG. 6.—UNPOLARIZED AND PLANE POLARIZED LIGHT VIBRATIONS

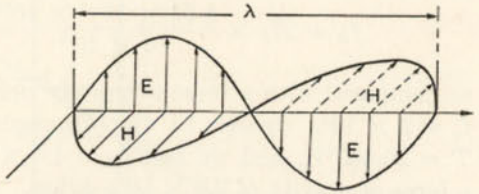

FIG. 7.—THE ELECTROMAGNETIC WAVE
(Adapted from a diagram in *Sky and Telescope*, August, 1945, p. 8.)

The transverse displacements consist of variations in the magnitude of electric and magnetic fields that are directed perpendicular to one another and to the direction of propagation of the light wave. (See Fig. 7.) The flux of the radiation, i.e., the amount of energy traveling in the beam, is proportional to $E^2 + H^2$, viz.,

$$\mathfrak{F} = \frac{c}{8\pi}[E^2 + H^2] \tag{27}$$

Classical electromagnetic theory relates the radiation of energy with the motions of the system of charge. Let us suppose that a stationary charge of ε is placed at the point A and a charge $-\varepsilon$ executes simple harmonic motion along the z axis with an amplitude z_0. If z_0 is much smaller than the wave length of the emitted light, an observer at O at a distance large compared with z_0 will receive an almost pure sine wave. As the charge moves up and down along the z axis, it emits radiation which has a maximum intensity in the xy plane and is zero along the z direction.

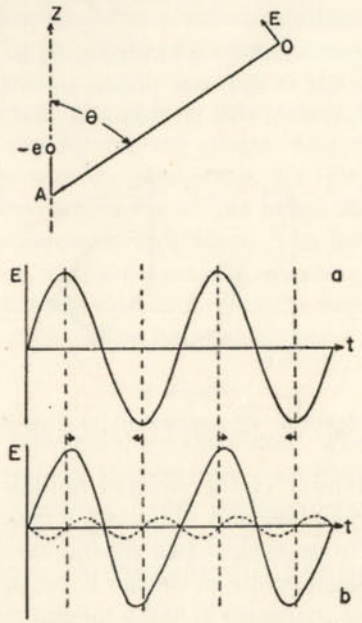

FIG. 8.—THE RADIATION FROM A DIPOLE

The electric charge $-e$ vibrates around A along the direction Z. The electric vector $\boldsymbol{E}$ of the wave emitted is observed in O. If the amplitude of vibrations of the electric charge is negligibly small, the vibration of $\boldsymbol{E}$ is represented by the sine curve (a). For an amplitude which is not very small in comparison to the wave length λ, a distortion occurs and the vibration of $\boldsymbol{E}$ can be decomposed into two vibrations with frequencies ν and 2ν (curve b), corresponding to electric dipole and electric quadrupole radiations. (Courtesy, S. Mrozowski, *Review Modern Physics* **16**, 164, 1944, Fig. 5.)

Now the distance of the charge $-\varepsilon$ from O varies as it executes its oscillations. The time interval between the maximum and minimum of the electric vector E will be smaller in the half of the cycle when the charge moves towards the observer than in the other half of the cycle. Hence there will be deviations from the pure sine pattern. It is found that the emitted wave can be represented as the sum of the two vibrations,

$$E = a_d \sin 2\pi\nu t + a_q \sin 4\pi\nu t \tag{28}$$

The ratio a_q/a_d is proportional to (z_0/λ). There are in fact also higher order terms but these fall off very rapidly in amplitude. We call the second term the electric quadrupole component of the radiation.

If z_0 is made smaller and smaller but the vibrating charge $-\varepsilon$ larger in such a way that the product,

$$P_0 = z_0\varepsilon \tag{29}$$

remains finite, in the limit the vibrating system will radiate a pure sine wave or pure dipole radiation.

Now consider a system where a charge $+2q$ is placed at the origin and 2 charges $-q$ vibrate in opposite phases on either side. The dipole radiation from such a system will be zero and only quadrupole emission

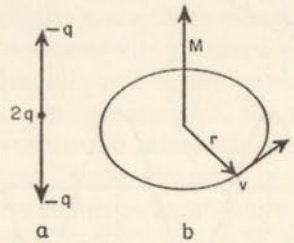

FIG. 9.—(a) THE ELECTRIC QUADRUPOLE; (b) THE MAGNETIC DIPOLE

will appear. The intensity of the emitted radiation is zero along the z axis and also in the xy plane and will attain a maximum value at some intermediate angle. In general, if two charges oscillate along a line as in an antenna, the system emits as though it contained a dipole radiating a pure sine wave of frequency ν, and a quadrupole radiating at twice this frequency. When both are present and the amplitude of motion is much smaller than the wave length of the emitted radiation, the quadrupole component is much smaller than the dipole component.

Suppose now that instead of oscillating along a straight line the charges move in a closed curved path as in a loop antenna. Such a closed circuit has the properties of a magnetic dipole and if the charges surge first one way and then another, the magnetic dipole will change sign and the system will radiate magnetic dipole radiation.

The concepts of electric dipole, electric quadrupole, and magnetic dipole radiation are useful for the treatment of the radiation of energy by atoms. Unless the electric dipole component of the radiation is missing, the others are of no importance.

On the classical theory of atoms radiating continuously, the energy emitted was simply proportional to the square of the amplitude of the emitted light wave. On the other hand, the quantum theory requires

that atoms radiate energy in discrete pulses or quanta in which energy and frequency are related by

$$E = h\nu$$

where h is Planck's constant and the frequency ν of the emitted quantum determines its energy.

8. The Classical Dipole

The simplest classical model of a radiating atom is a dipole wherein a charge ε is bound by an elastic restoring force, and is subject to a damping or dissipative force proportional to the velocity.

When such an atom is placed in a light beam, the atomic electron will try to follow the rapidly varying electric field and will bob up and down with the frequency of the light wave. If this frequency lies near the resonance or natural frequency of the atom, the oscillation of the charge may attain considerable amplitude. (In fact, the amplitude is limited only by the rate of dissipation of energy.)

We shall suppose that the electric field of the incident light wave has a sinusoidal variation that can be represented by

$$\boldsymbol{E} = \boldsymbol{E}_{0z}e^{i\omega t} \tag{30}$$

where the $\boldsymbol{E}$ vector is directed along the z axis. That is: $\boldsymbol{E} = E_z$.

Let m denote the mass of the electron, ε its charge, and K the harmonic restoring force constant. There is also a damping force gz' which we assume to be proportional to the velocity. At any instant, the disturbing force acting upon the charge is εE_z. The equation of motion is therefore

$$\underset{\text{mass times acceleration}}{mz''} = \underset{\text{dissipative force}}{-gz'} - \underset{\text{restoring force}}{Kz} + \underset{\text{external force}}{\varepsilon E_{0z}e^{i\omega t}} \tag{31}$$

If $g/m = \gamma$, $K/m = \omega_0^2$, eqn. (31) reduces to

$$z'' + \gamma z' + \omega_0^2 z = \frac{\varepsilon E_{0z}}{m}e^{i\omega t} \tag{32}$$

To solve this equation we assume a particular solution,

$$z = z_0 e^{i\omega t} \tag{33}$$

where z_0 may be a complex number. The transient solution is of no interest here as it represents momentary effects when radiation first strikes the atom. When eqn. (33) is put in eqn. (32) and use is made of the relations

$$\omega = 2\pi\nu \quad \text{and} \quad \omega_0 = 2\pi\nu_0 \tag{34}$$

there results

$$z = \frac{\frac{\varepsilon}{4\pi^2 m} E_{0z} e^{2\pi i \nu t}}{\nu_0^2 - \nu^2 + i\gamma \frac{\nu}{2\pi}} \tag{35}$$

The complex form of z_0 merely means that the displacement z of the charged particle is not in phase with the incident wave, although it vibrates with the same frequency ν.

With the aid of certain formulae from classical electricity and magnetism we shall now obtain expressions for the index of refraction and the absorption coefficient of the gas.

In any medium the velocity of light is

$$v = \frac{c}{n} = \frac{c}{\sqrt{\epsilon}} \tag{36}$$

where n is the index of refraction which may be complex, and ϵ is the dielectric constant. In free space $\epsilon = 1$.

The concept of a dielectric constant is usually introduced in connection with Coulomb's law. If two charges q_1 and q_2 are separated by a distance r in a medium, the electrostatic force between them will be

$$F = \frac{q_1 q_2}{\epsilon r^2}$$

If q_1 and q_2 are measured in e.s.u. and r in cm, F will be in dynes.

Now ϵ is related to the *polarizability* of the medium. Imagine a nonconducting slab placed between the plates of a condenser. The field between the plates tends to distort the atoms in such a way that the negative charges are pulled towards the positive plate and the positive charges towards the negative plate. An actual flow of electricity cannot take place in the medium; what happens is that the charges bound in the atoms are displaced from their normal positions. Although the material as a whole must remain neutral, the surfaces of the slab will become charged. The surface of the nonconducting slab near the positive condenser plate acquires an excess of negative charge while the other surface acquires a positive charge. These induced surface charges cancel some of the lines of force that originate on the condenser plate with the result that the field within the slab is weakened.

Under normal circumstances, the negative charges in an atom are symmetrically distributed about the nucleus, but if the atom is placed in an electric field, the electrons tend to be pushed one way and the positively charged nucleus the other. For small distortions the amount of this shift is proportional to the field. Let r denote the distance between

the center of gravity of the positive charge and that of the negative charge. If two opposite charges, $+q$ and $-q$, are separated by a distance r, they are said to constitute a dipole of moment

$$p = qr \tag{37}$$

Since p depends on the electric field we can write

$$p = \alpha E$$

where the constant of proportionality, α, is called the susceptibility of the medium. It is shown in textbooks on electricity and magnetism that*

$$\epsilon E = E + 4\pi N p = E(1 + 4\pi N\alpha), \quad \epsilon = 1 + 4\pi N\alpha \tag{38}$$

where N is the number of electrons/cm^3. Since z is the net shift between the two charges comprising the dipole, $p = \alpha E_z = \varepsilon z$, and from eqns. (30) and (35) we get

$$\alpha = \frac{\varepsilon z}{E_z} = \frac{\frac{\varepsilon^2}{4\pi^2 m}}{\nu_0^2 - \nu^2 + i\gamma \frac{\nu}{2\pi}} \tag{39}$$

From eqns. (38) and (39) the dielectric constant is

$$\epsilon = 1 + \frac{\frac{N\varepsilon^2}{\pi m}}{\nu_0^2 - \nu^2 + i \frac{\nu}{2\pi}\gamma} \tag{40}$$

The physical significance of the complex dielectric constant is that the medium not only refracts light but also absorbs it. The complete index of refraction may be represented by

$$\tilde{n}^2 = \epsilon = (n - i\kappa)^2 \tag{41}$$

We shall now demonstrate that n represents the ordinary index of refraction of the gas and κ represents the absorptivity. For gases, n is of the order of unity, so we can expand eqn. (40) by the binomial theorem and neglect all terms beyond the second,

$$n - i\kappa = 1 + \frac{N\frac{\varepsilon^2}{2\pi m}}{\nu_0^2 - \nu^2 + i \frac{\gamma}{2\pi}\nu} \tag{42}$$

* See, for example, L. Page and N. I. Adams, *Principles of Electricity* (New York: D. Van Nostrand Co., Inc., 1931), p. 44.

We may reduce this formula to real and imaginary parts by multiplying the second term on the right by its complex conjugate. Then

$$n = 1 + \frac{N\varepsilon^2}{2\pi m} \frac{\nu_0^2 - \nu^2}{(\nu_0^2 - \nu^2)^2 + \left(\frac{\gamma}{2\pi}\right)^2 \nu^2}$$

$$\kappa = \frac{N\varepsilon^2}{2\pi m} \frac{\nu\left(\frac{\gamma}{2\pi}\right)}{(\nu_0^2 - \nu^2)^2 + \nu^2\left(\frac{\gamma}{2\pi}\right)^2} \tag{43}$$

For many astrophysical applications we are interested in the behavior of the ordinary index of refraction n and the imaginary component κ near the resonance frequency ν_0. When $\nu \sim \nu_0$ we may put

$$\nu_0^2 - \nu^2 \sim 2\nu(\nu_0 - \nu)$$

and we obtain the following adequately accurate expressions,

$$n = 1 + \frac{N\varepsilon^2}{4\pi m\nu} \frac{\nu_0 - \nu}{(\nu_0 - \nu)^2 + \left(\frac{\gamma}{4\pi}\right)^2} \tag{44}$$

$$\kappa = \frac{N\varepsilon^2}{8\pi m\nu} \frac{\frac{\gamma}{2\pi}}{(\nu_0 - \nu)^2 + \left(\frac{\gamma}{4\pi}\right)^2} \tag{45}$$

The dependence of $n - 1$ and κ upon ν near the resonance frequency ν_0 is shown in Fig. 10. Notice that at ν_0, $n - 1$ changes sign while κ reaches a maximum. This behavior of n in the neighborhood of a resonance frequency is referred to as *anomalous dispersion.*

We shall now show how κ is related to the absorption coefficient, k, as defined in eqn. (18). Suppose a light beam of electric field E, and initial intensity I_0 and amplitude E_0 falls normally upon a slab of absorbing material. Let x denote the direction in which the beam is moving. Then E is a function of both x and t. From electromagnetic theory E satisfies

$$\frac{\partial^2 E}{\partial x^2} = \frac{1}{v^2}\frac{\partial^2 E}{\partial t^2} \tag{46}$$

where v is the phase velocity of light. The solution is

$$E = E_0 e^{2\pi i\nu\left(t - \frac{x}{v}\right)} \tag{47}$$

which is the equation of the wave. Since the velocity v is given by

$$v = \frac{c}{\tilde{n}}$$

where $\tilde{n} = n - i\kappa$ we have

$$E = E_0 e^{-\frac{2\pi\nu\kappa x}{c}} e^{2\pi i\nu\left(t - n\frac{x}{c}\right)} \tag{48}$$

which means that the amplitude dies away according to exp $(-\omega\kappa x/c)$, and since the intensity varies as the square of the amplitude we have

$$I = I_0 e^{-\frac{4\pi\nu\kappa}{c}x} = I_0 e^{-k\rho x} = I_0 e^{-k'x} \tag{49}$$

where k' is here defined as the absorption coefficient per unit volume.

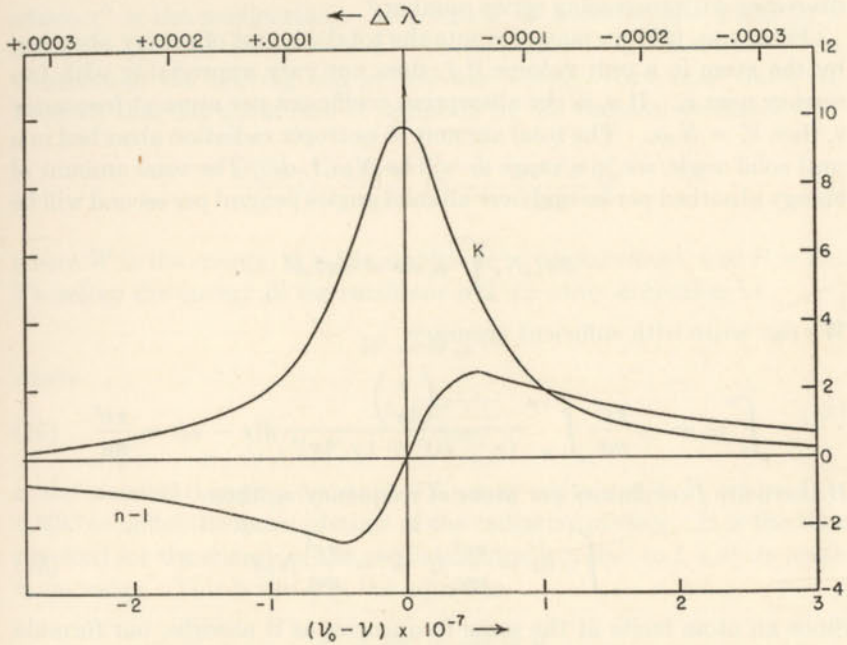

FIG. 10.—THE VARIATION OF $(n - 1)$ AND κ WITH FREQUENCY NEAR RESONANCE

The curves are computed for sodium atoms absorbing at the λ5889 (D_1) line. Notice the anomalous behavior of the index of refraction near resonance. The ordinates are arbitrary.

9. The Classical Atomic Absorption Coefficient

From eqns. (45) and (49) we may now write down an expression for the absorption coefficient per unit volume, k', viz.,

$$k' = \frac{4\pi\nu\kappa}{c} = \frac{N\varepsilon^2}{2mc}\frac{\gamma}{2\pi}\frac{1}{(\nu - \nu_0)^2 + (\gamma/4\pi)^2} \tag{50}$$

where N is the number of electrons per unit volume with a natural frequency ν_0.

Now the quantum theory employs the same formula with a somewhat modified meaning of γ and with N replaced by $N_0 f$. Here N_0 is the number of atoms/cm³ capable of absorbing the frequency ν_0 and f is called the *oscillator strength* or number of dispersion electrons of frequency ν_0 per atom. For example, for the first few members of the Balmer series the f values are

$$H\alpha = 0.6408, \quad H\beta = 0.1193, \quad H\gamma = 0.0447, \quad \text{and} \quad H\delta = 0.0221$$

according to the data of Menzel and Pekeris. Notice how f progressively decreases with increasing series number.*

From eqn. (50) we may compute the total amount of energy absorbed by the atom in a unit volume if I_ν does not vary appreciably with frequency near ν_0. If α_ν is the absorption coefficient per atom at frequency ν, then $k'_\nu = N_0\alpha_\nu$. The total amount of isotropic radiation absorbed in a unit solid angle/sec in a range $d\nu$ will be $N_0\alpha_\nu I_\nu\, d\nu$. The total amount of energy absorbed per second over all solid angles per cm³ per second will be

$$4\pi I_\nu N_0 \int_0^\infty \alpha_\nu\, d\nu = 4\pi I_\nu \bar{k}'$$

We can write with sufficient accuracy

$$\int_0^\infty \alpha_\nu\, d\nu = \frac{\pi\varepsilon^2}{mc} \int_{-\infty}^{+\infty} \frac{\left(\frac{\gamma}{4\pi^2}\right)}{(\nu - \nu_0)^2 + (\gamma/4\pi)^2}\, d(\nu - \nu_0) = \frac{\pi\varepsilon^2}{mc} \tag{51}$$

If there are f oscillators per atom of frequency ν_0, then

$$\int \alpha\, d\nu = \frac{\pi\varepsilon^2}{mc} f, \quad \bar{k}' = \frac{\pi\varepsilon^2}{mc} N_0 f \tag{52}$$

Since an atom emits at the same frequencies as it absorbs, our formula for $\bar{k}$ tells us the frequency-intensity character of a spectral line emitted by a classical oscillator.

The qualitative difference between natural broadening as expressed in eqn. (50) and Doppler broadening (Sec. 6 of Ch. 3) will be apparent from the character of the formulae. At distances $(\nu_0 - \nu)$ from the line center much larger than $(\gamma/4\pi)$, the absorption coefficient in a naturally broadened line falls off as $(\nu_0 - \nu)^{-2}$ while that of an intrinsically narrow line broadened only by the thermal motions of the radiating atoms falls off as $\exp[-C(\nu - \nu_0)^2]$.

The shape of the line absorption coefficient for natural broadening depends on the value of the classical damping constant γ. The electromagnetic theory gives the rate at which the dipole emits energy and hence the speed with which the oscillations of a dipole of initial amplitude r_0 die down. This decay takes place exponentially and the rate of the decay will determine γ.

* For the strongest doublets of alkali atoms f may be close to 1, e.g., for the two "D" lines of sodium, the sum of the f values is 0.98.

According to classical theory an accelerated electron of change ε will radiate energy at the rate*

$$\frac{dW}{dt} = -\frac{2}{3}\frac{\varepsilon^2(z'')^2}{c^3} \tag{53}$$

where z'' is the acceleration. Although z'' is a vector, the scalar $(z'')^2$ is always positive unless $z'' = 0$. Hence, whatever the direction of the acceleration the moving charge will lose energy. One may show (cf. Prob. 6) that the mean rate of radiation by the classical oscillator is

$$\overline{\frac{dW}{dt}} = -\frac{16\pi^4\nu^4}{3c^3} P^2 = -\frac{8\pi^2\nu^2\varepsilon^2}{3mc^3} W \tag{54}$$

where W is the energy, z_0 is the amplitude of displacement, and $P = \varepsilon z_0$. Therefore the energy of the oscillator will die away according to

$$W = W_0 e^{-\gamma t}$$

where

$$\gamma = \frac{8\pi^2\nu^2\varepsilon^2}{3mc^3} \tag{55}$$

is the classical damping constant. We may write $\gamma = 1/T$, where $T = 4.50\lambda^2$ is called the mean lifetime of the radiating system. It is the time required for the energy of the oscillating dipole to fall to $1/e$ of its maximum value. This is the γ in the equation

$$z'' + \gamma z' + \omega_0^2 z = 0$$

which is obtained from eqn. (32) when the external force is zero. The solution is

$$z = z_0 e^{-\frac{1}{2}\gamma t} \cos \omega t + \text{const}$$

From eqn. (54) we may compute the law of scattering for particles whose radii a are much smaller than the wave length of the incident light, λ. Such particles can be regarded as containing a multitude of oscillating electric dipoles all of which are in phase. Let P denote the electric moment per dipole. Then the total electric moment of a particle is proportional to its volume, i.e., the scattering or dissipation of energy

* See, for example, F. K. Richtmyer and E. H. Kennard, *Introduction to Modern Physics* (New York: McGraw-Hill Book Co., Inc., 1942), p. 73.

will be proportional to the (volume)^2 or a^6. Then the scattering coefficient S is proportional to

$$\frac{a^6}{\lambda^4} \quad \text{or to} \quad \pi a^2 \left(\frac{a}{\lambda}\right)^4$$

As an example consider absorption by the D lines of sodium. Since $\lambda = 5.893 \times 10^{-5}$ cm it follows from eqn. (55) that:

$$\gamma = \frac{0.2224}{\lambda^2} = 6.403 \times 10^7 \text{ sec}^{-1}$$

Now calculate the absorption coefficient per gram of sodium atoms at a distance of 2A from the center of $\lambda 5889 (D_1)$. Here Doppler broadening is not important. From eqn. (50), noting that

$$N = \frac{1}{23 \times 1.660 \times 10^{-24}} = 2.619 \times 10^{22} \text{ atoms/gram}$$

and

$$(\nu_0 - \nu) = 1.729 \times 10^{11} \text{ sec}^{-1}$$

we find that

$$k = 3.764 \times 10^4 f$$

The f value for the D_1 line is 2/3, however, so that the absorption coefficient/gram of neutral sodium is $k = 2.51 \times 10^4$ for the D_1 line.

We may use this result to make a rough estimate of the amount of neutral sodium above the photosphere of the sun. At a distance of 2A from the center of $\lambda 5889$, the depression of the line below the continuum is about 1 per cent. If we make the naïve assumption that the light of the continuous spectrum is simply extinguished by the sodium atoms, the actual amount of material may be estimated with the aid of eqn. (19),

$$\frac{I}{I_0} = e^{-k\overline{\rho h}} \sim 1 - k\overline{\rho h} = 0.99, \quad \text{or} \quad k\overline{\rho h} = 0.01$$

Here $\overline{\rho h}$ is the amount of neutral sodium above the photosphere, i.e.,

$$\overline{\rho h} = 4 \times 10^{-7} \text{ grams/cm}^2$$

Even if we allow for the fact that at a temperature 5700° and $P_e = 20$ dynes, 99.92 per cent of all sodium is ionized, the total amount of this metal above the photosphere of the sun would be of the order of 0.5 milligrams/cm^2.

10. Rayleigh and Thomson Scattering

We derived eqn. (43) from a consideration of the scattering of light. An electromagnetic wave of frequency ν_0 falling upon a charged particle sets it in motion with the same frequency. The vibrating particles then act as a new source of waves of the same frequency ν_0. The energy of these new waves is supplied at the expense of the incident wave. We say that the incident wave is *scattered*.

Scattering at frequencies considerably different from resonance frequencies is often important. Two limiting examples are of particular interest:

(a) The frequency of the light is much lower than the resonance frequency, i.e., $\nu \ll \nu_0$ as in the scattering of sunlight by air molecules.

(b) The frequency of the incident light is much greater than the resonance frequency, e.g., the scattering of X rays by the outer bound electrons of an atom or scattering by free electrons.

If we put eqn. (55) in eqn. (43), we find for $(\nu - \nu_0) \gg \gamma$

$$k' = \frac{4\pi\nu\kappa}{c} = \frac{8\pi N \varepsilon^4}{3m^2c^4} \frac{1}{\left[\left(\frac{\nu_0}{\nu}\right)^2 - 1\right]^2} \tag{56}$$

When $\nu_0 \gg \nu$, then the scattering coefficient per cm^3 is

$$k' = \frac{8\pi N \varepsilon^4}{3m^2c^4} \frac{\nu^4}{\nu_0^4} = \left[\frac{8\pi N \varepsilon^4 \lambda_0^4}{3m^2c^4}\right] \frac{1}{\lambda^4} \tag{57}$$

This is the Rayleigh scattering formula. When $\nu_0 \ll \nu$, eqn. (56) gives

$$k' = \frac{8\pi N \varepsilon^4}{3m^2c^4} = 0.6655 \times 10^{-24} N \qquad \text{(Thomson formula)} \tag{58}$$

which is the formula for scattering by free electrons. Note that electron scattering is independent of wave length, all colors being treated impartially, whereas with Rayleigh scattering there is a strong color dependence.

11. The Quantum Theory of Radiation

The quantum picture of the emission and absorption of energy differs markedly from the classical picture. Instead of escaping as continuous emission from an accelerated charge, the energy springs from the atom in a discrete packet or quantum when the atom jumps from one energy level to another.

Emission of energy takes place when an atom passes from a level of higher energy to one of lower energy; absorption, when there is a transition from a lower level to a higher one. The quantitative discussion of the emission and absorption of energy may be approached most suitably by means of the Einstein probability coefficients. Suppose an atom is initially in the excited state n. Unless the transition is forbidden, there is a finite probability, $A(n, n')\,dt$ that in the time dt, the atom will spontaneously (i.e., without any external influence) jump from level n to

level n' with the emission of energy, $h\nu = W_n - W_{n'}$. In other words, the Einstein coefficient $A(n, n')$ expresses the probability that, in a unit time, the atom will undergo the spontaneous downward transition from n to n' with the emission of energy. The total number of downward (n–n') transitions in a time dt will be, $N_n A(n, n')\, dt$, where N_n is the number of atoms in level n.

For example, if 10^8 atoms are maintained in level n by collisions, by absorption of radiation, by recapture from the continuum, etc., and if the A value for the n–n' transition is 10^6, the number of quantum emissions per second will be $10^8 \times 10^6 = 10^{14}$. That is, if the only permitted downward transition is n–n', a particular atom will remain in level n only 10^{-6} sec. We say that the level has a lifetime of 10^{-6} sec.

In actual practice, the A values are of the order of 10^8 or 10^9 sec^{-1}; for the first member of the principal series and in the higher members they may be as little as 10^3. For intercombination lines, the A values may be even smaller.

If the atom is exposed to radiation, two additional phenomena occur. For the moment, let us suppose the radiation to be isotropic and Planckian or "black body" in character. If we wish, we can think of the processes as taking place in an enclosure at some temperature T. The atoms will absorb energy. Transitions from a level n to a higher level n'' will take place at a rate proportional to the number in the level n, N_n, and to the intensity $I_{\nu''}$ of the radiation of frequency $\nu(n, n'')$, viz.,

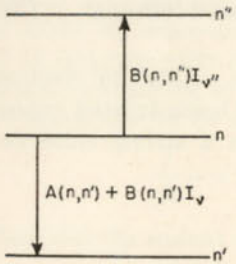

FIG. 11.—TRANSITIONS FROM A LEVEL n

Absorption, spontaneous emission, and induced emission are indicated.

$$N_n B(n, n'') I_{\nu''}$$

where $I_{\nu''}$ is given by Planck's law, eqn. (10), and $B(n, n'')$ is the *Einstein coefficient of absorption*. The second effect of the radiation upon the atom is not so obvious—we refer to the *induced emissions* (more correctly called *negative absorptions*). If an atom is in an excited level n and radiation of frequency $\nu(n, n')$ corresponding to the permitted n–n' transition falls upon it, the likelihood of its cascading to level n' with the emission of $\nu(n, n')$ is increased by an amount dependent upon the intensity of the incident light.

Hence we define a coefficient of negative absorption (induced emission), $B(n, n')$, such that the number of induced emissions of atoms from level n to n' per unit time will be $B(n, n')I_\nu N_n$. The total number of atoms leaving n for n' in a time dt will be

$$\text{(spontaneous plus induced emission)} = N_n[A(n, n') + B(n, n')I_\nu]\, dt \quad (59)$$

We shall avoid confusion if we call the induced emissions negative absorptions, since the induced radiation is put back in the beam in the same direction as the incident radiation. It is not emitted in a random direction as are the spontaneously emitted quanta.

Under conditions of thermal equilibrium, the relative population of the two levels n and n' is given by the Boltzmann formula

$$\frac{N_n}{N_{n'}} = \frac{g_n}{g_{n'}} e^{-\chi_{nn'}/kT} \quad (60)$$

where $\chi_{nn'} = W_n - W_{n'}$ is the energy difference between the two levels n and n', and g_n and $g_{n'}$ are the statistical weights of the two levels, $2J + 1$, $2J' + 1$, where J and J' are the respective inner quantum numbers of level n and n'.

By the principle of detailed balancing, the number of downward transitions from level n to n' must equal the number of upward transitions from n' to n, viz.,

$$N_n[A(n, n') + B(n, n')I_\nu] = N_{n'} B(n'n) I_\nu \quad (61)$$

Let us henceforth write $\nu(nn')$ as $\nu_{nn'}$ or ν and $B(nn')$ as $B_{nn'}$, etc. If we now use eqn. (60) and recall that under conditions of thermal equilibrium I_ν is given by the Planck formula eqn. (10) we have

$$\frac{g_n}{g_{n'}} A_{nn'} = \frac{2h\nu^3}{c^2} B_{n'n} \frac{\left[e^{h\nu/kT} - \dfrac{g_n}{g_{n'}} \dfrac{B_{nn'}}{B_{n'n}}\right]}{e^{h\nu/kT} - 1} \quad (62)$$

In order for $A_{nn'}$ to be independent of the temperature, i.e., a constant of the atom only, we must have

$$g_n B_{nn'} = g_{n'} B_{n'n} \quad (63)$$

and

$$\frac{g_n}{g_{n'}} A_{nn'} = B_{n'n} \frac{2h\nu^3}{c^2} \quad (64)$$

We emphasize that the Einstein coefficients are atomic constants, which may be determined for a given transition by experiment or by quantum mechanical calculation. If one coefficient is known, the others may be found from eqns. (63) and (64). Although we have considered conditions of thermal equilibrium in order to derive the relations between these atomic constants, it is important to realize that the same relations, eqns. (63) and (64), will hold under all conditions.*

* Many authors derive the relations for energy density and hence obtain a different form for eqn. (64). See Prob. 10.

12. The Absorption Coefficient According to Quantum Theory

By quantum mechanics Weisskopf and Wigner derived the rigorous formulae for the shape of the line absorption coefficient. The expression is identical with the classical formula if we replace γ by a new constant Γ and N by Nf, viz.,

$$k' = \frac{\pi e^2}{mc} Nf \frac{\Gamma}{4\pi^2(\nu - \nu_0)^2 + \left(\frac{\Gamma}{2}\right)^2} \tag{65}$$

where the value of Γ must be computed on the basis of the following considerations. Consider an atom in a level n. It can go to a certain lower level n'. The rate at which the atoms in the upper level descend to the lower states is proportional to the sum of the A values of the corresponding transitions, thus

$$dN_n/dt = - N_n \Sigma A_{nn'} = - N_n \Gamma_n \tag{66}$$

$$\Gamma_n = \Sigma A_{nn'} \tag{67}$$

By integration we obtain

$$N_n = N_n^0 e^{-\Gamma_n t} \tag{68}$$

where N_n^0 denotes the number of atoms in level n at $t = 0$. Now Γ_n is simply the reciprocal of the mean lifetime T_n, of an atom in the level n, i.e.,

$$\Gamma_n = 1/T_n \tag{69}$$

We have been neglecting the fact that the lower levels themselves may have finite lifetimes. A more exact treatment of the problem shows that while eqn. (69) is valid for the resonance line, the absorption coefficients for subordinate lines require a damping constant given by

$$\Gamma_{nn'} = 1/T_n + 1/T_{n'} = \Gamma_n + \Gamma_{n'} \tag{70}$$

or the sum of the reciprocal lifetimes of the upper and lower levels. Hence as soon as the A's are known, we can calculate the lifetime for pure radiation damping.

At high temperatures, the radiation density becomes large and the atoms in a level n may escape in considerable numbers by negative absorptions, excitations to higher levels, and by ionization as well as by spontaneous emission. Hence these additional processes will play a role in fixing Γ_n and we must write:

$$\Gamma_n = \sum_{n'} A_{nn'} + \sum_{n'} B_{nn'} I(\nu_{nn'}) + \sum_{n''} B_{nn''} I(\nu_{nn''}) \tag{71}$$

where the first term refers to spontaneous transitions to lower levels, the second to negative absorptions to lower levels, and the third to

ordinary absorption processes. With the aid of eqns. (10), (63), (75), and (64), we find

$$\Gamma_n = \frac{8\pi^2 e^2}{mc} \left\{ \sum \frac{g_{n'}}{g_n} \lambda^{-2} f_{n'n} (1 - e^{-h\nu/kT})^{-1} + \sum \lambda^{-2} f_{nn''} (e^{h\nu/kT} - 1)^{-1} \right\} \tag{72}$$

13. The Interpretation of Natural Line Broadening

It is evident that the process of line broadening must occur in two different ways in the two theories.

Classical broadening occurs because a bound electron can oscillate in frequencies on either side of resonance, much as a radio set will pick up a program even if it is not tuned precisely to the output frequency of the broadcasting station.

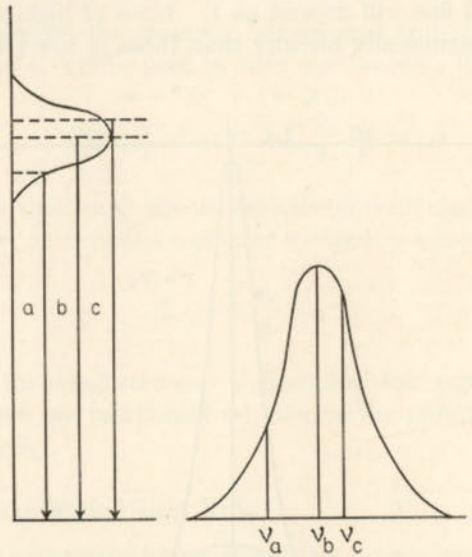

FIG. 12.—THE RELATION BETWEEN LEVEL BREADTH AND LINE PROFILE FOR A RESONANCE LINE

The transitions from three "substates" of the broadened upper level, denoted by *a*, *b*, and *c*, are correlated with three frequencies ν_a, ν_b, and ν_c in the resonance line.

There is another way of looking at classical broadening. A radiating atom emits a damped wave which gradually dies out, or a wave of fixed frequency ν for a short-time interval. If this wave is subjected to a Fourier analysis, it is found that it is not monochromatic but consists of a narrow range of frequencies whose intensity distribution is given by an expression similar to eqn. (50). That is, if the wave trains from a classical oscillator are analyzed by a spectrograph of infinite resolving power, each spectrum line gives a broadened profile.

Although, in the quantum picture, each emitted quantum has a precise energy E and frequency ν, the atomic energy levels themselves are slightly fuzzy. According to the Heisenberg uncertainty principle, if an atom has a lifetime, Δt, in a certain level, the level will have an energy breadth ΔE, such that

$$\Delta E\, \Delta t \sim h$$

The lifetime of the ground level is very long; hence ΔE is very small and the level is quite sharp. An excited level for which $A = 10^8$ has a $\Delta t = 1/A = 10^{-8}$ which is small. Hence ΔE will be relatively large. Since the transition may take place from any part of the broadened level, the observed spectral line will be slightly widened (see Fig. 12). Unlike lines emitted by classical oscillators, whose half-breadths as measured on a wave length scale are always the same, the natural breadth of a real spectral line will depend on Γ. Lines of high transition probability will be intrinsically broader than those of low transition probability.

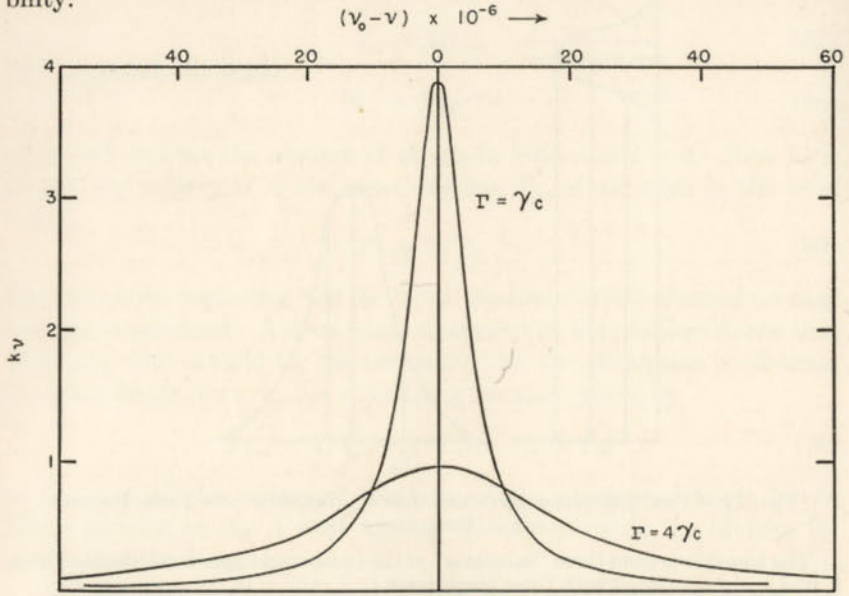

FIG. 13.—EFFECT OF THE DAMPING CONSTANT UPON A LINE ABSORPTION COEFFICIENT

14. The Relation Between the Einstein Coefficients and Oscillator Strengths

The relation between the f's and the Einstein A's or B's is useful for some problems. The energy absorbed per cm³ per second by atoms in level n' is

$$N_{n'} B_{n'n} I_\nu h\nu \tag{73}$$

and this must equal the energy absorbed as computed in terms of the conventional absorption coefficient, viz.,

$$N_{n'} \bar{\alpha}_\nu 4\pi I_\nu \overline{\Delta\nu} = 4\pi I_\nu N_{n'} \frac{\pi e^2}{mc} f_{n'n} \tag{74}$$

where we have averaged the absorption coefficient, α_ν, over the spectral line of effective width $\overline{\Delta\nu}$. Hence

$$B_{n'n} = \frac{\pi e^2}{mc} f_{n'n} \frac{4\pi}{h\nu} \tag{75}$$

and

$$A_{nn'} = \frac{g_{n'}}{g_n} \frac{8\pi^2 e^2 \nu^2}{mc^3} f_{n'n} = 3\frac{g_{n'}}{g_n} f_{n'n}\gamma_c = 3\frac{(2J'+1)}{(2J+1)} f_{n'n}\gamma_c \tag{76}$$

The relation between the quantum mechanical and classical damping constants Γ_n and γ_c will be used in later discussions. We can write

$$\Gamma_n = \sum_{n'} A_{nn'} = 3\sum \frac{g_{n'}}{g_n} f_{n'n}\gamma_c \tag{77}$$

Although we shall deal almost exclusively with oscillator strengths as defined above, an emission oscillator strength is sometimes used, viz.,

$$f'_{nn'} = -\frac{g_{n'}}{g_n} f_{n'n} \tag{78}$$

which is given for completeness. Unless otherwise explicitly specified, whenever f values are mentioned we refer to the ordinary (absorption) oscillator strength f.

15. The Thomas-Kuhn Sum Rule

The oscillator strengths for an atom obey a very important relationship called the Thomas-Kuhn sum rule. If we sum f over all possible transitions between all possible configurations, we should obtain the number of electrons in the atom, viz.,

$$\Sigma f(nl; n'l') = N \tag{79}$$

where N is the number of electrons in the atom or ion. In iron for example, the exact sum of f values over all X-ray and optical transitions will be 26.

If the electrons in the inner shell are so tightly bound that we need not consider interactions between them and the outer (valence) electrons, we can write

$$\Sigma f(nl; n'l') = r \tag{80}$$

where r is the number of valence electrons and the summation is carried out over all levels to which transitions can take place. Expressing our results in terms of the absorption oscillator strengths,

$$\sum_{n''} f_{nn''} - \sum \frac{g_{n'}}{g_n} f_{n'n} + \int_0^\infty f_{n\kappa}\, d\kappa = r \tag{81}$$

The first term written on the left represents the absorptions from the level n and the summation is carried out over all levels with $n'' > n$. The second term represents the emissions and the summation is carried out over all levels with $n' < n$, while the third term represents the bound-free absorptions in which the electron is lost from the atom. We shall explain the use of eqn. (81) with an application to the subordinate lines of helium. Care must be exercised in the choice of the value of r, e.g., for helium, r is 2 for the principal series since there are two 1s electrons in the ground level and either of these may jump during a transition to a higher level. Since only one of these electrons will exist in a higher level at any one time, the f values of subordinate lines should sum to unity as for hydrogen.

If the f values for single multiplets are given and it is required to find the appropriate f for the whole set of transitions between the two configurations involved, we do not simply form the sum of the f's. Rather, we calculate the sum of the products of the weights of each term and the f value of each multiplet arising from it and then divide by the weight of the whole configuration. Consider a line of the Balmer series. It is composed of $2^2S - n^2P$, and $2^2P - n^2S$, $2^2P - n^2D$ doublets. The weight of ^2S term is 2, that of ^2P term is 6. Hence

$$\begin{aligned} f_{2n} &= \tfrac{1}{8}[2f(2,0;n,l) + 6f(2,l;n,0) + 6f(2,l;n,2)] \\ &= \frac{1}{g_2}\sum_{l,l'} g_{2l} f(2,l;n,l') \end{aligned} \tag{82}$$

To illustrate some of these formulae, let us consider He I whose f values have been computed by Goldberg. Reference to the He I term diagram (Fig. 4 of Ch. 2) will be helpful here.

The f value for the $2^3P - 4^3D$ multiplet giving the unresolved λ4471 line is 0.129; we are to compute the A value. The statistical weights of the ^3P and ^3D terms are 9 and 15 respectively. Employing eqn. (76), we get $A = 2.59 \times 10^7$.

The damping constant for the line is calculated as follows: Atoms may escape from $4(^3D)$ to $2(^3P)$ and $3(^3P)$ and from the lower $2(^3P)$ level to $2(^3S)$ with the emission of λ10830 (see term diagram). Calculation shows a negligible number of transitions to $3(^3P)$. Hence

$$\Gamma_{4471} = A(4^3D - 2^3P) + A(2^3P - 2^3S) = (2.59 + 1.03) \times 10^7 = 3.62 \times 10^7$$

For the $2^3S - 2^3P$ line, $\Gamma = A(2^3S - 2^3P) = 1.03 \times 10^7$, since the lower level is metastable, i.e., it has an infinite lifetime. Similarly $A = \Gamma$ for the resonance line $(1^1S - 2^1P)$ for which $A = 2.34 \times 10^9$. Further illustrations are worked out in Chapter 8.

The sums of the f values provide an interesting illustration of the Thomas-Kuhn sum rule. For the $2^1S - n^1P^0$ series, Goldberg finds the sum of the f values for discrete transitions to be 0.666 while Huang finds the integral of the f value over the continuum to be 0.402. Hence Σf will be 1.068 instead of 1.00. The f values for the lines are in need of improvement.

Note that since the 2^1S level is metastable, there are no allowed downward transitions, i.e., $f' = 0$. From the 2^1P level, on the other hand, an atom may escape by going to n^1D or n^1S (with the absorption of energy) or by going to the ground ^1S level with the emission of energy. Goldberg finds

$$f(2^1P - n^1D) = 0.967 \text{ (lines)} + 0.157 \text{ (continuum)} = 1.124$$

Downward jumps to the singlet levels, 2^1S and 1^1S, must be considered. $f(2^1P - 2^1S) = 0.389$, $(2J' + 1)/(2J + 1) = 1/3$, so that the emission oscillator strength $f' = -\dfrac{0.389}{3} = -0.130$. Similarly, for the $2^1P - 2^1S$ transition, $f' = -0.116$. Hence we have,

$$0.967 + 0.157 - 0.130 - 0.116 = 0.878$$

instead of unity. The discrepancy here arises partly from the fact that Goldberg has not allowed for the $2^1P - n^1S$ transitions.

16. Calculation of f Values

For atoms of simple structure, notably hydrogen and helium, or the alkali metals, it is practical to calculate A or f by quantum mechanics.

The f values for hydrogen may be computed exactly by the formula

$$f_{n'n} = \frac{2^6}{3\sqrt{3}\pi}\frac{1}{g_{n'}}\frac{1}{\left[\dfrac{1}{n'^2} - \dfrac{1}{n^2}\right]^3}\left|\frac{1}{n^3}\frac{1}{n'^3}\right| g \tag{83}$$

Here $g_{n'} = 2n^2$ denotes the statistical weight of the lower level. It is not to be confused with the Gaunt factor g, a correction required by quantum mechanics. This factor has been tabulated by Menzel and Pekeris.

The problem for helium cannot be solved explicity and resort must be had to approximation techniques such as the variation method, which Goldberg has employed for the most important transitions in this atom. It is hoped that similar techniques may be applied to elements such as C, N, O, or Ne in various stages of ionization.

Quantum mechanical calculations have also been made for selected transitions in a few metals such as sodium, calcium, and magnesium, but for the most part we must content ourselves with relative f values for certain lines in the spectrum.

The Einstein A value for a transition between a level characterized by quantum numbers $nlLSJ$ (abbreviated simply as αJ) and one with quantum numbers $n'l'L'S'J'$ (denoted as $\alpha' J'$) may be expressed in terms of a parameter called the strength, S_1, of the line.

$$A(\alpha J\,;\,\alpha' J') = \frac{1}{2J+1}\frac{64\pi^4\nu^3}{3hc^3} S_1(\alpha J\,;\,\alpha' J') \tag{84}$$

where ν is the frequency of the line, and $g = 2J + 1$ is the statistical weight of the upper level. The absolute strength S_1 depends on both the radial and angular charge distribution within the atom, and consists of two factors, viz.:

$$S_1 = S\sigma^2 \tag{85}$$

Here σ^2 depends on the radial charge distribution in the upper and lower levels. At least, to the first approximation, it will be the same for all lines and multiplets connecting a given pair of configurations n_1l_1 and n_2l_2.

The factor S can be calculated for atoms in pure LS or pure jj coupling. Hence it is possible to obtain the relative strengths of all lines and multiplets belonging to a given pair of configurations $(n_1l_1;\ n_2l_2)$. In Section 17 we shall see how the factor S is to be found for LS coupling. If, in addition, the σ^2 factor can be calculated we may obtain the A or f values for the lines in question.

17. Calculation of Relative Strengths in *LS* Coupling

Before we turn to the formulae and tables for calculations of line strengths, let us summarize some important spectroscopic definitions.

The quantities $nlSLJM$ (where nl is given for all electrons and M is the magnetic quantum number, i.e., the projection of J on the magnetic field) define a *Zeeman state* of the atom.

The quantities $nlSLJ$ define a *level* which includes $2J + 1$ states, e.g., $2p^2\ {}^3P_2$.

The quantities, $nlSL$, define an *atomic term*, the whole set of $(2S + 1)(2L + 1)$ states characterized by the given values of L and S, e.g., $2p^2\ {}^3P$.

A *polyad* is a set of terms of the same multiplicity based on the same parent term by the addition of one electron to an atom, e.g., $p^3d(^2D)$ plus a d electron gives ${}^1S{}^1P{}^1D{}^1F{}^1G$ (one polyad) and ${}^3S{}^3P{}^3D{}^3F{}^3G$ (another polyad).

(1) Transitions between the individual states into which a given pair of levels is resolved by a magnetic field are called *Zeeman components*.

(2) A transition between 2 levels, e.g., ${}^3P_2 - {}^3D_3$, is called *a spectral line*.

(3) The totality of transitions between 2 terms, e.g., ${}^3P - {}^3D$, gives a *multiplet*.

(4) A *supermultiplet* comprises the totality of transitions between two polyads.

(5) All the jumps between two configurations constitute a *transition array*.

If the atom is in good LS coupling, relative strengths, and therefore relative f values, can be obtained for all the lines in a whole transition array. In the calibration of the intensities of absorption lines in terms of the numbers of atoms, it is useful to have a large number of lines whose relative f values are known, even if the absolute f values cannot be obtained.

We calculate S in two steps. First we find the strength of the line in question referred to that of the whole multiplet, $s/\Sigma s$, and then we compute the strength of the entire multiplet itself.

Even before the advent of quantum mechanics, Sommerfeld, Honl, Russell, and Kronig derived formulae for the relative strengths within an LS multiplet. It is convenient to look up the relative strengths in tables such as those computed by White and Eliason or by Russell.

In the White-Eliason plan the relative strength is tabulated for different values of L with J as argument.* The individual tables are then grouped according to different values of the spin. The strongest line of each multiplet is taken as 100. We find it more useful to have $s/\Sigma s$, i.e., the strength of each line is given in terms of the strength of the whole multiplet. Table 1 gives $\log \Sigma s/s$.

As an example, let us compute the strengths for a ${}^4P - {}^4D$ multiplet. The terms are quartets, $S = 3/2$, hence we use the table with spin $= 3/2$ and choose the box with $L_1 = 1$, $L_2 = 2$. The values of $\log \Sigma s/s$ from Table 1 are:

		${}^4D$			
		1/2	3/2	5/2	7/2
${}^4P$	1/2	1.08	1.08		
	3/2	1.77	0.97	0.68	
	5/2		2.00	1.05	0.40

e.g., for ${}^4P_{3/2} - {}^4D_{5/2}$, $\log s/\Sigma s = -0.68 = \bar{9}.32$ or $s/\Sigma s = 0.21$. That is, the 3/2–5/2 line contributes 0.21 of the total strength of the multiplet.

* These tables may also be used to compute the strengths of lines in jj coupling since the Sommerfeld, Russell, etc., formulae remain valid if we replace L by j_2 and S by j_1, and take j_1 as the quantum number that does not change during a transition.

TABLE 1. $\log \frac{\Sigma s}{s}$

DOUBLET TERMS (Spin = 1/2)

		P 1/2	P 3/2	D 3/2	D 5/2	F 5/2	F 7/2	G 7/2	G 9/2	H 9/2	H 11/2
S	1/2	0.48	0.18								
P	1/2	0.65	0.95	0.48							
	3/2	0.95	0.25	1.18	0.22						
D	3/2			0.44	1.40	0.40					
	5/2			1.40	0.25	1.54	0.24				
F	5/2					0.39	1.70	0.37			
	7/2					1.70	0.26	1.80	0.25		
G	7/2							0.36	1.92	0.35	
	9/2							1.92	0.27	2.00	0.26

TRIPLET TERMS (Spin = 1)

		P 0	P 1	P 2	D 1	D 2	D 3	F 2	F 3	F 4	G 3	G 4	G 5
S	1	0.95	0.48	0.26									
P	0		0.95		0.95								
	1	0.95	1.08	0.86	1.08	0.60							
	2		0.86	0.38	2.25	1.08	0.33						
D	1				0.82	1.30		0.70					
	2				1.30	0.64	1.29	1.42	0.53				
	3					1.29	0.38	3.05	1.42	0.37			
F	2							0.68	1.57		0.62		
	3							1.57	0.55	1.57	1.68	0.50	
	4								1.57	0.40	3.40	1.68	0.39
G	3										0.61	1.80	
	4										1.80	0.52	1.80
	5											1.80	0.41

TABLE 1 (*Continued*)

QUARTET TERMS

(Spin = 3/2)

		P 1/2	P 3/2	P 5/2	D 1/2	D 3/2	D 5/2	D 7/2	F 3/2	F 5/2	F 7/2	F 9/2	G 5/2	G 7/2	G 9/2	G 11/2
P	1/2	1.55	0.86		1.08	1.08										
	3/2	0.86	1.36	0.82	1.77	0.97	0.68									
	5/2		0.82	0.46		2.00	1.05	0.40								
D	1/2				1.30	1.30			1.00							
	3/2				1.30	1.10	1.15		1.40	0.80						
	5/2					1.15	0.76	1.24	2.52	1.28	0.61					
	7/2						1.24	0.46		2.70	1.39	0.45				
F	3/2								0.94	1.55			0.84			
	5/2								1.55	0.83	1.42		1.64	0.72		
	7/2									1.42	0.66	1.52	3.00	1.52	0.59	
	9/2										1.52	.49		3.00	1.64	0.48
G	5/2												0.83	1.74		
	7/2												1.74	0.74	1.62	
	9/2													1.62	0.63	1.74
	11/2														1.74	0.50

TABLE 1 (*Continued*)

QUINTET TERMS

(Spin = 2)

		P 1	P 2	P 3	D 0	D 1	D 2	D 3	D 4	F 1	F 2	F 3	F 4	F 5	G 2	G 3	G 4	G 5	G 6
P	1	1.28	0.82																
	2	0.82	1.55	0.81															
	3		0.81	0.51															
D	0	1.40				1.40				1.24	1.54				1.03	1.72			
	1	1.05	1.52		1.40	2.00	1.16			1.54	1.15	1.37			1.72	0.96	1.56		
	2	1.16	0.93	1.89		1.16	1.30	1.10			1.37	0.95	1.35			1.56	0.84	1.55	
	3		0.73	1.03			1.10	0.85	1.22			1.35	0.74	1.50			1.55	0.71	1.72
	4			0.44				1.22	0.52				1.50	0.55				1.72	0.57

		P 1	P 2	P 3	D 0	D 1	D 2	D 3	D 4	F 1	F 2	F 3	F 4	F 5	G 2	G 3	G 4	G 5	G 6
F	1	1.40	1.05	1.16	1.40	1.40	1.10			1.24	1.54				1.07				
	2		1.52	0.93		2.24	1.24	2.24		1.54	1.15	1.37			1.62	3.00			
	3		0.93	1.89		1.24	0.86	1.22	2.52		1.37	0.95	1.35		0.92	1.46	2.70		
	4		0.73	1.03			0.86	0.67	1.37			1.35	0.74	3.05		0.79	1.45	3.05	
	5			0.44				1.22	0.50				1.50	1.60			0.66	1.60	
														0.54				0.54	

		F 1	F 2	F 3	F 4	F 5	G 2	G 3	G 4	G 5	G 6
G	2	1.07	1.62	3.00			1.03	1.72			
	3		0.92	1.46	2.70		1.72	0.96	1.56		
	4			0.79	1.45	3.05		1.56	0.84	1.55	
	5				0.66	1.60			1.55	0.71	1.72
	6					0.54				1.72	0.57

TABLE 2

RELATIVE MULTIPLET STRENGTHS IN LS COUPLING

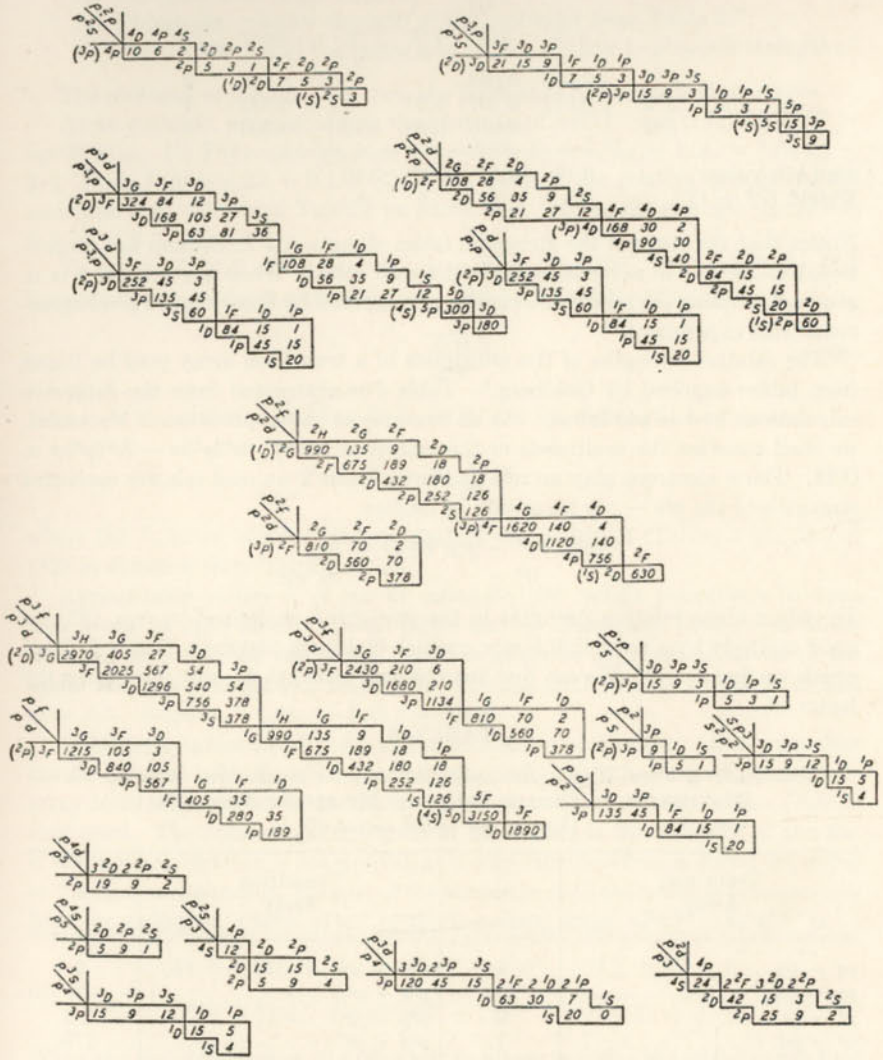

For checks on the calculations, the *sum rules* are of great importance. For a given multiplet these are:

(1) The sum of the strengths of all the lines of a multiplet that end on a common final level is proportional to $2J + 1$ for the level.

(2) The sum of the strengths of all the lines of a multiplet that start from a common initial level is proportional to the weight, $2J + 1$, of the initial level.

As an example, consider the $^4P - {}^4D$ multiplet. In terms of $s/\Sigma s$, the box now looks like,

		^4D 1/2	3/2	5/2	7/2	Sum	Weight $(2J+1)$
	1/2	0.083	0.083			0.166	2
^4P	3/2	0.017	0.107	0.21		0.334	4
	5/2		0.010	0.09	0.40	0.500	6
Sum of s values		0.10	0.20	0.30	0.40		
Weight $(2J+1)$		2	4	6	8		

Notice that the sums of the strengths taken along a row or column are proportional to $2J + 1$ in accordance with the sum rules. When the multiplet is in good LS coupling the relative strengths, s, computed by theory are in good agreement with experiment.

The relative strengths of the multiplets of a transition array may be found from tables supplied by Goldberg.* Table 2 is abstracted from the extensive calculations he has published. As an example of the application of his tables, we shall consider the multiplets of the transition array, $2s^22p^23s - 2s^22p^23p$ in O II. The s^2 electrons play no role and from Table 2 we read relative multiplet strengths of the $p^2s - p^2p$ transition as follows:

$$p^2s(^3P)^4P - p^2s(^3P)^4D = 10$$
$$^4P - \quad ^4P = 6, \text{ etc.}$$

To reduce these relative strengths to the strength S as defined by eqn. (85) we must multiply by a reduction factor a which Goldberg has given (Table 3) from which we find $a = 2$. We can find the absolute strength S_1, only if we know the factor σ^2.

TABLE 3

THE FACTOR a BY WHICH RELATIVE MULTIPLET STRENGTHS ARE TO BE MULTIPLIED TO OBTAIN ABSOLUTE MULTIPLET STRENGTHS†
(Except for radial factor σ^2)

Transition Array	a	Transition Array	a
$ps - pp$	1	$s^2p^2 - sp^3$	2
$pp - pd$	1/2	$p^3s - p^3p$	1
$p^2 - ps$	2	$p^3p - p^3d$	1/2
$p^2 - pd$	1	$p^3d - p^3f$	1/6
$pd - pf$	1/3	$p^4 - p^3s$	1
$p^2s - p^2p$	2	$p^4 - p^3d$	2
$p^2p - p^2d$	1	$p^5 - p^4s$	2
$p^2d - p^2f$	1/3	$p^5 - p^4d$	10
$p^3 - p^2s$	1		
$p^3 - p^2d$	5		

† From L. Goldberg, *Astrophysical Journal* (University of Chicago Press) **84**, 11, 1936.

* (Ref. 1) *Ap. J.* **82**, 1, 1935. The reduction factors "a" are given in Table 1 (Ref. 2), *Ap. J.* **84**, 12, 1936.

The steps for calculating the strength S of a line are as follows:

(1) Compute $s/\Sigma s$ from Table 1.
(2) Obtain the relative strength of the multiplet from Table 2.*
(3) From Table 3 find the factor a to reduce relative to absolute strengths.*

The strength of the line S is then the product of the three factors above.

As an example, let us compute the strength of λ4317.16 of O II, $3s(^3P)^4P - 3p(^3P)^4P_{3/2}$. (1) For a quartet, $S = 3/2$. With $L_1 = 1$, $L_2 = 1$, $J_1 = 1/2$, $J_2 = 3/2$, Table 1 gives $s/\Sigma s = 0.14$. (2) From Table 2, the relative strength of the multiplet is 6. (3) From Table 3 we find $a = 2$. Hence the strength of the line is $0.14 \times 6 \times 2 = 1.68$.

To get the f value of the line we now employ eqns. (76), (84), and (85). If λ is measured in angstrom units (10^{-8} cm) and S_1 in atomic units ($a_0^2\varepsilon^2$)

$$f = \frac{304}{g'\lambda} S_1 \tag{86}$$

Here a_0 is the radius of the first Bohr orbit, ε is the electronic charge, and

$$S_1 = S_0 \frac{s}{\Sigma s} \sigma^2 \tag{87}$$

where the S_0 factor refers to the strength of the multiplet (Tables 2 and 3) and $s/\Sigma s$ is obtained from Table 1.

Approximate values of σ^2 can be calculated for certain transitions between high levels in light atoms. D. R. Bates and A. Damgaard have given tables from which σ may be computed from the effective quantum numbers of the upper and lower levels of a transition. For the 4317.16 O II line, $g' = 2$, and $\sigma^2 = 5.5$. Since $S = 1.68$, we find $f = 0.325$.

Goldberg's tables cover most of the multiplets of interest. Other examples can be handled with the aid of certain sum rules. All the lines of a transition array that originate in (or terminate on) a given level constitute the J-file of that level. The sum of the strengths of these lines is the strength of the file. If the jumping electron is not equivalent to any other electron in either the initial or the final configuration, the sum of the strengths of all the multiplets originating from, or ending in, a term $nl^kn'l'$ of the transition array, $nl^kn'l' - nl^kn''l''$ is

$$(2S+1)(2L+1)(l'+1)(2l'+3)\sigma^2 \qquad \text{if } l' = l'' - 1$$

or

$$(2S+1)(2L+1)(l')(2l'-1)\sigma^2 \qquad \text{if } l' = l'' + 1$$

When the jumping electron is equivalent to others in either the initial or the final configuration, we may employ other sum rules given by Menzel.

As an example of the J-file sum rule consider the $2s2p3s\,{}^4P - 2s2p3p\,{}^4P$, multiplet of N III at λ3360. The only term in the $2s2p3s$ configuration with which the $3p^4P$ term can combine is the ^4P term, as transitions to ^2P terms are excluded in good LS coupling. Hence the sum of the strengths of all the transitions of the $2p3s - 2p3p$ array originating in the $3p^4P$ term is simply the strength

* Goldberg gives more complete tables, *Ap. J.* **82**, 1, 1935; **84**, 11, 1936.

of the λ3360 multiplet. For the upper level $S = 3/2$, $L = 1$, and $l = 1$; hence $S = 12$.

The validity of the foregoing methods depends on how well the atom in question follows LS coupling. For certain light atoms, such as carbon or oxygen, the results are probably good first approximations. For other atoms such as neon this is no longer true. The heavier elements usually show marked deviations from LS coupling and hence they have strong lines connecting terms of different multiplicity (intercombination lines).

It appears that the relative strengths of different multiplets belonging to a configuration array become affected first by deviations from LS coupling. The relative line strengths within a multiplet, however, become sensibly distorted only with appreciable deviations from LS coupling.*

18. Experimental Determinations of f Values

In many of the complex atoms, such as iron, the deviations from LS coupling become very large, accurate f values cannot be calculated by theoretical means, and recourse must be had to empirical determinations of line strengths and f values.

Dorgelo and others have measured relative f values within multiplets from emission line intensities. Other workers have measured the lifetimes of excited levels. Magneto-rotation effects (rotation of the plane of polarization in a medium placed in a magnetic field) and measures of the index of refraction of a gas in the neighborhood of an absorption line yield values of Nf where N is the number of atoms in the vapor column capable of absorbing the line. If N is known, f may be determined.

R. B. and A. S. King and their co-workers measured relative f values from the absorptions produced in thin layers of the absorbing gas. Then the amount of energy subtracted from the beam by the gas is very nearly proportional to the f value.

Consider a weak absorption line upon a continuous spectrum. We express its intensity as an equivalent width W, which is the width of the perfectly black line of rectangular profile that would remove the same amount of energy from the spectrum. We measure I_ν/I_0 at each point in the line profile and define

$$W_\nu = \int \frac{I_0 - I_\nu}{I_0}\, d\nu \tag{88}$$

* Calculations of line strengths wherein deviations from LS coupling are taken into account have been made by W. M. Gottschalk for the $3d^74s - 3d^74p$ configuration in Fe I. See *Ap. J.* **108,** 326, 1948. The relative strengths show fair agreement with the King relative f values, suggesting that much valuable information may be obtainable by this method for atoms in higher stages of ionization.

the equivalent width in frequency units. A beam of light passing through an absorbing medium of length h and density ρ with an absorption coefficient k will be extinguished according to the law

$$I = I_0 e^{-hk\rho} = I_0 e^{-hN\alpha}$$

where N is the number of atoms/cm³ in the tube. Both k and α depend on the frequency. If the optical thickness of the layer is small,

$$I = I_0(1 - hN + \text{small terms})$$

then by eqn. (52),

$$\rho h \int k\, d\nu = hN \int \alpha\, d\nu = hN \frac{\pi\varepsilon^2}{mc} f = \int \frac{I_0 - I_\nu}{I_0}\, d\nu = W_\nu$$

In wave length units,

$$W_\lambda = \frac{\lambda_0^2}{c} W_\nu \tag{89}$$

and

$$W_\lambda = hN\lambda_0^2 \frac{\pi\varepsilon^2}{mc^2} f \tag{90}$$

Hence if N can be found from the vapor pressure in the tube and W_λ can be measured, we may obtain the absolute value of f. If N is not known, only relative f values may be found. We emphasize that weak lines must be used.

In practice, the ideal condition of a layer of absorbing vapor whose optical depth at all wave lengths is much less than 1 is difficult to fulfill and allowance must be made for deviations from linearity in the W–Nf relationship (curve of growth). Fortunately this relationship is well known (see Ch. 8). Very strong lines yield an estimate of $Nf\Gamma$; hence Γ must be estimated as well as N, or if N and f are known from other data we can evaluate Γ. The fact that Γ depends on the density complicates the problem.

R. B. King determined absolute f values for iron lines from specially purified samples of this metal heated in a quartz tube in an electric furnace at an accurately known temperature. The vapor pressure of iron is known as a function of the temperature; hence the number of gaseous iron atoms in the quartz tube may be found. If the vacuum furnace is placed between a tungsten filament lamp and the spectrograph, the continuous spectrum formed by the lamp is crossed by dark lines arising from the iron vapor. If the vapor pressure of the metal is not known, it is possible to obtain only relative f values.

More recently, H. Kopfermann and G. Wessel at Göttingen have determined absolute f values by an experimental procedure involving the use of an iron-atom stream as an absorber. They find f values about

three times those obtained by King. Such discrepancies emphasize the need for further experimental work on the determination of both absolute and relative f values.

Attempts have been made to determine relative strengths from the intensities of the dark lines in the solar spectrum with the aid of the solar curve of growth (cf. Ch. 8) and from emission line intensities observed in the flash spectrum of the sun at times of solar eclipses (cf. Ch. 9). Although these astrophysical methods yield some results of interest, the uncertainties in our knowledge of certain basic parameters such as damping constants, excitation temperatures, etc., are such as to prevent us from getting any accurate information. Emphasis must be placed on laboratory methods and theoretical calculations.

19. The Continuous Absorption and Emission of Energy

For a discussion of continuous spectra of the sun and stars, of the gaseous nebulae, and of the physical state of atoms and molecules in interstellar space, we must study the continuous absorption of atoms and ions.

We have already mentioned Rayleigh and Thomson scattering as examples of processes wherein radiation is simply scattered by electrons. Transitions from one energy state of the atom to another are not involved. In the present context we are interested in processes that may be described by the general term of absorption, such as the photoionization of atoms from various discrete levels or the photodissociation of molecules. The inverse process is recombination with the release of the excess energy as radiation.

As an important astrophysical example we shall discuss in some detail the continuous absorption and emission of energy by hydrogen. We recall from Chapter 2 that the atom may be photoionized while occupying any one of its permitted levels. In a discrete transition, an atom may absorb only a particular frequency ν corresponding to the energy difference between the two levels. In photoionization processes, any amount of energy greater than that necessary to detach the electron may be absorbed.

For example, we have seen that the Balmer lines represent transitions from the second to higher levels. Toward the limit of the series they crowd closer and closer together until they coalesce into a continuum near λ3650. This continuous absorption beyond the Balmer limit corresponds to the photoelectric detachment of electrons from the second level. Similarly, the photoionizations from the third level produce a continuous absorption beyond the limit of the Paschen series in the infrared. This absorption extends into the visual region of the spectrum. In fact, in the visual region of the spectra of A- and B-type stars, the

continuous absorption comes mainly from the photoionization from third and higher levels. In the far ultraviolet there occurs the continuous absorption at the limit of the Lyman series which sets in at a frequency corresponding to 13.54 volts energy, i.e., $\lambda = 912\text{A}$, or $\bar{\nu} = 109{,}679\ \text{cm}^{-1}$.

Thus there is a continuous absorption associated with each of the hydrogen series, Lyman, Balmer, Paschen, Brackett, etc. In each of these continua, the absorption is strongest at the series limit and falls off gradually to the shorter wave lengths. We refer to these photoionizations as *bound-free transitions*. We shall now show how the absorption coefficient per atom in an excited level n' may be computed with the aid of eqn. (83) which gives explicitly the f value for a bound-bound transition. If a hydrogen atom in an excited level n absorbs a quantum of energy $h\nu$, that is greater than the energy necessary to detach the electron from the atom, the liberated electron will fly away with a velocity v given by

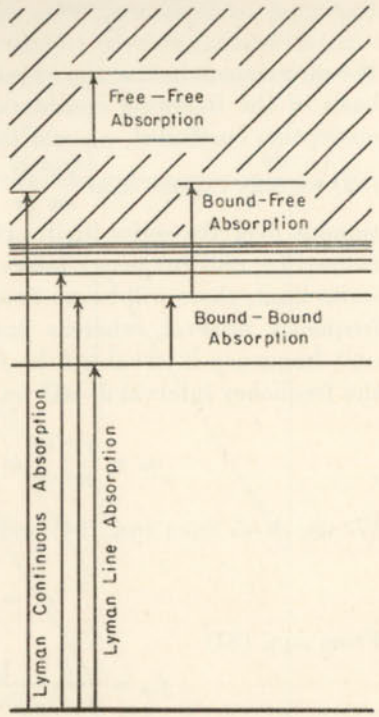

FIG. 14.—BOUND-BOUND, BOUND-FREE, AND FREE-FREE TRANSITIONS IN HYDROGEN

$$\frac{1}{2}mv^2 + \frac{hR}{n^2} = h\nu \qquad (91)$$

since the energy of any level n is $-hR/n^2$ (referred to the ionized atom as zero). In electron-volt units, hR is 13.54 ev. R is the Rydberg constant, $2\pi^2\varepsilon^4 m/h^3$, in the Balmer formula. (See Ch. 2, p. 24.) Then eqn. (11) of Ch. 2 becomes:

$$\nu = RZ^2\left(\frac{1}{n^2} - \frac{1}{n''^2}\right), \quad (n'' > n) \qquad (92)$$

where Z is the atomic number. Menzel and Pekeris suggested that this formula be applied to the transitions involving the continuum by means of the substitution,

$$n'' \to i\kappa$$

where κ is a real but not necessarily integral quantum number. We take the real part of the resultant expression. Thus

$$\nu = RZ^2\left(\frac{1}{n^2} + \frac{1}{\kappa^2}\right) \qquad (93)$$

and κ is defined by means of the relations

$$\frac{hRZ^2}{\kappa^2} = \frac{1}{2}mv^2, \quad \frac{-2hRZ^2}{\kappa^3}d\kappa = mv\,dv = h\,d\nu \tag{94}$$

We may calculate the absorption coefficient for the continuum on the basis of the following considerations. Since the relation between the absorption coefficient, α_ν, and the oscillator strength f is given by eqn. (52) we may express α_ν as $\frac{\pi e^2}{mc}\frac{df}{d\nu}$. The absorption coefficient will be continuous over the series limit. Hence, we must consider the f value as defined for unit frequency interval. Just to the low frequency side of a series limit, there will be Δn lines of mean oscillator strength f per unit frequency interval, whereas just on the violet side the f value per unit frequency interval will be $f\,\Delta\kappa$. Thus the f value corresponding to the frequency interval $d\nu$ will be $df = f\,d\kappa$. Hence

$$\alpha_\nu = \frac{\pi e^2}{mc}\frac{df}{d\nu} = \frac{\pi e^2}{mc}\frac{df}{d\kappa}\frac{d\kappa}{d\nu} = \frac{\pi e^2}{mc}f\frac{d\kappa}{d\nu} \tag{95}$$

We use $d\kappa/d\nu$ from eqn. (94) and drop the minus sign to obtain

$$\alpha_\nu = \frac{\pi e^2}{mc}f\frac{\kappa^3}{2RZ^2} \tag{96}$$

From eqn. (83)

$$f_{n\kappa} = \frac{2^6}{3\sqrt{3}\pi}\frac{1}{2n^2}\frac{1}{\left(\frac{1}{n^2}+\frac{1}{\kappa^2}\right)^3}\left|\frac{1}{n^3}\frac{1}{\kappa^3}\right| g \tag{97}$$

With the aid of eqn. (93) and the definition of R we find from eqn. (97):

$$\alpha_n(\nu) = \frac{32}{3\sqrt{3}}\frac{\pi^2 e^6}{ch^3}\frac{RZ^4}{n^5\nu^3}g \tag{98}$$

the absorption coefficient per atom in the nth level. Fortunately, the correction factor g is always near unity. For the Balmer continuum, the absorption coefficient at the series limit amounts to 1.38×10^{-17} c.g.s. units per atom in the second level. It gradually falls to about half this value at the limit of transmission of the earth's atmosphere, λ2900.

To compute the total absorption coefficient for a gram of neutral hydrogen at a particular temperature it is necessary to sum over the contributions of all levels that can produce the absorption at the wave length of interest. At λ4000, for example, transitions from the third and higher levels have to be taken into account; at λ3500 the contribution from the second level must be added, while the ionization from the first level need be considered only for wave lengths less than λ912. Fig. 15

shows the dependence of the mass absorption coefficient of hydrogen upon the frequency. Notice that between successive series limits the absorption coefficient falls off as ν^{-3} rises anew at each series limit and then falls off again as ν increases. The relative contributions of the various ionization limits to α_ν depend critically upon the temperature in

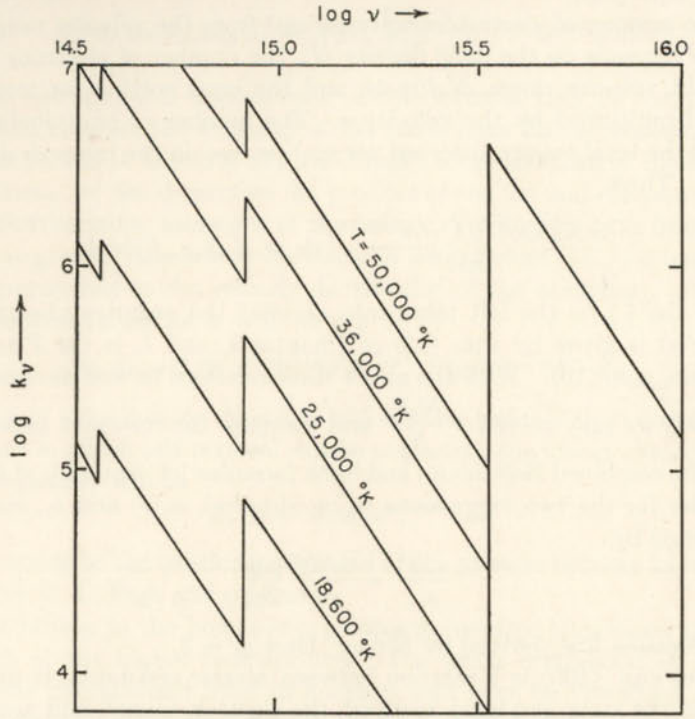

FIG. 15.—THE ABSORPTION COEFFICIENT OF ATOMIC HYDROGEN

We plot $\log k_\nu$ against $\log \nu$ for a gram of neutral hydrogen as a function of the temperature. The effect of negative absorptions (induced emissions) is not included.

accordance with the Boltzmann law. At low temperature the high levels are sparsely populated and appreciable absorption occurs only from the lowest level. At higher temperatures the increasing population of the upper levels produces more and more absorption in the ordinary spectral regions.

Continuous emission at the limit of the Balmer series is observed in the solar chromosphere and in the gaseous nebulae; it results from the recapture of electrons by ions.

The inverse of photoionization is the recapture of an electron by the ion. The capture coefficient, $\sigma_{\kappa n}$, for an electron of velocity v, is related to the absorption coefficient α_ν, ν and v being connected by eqn. (91).

That is, α_ν and $\sigma_{\kappa n}$ are atomic parameters; the relation between them may be evaluated with the aid of the principle of detailed balancing in thermodynamic equilibrium. Then the number of ionizations in the frequency interval $d\nu$ from a level n must equal the number of recombinations to this same level from the corresponding interval in velocity dv [cf. eqn. (94)].

The number of electron recaptures/cm³ from the velocity range v to $v + dv$ depends on the ionic density N_i, the number of electrons in the relevant velocity range, $N_e f(v)\, dv$, and the cross section for recapture $\sigma_{\kappa n}$, all multiplied by the velocity v. The number of photoionizations equals the total energy absorbed per cm³ per sec. in the range $d\nu$ divided by $h\nu$. Thus

$$\frac{4\pi N_n \alpha_n(\nu) I_\nu (1 - e^{-h\nu/kT})}{h\nu}\, d\nu = N_i N_e \sigma_{\kappa n} f(v) v\, dv \tag{99}$$

where the ( ) on the left takes into account the negative absorptions. Here $f(v)$ is given by eqn. (15) of Chapter 3, and I_ν is the Planckian function, eqn. (10). With the aid of these relations as well as eqns. (91) and (94) we may solve for $\frac{N_i N_e}{N_n}$ and compare the resultant expression with the combined Boltzmann and Saha formulae [cf. eqn. (26) of Ch. 4]. In order for the two expressions to be identical, $\alpha_n(\nu)$ and $\sigma_{\kappa n}$ must be connected by

$$\frac{\alpha_n(\nu)}{\sigma_{\kappa n}} = \frac{m^2 c^2 v^2}{\nu^2 h^2} \frac{g_e g_i}{2 g_n} \tag{100}$$

an expression first derived by Milne. Here $g_e = 2$.

Since eqn. (100) is a relation between atomic constants, it depends only on the atom and level involved, the electron energy, and not at all on the existence or absence of thermal equilibrium. In the practical calculation of recombination rates we shall assume that the velocity distribution is Maxwellian corresponding to some temperature T_e. Hence the number of recombinations/cm³/sec in the interval dv is

$$F_{\kappa n}\, d\nu = N_i N_e f(v, T_e) v \sigma_{\kappa n}\, dv \tag{101}$$

We now employ eqns. (98), (15) of Chapter 3, (91), (94), (100), and (101) together with the definitions:

$$\nu_n = \frac{RZ^2}{n^2}, \quad X_n = \frac{h\nu_n}{kT_e} = \frac{hRZ^2}{n^2 kT_e} \tag{102}$$

and the statistical weights, $g_i = 1$, $g_n = 2n^2$, for hydrogen to obtain

$$F_{\kappa n}\, d\nu = N_i N_e \frac{KZ^4}{T_e^{3/2}} \frac{g}{n^3} e^{-h(\nu - \nu_n)/kT_e} \frac{d\nu}{\nu} \tag{103}$$

where the constant K is given by

$$K = \left(\frac{h^2}{2\pi mk}\right)^{3/2} \frac{8\pi^2 e^2 R^2}{mc^3} \frac{2^4}{3\sqrt{3}\pi} = 3.260 \times 10^{-6} \tag{104}$$

and g is the Gaunt factor. The corresponding emission per unit volume and time is

$$E_{\kappa n}\, d\nu \equiv F_{\kappa n} h\nu_{\kappa n}\, d\nu = N_i N_e \frac{KZ^4}{T_e^{3/2}} \frac{g}{n^3} e^{-h(\nu - \nu_n)/kT_e} h\, d\nu \tag{105}$$

Two astrophysical applications of this formula may be mentioned. If we can measure the intensity of the continuous Balmer emission in a gaseous nebula in absolute units and make some estimate of the radiating volume, we can determine the product of the ion and electron densities. Furthermore, measures of the energy distribution with frequency ought to give an estimate of the electron temperature (i.e., the temperature appropriate to the velocity distribution of the electrons). Putting in numerical values for $n = 2$, we get

$$E_{\kappa 2}\, d\nu = 2.70 \times 10^{-33} N_i N_e T_e^{-3/2} g e^{-h(\nu - \nu_2)/kT_e}\, d\nu \tag{106}$$

That is, in a continuous spectrum which arises entirely from recombination and in which self-reversal can be neglected, the energy distribution with frequency will be

$$E_\nu\, d\nu = \text{const}\, e^{-h\nu/kT_e}\, d\nu \tag{107}$$

Applications to the continuous spectra of the gaseous nebulae have been made by T. L. Page and others.

In addition to the bound-free processes, free-free transitions are important at the higher temperatures. The latter correspond to jumps from one unquantized level to another, and may be visualized in the Bohr picture as follows. A free electron approaching a positive ion along a hyperbolic orbit may emit a quantum of energy and fly away in a second hyperbolic orbit of less energy. Conversely, it may absorb radiant energy in the neighborhood of the ion and move on with increased speed. Since the energy changes are unquantized the absorbed and emitted frequencies constitute a continuous spectrum. Small energy changes occur more frequently than large ones; hence free-free absorptions become particularly important in the infrared.

From the standpoint of the classical theory, the ion and the electron approximate a dipole and may radiate energy in accordance with the usual electromagnetic equations. The encounter between two electrons does not constitute a dipole and neither classical theory nor quantum mechanics permit radiation to be emitted or absorbed.

In the hottest stars, free-free absorptions become important in ordinary spectral regions. Minkowski finds evidence that the continuous

spectrum of the Crab nebula probably arises primarily from free-free emissions involving carbon and heavier elements.

The most important source of continuous absorption in stars such as the sun, however, is the negative hydrogen ion whose bound-free transitions produce most of the absorption in ordinary spectral regions. Beyond λ16,000 in the infrared spectrum of the sun the principal causes of

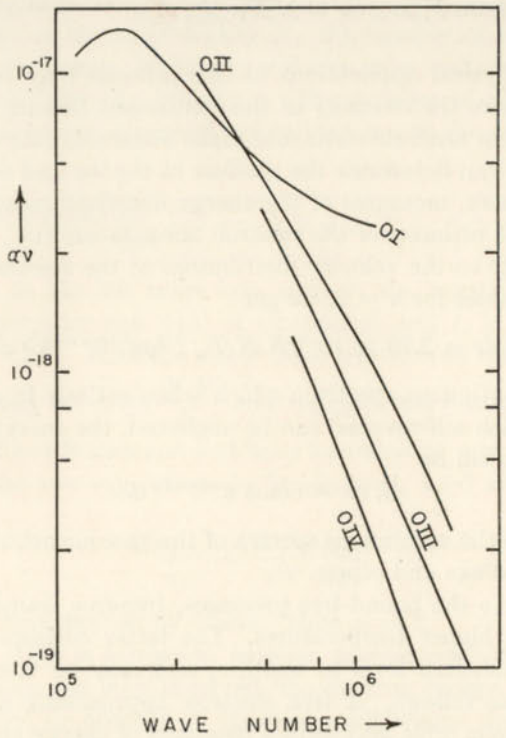

FIG. 16.—THE CONTINUOUS ABSORPTION COEFFICIENT OF OXYGEN FOR DIFFERENT STAGES OF IONIZATION

The absorption coefficient α_ν is computed from Hartree wave functions for p^n configurations and hydrogenic d-wave functions in the continuum. The contributions of the $p^n - p^{n-1}s$ transitions to the absorption coefficient have been neglected. A logarithmic scale is employed in both coordinates. (Leo Goldberg and L. H. Aller, 1941.)

continuous absorptions are the free-free transitions of this ion. The electric field of the proton is not fully screened by the valence electron of the neutral atom. An electron passing nearby experiences an attraction and may absorb or emit energy in a free-free transition.

Continuous absorption coefficients for bound-free transitions have been computed or measured experimentally for a number of atoms. Fig. 16 illustrates some results for oxygen in various stages of ionization.

References to some atoms of astrophysical interest are given at the end of this chapter.

20. Transition Probabilities of Forbidden Lines

The radiations of the night sky, the solar corona, and the gaseous nebulae contain strong emission lines corresponding to transitions between low lying metastable levels and the ground level. These are the *forbidden* lines: they all represent transitions between levels belonging to the same configuration and they all violate the Laporte parity rule. Whereas the ordinary "permitted" lines represent transitions of the dipole type, the forbidden lines correspond to magnetic dipole or to electric quadrupole type. When forbidden lines can be studied in the laboratory the angular distribution and polarization of the emitted radiation may be shown to be appropriate to these latter types of radiation.

Thus the "auroral" transition represents pure electric quadrupole radiation ($\Delta L = 2$), whereas the "nebular" transitions contain both magnetic dipole and electric quadrupole contributions.*

Bowen suggested that the forbidden lines in the gaseous nebulae are produced in the following manner. Electrons of several volts energy collide with atoms in the ground level and give up kinetic energy to excite the atoms to nearby metastable levels. Once in such a level the atom can return to the ground state in one of two ways; either it can unload its energy on a passing electron in a superelastic collision (inverse of an inelastic collision) or it can return to the ground level with the emission of a forbidden line. Which of these two processes will prevail depends on the temperature and particularly on the density of the gas. In any event the emission per unit volume will be $N_B A_{BA} h\nu_{BA}$ where N_B is the number of atoms in the upper level, B, of the transition, A_{BA} is the transition probability for the line in question and $h\nu_{BA}$ is the energy per quantum.

Generally the observational data give a numerical estimate of the emission per unit volume; hence if A_{BA} is known, the number of atoms in the upper level may be found. To find also the number in the ground level, N_0, we must determine the ratio N_B/N_0 which will depend on the temperature and density.

Condon, Pasternack, Shortley and his colleagues, and others have computed A values for the forbidden lines of light atoms by quantum mechanics. Many of the forbidden lines comprise both electric quadrupole and magnetic dipole radiation.

* In electric quadrupole radiation Δl can be ± 2, or 0 and J can change by 0, 1, or 2 units except that $0 \to 0$, $\frac{1}{2} \to \frac{1}{2}$, or $1 \to 0$ is not permitted. In magnetic dipole radiation, the transitions are restricted to levels of the same configuration, and J may change by ± 1, or 0, except that $0 \to 0$ cannot occur.

Neutral oxygen, which is responsible for some of the strongest lines of the permanent aurora, provides a good example. See Fig. 9, Ch. 2.

λ	Type	Transition	A
5577	a	$^1D_2 - {}^1S_0$	e 1.28
6300	n	$^3P_2 - {}^1D_2$	e 0.000024 m 0.0069
6364	n	$^3P_1 - {}^1D_2$	e 0.0000032 m 0.0022
6391	n	$^3P_0 - {}^1D_2$	e 0.0000011
2972	t	$^3P_1 - {}^1S_0$	m 0.078
2958	t	$^3P_2 - {}^1S_0$	e 0.00037

The first column of the table gives the wave lengths of the forbidden lines; a, n, and t denote whether the lines are of auroral, nebular, or transauroral nature. The A values according to Garstang are given in the last column. The symbols e and m denote electric quadrupole and magnetic dipole components of the radiation respectively. The total transition probability is $A = A_m + A_e$.

The transition probability of the λ5577 line is very much greater than that of the nebular lines. This result holds for the auroral transitions in other atoms and ions as well. Oxygen atoms in the upper atmosphere (ionsphere) of the earth are excited to the ^1S level by collisions with electrons. As they cascade to the ^1D level they emit the forbidden λ5577 line. The nebular lines, which result from transitions from the D term to the P term, are very much weaker. Even though many more atoms are excited to the D term by collision than to the S level, the A values are so very much lower that the nebular lines are weaker than the auroral line.

In the gaseous nebulae, on the other hand, the situation differs strikingly. The strongest lines are usually the green $^3P - {}^1D$ lines of [O III], while the auroral type transition $^1D_2 - {}^1S_0$, λ4363, is very much weaker. A glance at the transition probabilities involved shows the same situation as in O I, the A value for λ4363 is 1.6, whereas the A values for the $^3P_2 - {}^1D_2$ and $^3P_1 - {}^1D_2$ transitions are 0.021 and 0.0071 respectively. Yet the auroral line, despite its larger A value, often is a hundred times weaker than the nebular lines! We find these striking differences to be correlated with the densities of the media involved. The gaseous nebulae are much more rarefied than the ionosphere, the envelopes of novae fall in between these two extremes. In the novae the auroral λ4363 line is much stronger relative to the green λ4959 and λ5007 lines than in the gaseous nebulae.

21. Collisional Excitation of Forbidden Lines

When the density of a gas is high, most of the atoms entering a metastable level by collision will also be de-excited by collision, i.e., the number of collisional excitations will very nearly equal the number of collisional de-excitations. Hence the relative populations of the metastable and ground levels will be given with sufficient accuracy by Boltzmann's formula. As the density is decreased, the number of collisional excitations and de-excitations likewise falls off and a greater proportion of atoms will return to the ground level with the emission of a forbidden line. Since the principle of detailed balancing no longer holds, the population of the excited level depends on both the A value of the forbidden line and the target area for the collisional excitation of the metastable level.

Let σ_{AB} denote the target area in units of cm² for the collisional excitation of level B from level A. The number of collisional excitations /cm³/sec, by electrons with velocities between v and $v + dv$ will equal the number of ions in the lower level, N_A, multiplied by the number of electrons of velocity v to $v + dv$, $N_e f(v)\, dv$ in a column of volume $\sigma_{AB} v$ [cf. eqn. (15) of Ch. 3]. The total number of collisional excitations /cm³/sec, F_{col}, is then obtained by an integration over all velocities greater than v_0, the velocity of an electron whose energy is equal to the excitation energy of the level B above level A. That is,

$$F_{\text{col}} = N_A N_e \int_{v_0}^{\infty} \sigma_{AB} v f(v)\, dv \tag{108}$$

Attempts to calculate target areas have been made by D. H. Menzel and M. H. Hebb (O III), by T. Yamanouchi, T. Inui, and A. Amemiya (O I), by L. H. Aller (O II), and by L. H. Aller and M. L. White (N II). Unfortunately the quantum mechanical basis for such computations is unsound and it is possible to give only an upper limit to the cross-sections.

22. Roles of Emission and Absorption Lines in Astrophysical Sources

The normal spectrum of a star consists of a continuous spectrum upon which are superposed dark absorption lines due to the various elements that compose its atmosphere. The discussions in this and previous chapters have given us the necessary physical background to approach the theory of absorption line formation and to show how the temperatures, densities, and compositions of stellar atmospheres are determined.

Gaseous nebulae, on the other hand, show emission-line spectra and the problem of interpretation becomes one of finding the appropriate

mechanism for the formation of the line in question. The hydrogen lines, for example, are produced by the recombination of ions and electrons and subsequent cascading. The forbidden lines are all produced by the aforementioned mechanism of collisional excitation. Some permitted oxygen lines in the gaseous nebulae are produced by recombination but others owe their high intensities to fluorescent effects.

Extended stellar atmospheres exhibit every stage intermediate between a bona fide star and a nebula. In one class of objects, the novae, we witness a smooth transition between the spectrum of a star and that of a gaseous nebula. In many peculiar stars, forbidden lines are strong, indicating nebula-like conditions, and sometimes we observe permitted emission lines of Fe II, produced by collisional processes similar to those just discussed. In the solar system, comets furnish some of the outstanding puzzles for astrophysical interpretation.

In the analysis of all astrophysical data it is necessary to keep in mind at all times the assumptions and limitations of the underlying physical model.

PROBLEMS

1. A lens of 20-cm diameter and 100-cm focal length is used to form an image of the sun. How much brighter will the image be than a directly illuminated surface? The angular diameter of the sun is taken as 32′.

2. If the intensity distribution of the radiation emergent from the sun is given by

$$I(\theta) = a_0 + a_1 \cos\theta$$

compute the outward flux.

3. Compare the energy density of black body radiation at the following temperatures: 273°K, 5700°K, and 20,000,000°K.

4. If the temperature of the sun is 5700°K, what is the frequency ν_0 at which I_ν is a maximum? What is the wave length corresponding to this frequency? Why does it differ from λ_{max} given by Wien's law?

5. Calculate the rate of emission of a nebula, the brightness and color of which are described as equivalent to three fifth-magnitude G stars per square degree.

6. In the absence of an external field and with a small damping force, the equation of motion of the classical oscillator is very nearly

$$m\frac{d^2z}{dt^2} = -m\omega_0^2 z$$

With the aid of eqn. (53) calculate the instantaneous rate of energy radiation, average it over a cycle, verify eqn. (54), and derive the equation for γ (eqn. 55).

7. The f values for the multiplets based on the O II $3d$ terms in the $3d - 4f$ configuration array are as follows.

(^2D)	^2G	0.920	^2D	0.955	(^3P)	^4F	0.870	^2F	0.955
	^2F	0.880	^2P	0.984		^4D	0.930	^2D	0.995
						^4P	0.967	^2P	0.975
						$(^1S)^2D$	= 0.940		

What is the f value for the whole configuration?

8. Calculate the f value for O II λ4072.16 $2p^2(^3P)3p\,^4D_{5/2} - 3d\,^4F_{7/2}$ with the aid of Tables 1, 2, and 3.

9. Verify eqn. (100).

10. Derive the relation between the Einstein coefficients A and B defined for energy density instead of intensity.

REFERENCES

1. *Radiation Laws*

Milne, E. A. "Thermodynamics of the Stars," *Handbuch der Astrophysik*. Berlin: Julius Springer, 1930, Vol. III. Part 1, p. 65.

Chandrasekhar, S. *Stellar Structure*. Chicago: University of Chicago Press, 1940, chap. v.

Richtmyer, F. K., and E. H. Kennard. *Introduction to Modern Physics*. New York: McGraw-Hill Book Co., Inc., 1942, chap. v. (Derivation of Planck's law and other radiation relationships.)

The classical formulae of dispersion and absorption are developed in:

Slater, J. C., and N. H. Frank. *Theoretical Physics*. New York: McGraw-Hill Book Co., Inc., 1934, chap. xxiv.

Wood, R. W. *Physical Optics* (3d ed.). New York: The Macmillan Co., 1934, chap. xv.

Born, M. *Optik*. Berlin: Julius Springer, 1933, chap. viii.

For the modern treatment of the problem see:

Heitler, W. *Quantum Theory of Radiation* (2d ed.). New York: Oxford University Press, 1944.

2. *Transition Probabilities*

An extensive quantum mechanical treatment of radiation, line strengths, and related topics will be found in:

Condon, E. U., and G. Shortley. *Theory of Atomic Spectra*. London: Cambridge University Press, 1935.

Racah, G. *Phys. Rev.* **61,** 186, 1942; **62,** 438, 1942; **63,** 367, 1943; **76,** 1352, 1949.

For relative line strengths within a multiplet, see:

White, H. E. *Introduction to Atomic Spectra*. New York: McGraw-Hill Book Co., Inc., 1934, p. 439.

Russell, H. N. *Ap. J.* **83,** 129, 1936.

Relative multiplet strengths within a configuration array in LS coupling are tabulated by:

Goldberg, L. *Ap. J.* **82,** 1, 1935 (Ref. 1) and *ibid.* **84,** 11, 1936 (Ref. 2).

Tables for the calculation of the radial charge distribution coefficient σ for absolute line strengths are given by:

BATES, D. R., and A. DAMGAARD. *Phils. Trans. Roy. Soc.* A, **242**, 101, 1949.

Various sum rules are discussed by:

SHORTLEY, *op. cit.;* GOLDBERG, *op. cit.;* and MENZEL, D. H., *Ap. J.* **105**, 131, 1947.

Bibliographies of f-value determinations are given by

UNSÖLD, A. *Zeits. f. Ap.* **24**, 306, 1948.
CLAAS, W. J. *Astron. Researches Utrecht Obs.* **12**, No. 1, 1951.

More recent papers include

KING, R. B. *Ap. J.* **105**, 376, 1947 (VI), **108**, 87, 1948. (Ni I)
ESTABROOK, F. B. *Ap. J.* **113**, 684, 1951. (Absolute f values for Cr, Ni)
HILL, A. J., and R. B. KING. *J. Opt. Soc. Am.* **41**, 315, 1951. (Relative f values for Cr)
KOPFERMANN, H., and G. WESSEL. *Zeits. f. Phys.* **130**, 100, 1951.
TREFFETZ, E. *Zeits. f. Ap.* **28**, 67, 1950. (Mg I)
GARSTANG, R. H. *M. N.* **110**, 613, 1950. (Ne II)

See also

LANDOLT-BÖRNSTEIN. *Zahlenwerte U. Funktionen aus Physik, Chemie, Astronomie, Geophysik, U. Technik.* Berlin: Julius Springer, 1950, Vol. I. Part 1, p. 260.
CONDON, E. U. *Handbook of Physics.* New York: McGraw-Hill Book Co., Inc. (in press), Part 7, chap. iii.

3. *Continuous Absorption and Emission of Energy*

A general review of quantum mechanical calculations on this subject has been given by: BATES, D. R. *M. N.* **106**, 432, 1946, who gives a bibliography of the earlier work. Important recent papers on the continuous absorption coefficient include the following:

HUANG, SU SHU. *Ap. J.* **108**, 354, 1948. (He I)
GREEN, L. C. *Ap. J.* **109**, 289, 1949. (Ca I)
GREEN, L. C., and NANCY WEBER. *Ap. J.* **111**, 587, 1950; **113**, 690, 1951. ($4s-p$, $3d-f$), (Ca II)
BIERMANN, L., and K. LUBECK. *Zeits. f. Ap.* **26**, 145, 1949. (Mg II), (Si II)
BIERMANN, L. *Nach. Akad. Wiss. Gott. Math. Phys. Klasse* **3**, 12, 1947. (Mg II), (Si II)
BATES, D. R., and M. J. SEATON. *M. N.* **109**, 698, 1950. (C I, N I, O I)

4. *Transition Probabilities for Forbidden Lines*

The A values for many lines of astrophysical interest are given by:

PASTERNACK, S. *Ap. J.* **92**, 129, 1940.
OSTERBROCK, D. *Ap. J.* **114**, 469, 1951.
GARSTANG, R. H. *M. N.* **111**, 115, 1951.

The theory for the λ3727 lines of O II is given by:

UFFORD, C. W., J. H. VAN VLECK, and L. H. ALLER. *Ap. J.* **109**, 42, 1949.

Tables from which A values may be computed are given by:

SHORTLEY, G., L. H. ALLER, J. G. BAKER, and D. H. MENZEL. *Ap. J.* **93**, 178, 1941.

The present status of the theoretical calculations of target areas for the collisional excitation of forbidden lines is discussed by:

ALLER, L. H. *Ap. J.* **111**, 609, 1950.

CHAPTER 6

THE RADIATION OF THE STARS

1. The Significance of a Stellar Temperature

The masses, radii, and luminosities of the stars are fundamental quantities. The spectrum, for example, is intimately related to the surface temperature and gravity. The mass and radius fix the surface gravity, whereas the temperature depends essentially upon the rate of energy generation and upon the radius. The theoretical treatment of stellar atmospheres presupposes that we know the boundary temperature of the star, the surface gravity, and the chemical composition. The theory of stellar structure requires the luminosity, mass, and radius of a star and some information on its chemical composition.

In Chapter 1 we mentioned how stellar masses are found from the components of visual and eclipsing binaries, the radii from interferometer measures of stars of known parallax and from eclipsing binaries. In this chapter we shall concern ourselves with the determination of stellar luminosities. Our studies are hampered by the limitations imposed by the small region of the spectrum we can observe through the earth's atmosphere and by the wave length sensitivity of our detecting apparatus.

If we could measure the absolute energy output, $E_\lambda\, d\lambda$, of a star in some small spectral region λ to $\lambda + d\lambda$ and then could determine the complete distribution of energy with wave length, we would obtain the true luminosity of the star. Actually, such a rigorous procedure is not possible even for the sun, and we must content ourselves with measurements in accessible spectral regions and make the best guesses we can about the inaccessible regions.

Suppose, however, that a good estimate of the total energy output (luminosity), L, of a star of known radius, R, can be obtained. We define the effective temperature T_e of the star as that which a black sphere of the same radius must possess in order that its total energy output equal that of the star. That is, T_e is defined by

$$L = 4\pi R^2 T_e^4 \sigma \tag{1}$$

since $4\pi R^2$ is the surface area and σT_e^4 is the black body energy output/cm². The effective temperature is a datum of great theoretical interest, but we must emphasize that it is not directly observable for most stars!

A quantity that can be measured for a number of stars is the radia-

tion/cm²/sec/Angstrom, F_λ, for selected points in the continuous spectrum. We can define a brightness temperature, T_b, as that of the black body that would give the same energy output per angstrom as the star at wave length λ. Brightness temperatures are measurable only for stars of known angular diameter. At λ5300, Greaves estimates T_b's of 28,000°K for spectral type *O*8, 18,000°K for *B*0, 11,000°K for *A*0, and about 6100°K for *G*2 (the sun). The brightness temperature is really only a parameter that expresses the rate of energy radiation at certain wave lengths. It cannot be converted readily into the physical temperature of the emitting stellar surface. For example, from E. Pettit's measures of the radiation from the whole disk of the sun, the brightness temperature of that body is found to be 6200°K at λ4500 and 6000°K at λ6500, whereas the effective temperature of the sun is closer to 5760°K.

Still less representative of the physical temperatures of the stars are the so-called color temperatures. Suppose we compare the energy distribution of a star in the wave length region $\lambda_1 - \lambda_2$ with that of a blackbody source. We may find that in this interval the distribution of energy, not its absolute value, can be represented by a Planckian function for some temperature T_c. In another wave length region, $\lambda_3 - \lambda_4$, a different color temperature T_c' is found, etc. Stellar color temperatures do not represent the actual physical temperatures in the photospheric layers. A normal *A*0 star has a photospheric temperature near 10,000°K, but the color temperature obtained by fitting a Planckian curve with an arbitrary scale factor to the energy distribution near λ5000 is near 16,000°K, while that obtained in the vicinity of λ3500 is 10,000°K. Thus stellar color temperatures are parameters employed in Planck's formula to express the distribution of emitted energy with wave length, and no harm will be done provided we keep this fact in mind, but we must not confuse the number T_c with the physical temperature of the stellar atmosphere.

The distribution of atoms among the various stages of ionization in a stellar atmosphere serves to define an ionization temperature, while a comparison of the numbers of atoms in different energy levels by Boltzmann's formula introduces the concept of an excitation temperature. The fact that the parameter in Boltzmann's formula may not be the same as the effective temperature, or the temperature derived from an application of the ionization formula is a consequence of the circumstance that stellar atmospheres are not in strict thermal equilibrium and that they possess a temperature gradient.

2. The Energy Output of the Sun

The most extended measures of stellar radiation are those that have been carried out for the sun. The energy output from different parts of

the disk can be measured on an absolute scale as a function of wave length.

An estimate of the heat radiation of the sun follows most easily from a determination of the amount of energy absorbed when solar rays fall upon a blackened surface. Thus, in 1838, Pouillet filled a blackened vessel with water, exposed it to sunlight, and measured the rate of temperature rise. Corrections for cooling, for surface reflectivity, and for atmospheric extinction are necessary before the measure can be reduced to calories/cm²/sec received at the earth's mean distance from the sun.

Tyndall, and later Abbot, made use of Pouillet's principle in an improved instrument called the pyrheliometer. Unfortunately, the silver-disk pyrheliometer does not measure the solar energy on an absolute scale. It must be calibrated. To solve this problem, Abbot devised a water-flow pyrheliometer in which sunlight enters a hollow blackened chamber and heats, by a measurable amount, a stream of water which flows through a spiral tube at a known speed. The instrument is then pointed away from the sun, a resistance coil is placed in the same tube, and the amount of electric current necessary to raise the temperature of the stream of water by the same amount is measured. The heat developed by the coil ($0.24I^2R$ calories/sec, where I is the current in amperes and R is the resistance) must exactly equal the heat received from the sun.

Because the measurements are made within the earth's atmosphere, the effects of atmospheric extinction must be determined. The determination of the correction would be simple, were it not for the fact that the absorption depends strongly on wave length. Hence it is necessary to measure the wave length distribution of the solar energy at different altitudes of the sun in order to find the extinction effects at each wave length.

For the measurement of the solar energy curve, Abbot employed the spectrobolometer. This instrument involves the principle that when a metal wire is heated, its resistance is changed. A solar spectrum is formed in a conventional way and moved across a blackened wire. As regions of fluctuating intensity cross the wire, its temperature and therefore its resistance change, and a varying galvanometer deflection is obtained. Strong Fraunhofer lines give large depressions in the curve. When corrections are made for the transparency of the spectrograph, for reflection losses in the optical system, etc., the area under the reduced bolograph curve will be proportional to the total amount of energy received. Since the actual amount of energy is measured by the calibrated pyrheliometer, the area of the bolograph record is known in energy units, i.e., in calories.

The correction for atmospheric extinction requires both pyrheliometric and bolometric measures, at different zenith distances of the sun. The energy of wave length λ reaching the observer is

$$I_{z\lambda} = I_{0\lambda} e^{-k_\lambda m \sec z} \qquad (2)$$

where m is the total mass of air above the station, z is the zenith distance, and k_λ is the extinction coefficient. From a series of bolographs obtained at different zenith distances, $\log I_{z\lambda}$ may be plotted against $\sec z$. If a straight line is drawn through the points and extrapolated to zero air mass ($m \sec z = 0$), we obtain $\log I_{0\lambda}$, the intensity the radiation of wave length λ would have outside the earth's atmosphere. The same procedure is followed for other wave lengths and the totality of extrapolated

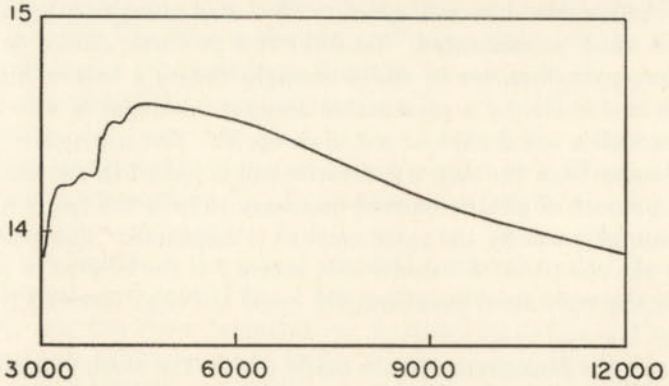

FIG. 1.—THE ENERGY DISTRIBUTION AT THE CENTER OF THE SUN'S DISK

We plot $\log I_\lambda$ against the wave length in angstroms. The intensity I_λ is expressed in ergs/sec/cm² of the solar surface per unit solid angle per centimeter interval of wave length.

$I_{0\lambda}$ values gives a curve which shows what the solar energy distribution would look like if we could observe it above the atmosphere. Since the units of the $I_{z\lambda}$ curves are known from the pyrheliometer measures, the area under the $I_{0\lambda}$ curve gives the solar constant, the amount of energy received from the sun per cm² per minute just outside the earth's atmosphere at the earth's mean distance from the sun.

Abbot found a value of 1.938 calories/cm²/min for the solar constant, which amounts to 1.36×10^6 ergs/cm²/sec, 0.136 watts/cm², or 1.81 H.P./meter²/sec. The total amount of energy passing through a sphere of the radius of the earth's orbit, 1.495×10^{13} cm, must equal the total energy output of the sun, 3.79×10^{33} erg/sec, or 5.08×10^{23} horsepower. The energy output/cm²/sec is 6.25×10^{10} ergs/cm²/sec. The corresponding effective temperature of the sun is obtained from Stefan's law [eqn. (13) of Ch. 5]. Putting in numerical values, we find

$$6.25 \times 10^{10} = 5.672 \times 10^{-5} T^4$$

whence $T = 5760°$K. Unsöld suggested that Abbot's value of the solar constant be corrected to 1.90 cals/cm²/min from which an effective temperature of 5732°K is derived.

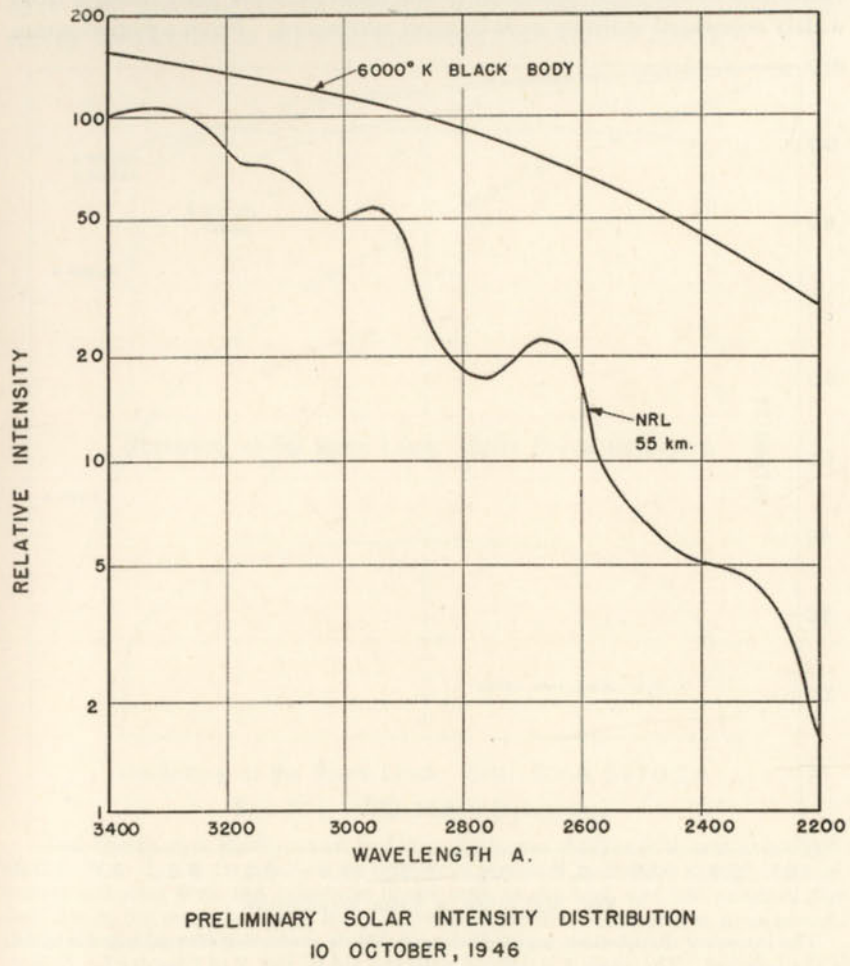

FIG. 2.—THE ENERGY DISTRIBUTION IN THE "ROCKET" ULTRAVIOLET

The solar energy distribution measured from a rocket at a height of 55 km is compared with that of a black body at 6000°K. (U. S. Naval Research Laboratory.)

It is necessary to try to allow for the infrared and ultraviolet solar radiation that is cut out by the earth's atmosphere. Abbot's measures excluded data beyond 2.5μ in the infrared. The recent measures by the Naval Research Laboratory group with the V-2 rockets show the solar ultraviolet radiation to be feeble. C. W. Allen concludes that the solar

constant should be increased by 3.7 per cent to 1.970 calories/cm². The effective temperature of the sun is then 5784°K.

The energy output of the sun may not be constant. Abbot found variations in the solar radiation of the order of 2 per cent; results from widely separated stations were in good agreement. From a periodogram

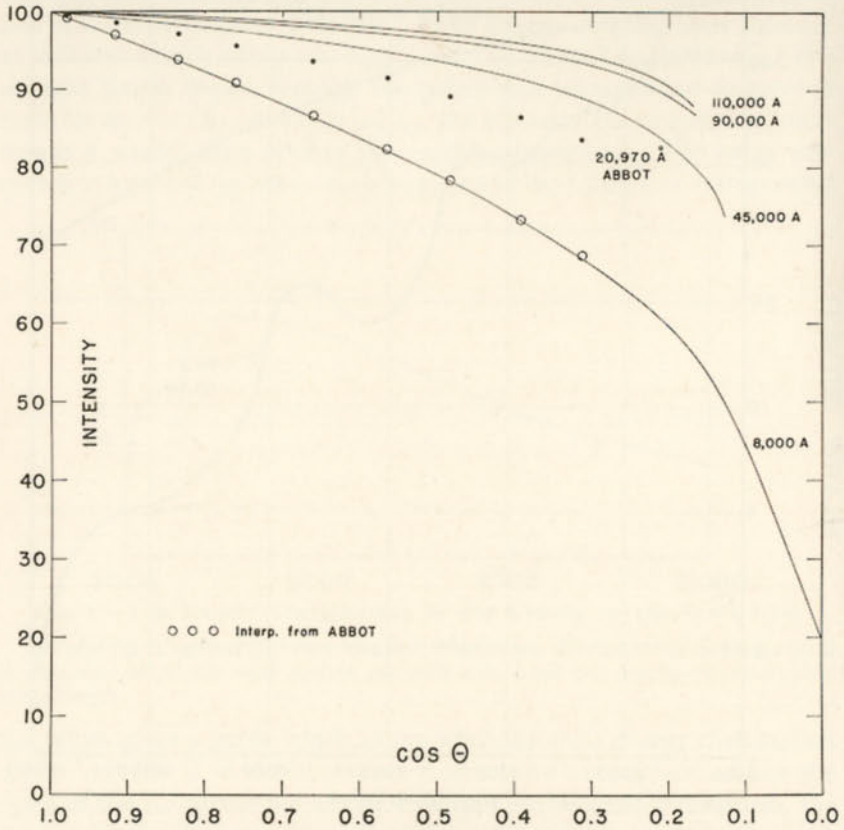

FIG. 3(a).—SOLAR LIMB DARKENING

The intensity distribution across the solar disk is shown for several wave lengths in the infrared. The angle θ is defined with the aid of Fig. 2 of Chapter 5. Notice the decrease of limb darkening with increasing wave length. Measures by C. G. Abbot are shown for comparison. (McMath-Hulbert Observatory, University of Michigan.)

analysis of Abbot's data, T. E. Sterne, K. Guthe, and W. O. Roberts concluded that there was some evidence for real changes in the solar constant with a period equal to that of the solar cycle, but the question can be finally settled only with more extended data.

Other investigations of the solar energy distribution have been published by Wilsing, by Buisson and Fabry, by R. Canavaggia and D. Chalonge, and by Pettit who studied the region λ2920–λ7700. Mulders compiled a definitive energy curve on the basis of the earlier work. Spectrograms obtained with rockets fired above the earth's atmosphere have been analyzed at the Naval Research Laboratory to obtain the energy distribution in the solar spectrum shortward of λ2900.

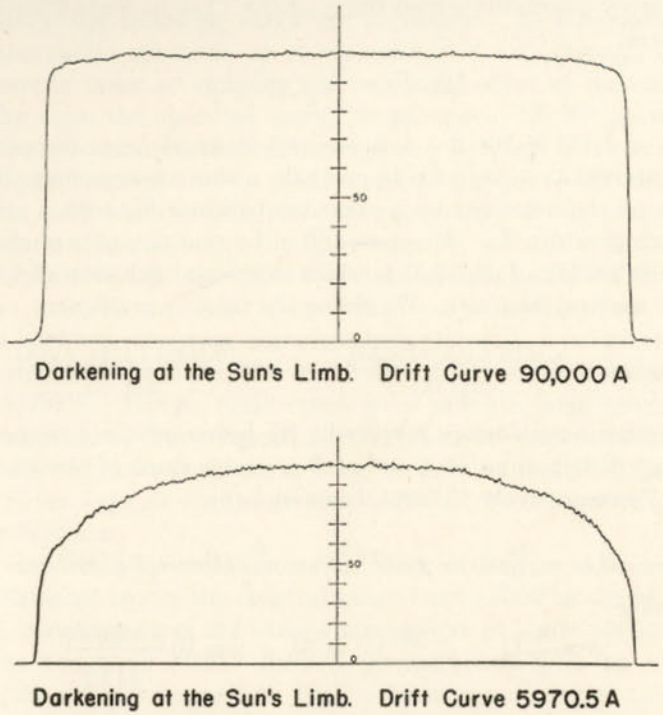

FIG. 3(b).—SOLAR LIMB DARKENING

These curves show the distribution of intensity across the disk of the sun at λ90,000 and λ5970.5. In the far infrared the opacity of the solar material is so high that we receive radiation from the outermost layers both at the limb and the center of the disk; hence the curve is almost flat. At λ5970.5 the limb darkening is pronounced. (McMath-Hulbert Observatory, University of Michigan.)

The discordances between various measurements show that new studies of the energy distribution are required. Water vapor complicates infrared studies; ozone introduces difficulties into the spectrophotometry of the ultraviolet. New measures by A. K. Pierce at Mount Wilson should provide good data on the solar energy distribution.

In Chapter 7 we shall see that in addition to the energy distribution, we must know the limb darkening $I_\lambda(\theta)/I_\lambda(0)$ as a function of wave length in order to undertake an analysis of the structure of the solar atmosphere. Measures were made by Abbot, by Moll, Burger, and van

der Bilt, by Miss Canavaggia and D. Chalonge, and recently by A. K. Pierce and his colleagues at the McMath-Hulbert Observatory.

3. Spectrophotometric Gradients

In descriptions of the energy distribution in stellar spectra it is useful to employ a quantity called the gradient. Let us write Planck's law in the form

$$I(\lambda, T) = \frac{c_1}{\lambda^5} \frac{1}{e^{c_2/\lambda T} - 1} \tag{3}$$

where $c_2 = 1.438 \times 10^8$ if λ is measured in angstroms. Suppose that for the interval λ_1–λ_2 we wish to compare a star whose energy distribution can be characterized by a color temperature T_A with a source of known temperature T_B. Measures, often by photographic photometry, give the ratio, $\log_{10} I_A(\lambda)/I_B(\lambda)$, which is a linear function of $1/\lambda$ even for large spectral intervals. We define the relative gradient:

$$G_{AB} = -\frac{d[\ln I_A(\lambda)/I_B(\lambda)]}{d(1/\lambda)} = -2.30 \frac{d \log_{10} I_A(\lambda)/I_B(\lambda)}{d(1/\lambda)} \tag{4}$$

for the wave length range involved. By hypothesis, we suppose that the energy distributions of A and of B resemble those of black bodies at T_A and T_B respectively. Hence, from eqn. (3),

$$G_{AB} = \frac{c_2}{T_A}(1 - e^{-c_2/\lambda T_A})^{-1} - \frac{c_2}{T_B}(1 - e^{-c_2/\lambda T_B})^{-1}$$

If we define

$$\phi = \frac{c_2}{T}(1 - e^{-c_2/\lambda T})^{-1} = 5\bar{\lambda} - \log_e 10 \frac{d \log_{10} I_\lambda}{d\left(\frac{1}{\lambda}\right)} \tag{5}$$

then

$$G_{AB} = \phi(T_A) - \phi(T_B) \tag{6}$$

If T is not large, λT will be small, and G_{AB} will approach

$$G_{AB} = c_2\left(\frac{1}{T_A} - \frac{1}{T_B}\right) \tag{7}$$

The observational quantity G_{AB} gives the relative energy distribution in the star and source over a selected wave length range. It is a more fundamental and useful quantity than the color temperature. Suppose we compare a certain number of stars with the same primary standard (star or laboratory source), for which a temperature T_B is assumed. If an error δT_B is subsequently found in T_B, the ϕ_A's will all be affected by the same amount $\delta\phi_B$, but the color temperatures will be affected in different ways. The changes in the color temperature will be much greater for the hot stars than for the cooler ones.

The experimental and observational difficulties in the comparison of a stellar spectrum with a laboratory source are formidable. A good account of the procedures is given by Robley Williams who compared the energy distribution of Vega with that of a carefully calibrated tungsten lamp as modified by a Corning Daylite filter.

To obtain the true energy curve of a stellar spectrum by photographic photometry the following steps are necessary. (1) We must photograph the stellar spectrum at several altitudes, i.e., through different air masses in order to estimate the reddening effect of the earth's atmosphere upon the observed energy distribution. (2) We must photograph the spectrum of a laboratory source of radiation whose spectral energy distribution is known. (3) We must employ some means of photographic calibration so the blackening (density) of the photographic emulsions can be related to the light intensity. Further, the star, the laboratory source, and the calibration must be photographed with equal exposure time, at the same temperature and humidity, and with the interval between successive exposures kept as small as practicable.*

The slopes of the energy curves change slowly with temperature beyond 12,000°K. Hence, small errors in ϕ produce large errors in the color temperature. For example, Kienle and his co-workers at Göttingen with a six-inch telescope and grating calibration system found T_c = 16,000°K for Vega as compared with 14,300°K from the 1938 observations of Williams.

The important spectrophotometric work of Barbier, Chalonge, and their colleagues covers the spectral range from λ5000 to the ultraviolet limit of transparency of the earth's atmosphere at about λ3000. These observers compared stellar spectra photographed with an objective prism with various lamps and with a hydrogen discharge tube. One trouble with their method is the large number of steps necessary to compare the stars with the ultimate standard lamp. A further difficulty is that the hydrogen source is bluer than the stars themselves.

Barbier and Chalonge tabulate the values of ϕ_1 and ϕ_2 which are defined for λ4250 and λ3500, respectively. (See Table 1.) These are the gradients above and below the Balmer limit. They also give the discontinuity D at the Balmer limit, defined by

$$D = \log_{10} \frac{I(\lambda > 3650\text{A})}{I(\lambda < 3650\text{A})} \tag{8}$$

Here $I_>$ refers to the intensity computed from a Planckian curve fitted to the longward side of the Balmer discontinuity, whereas $I_<$ refers to

* Photoelectric methods can yield a much higher precision as the investigations by Joel Stebbins, G. E. Kron, and J. Lynn Smith at the Lick Observatory and by Arthur Code at the Mount Wilson Observatory show.

the intensity derived from a curve drawn through the energy distribution on the shortward side. For an *A*0 star such as Vega, Barbier and Chalonge get $\phi_1 = 1.00$, corresponding to $T_1 = 16{,}500°\text{K}$, and $\phi_2 = 1.39$, which means $T_2 = 10{,}500°\text{K}$. They also give for each star, λ_1, the wave length that characterizes the position of the Balmer discontinuity. This parameter is useful in distinguishing between dwarfs and supergiants among early-type stars. Thus, in the *A*0 dwarf, Sirius, the Balmer lines merge at a longer wave length ($\lambda_1 = 3774$) than in the *A*2 supergiant, α Cygni ($\lambda_1 = 3697$).

TABLE 1

THE COLOR TEMPERATURES AND BALMER DISCONTINUITIES OF NORMAL STARS*

Spectrum	D	ϕ_1	$T_1 \times 10^{-3}$°K	ϕ_2	$T_2 \times 10^{-3}$°K
*Oe*5	0.03	0.57	52	0.62	29
*B*0	0.04	0.74	28	0.78	20
*B*1	0.07	0.74	28	0.78	20
*B*2	0.11	0.73	29	0.78	20
*B*3	0.17	0.79	25	0.86	18
*B*5	0.25	0.93	18	1.02	15
*B*8	0.33	0.86	21	1.10	13.5
*B*9	0.36	0.94	18	1.11	13
*A*0	0.47	1.00	16.5	1.39	10.5
*A*2	0.44	1.19	13	1.44	10
*A*3	0.42	1.31	11.5	1.43	10
*A*5	0.39	1.36	11	1.53	9.5
*F*0	0.28	1.70	8.6	1.74	8.3
*F*2	0.22	1.74	8.4	1.52	9.5
*gF*5	0.24	2.01	7.2	1.84	7.8
*dF*5	0.17	2.01	7.2	1.81	8.0
*dF*8	0.11	2.21	6.5	1.97	7.3
*gG*0	0.02	3.08	4.65	2.82	5.05
*dG*0	0.06	2.56	5.75	2.36	6.1
*gG*5		3.20	4.5		
*gK*0		3.86	3.75	3.26	4.4
*gK*5		5.40	2.65	3.73	3.8
gMa		5.72	2.5		

* Courtesy D. Barbier and D. Chalonge, *Annales d'Astrophysique* **3**, No. 2, 1940.

Barbier and Chalonge have observed other absolute magnitude effects in the continuous spectra. Earlier than *F*8, supergiants have the same gradients as main-sequence stars, whereas later than *F*8 the color temperatures of the more luminous stars are lower. The Balmer discontinuities are smaller in supergiants than in normal stars for spectral classes earlier than *A*5, whereas in later types the opposite is true. In fact, between *B*0 and *F*5 the two parameters D and λ_1 should suffice in principle to fix the spectral class and luminosity.

The comparison of stellar energy distributions with one another, i.e., the determination of relative gradients, achieves a much higher precision than does the measurement of absolute values. Among the more extensive programs of this nature are those of the Greenwich observers, Greaves, Davidson, and Martin, and of Kienle, Strassl, and Wempe in Germany.

The most accurate relative spectrophotometry can be done photoelectrically. With the aid of gratings, John Hall measured the relative gradients of 67 bright stars in the interval from λ4560 to λ10,300 with the caesium-oxide-on-silver cell. His results compare well with those obtained at Göttingen, but the attainable accuracy is greater.

TABLE 2

MEAN COLOR TEMPERATURES AND COLORS AS A FUNCTION OF SPECTRAL TYPE*

Spectrum	Mean Color Temperature		*V–I*	
	Main Sequence	Giants	Main Sequence	Giants
0	23,000°K		−2.52	
*B*0	21,000		−2.47	
*B*5	16,000		−2.24	
*A*0	11,000		−1.76	
*A*5	8,700		−1.30	
*F*0	7,300		−0.92	
*F*5	6,400		−0.52	
*G*0	5,950	5,100°K	−0.28	+0.30
*G*5	5,570	4,360	−0.05	+1.00
*K*0	5,280	3,830	+0.16	+1.68
*K*5	4,550	3,440	+0.80	+2.30
*M*0	3,590	3,160	+2.04	+2.86
*M*5		2,710		+4.00

* Courtesy J. Stebbins and A. E. Whitford, *Astrophysical Journal* (University of Chicago Press) **102**, 336, 1945.

Stebbins and Whitford employed a photocell and filter combination that gives effective wave lengths at λ3350, λ4220, λ4880, λ5700, λ7190, and λ10,300 to measure the relative-energy output of various stars. The zero point must be established from other data. Table 2 gives the color temperatures based on an assumed value of 5500°K for a dwarf *G*6 star. The *V–I* columns give the corresponding magnitude difference at effective wave lengths λ4220 and λ10,300. The accuracy of these measures permitted the separation of giants from supergiants, the limitations being imposed by inaccuracies in spectral classification rather than in color. Errors in spectral classification become particularly important

for the cooler stars and have, as Wildt noted, an important influence on the interpretation of the continuous spectra of the M stars.

Milford has considered the effects of lines on measured stellar magnitudes and has derived corrections to get the photovisual magnitude of the continuum. He has also derived the absolute fluxes of stars from $B3$ to $K5$ for the continuum at $\lambda 5450$. He suggests comparing stars by means of their monochromatic fluxes at one point in the continuum. Woolley and Gascoigne did this for Sirius at four wave lengths and Code has compared the fluxes of several stars by photoelectric methods.

The important point to realize is this: we observe in only a small number of stars the fundamental parameters (twenty or so effective temperatures, for example), while by contrast we have observed in a great number of stars other quantities such as spectrophotometric gradients, Balmer discontinuities, total intensities, and profiles of lines. Our task is to utilize these data with the aid of suitable theories to obtain such fundamental quantities as effective temperatures and absolute luminosities.

4. Relation Between Stellar Radii and Temperature

If a star is photographed or observed photoelectrically, the recorded light will cover a considerable range of wave length. The interval embraced will depend on the spectral sensitivity of the receiver and the filters employed. Unless the star shows abrupt variations of energy distribution in its spectrum, caused, for example, by intense emission lines or strong molecular bands, the magnitude of the star will be nearly the same as it would be if all the recorded light were lumped together at one wave length, called the effective wave length. For any combination of telescope, plate, and filter, the effective wave length can be determined with the aid of a wire grating placed over the objective. The effective wave length for conventional photographic magnitudes is $\lambda 4250$. In photoelectric work, λ_{eff} is found from the filter transmission and cell sensitivity.

The effective wave length changes in going from hot to cool stars in the sense that λ_{eff} becomes greater for the cooler stars. The effect will be more serious the greater the wave length range covered in a given filter and plate combination. For a small range of wave length and of spectral type, λ_{eff} usually may be regarded as constant.

The impression upon the photographic plate will be proportional to $r^{-2}\pi R^2 E(\lambda_e, T) Q\, \Delta\lambda$, where R is the radius of the star whose distance is r and E is the emission at the effective wave length λ_e over a wave length interval $\Delta\lambda$. Q is a factor which depends on the sensitivity of the apparatus and the transparency of the optical system. We assume that atmospheric extinction has been determined and taken into account.

Further, let us suppose that the stellar energy distribution may be represented by the Planckian function, eqn. (3), for some temperature. That is,

$$E(\lambda_e, T) = \pi K I(\lambda_e, T) \tag{9}$$

where the factor K takes account of the fact that although T may represent the wave length distribution of the energy, it does not necessarily describe the quantity of the radiation. For a given λ_e K will depend slightly on the temperature. If we assume I is given by eqn. (3) and express the measured brightness in magnitudes, we obtain

$$m_\lambda = -2.5 \log \pi^2 Q - 2.5 \log K c_1 \lambda_e^{-5}\, \Delta\lambda - 5 \log R + 5 \log r + \frac{2.5 c_2}{\lambda_e T} \log_{10} e + 2.5 \log (1 - e^{-c_2/\lambda_e T}) \tag{10}$$

where log means $\log_{10}$. Eqn. (10) can be written in the form

$$m_\lambda = a - 5 \log R + \frac{1.561}{\lambda_e T} + x + 5 \log r \tag{11}$$

Here, a represents the first two terms of eqn. (10) and x is the last term on the right of eqn. (10). If the distance r of the star is known, we may use eqn. (5) of Ch. 1 to obtain an expression for the absolute magnitude of the star for the wave length in question, viz.:

$$M = C_\lambda - 5 \log R + \frac{1.561}{\lambda_e T} + x \tag{12}$$

The correction factor, x, has been tabulated by Russell-Dugan-Stewart* as follows:

$\frac{1.561}{\lambda_e T}$	1.0	2.0	3.0	4.0	5.0
x	−0.55	−0.19	−0.07	−0.03	−0.01

For Harvard photovisual magnitudes, $\lambda_e = 5480$. We may evaluate the constant, $C_\lambda = 5 + a$ with the aid of the known absolute photovisual magnitude (+4.73), the diameter, and the temperature (5700°K) of the sun. We express stellar radii in terms of the solar radius. Then $C_\lambda = -0.27$ and we have

$$M_{vis} = -0.27 - 5 \log R + \frac{28{,}500}{T} \tag{13}$$

as the relation between absolute visual magnitude, radius, and temperature for the stars like the sun. Thus, given the gradient and the absolute

* *Astronomy* (Boston: Ginn & Co., 1927), II, p. 732.

visual magnitude, we may estimate the stellar diameter.* It is evident that the procedure is rough since the factor K, here treated as a constant, varies slightly with the temperature.

5. Color Indices

For photographic magnitudes, the effective wave length is λ4250 and from eqn. (12) there results:

$$M_p = C_p - 5 \log R + \frac{36{,}700}{T} \tag{14}$$

By definition, for an $A0$ star, $m_v = m_p$, and $M_v = M_p$. If T is taken as 12,000°K (as a compromise between the effective and color temperatures), C_p will be -0.95. For any star undimmed by space absorption, the color index,

$$\text{C.I.} = M_p - M_v$$

is related to the temperature T by

$$T = \frac{8200}{\text{C.I.} + 0.68} \tag{15}$$

In view of the crudeness of the assumption that stars radiate like black bodies, we have neglected the small correction factor x in eqns. (13), (14), and (15). Furthermore, the temperature determined from eqn. (15) is rather loosely defined, correlated with, but not identical with, either the effective or color temperature.

One may also determine red indices, i.e., the difference between visual and photo-red magnitudes. The zero-point of the red magnitude system is so chosen that the red index will vanish for an $A0$ star.

It is sometimes necessary to compare the luminosities of two stars with reference to the total radiation they emit, i.e., to compare their bolometric magnitudes. The bolometric correction is defined as the difference between the bolometric and photovisual magnitude, i.e.,

$$\text{B.C.} = m_{\text{bol}} - m_{pv}$$

The scale is so adjusted that the bolometric corrections are small for stars such as the sun ($G2$). They become large for high-temperature stars which radiate mostly in the far ultraviolet and for the cool stars whose principal energy output is in the infrared. Much of the infrared radiation may be measured with the thermocouple, although the corrections for absorption by water-vapor in the earth's atmosphere are troublesome. From such data, together with information supplied by eclipsing binaries, Kuiper has derived empirical bolometric corrections. At the other end of the temperature scale, bolometric corrections must be computed by theory. Here it is necessary to take into account, as best we can, the deviations of the energy distribution from that of a black body. (See Ch. 7.) For the hotter stars, the uncertainty in the temperature introduces a further uncertainty in the bolometric correction. Tables 3 and 4 give the empirical and theoretical bolometric corrections published by Kuiper.

* The stellar interferometer has been employed to measure angular diameters of red giant and supergiant stars. Thus, if the angular diameter of a star is known and its distance can be measured, R and M_{vis} are determined. From eqn. (13) one can then find the temperature.

TABLE 3

EMPIRICAL BOLOMETRIC CORRECTIONS IN MAGNITUDES FOR THE COOLER STARS*

(After Kuiper)

Spectrum	Main Sequence	Giants $M = 0.0$	c Stars $M = -4.0$	Spectrum	Main Sequence	Giants $M = 0.0$	c Stars $M = -4.0$
$F2$	−0.04	−0.04	−0.04	$K4$	−0.55	−1.11	−1.56
$F5$	0.04	0.08	0.12	$K5$	0.85	1.35	1.86
$F8$	0.05	0.17	0.28	$K6$	1.14		
$G0$	0.06	0.25	0.42	$M0$	1.43	1.55	2.2
$G2$	0.07	0.31	0.52	$M1$	1.70	1.72	2.6
$G5$	0.10	0.39	0.65	$M2$	2.03	1.95	3.0
$G8$	0.10	0.47	0.80:	$M3$	(2.35)	2.26	−3.6
$K0$	0.11	0.54	0.93:	$M4$	(2.7)	2.72	
$K2$	0.15	0.72	1.20	$M5$	−(3.1)	−3.4	
$K3$	−0.31	−0.89	−1.35				

* From *Astrophysical Journal* (University of Chicago Press) **88**, 429, 1938.

TABLE 4

THEORETICAL BOLOMETRIC CORRECTIONS IN MAGNITUDES FOR THE HOT STARS†

(After Kuiper)

Temperature °K	B.C.	Temperature °K	B.C.	Temperature °K	B.C.
6000	−0.06	10,000	−0.57	20,000	−2.18
6500	0.00	11,000	−0.78	22,000	−2.40
7000	−0.01	12,000	−0.98	25,000	−2.69
7500	−0.12	14,000	−1.36	30,000	−3.12
8000	−0.22	16,000	−1.66	40,000	−3.8
9000	−0.40	18,000	−1.94	50,000	−4.3

† *Ibid.*

The giant star Aldebaran, $K5$, has an apparent magnitude of 1.06. The bolometric correction is -1.35 and, hence, the star has a bolometric magnitude of $1.06 - 1.35 = -0.29$. Bolometrically, the irregular variable, α Orionis, $M2$, mag. 0.1 to 1.2, becomes brighter than Sirius ($m = -1.58$, $T = 10{,}000°\text{K}$), since the bolometric correction of α Orionis is -3.0.

Magnitudes measured with a thermocouple are called radiometric magnitudes. The thermocouple responds to all radiation that reaches it, but the resultant magnitudes still must be corrected for the effects of atmospheric extinction in order to obtain bolometric magnitudes. The difference between the visual and radiometric magnitude of a star,

$$m_{\text{visual}} - m_{\text{radiometric}}$$

is called its heat index. The zero-point of the radiometric magnitude scale is so chosen that the heat index is zero at class $A0$. Heat indices are positive and large for cool, red stars.

PROBLEMS

1. Derive the formula for the gradient in terms of frequencies rather than wave lengths.

2. If the maximum and minimum temperatures of χ Cygni are 2240°K and 1640°K respectively, what are the color indices?

3. If the absolute visual magnitude of τ Scorpii is -2.4, $T = 28{,}150°\text{K}$, $m_{\text{vis}} = 2.9$, calculate the distance of the star, its bolometric magnitude, and diameter. If the surface gravity is 8.5×10^4 cm/sec^2, what is its mass? How does this value of g compare with that derived from the empirical relation eqn. (11) of Chapter 1?

4. The star ε Eridani has an apparent visual magnitude of 3.8, a parallax of 0".301, and a spectrum of class $K0$. Compute the absolute visual magnitude, the diameter, the luminosity in terms of the sun. Estimate the mass from the empirical mass-luminosity relationship and compute the surface gravity.

5. A star whose temperature is 32,000°K has an apparent magnitude of 11.6 and a distance of 3000 parsecs. Calculate its diameter and absolute bolometric magnitude.

REFERENCES

Textbooks:

Russell, H. N., R. S. Dugan, and J. Q. Stewart. *Astronomy.* Boston: Ginn & Co., 1927, Vol. II, chap. xxi.

Unsöld, A. *Sternatmosphären.* Berlin: Julius Springer, 1938, pp. 21–61.

Among the measurements of the energy distribution in the sun, we mention:

Abbot, C. G. *Annals of the Astrophysical Observatory of the Smithsonian Institution,* Washington, D. C., **2,** 1908; **3,** 1913; **4,** 1922; **5,** 1932; **6,** 1942. (See also *Smithson. Misc. Coll.* **87,** 15, 1932.)

Pettit, E. *Ap. J.* **91,** 159, 1940; **75,** 185, 1932. (See also his chapter in Hynek's *Astrophysics.*)

Chalonge, D., and R. Canavaggia. *Ann. d'Ap.* **9,** 143, 1946.

The earlier measures were combined in a definitive energy curve for the sun by:

Mulders, G. *Zeits. f. Ap.* **11,** 132, 1936.

Limb-darkening measurements have been made by:

Abbot, C. G. *Ann. Smithson. Inst.* **3,** 159, 1913; **4,** 220, 1922.

Moll, W. J. H., H. C. Burger, and J. van der Bilt. *B. A. N.* **3,** 83, 1925.

Raudenbush, H. *A. N.* **266,** 301, 1938.

Chalonge, D., and R. Canavaggia. *Ann. d'Ap.* **9,** 143, 1946.

Minnaert, M., E. van den Hoven van Genderen, and J. van Diggelen. *B. A. N.* **11,** 55, 1949.

Pierce, A. K., R. R. McMath, Leo Goldberg, and O. C. Mohler. *Ap. J.* **112,** 289, 1950.

The numerical value of the solar constant has been discussed by:

Allen, C. W. *Observatory* **70,** 154, 1950.

For a discussion of stellar color temperatures and spectrophotometry see:

Williams, R. *Publ. Obs. Michigan* **7,** 93, 1938; 147, 159, 1939.

Kienle, Strassl, and Wempe. *Zeits. f. Ap.* **16,** 201, 1938.

Kienle, Wempe, and Beileke. *Zeits. f. Ap.* **20,** 91, 1940.

Barbier, D., and D. Chalonge. *J. des Obs.* **19,** 166, 1936; *Ann. d'Ap.* **3,** No. 2, 1940; **4,** 30, 1941; *Observatory* **62,** 273, 1939.

Greaves, Davidson, and Martin. *M. N.* **94,** 488, 1934; *Observatory* **62,** 252, 1939.

Greaves, W. M. H. *M. N.* **108,** 131, 1948.

Hall, J. S. *Ap. J.* **94,** 71, 1941.

Stebbins, J., and A. E. Whitford. *Ap. J.* **102,** 273, 1945.

The empirical relation between color and radiation temperatures for eclipsing stars is discussed by:

Becker, W. *Zeits. f. Ap.* **25,** 145, 1948.

Radiometric measurements and heat indices are discussed by:

Pettit, E., and S. B. Nicholson. *Ap. J.* **68,** 279, 1928; **78,** 320, 1933.

Monochromatic stellar fluxes have been determined by:

Milford, N. *Ann. d'Ap.* **13,** 251, 1950.

Code, A. D. *Observatory,* **72,** 201, 1952.

CHAPTER 7

The Continuous Spectra of the Sun and Stars

1. The Problem of the Continuous Spectrum

Although many stars radiate roughly like black bodies, important exceptions exist. The continuous spectra of the cooler stars are blighted by numerous absorption lines. In hotter stars such as those of spectral class *A*, the strong wave length dependence of the continuous hydrogen absorption plays havoc with the black body approximation.

Thus, two effects—the discrete absorptions of the spectral lines and the continuous absorption of hydrogen—distort the continuous energy curves of many stars.

Yet, it is worthwhile to pose this question: if the continuous stellar absorption coefficient were independent of wave length (as is actually true for electron scattering) and each volume element of the atmosphere radiated like a *grey* body, would the stellar energy curve be Planckian? The observed energy distribution is the sum of contributions from all layers from which radiation may escape to the surface. The uppermost strata are coolest and the underlying layers become increasingly warmer. If each stratum radiates according to Kirchhoff's law, then the energy distribution contributed by each zone of constant temperature will be Planckian in character, and the resultant energy output of the star will be the sum of many black body curves, each weighted according to the amount of radiation from that particular stratum that reaches the surface. Almost all the radiation from the upper, cooler layers reaches the surface, while the light from the deeper layers is dimmed by absorption in the intervening strata. From great depths but little of the radiation is able to reach the surface.

In most stars the absorption coefficient is not independent of wave length, with the consequence that in spectral regions where the absorption coefficient is high, the emergent radiation all comes from the uppermost layers, whereas in other spectral regions much of the observed radiation comes from relatively hot, deep strata. The continuous absorption coefficient in an *A* star provides an illustration. To the longward side of the Balmer limit at λ3650 the continuous absorption coefficient is less than it is on the shortward side of the Balmer limit. Hence to the red of λ3650 and between the Balmer lines, the observed radiation comes from much greater depths than does the radiation to the violet of the

Balmer limit. At λ3600, for example, radiation reaches us only from the coolest, outermost levels of the atmosphere.

For most stars we observe only a quantity proportional to the energy distribution in the integrated light, viz., $F_\lambda \frac{R^2}{d^2}$ where R is the radius of the star and d is its distance. For the sun we can observe both the intensity distribution at the center of the disk, $I_\lambda(0)$, and the variation of the intensity distribution across the disk, $I_\lambda(\theta)/I_\lambda(0)$, the so-called darkening to the limb. This latter effect provides the most elementary argument for the existence of a temperature gradient in the sun. At the

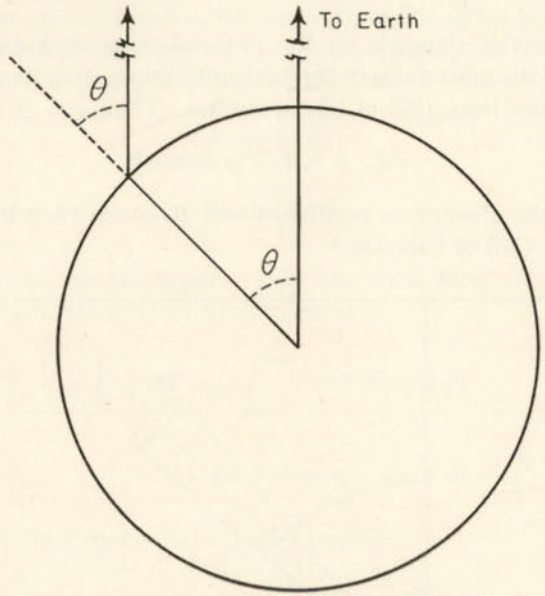

Fig. 1.—Emergent Ray from the Sun

center of the disk we see to much deeper and hotter layers than we do near the limb where our line of sight enters the solar atmosphere at a glancing angle. From the limb-darkening data and $I_\lambda(\theta)$ it is possible to find both the variation of the absorption coefficient with wave length and the temperature gradient in the solar atmosphere.

In order to interpret the observations we shall derive an expression for $I_\lambda(0, \theta)$, the intensity of the radiation emitted by a star in any wave length, λ, and at any angle θ with respect to the normal drawn to the surface. We may express our results in terms of either the wave length λ, or the frequency ν.

In Fig. 1, the ray reaching the observer from the point on the surface of the sun emerges at an angle θ with respect to the outward normal.

This ray comprises contributions from heated strata at many different depths.

Consider a layer at a depth x and temperature T, and let us fix our attention upon a small cylinder of unit area and thickness

$$ds = \sec\theta\, dx \tag{1}$$

(see Fig. 2). The total emissivity per gram of material is j_ν and since a volume ds contains a mass $\rho\, ds$, the intensity of the radiation emitted by the box will be

$$dE_\nu = \frac{1}{4\pi} j_\nu \rho\, ds \tag{2}$$

The emissivity depends on the physical conditions existing in the cylinder. If the material is in thermal equilibrium with its surroundings, Kirchhoff's law [eqn. (22) of Ch. 5] applies. Then

$$dE_\nu = k_\nu B_\nu(T)\rho\, dx \sec\theta \tag{3}$$

where k_ν is the absorption coefficient and B_ν is the Planck function defined in eqn. (10) of Chapter 5.

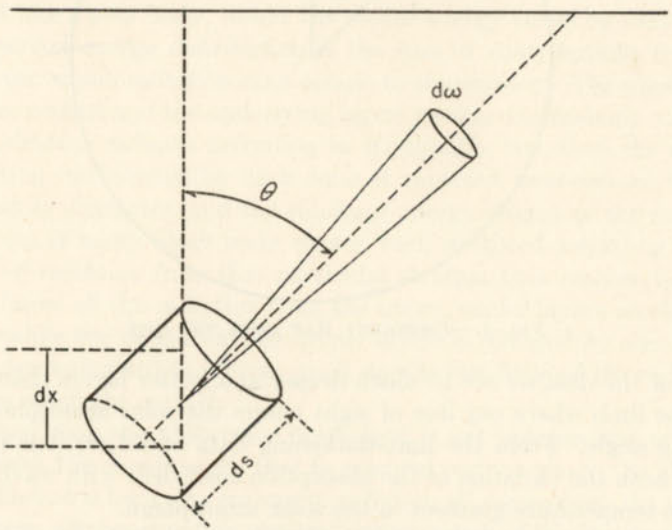

FIG. 2.—ELEMENTARY EMITTING VOLUME

The radiation emitted by the elementary cylinder in the direction of the observer is weakened by the absorption of the overlying strata, such that the contribution dI_ν which actually reaches the surface is

$$dI_\nu = e^{-\tau_\nu \sec\theta}\, dE_\nu \tag{4}$$

where the optical depth τ_ν is defined by eqn. (20) of Chapter 5. Therefore, the intensity of the emergent beam is the integral taken over all the elementary cylinders in the line of sight:

$$I_\nu(0,\theta) = \int_0^\infty B_\nu(T)\, e^{-\tau_\nu \sec\theta} \sec\theta\, d\tau_\nu \tag{5}$$

This is the fundamental relation expressing the connection between the emissivity of the radiating layers, the optical depth, and the observed intensity of the emergent beam. Since the absorption coefficient depends on wave length, it is clear that the temperature will be a different function of the optical depth τ_ν [cf. eqn. (20) of Ch. 5] for one frequency, say ν_1, than for another frequency, say ν_2. Hence, it is often desirable to define an optical depth in terms of some kind of an average coefficient of absorption $\bar{k}$. Thus

$$d\tau = \bar{k}\rho\, dx \tag{6}$$

or

$$d\tau_\nu = \frac{k_\nu}{\bar{k}}\, d\tau \tag{7}$$

In most stars we can observe only the total flux, πF_ν. Substitute eqn. (5) into eqn. (4) of Chapter 5 to obtain

$$F_\nu = 2\int_0^\infty B_\nu(T)\, d\tau_\nu \int_0^{\pi/2} e^{-\tau_\nu \sec\theta} \sin\theta\, d\theta \tag{8}$$

Now let

$$\sec\theta = y, \qquad \sin\theta\, d\theta = \frac{dy}{y^2}$$

and introduce the exponential integral function

$$E_n(x) = \int_{y=1}^\infty \frac{e^{-xy}}{y^n}\, dy \tag{9}$$

where E_1 is called simply E, and $E_0 = e^{-x}/x$. Then eqn. (8) becomes

$$F_\nu = 2\int_0^\infty B_\nu(\tau_\nu) E_2(\tau_\nu)\, d\tau_\nu \tag{10}$$

The flux (or intensity) of the emergent radiation depends on the rate at which the temperature increases with optical depth, i.e., on the temperature gradient, and on the absorptivity of the stellar material. The formula says nothing about the way in which the temperature gradient is maintained. The particular value the gradient will assume at any point will depend on the mode of energy transport, whether it is by molecular conduction, convection currents, or radiation.

Since the thermal conductivity of gas is low, e.g., that of helium is 0.344×10^{-3} cal/cm^2/sec/deg at N.T.P., we can easily show that thermal conduction can play no important role. In order for this process to supply the energy output of the sun, the required temperature gradient would be so high that actually the lower layers would lose more energy by thermal emission than by conduction, thus contradicting our hypothesis.

Convection currents require for their continued existence a different temperature gradient than that needed for the radiative transport of energy. Although the photospheric granules suggest that convection currents play some role in the outer layers of the sun, the temperature gradient demanded by the observations for the uppermost strata is more nearly in accord with that appropriate to the transport of energy by radiation than with that valid for a state of convective equilibrium. Below the radiative zone there is a zone in convective equilibrium. (See Ch. 9.)

Our principal tasks in this chapter will be not only to obtain solutions of eqns. (5) and (10) but also to show how these expressions may be employed in the interpretation of observable features of stellar spectra.

For example, the determination of the color temperature of a star amounts to fitting a Planckian curve to F_ν over a definite wave length interval, e.g., λ4000–λ6500. Thus, the so-defined temperature is only the parameter inserted in Planck's formula when the latter is used as a convenient interpolation device. Its relation to the physically significant effective temperature will depend on the temperature gradient and the absorption coefficient and is often complicated.

Our plan of attack will be as follows: First we shall investigate the theory of the stellar absorption coefficient both for a hot star and for a relatively cool one such as the sun. Then we shall show how the absorption coefficient in the solar atmosphere may be found empirically from the law of limb darkening and $I_\lambda(\theta)$. The agreement between theory and observation confirms our belief that the negative hydrogen ion is the principal source of opacity in the sun. The relation between color and effective temperature likewise may be explained in a satisfactory fashion.

The flow of radiation through a stellar atmosphere is a topic of utmost importance. We shall derive the equation of transfer and show how the temperature may be expressed in terms of the optical depth for a grey atmosphere. This is a problem of pure mathematics which has been treated by methods similar to those employed for the study of neutron diffusion in a radioactive pile, as well as by an elegant procedure suggested by Chandrasekhar. Unfortunately, the material of which stellar atmospheres are composed is not grey. Modifications are therefore required in the theory. The problem of radiative transfer in monochromatic light cannot be reduced easily to that of a grey body. We shall discuss the limb-darkening observations from the point of view of the temperature gradient and show how radiative equilibrium rather than convective equilibrium accounts for the temperature gradient of the outer atmosphere.

With the temperature gradient established we can derive the march of gas pressure, electron pressure, and continuous absorption coefficient with depth in a stellar atmosphere, i.e., the *model* of the atmosphere. Such model atmospheres will assume considerable importance in the interpretation of the dark-line spectra of the sun and stars. Finally, we return to the question of effective temperatures and show how measures of color temperatures and Balmer discontinuities together may determine both the effective temperature and the mean electron pressure in the atmosphere of a star.

2. The Stellar Absorption Coefficient

Because of its overwhelming predominance, hydrogen is the leading source of opacity in stellar atmospheres. In Chapter 5 we enumerated the processes responsible for the continuous absorption in stellar atmospheres. They were:

(1) Photoionization from discrete levels of hydrogen to the continuum (bound-free transitions).
(2) Free-free transitions wherein an electron traveling in one hyperbolic orbit near an atom jumps to another hyperbolic orbit with the absorption of energy.
(3) Electron scattering.
(4) Photodissociation of the negative hydrogen ion with consequent absorption of energy.
(5) Continuous absorption by molecules resulting in their dissociation.

In stars such as the sun, the negative hydrogen ion primarily determines the absorption coefficient. In the hotter *A* and *B* stars, the photoionization of atomic hydrogen and free-free transitions play the major roles, whereas in the *O* stars, electron scattering and even the photoionization of helium may make important contributions to the opacity. In the coolest stars, continuous molecular absorption (corresponding to their photodissociation) and the blocking of outgoing radiation by strong absorption lines become important. For most of the spectral sequence, from *B*0 to the late *K*'s, absorption processes involving hydrogen primarily determine the continuous absorption.

3. The Absorption Coefficient of Atomic Hydrogen

We shall now show in detail how one may calculate the absorption coefficient for atomic hydrogen. We first consider the photoionizations from discrete levels, which produce the bulk of the absorption in spectral regions normally accessible to observation.

The absorption coefficient per hydrogen atom in the nth level, $\alpha_n(\nu)$, is given by eqn. (98) of Chapter 5. Under conditions of thermal equilibrium, the number of atoms in level n, N_n, will be given by the Boltzmann formula (Ch. 4). Hence the contribution of atoms in level n to the absorption coefficient will be

$$N_n\alpha_n(\nu) = n^2N_1e^{-(X_1-X_n)}\alpha_n(\nu) \tag{11}$$

where N_1 denotes the number in the ground level, X_n is defined by eqn. (102) of Chapter 5, and $2n^2$ is the statistical weight of the level n.

At any particular wave length the absorption will comprise contributions from a number of different levels. At λ4000, for example, transitions from the third and higher levels are responsible for the continuous absorption. Photoionizations from the second level involve only quanta of wave lengths shorter than λ3650 and therefore cannot play any role at λ4000. At λ3600, contributions from $n = 2$ would have to be taken into account, whereas ionizations from the ground level, $n = 1$, need be considered only at wave lengths shorter than λ912. Our procedure will be to calculate the absorption coefficient for each level n by eqn. (98) of Chapter 5 and eqn. (11) of this chapter and then to sum over all levels that can contribute to the absorption at the wave length in question.

The number of hydrogen atoms per gram will be $1/M$. Here, M denotes the mass of one hydrogen atom. The absorption coefficient per gram of neutral hydrogen for bound-free transitions is

$$k_1(\nu) = \frac{32}{3\sqrt{3}}\frac{\pi^2\varepsilon^6RZ^4}{Mch^3}\frac{e^{-X_1}}{\nu^3}\sum\frac{1}{n^3}e^{X_n}g \tag{12}$$

where the summation is taken only over those levels for which ν exceeds ν_n [cf. eqn. (102) of Ch. 5]. For the interval λ8200–λ3650, for example, we sum over all terms, $n \geq 3$; from λ3650–λ3000 we sum over all terms, $n \geq 2$, etc. Unsöld and Pannekoek have carried out detailed calculations of $k_1(\nu)$. Unsöld set $g = 1$ throughout and performed the indicated summations for levels 1 to 4, while for the higher levels he replaced the summation by an integral

$$\sum\frac{1}{n^3}e^{X_n} \rightarrow -\frac{1}{2}\int e^{X_n}\,d\left(\frac{1}{n^2}\right) = -\frac{1}{2X_1}\int e^{X_n}\,dX_n = \frac{(e^{X_5}-1)}{2X_1} \tag{13}$$

where the integration is extended from X_5 to $X_n = 0$.

Finally, we must add to $k_1(\nu)$ the contributions from the free-free absorptions. The absorption coefficient per proton and free electron with velocity between v and $v + dv$ is

$$\alpha_\kappa(\nu)\,dv = \frac{2}{3\sqrt{3}}\frac{RZ^2h^2\varepsilon^2}{m^3\pi cv}\frac{g}{\nu^3}\,dv \tag{14}$$

If there are N_i protons/cm³ and $N_ef(v)\,dv$ electrons/cm³ with a velocity v to $v + dv$, the free-free absorption coefficient per cm³ will be

$$N_iN_ef(v)\alpha_\kappa(\nu)\,dv = \rho\,dk_\nu \tag{15}$$

where the velocity distribution of the electrons is given by eqn. (15) of Chapter 3. Furthermore N_iN_e may be expressed in terms of N_1 by means of the combined Boltzmann and Saha eqns. (26) of Chapter 4. Since electrons moving with any velocity v may absorb at the frequency ν, we must integrate eqn. (14) for a fixed frequency, over all velocities. Making use of the notation of eqn. (102) of Chapter 5 we get

$$ve^{-\frac{mv^2}{2kT}}\,dv = \frac{kT}{m}e^{-X_\kappa}\,dX_\kappa \tag{16}$$

Then, with the aid of eqns. (15) of Chapter 3, (26) of Chapter 4, (94) of Chapter 5, and (14) and (16) of this chapter we write eqn. (15) in the form

$$\rho\,dk_\nu = \frac{8}{3\sqrt{3}}\frac{RZ^2\varepsilon^2}{hmc}\frac{N_1kTg}{\nu^3}e^{-(X_1+X_\kappa)}\,dX_\kappa \tag{17}$$

Note that the density $\rho = N_1M$. Integrate eqn. (17) from $X_\kappa = 0$ to $X_\kappa = \infty$. Then add the resultant expression to eqn. (12), making use of eqn. (13) to obtain the complete absorption coefficient of atomic hydrogen per gram of neutral hydrogen,

$$k(\nu) = \frac{32}{3\sqrt{3}}\frac{\pi^2\varepsilon^6RZ^4}{ch^3M}\frac{e^{-X_1}}{\nu^3}\left\{\sum_{\nu_n<\nu}^{X_5}\frac{e^{X_n}}{n^3}\bar{g}_n + \frac{e^{X_5}}{2X_1}\bar{g}\right\} \tag{18}$$

A plot of the absorption coefficient against frequency has a jagged appearance (Fig. 15 of Ch. 5). Between successive series limits the absorption coefficient falls off as ν^{-3} but rises abruptly as the series limit is approached and successive hydrogen lines coalesce to form a continuum. The confluence of the Balmer series near λ3650 well illustrates this phenomenon.

The continuous absorption coefficient of atomic hydrogen varies with the temperature. At low temperatures nearly all hydrogen atoms are in the ground state and practically all absorption takes place from this lowest level, i.e., in wave lengths shorter than λ912. Since little radia-

tion falls in this spectral region, the contribution of atomic hydrogen to the opacity is small.

At higher temperatures the upper levels begin to be populated. Photoionizations may occur from the second and higher levels with the consequence that considerable absorption occurs in ordinary wave lengths.

Simultaneously, the fraction of radiation in the ultraviolet steadily increases. Photoionizations from the ground level become increasingly frequent. Atomic hydrogen then determines the opacity until it becomes practically all ionized. Only for stars somewhat hotter than the sun ($T > 8000°$K) are the bound-free absorptions important, and only in the very hottest stars do the free-free absorptions make any appreciable contribution.

4. Continuous Absorption in the Hotter Stars

The calculation of the coefficient of continuous absorption for the hotter stars involves a consideration not only of the contribution of atomic hydrogen but also of the effects of electron scattering, and sometimes also of helium, although in most instances the contribution of the latter will be small. The theory for helium is formally similar to that for hydrogen, but photoionization from the ground level corresponds to transitions in the far ultraviolet and the Boltzmann factor cuts down the role of the excited levels even in the hottest stars. In most instances, we need consider only atomic hydrogen in the range from 10,000°K to 20,000°K.

We shall now illustrate, by means of a practical example, the computation of the absorption coefficient for a hot star. Let us assume

$$\theta = \frac{5040}{T} = 0.17 \quad (T = 29{,}600°\text{K})$$

and

$$\log P_e = 3.0$$

First of all we shall compute the absorption coefficient for atomic hydrogen which will be the largest contributor. Write the expression eqn. (18) for $k(\nu)$ in the form

$$k(\nu) = D\frac{1}{\alpha^3}\left\{\sum \frac{e^{X_n}}{n^3}\bar{g}_n + \frac{e^{X_5}}{2X_1}\bar{g}\right\} = \frac{H}{\alpha^3} \tag{19}$$

where, now:

$$\alpha = h\nu/kT$$

and D is a numerical coefficient that depends on the temperature. For $\theta = 0.17$ we find $\log D = 6.553$. The factor in brackets is multiplied by D to form the quantity H, which is computed in Table 1. The first column gives n, the second the corresponding wave length, the third column the corresponding value of the frequency, and the fourth column X_n. Next we compute e^{X_n}/n^3 (column 5), estimate the Gaunt factor $\bar{g}_n$ (column 6) from the data of Menzel and Pekeris,

TABLE 1

CALCULATION OF THE ABSORPTION COEFFICIENT FOR ATOMIC HYDROGEN

(1) n	(2) λ	(3) $\nu \times 10^{-15}$	(4) X_n	(5) $\frac{e^{X_n}}{n^3}$	(6) $\bar{g}_n$	(7) $\bar{g}_n\frac{e^{X_n}}{n^3}$	(8) $\sum \bar{g}_n\frac{e^{X_n}}{n^3}$	(9) H
1	912	3.29	5.30	201.5	0.83	167.0	167.6	5.98×10^8
2	3650	0.823	1.324	0.470	0.925	0.435	0.643	2.29×10^6
3	8200	0.366	0.588	0.067	1.0	0.067	0.208	0.743×10^6
4		0.205	0.331	0.022	1.0	0.022	0.141	0.504×10^6
5		0.132	0.212	0.119*	1.0	0.119*	0.119*	0.425×10^6

and calculate the product $\bar{g}_n e^{X_n}/n^3$ (column 7). The entry for $n = 5$ is $e^{X_5}/2X_1$ and is denoted by an asterisk (*). In the eighth column we perform the indicated summation. Thus, $0.141 = 0.119 + 0.022$, $0.208 = 0.141 + 0.067$, etc. Finally, multiplication by D gives the coefficient of $1/\alpha^3$ which we call H. The value 5.98×10^8 is to be applied for wave lengths less than λ912, 2.29×10^6 in the interval λ912–λ3650, and 0.743×10^6 in the λ3650–λ8200 region. To derive $k(\nu)_H$, the absorption coefficient per gram of neutral hydrogen, we note that for $T = 29{,}600°$K, $\alpha = 1.62 \times 10^{-15}\nu$.

Table 2 gives $\log k(\nu)_H$ per gram of neutral hydrogen as a function of ν. At the series limits, approximately λ8200, λ3650, and λ912, there are two entries corresponding to the absorption coefficient above and below the limit. To

TABLE 2

DEPENDENCE OF THE HYDROGEN ABSORPTION COEFFICIENT ON WAVE LENGTH

$\nu \times 10^{15}$	α	Log $k_{gm}(\nu)_H$	Log $k_s(\nu)_H$	Corr.
0.30	0.48	6.64	1.09	
0.366	0.59	6.38	0.83	
0.366	0.59	6.55	1.00	0.00
0.60	0.97	5.90	0.35	0.00
0.82	1.33	5.49	−0.06	−0.02
0.82	1.33	5.98	0.43	−0.01
1.00	1.62	5.73	0.18	0.00
2.00	3.24	4.83	−0.72	0.03
3.29	5.33	4.18	−1.37	0.05
3.29	5.33	6.60	1.05	0.00
4.00	6.48	6.35	0.80	0.02
5.00	8.10	6.05	0.50	0.03
6.00	9.72	5.83	0.28	0.05
7.00	11.32	5.62	0.07	0.06
8.00	13.00	5.44	−0.11	0.07
10.00	16.20	5.15	−0.40	0.08
12.00	19.50	4.91	−0.64	0.08

apply the results of column 3 of Table 2 to an actual stellar atmosphere we must take into account the composition of the atmosphere and the ionization of hydrogen. From the ionization equation and the given T and P_e we find the ratio of ionized to neutral hydrogen to be 2.5×10^5, i.e., $\log k$ must be diminished by 5.40 to allow for the ionization of hydrogen. Secondly, on the basis of analyses of stellar atmospheres, we adopt abundance ratios (by weight) of 1000, 400, and 20 for H, He, and the elements of the oxygen group respectively. Hence, each gram of stellar material is assumed to contain 0.70 grams of hydrogen, and therefore

$$\log k_s(\nu) = \log k_{gm}(\nu) - 5.55 \tag{20}$$

gives the hydrogenic contribution to the stellar absorption coefficient. The last column gives the correction that is to be applied because the g factor is not constant but depends on wave length. The correction becomes large only at some distance from the absorption maximum and the practical effect upon the absorption is small.

Next, let us add the helium contribution.* The absorption coefficients for $\theta = 0.17$ are given in the second column of Table 3. With an electron pressure of 10^3 dynes, the ionization of He I is nearly complete, log He II/He I = 4.15,

TABLE 3

THE STELLAR ABSORPTION COEFFICIENT

$T = 29{,}600°K$, $\log P_e = 3.0$

(1)	(2)	(3)	(4)	(5)	(6)
$\nu \times 10^{-15}$	$\log k_{gm}(\nu)_{He}$	$\log k_s(\nu)_{He}$	k_{star}	$(1 - e^{-\alpha})$	$k'_\nu + \sigma$
0.30		(−0.6)	12.4	0.385	5.11
0.366		(−0.6)	7.0	0.447	3.45
0.366		(−0.6)	10.3	0.447	4.91
0.60	4.07	−0.64	2.47	0.623	1.85
0.82	3.83	−0.88	1.00	0.737	1.05
0.82	3.83	−0.88	2.84	0.737	2.41
1.00	3.83	−0.88	1.65	0.802	1.63
1.5	3.53	−1.18	0.52	0.905	0.78
2.0	3.21	−1.50	0.21	0.961	0.51
2.5	2.97	−1.74	0.12	0.982	0.42
3.29	2.57	−2.14	0.05	1.00	0.36
3.29	2.57	−2.14	11.2	1.00	11.5
4.0	2.46	−2.25	6.46	1.00	6.8
5.0	2.18	−2.53	3.40	1.00	3.7
6.0	6.06	+1.36	24.7	1.00	25.0
7.0	5.93	+1.22	17.8	1.00	18.1
8.0	5.84	+1.13	14.4	1.00	14.7
10.0	5.62	+0.91	8.6	1.00	8.9
12.0	5.45	+0.74	5.8	1.00	6.1

* Our numerical values are interpolated from a table by Greenstein (who employed absorption coefficients computed by Goldberg) and from the work of Vinti. Su Shu Huang has published improved values recently.

but double ionization is not yet appreciable. Since each gram of the stellar material is assumed to contain 400/1420 (antilog − 0.55) grams of helium, the contribution of this gas to the stellar absorption coefficient is (see column 3 of Table 3):

$$\log k_s(\text{He}) = \log k_{\text{gram}}(\text{He}) - 0.55 - 4.15 - 0.01 \tag{21}$$

Here 0.01 allows for the fact that helium is 97 per cent singly ionized. For the absorption by ionized helium we have

$$\log k_s(\text{He}^+) = \log k_{\text{gram}}(\text{He}^+) - 0.56 \tag{22}$$

which follows from the hydrogenic formula with $Z = 2$, $X_n(\text{He II}) = 4X_n(\text{H})$, and $M_0(\text{He}) = 4M_0(\text{H})$. For temperatures less than 30,000°K, ionized helium makes no appreciable contribution to the stellar absorption coefficient, and we neglect it in our calculations. Thus the stellar absorption coefficient is (see column 4, Table 3):

$$k_\nu = k_\nu(\text{H}) + k_\nu(\text{He}) \tag{23}$$

The negative absorptions increase the transparency of the stellar material to outgoing radiation so that the effective absorption coefficient becomes (see column 5, Table 3):

$$k'_\nu = (1 - e^{-\alpha})k_\nu \tag{24}$$

In addition to the absorption processes of hydrogen and helium, we must now take into account the effect of electron scattering. In Chapter 5, Sec. 10, we showed that the scattering coefficient for free electrons is

$$\sigma = 0.665 \times 10^{-24} N_e \tag{25}$$

where N_e is the number of electrons/gram. If μ_0 is the mean molecular weight of the stellar material when neutral, and M_0 is the mass of a hydrogen atom, and if β is the number of electrons supplied per atom, the scattering coefficient due to the free electrons will be

$$\sigma = a \frac{\beta}{M_0 \mu_0} \tag{26}$$

The molecular weight of a neutral stellar atmosphere in which hydrogen, helium, and the elements of the oxygen group are in the ratio 1000:400:20 is 1.29. The number of atoms per gram is then $0.466 \times 10^{+24}$ and if each atom contributes one electron, the scattering coefficient for free electrons will be

$$\sigma = 0.466 \times 10^{24} \times 6.65 \times 10^{-25} = 0.310 \tag{27}$$

In the first approximation we often simply add the contribution of electron scattering to k'_ν. Thus (see column 6, Table 3),

$$k_{\text{eff}} = \sigma + k'_\nu \tag{28}$$

Actually, as reference to Problems 5 and 6 or eqn. (56) will show, this procedure is not rigorous and electron scattering should be handled in a different way.

Since the electron pressure, gas pressure, and temperature all change with optical depth in the star, k_ν varies also. Nevertheless, an absorption coefficient calculated for some mean optical depth will enable us to interpret some results of observation.

It is easy to understand why the color temperature is greater than the effective temperature in A stars. The absorption coefficient is much larger at λ6500 than at λ4000; hence, we receive radiation from deeper

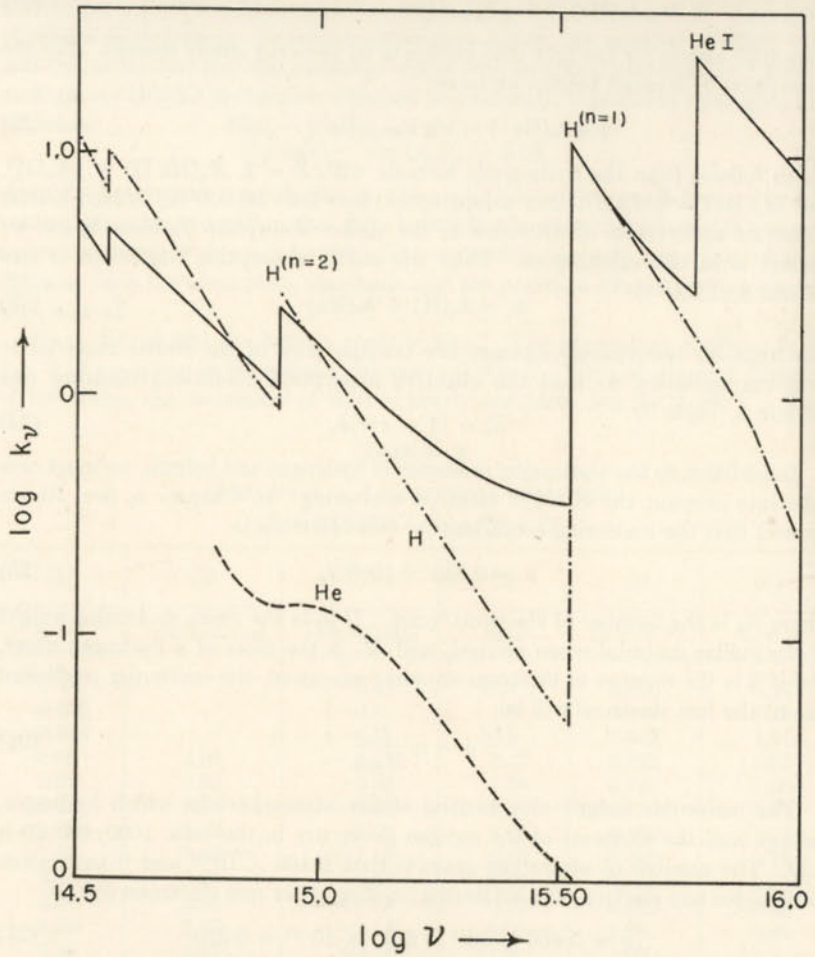

FIG. 3.—THE ABSORPTION COEFFICIENT FOR A HOT STAR

The solid line denotes the value of $k_\nu(1 - e^{-\alpha}) + \sigma$, while the dashed lines give the contributions of hydrogen and helium, respectively, to the absorption coefficient. We assume $T = 29{,}600°$K and $\log P_e = 3.0$. In a giant star the contribution of electron scattering to the total opacity would be much more pronounced.

and hotter layers at λ4000 than at λ6500. A black body curve fitted to the energy curve of the star will correspond to a temperature appreciably higher than the effective temperature. Barbier and Chalonge found that the color temperatures in the ultraviolet are lower than those in the

visible. The absorption coefficient beyond the Balmer limit is greater than that on the redward side and the radiation emerges from higher layers. If the absorption coefficient were infinite, the color temperature in the ultraviolet would be exactly the boundary temperature of the star. Under certain idealized conditions, one may observe a color temperature which is nearly the same as the boundary temperature of the star. Imagine an eclipsing binary in which the fainter star emits a negligible amount of light. When the eclipse is almost total, we observe radiation only from the extreme limb, i.e., the uppermost layers which are nearly at the boundary temperature T_0. Hence, the color temperature should equal the boundary temperature. At a wave length where the absorption coefficient is high, we obtain radiation only from the outermost layers at all phases and hence the color temperature would not change much during an eclipse. In a more transparent region of the spectrum, appreciable changes should be observed.

Barbier and Chalonge made a beautiful observational test of this idea with the eclipsing binary, Algol. The gradient ϕ_1, which measures the color temperature in the blue region of the spectrum, changed appreciably during an eclipse, when most of the primary star was covered, while ϕ_2, which refers to the ultraviolet, changed hardly at all, indicating that in a region of the spectrum where the absorption coefficient is large, one observes the outermost layers at all times. The effect of the secondary star does not appear to be important.

The amount of the Balmer discontinuity is readily observable in the hotter stars (Ch. 6). It depends on the relative numbers of atoms in levels $n = 2$, and $n = 3$ and therefore on the temperature, and also on the extent to which hydrogen contributes to the total opacity. Among the main-sequence high-temperature stars, the Balmer discontinuity is a good indicator of spectral type and therefore of temperature. Barbier and Chalonge found that supergiants show smaller Balmer discontinuities than do main-sequence stars of the same spectral class. Greenstein pointed out that hydrogen is more highly ionized in the supergiants. Therefore electron scattering provides a larger percentage of the opacity in the atmosphere of a supergiant than in that of a main-sequence star.

5. The Absorption Coefficient in the Cool Stars

Although absorption by neutral hydrogen explains the continuous absorption in the hotter stars, it fails by many orders of magnitude for the cool ones. Suppose we compute $k_\nu/\bar{k}$ for neutral hydrogen and evaluate the flux above and below the Balmer limit as a function of temperature from eqn. (10). We find that the Balmer discontinuity D increases without bound as the temperature decreases. On the other hand, if we plot D from the data of Barbier and Chalonge as a function

of spectral type we find that it rises from *B*0 to a maximum at *A*0 and then decreases at still lower temperatures. Evidently some other source of continuous absorption must replace atomic hydrogen at the lower temperatures.

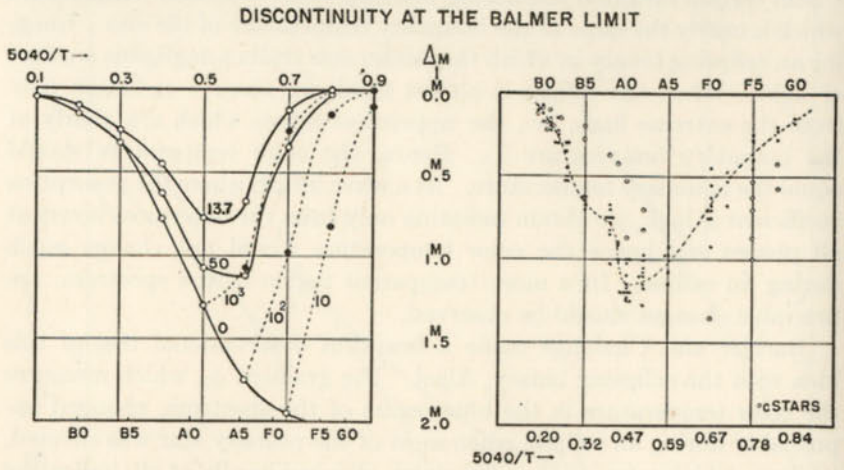

FIG. 4.—THE BALMER DISCONTINUITY AND ITS THEORETICAL INTERPRETATION

The diagram on the right shows the Balmer discontinuity (as measured by Barbier and Chalonge) and expressed in magnitudes plotted as a function of spectral type and $5040/T$ (Kuiper's temperature scale). The ordinates on the left are the theoretical magnitude differences computed for the Balmer discontinuity by means of the integral, eqn. (10), on the assumption $k_\nu/\bar{k}$ is constant with optical depth. The heavy lines computed for an electron pressure of 100 dynes/cm² refer to hydrogen/metal ratios of 13.7:1, 50:1, and ∞:1. Notice that a hydrogen/metal ratio of about 50 is required if only hydrogen and the metals produce opacity in the solar atmosphere.

The broken curves correspond to the effect of H^- absorption at electron pressures of 10, 100, and 1000 dynes/cm² and no metallic absorption. Notice that the Balmer discontinuity can be explained by the assumption that hydrogen and the negative hydrogen ion produce absorption in the solar atmosphere if the electron pressure is somewhat greater than 100 dynes/cm². The agreement is improved with the new calculations by Chandrasekhar. (Courtesy, R. Wildt, *Astrophysical Journal*, University of Chicago Press, **90**, 616, 1939.)

Initially, it was assumed that the metals were responsible for the opacity. If, following Pannekoek, we take a hydrogen to metal ratio of a thousand to one, the atmospheres of the cooler stars will be relatively transparent and the amount of material above the photosphere will be measured in hundreds of grams. On the other hand, if we choose a hydrogen/metal ratio to fit the Balmer discontinuity we find a ratio of about 15. In either event, the metallic line intensities in the cooler stars should be much greater than those observed unless some other agent is responsible for the continuous absorption.

The way out of this difficulty was found by Wildt who suggested

that *negative ions* of hydrogen produce most of the continuous absorption in late-type stars. One interesting aspect of his proposal was that the negative hydrogen ion had not been isolated in the laboratory, but had been predicted on the basis of quantum-mechanical calculations, independently, by H. Bethe and E. A. Hylleraas in 1930. Recently, R. Fuchs has observed the negative hydrogen ion continuum in the laboratory.

The single electron of a hydrogen atom does not completely screen the charge on the nucleus in its immediate neighborhood. An electron that passed sufficiently close to the atom would find itself in an attractive field. It would have a definite chance of becoming attached to the atom to form a negative ion, H^-. Chandrasekhar's exact calculation of the binding energy shows it to be near to 0.75 ev and confirms the fact that there exists only one stable energy state.

The astrophysical importance of the H^- ion lies in the fact that quanta of energy in the ordinary and near infrared spectral regions may photodissociate it into a neutral hydrogen atom and a free electron. The absorption spectrum of H^- in its ground state is a continuum whose edge falls at the wave length corresponding to 0.75 ev (i.e., λ16,650), rises steadily to a maximum near λ8500 and decreases to the shorter wave lengths. In addition to the "bound-free" absorption by the H^- ion, there are also "free-free" transitions, corresponding to the interactions of neutral hydrogen atoms with free electrons.

Calculation of the absorption coefficient of H^- is extremely difficult. Wildt, Massey and Bates, Williamson, and Henrich have discussed this problem, but the most satisfactory treatment is that by Chandrasekhar. An abstract of his results is reproduced in Table 4. Notice that the absorption coefficient is given per neutral hydrogen atom and for an electron pressure of one dyne. Hence, the effect of the temperature upon the dissociation of H^- is already taken into account. To obtain the absorption coefficient for P_e dynes it is necessary only to multiply the tabular value by P_e. Fig. 5, prepared by Chandrasekhar, gives the theoretical absorption coefficient computed for $T = 6300°\text{K}$.

It is of interest to compute the fraction of hydrogen atoms that go to form H^- ions at any temperature and pressure. The H^- ion to H atom ratio obeys an "ionization" equation of the form

$$\frac{N(\text{H}^-)}{N(\text{H})} = \phi(T)P_e \tag{29}$$

where

$$\log \phi(T) = -0.12 + 0.75\theta - 2.5 \log T \tag{30}$$

and P_e is the electron pressure in dynes. For example, at $T = 5600°\text{K}$, $P_e = 10$ dynes, the concentration is antilog $(-7.82) = 1.51 \times 10^{-8}$

TABLE 4

ABSORPTION COEFFICIENT OF THE NEGATIVE HYDROGEN ION

The Continuous Absorption Coefficient of the Negative Hydrogen Ion due to the free-free and bound-free transitions for various temperatures and wave lengths after allowing for the negative absorptions.

λ	$T = 10{,}080°K$ $\theta = 0.5$	$T = 8400°K$ $\theta = 0.6$	$T = 7200°K$ $\theta = 0.7$	$T = 6300°K$ $\theta = 0.8$	$T = 5600°K$ $\theta = 0.9$	$T = 5040°K$ $\theta = 1.0$	$T = 4200°K$ $\theta = 1.2$	$T = 3600°K$ $\theta = 1.4$
11,390Å	0.9599(−26)	1.580(−26)	2.517(−26)	3.910(−26)	5.953(−26)	8.902(−26)	1.902(−25)	3.861(−25)
10,130	0.9701	1.665	2.741	4.366	6.770	10.261	2.229	4.565
9,113	0.9638	1.695	2.838	4.575	7.152	10.901	2.383	4.894
7,594	0.9118	1.640	2.786	4.532	7.124	10.895	2.390	4.915
6,509	0.8344	1.513	2.581	4.206	6.618	10.126	2.222	4.570
5,695	0.7531	1.369	2.337	3.809	5.993	9.169	2.012	4.140
5,063	0.6768	1.230	2.100	3.423	5.385	8.238	1.808	3.721
4,556	0.6086	1.1058	1.887	3.074	4.837	7.401	1.625	3.346
4,050	0.5347	0.9710	1.656	2.698	4.246	6.499	1.428	2.941

The coefficients are per neutral hydrogen atom and per unit electron pressure. The numbers in parentheses give the powers of 10 by which the corresponding entries should by multiplied to get the coefficient in the unit cm²/dyne.

Courtesy, S. Chandrasekhar, *Astrophysical Journal* (University of Chicago Press) **104**, 444, 1946.

ions/cm³. If we let α_I denote the absorption coefficient per H^- ion, the absorption coefficient given by Chandrasekhar is

$$\alpha_\lambda = \alpha_I(H^-)\phi(T) \tag{31}$$

and the absorption coefficient per gram of neutral hydrogen is

$$k_\lambda(H^-) = \alpha_\lambda(H^-)\frac{P_e}{M_H} \tag{32}$$

since M_H is the mass of the hydrogen atom. Here, $k_2(H^-)$ includes the effect of the negative absorptions.

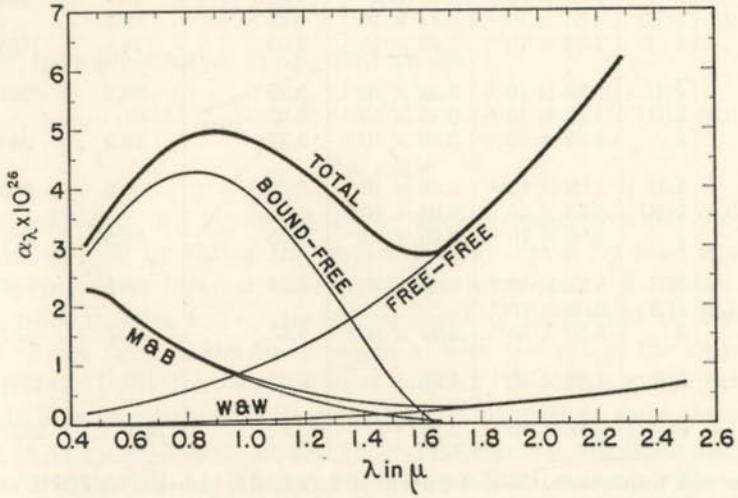

FIG. 5.—THE ABSORPTION COEFFICIENT OF THE NEGATIVE HYDROGEN ION

The curves are drawn for an atmosphere at a temperature of 6300°K, an electron pressure of one dyne/cm², and per neutral hydrogen atom. The curves M and B, W and W, and their sum are the results of earlier theoretical determinations by Massey and Bates, and by Wheeler and Wildt. The results of more recent calculations by Chandrasekhar and Breen are illustrated by the remaining curves. (Courtesy, S. Chandrasekhar, *The Scientific Monthly* **64**, 318, April, 1947.)

The straight mean absorption $\bar{k}$ [cf. eqn. (154)] calculated for an optical depth of 0.6 has been tabulated by Chandrasekhar and Münch (cf. Table 5). Let $\bar{\alpha}(H)$ denote the contribution of purely atomic hydrogen, and $\bar{\alpha}(H^-)$ that of the negative hydrogen ion for 1 dyne electron pressure. If x is the fraction of hydrogen ionized, the total mean absorption coefficient per gram of hydrogen will be

$$\bar{k} = \frac{1-x}{M_H}[\bar{\alpha}(H^-)P_e + \bar{\alpha}(H)] \tag{33}$$

TABLE 5

THE MEAN ABSORPTION COEFFICIENT FOR THE COOLER STARS

		$P_e = 1$	$P_e = 10$	$P_e = 10^2$	$P_e = 10^3$	$P_e = 10^4$
$\theta_e = 0.5$	$\bar{k}(H^-)$	5.85×10^{-6}	3.70×10^{-4}	4.98×10^{-2}	2.12	32.1
	$\bar{k}(H)$	1.71×10^{-1}	1.08	14.5	61.8	93.5
	$\bar{k}$	1.71×10^{-1}	1.08	14.6	63.9	126
$\theta_e = 0.6$	$\bar{k}(H^-)$	3.93×10^{-4}	2.60×10^{-2}	5.82×10^{-1}	6.68	68.4
	$\bar{k}(H)$	4.18×10^{-1}	2.76	6.19	7.10	7.27
	$\bar{k}$	4.18×10^{-1}	2.79	6.77	13.8	75.7
$\theta_e = 0.7$	$\bar{k}(H^-)$	9.08×10^{-3}	1.28×10^{-1}	1.34	13.4	134
	$\bar{k}(H)$	4.54×10^{-1}	6.41×10^{-1}	0.67	0.7	1
	$\bar{k}$	4.63×10^{-1}	7.69×10^{-1}	2.01	14.1	135
$\theta_e = 0.8$	$\bar{k}(H^-)$	2.26×10^{-2}	2.32×10^{-1}	2.32	23.2	232
	$\bar{k}(H)$	4.66×10^{-2}	0.48×10^{-1}	0.05		
	$\bar{k}$	6.92×10^{-2}	2.80×10^{-1}	2.37	23.2	232
$\theta_e = 0.9$	$\bar{k}(H^-)$	3.63×10^{-2}	3.63×10^{-1}	3.63	36.3	363
	$\bar{k}(H)$	0.33×10^{-2}	0.03×10^{-1}			
	$\bar{k}$	3.96×10^{-2}	3.66×10^{-1}	3.63	36.3	363
$\theta_e = 1.0$	$\bar{k}(H^-)$	5.57×10^{-2}	5.57×10^{-1}	5.57	55.7	557
	$\bar{k}(H)$	0.02×10^{-2}				
	$\bar{k}$	5.59×10^{-2}	5.57×10^{-1}	5.57	55.7	557
$\theta_e = 1.2$	$\bar{k}(H^-)$	1.20×10^{-1}	1.20	12.0	120	1200
$\theta_e = 1.4$	$\bar{k}(H^-)$	2.33×10^{-1}	2.33	23.3	233	2330

For each temperature, the contributions of the negative hydrogen ion $\bar{k}(H^-)$, atomic hydrogen $\bar{k}(H)$, and the total mean absorption coefficient $\bar{k}$ are listed. At the lowest temperatures the contribution of atomic hydrogen is negligible.

Courtesy, S. Chandrasekhar and G. Münch, *Astrophysical Journal* (University of Chicago Press) **104**, 449, 1946.

6. Empirical Determination of the Absorption Coefficient

Measurements of the energy distribution in the continuous spectrum of the center of the sun's disk, $I_\lambda(0, 0)$, and of the limb darkening,

$$\phi_\lambda(\theta) = \frac{I_\lambda(0, \theta)}{I_\lambda(0, 0)} \tag{34}$$

may be analyzed with the aid of eqn. (5) to determine the wave length variation of the solar continuous absorption coefficient. We describe the method proposed by Chalonge and Kourganoff and utilized more recently for the treatment of the limb-darkening observations secured by A. K. Pierce and his colleagues at the University of Michigan.

If we divide eqn. (5) by $I_\lambda(0, 0)$, the expression for limb darkening at wave length λ will be:

$$\phi_\lambda(\theta) = \int_0^\infty b_\lambda(T) e^{-\tau_\lambda \sec\theta} \sec\theta \, d\tau_\lambda \tag{35}$$

where

$$b_\lambda(T) = \frac{B(\tau_\lambda)}{I_\lambda(0, 0)} \tag{36}$$

and we notice that

$$b_\lambda(\tau_\lambda) = b_\lambda(T) \tag{37}$$

Kourganoff suggested that $b_\lambda(\tau_\lambda)$ be developed in terms of the exponential functions [cf. eqn. (9)], viz.,

$$b_\lambda(\tau_\lambda) = A_\lambda + B_\lambda \tau_\lambda + C_\lambda E_2(\tau_\lambda) \tag{38}$$

Then, from substitution in eqn. (36) we get

$$\phi_\lambda(\mu) = A_\lambda + B_\lambda \mu + C_\lambda[1 - \mu \ln(1 + \mu^{-1})] \tag{39}$$

where

$$\mu = \cos\theta \tag{40}$$

The coefficients, A_λ, B_λ, and C_λ are to be determined from the observed values of $\phi_\lambda(\theta)$ by fitting the empirical $\phi_\lambda(\theta)$ curves by least squares. Now, consider a layer at some particular temperature T. From eqn. (38) we may solve for τ_λ, the optical depth of this particular layer as seen in the light of the wave length λ, with the aid of the empirical A_λ, B_λ, and C_λ. At some other wave length λ', this layer at temperature T will lie at some other optical depth $\tau_{\lambda'}$. Calculations show the variation of $\tau_\lambda(T)$ with wave length to be pronounced, and hence k_λ must vary strongly with λ. We may not compare the τ_λ directly with $k_\lambda(H^-)$ on the assumption that the latter is responsible for the continuous absorption in the sun, because the tabulated $k_\lambda(H^-)$ refers to a given value of the temperature, whereas the empirical $\tau_\lambda(T)$ is the integral of $k_\lambda \rho$ through regions of varying density and temperature. Let us write

$$\tau_\lambda = \int_0^x k_\lambda(T)\rho \, dx = \int_{T_0}^T k_\lambda(T)\left[\rho(T)\frac{dx}{dT}\right] dT = \int_{T_0}^T k_\lambda(T) a_T \, dT \tag{41}$$

Then, by differentiation,

$$\frac{d\tau_\lambda}{dT} = a_T k_\lambda(T) \tag{42}$$

where a_T depends only on the temperature.

Hence, for a fixed temperature, $d\tau_\lambda/dT$ must be a linear function of k_λ. If we plot $d\tau_\lambda/dT$ against the theoretical k_λ for the temperature in question, the points should fall on a straight line. This expectation is confirmed for wave lengths greater than $\lambda 4000$ and permits the deter-

mination of a_T. Then one may compute τ_λ as a function of T from an integration of eqn. (42), and compare the predicted (or synthetic) and observed τ_λ curves.

When this program is carried out, it is found that the empirical and theoretical k_λ's show good qualitative agreement, but quantitatively there are some discrepancies (see Fig. 6). The τ_λ curves are sensitive to the adopted $I_\lambda(0, 0)$ and the uncertainties introduced by errors in the observed energy distribution at the center of the sun's disk are probably greater than the inaccuracies in the theory of the absorption coefficient. The boundary temperature of the sun appears to be near 4500°K.

An alternate approach to the same problem is that of G. Münch who determined the $k_\lambda/\bar{k}$ variation from the data of Mulders on the continuous spectrum at the center of the disk, and also from the total flux, $F_\lambda(0)$, emitted from the sun [cf. eqn. (10)].* Both methods yielded very nearly the same values of $k_\lambda/\bar{k}$, and since the flux included the effect of limb darkening, the agreement between the two evaluations implies that the same wave length variation of the absorption coefficient suffices to account for the wave length distribution of the intensity and for the limb darkening.

7. Theoretical Interpretation of Stellar Color Temperatures

We recall from Chapter 6 that stellar color temperatures (obtained from a fit of a Planckian curve to the observed energy distribution) often did not agree with the effective temperatures as defined by the total amount of radiated energy. Chandrasekhar and Münch showed that the color temperatures of main-sequence (*A*0–*G*0) stars, as determined by the Greenwich observers and by Barbier and Chalonge, could be interpreted with the aid of atomic hydrogen and H^- absorption.

They computed theoretical gradients (cf. Ch. 6) from the predicted $k_\lambda/\bar{k}$, assumed effective temperatures and electron pressures, and compared the results with the observations.

The relative energy distribution (flux) in the continuum of the star is represented by Planck's law with the temperature so chosen that the theoretical curve fits the observed curve at two wave lengths, say λ_1 and λ_2. If πF_1 and πF_2 denote the fluxes at these wave lengths, and if ϕ is the mean gradient in this interval, there follows from eqn. (5) of Chapter 6

$$\phi = 5\bar{\lambda} - 2.303 \frac{\log_{10} F_1/F_2}{\frac{1}{\lambda_1} - \frac{1}{\lambda_2}} \tag{43}$$

* To compute the flux from eqn. (10), we must know the temperature variation with optical depth. It is usually assumed that the energy transfer in the outermost layers takes place by radiative processes. (See Sec. 8.)

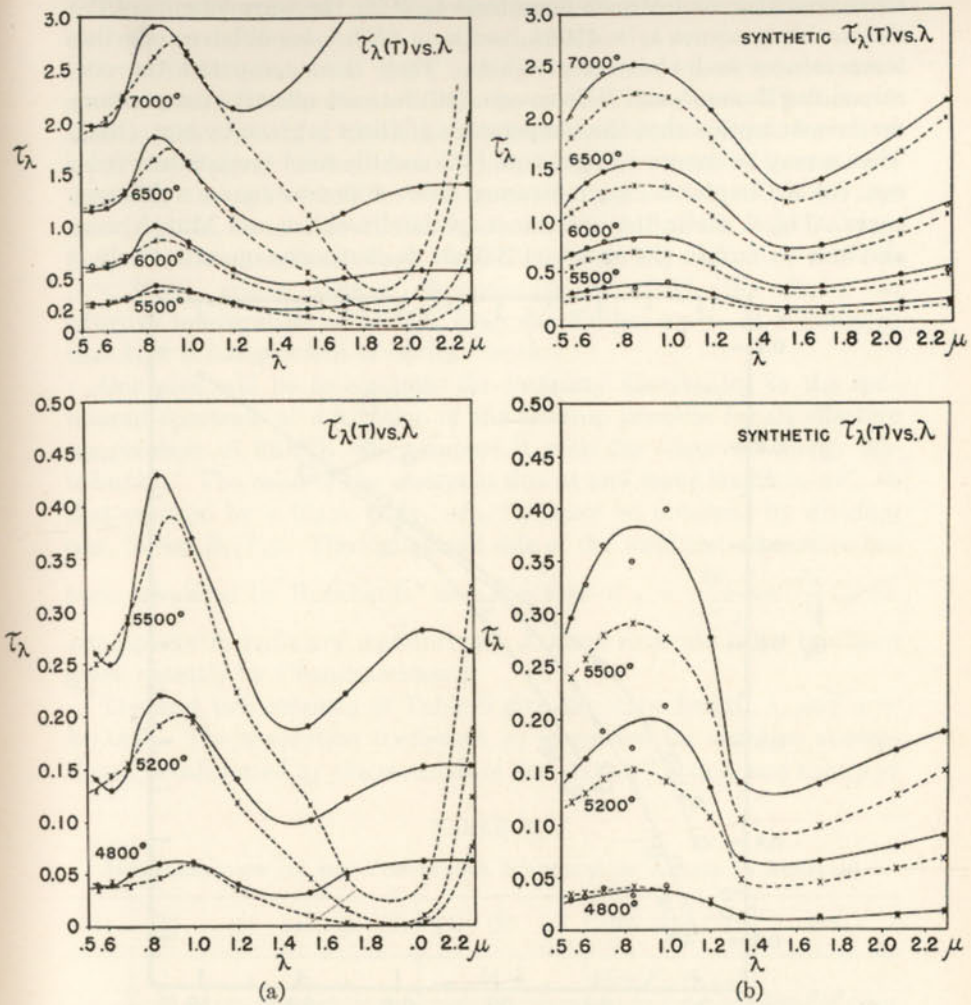

FIG. 6.—COMPARISON OF EMPIRICAL AND SYNTHETIC τ_λ'S FOR A FEW TYPICAL TEMPERATURES

(a) *Dotted curves:* Empirical τ_λ's computed from the observed limb darkening and Mulders' intensity distribution for center of the sun's disk, $I_\lambda(0, 0)$. *Solid curves:* Empirical τ_λ's computed from the observed limb darkening and from $I_\lambda(0, 0)$ as derived from the limb-darkening curves with the intensity at the limb, $I_\lambda(0, \pi/2)$ taken as appropriate to 4500°K.

(b) *Dotted curves:* Synthetic τ_λ's obtained from integration of eqn. (42). These are based on Chandrasekhar's absorption coefficient for H^- and Mulders' intensity distribution. *Solid curves:* Synthetic τ_λ's obtained from integration of eqn. (42). These are based on Chandrasekhar's absorption coefficient for H^- and $I_\lambda(0, 0)$ as derived from the boundary temperature of 4500°K. (A. Keith Pierce and L. H. Aller, McMath-Hulbert Observatory, University of Michigan.)

Chandrasekhar and Münch computed $k_\lambda/\bar{k}$ for the wave lengths of the Greenwich measures $\lambda_1 = 4100$A, and $\lambda_2 = 6500$A, for different effective temperatures and electron pressures. They then computed the corresponding fluxes F_1 and F_2 from eqn. (10) for each effective temperature on the assumption that the temperature gradient is given by eqn. (104). Then ϕ may be computed from eqn. (43) and the color temperature from eqn. (5) of Chapter 6. Each assumed electron pressure gives a different curve. Fig. 7 shows the agreement. Chandrasekhar and Münch were also able to explain the observed Balmer discontinuity quantitatively.

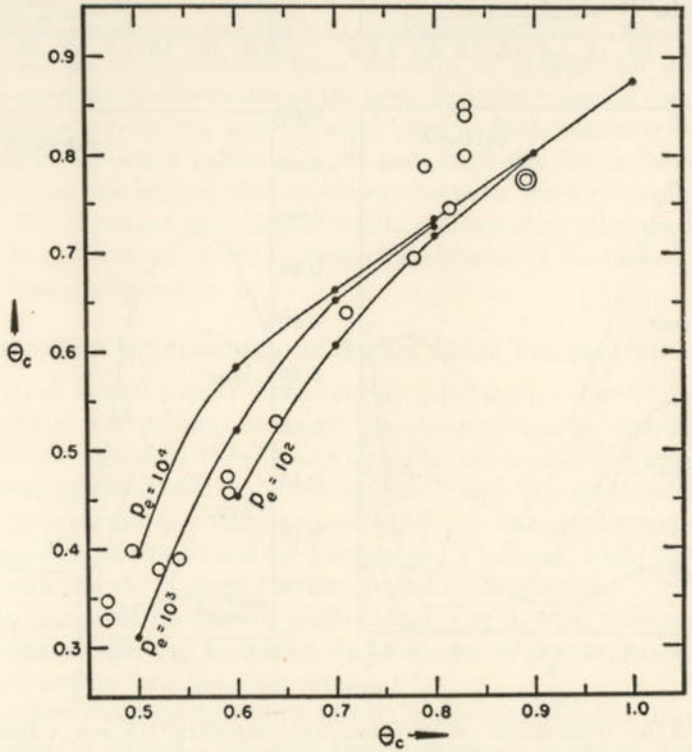

FIG. 7.—INTERPRETATION OF STELLAR COLOR TEMPERATURES

Comparison of the observed and theoretical color-effective temperature relations for the wave length interval λ4100–λ6500. The ordinates denote the reciprocal color temperatures and the abscissae the reciprocal effective temperatures in terms of $\left(\theta = \frac{5040}{T}\right)$. The circles represent the Greenwich color determinations reduced to the system of the Morgan-Keenan-Kellman spectral classification. At the low temperature end of the scale, the points fall above the curve because (except for the sun) no correction was made for the increased ultraviolet absorption. Note that the double circled point representing the sun falls below the others and close to the theoretical curve. (Courtesy, S. Chandrasekhar and G. Münch, *Astrophysical Journal*, University of Chicago Press, **104,** 455, November, 1946.)

As a further example of these considerations let us see what information can be determined from a star whose effective temperature can be inferred from its spectral class, and for which the spectrophotometric gradients and Balmer discontinuity have been measured. That is, we shall consider a star for which the gradient has been measured above and below the Balmer limits instead of confining our attention to measurements to the red of λ4000. For a specific application we choose the dwarf, Altair, Spectrum *A*7 (Morgan), for which Barbier and Chalonge find color temperatures $T_c = 10{,}400°\text{K}(\lambda > 3650)$, and $T_c = 8400°\text{K}$ $(\lambda < 3650)$, and a Balmer discontinuity $D = 0.38$. We choose an effective temperature of 8400°K from the Kuiper scale. It is assumed that $k_\lambda/\bar{k}$ is independent of optical depth.

Our plan will be to compute the intensity distribution in the continuous spectrum as a function of the electron pressure for an effective temperature of 8400°K and compare it with the observed energy distribution. The ratio of the emergent flux at any wave length λ, πF_λ, to that emitted by a black body, $\pi B_\lambda(T_e)$, may be obtained by dividing eqn. (5) by $B_\lambda(T_e)$. The right-hand side of the resultant expression has been tabulated by Burkhardt* as a function of $\alpha = \frac{hc}{\lambda k T_e}$ and $\frac{k_\lambda}{\bar{k}}$ for an atmosphere in radiative equilibrium. A more accurate table has been given recently by Chandrasekhar.†

The first two columns of Table 6 give the wave length, λ, and $\alpha = hc/\lambda k T_e$. The absorption coefficient, k_λ (corrected for negative absorptions), is calculated by the methods of Sec. 4, and Table 4, and shown in

TABLE 6

INTERPRETATION OF THE CONTINUOUS SPECTRUM OF ALTAIR (α AQUILAE)

(1)	(2)	(3) (4) (5) (6)	(7) (8) (9)	(10) (11) (12)	(13)
λ	$\frac{hc}{\lambda k T_e}$	k_λ Log P_e = 2.0 3.0 3.5 4.0	$k_\lambda/\bar{k}$ Log P_e = 3.0 3.5 4.0	Log $F_\lambda/F_{\lambda 6500}$ Log P_e = 3.0 3.5 4.0	Log $F_\lambda F/_{\lambda 6500}$ Observed
3000	5.72	15.4 21.5 31.2 61	1.56 0.71 0.81	0.21 0.46 0.45	0.08
3650	4.70	27.9 36.5 48.3 84 1.3 6.2 17.7 54	2.63 1.11 1.12 0.45 0.40 0.71	0.06 0.29 0.36 0.63 0.58 0.48	0.10 0.49
4000	4.28	1.63 7.0 19.5 59	0.51 0.44 0.78	0.49 0.49 0.41	0.44
5000	3.43	2.71 9.5 25.3 75	0.69 0.57 0.99	0.28 0.29 0.25	0.27
6500	2.64	5.04 13.7 33.3 95	0.99 0.76 1.25	0.00 0.00 0.00	0.00

* *Zeits. f. Ap.* **13,** 56, 1936; see also G. Münch, *Ap. J.* **102,** 388, 1945.

† *Radiative Transfer* (New York: Oxford University Press, 1950), pp. 304–7, especially eqns. (73) and (78), and Table XXX.

columns 3 to 6 of Table 6. Then $\bar{k}$ is taken from Table 5 and $k_\lambda/\bar{k}$ is computed (columns 7, 8, and 9 of Table 6). With the aid of Chandrasekhar's data and with α and $k_\lambda/\bar{k}$ as parameters, we compute log $(F_\lambda/F_{\lambda 6500})$, (columns 10, 11, and 12 of Table 6) for comparison with the observed log $(F_\lambda/F_{\lambda 6500})$, (column 13 of Table 6).

Although a reasonably good fit may be obtained to the red of the Balmer limit with an electron pressure near 6000 dynes, the Balmer discontinuity would require an electron pressure nearer 2000 dynes. The difference is not surprising since the higher layers contribute a larger fraction to the emission shortward of the Balmer limit than they do to the emission on the redward side of this limit. The fit in the ultraviolet is poor. Furthermore, the electron pressures seem much too high when compared with the results from the broadening of the hydrogen lines. Perhaps this is not surprising since line absorption originates in higher layers, on the average, than does the continuous absorption. Probably the major source of the discrepancy is the variation of $k_\lambda/\bar{k}$ with optical depth. In so far as the contribution of atomic hydrogen to the opacity is concerned, this ratio varies steeply with the temperature and therefore with τ.

8. The Flow of Radiation Through a Stellar Atmosphere

Measures of the limb darkening and the intensity distribution at the center of the disk give a clue not only to the absorption coefficient but to the temperature gradient as well. As we noted in Sec. 1, the latter depends on the mode of energy transport in the upper layers of the atmosphere. The observations show that radiative transfer rather than convection plays the dominating role.

We may easily see qualitatively how the intensity and directional distribution of the radiation vary as a function of depth in the star. At the surface there will be no backward flow of radiation and $I(\theta)$ will be zero for $\theta > \frac{\pi}{2}$. Below the surface, $I(\theta)$ will be positive for all θ, i.e., there will be backward as well as forward flowing radiation, but the outward directed radiation will still predominate. At great depths below the surface, $I(\theta)$ will be only slightly larger for $\theta < \pi/2$ than for $\theta > \pi/2$ Almost as large a fraction of the radiation will be flowing backwards as forwards. In so far as the integrated radiation is concerned, however, the flux must remain constant

$$F = \text{constant} \tag{44}$$

Even at great depths the same general properties of the radiation field are preserved and there is a net outward flow of radiation.

At a point x below the surface of the star, consider a pencil of radiation of intensity $I(\theta)$ defined by a cone of solid angle $d\omega$ which makes an angle θ with respect to the outward normal. Let this radiation fall upon an elementary cylinder of unit cross section and height ds, so placed that

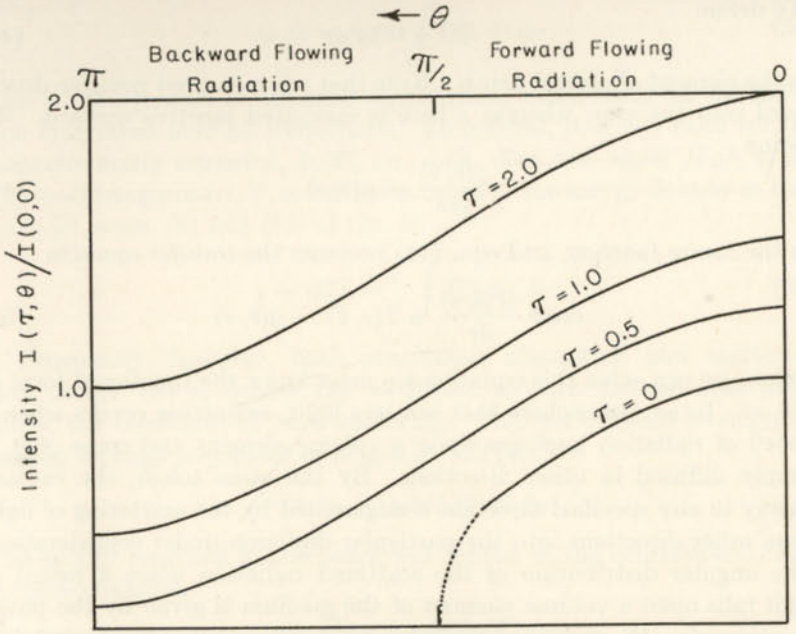

FIG. 8.—ANGULAR DISTRIBUTION OF THE INTENSITY $I(\theta)$ AS A FUNCTION OF OPTICAL DEPTH

These curves are intended to show the qualitative behavior of the intensity $I(\tau, \theta)$ as a function of the angle θ at different optical depths τ.

the axis of the radiation pencil is coincident with the axis of the cylinder. (See Fig. 2.) In passing through the cylinder the intensity will be cut down by an amount

$$dI(\theta, x)\, d\omega = -k\rho I(\theta, x)\, ds\, d\omega \tag{45}$$

where k is the mean absorption coefficient and ρ is the density. Our elementary cylinder also receives radiation from all sides and since a steady state exists, it must either scatter or diffuse this radiation, or absorb and re-emit it as thermal radiation. Both processes occur simultaneously. Let the mass emissivity of the material be denoted by j. In the most general problems of energy transfer, j will depend on θ as well as on x. The amount of energy emitted per second in solid angle $d\omega$ will be $\frac{d\omega}{4\pi}\rho j\, ds$. Hence, in passing through the elementary cylinder the beam suffers a net change in intensity

$$dI(\theta, x)\, d\omega = -k\rho I(\theta, x)\, ds\, d\omega + \frac{j(x, \theta)}{4\pi}\rho\, ds\, d\omega \tag{46}$$

(net change) = −(energy absorbed) + (energy re-emitted)

From the geometry of the problem,

$$ds = dx \sec\theta \tag{47}$$

We define

$$d\tau = -k\rho\, dx \tag{48}$$

as the element of optical depth. Note that τ is measured positive downward into the star, whereas x here is measured positive upward. We define

$$\frac{j(\theta, \tau)}{4\pi k} = \mathcal{J}(\theta, \tau) \tag{49}$$

as the *source function*, and eqn. (46) becomes the *transfer equation*

$$\cos\theta \frac{dI(\theta, \tau)}{d\tau} = I(\tau, \theta) - \mathcal{J}(\theta, \tau) \tag{50}$$

Before we can solve this equation we must know the functional form of $\mathcal{J}(\theta, \tau)$. In an atmosphere that scatters light, extinction occurs when a pencil of radiation impinges upon a volume element and some of it is simply diffused in other directions. By the same token, the radiant energy in any specified direction is augmented by the scattering of light from other directions into the particular direction under consideration. The angular distribution of the scattered radiation when a pencil of light falls upon a volume element of the medium is given by the phase function $p[\cos\Theta]$, so defined that $p[\cos\Theta]\, d\omega/4\pi$ specifies the probability of radiation being scattered in a direction Θ with respect to the direction of the incident beam. If scattering occurs according to Rayleigh's law, as with gas molecules,

$$p[\cos\Theta] = \tfrac{3}{4}[1 + \cos^2\Theta] \tag{51}$$

while for isotropic scattering,

$$p[\cos\Theta] = 1 \tag{52}$$

In a purely scattering atmosphere with no energy losses by heating, etc.

$$\int p[\cos\Theta] \frac{d\omega}{4\pi} = 1$$

In the present context, the state of greatest interest is that of thermal radiation. The volume element is heated by radiation received from its incandescent surroundings, and because it is hot it radiates energy. If the total emission is of strictly thermal origin, i.e., if all the impinging radiation that is absorbed is re-emitted as purely thermal energy uniformly over all directions, the emission at each frequency will be given by Kirchhoff's law [cf. eqn. (49) and eqn. (22) of Ch. 5.

$$\mathcal{J}_\nu(\tau) = B_\nu(\tau) \tag{53}$$

The local temperature, T, is governed by the condition that the total amount of energy absorbed over all frequencies must equal that emitted, viz.,

$$j\rho\, ds = k\rho\, ds \int I(\theta, x)\, d\omega \tag{54}$$

This is the equation of radiative equilibrium, which holds for the radiation integrated over all frequencies. In general, it is not valid for the monochromatic intensity, $I_\lambda(\theta)$, i.e., j_ν/k_ν does not equal $\int I_\nu(\theta, x)\, d\omega$. The local temperature, T, is defined in terms of the energy density at that point [cf. eqns. (8) and (12) of Ch. 5],

$$u = aT^4 = \frac{1}{c} \int I(\theta, x)\, d\omega \tag{55}$$

Frequently, however, both continuous absorption and scattering may occur. Let k_ν denote the coefficient of pure thermal absorption and σ_ν the coefficient of pure scattering. The loss of beam intensity in passing through a cylinder of length ds will be

$$-(k_\nu + \sigma_\nu)\rho\, ds\, I_\nu(\theta, x)\, d\omega$$

The energy returned to the beam will consist of the contribution from thermal emission,

$$j_\nu\rho\, ds \frac{d\omega}{4\pi} = k_\nu\rho\, ds\, B_\nu(T)\, d\omega$$

plus the light that is simply scattered from other directions

$$ds \frac{d\omega}{4\pi} \int \sigma_\nu p(\cos\Theta) I_\nu\, d\omega$$

where the integration is carried out over all angles, Θ being the angle between the direction of the beam and the direction from which the light is scattered. Adding up the gains and losses we find for the equation of transfer,

$$\cos\theta \frac{dI_\nu}{\rho\, dx} = -(k_\nu + \sigma_\nu) I_\nu + \sigma_\nu \int I_\nu p(\cos\Theta) \frac{d\omega}{4\pi} + k_\nu B_\nu(T) \tag{56}$$

where $dx = ds \cos\theta$. Recall that s is measured positive towards the surface of the star.

The nature of this equation shows that absorption and scattering cannot be regarded as equivalent processes, even if the scattering is isotropic, unless both k_ν and σ_ν are independent of wave length. In so far as the continuous spectra of the stars are concerned, we are mostly involved with thermal absorption and emission according to Kirchhoff's law. Only in the hottest stars and in certain supergiants does electron scat-

tering become important. Then one must employ eqn. (56) and take into account the anisotropy of the radiation. Chandrasekhar has solved this difficult problem for a grey atmosphere. Here, however, we confine our attention to the problem of pure absorption and show how a solution to the transfer equation may be obtained for the simplest example, an atmosphere composed of grey material.

The equations are to be solved with the boundary condition that there is no radiation incident on the surface of the star, and that J increases linearly with τ at large optical depths.

For an atmosphere in which pure absorption occurs, it will be useful to establish certain integral relations between the Planck function, the intensity I, and the flux πF.

The mean intensity of the radiation, J_ν [eqn. (2) of Ch. 5] at a given point τ will be the sum of contributions from radiating elements on all sides. The contribution to J_ν from an elementary volume at an optical depth t_ν in a direction θ as seen from the point τ_ν will be

$$dI_\nu = B_\nu(t_\nu) \exp(-|(t_\nu - \tau_\nu) \sec\theta|) \sec\theta \, dt_\nu \tag{57}$$

and the contribution from all such elements integrated over all angles and to all depths will be

$$\begin{aligned} 4\pi J_\nu(\tau_\nu) = {} & 2\pi \int_{\tau_\nu}^{\infty} B_\nu(t_\nu) \int_0^{\pi/2} \exp[-(t_\nu - \tau_\nu)\sec\theta] \sec\theta \sin\theta \, d\theta \, dt_\nu \\ & - 2\pi \int^{\tau_\nu} B_\nu(t_\nu) \int_{+\pi/2}^{\pi} \exp[-(t_\nu - \tau_\nu)\sec\theta] \sec\theta \sin\theta \, d\theta \, dt_\nu \end{aligned} \tag{58}$$

Now put $\sec\theta = y$ in the first integral and $\sec\theta = -y$ in the second. Notice that in the first integral $(t_\nu - \tau_\nu)$ is positive and in the second it is negative. Making use of eqn. (9) we find that eqn. (58) may be written in the form

$$J_\nu(\tau_\nu) = \tfrac{1}{2} \int_0^{\infty} B_\nu(t_\nu) E_1(|t_\nu - \tau_\nu|) \, dt_\nu \tag{59}$$

Similarly, the flux is given by

$$F_\nu(\tau_\nu) = 2 \int_{\tau_\nu}^{\infty} B_\nu(t_\nu) E_2(t_\nu - \tau_\nu) \, dt_\nu - 2 \int_0^{\tau_\nu} B_\nu(t_\nu) E_2(\tau_\nu - t_\nu) \, dt_\nu \tag{60}$$

In many problems B_ν is known as a function of τ or τ_ν and a rapid method for the evaluation of F_ν and J_ν is desirable. The approximation formula,

$$\tfrac{1}{2} \int_0^{\tau} f(t) E_1(\tau - t) \, dt = a_1 f(t_1) + a_2 f(t_2) \tag{61}$$

suggested by A. Reiz facilitates the calculation of integrals of the type of eqn. (59). Table 7 lists the weights a_1 and a_2 and the points t_1 and t_2

TABLE 7

DATA FOR EVALUATION OF INTENSITY INTEGRALS

$$J(\tau) = \tfrac{1}{2}\int_0^{\infty} B(t)E_1(|\tau - t|)\,dt = a_1B(t_1) + a_2B(t_2) + 0.4532B(\tau + 0.292) + 0.0468B(\tau + 2.507)$$

Weighting coefficients a_1, a_2 and points t_1, t_2 at which function $B(t)$ is to be evaluated

τ	t_1	a_1	t_2	a_2
0.20	0.051	0.0851	0.169	0.1278
0.40	0.106	0.1094	0.342	0.1959
0.60	0.167	0.1198	0.520	0.2421
0.80	0.232	0.1224	0.699	0.2772
1.00	0.303	0.1214	0.881	0.3044
1.20	0.378	0.1182	1.064	0.3262
1.40	0.459	0.1138	1.249	0.3442
1.60	0.544	0.1090	1.436	0.3591
1.80	0.635	0.1040	1.624	0.3716
2.0	0.731	0.0991	1.812	0.3821
2.2	0.832	0.0944	2.002	0.3912
2.4	0.939	0.0899	2.193	0.3989
2.6	1.051	0.0857	2.385	0.4056
2.8	1.168	0.0819	2.577	0.4113
3.0	1.290	0.0783	2.770	0.4164
3.2	1.417	0.0751	2.964	0.4208
3.4	1.549	0.0721	3.158	0.4246
3.6	1.686	0.0694	3.353	0.4280
3.8	1.828	0.0670	3.548	0.4310
4.0	1.974	0.0648	3.744	0.4336
4.2	2.125	0.0628	3.940	0.4359
4.4	2.280	0.0610	4.137	0.4380
4.6	2.438	0.0594	4.334	0.4398
4.8	2.601	0.0580	4.531	0.4414
5.0	2.766	0.0567	4.728	0.4428
6.0	3.640	0.0521	5.719	0.4477
8.0	5.530	0.0482	7.710	0.4518
10.0	7.500	0.0472	9.708	0.4528

Courtesy, S. Chandrasekhar, *Radiative Transfer* (New York: Oxford University Press, 1950), p. 67, for entries 0.20 to 4.8. The values 5.0 to 10.0 were kindly supplied by Jean K. McDonald in advance of publication.

at which $f(t)$, which is to be identified with $B(t)$ in the present instance, is to be evaluated. Similarly,

$$\tfrac{1}{2} \int_0^{\infty} f(y) E_1(y) \, dy = b_1 f(y_1) + b_2 f(y_2) \tag{62}$$

where

$$\begin{aligned} y_1 &= 0.292 \qquad b_1 = 0.4532 \\ y_2 &= 2.507 \qquad b_2 = 0.0468 \end{aligned} \tag{63}$$

Thus

$$\tfrac{1}{2} \int_{\tau}^{\infty} f(t) E_1(t - \tau) \, dt = 0.4532 f(\tau + .292) + 0.0468 f(\tau + 2.507) \tag{64}$$

TABLE 8

DATA FOR THE EVALUATION OF THE FLUX INTEGRALS

$$F(\tau) = 2\int_{\tau}^{\infty} B(t)E_2(t-\tau)\,dt - 2\int_{0}^{\tau} B(t)E_2(\tau - t)\,dt$$
$$= 0.8839B(\tau + 0.397) + 0.1161B(\tau + 2.723) - d_1B(t_1) - d_2B(t_2)$$

Weighting coefficients d_1, d_2 and points t_1, t_2 at which function $B(t)$ is to be evaluated

τ	t_1	d_1	t_2	d_2
0.10	0.022	0.0786	0.080	0.0889
0.20	0.046	0.1346	0.162	0.1615
0.30	0.071	0.1753	0.244	0.2247
0.40	0.096	0.2055	0.328	0.2800
0.50	0.124	0.2279	0.412	0.3289
0.60	0.152	0.2443	0.498	0.3726
0.70	0.181	0.2561	0.584	0.4118
0.80	0.212	0.2642	0.671	0.4472
0.90	0.244	0.2694	0.758	0.4792
1.00	0.276	0.2723	0.846	0.5083
1.10	0.311	0.2734	0.935	0.5349
1.20	0.346	0.2730	1.024	0.5591
1.30	0.382	0.2715	1.114	0.5814
1.40	0.420	0.2690	1.204	0.6018
1.50	0.459	0.2659	1.294	0.6206
1.60	0.499	0.2622	1.386	0.6380
1.70	0.540	0.2581	1.477	0.6540
1.80	0.583	0.2537	1.569	0.6688
1.90	0.627	0.2492	1.661	0.6826
2.00	0.672	0.2444	1.753	0.6953
2.2	0.766	0.2348	1.940	0.7182
2.4	0.865	0.2252	2.127	0.7380
2.6	0.970	0.2158	2.315	0.7553
2.8	1.079	0.2070	2.504	0.7704
3.0	1.194	0.1986	2.695	0.7836
3.2	1.314	0.1907	2.886	0.7952
3.4	1.439	0.1834	3.078	0.8054
3.6	1.569	0.1767	3.270	0.8145
3.8	1.704	0.1706	3.464	0.8225
4.0	1.844	0.1650	3.658	0.8295
6.0	3.457	0.1311	5.621	0.8684
8.0	5.324	0.1201	7.608	0.8798
10.0	7.287	0.1170	9.604	0.8830

As τ becomes larger, d_1 approaches 0.1161 and d_2 approaches 0.8839 while $(\tau - t_1)$ approaches 2.723 and $(\tau - t_2)$ approaches 0.397.

Courtesy, S. Chandrasekhar, *Radiative Transfer*, p. 68 for entries $\tau = 0.10$ to $\tau = 2.0$. The values for $\tau = 2.2$ to 3.8 are taken from a table by B. Strömgren kindly supplied in advance of publication. The values for $\tau = 4.0$ to 10.0 were calculated by Jean K. McDonald.

For the evaluation of the flux integral eqn. (60), Reiz has given an expression similar to eqn. (61) and has calculated the appropriate coefficients (see Table 8). The emergent flux at the surface of the star is given by

$$F_\nu(\tau = 0) = c_1B(t_1) + c_2B(t_2) \tag{65}$$

where

$$\begin{aligned} t_1 &= 0.397 \qquad c_1 = 0.8839 \\ t_2 &= 2.723 \qquad c_2 = 0.1161 \end{aligned} \tag{66}$$

For an illustrative example involving the use of these formulae see Sec. 9c of Chapter 8.

9. The Eddington Approximation

Various approximate solutions illustrate the character of the radiation flow. The earliest approximation is that employed by Schuster and Schwarzschild who simply divided the radiation field into an incoming and an outgoing beam. This method fails to give the correct flux. Eddington gave a useful approximate solution that yields the correct flux. It has been employed in a great number of problems. He defines three quantities:

$$\begin{aligned} J &= \frac{1}{4\pi}\int I(\theta)\,d\omega \\ H &= \frac{1}{4\pi}\int I(\theta)\cos\theta\,d\omega \\ K &= \frac{1}{4\pi}\int I(\theta)\cos^2\theta\,d\omega \end{aligned} \tag{67}$$

where the integration is taken over all solid angles. J is the mean intensity of the radiation, H is the net outward flow of the radiant energy, and K is the radiation pressure at each point multiplied by the velocity of light. [Cf. eqns. (2), (4), and (23) of Ch. 5.]

First multiply eqn. (50) by $\frac{d\omega}{4\pi}$ and integrate over all angles to obtain

$$\frac{dH}{d\tau} = J - J = 0, \quad \text{i.e., } H = \text{constant} \tag{68}$$

in accordance with the definition of J and the constancy of the flux [see eqns. (49) and (54)]. Next multiply eqn. (50) by $\cos\theta\frac{d\omega}{4\pi}$ and integrate over all angles. Since J is independent of θ in accordance with our assumption concerning thermal emission,

$$\frac{1}{4\pi}\frac{d}{d\tau}\int I(\theta)\cos^2\theta\,d\omega = \frac{dK}{d\tau} = H \tag{69}$$

and

$$K = H\tau + \text{constant} \tag{70}$$

Thus the radiation pressure varies linearly with the optical depth with H appearing as the constant of proportionality.

To this point the development has been rigorous. To make further progress, Eddington reasoned as follows: In the deep interior of the star,

I must be nearly independent of θ, in which event one may take it outside the integral sign, and write:

$$K \sim \frac{I}{4\pi} \int \cos^2 \theta \, d\omega \quad \text{or} \quad K \sim \frac{J}{3} \tag{71}$$

Eddington's approximation consists in supposing that quite generally we may take $K = \frac{J}{3}$ so that,

$$\frac{dJ}{d\tau} = 3H \tag{72}$$

and

$$J = 3H\tau + \text{constant} \tag{73}$$

In the first approximation the variation of I with θ is neglected, except for a general distinction between inward and outward flow. That is

$$I(\theta) = I_1, \quad 0 < \theta < \frac{\pi}{2}; \qquad I(\theta) = I_2, \quad \frac{\pi}{2} < \theta < \pi \tag{74}$$

At the surface of the star, I is assumed uniform over the entire hemisphere, and $H_0 = \frac{J_0}{2}$, since the mean value of the cosine averaged over a hemisphere is $\frac{1}{2}$. Thus we find:

$$J(\tau) = 2H(1 + \tfrac{3}{2}\tau) = \tfrac{1}{2}F(1 + \tfrac{3}{2}\tau) \tag{75}$$

In any application of eqn. (5) or (10) to predict the theoretical energy curve of a star, a fundamental datum is the variation of the temperature with optical depth. Different approximate solutions of the transfer equation differ from one another in that they predict different temperature gradients.

From eqn. (75) we see that the source function $\mathcal{J}(\tau) = J(\tau)$ is related, in accordance with eqn. (55) and eqn. (2) of Chapter 5, with the local temperature T and optical depth τ by

$$\frac{4\pi J}{c} = aT^4 = \frac{2\pi F}{c}\left(1 + \frac{3}{2}\tau\right) \tag{76}$$

The effective temperature T_e of the star is defined in terms of the flux by

$$\pi F = \sigma T_e^4 \tag{77}$$

From eqn. (76), the definition of a [cf. eqn. (12) of Ch. 5], and eqn. (77) it follows that

$$T_e = \sqrt[4]{2}\,T_0 = 1.19T_0 \tag{78}$$

If the effective temperature of the sun is taken as 5750°K, the boundary temperature is 4800°K.

To derive an expression for the darkening to the limb put eqn. (75) into eqn. (5), noting that $J = B$, to obtain

$$I_0(\theta) = \frac{F}{2}\left(1 + \frac{3}{2}\cos\theta\right) \tag{79}$$

The limb darkening in the integrated radiation is

$$\frac{I_0(\theta)}{I_0(0)} = 0.4 + 0.6\cos\theta \tag{80}$$

where the subscript "0" denotes that the intensity is to be evaluated at the surface of the star. This law of darkening gives a surprisingly good representation of the observations and suggests that radiative equilibrium prevails in the uppermost strata of the solar atmosphere.

10. The Chandrasekhar Method for the Solution of the Transfer Equation

We now give a brief sketch of the most powerful method that has been devised for the treatment of the transfer equation. For the time being we continue to confine our attention to grey material (for which the absorption coefficient is independent of wave length). With $\mu = \cos\theta$, the equation of transfer eqn. (50) becomes

$$\mu \frac{dI}{d\tau} = I - \frac{1}{2}\int_{-1}^{+1} I \, d\mu \tag{81}$$

Our problem is to find how $I(\tau, \mu)$ depends on μ and τ, the optical depth in the star, given the appropriate boundary conditions. The appearance of the μ factor on the left-hand side complicates the solution of the equation in the neighborhood of the boundary. The equation of transfer for a grey body is formally equivalent to the problem of the diffusion of neutrons in a pile. Among the solutions of this problem was that proposed by Wick, which was amplified and extended by Chandrasekhar. In a manner analogous to that employed in the kinetic theory of gases where it is customary to resolve the motions of the molecules in a box into three equivalent streams parallel to the walls, one may divide the radiation I into several elementary pencils, each of which corresponds to a different μ. That is, we replace $I(\tau, \mu)$ which is a function of two variables by a set of $2n$ quantities, $I(\tau, \mu_i)$, $i = \pm 1, 2, \cdots, n$, each of which is a function of the one variable τ since μ is held fixed. This is an example of the Gaussian method of integration, wherein the choice of the μ_j's is made so that as closely as possible,

$$\int_{-1}^{+1} I(\tau, \mu) \, d\mu = \sum_{j=-n}^{+n} a_j I(\tau, \mu_j) \tag{82}$$

where the a_j's are the appropriate weight factors. Thus to calculate the integral we evaluate the integrand at certain specified points, multiply by pre-assigned weight factors, and add the products. Since I is symmetrical with respect to μ, it follows that

$$a_j = a_{-j}; \quad \mu_j = -\mu_{-j} \tag{83}$$

In order to achieve the highest accuracy with a limited number of points (at least for a function which may be well represented by a polynomial), Gauss showed that the proper procedure was to choose the μ_j's as zeros of the Legendre polynomial $P(\mu)$. When $n = 1$, $\mu_1 = -\mu_{-1} = 3^{-1/2}$. In the second approximation, the μ's are the zeros of $P_4(\mu)$; in the third the zeros of $P_6(\mu)$; in the fourth the zeros of $P_8(\mu)$, etc.*

Chandrasekhar replaces eqn. (81) by a system of $2n$ ordinary linear differential equations,

$$\mu_i \frac{dI_i}{d\tau} = I_i - \frac{1}{2}\sum a_j I_j, \qquad i = \pm 1, \pm 2, \cdots \pm n \tag{84}$$

To solve this equation Chandrasekhar tries an expression of the form,

$$I_i = g_i e^{-k\tau} \qquad (i = \pm 1, \cdots \pm n) \tag{85}$$

where the g's and k's are constants to be determined. If eqn. (85) is put in eqn. (84) there results,

$$g_i(1 + \mu_i k) = \tfrac{1}{2}\Sigma a_j g_j \tag{86}$$

Hence,

$$g_i = \frac{\text{constant}}{1 + \mu_i k} \qquad (i = \pm 1, \cdots \pm n) \tag{87}$$

The "constant" is independent of i. If we substitute eqn. (87) under the summation sign in eqn. (86) and employ eqn. (83), we obtain the equation for k,

$$1 = \frac{1}{2}\sum \frac{a_j}{1 + \mu_j k}$$

or

$$1 = \sum_{j=1}^{n} \frac{a_j}{1 - \mu_j^2 k^2} \tag{88}$$

Thus the "k's" must satisfy an algebraic equation of degree $2n$. Now

$$\sum_{j=1}^{n} a_j \mu_j^m = \int_0^1 \mu^m \, d\mu = \frac{1}{m+1} \tag{89}$$

* For the evaluation of a_j see Chandrasekhar's *Radiative Transfer*, p. 61. The μ_j's and a_j's are tabulated on p. 62.

and in particular,

$$\sum_{j=1}^{n} a_j = 1 \tag{90}$$

which means that $k^2 = 0$ is a root of eqn. (88). Hence eqn. (88) can have only $2n - 2$ distinct roots, which will appear in pairs as

$$\pm k_\alpha \qquad (\alpha = 1, \cdots, n-1) \tag{91}$$

That is, eqn. (84) will have $2n - 2$ linearly independent solutions corresponding to the $2n - 2$ distinct roots.

In addition to the solution eqn. (85) we notice that an expression of the form,

$$I_i = b(\tau + Q + \mu_i) \tag{92}$$

will also satisfy eqn. (84). Q and b are to be found from the boundary conditions and the total flux of radiation. The sum of eqns. (85) and (92)—the general solution—then has the form

$$I_i = b\left\{\sum_{\alpha=1}^{n-1} \frac{L_\alpha e^{-k_\alpha \tau}}{1 + \mu_i k_\alpha} + \sum_{\alpha=1}^{n-1} \frac{L_{-\alpha} e^{+k_\alpha \tau}}{1 - \mu_i k_\alpha} + \tau + \mu_i + Q\right\} \tag{93}$$

where b, Q, $L_{\pm\alpha}$ are the $2n$ constants of integration. The first term is reminiscent of the transient term in an electrical circuit. It will be important only at a small optical depth. The last three terms correspond to the steady state solution, valid at large τ.

We must now impose the boundary conditions of the problem. Since the positive exponential would give an intensity increasing exponentially with depth in contradiction to the requirements of astrophysical theory, we must set $L_{-\alpha} = 0$. Furthermore, at the surface of the star, there is no backward flowing radiation which means

$$I_{-i} = 0 \quad \text{at} \quad \tau = 0, \quad \text{for} \quad i = 1, \cdots n$$

With the aid of eqns. (83) and (93), we find

$$\sum_{\alpha=1}^{n-1} \frac{L_\alpha}{1 - \mu_i k_\alpha} + Q = \mu_i \qquad (i = 1, \cdots n) \tag{94}$$

Thus there are n equations to determine the $n - 1$ values of L and Q. This process does not fix the constant b, which we shall show to be related to the constant net flux of radiation in the atmosphere, πF. In our present notation

$$F = 2\int_{-1}^{+1} I\mu \, d\mu \tag{95}$$

We replace the integral by the sum over the $I_i\mu_i$'s and use eqn. (93) to obtain:

$$F = 2b\left\{\sum_{\alpha=1}^{n-1} L_\alpha e^{-k_\alpha \tau} \sum_i \frac{a_i \mu_i}{1 + \mu_i k_\alpha} + \sum_i a_i \mu_i^2 + (Q + \tau)\sum_i a_i \mu_i\right\} \tag{96}$$

Making use of eqns. (83) and (89) we have

$$\Sigma a_i \mu_i^2 = \tfrac{2}{3}, \quad \Sigma a_i \mu_i = 0 \tag{97}$$

From eqn. (88) we have the identity,

$$\Sigma \frac{a_i \mu_i}{1 + \mu_i k_\alpha} = \frac{1}{k_\alpha} \Sigma a_i \left(1 - \frac{1}{1 + \mu_i k_\alpha}\right) = \frac{1}{k_\alpha}\left(2 - \Sigma \frac{a_i}{1 + \mu_i k_\alpha}\right) \tag{98}$$

which is equal to zero. Then

$$F = \tfrac{4}{3} b = \text{constant} \tag{99}$$

Furthermore,

$$J = \tfrac{1}{2} \int_{-1}^{+1} I \, d\mu = \tfrac{1}{2} \Sigma a_i I_i \tag{100}$$

Making use of eqns. (88), (89), (93), (97), and (98) we get

$$J = \tfrac{3}{4} F \left(\tau + Q + \sum_{\alpha=1}^{n-1} L_\alpha e^{-k_\alpha \tau}\right) \tag{101}$$

If we define

$$q(\tau) = Q + \sum_{\alpha=1}^{n-1} L_\alpha e^{-k_\alpha \tau} \tag{102}$$

we may write

$$J = \tfrac{3}{4} F[\tau + q(\tau)] \tag{103}$$

and the temperature distribution with depth is given by

$$T^4(\tau) = \sqrt{3} T_0^4 [\tau + q(\tau)] \tag{104}$$

Notice that $q(\tau)$ corresponds to the constant, 2/3, in the Eddington approximation [cf. eqn. (76)]. Finally, the law of limb darkening follows from a substitution of eqn. (101) into eqn. (5) to yield

$$I(0, \mu) = \frac{3F}{4}\left(\mu + Q + \sum_{\alpha=1}^{n-1} \frac{L_\alpha}{1 + k_\alpha \mu}\right) \tag{105}$$

We now illustrate the calculation of J and $I(0, \mu)$ in the first two approximations.

First Approximation. Here

$$a_1 = a_{-1} = 1, \quad \text{and} \quad \mu_1 = -\mu_{-1} = 3^{-1/2} \tag{106}$$

Eqn. (88) has only the one root $k = 0$ and from eqn. (94), $Q = \mu_1 = 3^{-1/2}$, while from eqn. (102), $q(\tau) = 3^{-1/2}$ and J may be found from eqn. (103). The law of limb darkening, eqn. (105), is

$$I(0, \mu) = \frac{3F}{4}\left(\mu + \frac{1}{\sqrt{3}}\right) \tag{107}$$

The inward and outward beams obey the equations

$$\frac{1}{\sqrt{3}} \frac{dI_1}{d\tau} = I_1 - \frac{1}{2}(I_1 - I_{-1}), \quad -\frac{1}{\sqrt{3}} \frac{dI_{-1}}{d\tau} = I_{-1} - \frac{1}{2}(I_1 + I_{-1}) \tag{108}$$

These equations are analogous to those derived by Schuster and Schwarzschild many years ago except for a factor $\frac{1}{2}$ instead of $3^{-1/2}$.

Second Approximation. Here

$$\begin{aligned} a_1 &= 0.65214 \qquad \mu_1 = 0.33998 \\ a_2 &= 0.34785 \qquad \mu_2 = 0.86114 \end{aligned} \tag{109}$$

The summation eqn. (88) consists of two terms from which we may derive

$$\mu_1^2 \mu_2^2 k^2 = a_1 \mu_1^2 + a_2 \mu_2^2 = \tfrac{1}{3} \tag{110}$$

Then

$$k = \frac{1}{\sqrt{3 \mu_1 \mu_2}} = 1.97203 \tag{111}$$

and from eqn. (94)

$$\frac{L}{1 - \mu_1 k_1} + Q = \mu_1 = 0.33998 \tag{112}$$

$$\frac{L}{1 - \mu_2 k_1} + Q = \mu_2 = 0.86114 \tag{113}$$

Thus

$$Q = 0.69402 \quad \text{and} \quad L_1 = -0.11668 \tag{114}$$

Then we may calculate J from eqn. (101) and $I(0, \mu)$ from eqn. (105). The summation consists of one term.

Chandrasekhar also carried out solutions for the third and fourth approximations. The procedure should be clear from the foregoing discussion. He was also able to derive a rigorous solution of the transfer equation in a closed form. If we compare eqn. (105) which gives $I(0, \mu)$, the angular distribution of the radiation emergent from the surface of the star, with eqn. (94) which determines the constants, L_α and Q, we note that $I(0, \mu)$ which exists for $1 > \mu > 0$, is determined in terms of a function that has zeros in the complementary interval, $-1 < \mu < 0$. Let

$$S(\mu) = \sum_{\alpha=1}^{n-1} \frac{L_\alpha}{1 - \mu k_\alpha} - \mu + Q \tag{115}$$

The boundary condition at the surface asserts that

$$S(\mu_i) = 0 \qquad (i = 1, 2, \cdots n) \tag{116}$$

while at the same time, the angular distribution of the emergent radiation, eqn. (105), may be written as

$$I(0, \mu) = \tfrac{3}{4} F S(-\mu) \tag{117}$$

Chandrasekhar shows how we may find an explicit formula for $S(\mu)$ without actually solving for the constants L_α and Q. To find such a solution, consider the product function

$$\prod_{\alpha=1}^{n-1}(1-\mu k_\alpha)S(\mu) = (1-\mu k_1)(1-\mu k_2)\cdots(1-\mu k_{n-1})S(\mu) \quad (118)$$

which must be a polynomial of degree n, with roots, $\mu = \mu_1 \cdots \mu_i \cdots \mu_n$. Thus there must be a proportionality of the form

$$\prod_{\alpha=1}^{n-1}(1-k_\alpha\mu)S(\mu) \sim \prod_{i=1}^{n}(\mu-\mu_i) \quad (119)$$

We find the constant of proportionality by considering the coefficient of μ^n. For example, if $n = 3$,

$$(1-\mu k_1)(1-\mu k_2)\left[\frac{L_1}{1-\mu k_1}+\frac{L_2}{1-\mu k_2}-\mu+Q\right] = -k_1k_2\mu^3+\cdots = \text{const}\,(\mu-\mu_1)(\mu-\mu_2)(\mu-\mu_3) \quad (120)$$

from which the constant is $(-1)^3k_1k_2$. In general,

$$S(\mu) = (-1)^n k_1\cdots k_{n-1}\frac{\prod_{i=1}^{n}(\mu-\mu_i)}{\prod_{\alpha=1}^{n-1}(1-k_\alpha\mu)} \quad (121)$$

which is the required expression. Similarly,

$$S(-\mu) = k_1\cdots k_{n-1}\frac{\prod_{i=1}^{n}(\mu+\mu_i)}{\prod_{\alpha=1}^{n-1}(1+k_\alpha\mu)} \quad (122)$$

It can be shown that

$$k_1\cdots k_{n-1}\mu_1\cdots\mu_n = \frac{1}{\sqrt{3}} \quad (123)$$

whence,

$$S(-\mu) = \frac{1}{\sqrt{3}}H(\mu) \quad (124)$$

where $H(\mu)$ is the function defined by

$$H(\mu) = \frac{1}{\mu_1\cdots\mu_n}\frac{\prod_{i=1}^{n}(\mu+\mu_i)}{\prod_{\alpha=1}^{n-1}(1+k_\alpha\mu)} \quad (125)$$

Then the angular distribution of the emergent radiation $I(0, \mu)$, eqn. (105), can be written as

$$I(0,\mu) = \frac{\sqrt{3}}{4}FH(\mu) \quad (126)$$

Chandrasekhar has considered a large number of transfer problems, for example, the scattering of light with or without absorption, and with different phase function, diffuse reflection in an extended atmosphere, scattering where polarization must be taken into account (as in the atmospheres of hot stars where electron scattering is primarily responsible for the opacity), and atmospheres of finite optical thickness, such as those of planets.

In all of these problems, the observed quantity is the emergent or reflected radiation defined for μ's in the interval $0 < \mu < 1$. The boundary conditions, however, fix the zeros of the same analytic function in the interval $0 > \mu > -1$. The result is that in any approximation, the Q and L_α constants may be eliminated and the solutions may be reduced to a closed form in the nth approximation. Except for certain constants, these equations involve $H(\mu)$ functions of the form of eqn. (125) where the k_α's are the positive or zero roots of a characteristic equation analogous to eqn. (88), viz.,

$$1 = 2\sum_{j=1}^{n}\frac{a_j\Psi(\mu_j)}{1-k^2\mu_j^2} \quad (127)$$

As usual, the μ_i's are zeros of the Legendre polynomial, $P_{2n}(\mu)$. Here $\Psi(\mu)$ is an even polynomial in μ which must satisfy the condition

$$\int_0^1 \Psi(\mu)\,d\mu \leq \tfrac{1}{2} \quad (128)$$

In the transfer problem we have taken $\Psi(\mu) = \frac{1}{2}$. Other problems lead to different $\Psi(\mu)$ functions and hence to $H(\mu)$ functions that differ from one another only in the way the roots k_α are defined.

Then the $H(\mu)$ function satisfies identically the equation

$$H(\mu) = 1 + \mu H(\mu)\sum_{j=1}^{n}\frac{a_jH(\mu_j)\Psi(\mu_j)}{\mu+\mu_j} \quad (129')$$

To prove this, consider first the case when the inequality holds in eqn. (128). Then eqn. (127) has n distinct positive roots. Consider the function

$$S_0(\mu) = \sum_{\alpha=1}^{n}\frac{L_\alpha}{1-k_\alpha\mu} + 1$$

(cf. eqn. 115). Here the constants L_α ($\alpha = 1, \cdots n$) are to be determined from the set of n equations

$$\sum_{\alpha=1}^{n}\frac{L_\alpha}{1-k_\alpha\mu_i} + 1 = S_0(\mu_i) = 0 \quad (i = 1, \cdots n)$$

Then we may write

$$S_0(\mu) = k_1 \cdot \cdot \cdot k_n\mu_1 \cdot \cdot \cdot \mu_n \frac{(-1)^n}{\mu_1\mu_2 \cdot \cdot \cdot \mu_n} \frac{\prod_i (\mu - \mu_i)}{\prod_\alpha (1 - k_\alpha\mu)}$$

$$= k_1 \cdot \cdot \cdot k_n\mu_1 \cdot \cdot \cdot \mu_n H(-\mu) = S_0(0)H(-\mu)$$

since $H(0) = 1$. Thus

$$S_0(0) = k_1 \cdot \cdot \cdot k_n\mu_1 \cdot \cdot \cdot \mu_n = \sum_{\alpha=1}^{n} L_\alpha + 1$$

Since $\Psi(\mu)$ is an even function in μ, the characteristic root will satisfy an equation which can be written either as

$$1 = \sum_j \frac{a_j\Psi(\mu_j)}{1 + k\mu_j} \quad \text{or as} \quad 1 = \sum_j \frac{a_j\Psi(\mu_j)}{1 - k\mu_j}$$

Denoting a particular characteristic root as k_α, and making use of the above expressions which are satisfied by any of these characteristic roots, we obtain the identity

$$S_0(0) = \sum_{\beta=1}^{n} L_\beta + 1 = \sum_{\beta=1}^{n} \frac{L_\beta}{k_\alpha + k_\beta} \left\{ \sum_j a_j\Psi(\mu_j) \left[\frac{k_\alpha}{1 + k_\alpha\mu_j} + \frac{k_\beta}{1 - k_\beta\mu_j} \right] \right\} + \sum_j \frac{a_j\Psi(\mu_j)}{1 + k_\alpha\mu_j}$$

$$= \sum_{\beta=1}^{n} L_\beta \left[\sum_j \frac{a_j\Psi(\mu_j)}{(1 + k_\alpha\mu_j)(1 - k_\beta\mu_j)} \right] + \sum_j \frac{a_j\Psi(\mu_j)}{1 + k_\alpha\mu_j}$$

$$= \sum \frac{a_j\Psi(\mu_j)}{1 + k_\alpha\mu_j} \left[\sum_{\beta=1}^{n} \frac{L_\beta}{1 - k_\beta\mu_j} + 1 \right]$$

In the last expression the order of summation has been inverted and the term in brackets is $S_0(\mu)$, so that

$$S_0(\mu) = \sum_j \frac{a_jS_0(\mu_j)\Psi(\mu_j)}{1 + k_\alpha\mu_j}$$

In this expression the summation is taken over both positive and negative values of j. We have seen, however, that $S_0(+\mu_j) = 0$, so that only terms with negative j make a non-zero contribution to the above summation. Thus

$$S_0(0) = \sum_{j=1}^{n} \frac{a_jS_0(-\mu_j)\Psi(\mu_j)}{1 - k_\alpha\mu_j} \quad (\alpha = 1, 2, \cdot \cdot \cdot n)$$

Since $S_0(-\mu) = S_0(0)H(\mu)$, we have

$$1 = \sum_{j=1}^{n} \frac{a_jH(\mu_j)\Psi(\mu_j)}{1 - k_\alpha\mu_j} \quad (\alpha = 1, 2, \cdot \cdot \cdot n)$$

In accordance with this relation, the function

$$1 - \mu \sum_{j=1}^{n} \frac{a_jH(\mu_j)\Psi(\mu_j)}{\mu + \mu_j}$$

will vanish if $\mu = -1/k_\alpha$ ($\alpha = 1, 2, \cdot \cdot \cdot n$), since

$$1 + \frac{1}{k_\alpha} \sum_{j=1}^{n} \frac{a_jH(\mu_j)\Psi(\mu_j)}{(-1/k_\alpha) + \mu_j} = 1 - \sum_{j=1}^{n} \frac{a_jH(\mu_j)\Psi(\mu_j)}{1 - k_\alpha\mu_j} = 0$$

Therefore, if we set $\mu = -1/k_\alpha$ ($\alpha = 1, 2, \cdot \cdot \cdot n$), the expression

$$\prod_{j+1}^{n} (\mu + \mu_j) - \mu \sum_{j=1}^{n} a_jH(\mu_j)\Psi(\mu_j) \prod_{i \neq j} (\mu + \mu_i) = \mu_1\mu_2 \cdot \cdot \cdot \mu_n + \text{etc.}$$

likewise vanishes. This product function is an nth degree polynomial which differs from

$$\prod_{\alpha=1}^{n} (1 + k_\alpha\mu) = 1 + \mu \sum k_\alpha + \cdot \cdot \cdot$$

only by the constant of proportionality, $\mu_1\mu_2 \cdot \cdot \cdot \mu_n$, which is established by comparing the two functions with μ set equal to zero. Hence

$$1 - \mu \sum_{j=1}^{n} \frac{a_jH(\mu_j)\Psi(\mu_j)}{\mu + \mu_j} = \mu_1 \cdot \cdot \cdot \mu_n \frac{\prod_{\alpha=1}^{n} (1 + k_\alpha\mu)}{\prod_{j=1}^{n} (\mu + \mu_i)} = \frac{1}{H(\mu)}$$

and eqn. (129′) follows at once.

When the integral (128) equals $\frac{1}{2}$, there are $(n - 1)$ positive roots and $k = 0$ is a root of the characteristic equation. The proof follows in a manner similar to the one we sketched. Eqn. (129′) holds for any value of n, however large.

When n increases without bound, Chandrasekhar shows that $H(\mu)$ satisfies the equation

$$H(\mu) = 1 + \mu H(\mu) \int_0^1 \frac{H(\mu')\Psi(\mu')}{\mu + \mu'} d\mu' \tag{129}$$

first found by Ambarzumian by a different line of reasoning.

Eqn. (129) may be solved by iteration. We obtain an initial $H(\mu)$ by the approximate methods previously described, substitute it as $H(\mu')$ under the integral sign and compute a new $H(\mu)$. We continue until the $H(\mu)$ of the $(j + 1)$st approximation does not differ from that of the jth approximation.

For example, to solve the limb-darkening problem, we could start with eqn. (105) with the constant L and Q from eqn. (114), solve for $H(\mu)$ from eqn. (126), and substitute in eqn. (129). The final $H(\mu)$ obtained

by iteration from eqn. (129) is then replaced in eqn. (126) to get the limb darkening.

In all approximations, the boundary temperature of the star is related to the effective temperature by

$$T_e^4 = \frac{4}{\sqrt{3}} T_0^4 \tag{130}$$

since $q(0) = 3^{-1/2}$. This is the exact solution obtained by Hopf and Bronstein some years ago. Thus

$$T_e = 1.233 T_0 \tag{131}$$

If the effective temperature of the sun is 5700°K, the boundary temperature is 4623°K. Further, $q(\infty) = 0.71045$.

We have confined our attention to the simplest practical application of Chandrasekhar's method and have indicated only in the sketchiest terms how the procedure is to be generalized to obtain an exact solution. For details the reader should consult Chandrasekhar's *Radiative Transfer*, where a full account is given of these powerful new methods and their applications to astrophysical problems.

11. Other Solutions of the Transfer Equation

The Chandrasekhar method is primarily adapted to the prediction of the observed quantity $I(0, \mu)$. On the other hand, it often does not permit a simple determination of the source function itself. In contrast, Kourganoff has found a method which gives the source function directly. For a grey atmosphere in thermal equilibrium we may equate B, J, and the source function, viz.,

$$B = J = \mathcal{J} \tag{132}$$

Now J is given by eqn. (103) and we shall expand the quantity in brackets $\tau + q(\tau)$, in a series of the form

$$\tau + q(\tau) = A_0 + A_1\tau + A_2 E_2(\tau) + \cdots \tag{133}$$

where $A_1 = 1$, and E_n is given by eqn. (9). Kourganoff's method of solution consists in expressing the constancy of flux by a minimum condition (variational method) which gives the A_i's very easily.

The flux at any optical depth τ is given by eqn. (60). For brevity we introduce the operator

$$P(X) = 2\int_\tau^\infty X E_2(t - \tau)\, dt - 2\int_0^\tau X E_2(\tau - t)\, dt \tag{134}$$

We obtain from eqns. (60), (103), (132), and (134)

$$F(\tau) = P(B) = \frac{3F}{4} P[\tau + q(\tau)] \tag{135}$$

Now put eqn. (133) into eqn. (135) to obtain

$$\frac{F(\tau)}{F} = \frac{3}{4}[A_0 p_0(\tau) + p_1(\tau) + A_2 p_2(\tau) + \cdots] \tag{136}$$

where

$$p_0(\tau) = P(1), \quad p_1(\tau) = P(\tau), \quad p_n(\tau) = P(E_n) \tag{137}$$

The p's may be computed once and for all, e.g.,

$$p_0 = 2E_3(\tau), \quad p_1 = \tfrac{4}{3} - 2E_4(\tau) \tag{138}$$

(see Problem 10). Others have been tabulated by Kourganoff. The A's are determined by the condition that

$$F(\tau) = F = \text{constant} \tag{139}$$

Kourganoff insures that eqn. (139) be fulfilled as closely as possible by requiring that the "functional resolvant,"

$$s(A_0, A_2, \cdots A_n) = \int_0^\infty \left[\frac{F(\tau)}{F} - 1\right]^2 d\tau \tag{140}$$

is a minimum. Take the partial derivatives of s with respect to each of the A's. Thus n linearly independent equations involving the A's as the unknown coefficients are obtained. To evaluate these coefficients, he assigns τ a series of values $\tau_1, \tau_2, \ldots \tau_i (i > n)$, and solves the linear system of i equations by least squares. Kourganoff illustrates the procedure for $n = 6$, and $i = 16$. He has also given an alternate solution which is more precise. Once $q(\tau)$ is known, the emergent intensity $I(0, \mu)$ may be computed at once from equation (5). The process converges rapidly, but q approaches the exact solution faster for large τ than for small τ. If a good initial guess for J is available, in particular one which gives the correct value of J for large τ, the variational solution just described can be improved by an iteration method as Kourganoff has shown.

Let us define the operator L by

$$L(X) = \tfrac{1}{2}\int_0^\infty X E_1(|\tau - t|)\, dt \tag{141}$$

Then, for a grey atmosphere [cf. eqn. (132)] we obtain from an integration of eqn. (59) over all frequencies,

$$J = L(J) \tag{142}$$

Unsöld, who generalized a discussion by Hopf, has shown that if we start with an initial solution J_0 and apply the operator L, $J_1 = L(J_0)$ will lie closer to the true solution J. We then construct a new solution $J_2 = L(J_1)$ and continue until $J_n = J_{n-1}$. Unsöld used the iteration procedure

with Eddington's approximation. It converges most rapidly at small optical depths where the variational solution converges most slowly. Hence it can be used to improve the variational solution. Consider an expansion of the type eqn. (133) and apply eqn. (141) term by term. We get

$$u_0 = L(1) = 1 - \tfrac{1}{2}E_2(\tau) \tag{143}$$

$$u_1 = L(\tau) \tag{144}$$

$$u_n = L(E_n), \text{ etc.} \tag{145}$$

These functions may be computed from the previously obtained p's. The iterated "variational solution" is then

$$q_i(\tau) = A_0u_0 + A_1u_1 + A_2u_2 + A_3u_3 + \cdots + A_nu_n \tag{146}$$

The variational procedure gives an exact q at large τ whereas the iteration method gives best results for small τ. Hence a combination of the two procedures leads to an exact solution most rapidly.* The error in the iterated sixth approximation is less than one part in a million.

D. H. Menzel and H. K. Sen solved the transfer equation by an operational method. Other treatments of the transfer equation were developed by physicists to handle neutron diffusion problems. In this connection we mention the work of R. E. Marshak, G. Placzek, W. Seidel, C. Mark, J. LeCaine, and B. Davison and the earlier work of N. Wiener and E. Hopf.

D. Labs has suggested the representation of the function $B(\tau)$ for a grey body by a formula of the form

$$B(\tau) = \tfrac{3}{4}F(a + \tau - Ae^{-\alpha\tau}) \tag{147}$$

for which he finds $a = 0.7104$, $A = 0.1331$, and $\alpha = 3.4488$.

* In order to discuss the radiative equilibrium of stellar atmospheres composed of *nongrey* material, Unsöld adopts a zeroth approximation to the source function, $\mathcal{J}_{0\nu}(\tau_\nu)$, where τ_ν is the optical depth at the frequency ν. Then $F_{0\nu}(\tau_\nu)$ is found from eqn. (134),

$$F_{0\nu}(\tau_\nu) = P(\mathcal{J}_{0\nu}(\tau_\nu))$$

For a given geometrical depth which corresponds to an optical depth $\bar{\tau}$ in the integrated radiation, one finds the total flux:

$$\pi F_0(\bar{\tau}) = \int_0^\infty \pi F_{0\nu}(\tau_\nu(\bar{\tau}))\, d\nu$$

which departs from the assumed constant flux, πF, by

$$\pi\Delta F(\bar{\tau}) = \pi F_0(\bar{\tau}) - \pi F$$

Next, one must compute a correction $\Delta\mathcal{J}$ to the source function $\mathcal{J}$ so that $\Delta F(\bar{\tau})$ can be made to vanish. Using the Eddington approximation and the equations of transfer, one may show that for the integrated radiation:

$$-\Delta\mathcal{J} = \frac{1}{2}\Delta F(0) + \frac{3}{4}\int_0^{\bar{\tau}} \Delta F(\bar{\tau})\, d\bar{\tau} - \frac{1}{4}\frac{d\,\Delta F(\bar{\tau})}{d\bar{\tau}}$$

12. The Mean Absorption Coefficient

Unfortunately the material of which stellar atmospheres are composed is not grey. As we saw in Secs. 2 and 3, the absorption coefficient varies with wave length in the examples of principal astrophysical interest. The coloring effect of the gases may have a pronounced effect on the outward flow of radiation. The questions we ask are these: To what extent will the temperature distribution derived in Secs. 10 and 11 be valid in a nongrey atmosphere? Can we define a mean absorption coefficient, $\bar{k}$, in such a way that the grey-body solution will remain valid? That is, the optical depth $\bar{\tau}$ in the integrated radiation defined by $\bar{\tau} = \int \bar{k}\rho\, dx$, is to be identified with the optical depth in the corresponding grey atmosphere.

Let us return to the equations of transfer in the Eddington notation [cf. eqns. (69) and (68)]. We have:

Monochromatic Radiation	Integrated Radiation
$\dfrac{dH_\nu}{k_\nu\rho\, dx} = J_\nu - B_\nu$	$\dfrac{dH}{\bar{k}\rho\, dx} = 0$ (148)
$\dfrac{dK_\nu}{k_\nu\rho\, dx} = H_\nu = \tfrac{1}{4}F_\nu$ (149)	$\dfrac{dK}{\bar{k}\rho\, dx} = H = \tfrac{1}{4}F$ (150)

Eqn. (148) [our old eqn. (68)] expresses the constancy of the total radiation flux:

$$\int H_\nu\, d\nu = H \tag{151}$$

also

$$\int K_\nu\, d\nu = K \tag{152}$$

At a given point in the atmosphere, we have from eqns. (149), (150), and (151)

$$\int \frac{1}{k_\nu}\frac{dK_\nu}{\rho\, dx}\, d\nu = \frac{1}{\bar{k}}\int \frac{dK_\nu}{\rho\, dx}\, d\nu \tag{153}$$

which defines the *mean absorption coefficient* or *opacity*. We suppose that k_ν and $\bar{k}$ contain the negative absorptions.

In the Rosseland mean (see Ch. 10) K_ν is replaced by $\frac{1}{3}J_\nu$ (Eddington approximation) and this in turn is replaced in eqn. (153) by B_ν. But $J_\nu = B_\nu$ implies monochromatic radiative equilibrium, whereas the essence of local thermodynamic equilibrium is that there is a shift in the

frequency distribution of the energy with depth. Even in a strictly grey atmosphere, J_ν could not be replaced rigorously by B_ν. At large optical depths, however, the replacement of K_ν by $\frac{1}{3}B_\nu$ will make little difference and the Rosseland mean coefficient will be valid.

From eqns. (149) to (153) we can write

$$\bar{k} = \frac{1}{F}\int_0^\infty k_\nu F_\nu \, d\nu \tag{154}$$

The only difficulty with this equation is that the variation of F_ν with frequency is not known. Chandrasekhar suggested that if $k_\nu/\bar{k}$ is constant with optical depth and does not vary with wave length by a large factor, F_ν may be taken as the net monochromatic flux of radiation of frequency ν in a grey atmosphere.* Then the grey body temperature distribution remains valid if $\bar{k}$ is defined by eqn. (154), at least in the first approximation. Corrections to the temperature distributions can be calculated if a refined treatment is necessary. At large optical depths the $\bar{k}$ computed by eqn. (154) must go over into the Rosseland mean. In stars such as the sun where k_ν varies smoothly on account of the negative hydrogen ion absorption, or in supergiant B stars where electron scattering does the smoothing, the Chandrasekhar mean appears to give excellent results. Münch studied the temperature distribution in the solar atmosphere in a higher approximation wherein departures from greyness were taken into account. He found that the difference between this temperature distribution and the grey atmospheric value is sufficiently small to justify the use of the temperature distribution of the grey body as a good first approximation.†

If $k_\nu/\bar{k}$ varies abruptly with wave length or optical depth, as in the early-type stars, the Chandrasekhar mean may still give a good first approximation, as is shown by Miss Underhill's calculations of a model atmosphere for an 09.5 main-sequence star, by Jean McDonald's calculations for a $B2.5$ star, as well as by computations for $B1$ and $B5$ stars and for pure helium stars. We return to this topic in Sec. 16.

13. Limb Darkening in the Integrated Radiation

Once the temperature distribution with optical depth is known for a grey atmosphere, one can compute $I_\nu(0,\theta)/I(0,0)$ for the integrated solar radiation on the hypothesis that radiative transfer determines the energy flow. In practice, two effects conspire to limit the theoretical accuracy of $T(\tau)$ and $I(0,\theta)$.

* For a Table of F_ν/F as a function of τ see Chandrasekhar's *Radiative Transfer*, p. 295.

† In the light of Münch's work, Unsöld's criticism of the Chandrasekhar mean appears unjustified for stars like the sun.

First, the continuous absorption coefficient varies with wave length. Münch found the grey-body distribution to be a good approximation if the mean absorption coefficient is computed in the manner indicated by Chandrasekhar.

Second, the outward flow of radiation is impeded not only by continuous absorption but also by discrete line absorption in the Fraunhofer lines. Mulders estimated the total fraction of energy subtracted from the outgoing radiation to be 0.083, but the depletion is particularly serious in the ultraviolet. G. Münch, who solved the transfer equation by the Chandrasekhar method, under the conditions of a constant net flux, found about 4600°K, a result in harmony with excitation temperatures derived by a number of workers and with the boundary temperature found from an analysis of limb-darkening measures made at the McMath-Hulbert Observatory. The most detailed treatment of the problem is that by D. Labs who took into account the variation of the line absorption coefficients with optical depth for different regions of the spectrum. With the aid of the condition of radiative equilibrium for nongrey material he was able to improve the temperature distribution in the outer layers. He finds that in spite of the numerous Fraunhofer lines the temperature departs substantially from that of a grey body only for $\tau < .01$ where there is a sharp decline of the temperature to 4300°K at the boundary. Limb-darkening measures are not capable of distinguishing between such a sharp drop at the very boundary of the sun and a more gradual fall off to 4600°K. The effect of line absorption upon the temperature distribution in the solar atmosphere is called the *blanketing effect.*

TABLE 9

LIMB DARKENING IN THE SUN

cos θ	First Approximation	Exact Solution (Chandrasekhar)	Münch (Blanketing Effect)	Observed Intensity
1.00	1.000	1.000	1.000	1.000
0.90	0.940	0.939	0.946	0.944
0.80	0.880	0.878	0.892	0.898
0.70	0.820	0.816	0.838	0.842
0.60	0.760	0.755	0.781	0.788
0.50	0.700	0.692	0.725	0.730
0.40	0.640	0.629	0.666	0.670
0.30	0.580	0.565	0.615	0.602
0.20	0.520	0.499	0.541	0.485
0.10	0.460	0.429	0.467	
0.00	0.400	0.344	0.363	

Table 9 compares theoretical predictions with the observed values of the limb darkening in integrated light as deduced from the measures by

Abbot, Aldrich, and Fowle, and by Moll, Burger, and van der Bilt. Successive columns in Table 9 give the values predicted by the simple law, eqn. (80); those from Chandrasekhar's exact solution [cf. eqn. (126)]; Münch's results taking the blanketing effect into account, and finally the observed data. Notice that the limb darkening predicted by the simple theory is too small, whereas Münch's predictions agree with the observations until $\cos\theta = 0.30$ is reached, beyond which point both theory and observation encounter difficulties.

The observed results are in harmony with the suggestion that the temperature gradient of the upper atmosphere is determined by radiative equilibrium. An atmosphere in complete convective equilibrium would be totally darkened to the limb as K. Schwarzschild showed many years ago (see Problem 2). At some depth below the surface, however, convective equilibrium must set in (see Chs. 9 and 10). At the present time the theory of this convection zone has not been worked out completely.

Further complications are introduced if the solar gases are not stratified in plane parallel layers, because the solar surface may have an undulatory character associated with the granules (see Ch. 9).

14. Model Stellar Atmospheres

With a knowledge of the coefficient of continuous absorption and of the temperature distribution with optical depth we may now investigate the structure of stellar atmospheres. One reason for calculating the temperature and density distribution is to obtain the basic data needed for a precise theoretical study of the profiles of absorption lines. If the variations of gas pressure, electron pressure, density, temperature, and absorption coefficient are known as a function of depth, the change of ionization of the element of interest and the line absorption coefficient may be calculated.

Another reason for studying the structure of a stellar atmosphere, particularly the variation of k_ν/k and T with optical depth, is to provide a basis for the interpretation of the observable characteristics of continuous stellar spectra, e.g., color temperatures and Balmer discontinuities.

To make headway with this problem, we shall suppose the atmosphere to be in hydrostatic equilibrium, i.e., at each point the gas pressure supports the weight of the overlying layers. A slab of density ρ of unit cross-sectional area, and of thickness dx, subject to an acceleration of gravity g will weigh $g\rho\,dx$; hence the increase in pressure with an increment dx in depth must be

$$dP = g\rho\,dx \tag{155}$$

where x is measured downward into the star. Now introduce the optical depth defined in terms of the integrated radiation,

$$d\tau = k\rho\,dx \tag{156}$$

and there results

$$\frac{dP}{d\tau} = \frac{g}{k} \tag{157}$$

as the equation that must be satisfied to obtain the variation of gas pressure with τ.* For the moment g may be taken as the gravitational acceleration; we shall temporarily assume that the levitational effects of radiation pressure, turbulence, etc. can be neglected. The gas pressure, P_g, is characterized by a kinetic temperature T which is customarily identified with the local temperature given by the theory of radiative equilibrium [cf. eqn. (104)].

To determine the gas pressure, P_g, as a function of τ, it is necessary to determine k as a function of P_g and $\theta = \dfrac{5040}{T}$ and to solve eqn. (157). Now k is given as a function of the electron pressure, P_e, and the temperature. The relation between P_e and P_g will depend on the assumed composition (cf. Sec. 9 of Ch. 4). For numerical calculations we have assumed a mixture in which hydrogen contributes 540 mg of each gram of stellar material. With the aid of the P_g, P_e, θ curves of Fig. 9, which

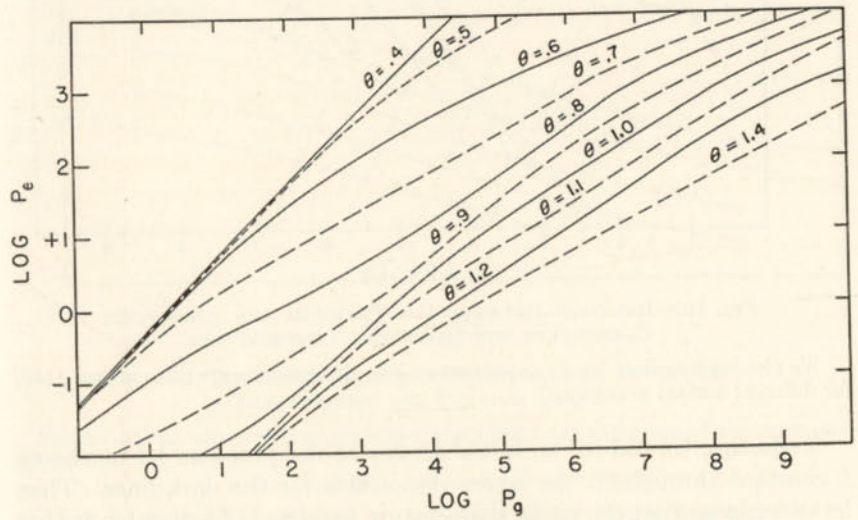

FIG. 9.—RELATION BETWEEN GAS AND ELECTRON PRESSURE FOR DIFFERENT TEMPERATURES

Ordinates are log P_e; abscissae are log P_g computed for relative abundances: H, He, (Fe, Si, Mg, Ni), and (Al, Ca, Na) 1000/200/0.43/0.11 (see Chapter 4). Curves are given for values of the parameter, $\theta = \dfrac{5040}{T}$, from 0.4 to 1.4.

* In this section we omit the bars from $\bar{\tau}$ and $\bar{k}$. It is understood that k refers to the mean absorption coefficient in a nongrey atmosphere, and $T(\tau)$ to the grey body temperature distribution.

are based on Table 3 of Chapter 4, the relation between electron pressure, temperature, and absorption coefficient (Table 5) may be transformed into a relation between gas pressure, temperature, and absorption coefficient, $k(P_g, T)$ or rather $k(P_g, \theta)$, cf. Fig. 10.

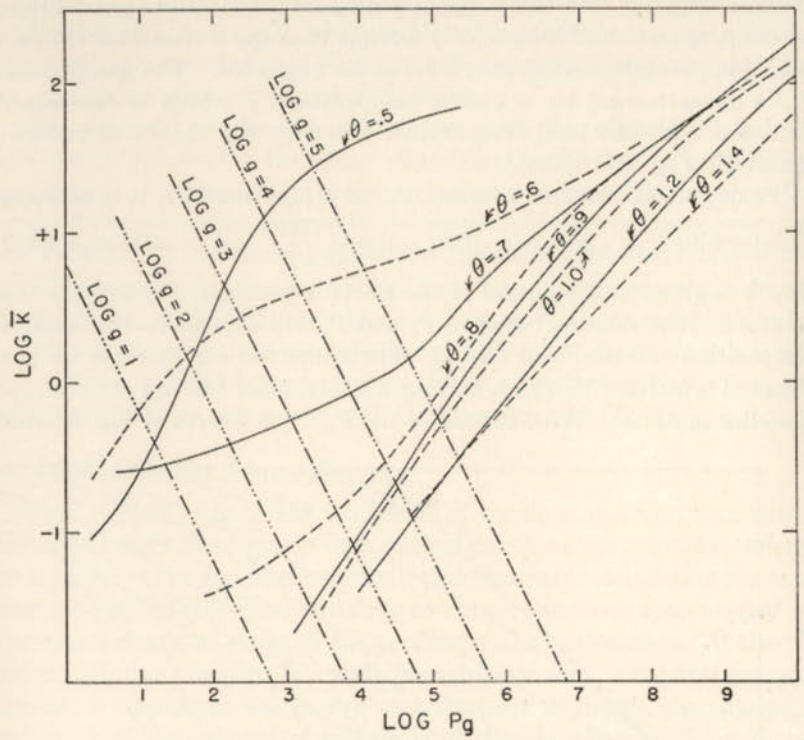

FIG. 10.—RELATION BETWEEN GAS PRESSURE AND ABSORPTION COEFFICIENT FOR DIFFERENT TEMPERATURES

We plot log k against log P_g as abscissae. The straight lines are plots of eqn. (159) for different surface gravities.

Following Unsöld for an initial survey of the problem, let us choose k constant throughout the layers responsible for the dark lines. Then let us suppose that the mean temperature and level of ionization is that appropriate to a characteristic optical depth τ_0 which we tentatively take as 0.63.* Then

$$P_g = \frac{g}{k_0}\tau_0 \tag{158}$$

or

$$\log P_g = \log g - \log k - 0.20 \tag{159}$$

* For atoms that become rapidly ionized with depth, e.g., sodium in the sun, we should choose a much smaller τ_0, e.g., 0.25.

For each value of log g this equation gives a line of 45° slope in the P_g–k plane. Its intersection with a particular $k(P_g, T)$ curve gives k and log P_g for a star of temperature T and surface gravity g. Then from Fig. 9, we read off log P_e for a given T.

Example: Let

$$\log g = 4.0, \quad \theta = 0.50$$

The line,

$$\log P_g + \log k = 4.00 - 0.20$$

intersects the $k(P_g, \theta = 0.5)$ curve at $\log P_g = 2.68$ and $\log k = 1.10$. From Fig. 9, we find that for $\theta = 0.5$, $\log P_e = 2.25$, or $P_e = 178$ dynes. The "amount of material above the photosphere," i.e., above optical depth $\tau_0 = 0.63$ is $\int \rho\, dx = \bar{\rho} h = \tau_0/k = 0.63/12.6 = 0.05$ gm. Next, consider a giant for which $\log g = 3.0$, $\theta = 0.9$. A similar computation shows $\log P_g = 3.90$, $\log k = -1.10$, $\log P_e = 0.58$.

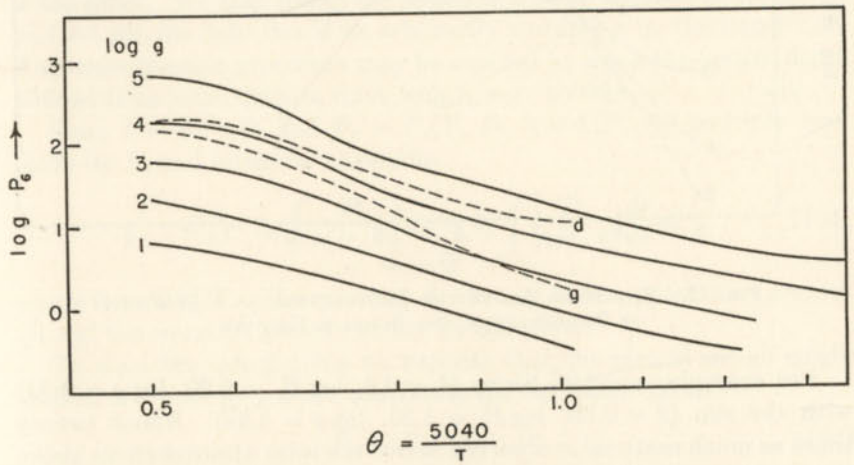

FIG. 11.—THE MEAN ELECTRON PRESSURE AS A FUNCTION OF TEMPERATURE AND SURFACE GRAVITY

Broken curves are drawn to represent giant stars (g) and stars of the main sequence (d).

Figs. 11 and 12, computed on the basis of the above considerations, show how the electron pressure and mass above the photosphere vary with temperature for different values of the surface gravity g. For a given surface gravity, notice how the electron pressure increases and the mass above the photosphere decreases as the temperature rises. Hydrogen is the most abundant constituent of stellar atmospheres. At the lower temperatures, it is mainly neutral, and free electrons are contributed only by the metals. Hence the electron pressure is quite a small fraction of the gas pressure. As the temperature rises, hydrogen be-

comes ionized and both the electron pressure and absorption coefficient increase. Atomic hydrogen becomes more effective in blocking the outgoing radiation than is the H^- ion.

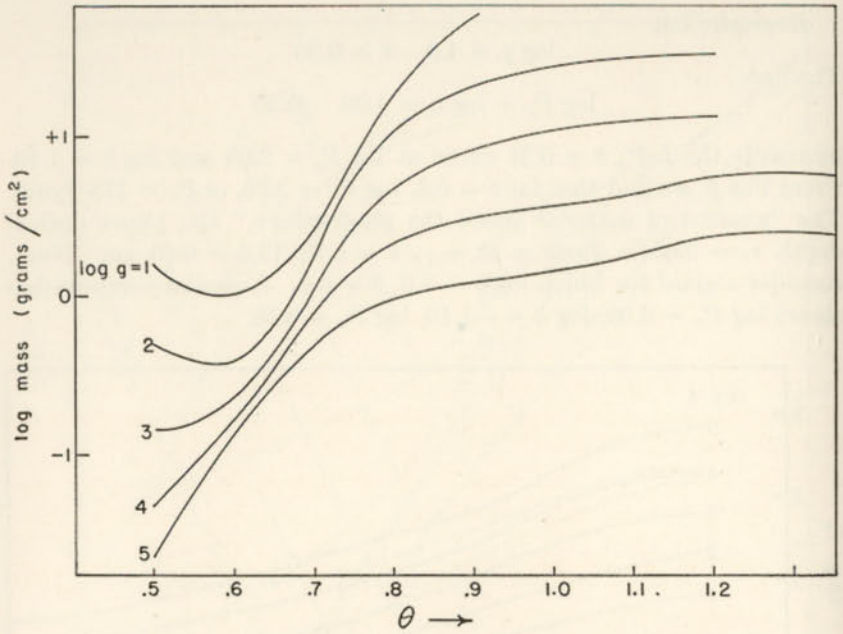

FIG. 12.—THE MASS ABOVE THE PHOTOSPHERE AS A FUNCTION OF TEMPERATURE AND SURFACE GRAVITY

For example, compare Sirius ($\theta = 0.5$, $\log P_e = 2.20$, $\log g = 4.31$) with the sun ($\theta = 0.88$, $\log P_e = 1.30$, $\log g = 4.44$). About twenty times as much material is observed above the solar atmosphere as above that of Sirius, a result in harmony with the predictions of theory.

15. A Model Solar Atmosphere

The foregoing approach is adequate for only a first reconnaisance of the problem of absorption line formation. In refined work we must know the variation of P_g, P_e, k, and T with optical depth τ. Let us integrate the equation (157) for the solar atmosphere. We proceed by a method of successive approximations along the lines followed by Strömgren and more recently by Münch.

First we must know the variation of the temperature with τ. Analysis of limb-darkening observations made at the McMath-Hulbert Observatory gives $T(\tau_\lambda)$ where τ_λ is the optical depth at the wave length λ. In order to convert $T(\tau_\lambda)$ to $T(\tau)$, it is necessary to know k/k_λ as a function of temperature. We suppose that the negative hydrogen ion and atomic hydrogen produce the opacity. Then $\bar{k}(\tau)$ may be found from eqn. (33) with the understanding that $\bar{\alpha}(H)$ and $\bar{\alpha}(H^-)$ are calculated with the grey body weighting function F_ν/F chosen for the appropriate optical depth (see columns 3 and 4 of Table 10). In the first approximation the contribution of atomic hydrogen is neglected. Then

$$\tau = \int \frac{k}{k_\lambda} d\tau_\lambda \tag{160}$$

and $T(\tau)$ may be found from the known $T(\tau_\lambda)$. When this program is carried out, the predicted flux is found to be 1.35 times the observed flux. A similar result was obtained by Chandrasekhar and Münch. While line absorption may account for some of the discordances it does not seem possible to explain all of the discrepancy in this way. Thus $\bar{k}$ is too small. We may retain the notion of a mean absorption coefficient and yet get the right flux if we arbitrarily multiply $\bar{k}$ by the factor 1.35. This objectionable procedure may be avoided by using the optical depth defined from some definite wave length, e.g., λ5000A.

Since $k = k(P_e, \theta)$ and $P_g = P_g(P_e, \theta)$, $k = k(P_g, \theta)$, multiply eqn. (157) by P_g and integrate to obtain:

$$P_g^2 = 2g \int \frac{P_g}{k(P_g, \theta)} d\tau = 2g \int \frac{P_g}{k(P_g, \theta)} \frac{d\tau}{d\theta} d\theta \tag{161}$$

where $\theta = 5040/T$. The quantity $d\tau/d\theta$ may be computed once and for all and the equation solved quickly by iteration.

To start the integrations we suppose that the metals are all singly ionized and that they alone contribute the electrons. Then

$$P_g \sim P_e A(1 + D) \tag{162}$$

where D is the He/H ratio by numbers of atoms (here adopted as 0.2) and A, the ratio of hydrogen to the metals, is adopted as 2260 (cf. Ch. 4). Neglecting the influence of atomic hydrogen we obtain

$$k = 1.35\beta k(H^-) \tag{163}$$

where β is the mass of hydrogen per gram of stellar material. Then eqn. (32) and eqn. (161) yield

$$P_g^{(0)} = \left[\frac{2gM_H A(1 + D)}{1.35\beta} \int \frac{d\tau}{\bar{\alpha}(H^-)}\right]^{1/2} \tag{164}$$

our initial estimate of P_g (see column 5 of Table 10). To perform the second iteration, P_e is found with the aid of Fig. 9, k is calculated with the aid of $\bar{\alpha}(H^-)$ and $\bar{\alpha}(H)$ from columns 3 and 4 of Table 10, and P_g' is

computed with the aid of eqn. (161). The process is repeated until two successive integrations give the same dependence of P_g on τ (last column of Table 10).

TABLE 10

NUMERICAL INTEGRATION OF THE SOLAR ATMOSPHERE

θ	τ	$\bar{\alpha}(H^-) \times 10^{24}$	$\bar{\alpha}(H) \times 10^{24}$	$\log P_g^e$	$\log P_g^I$	$\log P_g$
1.10	0.01	0.1221		3.750	3.744	3.74
1.05	0.04	0.1020		4.142	4.215	4.22
1.00	0.11	0.0838		4.368	4.426	4.44
0.95	0.22	0.0673	0.001	4.556	4.578	4.59
0.90	0.38	0.0547	0.005	4.729	4.710	4.72
0.85	0.68	0.0430	0.021	4.891	4.840	4.84
0.80	1.17	0.0334	0.081	5.048	4.957	4.95
0.75	1.87	0.0250	0.276	5.201	5.048	5.04
0.70	2.94	0.0185	0.977	5.350	5.119	5.10

The results of the integration are listed in Table 11 where we give $\tau(5500)$, the optical depth at 5500A, as well as τ.* Successive columns

TABLE 11

MODEL SOLAR ATMOSPHERE

τ	$\tau(5500)$	θ	Log P_g	Log P_e	Log $\bar{k}$	x
0.00	0.00	1.120				
0.05	0.04	1.045	4.22	0.46	9.10 − 10	−46
0.10	0.08	1.006	4.41	0.74	9.31	0
0.20	0.16	0.956	4.58	0.99	9.47	39
0.30	0.24	0.923	4.67	1.13	9.55	61
0.40	0.32	0.897	4.73	1.23	9.61	76
0.50	0.39	0.877	4.78	1.32	9.65	89
0.60	0.47	0.860	4.82	1.38	9.69	99
0.80	0.63	0.835	4.88	1.52	9.77	115
1.00	0.78	0.816	4.92	1.64	9.84	126
1.20	0.94	0.797	4.96	1.75	9.92	138
1.40	1.10	0.781	4.99	1.85	9.99	146
1.60	1.25	0.767	5.01	1.94	0.05	151
1.80	1.42	0.754	5.03	2.02	0.11	158
2.00	1.57	0.743	5.05	2.10	0.16	164

* We could have eliminated the use of τ entirely by writing

$$\frac{dP_g}{d\tau_\lambda} = \frac{g}{k_\lambda},$$

and using the known dependence of T on τ_λ. The results are essentially the same as those already given. In future calculations of model solar atmospheres it is probably better to use τ_λ and k_λ rather than τ and k.

list θ, log P_g, log P_e, and log k as functions of optical depth. Similar calculations for other hydrogen and helium abundances and the same empirical temperature distribution have been given elsewhere.

For other stars the temperature variation with optical depth cannot be found empirically. The outermost layers of most stars are usually in radiative equilibrium. Immediately below these strata often lies a zone in convective equilibrium (see Ch. 10, Sec. 5).

The relation between τ and the linear depth x measured downward in the atmosphere is of interest. The gas pressure, density and temperature satisfy eqn. (4) of Chapter 3, wherein the molecular weight μ depends on the level of ionization of the material in accordance with Sec. 3 of Chapter 3. For our assumed solar composition, $\mu = 1.54$, since the material is mostly neutral. Eliminating the density from eqn. (155), with the aid of the gas law, eqn. (4) of Chapter 3, we find

$$dx = \frac{\Re T}{\mu g} d \ln P_g \tag{165}$$

which must be solved numerically to relate P_g with x and ultimately τ with x (last column of Table 11). The zero point of x is, of course, arbitrary.

16. Model Atmospheres for Early-type Stars

The high temperature stars where the opacity is produced almost entirely by atomic hydrogen present a very different problem from that of the sun. Among the hotter stars (O–$B3$) of the main sequence, radiation pressure may support an appreciable fraction of the weight of the gases. In the first approximation, it has been customary to replace g by an effective surface gravity

$$g_{\text{eff}} = g - g' \tag{166}$$

where g' represents the force/gram exerted by the radiation, viz.,

$$g' = \frac{\pi}{c} \int F_\nu k_\nu \, d\nu \tag{167}$$

of eqn. (26) of Chapter 5. Since F_ν and k_ν vary with the temperature, g' unlike the "mechanical" surface gravity, $g = GM/R^2$, varies with depth in the star. The correct equation of hydrostatic equilibrium may be shown to be

$$\frac{dP_g}{d\tau} = \frac{g}{\bar{k} + \sigma} - \frac{\sigma}{c} T_e^4 \tag{168}$$

where σ is the Stefan-Boltzmann constant.

The extreme nongrey character of the continuous absorption coefficient in early-type stars introduces enormous complications. Reference to Fig. 3 shows that k_ν varies in a jagged fashion. It is small just longward of the Lyman limit and then becomes so very large that the outgoing radiation is effectively blocked. Qualitatively the strong Lyman absorption has a blocking effect similar to that produced by the Fraunhofer lines in the solar spectrum. Many years ago Chandrasekhar and Hopf showed that if the spectrum is crossed by a "picket-fence" of evenly spaced absorption lines, the temperature at the boundary will be depressed below that appropriate to a grey body, will then rise steeply, overshoot the grey body curve and finally asymptotically approach the latter with increasing τ. If a_1 is the fraction of outgoing radiation blocked by the absorption lines, $x_1 = k_L/\bar{k}$, and $x_2 = k_c/\bar{k}$ where k_L and k_c are the absorption coefficients in the lines and between the lines, respectively, E. Hopf showed that in eqn. (102), $q(\tau = 0)$ becomes

$$q(0) = \frac{1}{\sqrt{3(a_1x_1 + a_2x_2)}} \tag{169}$$

Chandrasekhar* derived an expression for $q(\tau)$ that enables one to correct an initially assumed temperature distribution for the effects of line absorption. The strong absorption beyond the Lyman limit plays a qualitatively similar role to the Fraunhofer lines. Thus the Chandrasekhar-Hopf theory may be employed as a guide to set up a plausible initial temperature distribution for the calculation of a model atmosphere. In order to obtain an initial temperature distribution one must first estimate the mean absorption coefficient. At large optical depths the Rosseland mean absorption coefficient is valid. For the region near the surface one may calculate k by a formula suggested by Chandrasekhar, viz.,

$$\bar{k} = \frac{\int k_\nu F_\nu \, d\nu}{\int F_\nu \, d\nu} \tag{170}$$

where the integration is carried from 0 to the frequency of the Lyman limit, and πF_ν is the black body flux which depends on τ. In intermediate optical depths one may interpolate $\bar{k}$ between these two extremes. The model atmosphere is next calculated by eqn. (157) with the assumption that T is given as a function of τ by an expression of the form, eqn. (104). The effect of the Lyman absorption is taken into account roughly by the choice of $q(\tau)$. With the assumed temperature distribution we now calculate $B_\nu(T)$ as a function of τ. At each point the condition of radiative equilibrium

$$\int_0^\infty k_\nu J_\nu \, d\nu = \int_0^\infty k_\nu B_\nu \, d\nu \tag{171}$$

must be fulfilled. We may compute J_ν at each τ with the aid of eqn. (59). If this J_ν be put in eqn. (171), a new B_ν, call it B_ν^I, will be demanded, which leads to a new temperature determination by the condition that

$$caT^4 = 4\pi \int_0^\infty B_\nu^I \, d\nu \tag{172}$$

The condition of radiative equilibrium is not very sensitive to changes in the assumed temperature distribution.

After the model atmosphere is calculated and P_g, P_e, and k are found as functions of τ, it is necessary to calculate the integrated flux as a function of optical depth. If the atmosphere is in radiative equilibrium, F will be constant with τ. The presence of electron scattering complicates the problem. In the integrals (59) and (60) the Planckian function is replaced by a source function defined in eqn. (60) of Chapter 8, which involves both B and J and the ratio of the coefficients of electron scattering to thermal absorption. The equation for the source function is solved by an iteration procedure [Sec. 8(c) of Ch. 8] and the total flux integrated over all frequencies is computed as a function of optical depth in the integrated radiation.

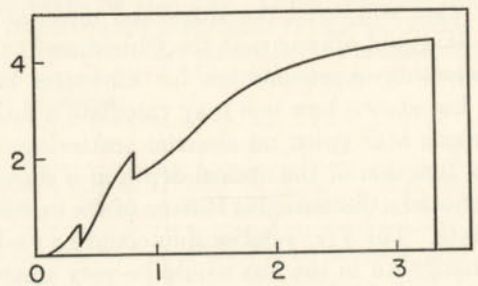

FIG. 13.—THE EMERGENT FLUX FROM AN ATMOSPHERE COMPOSED OF PURE HYDROGEN

We assume $\log g_{eff} = 4.20$. The temperature distribution is taken as follows:

τ	T	τ	T	τ	T	τ	T	τ	T
0.00	18,000	0.10	21,250	0.40	23,000	0.80	24,700	1.40	26,900
0.05	20,700	0.20	21,850	0.60	23,900	1.00	25,600	2.00	28,700

Ordinates are flux $F_\nu \times 10^{-3}$ ergs/cm²/sec; abscissae are $\nu \times 10^{-15}$ sec^{-1}. The effective temperature is about 26,500°K. Notice the profound effect of the continuous absorption at the limit of the Lyman Series, $\nu = 3.29 \times 10^{15}$ sec^{-1}.

* *M.N.* **96**, 21, 1936, cf. eqn. (52).

If the flux is not constant, a new temperature distribution must be chosen and the entire process repeated. We illustrate the emergent flux for model atmospheres with log $g_{\text{eff}} = 4.20$ and excitation temperatures near 24,000°K. One atmosphere is assumed composed of pure hydrogen, the other of pure helium. Notice the sharp cut-off at the Lyman limit in the hydrogen atmosphere (somewhat exaggerated because the Lyman line absorption is not included). A comparison of the energy distribution with that of a black body that emits the same amount of energy illustrates the copious flow of energy through the window on the redward side of the Lyman limit.* See Figs. 13 and 14.

In the atmosphere of the pure helium star the first ionization is almost complete, but second ionization has not yet become important in the layers relevant to the production of the absorption lines. At corresponding optical depths the electron pressure and the contribution of electron scattering to the total opacity is greater than in the pure hydrogen star. Notice the irregular behavior of the flux and the influence of the absorption limits of He II at λ912 and He I near λ3420.

These calculations as well as the earlier investigations by Rudkjobing, by Pecker, by Miss Underhill, and by Miss McDonald show that the effective and boundary temperatures are no longer connected by eqn. (131). Indeed, it would seem impossible to define a mean absorption coefficient in the sense that the temperature dependence on the resultant τ would be the same as for a grey body. Underhill and McDonald based their calculations on the Chandrasekhar mean and secured models in which the flux in the outer layers was nearly constant in the first approximation. Pecker employed the Rosseland mean and required several iterations. It would appear that the Chandrasekhar mean is to be preferred as a starting approximation for the outer layers. Allan F. Cook, however, has shown how one may calculate a model atmosphere for a pure hydrogen star (with no electron scattering) and obtain the temperature as a function of the optical depth at a standard frequency. Miss McDonald noted a discouraging feature of the calculation of models for early-type stars. The $T(\tau)$ relationship could be varied over a large range and the change $\Delta\mathfrak{F}$ in the flux would be very small.†

* The sharpness of the Lyman discontinuity may be inferred from the spectra of shells in certain stars. Ions such as Ca II and Sr II whose ionization potentials are less than 13.54 ev would be exposed to strong radiation through the "window" to the redward of the Lyman series limit. Hence, calcium and strontium should be mostly doubly ionized and the Ca II and Sr II lines should be quite weak, while ions of Ni II, Cr II, Fe II, Ti II, and Mn II whose ionization potentials are greater than 13.54 ev should be protected from the second ionization by the strong Lyman absorption. Struve finds that such differences do not appear to exist, probably because of the overlapping of the Lyman lines near the series limit.

† The profiles and intensities of observable spectral lines, however, are sensitive to the temperature as all of them arise from high levels for which the Boltzmann factor is important. The predicted profiles of the hydrogen lines in γ Pegasi (*B*2.5) disagree with the observed ones. The correction to the grey-body temperature distribution suggested by the Chandrasekhar-Hopf theory tends to lessen the discordance, but it remains to be seen if it can remove it entirely.

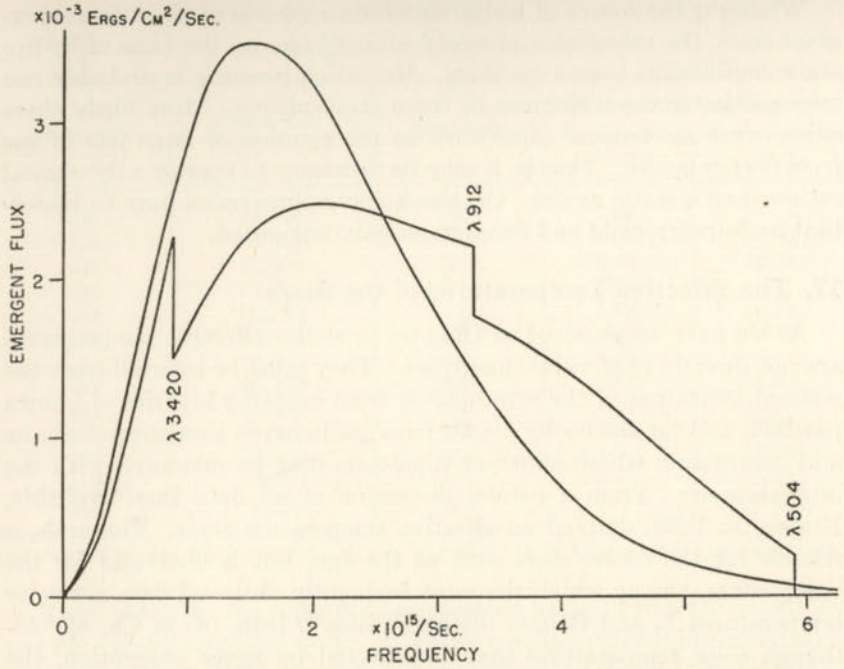

FIG. 14.—THE EMERGENT RADIATION FLUX FROM A HELIUM ATMOSPHERE

Here log $g_{\text{eff}} = 4.20$. The effective temperature is 26,560°K and the corresponding black body curve is shown. In the region λ4000–λ9000 the brightness temperature is close to 23,600°K. Notice the discontinuities produced by the He I absorption at λ3420 and λ504 and by He II at λ912. To the redward of the He II λ912 limit the He I absorption rises so rapidly that the He II limit at λ2052 is masked. In observable spectral regions only the He I absorption and electron scattering contribute to the blocking of the outward flux. The temperature distribution at the smaller optical depths is adopted as follows:

τ	T	τ	T	τ	T
0.00	18,000	0.10	20,900	0.40	22,700
0.05	20,500	0.20	21,500	0.60	23,800

At the larger optical depths it is assumed to be the same as in the hydrogen model.

Giant and supergiant stars present even more difficult problems since they often show

$$g_{\text{eff}} \sim 10^{-2}\frac{GM}{R^2} \tag{173}$$

Such an effect is demonstrated not only by the line profiles whose shapes depend on the surface gravity but also by the density gradients in the atmospheres of eclipsing systems such as ζ Aurigae or 31 Cygni.

Whatever the source of levitation of atmospheres of giant and supergiant stars, the calculation of model atmospheres on the basis of hydrostatic equilibrium seems excluded. Radiation pressure is probably not responsible for the distention of these atmospheres. More likely there exists some mechanical cause such as the ejection of large jets of gas from deeper layers. That is, it may be necessary to employ a dynamical rather than a static model. Or, shock wave phenomena may be important as Schwarzschild and Schatzman have suggested.

17. The Effective Temperatures of the Stars

As we have emphasized in Chapter 6, stellar effective temperatures are not directly observable quantities. They must be inferred from the state of ionization of the atmosphere, from eclipsing binaries of known parallax, and for the cooler stars—from radiometric measures of giants and supergiants whose apparent diameters may be measured with the interferometer. From a careful discussion of all data then available, Kuiper, in 1938, derived an effective temperature scale. The scale is reliable for the cooler stars such as the sun, but is uncertain for the hotter stars, among which the most frequently observed data are color temperatures T_c and Balmer discontinuities D [eqn. (8) of Ch. 6]. Although color temperatures may be affected by space absorption, the Balmer discontinuities are not so affected.

As described in Sec. 7, the continuous absorption by atomic hydrogen and the negative hydrogen ion explained the $T_c - T_{\text{eff}}$ relation for stars of spectral classes A to G. As our numerical example showed, however, the quantitative representation of both color temperature and Balmer discontinuity appeared impossible with an atmosphere for which k_ν/k is constant. The answer to these difficulties probably lies in a thorough analysis of atmospheres wherein k_ν/k varies not only with wave length but with optical depth as well.

In Chapter 6 we mentioned how Barbier's work showed that the Balmer discontinuity D provided a useful criterion for absolute magnitudes of early-type stars. Furthermore, Barbier has derived a theoretical relationship between the Balmer discontinuity, the temperature, and the electron pressure, with the aid of which an effective temperature scale may be found for the main-sequence stars from their observed D's.*

* With an assumed $\log P_e = 3.0$, we find the following $\log T_c$'s:

*B*0	4.45	*B*2	4.27	*B*5	4.15	*B*9	4.07
*B*1	4.35	*B*3	4.19	*B*8	4.10	*A*0	4.03

Ionization theory suggests that the temperatures for spectral classes *B*2 and *B*3 are too low.

TABLE 12

THE EFFECTIVE TEMPERATURE SCALE*

Spectrum	Effective Temperature	Spectrum	Effective Temperature	
			Dwarfs	Giants
*O*5	36,300	*F*0	7500	—
*O*6	34,600	*F*5	6470	—
*O*7	32,900	*G*0	6000	5200
*O*8	31,700	*G*2	5710	—
*O*9	30,700	*G*5	5360	4620
*B*0	28,600	*K*0	4910	4230
*B*1	23,000	*K*2	4650	—
*B*2	20,400	*K*5	3900	3580
*B*3	18,600	*M*0	—	3400
*B*5	15,500	*M*2	3200	3200
*B*8	12,300	*M*4	—	2930
*A*0	10,700	*M*6	—	2750
*A*5	8,530	*M*8e	—	2590

* R. M. Petrie, *Publ. Dom. Ap. Obs.* **7**, 321, 1948; G. P. Kuiper, *Ap. J.* **88**, 429, 1938.

Table 12 gives the effective temperature scale. From *O*5 to *B*0 we use the values suggested by R. M. Petrie who interpreted line intensities with the ionization theory. Recent theoretical work by Miss Underhill indicates that these ionization temperatures are probably lower than the effective temperatures. The rest of the scale is taken from Kuiper's paper. Radiometric measures and studies of line excitation carried out at Mount Wilson indicate that the temperature of the later-type giants are lower than the values assigned by Kuiper. Thus *gM*6 should be about 2350°K and *gM*10 about 1750°K.

We conclude with some remarks on the problem of model stellar atmospheres and on the coefficient of continuous absorption. More accurate measures of the specific intensity $I_{0\lambda}$ at the center of the sun's disk are urgently needed. A study of limb darkening above and below the Balmer limit in early-type eclipsing stars might reveal much about their atmospheres and the relative importance of absorption and scattering.

It is fortunate that the existence and absorptivity of the negative hydrogen ion can be confirmed by experiment. R. Fuchs employed a capillary hydrogen-filled tube which was excited by the discharge of a $0.5\mu F$ condenser charged to a potential of 30 kev. The discharge lasted long enough for thermal equilibrium at about 12,000°K to be established at a pressure near 50 atmospheres. The resultant continuous spectrum could be shown to consist of contributions from the negative hydrogen ion as well as from atomic hydrogen. W. Lochte-Holtgreven and

W. Nissen used a water-cooled quartz discharge tube of 8 mm diameter and blew hydrogen into it through a tangential nozzle in such a way as to form a whirling gas stream about the arc and tungsten electrodes. With this relatively stable arc, they observed the Balmer lines superposed on a continuous background. Since they were able to derive the electron density and temperature from the intensity and profile of Hβ, they could calculate the contributions of atomic hydrogen and the negative hydrogen ion to the continuum. At a temperature of 10,000°K and a pressure of one atmosphere these contributions were about equal, the experimental results being in excellent agreement with the theory. They also found that if an H_2^+ continuum exists, its contribution must be very small.

Although the negative hydrogen ion and atomic hydrogen account for most of the continuous absorption in stars like the sun, an appreciable fraction of the blocking of outflowing solar radiation may be done by agents not yet specifically identified. Among the possibilities are discrete line absorption, discrete and continuous molecular absorption, and possibly absorption by other negative ions.* Beyond the H and K lines we probably do not see the continuous spectrum; it is smothered by a host of strong overlapping lines, which become stronger and more pronounced toward the "rocket" ultraviolet, λ2900–2000A, so that ultimately the "continuous" spectrum is depressed well below that of a black body at 5700°K. Liller and Lewis showed that in the neighborhood of the K line in the $K0$ dwarf ε Eridani the continuum is depressed about 35 per cent because of the overlapping wings of strong lines. The calculation of model atmospheres for such objects becomes very difficult because of the blocking of the radiation by strong lines.

Much information on the structure of stellar atmospheres may be derived from studies of line profiles to which problem we now turn our attention.

PROBLEMS

1. Show that the temperature gradient in an atmosphere in adiabatic equilibrium

$$P = K\rho^{\gamma} \tag{174}$$

is constant and equal to

$$\frac{dT}{dx} = \frac{\gamma - 1}{\gamma}\frac{\mu}{\mathfrak{R}}g \tag{175}$$

* Negative ions other than those of hydrogen probably play no important role in stellar atmospheres. Wildt and Chandrasekhar suggested that the negative oxygen ion might produce some absorption in cooler stars, but this possibility hangs on an insecurely determined electron affinity. The halogens, which have large electron affinities, are not sufficiently abundant to exert any important influence.

where $\mathfrak{R}$ is the gas constant, γ is the ratio of specific heats, and g is the acceleration of gravity.

2. Consider an atmosphere in adiabatic equilibrium, and in which the absorption coefficient is proportional to the gas pressure. Show that the limb-darkening law is

$$\frac{I(0,\theta)}{I(0,0)} = (\cos\theta)^{\frac{2(\gamma-1)}{\gamma}} \tag{176}$$

3. Assume that the temperature distribution with optical depth is given by the Eddington approximation, eqn. (76). Show that if the Planck function is expanded as $B = a + b\tau$, then

$$\frac{b}{a} = \frac{3}{8}u(1 - e^{-u})^{-1} \tag{177}$$

where

$$u = \frac{h\nu}{kT_0} \tag{178}$$

and T_0 is the boundary temperature and a, b, and B all depend on the wave length.

4. Verify eqns. (17) and (18).

5. Consider an atmosphere in which both absorption and isotropic scattering occur. Show that if k and σ are both independent of wave length, the equation reduces to the one already treated. When k and σ depend on frequency, let us define:

$$d\bar{\tau} = (\overline{k+\sigma})\rho\,dx, \quad d\tau = k\rho\,dx, \quad \text{and} \quad dt = (k+\sigma)\rho\,dx \tag{179}$$

Then

$$B_\lambda = a_\lambda\left(1 + \frac{b_\lambda}{a_\lambda}\frac{\overline{k+\sigma}}{k}\tau\right) \tag{180}$$

where the ratio b/a is given by eqn. (177). Solve the appropriate eqn. (56), with Eddington's approximation under the assumption that σ/k and $k/(\overline{k+\sigma})$ are independent of the optical depth. Show that

$$J_\lambda = B_\lambda + A_\lambda e^{-\beta t} \tag{181}$$

where

$$\beta = \left(\frac{3k}{k+\sigma}\right)^{1/2} \tag{182}$$

and the boundary conditions require that

$$A_\lambda = a_\lambda\frac{\frac{2}{3}\frac{b_\lambda}{a_\lambda}\frac{\overline{k+\sigma}}{k+\sigma} - 1}{1 + \frac{2}{3}\beta} \tag{183}$$

6. With the aid of the results from Problem 5 show that the emergent flux πF_λ is given by

$$F_\lambda = 2\int_0^\infty B(\bar{\tau})E_2(t)\,dt + 2A_\lambda \frac{\sigma}{k+\sigma}\int_0^\infty E_2(t)e^{-\beta t}\,dt \qquad (184)$$

7. Calculate the relative numbers of atoms above the photosphere capable of absorbing the λ3933 lines of Ca II for stars on the main sequence at $\theta = \dfrac{5040}{T} = 0.5$, 0.6, 0.8, 1.0, 1.2, and 1.4.

8. Prove eqn. (168).

9. Calculate a model atmosphere for a giant star of effective temperature 5100°K, and $\log g = 2.0$, including the relation between x and τ. Compare the structure of the atmosphere with that of the sun (cf. Table 10), and that of a dwarf star with $T_{\text{eff}} = 5100$°K and $\log g = 4.61$.

10. With $E_n(x)$ defined by eqn. (9), and

$$E_0 = \frac{e^{-x}}{x}, \quad E_1 = E \qquad (185)$$

prove the following relations:

$$(n-1)E_n(x) = e^{-x} - xE_{n-1}(x), \quad n \geq 2 \qquad (186)$$

$$E_n(0) = \frac{1}{n-1}, \quad n \geq 2 \qquad (187)$$

$$\int_x^\infty E_n(x)\,dx = E_{n+1} \qquad (188)$$

$$\frac{d}{dx}E_n(x) = -E_{n-1}(x), \quad (n \geq 1) \qquad (189)$$

$$\int_x^\infty xE_n(x)\,dx = xE_{n+1}(x) + E_{n+2}(x) \qquad (190)$$

$$A(\alpha, x) = \int_0^x e^{\alpha z}E(x)\,dx = -\frac{1}{\alpha}[\ln(|1-\alpha|) + E[(1-\alpha)x] - e^{\alpha x}E(x)] \qquad (191)$$

11. Consider an atmosphere in which the radiative flux is no longer constant with optical depth (as in an atmosphere where convection occurs). Show that in the Eddington approximation:

$$B = \frac{F_0}{2} + \frac{3}{4}\int F\,d\tau - \frac{1}{4}\frac{dF}{d\tau} \qquad (192)$$

REFERENCES

1. *General*

An account of the powerful new methods for the treatment of the flow of radiation through a stellar atmosphere is given in:

CHANDRASEKHAR, S. *Radiative Transfer*. London: Oxford University Press, 1950. See especially chaps. i–v, xi, and xii. An extensive bibliography is given. The discussion in our Sec. 10 is taken largely from *Ap. J.* **100,** 76, 1944.

Among the best older references are:

UNSÖLD, A. *Physik der Sternatmosphären*. Berlin: Julius Springer, 1938.
EDDINGTON, A. S. *Internal Constitution of the Stars*. London: Cambridge University Press, 1926.
MILNE, E. A. *Handbuch der Astrophysik*, Vol. 3, Part 1. Berlin: Julius Springer, 1930.

The operational method for the treatment of transfer problems is given by:

MENZEL, D. H., and H. K. SEN. *Ap. J.* **110,** 1, 1949; **113,** 482, 1951.

An account of the variation method together with an excellent bibliography is given by:

KOURGANOFF, V. *Ann. d'Ap.* **12,** 169, 1949.

Numerical integration formulae are discussed by:

CHANDRASEKHAR, S. *Op. cit.*, chap. ii.
KOURGANOFF, V., and C. PECKER. *Ann. d'Ap.* **12,** 247, 1949.

2. *Stellar Absorption Coefficient*

Atomic hydrogen:

UNSÖLD, A. *Sternatmosphären*, p. 116.
PANNEKOEK, A. *Publ. Astron. Instit. Amsterdam* **4,** 1935.

Negative hydrogen ion:

CHANDRASEKHAR, S. *Ap. J.* **104,** 430, 1946.
FUCHS, ROLAND. *Zeits. f. Phys.* **130,** 69, 1951.
LOCHTE-HOLTGREVEN, W., and W. NISSEN, *Zeits. f. Phys.* **133,** 124, 1952.

Atomic helium:

HUANG, S. S. *Ap. J.* **108,** 354, 1948.
GREENSTEIN, J. L. *Ap. J.* **95,** 299, 1942.

General:

VITENSE, E. *Zeits. f. Ap.* **28,** 51, 1951.

3. *Interpretation of Continuous Spectra of Sun and Stars*

CHALONGE, D. *Physica* **12,** 721, 1946.
CHALONGE, D., and V. KOURGANOFF. *Ann. d'Ap.* **9,** 69, 1946.
MÜNCH, G. *Ap. J.* **102,** 385, 1945; **104,** 87, 1946.
CHANDRASEKHAR, S., and G. MÜNCH. *Ap. J.* **104,** 446, 1946.
BARBIER, D. *Ann. d'Ap.* **6,** 36, 1943; **7,** 113, 1944; **9,** 173, 1946.
LABS, D. *Zeits. f. Ap.* **29,** 199, 1951.

4. *Model Atmospheres*

Theoretical considerations and illustrative examples are given for example by

Strömgren, B. *Publ. Copenhagen Obs. No. 138*, 1944.
Neven and C. de Jager. *B.A.N.* **11**, 291, 1951.
Münch, G. *Ap. J.* **106**, 217, 1947; **107**, 265, 1948.
Pierce, A. K., and L. H. Aller. *Ap. J.* **114**, 145, 1951; **116**, 175, 1952.
Cook, A. F. *Ap. J.*, in press.
Pecker, J. C. *Ann. d'Ap.* **13**, 294, 319, 433, 1950.
Underhill, A. *Publ. Copenhagen Obs. No. 151*, 1950. *Publ. Dom. Ap. Obs.* **8**, 357, 1951.

A number of basic calculations for model atmospheres are published by

Rosa, A. *Zeits. f. Ap.* **25**, 1, 1948.
Unsöld, A. *Zeits. f. Ap.* **25**, 11, 20, 1948.

5. *Effective Surface Gravity*

Elvey, C. T., and O. Struve. *Ap. J.* **79**, 409, 1934.
Pannekoek, A. *B.A.N.* **8**, 175, 1937.

The effect of radiation pressure in early-type stars is discussed by

Underhill, A. *M. N.* **109**, 562, 1949.

6. *Radiative Equilibrium*

The integral equation of radiative equilibrium is discussed by:

Unsöld, A. *Zeits. f. Ap.* **24**, 363, 1948; *Naturswissenschaften* **22**, 525, 1951.

The formal theory of near thermodynamic radiative equilibrium is given by

Henyey, L. G. *Ap. J.* **103**, 332, 1946.

A general discussion of transfer problems with applications to nuclear physics is given in

Kourganoff, V. (with collaboration of Ida W. Busbridge). *Basic Methods in Transfer Problems*. London: Oxford University Press, 1952.

CHAPTER 8

The Fraunhofer Spectrum

1. Introduction

The fundamental problem of stellar atmospheres is the following: Given the intensities of the absorption lines, to determine the composition and physical state of the atmosphere and the surface gravity of the star. From the spectrum we should be able to tell whether the star has a normal or an unusual composition and whether it is a dwarf, giant, or supergiant.

First of all we need to define the "intensity" of a line. Rowland made eye estimates of the intensities of the dark lines in the solar spectrum on an arbitrary scale, and these estimates, when properly calibrated, are useful for many problems. Unfortunately, no single parameter will completely describe an absorption line. A Fraunhofer line may be represented by an intensity curve, with a certain depth, width, and shape. Since every one of these features arises from a definite physical cause, an adequate theory should be able to account for the complete intensity distribution or profile of the line. It is true that spectral lines have certain common characteristics as regards shape. Usually they are symmetrical (notable exceptions are certain helium lines in hot dwarf stars) and possess a single minimum. But in other features they may differ markedly. The strong lines show broad "wings" —extensions on either side of the minimum. Weak lines do not have such wings, and if they are photographed with an instrument of sufficient resolving power, they show a bell-shaped profile. Also some lines, e.g., λ4227 of Ca I, are nearly black at the center; others have appreciable central intensities. Thus it is not possible to write an empirical equation with a single parameter that would represent the profiles of all the lines in the solar spectrum, for example. We shall see that these differences in shape arise from the differences in the number of atoms acting to produce the lines, from differences in the physical conditions under which the lines are formed, and from the fact that processes important for strong lines, e.g., collisional broadening, are not significant for the weaker lines.

The experimental determination of line profiles is a difficult problem. The finite resolving power of the spectrograph and photographic turbidity tend to blur out the lines. Furthermore, with a grating, light will

be scattered from the adjacent continuous spectrum into the lines and will give too high a central intensity, i.e., too shallow a line. If the line is deep and narrow, the photographic Eberhard effect may become serious. Hence painstaking care is necessary for the accurate determination of line profiles. We mention the investigations of Shane (Na "*D*" lines); Plaskett, d'Azambuja, Cherrington, and others (Mg "*b*" group); Redman (λ4227 Ca I); and Houtgast (center-limb variations of a number of strong lines). Shane employed an elaborate interference method to determine the amount of scattered light and to eliminate the photographic Eberhard effect; his method gives results of high accuracy. Redman placed an auxiliary spectroscope in front of his spectrograph and isolated the small spectral region he wished to investigate. Thus scattered light from distant parts of the spectrum is avoided.

Although line profiles are of the utmost importance in studies of the atmosphere of the sun and other stars, the labor involved in getting good measurements has limited the amount of available data. Astronomers have often worked with the equivalent widths of lines, i.e., the total amount of energy subtracted from the continuous spectrum by the absorption line. By the "intensity" of an absorption line we shall mean, unless otherwise specified, the equivalent width of the line. The shapes of lines of the same equivalent width in the solar spectrum are often, but not always, nearly the same. We shall describe what can be learned both from line profiles and from equivalent widths.

Clearly, the intensity of a line must be related to the number of atoms acting to produce it: the stronger the line the greater the number of atoms. At first, one might suppose the intensity of a line to be simply proportional to the effective number of atoms, Nf, and this is indeed true for the very weakest lines. Lines of intermediate and large equivalent width are not related to the number of effective atoms in such a simple way. The character of the line broadening plays the decisive role, such that the exact relationship will depend on the importance of the Doppler effect, radiation and collision damping, broadening by charged ions, etc. Consider what happens as an increasing number of atoms is added to an atmosphere. (We can get the same effect by considering lines of the same atom but of different oscillator strength f, since Nf, not just N, is the important factor.) When the number of atoms is small, the amount of energy subtracted from the continuous spectrum is small and is proportional to the number of atoms, i.e., W varies as Nf. As Nf increases, the energy in the center of the line is depleted and further absorption has to take place in the wings. Thus the total amount of energy subtracted from the outgoing radiation as Nf increases will depend upon how much energy the atoms can absorb at great distances from the line center, i.e., on how the absorption coefficient depends on the distance $(\lambda - \lambda_0)$ from the line center. Hence we must first consider sources of line broadening and their influence on the absorption coefficient.

2. Sources of Broadening of Spectral Lines in Stellar Spectra

Absorption lines in stellar spectra are intrinsically broadened by the following causes:

(a) Doppler effect arising from the random kinetic motions of atoms. To this may be added a possible "turbulence" broadening because of large scale motions of large masses of gas especially in the atmospheres of giant and supergiant stars.

(b) Radiation damping which is a consequence of the finite lifetimes of excited levels. Classically, it corresponds to the fact that the finite wave train emitted by a radiating atom is nonmonochromatic.

(c) Collision damping.* A radiating atom may be perturbed by its neighbors and emit a broadened spectral line. The perturbing particles may be neutral atoms, ions, or electrons.

(d) Stark effect on hydrogen and helium lines, because of statistically fluctuating fields produced by ions and electrons.

(e) Hyperfine structure is responsible for the broadening of certain lines in the solar spectrum.

(f) Zeeman effect. Lines produced in sunspots or magnetic stars are broadened or split by the magnetic field.

Finally, there are extrinsic causes of broad lines in stellar spectra. An absorption line profile in a rapidly spinning star is a composite of contributions from different parts of the disk, some of which are approaching and some of which are receding. The net result will be a broad, dish-shaped line. Expanding shells in novae, peculiar stars, or Cepheids also produce broadened lines. If large scale convection currents occur, widened lines may also result.

The absorption coefficient of a line broadened by thermal motions alone [cf. eqn. (21) of Ch. 3] has a bell shape, falling off as exp $[-\text{const}\ (\delta\lambda)^2]$ in the wings. Radiation damping gives a narrow absorption coefficient with broad wings in accordance with eqn. (65) of Chapter 5. In resonance lines the quantum mechanical damping constant Γ may be of the order of the classical damping constant γ. Observations show, however, that damping constants of five, ten, or even fifty times

* Both (c) and (d) may be regarded as collisional broadening, but (c) is usually treated on the basis of discrete encounters whereas (d) is regarded as a statistical phenomenon. See Sec. 3.

the classical value are required to explain the profiles of certain strong Fraunhofer lines. Collisional broadening appears to be responsible for these large damping constants.

3. Collisional Broadening of Spectral Lines

We may employ two limiting points of view in the discussion of the collisional broadening of spectral lines. Following Lorentz, Lenz, Weisskopf and Lindholm we regard the emitting and absorbing atoms as being disturbed by separate, i.e., discrete, encounters with other particles.* Or, alternatively, following Stark, Debye, Holtsmark, or Margenau, we can ask what will be the value, at a given atom, of the electric field F produced by the surrounding particles. The value of F will fluctuate as the configuration of the particles change, but we can compute the probability, $W(F/F_0)$, for a field of strength F at a given instant. F_0 is the time average value of the field. Since to each F there corresponds a shift $\delta\nu$ in the frequency of the emitted radiation, we can compute for what fraction of time the spectral line is shifted by amounts, $\delta\nu_1$, $\delta\nu_2$, $\cdots$, etc. Then by summing over all shifts according to their statistical probabilities, we get the shape of the broadened emission line and hence the wave length dependence of the absorption coefficient, since it must have the same form (cf. Ch. 5). On the other hand, in the discrete encounter theory, the time dependence of the perturbation is the strategic factor. The wave emitted by the radiating atom is interrupted by collisions with perturbing particles and the intensity distribution in the emitted line is obtained by a Fourier analysis as a function of density and temperature.

In the limiting extreme of no relative motion between radiating atom and perturber, the Holtsmark theory would be valid. When there is relative motion, the central part of the line is governed by the discrete encounter theory and the statistical theory applies in the wings. Under conditions prevailing in stellar atmospheres, usually one or the other of these two extremes applies for a given line, e.g., for the broadening of Ca II λ3933 or Ca I λ4227 we apply the discrete encounter theory, while for the hydrogen lines we apply the Holtsmark theory.

Before we derive an expression for the shape of the broadened emission line which will give the absorption coefficient, let us consider the line broadening process from the point of view of the quantum theory. The undisturbed atom will radiate a frequency, ν_0, given by $h\nu_0 = W_2^0 - W_1^0$. If the atom is perturbed by an intruder, the energy levels will be shifted. A plot of W_1 and W_2 against r, the separation of the radiating atom and the perturbing particle, yields curves resembling the

* Encounters between neutral particles involve only short-range electric fields.

potential energy curves of a diatomic molecule. If the atom radiates when the separation is r, then $h\nu = W_2(r) - W_1(r)$. This energy will differ from that ordinarily radiated since $W_2 - W_1$ will change with r and the position of the spectral line will be shifted. Throughout the radiating volume, emissions will occur at differing r values and the resultant spectral line will not only be shifted but broadened as well.

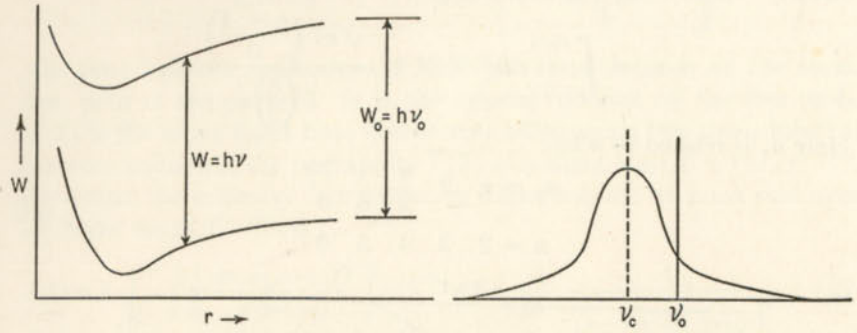

Fig. 1.—Collisional Displacement of a Spectral Line

The left part of the figure depicts the distortion of the energy levels as a function of the separation r between the atom and perturber. The undisturbed frequency is ν_0. The resultant spectral line (right) not only is broadened because encounters take place at different r values but is shifted as well.

In the classical, discrete-collision picture an atom radiating a wave train suffers an encounter with another particle which quenches the wave or changes its phase so appreciably that the net effect is as though two distinct wave trains were emitted. In all encounters the phase of the wave will be advanced or retarded. Sometimes the phase shift is large (cf. Fig. 2); at other times it is so small that the net effect is negligible.

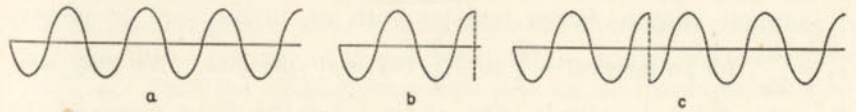

Fig. 2.—Quenching of a Wave Train in an Encounter

(a) Normal classical wave of finite duration, (b) quenched wave, (c) collision with a phase shift of 180°.

Let us suppose, following Weisskopf, that the phase shift depends on an inverse power of the separation, r^{-n}, viz.,

$$\delta\omega = \frac{2\pi C}{r^n} \tag{1}$$

where ω is measured in circular frequency units and C is a constant. The total phase shift is found by integrating $\delta\omega$ over the duration of the encounter. That is,

$$\eta = \int_{-\infty}^{+\infty} \delta\omega \, dt = 2\pi C \int_{-\infty}^{+\infty} \frac{dt}{(\rho^2 + v^2t^2)^{n/2}} = \frac{2\pi C}{v\rho^{n-1}} a_n \tag{2}$$

since $r = \rho \sec\theta$ (cf. Fig. 3); whence

$$a_n = \int_{-\pi/2}^{+\pi/2} \cos^{n-2}\theta \, d\theta = \frac{\sqrt{\pi}\,\Gamma\left(\frac{n-1}{2}\right)}{\Gamma\left(\frac{n}{2}\right)}$$

Here a_n is related to n by:

$$\begin{array}{lccccc} a_n = \pi & 2 & \frac{\pi}{2} & \frac{4}{3} & \frac{3\pi}{8} \\ n = 2 & 3 & 4 & 5 & 6 \end{array} \tag{3}$$

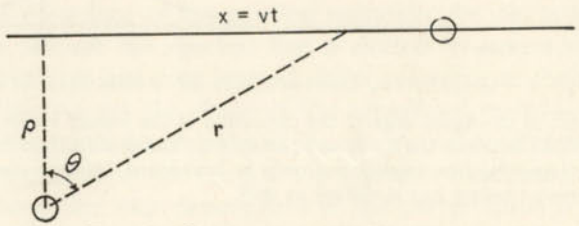

FIG. 3.—GEOMETRY OF AN ENCOUNTER

The perturbing particle whose velocity is v passes the radiating atom at a minimum distance ρ.

Weisskopf supposed, arbitrarily, that if the phase shift was greater than a critical value, η_0, which he set equal to 1, the atom would be so disturbed by the collisions that the emissions before and after should be regarded as independent processes, insofar as their influence on the shape of the spectral line is concerned.

Suppose that an atom radiates with an undisturbed frequency, $\nu_0 = \frac{\omega_0}{2\pi}$, for an interval $-\frac{T}{2}$ to $+\frac{T}{2}$ between collisions. We may analyze this finite wave train, $e^{i\omega_0 t}$, of time duration T by means of the Fourier integral theorem. We write

$$F(t) = \int_{-\infty}^{+\infty} e^{i\omega t} \, d\omega \int_{-a}^{+a} F(u) e^{i\omega u} \, du \tag{4}$$

where $F(t) = 0$ outside the interval $-a$ to $+a$. With $a = \frac{T}{2}$, and $F(t) = e^{i\omega_0 t}$, we find

$$e^{i\omega_0 t} = \int_{-\infty}^{+\infty} e^{i\omega t} \, d\omega \int_{-T/2}^{+T/2} e^{i(\omega-\omega_0)y} \, dy$$

which means that the finite wave train $-T/2$ to $+T/2$ is equivalent to the superposition of infinite wave trains, $e^{i\omega t}$, having an amplitude $\int_{-T/2}^{+T/2} e^{i(\omega-\omega_0)y} \, dy$, and therefore an intensity dependence on frequency given by

$$I(\nu) \propto \left[\int_{-T/2}^{+T/2} e^{i(\omega-\omega_0)t} \, dt\right]^2 = \left[\frac{\sin\left(\frac{\omega-\omega_0}{2}\right)T}{\frac{\omega-\omega_0}{2}}\right]^2$$

The time between encounters, T, or flight time, depends on the mean free path of the particle. It is the velocity divided by the free path. If T_0 is the mean flight time (sometimes called mean free time) interval between collisions, the probability $F(T)$ of a flight time T is $1/T_0 e^{-T/T_0}$. To obtain the intensity distribution in a spectral line we must sum over all flight times T. Then

$$I(\nu) = A\int_0^\infty \frac{1}{T_0}\left[\frac{\sin\pi(\nu-\nu_0)T}{\pi(\nu-\nu_0)}\right]^2 e^{-T/T_0}\,dT = \frac{A}{2\pi^2}\frac{1}{(\nu-\nu_0)^2+\left(\frac{1}{2\pi T_0}\right)^2} \tag{5}$$

where A is determined by the condition that

$$\int I(\nu)\,d\nu = I_{\text{total}} \tag{6}$$

Since the shape of the absorption coefficient is the same as that of the corresponding emission line, the absorption coefficient per atom is

$$\alpha_\nu = \frac{\pi e^2}{mc} f \frac{1}{2\pi^2 T_0}\frac{1}{(\nu-\nu_0)^2+\left(\frac{1}{2\pi T_0}\right)^2} \tag{7}$$

This expression shows the same frequency dependence as the radiation damping formula (eqn. 50, Ch. 5) if the constant γ be replaced by $2/T_0$.

Weisskopf supposed that those collisions that change the phase, η, by an amount greater than η_0 contributed to the broadening. Let us suppose that a distance of closest encounter, ρ_0, corresponds to a phase shift, η_0. Then the collision cross-section is $\pi\rho_0^2$ for line-broadening encounters. Let N_b denote the number of particles/cm^3 responsible for the broadening. For problems such as the widening of metallic lines in the solar spectrum, N_b will be the number of hydrogen atoms/cm^3. That is, the perturbers will be vastly more numerous than the number of emitting particles. The number of line-broadening collisions/sec for each radiating particle will be

$$S = \frac{1}{T_0} = \pi\rho_0^2 N_b V \tag{8}$$

where V, the mean relative speeds of radiating and perturbing particles, is given by kinetic theory as

$$V = \sqrt{\frac{8kT}{\pi M_0}\left(\frac{1}{A_1} + \frac{1}{A_2}\right)} \tag{9}$$

M_0 is the mass of a particle of unit atomic weight and A_1 and A_2 are the atomic weights of the radiating and perturbing atoms. Since the density of stellar atmospheres is always low, the mean distance between particles $r_0 = \sqrt[3]{\frac{3}{4\pi N}} >> \rho_0$, and we may neglect multiple collisions.

With $\eta = \eta_0$, ρ_0 follows from eqn. (2), viz.,

$$\rho_0 = \left[\frac{2\pi C a_n}{V\eta_0}\right]^{1/n-1} \tag{10}$$

The collisional damping constant will be

$$\begin{aligned}\Gamma_{\text{coll}} &= \frac{2}{T_0} = 2\pi V N_b \rho_0^2 = 2\pi N_b \left[\frac{2\pi C a_n}{\eta_0}\right]^{\frac{2}{n-1}} V^{1-\frac{2}{n-1}} \\ &= 2^{\left(\frac{5n-7}{2n-2}\right)} C^{\left(\frac{2}{n-1}\right)} \pi^{\frac{n+5}{2(n-1)}} a_n^{\frac{2}{n-1}} \left[\frac{kT}{M_0}\left(\frac{1}{A_1} + \frac{1}{A_2}\right)\right]^{\frac{n-3}{2n-2}} \eta_0^{-\frac{2}{n-1}} N_b\end{aligned} \tag{11}$$

if the force law is of the form r^{-n}. When elements other than hydrogen and helium are perturbed by ions or electrons, the quadratic Stark effect obtains and $n = 4$. Collisional broadening that arises when other absorbing atoms suffer encounters with neutral hydrogen atoms involves a van der Waals type of force for which $n = 6$.

The difficulty with the elementary approach lies in the choice of η_0. Weisskopf and Lorentz made the simple assumption that no relation existed between the phases before and after collision and that $\eta_0 = 1$. Actually, in some collisions that influence line broadening, there does exist a relation between the initial and final phases.

Lindholm gave a more detailed discussion of this problem wherein he took into account the cumulative effect of numerous encounters in which the phase is changed by varying amounts. In practice, there are few collisions in which η is large but many in which η is small. In agreement with experiment and in contrast with eqn. (7), Lindholm found a frequency shift as well as a line broadening so that the intensity is given by

$$I(\nu) = I_0\left(\frac{\gamma}{4\pi^2}\right)\frac{1}{(\nu - \nu_0 + \beta')^2 + (\gamma/4\pi)^2} \tag{12}$$

in agreement with the predictions of quantum theory.

The encounters for which $\eta \geq 1$ are most important for line broadening, whereas encounters for which $\eta < 1$ play the more significant role in causing line shifts.

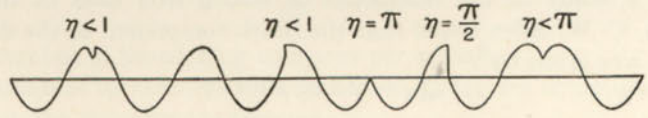

FIG. 4.—PHASE SHIFTS IN ENCOUNTERS

Assuming that the phase shifts are produced in accordance with the law expressed in eqn. (1), Lindholm has derived values of γ, $\beta = 2\pi\beta'$, and η_0 for different values of n. We quote here his results for the two special cases of greatest interest, namely, $n = 4$ (quadratic Stark effect) and $n = 6$ (van der Waals forces).

	$n = 4$	$n = 6$
γ	$38.8C^{2/3}V^{1/3}N$	$17.0C^{2/5}V^{3/5}N$
β	$33.4C^{2/3}V^{1/3}N$	$6.16C^{2/5}V^{3/5}N$
γ/β	1.16	2.80
η_0	0.64	0.61

The last row gives the correct value of η_0 to employ in eqn. (10) to get ρ_0.

As an example, let us consider the quadratic Stark effect in iron, wherein the radiating atom is disturbed by a passing electron or ion. Panter and Foster measured the displacements of iron lines in a strong electric field. If the shift in wave numbers is $\Delta\tilde{\nu}$ in a field of E_0 volts, then we may compute C from

$$c\,\Delta\tilde{\nu} = \frac{C}{\varepsilon^2}\left(\frac{E_0}{300}\right)^2 \tag{13}$$

or numerically,

$$C = 6.21 \times 10^{-4}\frac{\Delta\tilde{\nu}}{E_0^2} \tag{14}$$

For a field of 81,000 ev/cm, Panter and Foster found the λ5162.28 line broken into components polarized parallel and perpendicular to the fields and displaced by 5.76 and 4.02 cm^{-1}, respectively. With $\Delta\tilde{\nu} = 4.89$, we find $C = 46.3 \times 10^{-14}$. The C values for other lines can be found from the experimental data in a similar fashion. The Stark damping constant is then

$$\Gamma_{\text{Stark}} = 2^{3/2}\pi^{13/6}\left(\frac{kT}{M_0}\right)^{1/6}\left(\frac{1}{A_1} + \frac{1}{A_2}\right)^{1/6} N\eta_0^{-2/3}C^{2/3} \tag{15}$$

N here refers to the number of charges/cm³ active in producing line broadening. Since $A_2 = \frac{1}{1847}$ for an electron, their contribution to line broadening much exceeds that of other charges.

From a study of the intensities of strong iron lines in the solar spectrum, C. W. Allen found that the Stark component of the damping constant was given by

$$\Gamma_{\text{Stark}} = 2.2 \times 10^{17} C^{2/3} \tag{16}$$

Some contribution to this damping constant arises from electrons, some from ions. Now $A_1 = 56$, and if we suppose that most of the electrons are supplied by ionization of elements like sodium, calcium, etc.,* A_2 is about 40 for the ions as compared with $\frac{1}{1847}$ for the electrons. Hence 86 per cent of Γ_{Stark} is contributed by the electrons, or $\Gamma_e = 1.9 \times 10^{17} C^{2/3}$. If we put in the numerical values for k and M_0, choose $T = 5700°\text{K}$ (for the sun), and adopt $\eta_0 = 0.64$, which is appropriate for $n = 4$, we find $N_e = 1.34 \times 10^{13}$ or $P_e \sim 10$ dynes/cm².

Collisions between radiating atoms or ions and neutral hydrogen atoms are characterized by the van der Waals force law ($n = 6$). Then $\eta_0 = 0.61$, and by eqns. (10) and (3)

$$\rho_0 = \left(\frac{3\pi^2}{4V}\frac{C}{\eta_0}\right)^{1/5} = \left(12.15\,\frac{C}{V}\right)^{1/5} \tag{17}$$

where C, the van der Waals constant of interaction, can be found by experiment in some instances or calculated by quantum mechanics in others. With hydrogen as the principal perturbing atom, we may write C as

$$C = \frac{\varepsilon^2}{h}\alpha R_k^2 \tag{18}$$

where $\alpha = 6.77 \times 10^{-25}$ cm³ is the polarizability of the hydrogen atom (computed from quantum mechanics), and R_k^2 is the mean square radius appropriate to the upper level of the broadened absorption line. If R_k is measured in units of a_0, the radius of the first Bohr orbit,

$$C = 6.56 \times 10^{-34}\frac{R^2}{a_0^2} \tag{19}$$

As an example, consider the broadening of the H and K lines of Ca II, for which we take $R_k^2 = 23a_0^2$, whence $C = 1.51 \times 10^{-32}$. From eqn. (9) we obtain $V = 1.11 \times 10^6$ cm/sec since $A_1 = 40$, $A_2 = 1$, and $T = 5700°$ K. The target radius for collisional broadening in the Lorentz-Weisskopf sense is then, from eqn. (17), $\rho_0 = 4.40 \times 10^{-8}$ cm $= 4.40$A.

* In the solar atmosphere hydrogen supplies few electrons.

At an optical depth of 0.6 in the solar atmosphere we may take $\log P_g = 4.86$, and $T = 5700°$K so that,

$$S = \pi V \frac{P_g}{kT}\rho_0^2 = 6.2 \times 10^8 \tag{20}$$

is the number of broadening collisions per second.

If quantum mechanical calculations of R_k^2 are not available, we may often use the approximate formula,

$$\frac{R_k^2}{a_0^2} = \frac{n^{*2}}{2Z^2}\{5n^{*2} + 1 - 3l(l+1)\}$$

valid for the hydrogen-like levels of many light atoms. Here n^* is the effective quantum number, l is the azimuthal quantum number, $Z = 1$ for neutral atoms, 2 for singly ionized atoms, etc.

For the lines of most atoms, the above theory of collisional broadening appears to be adequate, but for hydrogen and helium where $\delta_\nu = \frac{c}{\nu^2}$, the Holtsmark statistical theory (Sec. 16) is valid.

The complete theory of collisional encounters shows that the discrete encounter picture and the statistical picture represent asymptotic forms of a general theory.

The Zeeman splitting of lines in a macroscopic magnetic field, such as exists in sunspots and certain peculiar A stars, depends on the number and separation of the components and on the intensity of the field. A single line may become replaced by a number of components each acting to block the outward flow of radiation. We shall treat this problem in Sec. 19 of this chapter.

4. The Line Absorption Coefficient

We shall now compute the shape of the absorption coefficient of a line broadened both by Doppler effect and by radiation or collisional damping. The latter two effects can be handled together by a suitable definition of the damping constant.

An atom moving with the velocity v toward the observer will emit a line centered on a frequency ν' given by

$$\nu' = \nu_0 + \frac{v}{c}\nu_0 \tag{21}$$

and for this atom the absorption coefficient will be

$$\alpha_\nu = \frac{\pi\varepsilon^2}{mc}f\frac{\Gamma}{4\pi^2}\frac{1}{\left(\nu_0 + \frac{v}{c}\nu_0 - \nu\right)^2 + \left(\frac{\Gamma}{4\pi}\right)^2} \tag{22}$$

To obtain the total absorption coefficient per atom in unit frequency interval at ν, we must multiply eqn. (22) by the fraction of atoms moving with the velocity v to $v + dv$ and then integrate over all velocities. The number moving in the velocity range v to $v + dv$ is given by Maxwell's equation for velocities [cf. eqn. (11) of Ch. 3]:

$$dN = N\sqrt{\frac{M}{2\pi kT}}\, e^{-\frac{Mv^2}{2kT}}\, dv \tag{23}$$

where $M = AM_0$ is the mass of the atom in question. A is the atomic weight and M_0 the mass of an atom of unit atomic weight. To obtain the absorption coefficient α_ν at a frequency ν we now integrate over all velocities that may contribute to the absorption coefficient at this frequency. Thus from eqns. (22) and (23),

$$\alpha_\nu = \frac{\pi e^2}{mc} f \frac{\Gamma}{4\pi^2} \int_{-\infty}^{+\infty} \frac{\left(\frac{M}{2\pi kT}\right)^{1/2} e^{-\frac{Mv^2}{2kT}}}{\left(\nu_0 + \frac{v}{c}\nu_0 - \nu\right)^2 + \left(\frac{\Gamma}{4\pi}\right)^2} dv \tag{24}$$

We transform this integral with the aid of the following substitutions. First let,

$$\Delta\nu_0 = \frac{\nu_0}{c}\sqrt{\frac{2kT}{M}} \tag{25}$$

$$\Delta\nu = \frac{\nu_0}{c} v \tag{26}$$

so that

$$dv = \frac{c}{\nu_0} d(\Delta\nu) \tag{27}$$

Then let us define,

$$y = \frac{\Delta\nu}{\Delta\nu_0} \tag{28}$$

$$u = \frac{\nu - \nu_0}{\Delta\nu_0} \tag{29}$$

$$\delta' = \Gamma/4\pi \tag{30}$$

$$a = \frac{\delta'}{\Delta\nu_0} \tag{31}$$

where Γ is the effective damping constant. The absorption coefficient at the line center for zero radiation damping (sometimes called the fictitious absorption coefficient) is (cf. eqn. 76 of Ch. 5):

$$\alpha_0 = \frac{\pi e^2}{mc} f \frac{1}{\Delta\nu_0}\frac{1}{\sqrt{\pi}} \tag{32}$$

or

$$\alpha_0 = \frac{g_n}{g_{n'}} A_{nn'} \frac{\lambda^2}{8\pi^{3/2}} \frac{1}{\Delta\nu_0} \tag{33}$$

where $A_{nn'}$ is the Einstein coefficient for the transition and g_n and $g_{n'}$ are the weights of the upper and lower levels respectively. Then,

$$\alpha_\nu = \alpha_0 \frac{a}{\pi} \int_{-\infty}^{+\infty} \frac{e^{-y^2}}{a^2 + (u - y)^2}\, dy \tag{34}$$

When both radiation damping and collisional broadening occur, we can write

$$\delta' = \delta_1 + \delta_2 = \frac{\Gamma_{\text{rad}}}{4\pi} + \frac{S}{2\pi} \tag{35}$$

where Γ_{rad} is the sum of the reciprocal lifetimes of levels n and n' for radiative processes, and S is the number of damping collisions/sec. Then,

$$\delta' = \frac{1}{4\pi}\sum A_{nn'} + \frac{1}{2} N_b \rho^2 V \tag{36}$$

To obtain the damping constant of any line, we must know the number of broadening particles/cm^3, N_b, and the damping collisional cross-section for the two levels of the transition in question.

At a fixed temperature and pressure, a is constant and the integration may be carried out over y. Helpful tables for the calculation of α_ν/α_0 as a function of v and a have been given by Hjerting, by Mitchell and Zemansky, and most recently by D. Harris who writes α_ν/α_0 in the form,

$$\frac{\alpha_\nu}{\alpha_0} = H_0(u) + aH_1(u) + a^2H_2(u) + a^3H_3(u) + \cdots \tag{37}$$

and tabulates H_0, H_1, etc. (see Table 1).

Example: Calculate the line absorption coefficient for λ3933 of Ca II, $4^2S_{1/2} - 4^2P_{3/2}$ at $T = 5700°$K. The f value for this line is $\frac{2}{3} \times 1.19$; hence from eqn. (77) of Chapter 5,

$$\Gamma_{\text{rad}} = 3\sum \frac{g_{n'}}{g_n} f_{n'n}\gamma_c = 3 \times \frac{2}{4} \times 1.19 \times \frac{2}{3}\gamma_c = 1.19\gamma_c \tag{38}$$

Then,

$$\Delta\lambda_0 = \frac{c}{\nu_0^2}\Delta\nu_0 = \frac{\lambda}{c}\sqrt{\frac{2kT}{M}} = \frac{3933}{3 \times 10^{10}}\sqrt{\frac{2 \times 1.38 \times 10^{-16} \times 5700}{40.07 \times 1.67 \times 10^{-24}}}$$
$$= 0.0202\text{A}, \tag{39}$$

or

$$(\lambda - \lambda_0) = 0.0202u\text{A} \tag{40}$$

while $\Delta\nu_0 = 0.392 \times 10^{10}$ sec^{-1}. Let us first consider the limiting case of pure radiation damping. From eqns. (38) and (55) of Chapter 5 we obtain

$$\delta' = \frac{\Gamma_{\text{rad}}}{4\pi} = \frac{1.19\gamma_c}{4\pi} = \Delta\nu_R \tag{41}$$

TABLE 1*

THE FUNCTIONS H_0, H_1, H_2, H_3, AND H_4

u	$H_0(u)$	$H_1(u)$	$H_2(u)$	$H_3(u)$	$H_4(u)$
0.0	+1.000 000	−1.128 38	+1.000 0	−0.752	+0.50
0.1	+0.990 050	−1.105 96	+0.970 2	− .722	+ .48
0.2	+0.960 789	−1.040 48	+0.883 9	− .637	+ .40
0.3	+0.913 931	−0.937 03	+0.749 4	− .505	+ .30
0.4	+0.852 144	−0.803 46	+0.579 5	− .342	+ .17
0.5	+0.778 801	−0.649 45	+0.389 4	− .165	+ .03
0.6	+0.697 676	−0.485 52	+0.195 3	+ .007	− .09
0.7	+0.612 626	−0.321 92	+0.012 3	+ .159	− .20
0.8	+0.527 292	−0.167 72	−0.147 6	+ .280	− .27
0.9	+0.444 858	−0.030 12	−0.275 8	+ .362	− .30
1.0	+0.367 879	+0.085 94	−0.367 9	+ .405	− .31
1.1	+0.298 197	+0.177 89	−0.423 4	+ .411	− .28
1.2	+0.236 928	+0.245 37	−0.445 4	+ .386	− .24
1.3	+0.184 520	+0.289 81	−0.439 2	+ .339	− .18
1.4	+0.140 858	+0.313 94	−0.411 3	+ .280	− .12
1.5	+0.105 399	+0.321 30	−0.368 9	+ .215	− .07
1.6	+0.077 305	+0.315 73	−0.318 5	+ .153	− .02
1.7	+0.055 576	+0.300 94	−0.265 7	+ .097	+ .02
1.8	+0.039 164	+0.280 27	−0.214 6	+ .051	+ .04
1.9	+0.027 052	+0.256 48	−0.168 3	+ .015	+ .05
2.0	+0.018 3156	+0.231 726	−0.128 21	− .010 1	+ .058
2.1	+0.012 1552	+0.207 528	−0.095 05	− .026 5	+ .056
2.2	+0.007 9071	+0.184 882	−0.068 63	− .035 5	+ .051
2.3	+0.005 0418	+0.164 341	−0.048 30	− .039 1	+ .043
2.4	+0.003 1511	+0.146 128	−0.033 15	− .038 9	+ .035
2.5	+0.001 9305	+0.130 236	−0.022 20	− .036 3	+ .027
2.6	+0.001 1592	+0.116 515	−0.014 51	− .032 5	+ .020
2.7	+0.000 6823	+0.104 739	−0.009 27	− .028 2	+ .015
2.8	+0.000 3937	+0.094 653	−0.005 78	− .023 9	+ .010
2.9	+0.000 2226	+0.086 005	−0.003 52	− .020 1	+ .007
3.0	+0.000 1234	+0.078 565	−0.002 10	− .016 7	+ .005
3.1	+0.000 0671	+0.072 129	−0.001 22	− .013 8	+ .003
3.2	+0.000 0357	+0.066 526	−0.000 70	− .011 5	+ .002
3.3	+0.000 0186	+0.061 615	−0.000 39	− .009 6	+ .001
3.4	+0.000 0095	+0.057 281	−0.000 21	− .008 0	+ .001
3.5	+0.000 0048	+0.053 430	−0.000 11	− .006 8	.000
3.6	+0.000 0024	+0.049 988	−0.000 06	− .005 8	.000
3.7	+0.000 0011	+0.046 894	−0.000 03	− .005 0	.000
3.8	+0.000 0005	+0.044 098	−0.000 01	− .004 3	.000
3.9	+0.000 0002	+0.041 561	−0.000 01	− .003 7	.000
4.0	+0.000 0001	+0.039 250	0.000 00	−0.003 3	0.000

u	$H_1(u)$	$H_3(u)$	u	$H_1(u)$	$H_3(u)$
4.0	+0.039 250	−0.003 29	8.0	+0.009 0306	−0.000 15
4.2	+ .035 195	− .002 57	8.2	+ .008 5852	− .000 13
4.4	+ .031 762	− .002 05	8.4	+ .008 1722	− .000 12
4.6	+ .028 824	− .001 66	8.6	+ .007 7885	− .000 11
4.8	+ .026 288	− .001 37	8.8	+ .007 4314	− .000 10
5.0	+ .024 081	− .001 13	9.0	+ .007 0985	− .000 09
5.2	+ .022 146	− .000 95	9.2	+ .006 7875	− .000 08
5.4	+ .020 441	− .000 80	9.4	+ .006 4967	− .000 08
5.6	+ .018 929	− .000 68	9.6	+ .006 2243	− .000 07
5.8	+ .017 582	− .000 59	9.8	+ .005 9688	− .000 07
6.0	+ .016 375	− .000 51	10.0	+ .005 7287	− .000 06
6.2	+ .015 291	− .000 44	10.2	+ .005 5030	− .000 06
6.4	+ .014 312	− .000 38	10.4	+ .005 2903	− .000 05
6.6	+ .013 426	− .000 34	10.6	+ .005 0898	− .000 05
6.8	+ .012 620	− .000 30	10.8	+ .004 9006	− .000 04
7.0	+ .011 8860	− .000 26	11.0	+ .004 7217	− .000 04
7.2	+ .011 2145	− .000 23	11.2	+ .004 5526	− .000 04
7.4	+ .010 5990	− .000 21	11.4	+ .004 3924	− .000 03
7.6	+ .010 0332	− .000 19	11.6	+ .004 2405	− .000 03
7.8	+ .009 5119	− .000 17	11.8	+ .004 0964	− .000 03
8.0	+0.009 0306	−0.000 15	12.0	+0.003 9595	−0.000 03

* Courtesy, D. L. Harris, *Astrophysical Journal* (University of Chicago Press), **108**, 114, 1948.

while in wave length units the classical damping constant yields

$$\delta_c'(\lambda) = \frac{\gamma_c(\lambda)}{4\pi} = \frac{c}{\nu_0^2}\frac{\gamma_c}{4\pi} = \frac{2\pi e^2}{3mc^2} = 0.000059\text{A} \tag{42}$$

which is a constant independent of wave length. For λ3933,

$$\delta'(\lambda) = 1.19\delta_c(\lambda) = \Delta\lambda_R = 7.02 \times 10^{-5} \tag{43}$$

Then

$$a = \frac{\delta'}{\Delta\nu_0} = \frac{\Delta\lambda_R}{\Delta\lambda_0} = \frac{0.702 \times 10^{-4}}{0.0202} = 0.0035 \tag{44}$$

We may now compute α_ν/α_0 with the aid of Table 1. For example, the value of α_ν/α_0 for $u = 0.4$ is

$$\alpha_\nu/\alpha_0 = 0.85214 - 0.0035 \times 0.80346 + (0.0035)^2 \times 0.5795 = 0.84934 \tag{45}$$

From eqn. (33) with $g_n = 4$, $g_{n'} = 2$, $A_{nn'} = 1.72 \times 10^8$, we compute

$$\begin{aligned}\alpha_0 &= \frac{4}{2} \times 1.72 \times 10^8 \frac{(3.933 \times 10^{-5})^2}{8 \times \pi^{3/2}} \times \frac{1}{0.392 \times 10^{10}} \\ &= 3.05 \times 10^{-12}\end{aligned} \tag{46}$$

Now consider the case in which both radiation and collision damping have to be taken into account. From eqns. (20) and (36) we find with $\log P_g = 4.86$, and $A_{nn'} = 1.72 \times 10^8$ that,

$$\delta' = 0.137 \times 10^8 + 0.99 \times 10^8 = 1.127 \times 10^8 \tag{47}$$

and

$$a = \frac{\delta'}{\Delta\nu_0} = \frac{1.127 \times 10^8}{0.392 \times 10^{10}} = 0.0287 \tag{48}$$

for the combined effects of natural damping and collisional broadening. The resultant values are given in Fig. 5. Notice how radiation damping plus collision damping gives a much larger absorption coefficient at great distances from the line center than does radiation damping alone. Near the line center, Doppler broadening alone determines the absorption coefficient. At distances much larger than $\Delta\lambda_0$, the Doppler contribution is small; there collision and radiation damping fix α_ν/α_0.

To summarize: the Doppler motions of the atoms determine the shape of the absorption coefficient near the line center, whereas radiation and collision damping fix the absorptivity at greater distances from the line center. In the sun and similar stars, collisions primarily determine Γ, so that an accurate knowledge of the collision damping parameter ρ and the gas pressure P_g is needed for the precise specification of α_ν throughout the layers that play a role in the production of absorption lines.

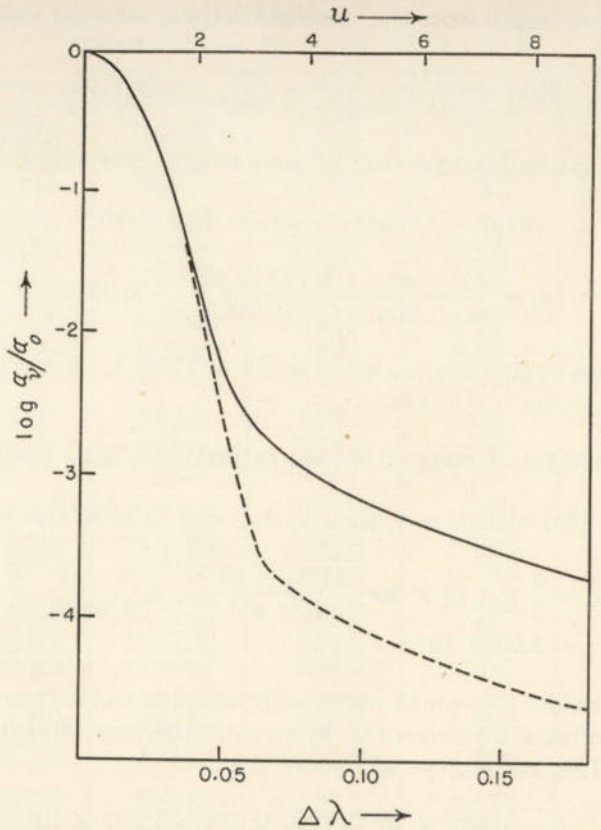

FIG. 5.—THE LINE ABSORPTION COEFFICIENT FOR CA II λ3933

We plot $\log \alpha_\nu/\alpha_0$ against u and $\Delta\lambda$ as abscissa for $T = 5700°K$. The solid curve applies to combined radiation and collisional broadening at a gas pressure of 7.2×10^4 dynes; the dotted curve applies for radiation damping alone.

5. The Formation of Absorption Lines

The interpretation of the absorption line spectra of the stars requires the answers to two questions. In what layers are the absorption lines formed and what are the physical mechanisms involved? Let us consider these questions in turn:

The same strata that provide the continuous absorption also contribute to the formation of the Fraunhofer lines. The ratio of line to continuous absorption, l_λ/k_λ, will differ for different elements. For neutral metals such as Ca I and Na I in the sun, this ratio will diminish with optical depth because of increased ionization with increased temperature. The approximation is sometimes made by regarding such lines as formed in a "reversing layer" which overlies a photosphere that produces a pure

continuous spectrum. This schematic model in which the upper layer produces line absorption or scattering only, whereas all the continuous radiation comes from the photosphere below, is called the Schuster-Schwarzschild model. It is the one we have in mind when we speak of the "number of atoms above the photosphere," i.e., the number of atoms required in the hypothetical reversing layer to produce lines of the same intensities as those observed in real stars. In the Milne-Eddington atmospheric model, on the other hand, l_λ/k_λ is constant with optical depth, i.e., all strata are equally effective in producing line and continuous absorption. This approximation is reasonably good for ionized metals, Ca II, Fe II, etc., for which second ionization is not important in the relevant layers.

The true situation for any line lies between the two extremes. The "reversing layer" and photosphere merge gradually into one another, and the factor that distinguishes the latter is the gradual increase in the opacity.

We may regard the physical processes of line formation from two extreme points of view. One might, for example, suppose that a unique temperature completely determines the emission and absorption processes in a given volume element, i.e., Kirchhoff's law holds. This condition is called local thermodynamic equilibrium (*LTE*) and is sometimes referred to as absorption. From this point of view, the radiation from the center of a strong line, therefore, will correspond to the temperature of the uppermost stratum since l_λ at this wave length is large and radiation reaches us only from the surface. In the nearby continuum, the bulk of the radiation comes from hotter, deeper layers. Toward the limb of the sun, the emergent radiation arises only from the uppermost layers both in the continuum and in the lines, and the latter should disappear.

In the other extreme, the atoms are not in temperature equilibrium with the radiation field at all, but simply scatter quanta reaching them from (mostly) greater depths. Thus a particular light quantum may be absorbed and re-emitted many times on its way through the atmosphere, and since it may be thrown either forward, sideways, or backward, its chance of reaching the surface is small. A line formed according to the mechanism of scattering* will have a black center unless it is weak.

Most Fraunhofer lines are neither black at the center nor invisible at the limb. Some lines, e.g., the resonance line λ4227 of Ca I, have low central intensities, about 3 to 5 per cent, whereas the infrared subordinate lines of O I are observed to fade out as the limb is approached. There

* Milne labeled this process monochromatic radiative equilibrium (*MRE*). We prefer to call it simply scattering.

seems to be a tendency for resonance lines to favor the scattering mechanism and high level subordinate lines to lean towards the *LTE* mechanism.

Scattering requires that the absorption of a quantum be followed by the re-emission of the same quantum. The absorption of a strong resonance line, e.g., λ5896 Na I or λ4227 Ca I, is likely to be followed by the re-emission of the same quantum. Sometimes, however, an atom may be immediately ionized from the higher level and a resonance quantum disappears. Conversely, an ion may recapture an electron in the upper level and cascade downward with the rebirth of a resonance quantum.

The emission and absorption of subordinate quanta will not follow the scattering mechanism since upper levels are populated to a large extent by transitions from the ground level, by cascade from higher levels and by recombination. For example, the $(n = 2) - (n = 6)$ absorption transition in hydrogen (Hδ) is not likely to be followed by the inverse. Whenever the re-emission of the particular quantum absorbed is improbable, scattering is unimportant and the *LTE* mechanism prevails.

In the hydrogen spectrum, for example, Lyman α tends to follow the scattering mechanism, whereas the Balmer lines, and more particularly the Paschen and Brackett lines, will follow the *LTE* scheme.

6. The Equation of Transfer for Line Radiation

The theoretical study of absorption line formation was initiated by Schuster and Schwarzschild many years ago and has been developed in more recent times by Milne, Eddington, Unsöld, Pannekoek, Minnaert, Strömgren, Chandrasekhar, and others. A simple model atmosphere, stratified in plane parallel layers, and subject to no large scale or turbulent motions is postulated. Usually the formation of a given line is treated as though one can ignore all the other lines in the spectrum.

The attack on the problem consists of two phases: (1) the determination of the appropriate absorption and emission coefficients for the line and continuum from the data of atomic physics, and (2) the study of the outward flow of radiation through the atmosphere of a star of assumed chemical composition, surface gravity, and temperature.

The line intensity calculation can attain any level of complexity depending on the assumed initial conditions. First we need a standard solution for the formation of a line under simplified self-consistent conditions. This standard solution can serve then as a basis for more elaborate treatments, wherein the deviations from our idealized model are taken into account.

We follow Eddington in setting up the fundamental equation. Let $\bar{k}$ denote the mean absorption coefficient so that $\bar{\tau} = \int \bar{k}\rho\, dx$. Let k denote the coefficient of continuous absorption in the neighborhood of a line and l the coefficient of line absorption. Both k and l depend on the frequency or wave length; l varies sharply across a line; k varies so slowly that it may be taken as constant in the neighborhood of the line.

To derive the equation of transfer, we again fix our attention on events transpiring in an elementary cylinder of unit area and length ds placed at a depth x below the surface (see Fig. 2 of Ch. 7). In the distance ds, $I(\theta)$ suffers a loss from both continuous and line absorption, viz.,

$$dI(\theta) = -kI(\theta)\rho\, ds - lI(\theta)\rho\, ds \tag{49}$$

If the line radiation is simply re-emitted in the same frequency, simple scattering obtains. Often, however, while the atom lingers in the excited level, it may collide with a passing electron which carries away the excess energy in a superelastic collision (collision of the second kind). The atom may become ionized from the upper state, or further excited, or it may cascade to a lower level other than the initial one. We shall suppose that of the quanta initially absorbed, the portion $(1 - \varepsilon)$ is re-emitted. The total number of ν-quanta absorbed in the cylinder is

$$l\rho\, ds \int I(\theta)\, d\omega$$

of which the fraction re-emitted in $d\omega$ will be

$$(1 - \varepsilon) l \frac{d\omega}{4\pi} \rho\, ds \int I(\theta)\, d\omega = (1 - \varepsilon) lJ\rho\, ds\, d\omega \tag{50}$$

where J is given by eqn. (2) of Chapter 5.

We must now take into account the fact that additional line emission is provided by inelastic collisions, by electron recaptures on the higher levels, and by cascading. In practice, the rate of these processes will depend on the local temperature T. The amount of energy emitted will be $\varepsilon l B(T)\rho\, ds$, where $B(T)$ is the Planckian function. If we set $ds = -\sec\theta\, dx$, and add up the gains and losses in our elementary cylinder, we obtain Eddington's transfer equation:*

$$\cos\theta \frac{dI}{\rho\, dx} = (k + l)I - kB(T) - (1 - \varepsilon)lJ - \varepsilon l B(T) \tag{51}$$

* An alternative form of this equation is often useful. We think of the absorption occurring in the line as being compounded of two processes; a straight scattering of the radiation, and a thermal absorption at the local temperature $T(x)$, followed by emission at the same temperature. We define a scattering coefficient

$$s = (1 - \epsilon)l$$

and a line absorption coefficient, $a = \varepsilon l$, which refers to the thermal processes. Thus, $l = a + s$, and

$$\cos\theta \frac{dI}{\rho\, dx} = (k + s + a)I - sJ - (k + a)B \tag{51a}$$

The optical depth in the line is defined by

$$dt = (k + l)\rho\, dx \tag{52}$$

The ratio of line to continuous absorption is

$$\eta = \frac{l}{k} \tag{53}$$

If we introduce

$$L = \frac{1 + \varepsilon\eta}{1 + \eta} \tag{54}$$

eqn. (51) becomes

$$\cos\theta \frac{dI}{dt} = I - LB(T) - (1 - L)J \tag{55}$$

The source function [compare eqn. (50) of Ch. 7] will be

$$\mathcal{J} = LB(T) + (1 - L)J \tag{56}$$

We can grasp the physical significance of the source function perhaps a little more clearly with the aid of the following considerations. Consider our elementary radiating volume at an optical depth t in the line. The thermal emissivity in the continuum per unit solid angle is $\frac{1}{4\pi} j\rho\, ds = B \sec\theta\, d\tau$, the light scattered by the volume is $(1 - \varepsilon)Jl\rho\, ds = (1 - \varepsilon)\eta J \sec\theta\, d\tau$, and the thermal emission in the line is $\varepsilon B\eta \sec\theta\, d\tau$. Since $dt = (1 + \eta)\, d\tau$, the total emission of the volume element is

$$[LB + (1 - L)J]\, dt \sec\theta = \mathcal{J} \sec\theta\, dt \tag{57}$$

The contribution from this volume element is dimmed by absorption in the upper strata, the extinction factor being $\exp(-t \sec\theta)$. The intensity in the line therefore is the integral over all radiating elements, viz.,

$$I(0, \theta) = \int_0^\infty \mathcal{J}(t) e^{-t \sec\theta} \sec\theta\, dt \tag{58}$$

By the method employed in the derivation of eqn. (59) of Chapter 7, we find an expression for the mean intensity J to which a volume element at t is exposed because of the emission of the surrounding strata. We obtain

$$J = \tfrac{1}{2} \int_0^\infty \mathcal{J}(t') E_1(|t' - t|)\, dt' \tag{59}$$

and

$$\mathcal{J} = LB + \tfrac{1}{2}(1 - L) \int_0^\infty E_1(|t' - t|) \mathcal{J}(t')\, dt' \tag{60}$$

The flux πF at t will be computed with the aid of [cf. eqn. (60) of Ch. 7]

$$F = 2 \int_t^\infty \mathcal{J}(t') E_2(t' - t)\, dt' - 2 \int_0^t \mathcal{J}(t') E_2(t - t')\, dt' \tag{61}$$

where E_1 and E_2 have been defined by eqn. (9) of Chapter 7.

Notice that eqn. (60) is an integral equation of the form

$$f(x) = g(x) + \int h(x - y) f(y)\, dy \tag{62}$$

where g and h are known functions, and f is to be determined. In general, g and h will be given in tabular form and the equation must be solved by an iteration method.

The solution of eqn. (55) may be found if we know the dependence of L and B upon t, the optical depth at the particular point in the line. Both L and J depend strongly on $(\lambda - \lambda_0)$, the distance from the line center.

7. Solution of the Transfer Equation for a Constant Ratio of Line to Continuous Absorption

Although numerical methods must be employed to solve eqn. (55) if $L(t)$ is arbitrary, an exact solution may be found if L is constant with optical depth. For some purposes, however, it suffices to use a Schuster-Schwarzschild type of approximation with modifications proposed by Chandrasekhar.

Analogous to eqn. (108) of Chapter 7 we now have:

$$\frac{1}{\sqrt{3}} \frac{dI}{\rho\, dx} = (k + l)I - (k + \varepsilon l)B - (1 - \varepsilon) l \frac{1}{2}(I + I') \tag{63}$$

$$-\frac{1}{\sqrt{3}} \frac{dI'}{\rho\, dx} = (k + l)I' - (k + \varepsilon l)B - (1 - \varepsilon) l \frac{1}{2}(I + I') \tag{64}$$

Here I, I', B, k, and l all depend on the wave length. The flux πF and mean intensity J are defined with the aid of

$$F = 2 \sum I \mu_j a_j = \frac{2}{\sqrt{3}} (I - I') \tag{65}$$

and

$$J = \tfrac{1}{2}(I + I') \tag{66}$$

respectively, since $n = 1$ [cf. eqn. (106) of Ch. 7].

These equations must be solved subject to the boundary condition that J does not increase exponentially with t, and that

$$I' = 0 \text{ when } t = 0 \tag{67}$$

since there is no inward flux on the outer boundary. Also we shall suppose

$$B = a + b\bar{\tau} \tag{68}$$

or

$$B = B_0 + \left(\frac{dB}{dt}\right)_0 t = a + pt \tag{69}$$

where $\bar{\tau}$ is the optical depth defined in terms of the mean absorption coefficient $\bar{k}$ (cf. Sec. 12 of Ch. 7). The subscript "0" indicates that the quantity is computed for $\tau = 0$. Let τ denote the optical depth in the continuous spectrum at the spectral region in question. Then

$$d\tau = \frac{k}{\bar{k}}\, d\bar{\tau} \tag{70}$$

Here $d\tau$ is the $d\tau_\nu$ defined by eqn. (7) of Chapter 7. Let

$$M = \frac{1}{1+\eta} \tag{71}$$

and

$$n = \frac{k}{\bar{k}} \tag{72}$$

Then from eqn. (52) and from the definition of $d\tau$,

$$dt = \frac{k+l}{k}\, d\tau = \frac{n}{M}\, d\bar{\tau} \tag{73}$$

Hence,

$$p = \frac{M}{n}\, b \tag{74}$$

Following the notation of Problem 3 of Chapter 7, let us write,

$$\frac{b}{a} = \frac{3}{8}\, x_0 \tag{75}$$

where with $u = h\nu/kT_0$

$$x_0 = u(1 - e^{-u})^{-1} \tag{76}$$

Subtract eqn. (64) from eqn. (63) to obtain

$$\frac{1}{\sqrt{3}}\, \frac{d(I + I')}{dt} = (I - I') \tag{77}$$

If we add eqns. (63) and (64) and employ eqns. (52), (54), (77), and (66), we find

$$\frac{d^2J}{dt^2} = 3L(J - B) \tag{78}$$

Now employ eqns. (67), (65), and (66) to obtain

$$F_0 = \frac{4}{\sqrt{3}}\, J_0 \tag{79}$$

for $t = 0$. Similarly from eqns. (77) and (66) we find at $t = 0$

$$\frac{1}{\sqrt{3}} \left(\frac{dJ}{dt}\right)_0 = J_0 \tag{80}$$

Now let

$$y = J - B \tag{81}$$

Then from eqn. (78) and the condition imposed on B by eqn. (69), we find

$$\frac{d^2y}{dt^2} = 3Ly \tag{82}$$

or

$$y = y_0 e^{-\sqrt{3L}t} \tag{83}$$

From eqns. (69), (80), (81), and (83) there results

$$\frac{1}{\sqrt{3}} \left(\frac{dy}{dt}\right)_0 = -\sqrt{L}y_0 = a - \frac{1}{\sqrt{3}}\, p + y_0 \tag{84}$$

Solving for y_0, and employing eqns. (81) and (69) we find

$$J = a + pt - \frac{\left(a - \frac{1}{\sqrt{3}}\, p\right)}{1 + \sqrt{L}}\, e^{-\sqrt{3L}t} \tag{85}$$

Using eqn. (79), the emergent flux is computed from

$$F = \frac{\frac{4}{3}a\sqrt{3L} + \frac{4}{3}p}{1 + \sqrt{L}} \tag{86}$$

In the continuum, $L = M = 1$, so that the residual intensity in the line is

$$r = \frac{F}{F_0} = \frac{2}{\frac{4}{\sqrt{3}} + \frac{1}{2}\frac{x_0}{n}}\, \frac{\frac{4}{3}\sqrt{3L} + \frac{1}{2}\frac{x_0}{n}M}{1 + \sqrt{L}} \tag{87}$$

which is the solution of the problem. For an adopted mean temperature and electron pressure we calculate first k and $\bar{k}$. Then we find l, η, and L as functions of $(\lambda - \lambda_0)$ if ε is known. Finally with the aid of eqn. (87) it is possible to compute r for selected values of $(\lambda - \lambda_0)$ and draw the profile.

TABLE 2

THE FIRST AND SECOND MOMENTS OF CHANDRASEKHAR'S $H(\mu)$ FUNCTION*

L	α_1	α_2
1.0	0.500000	0.333333
0.9	0.515609	0.344357
0.8	0.533154	0.356787
0.7	0.553123	0.370985
0.6	0.576210	0.387466
0.5	0.603495	0.407030
0.4	0.636636	0.430922
0.3	0.678674	0.461423
0.2	0.735808	0.503218
0.1	0.825318	0.569449
0.075	0.858734	0.594404
0.050	0.901864	0.626785
0.025	0.964471	0.674134
0.00	1.154701	0.820352

* Courtesy S. Chandrasekhar, *Astrophysical Journal* (University of Chicago Press) **106**, 151, 1947, Table 1.

Chandrasekhar has given an exact solution of the transfer equation for L = constant, in terms of his H functions and their first and second moments.† In place of eqn. (87), the expression for the residual intensity for pure scattering becomes

$$r(\lambda) = \frac{L^{3/2}}{\frac{1}{3} + \frac{4}{3}\frac{n}{x_0}}\left[\alpha_2 + \frac{8}{3}\frac{n}{Lx_0}\alpha_1 + \frac{1-L}{2\sqrt{L}}\alpha_1^2\right] \tag{88}$$

where α_1 and α_2 are respectively the first and second moments of the H functions (see Table 2). For the center-limb variations, Chandrasekhar gives the following expression for the residual intensity:

$$r(\mu) = \frac{L^{3/2}}{\mu + \frac{8n}{3x_0}} H(\mu)\left[\mu + \frac{8n}{3Lx_0} + \frac{1-L}{2\sqrt{L}}\alpha_1\right] \tag{89}$$

where $\mu = \cos\theta$.

8. Solution of the Transfer Equation for η Variable with Optical Depth

(a) *Method Based on Choice of a Mean Value of $\bar{L}$ and $\sqrt{\bar{L}}$*

We might expect the assumption η = constant to hold for such a line as λ3933 of Ca II where both l and k increase with increasing optical depth. Actual calculation (Sec. 9) shows that even for this line, η varies with τ. If the variations in η are not too large, Strömgren showed that one can employ eqn. (87) with a $\sqrt{\bar{L}}$ and $\bar{M}$ defined by

$$\sqrt{\bar{L}} = \int_0^\infty \sqrt{L}e^{-2z}\,2\,dz \tag{90}$$

and

$$\bar{M} = \int_0^\infty Me^{-z}\,dz \tag{91}$$

where

$$z = \left(\frac{3}{L_0}\right)^{1/2}\tau \tag{92}$$

The best procedure is to choose $\sqrt{\bar{L}} = \sqrt{L_0}$ by a process of iteration as illustrated in Sec. 9. We may employ eqns. (88) and (89) with the following substitutions:

$$L^{3/2} \to \bar{L}\sqrt{\bar{L}};\quad (1-L) \to (1-(\sqrt{\bar{L}})^2);\quad \frac{8n}{3Lx_0} \to \frac{8n}{3\bar{L}x_0} \tag{93}$$

Given $\eta(t)$, one computes $\bar{L}$ or $\sqrt{\bar{L}}$ for several points in the line profile by eqns. (90) and (91), and then obtains $r(\lambda)$ from eqn. (88) with the replacements as noted in eqn. (93). The center-limb variations follow from eqns. (89) and (93). In the calculation of the center-limb variations we note that $\bar{L}$ and $\sqrt{\bar{L}}$ will vary with μ. Toward the limb, radiation is emitted from successively higher layers. Hence in eqn. (92), τ must be replaced by τ/μ.

The computed profile is sensitive to the choice of L_0. Also the method requires that the variations of η with optical depth be small. The method fails for the hydrogen lines in the sun.

One difficulty is that the formulae (87), (88), and (89) rest on the assumption that B varies linearly with the optical depth, eqn. (68). There are three possibilities for fixing the ratio b/a:

(1) One can determine it from the variation of the Planck function with optical depth, using either the first derivative computed for some representative optical depth or the empirical value from the plot of B against τ;
(2) One may estimate it from the computed law of darkening for the continuum; or
(3) One may guess it from the observed law of darkening for the continuum.

In his discussion of the sodium "D" lines, D. Harris found that the constants in eqn. (88) had no relation to the constants in the limb-darkening law, as theory required that they should. Actually, a second-degree

† See *Radiative Transfer*, p. 321 et seq., especially his eqns. (71) and (70). $H(\mu)$ is tabulated on page 125.

polynomial in $\mu = \cos\theta$ is required to fit the observations. If the ratio b/a was computed from the theoretical and observed law of limb darkening respectively, a considerable discrepancy resulted.

(*b*) *Method of Direct Numerical Integration*

A number of years ago Pannekoek suggested a method of direct integration of the transfer equation based on the Eddington approximation. We divide eqn. (51a) by k, substitute $d\tau = +k\rho\, dx$, multiply by $\frac{d\omega}{4\pi}$, integrate over all solid angles, and use the Eddington J, H, and K with the understanding that these quantities here depend on the wave length [eqn. (67) of Ch. 7]. We obtain:

$$\frac{dH}{d\tau} = \left(1 + \frac{a}{k}\right)(J - B) \tag{94}$$

If we multiply eqn. (51a) by $\cos\theta \frac{d\omega}{4\pi}$ and integrate we find

$$\frac{dK}{d\tau} = \left(1 + \frac{a+s}{k}\right)H \tag{95}$$

In the Eddington approximation we assume

$$K = \tfrac{1}{3}J \tag{96}$$

Hence,

$$\frac{dJ}{d\tau} = 3\left(1 + \frac{a+s}{k}\right)H \tag{97}$$

Here k denotes the coefficient of continuous absorption in the neighborhood of the line. Also,

$$a = \varepsilon l \tag{98}$$

is the coefficient of line absorption as distinct from the coefficient of line scattering

$$s = (1 - \varepsilon)l \tag{99}$$

Let us express J, H, and B in units of B_0 (the Planck function evaluated for the boundary temperature). Denote the corresponding quantities by primes. Then eqns. (94) and (97) are replaced by the expressions:

$$\Delta J' = 3(1 + \eta)H'\,\Delta\tau \tag{100}$$

$$\Delta H' = (J' - B')\,\Delta\tau \tag{101}$$

for lines formed according to the mechanism of pure scattering. To start the integrations we adopt an arbitrary J_0' at the surface of the star. The boundary condition

$$H_0' = \tfrac{1}{2}J_0' \tag{102}$$

or

$$H_0' = \frac{1}{\sqrt{3}}J_0' \tag{103}$$

(depending on whether we use the Eddington or exact condition) will fix H_0'. We then compute the increments $\Delta J'$ and $\Delta H'$ from eqns. (100) and (101) for a small step $\Delta\tau$, find new values of H' and J', and continue the process. If J_0' has been chosen correctly, J' will approach B' deeper in the atmosphere. Usually J will deviate sharply from B and new J_0' values will have to be tried until a solution is found. The corresponding H_0' will be the correct flux in the line. Finally,

$$r(\lambda) = \frac{H_0'}{H_{0c}'} \tag{104}$$

where H_{0c}', the flux in the continuum, is obtained from the solution of eqns. (100) and (101) with $\eta = 0$. The method has the advantage that variations of B, ε, and η with τ may be taken into account exactly and is readily adapted to punch-card and other modern computational techniques.

(*c*) *Solution of the Radiative Integral Equation by Iteration*

Instead of integrating the differential equation of radiative transfer directly, one may attack the corresponding integral equation (60). We follow a procedure suggested by Strömgren. Let

$$Y = J - B \tag{105}$$

Then from eqns. (56) and (59) we obtain

$$Y = -B + \overline{B} + \tfrac{1}{2}\int_0^\infty E_1(|t' - t|)(1 - L)Y\, dt' \tag{106}$$

where

$$\overline{B} = \tfrac{1}{2}\int_0^\infty BE_1(|t' - t|)\, dt' \tag{107}$$

Here B, $\overline{B}$, Y, J, L, and t all depend on the wave length. Suppose that $Y(t)$ can be expressed as a series of terms of the form

$$Y(t) = Y^0 + \Delta^1 Y + \Delta^2 Y + \cdots + \Delta^n Y \tag{108}$$

where

$$Y^0 = -B + \overline{B} \tag{109}$$

and

$$\Delta^n Y = \tfrac{1}{2}\int_0^\infty E_1(|t' - t|)(1 - L)\,\Delta^{n-1}Y\, dt' = \overline{(1 - L)\,\Delta^{n-1}Y} \tag{110}$$

The solution may be obtained as follows: First prepare a table of $B(t)$ and compute Y^0. Substitute Y^0 in the second integral of eqn. (106) to obtain $\Delta^1 Y$. Next calculate $(1 - L)\,\Delta^1 Y$, evaluate $\Delta^2 Y$, and continue

the process until successive terms become negligible. Once Y is found, the source function may be calculated with the aid of eqn. (56) and the intensity of the emergent ray found from eqn. (58). The intensity in the continuum follows from eqn. (58) with $L = 1$. The evaluation of the integrals (107) and (110) is facilitated by approximation formulae of the type of eqns. (61) and (64) of Chapter 7. In eqn. (65) of Chapter 7 B is replaced by the source function (56). The smaller the value of L, the slower the convergence of the series, eqn. (108).

This method may be employed to treat the flow of continuous radiation in an atmosphere in which both thermal absorption and electron scattering occur [cf. eqn. (56) and Sec. 16 of Ch. 7].

Finally, for the outer wings of a line, M. Minnaert and also A. Unsöld have given important methods based on the idea of a weighting function (Sec. 10).

The precise calculation of a line profile involves the following steps:

(1) Calculate a model atmosphere for an assumed hydrogen/metal ratio and known dependence of temperature on optical depth in the integrated radiation $\bar{\tau}$. Thus one finds the gas pressure, the electron pressure, and the absorption coefficient as functions of $\bar{\tau}$.

(2) The theory of the continuous absorption coefficient gives k_λ and $\bar{k}$ from which we find the relation between $\bar{\tau}$ and τ, the optical depth at the wave length in question.

(3) From the ionization and Boltzmann equations, calculate the fraction of all atoms of a given element capable of absorbing the line in question, N_r/N_{total}. The electron pressure and temperature are known as a function of τ.

(4) Calculate the fictitious absorption coefficient at the center of the line, α_0, from eqn. (33). For an adopted abundance of the element in question compute $N_r\alpha_0$, where N_r is the number of atoms per gram of stellar material capable of absorbing the line.

(5) With the aid of the gas pressure, temperature, and the damping parameter ρ_0 [see e.g., eqn. (17)] calculate a [eqn. (31)] and $\Delta\lambda_0$ [cf. eqn. (39)] as a function of optical depth.

(6) From eqn. (37), with a and $u = \dfrac{\lambda - \lambda_0}{\Delta\lambda_0}$ as parameters, compute α_λ/α_0 at selected optical depths and values of $\lambda - \lambda_0$.

(7) Derive the line absorption coefficient, $l_\lambda = N_r\alpha_0\left(\dfrac{\alpha_\lambda}{\alpha_0}\right)$, and form $\eta = \dfrac{l}{\bar{k}}$,

(8) If the variation of η with optical depth is small, one may employ the method (a); whereas if η varies over a large range in the relevant atmospheric layers (e.g., H in the sun) (a) cannot be used, and we may employ (b) or (c), or the method of weighting functions (Sec. 10).

9. The Profile of the *K*-Line in the Solar Spectrum

To illustrate some of the preceding formulae and methods we shall compute the profile of the Ca II λ3933 (K) line.

First, let us assume we can take η constant throughout the relevant layers of the solar atmosphere and calculate $r(\lambda)$ by eqns. (87) and (88). We assume $T = 5700°\text{K}$, $\log P_g = 4.86$ ($\bar{\tau} = 0.6$). From eqn. (47) we had $\delta' = 1.127 \times 10^8$, whereas δ_c' in frequency units is 1.145×10^7. Also $f = \frac{2}{3} \times 1.19 = 0.793$. For distances from the line center greater than 0.2A, we may use the results of Problem 1, noting that $\delta'/\delta_c = \Gamma/\gamma_c = 9.8$, to obtain

$$\alpha_\lambda = 19.8 \times 10^{-18}\,(\Delta\lambda)^{-2} \tag{111}$$

where $\Delta\lambda$ is expressed in angstrom units. From the model atmosphere we adopt $P_e = 21$ dynes. Furthermore, $\bar{k} = 0.65$ at $\tau = 0.6$, and $k = 0.451$ (we adopt Münch's estimate of $n = 0.70$ at λ3933). With a boundary temperature $T_0 = 4610°\text{K}$ we find $x_0 = 7.94$, and $x_0/n = 11.3$.

An application of the ionization equation shows that calcium is almost all singly ionized. This means that effectively every one of the calcium atoms in the solar atmosphere will be capable of absorbing λ3933. If N is the number of calcium atoms per gram of solar material,

$$\eta = \frac{N\alpha_\lambda}{k} = 44.0 \times 10^{-18}\frac{N}{(\Delta\lambda)^2} \tag{112}$$

If pure scattering obtains, $\varepsilon = 0$, and $L = M$ [cf. eqns. (54), (71)]. Upon the substitution of appropriate numerical values, eqn. (87) becomes:

$$r = \frac{0.58\sqrt{L} + 1.42L}{1 + \sqrt{L}} \tag{113}$$

TABLE 3

PROFILE OF λ3933 FOR $N = 1.8 \times 10^{18}$

$\Delta\lambda$	η	L	Approx. r_λ eqn. (87)	α_1	α_2	Exact r_λ eqn. (88)
0.5	316	0.0024	0.030	1.139	0.809	0.022
1.0	79.2	0.0125	0.074	1.063	0.699	0.073
2.0	19.8	0.048	0.160	0.907	0.631	0.150
4.0	4.95	0.168	0.337	0.764	0.524	0.323
6.0	2.20	0.312	0.491	0.674	0.458	0.471
8.0	1.24	0.446	0.610	0.621	0.420	0.60
10.0	0.79	0.557	0.699	0.588	0.396	0.681
15.0	0.37	0.731	0.825	0.547	0.367	0.813
20.0	0.20	0.835	0.894	0.527	0.352	0.886

Table 3, computed for $N = 1.8 \times 10^{18}$, gives $\Delta\lambda$ (distance from the line center in angstrom units), η, L, and r, calculated from eqn. (113) and the moments employed in the exact expression, eqn. (88). Fig. 6 compares three profiles calculated for 0.9×10^{18}, $1.8 \times 10^{+18}$, and 3.6×10^{18} calcium atoms per gram of solar material, with the observed profile. Apparently the abundance of calcium lies between 0.9 and 1.8×10^{18} atoms/gram and a little closer to the latter. The deviations in the far wings arise partly from uncertainties in locating the continuous spectrum and partly from our assumption that the solar atmosphere can be regarded as a layer at a uniform temperature and pressure. The departure at the line center comes from the fact we assumed $\varepsilon = 0$, i.e., pure scattering. The differences between the approximate formula, eqn. (87), and the exact formula (88) are small.

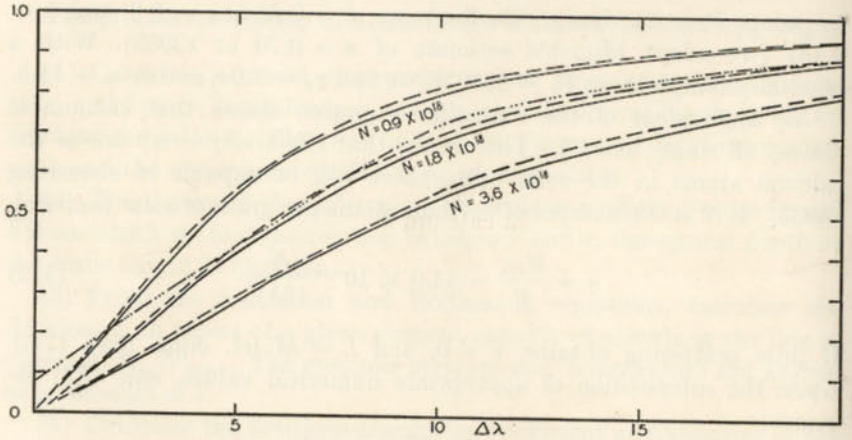

FIG. 6.—THE THEORETICAL PROFILE OF λ3933 FOR CONSTANT η (TOTAL FLUX)

The solid curves give the profiles calculated by eqn. (88), the dashed curves those calculated by eqn. (87) for $N = 0.9$, 1.8, and 3.6×10^{18} atoms/gram. The dash-dot curve is the observed total flux as derived from Houtgast's observations. Since pure scattering is assumed, agreement at the center of the line is not to be expected. Compare with Fig. 7 of Chapter 8, where the variation of η with optical depth is taken into account.

Let us now calculate the K-line profile taking into account the variation of η with optical depth. First we adopt a model atmosphere similar to that discussed in Chapter 7, and based on the chemical composition adopted in Sec. 9, Chapter 4. The model resembles those computed by Münch and Strömgren except that helium has been included. The gas pressure at corresponding optical depths is greater, since helium contributes to the mass but not to the opacity of the layers. Throughout the relevant layers $k/\bar{k}$ is very nearly constant at 0.7. Table 4 gives the

adopted variation of $\theta = \dfrac{5040}{T}$, $\log P_g$, $\log P_e$ and k with the optical depth in the integrated radiation as argument.

TABLE 4

DATA FOR CALCULATION OF PROFILE OF λ3933

τ	$\theta = \frac{5040}{T}$	Log P_g	Log P_e	k_λ	$\Delta\lambda = 1$ η
0.05	1.056	4.20	0.40	0.092	69
0.10	1.032	4.33	0.58	0.121	65
0.15	1.01	4.45	0.72	0.159	61
0.20	0.99	4.55	0.84	0.193	58
0.30	0.96	4.67	0.95	0.248	54
0.40	0.93	4.75	1.15	0.306	50.5
0.50	0.91	4.80	1.20	0.325	47.5
0.60	0.89	4.85	1.32	0.431	45
0.80	0.85	4.91	1.50	0.530	40
1.00	0.82	4.95	1.64	0.583	37
1.40	0.77	5.01	1.90	0.967	26
1.80	0.73	5.05	2.20	1.28	20.3
2.0	0.715	5.06	2.30	1.40	18.3

With the aid of eqns. (9), (20), (36), (47), and (111), we obtain

$$\alpha_\lambda = 2.41 \times 10^{-18}\left[1 + 7.22\,\frac{P_g}{P_a}\left(\frac{T_a}{T_g}\right)^{1/2}\right]\frac{1}{(\Delta\lambda)^2} \qquad (114)$$

where P_a and T_a refer to the gas pressure and temperature at an optical depth of 0.6. If there are N(Ca II) ionized calcium atoms per gram of stellar material, the line absorption coefficient will be

$$l = N(\text{Ca II})\alpha_\lambda \qquad (115)$$

Now N(Ca II) will depend on the abundance of calcium and the stage of ionization. Throughout the layers of interest, which are assumed to be in radiative equilibrium, essentially all the calcium is singly ionized. Even at an optical depth of 4.0, 92 per cent of the calcium is still singly ionized. For an element such as sodium, the variation of N(Na I)/N(Na-total) would be important. The last column* of Table 4 gives the smoothed values of

$$\eta_l = \frac{N(\text{Ca II})\alpha_\lambda}{k} \qquad (116)$$

* Near the line center ($\Delta\lambda \sim 1$A), only the uppermost layers will contribute. Hence we must include η for the interval 0.00–0.05. Similarly in the far wings η values for $\tau > 2.0$ will be needed. Lack of space prevents our inclusion of these calculations here.

for $\Delta\lambda = 1$A where α_λ is taken from eqn. (114), and N is chosen as 1.0×10^{18} calcium atoms/gram. Values for the outer part of the line are found from the relation

$$\eta\,(\Delta\lambda) = \frac{\eta_1}{(\Delta\lambda)^2} \tag{117}$$

The optical depth at any point in the line will be related to the optical depth in the nearby continuum by

$$t = \int_0^\tau (1 + \eta)\, d\tau \tag{118}$$

Since $k/\bar{k} = 0.7 =$ constant,

$$\tau = 0.7\bar{\tau} \tag{119}$$

Because of the rapid increase of gas pressure with τ, k rises more rapidly than α_λ and η declines steadily with optical depth.

To evaluate the line profile by eqns. (87), (88), and (89) we must compute $\sqrt{\bar{L}}$ and $\bar{L}$ by eqns. (90) and (91). For the computation of these integrals one often may employ the 3-term approximation formula:

$$\int_0^\infty e^{-x} f(x)\, dx \sim q_1 f(x_1) + q_2 f(x_2) + q_3 f(x_3) \tag{120}$$

where:

i	x	q
1	0.41577	0.71109
2	2.2943	0.27852
3	6.290	0.01039

Example: ($\Delta\lambda = 1$) To obtain an initial estimate of L_0, choose the value appropriate to an optical depth $t = 0.5$ in the line,

$$\overline{(1 + \eta)\tau} = 0.5 \tag{121}$$

Since η is near 72 (see Table 3), L is chosen for $\tau \sim 0.01$, which gives $L_1 = 0.0137$. See eqn. (54). Then $\sqrt{\bar{L}_1} = 0.117$. In this example,

$$x = \frac{2\sqrt{3}}{0.117}\,\tau \tag{122}$$, or

(cf. eqn. 119)

$$\bar{\tau} = 0.0483x \tag{123}$$

The calculation according to eqn. (120) proceeds as follows:

n	$\bar{\tau}$	η	L	$\sqrt{L}$	
1	0.0201	73.0	0.0135	0.116	
2	0.1108	64.0	0.0154	0.124	$\sqrt{\bar{L}} = 0.118$
3	0.304	53.8	0.0182	0.135	

A retrial with $\sqrt{L_2} = 0.118$ reproduces $\sqrt{L_3} = 0.118$. For the computation of L we have $\bar{\tau} = 0.0973x$, and $\bar{L} = 0.0150$.

In this fashion we compute $\bar{L}$ and $\sqrt{\bar{L}}$ for each point in the profile. Then we interpolate α_1 and α_2 from Table 2 with $(\sqrt{\bar{L}})^2$ as argument. Finally, eqn. (88), with the substitutions noted in eqn. (93), yields the value of $r(\lambda)$, the residual intensity in the line.

The resultant profile differs but little from that obtained with a constant η computed for $\bar{\tau} = 0.6$. In fact, the differences are comparable with those found between observational determinations of the profiles.

Instead of calculating $r(\lambda)$ by eqn. (88), we can compute $r_\lambda(\theta)$ by eqn. (89), and integrate the profile over the disk of the sun, taking into account the observed limb darkening at λ3933. The $r(\lambda)$ profile computed in this way agrees reasonably well with the profile computed directly from eqn. (88); see Table 5.

TABLE 5

THE PROFILE OF λ3933 IN INTEGRATED SUNLIGHT

$\Delta\lambda$	$\sqrt{\bar{L}}$	$\bar{L}$	α_1	α_2	r_λ eqn. (88)	r_λ eqn. (89)
1	0.118	0.0150	1.049	0.7391	0.087	0.085
3	0.353	0.140	0.7426	0.5532	0.272	0.273
6	0.618	0.429	0.6442	0.4364	0.586	0.560
9	0.771	0.645	0.5777	0.3886	0.758	0.790
12	0.755	0.767	0.5469	0.3666	0.845	0.822
15	0.898	0.838	0.5320	0.3560	0.894	0.910
18	0.926	0.883	0.5231	0.3496	0.925	

When the computed profile is compared with the observed profile (cf. Fig. 7), it is found that in order to secure a good fit, the number of atoms should be increased to about 1.37×10^{18} atoms per gram. Hence the $\Delta\lambda$'s in the first column of Table 5 should be multiplied by $\sqrt{1.37} = 1.17$. Similarly, a value of 1.55×10^{18} atoms/gram is found from the calculations by the Strömgren iteration method.

Let us now illustrate the Strömgren iteration method by calculating

the residual intensity of a point in the profile at $\Delta\lambda = 3\text{A}$ at the center of the disk. By eqn. (117),

$$\eta_3 = \tfrac{1}{5}\eta_1 \tag{124}$$

First we derive t as a function of τ by eqn. (118). The first two columns of Table 6 express this relationship. Table 4 gives $T(\bar{\tau})$. Since $\tau = 0.7\bar{\tau}$, and t is known as a function of τ, we can express the temperature, or more precisely the Planckian function $B(t)$, as a function of t.

The emergent intensity in the continuous spectrum $I(0, \theta)$ will be given by eqn. (5) of Chapter 7. The ratio, $B(\tau)/B(0)$, is known for the frequency under consideration as a function of τ. If we set $I_c(0, \theta) = 1$, we shall define $B'(0)$ by the condition.

$$1 = B'(0)\int_0^\infty \frac{B(\tau)}{B(0)}\, e^{-\tau \sec\theta} \sec\theta \, d\tau \tag{125}$$

We evaluate the integral in eqn. (125) with the aid of eqn. (120) where $\tau \sec\theta = x$. With $\sec\theta = 1$, we find $B'(0, 0) = 0.0959$. Column 3 of Table 6 gives $B(t)$ on this scale. The next step is to evaluate $\overline{B}(t)$ as defined by eqn. (107) with the aid of eqns. (61), (62), and (64) of Chapter 7. As a typical example, let us compute $\overline{B}$ for $t = 0.2$ by means of eqns. (61) and (64) of Chapter 7, and Table 7 of Chapter 7.

$t = 0.2$

Point	$t_1 = 0.051$	$t_2 = 0.169$	$t + y_1 = 0.492$	$t + y_2 = 2.707$
$B(t)$	0.100	0.109	0.135	0.363
Weight	$a_1 = 0.0851$	$a_2 = 0.1278$	$b_1 = 0.4532$	$b_2 = 0.0468$

Then the second number in the 4th column of Table 6 is

$$\overline{B}(0.2) = 0.0851 \times 0.100 + 0.1278 \times 0.109 + 0.4532 \times 0.135 + 0.0468 \times 0.363 = 0.101$$

Column 4 gives $\overline{B}$, column 5 gives $(1 - L)$ and column 6 gives $Y^0 = \overline{B} - B$. We next form the product $(1 - L)Y^0$, plot it on a graph, draw a smooth curve and compute $\Delta^1 Y$ by means of eqn. (110) with the aid of eqns. (61) and (64) of Chapter 7, and Table 7 of Chapter 7. We then form $(1 - L)\,\Delta^1 Y$, compute $\Delta^2 Y$, and repeat the process until $\Delta^n Y$ is negligible. We then compute $Y(t)$ from eqn. (108), and from eqns. (56) and (105) we get

$$\mathcal{J} = B + (1 - L)Y \tag{126}$$

Finally we calculate the intensity in the line by eqn. (58). By our choice of $B'(0)$ in eqn. (126), the intensity of the continuum $I_c(0, 0)$ at the

TABLE 6

CALCULATION OF A POINT IN A LINE PROFILE BY STRÖMGREN'S ITERATION METHOD ($\Delta\lambda = 3\text{A}$)

t_λ	τ_λ	$B_\lambda(t)$	$\bar{B}_\lambda$	$1 - L$	Y^0	$\Delta^1 Y$	$\Delta^2 Y$	$\Delta^3 Y$	$\Delta^4 Y$	$\Delta^5 Y$	$\mathcal{J}_\lambda$
0.0	0.00	0.095	0.069	0.894	−0.026	−0.0028	−0.0014	−0.0005	−0.0003	−0.0001	0.067
0.2	0.022	0.112	0.101	0.889	−0.011	−0.0040	−0.0015	−0.0006	−0.0003	−0.0002	0.096
0.4	0.045	0.127	0.123	0.883	−0.004	−0.0028	−0.0012	−0.0006	−0.0002	−0.0001	0.119
0.6	0.068	0.144	0.142	0.879	−0.002	−0.0013	−0.0006	−0.0003	−0.0001	+0.0001	0.140
0.8	0.093	0.162	0.162	0.874	0.000	−0.0002	−0.0001	+0.0001	+0.0002	+0.0001	0.162
1.0	0.119	0.179	0.181	0.870	+0.002	+0.0009	+0.0006	+0.0005	+0.0004	+0.0003	0.183
1.2	0.146	0.197	0.200	0.865	+0.003	+0.0019	+0.0014	+0.0010	+0.0007	+0.0005	0.205
1.4	0.173	0.215	0.218	0.862	+0.003	+0.0029	+0.0020	+0.0014	+0.0010	+0.0006	0.225
1.6	0.201	0.234	0.240	0.858	+0.006	+0.0037	+0.0026	+0.0017	+0.0010	+0.0007	0.248
1.8	0.230	0.256	0.262	0.854	+0.006	+0.0044	+0.0029	+0.0018	+0.0010	+0.0005	0.270
2.0	0.259	0.278	0.285	0.851	+0.007	+0.0046	+0.0029	+0.0017	+0.0007	+0.0004	0.293
—	—	—	—	—	—	—	—	—	—	—	—

center of the disk is unity, and $I_\lambda(0, 0)$ is the residual intensity in the line. By eqn. (120) we find

$$\begin{aligned} I_\lambda(0, 0) &= r_\lambda(0) \\ &= 0.711g(0.416) + 0.279g(2.29) + 0.0104g(6.29) \\ &= 0.711 \times 0.121 + 0.279 \times 0.328 + 0.0104 \times 1.131 \\ &= 0.189 \end{aligned} \tag{127}$$

We may calculate the values of the residual intensity $r_\lambda(\theta)$ for other angles with the aid of eqns. (58) and (125).

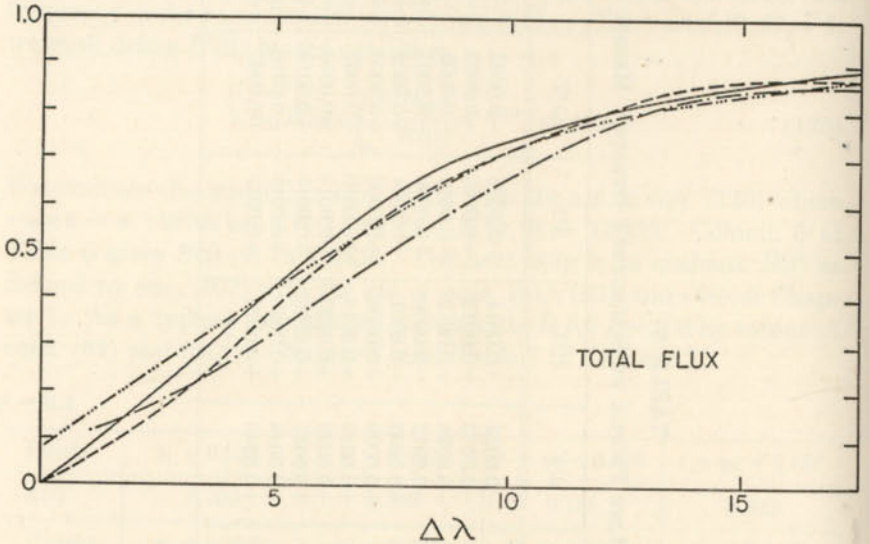

FIG. 7.—COMPARISON OF PROFILES OF λ3933 IN TOTAL FLUX COMPUTED FOR VARIABLE η BY DIFFERENT METHODS

The observational curve (dash–3 dots) is taken from the work of Houtgast. The solid curve was computed by eqn. (88) with L and $\sqrt{L}$ replaced by $\bar{L}$ and $\sqrt{\bar{L}}$ as indicated by eqn. (93). The dashed curve was obtained by Strömgren's iteration method, and the dash-dot curve is the latter corrected for noncoherent scattering.

The emergent flux, πF, can be obtained from eqn. (61) with the aid of an approximation formula [compare eqn. (65) of Ch. 7] which we may write as

$$\begin{aligned} F(0) &= 0.8839g(0.397) + 0.1161g(2.723) \\ &= 0.8839 \times 0.119 + 0.1161 \times 0.378 = 0.1491 \end{aligned} \tag{128}$$

Similarly the flux in the continuum is obtained from eqn. (65) of Chapter 7 as follows:

$$F_c(0) = 0.8839 \times 0.382 + 0.1161 \times 2.802 = 0.6630 \tag{129}$$

and the residual intensity in the line at 3A is

$$r = \frac{F(0)}{F_c(0)} = \frac{0.1491}{0.6630} = 0.225 \tag{130}$$

The iteration method converges slowly when η is large. On the other hand, a precise line profile may be calculated for an arbitrary variation of η and $B(t)$.

We find, for example, that the shape of the line is sensitive to the assumed $k/\bar{k}$ variation.

The calculated profiles for different positions on the disk are shown in Fig. 8. The iteration method indicates that the line wings tend to go into emission at the limb. This result is in contradiction with that obtained by the mean value method, and evidently with the observations as well (cf. Sec. 12). The introduction of noncoherent scattering (cf. Sec. 11) tends to remove this discrepancy with the observations.

Notice that the profiles calculated by eqn. (88) or (89) give zero central intensities since we assumed pure scattering. The non-zero central intensities of lines such as λ3933 suggest that pure scattering does not obtain. If we take ε different from zero, the computed line profile will have a finite central intensity, or conversely if we make the observed and computed central intensities agree, we can obtain an estimate of ε. At the center of the line η becomes very large, L approaches ε, and M [cf. eqn. (71)] approaches zero. Hence from eqn. (87),

$$r_c = \frac{2}{\frac{4}{3}\sqrt{3} + \frac{1}{2}\frac{x_0}{n}} \frac{\frac{4}{3}\sqrt{3\varepsilon}}{1 + \sqrt{\varepsilon}} \tag{131}$$

For a given value of r_c we can compute ε. For λ3933, r_c is about 0.08 whence $\sqrt{\varepsilon}$ would be 0.16 and ε would be 0.026.

Notice that the central intensity of the line depends only on the value of ε and not at all on the abundance of the element in question. On the other hand, the intensity in the wings does depend on the abundance of the atom responsible for the line.

A complete theory of absorption line formation would enable the prediction of ε as a function of optical depth for any line. The problem is intimately connected with that of interlocking (Sec. 11). The formation of each line has to be treated in connection with the energy level scheme of the whole atom. In general, ε will tend to be small for resonance lines like λ4227 of calcium and larger for the subordinate lines, e.g., the Paschen lines of hydrogen.

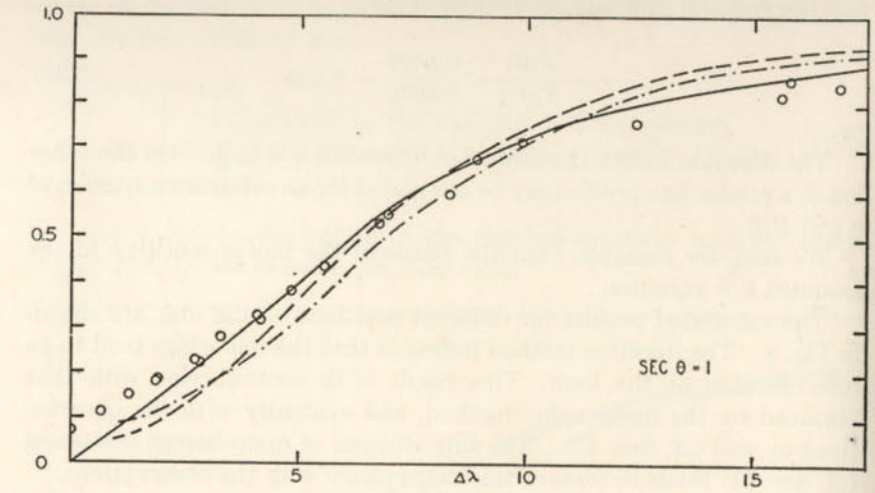

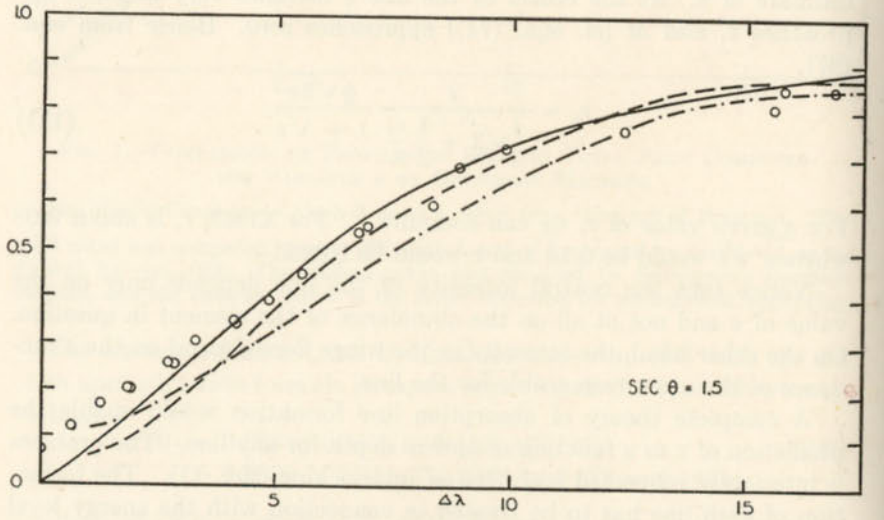

FIG. 8.—THE CENTER-LIMB VARIATIONS IN λ3933

We compared Houtgast's observations (circles) with the theoretical curves. At sec $\theta = 1.5$ and 3 the plotted points are interpolated from the observations. The solid curves give the profile computed by eqn. (89) with the modifications suggested by eqn. (93). The dashed curve is computed by the iteration method, while the dot-dash curve gives the latter corrected for noncoherent scattering. Notice that although there is fair agreement between the theoretical curves near the center of the disk, the curves show significant departures from one another toward the limb. The noncoherent scattering curve seems to give a better representation of the center-limb variations than does the completely coherent theory. The model atmosphere for the sun needs improvement.

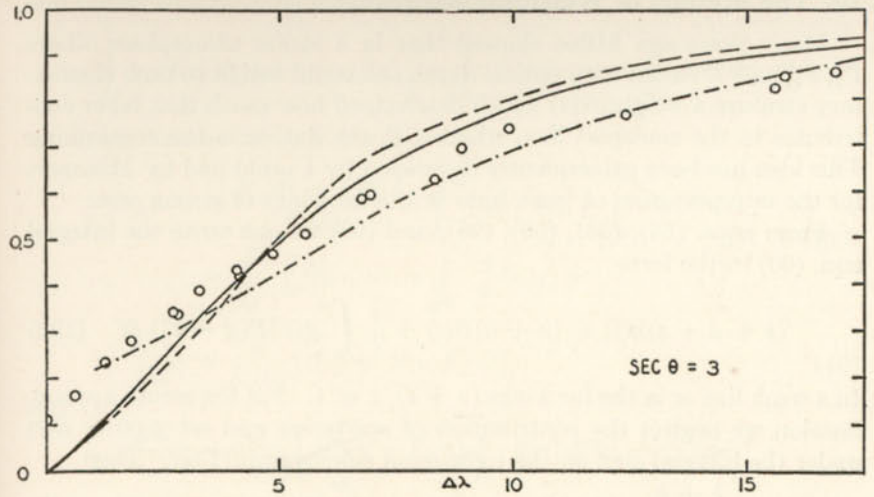

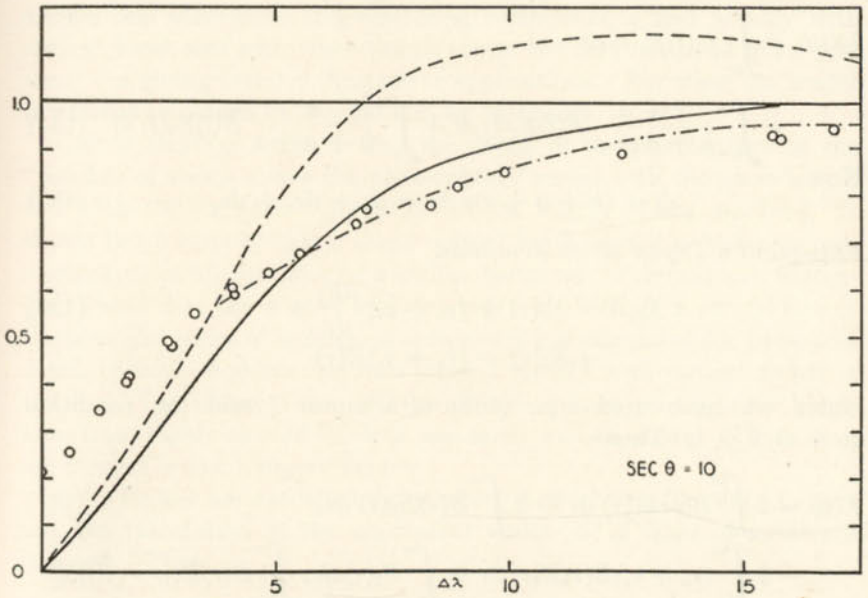

10. The Method of Weighting Functions

Many years ago Milne showed that in a stellar atmosphere where P_g, P_e, and T varied with optical depth one could assign to each elementary stratum a weight $G(\tau)$ which determined how much that layer contributes to the emergent flux, whether in the line or in the continuum. This idea has been subsequently developed by Unsöld and by Minnaert for the interpretation of weak lines or the far wings of strong ones.

From eqns. (54), (56), (59), (98), and (99) we can write the integral eqn. (60) in the form

$$(k + a + s)\mathcal{J}(t) = (k + a)B(t) + \frac{s}{2}\int_0^\infty \mathcal{J}(t')E(|t - t'|)\,dt' \quad (132)$$

In a weak line or in the far wings $(a + s)/k \ll 1$. For the zeroth approximation we neglect the contribution of scattering and set $\mathcal{J}_0(t) = B(t)$ under the integral sign on the right-hand side of eqn. (132). Then

$$\mathcal{J}_1(t) = \frac{k + a}{k + a + s}B(t) + \frac{s}{2(k + a + s)}\int_0^\infty B(t')E(|t - t'|)\,dt' \quad (133)$$

Using eqns. (61) and (107) we compute the emergent flux $\pi F(0)$ from

$$\tfrac{1}{2}F(0) = \int_0^\infty \mathcal{J}_1(t)E_2(t)\,dt$$

$$= \int_0^\infty \frac{k + a}{k + a + s}B(t)E_2(t)\,dt + \int_0^\infty \frac{s}{k + a + s}\bar{B}(t)E_2(t)\,dt \quad (134)$$

Now

$$dt = (k + a + s)\rho\,dx = d\tau + d\tau_a + d\tau_s \quad (135)$$

Expand in a Taylor series to obtain:

$$E_2(t) = E_2(\tau) + (\tau_a + \tau_s)\frac{dE_2}{d\tau} + \cdots \quad (136)$$
$$= E_2(\tau) - (\tau_a + \tau_s)E(\tau)$$

where we have used eqn. (189) of Chapter 7 and the condition $(a + s)/k \ll 1$. Then

$$F(0) = 2\int_0^\infty B(\tau)E_2(\tau)\,d\tau + 2\int_0^\infty B(\tau)E_2(\tau)\,d\tau_a \quad (137)$$
$$- 2\int_0^\infty (\tau_a + \tau_s)B(\tau)E(\tau)\,d\tau + \int_0^\infty E_2(\tau)\,d\tau_s\int_0^\infty B(\tau)E(|\tau - \tau'|)\,d\tau'$$

The first term on the right represents $F_c(0)$, the flux in the continuum divided by π. If we define

$$f(x) \equiv \int_x^\infty B(x)E(x)\,dx \quad (138)$$

and notice that by integration by parts

$$-\int_0^\infty \tau_a B(\tau)E(\tau)\,d\tau = \tau_a f(\tau)\Big|_0^\infty - \int_0^\infty f(\tau)\,d\tau_a = -\int_0^\infty f(\tau)\,d\tau_a, \text{ etc.}$$

we obtain for the depth of the line

$$1 - r = \frac{F_c(0) - F(0)}{F_c(0)} = \int_0^\infty G_1(\tau)\,d\tau_a + \int_0^\infty G_2(\tau)\,d\tau_s$$
$$= \int_0^\infty \frac{a}{k}G_1(\tau)\,d\tau + \int_0^\infty \frac{s}{k}G_2(\tau)\,d\tau \quad (139)$$

$$G_1(\tau) = \frac{2}{F_c(0)}[f(\tau) - B(\tau)E_2(\tau)] \quad (140)$$

and

$$G_2(\tau) = \frac{1}{F_c(0)}\left[2f(\tau) - E_2(\tau)\int_0^\infty B(\tau')E(|\tau - \tau'|)\,d\tau'\right]$$

G_1 represents the weighting function for absorption processes, G_2 that for scattering processes. The important point is that these functions may be calculated once and for all for a given model atmosphere. The atomic line absorption and scattering coefficients, a and s, vary with optical depth and with wave length across the line. Lack of space prevents our giving detailed illustrative applications. For these the reader is referred to papers by Unsöld and by Minnaert.

One interesting result is that the depth of the photosphere or the "number of atoms above the photosphere" varies with the wave length and with the excitation potentials of the energy states involved. It should be no surprise that a single optical depth cannot be taken as representative of all the lines of a stellar spectrum. For example, Strömgren found that the correct total intensity of λ3302 (the second line of the principal series of sodium) is obtained if η is calculated for an optical depth of 0.25. Sodium becomes ionized rapidly with optical depth in the sun. The Balmer lines or infrared carbon lines, on the other hand, arise from highly excited levels of less easily ionized atoms. These lines are formed in much deeper layers.

J. C. Pecker has extended the method of weighting functions to permit the calculation of the equivalent width W of lines of moderate strength. Thus

$$W \sim \int_0^\infty g(\tau)b(\tau)\Psi[x(\tau), a(\tau)]\,d\tau$$

where $g(\tau)$ is the weighting function that depends only on the model of the atmosphere. The function $b(\tau)$ depends on the ionization and excitation of the atoms capable of absorbing the line considered [the function

$x(\tau)$ is deduced from the function $b(\tau)$]. The saturation function Ψ is equal to 1 near the surface and decreases to zero at large optical depths, the stronger the line the more rapid the decrease of Ψ. For weak lines $\Psi = 1$ throughout the whole atmosphere. The quantity a, defined by eqn. (31), also varies with optical depth.

11. Interlocking and Noncoherent Scattering

The theory of line profiles suffers from two important defects, interlocking and noncoherent scattering. For convenience in the calculation of line profiles, we often set $\varepsilon = 0$, i.e., we assume pure scattering. But $\varepsilon = 0$ predicts profiles with black centers in contradiction to observation. We can introduce an empirical value of ε to make the observed and computed central intensities agree, but ε can be computed by theory only if we have some definite mechanism in mind. The upper levels can be populated by captures from the continuum, by cascading from higher levels, or by collisional excitations. Collisions are not likely to be important in the upper atmosphere of the sun, but recaptures in higher levels and cascading can become important for subordinate lines as Strömgren and others have emphasized. The Balmer lines provide a good illustration. An atom may be raised from the ground level by the absorption of Lyman β, for example. As it cascades to the second level it emits a λ6563 quantum, so Hα will tend to be filled in. Woolley suggested that this interlocking effect might account for the observed central intensities of the Balmer lines. Shane found the sodium "*D*" lines to have central intensities of 0.058 and 0.051. Dempster worked out a theory for the formation of these lines in which he took recaptures into account. With the aid of precise f values he was able to account for about half the observed central intensity. The solar ultraviolet radiation field may explain the discrepancy, but at present no decision on this question is possible.

The second important question is whether light absorbed in one part of the line is re-emitted at precisely the same part of the line. If this is true, as we assumed in our line profile calculations, the darkening in each frequency is independent of what happens in other frequencies.

On the other hand, the re-emitted frequency may be correlated with, but not determined by, the absorbed frequency. Under this condition, which is called noncoherent scattering, re-emission is not the exact inverse of absorption. When a transition occurs between two broadened levels, the atom is not likely to return to the same spot in the broadened lower level from which it started.

W. Orthmann and P. Pringsheim showed that when mercury vapor is exposed to radiation of a narrow resonance line from an auxiliary mercury lamp, the profile of the re-emitted line is independent of perturbing

atoms in the auxiliary lamp and is determined only by the Lorentz widening in the gas exposed to the radiation. Hence, we may conclude damping by collision produces noncoherent scattering.

The discussions by Spitzer, Woolley, and others show that noncoherent scattering is to be expected in many absorption lines of astronomical importance. It has little effect on the total intensities of the absorption lines, but the cores of strong lines will be stronger than on the older theory. The profiles of the hydrogen lines in early-type stars and Shane's data on the sodium "*D*" lines in the sun are qualitatively in harmony with the hypothesis of noncoherent scattering.

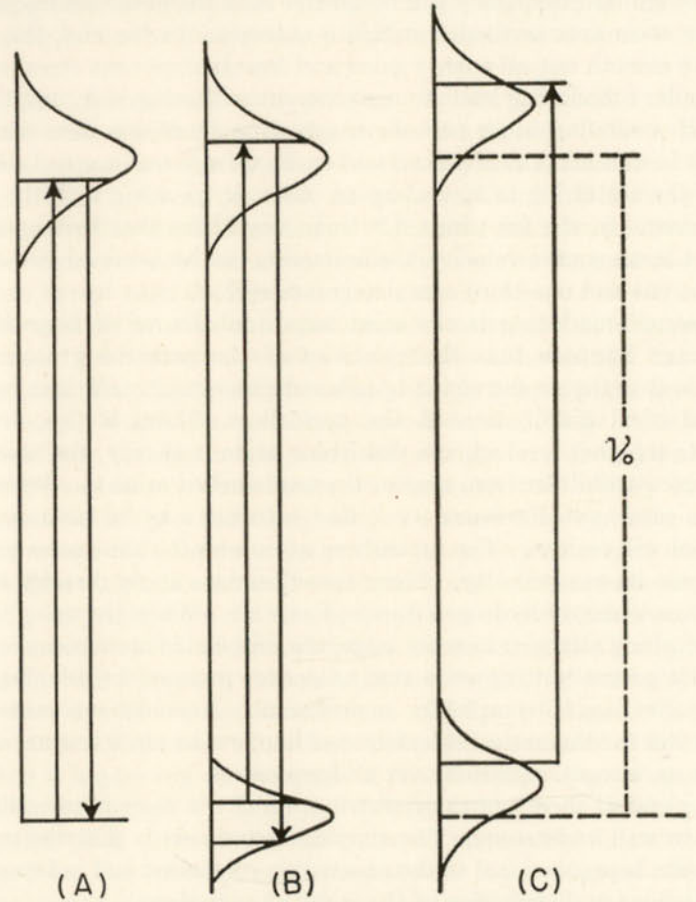

FIG. 9.—NONCOHERENT SCATTERING

(A) A resonance line arising from a perfectly sharp lower level follows coherent scattering if the radiating atoms are at rest. (B) Noncoherent scattering occurs if both upper and lower levels are broadened by radiation damping, or by collisions as in (C) where ν_0 denotes the undisturbed frequency.

Following the discussion by Spitzer, let us first describe noncoherent scattering by atoms subject to natural broadening only. In the first example (Fig. 9A), the ground level is sharp and the atom must emit the same frequency as it absorbs. If as for subordinate lines, however, both upper and lower levels are fuzzy, as indicated in Fig. 9B, the atom may emit a different amount of energy than it absorbs. In the long run, the sum of the energies of all absorbed quanta must equal the sum of the energies of all emitted quanta. If the atom, upon returning to the ground level, emits a quantum of frequency less than the frequency of the quantum previously absorbed, then in the next capture of a quantum, the emitted frequency will be greater than the absorbed frequency, i.e., the atom acts as though it had a memory. In the end, the atom tends to smooth out all energy gains and losses.

Doppler broadening leads to noncoherent scattering in a complicated way. If a moving atom absorbs a quantum from one direction and emits it in another, the absorbed and emitted frequencies are not equal, even if the scattering as viewed by an observer traveling with the atom is coherent. In the far wings, for frequency shifts that correspond to the root mean square velocity, the scattering can be assumed two-thirds noncoherent and one-third completely coherent.

Pressure broadening is the most important source of noncoherent scattering. Suppose that the velocities of the perturbing atoms are small, so that the profile of the broadened absorption coefficient reflects the statistical distribution of the perturbers. Then, if the electron jumps to a higher level when a disturbing atom is nearby, the absorbed frequency ν will differ from that of the undisturbed atom ν_0. When the electron returns to the lower level, the perturber may be far away and the atom will emit ν_0. The perturbing atom absorbs the excess energy to increase its own velocity. These considerations apply directly to the Stark broadening of hydrogen lines in hot stars. When the velocities of the perturbing atoms or ions are large, the problem is more complicated, but quite generally it appears that whenever pressure broadening prevails, scattering is completely noncoherent. Noncoherent scattering complicates the theoretical calculation of line profiles since it is necessary to solve an integral equation over all frequencies.

The physical theory of the redistribution of the re-emitted radiation is not too well understood. The simplest hypothesis is that the energy re-emission is proportional to the absorption coefficient and independent of the frequency distribution of the incident radiation.

Following the discussion by Zanstra and Spitzer, one may suppose that if the line has a damping constant Γ, comprising a contribution Γ_r due to radiation damping and a collision damping term Γ_c, the fraction

$\frac{1}{3}\Gamma_r/\Gamma_c$ will be re-emitted in the same frequency as absorbed (coherent scattering) while the rest is re-emitted with a frequency distribution proportional to the absorption coefficient. Then the usual equation of transfer, eqn. (51), must be modified for the fact that the fraction $(\Gamma_c + \frac{2}{3}\Gamma_r)/\Gamma$ of the absorbed radiation is redistributed over all frequencies. If the difference between the coherent radiation field J and the noncoherently scattered radiation characterized by J' is small, the effect upon the line profile may be evaluated. (See Fig. 8.)

Münch has derived an explicit solution for η = constant and has shown that a formal representation of the center-limb variation of the K-line profile is obtainable. Unfortunately, the role of noncoherent scattering cannot be predicted entirely from theory and certain empirical adjustments are required.

Further discussions have been given by D. Labs and by Suemoto, but the most satisfactory treatment is that by M. P. Savedoff who handles the problem of noncoherent scattering with and without selective absorption by iterating the exact integral equation for the average value of J over the line minus B, viz., $\bar{J} - B$, where ϵ and η are independent of depth. Even for $\epsilon = 0$ the line profiles lie close to the pure absorption solution except near the line center.

The qualitative effects of noncoherent scattering on the radiation field may be summarized briefly. In our discussion of the K-line profile we saw that $J_{\nu_0}(\tau)$, while small at the surface, rapidly rose to the black body value with increasing optical depth. Away from the line center where the absorption coefficient is smaller, J_ν approached B_ν much more slowly. Noncoherent scattering cannot directly alter the total net flux in the whole line, but it can transfer energy from one frequency to another. Let us suppose that the mean intensity at the center of the line, $J_{\nu_0}(\tau)$, computed for coherent scattering can be used as a starting approximation in the treatment of noncoherent scattering. Then, at large optical depths, radiation taken up by the line will be re-emitted in the wings at a rate proportional to $\alpha_\nu B_\nu$ for each atom, since the redistribution is proportional to α_ν and the radiation field J_{ν_0} is B_ν at the center of the line. In other words, the re-emission is determined by what is happening at the center of the line where the energy density is $B_\nu(\tau)$, rather than by $J_\nu(\tau)$, the average intensity at the frequency ν in the line wing. Toward the line center J_ν approaches J_{ν_0} and the deviations from the coherent scattering picture are not great. Near the surface, the energy absorbed in the wings tends to be put back near the line center and there is extinction with no re-emission in the wings. Hence noncoherent scattering should show up as a combination of absorption and extinction in the far wings of absorption lines.

12. Variations of Line Profiles Across the Solar Disk

At different distances from the center of the solar disk we observe radiation from effectively different depths of the solar atmosphere. Hence line profile variations should reveal something of the stratification of the radiating atoms. Theory predicts that the behavior of the line wings is insensitive to whether scattering or absorption prevails but is sensitive to the variation of η with depth. At the limb itself, the wings vanish for pure absorption, whereas lines formed in strict monochromatic radiative equilibrium may actually appear in emission at the limb! (Compare Fig. 8.) If we represent $B_\nu(\tau)$ by a linear expression,

$$B_\nu = B_0 + B_1\tau \tag{141}$$

we find that to the violet of the energy maximum B_1 will be so large that B_ν will rise rapidly with τ. A volume element in local thermal equilibrium near the surface will absorb a greater amount of radiation of frequency ν than it will emit as thermal energy of the same frequency, since the emission depends on the local temperature in accordance with Kirchhoff's law. On the other hand, purely scattering atoms will emit all the radiation absorbed at ν in the same frequency ν. Thus they may emit more energy than the atoms responsible for the continuous spectrum, provided that the flux in the line is comparable with that in the continuum, a condition which is fulfilled for the far wings of the line. Hence the wings may appear in emission. On the other hand, to the red of the energy maximum in the spectrum, scattering may act to intensify the dark wings.

Center-limb variations of solar line profiles have been studied by many observers, among whom we may mention K. Schwarzschild, A. Unsöld, H. H. Plaskett, G. Righini, T. Royds, and A. L. Narayan, M. Minnaert, R. O. Redman, C. W. Allen, D. S. Evans, E. Cherrington, D. C. Shane, and J. Houtgast. The most extensive series is that of Houtgast who studied 23 representative lines of Fe I, Mg I, Ca I, Ca II, and Na I across the solar disk. In spite of great care, his observations show systematic differences from those of other observers, for example, from the precise measures by C. D. Shane on the sodium "*D*" lines.

The central intensities of the strong lines simply mirror the center-limb variations in the continuous background. The variations in the line wings are of great interest in the evaluations of the relative roles of scattering, absorption, and noncoherency. Towards the limb, scattering must predominate in the wings, since radiation is received from only the uppermost layers. It follows that since it appears necessary to introduce an absorption coefficient to explain the profiles near the limb, we are really dealing with noncoherent scattering which transfers energy

from the wing towards the center of the line! Towards the line center, in accordance with our expectations, a formal representation by coherent scattering becomes possible. In order to explain the measured profiles, Houtgast found it necessary to invoke noncoherent scattering. On the other hand, Miss Tuberg's detailed calculations of the center-limb variations of λ3933, Na "*D*," and λ4227 showed a general qualitative agreement with Houtgast's observations without invoking noncoherent scattering. More recent work, however, suggests that noncoherent scattering does play a role.

The most accurate study of center-limb variations in line profiles is C. D. Shane's investigation of the sodium "*D*" lines by an interferometer method. He measured the line profiles at the center of the disk and near the limb and showed the observations to be inconsistent with the assumption of an η constant with optical depth, although a constant η would reproduce the profile at the center of the disk. The observations suggested an η decreasing with optical depth. Spitzer concludes that the profile variations found by Shane for sodium "*D*" can be explained by appeal to noncoherent scattering.

With the aid of the considerations of Sec. 11, we may correct the profiles calculated in Sec. 9 for noncoherent scattering. (See Fig. 8.) It appears that the center-limb behavior of the wings can be explained in at least a qualitative fashion. The behavior of the computed profile near the center of the line is quite unsatisfactory from both points of view. More accurate information on the ratio $k/\bar{k}$ and on the temperature gradient in the uppermost layers is necessary, as well as an adequate theory of central intensities.

Fortunately, the problem of center-limb variations in line profiles can be attacked from another point of view, developed by H. Zanstra. A resonance line like λ4227 of Ca I should behave like a classical oscillator with negligible true absorption. The scattered light should be polarized such that the intensity of the component along the solar radius, I_r, differs from that parallel to the solar limb, I_L. The difference, $I_L - I_r$ expressed in units of the nearby continuum depends on the position on the disk and the limb-darkening coefficient. Redman found a polarization effect in λ4227 ten times smaller than the value predicted by Zanstra for pure scattering. The conclusion is that collisional damping rather than radiation damping prevails for the line. The scattering is noncoherent; only a tenth of the radiation absorbed in the line wings is re-emitted in the same frequency; the rest is distributed over the entire line.

A possible influence of the granulation upon the spectrum at the extreme limb of the sun has been discussed by Redman, who studied the Fraunhofer line spectrum, freed from chromospheric emission, less than

one second of arc from the limb. At this point, the weak lines are stronger than at the center of the disk, but lines with equivalent widths a bit greater than 0.13A become weakened at the limb, and the greater the intensity, the greater is the weakening. The ordinary Fraunhofer line theory does not explain the result. The clue to the puzzle seems to lie in the roughness of the solar surface associated with the solar granulation, which reduces the value of θ of the emergent ray for observations near the limb. Quantitative estimates show that an apparent cos θ of 0.05 can be changed to 0.20 by this process. These results imply that the effects of an unevenness in the solar surface cannot always be ignored in a precise theory of absorption line formation.

In certain eclipsing binaries, center-limb variations of line profiles can be observed. We do not obtain the spectra of separate points of the star's surface, but merely the integrated spectrum of the noneclipsed portion of the primary.* Redman studied the changes in the line intensities from center to limb in the primary components of U Cephei and U Sagittae. His observations and those of Otto Struve favor the conclusion that the lines of H and He in late *B* stars are weak at the edge, although the Mg II lines appear not to vanish at the limb. Struve suggests that we see here an effect of Stark broadening in H and He which diminishes at the limb (because we observe only the highest layers). The vanishing of the lines is not a consequence of their being formed under *LTE*. If the latter scheme prevailed, the Mg II lines should disappear at the limb.

13. The Curve of Growth

In practice, it is often not possible to obtain profiles for all absorption lines of interest. Except for lines with rather broad wings observed with high dispersion, the profiles are always seriously distorted by the finite resolution of the spectrograph. The total energy subtracted by the line, expressed in units of one angstrom of the nearby continuum, i.e., the equivalent width, is less seriously disturbed than the line shape by the finite resolution of the spectrograph and may be determined readily.

How will the equivalent width (intensity) of a spectral line change as the number of atoms acting to produce it increases? The significant parameter is not simply N, the number of atoms, but Nf, the number of atoms times the f value. When Nf is small, we observe only a small depression in the continuous spectrum. As it increases, the line center deepens and widens until, when Nf becomes very large, prominent "wings" begin to appear. We depict the process in Fig. 10a, which

* The spectrum of the fainter component is superposed and its effect has to be subtracted from the measured intensities. The most favorable pairs are those stars where a small early-type primary revolves around a large late-type secondary.

shows the growth of a line formed by atoms in a thin layer (Schuster-Schwarzschild model) according to the mechanism of pure scattering. The number, N_0, is so chosen that for this number of atoms above the

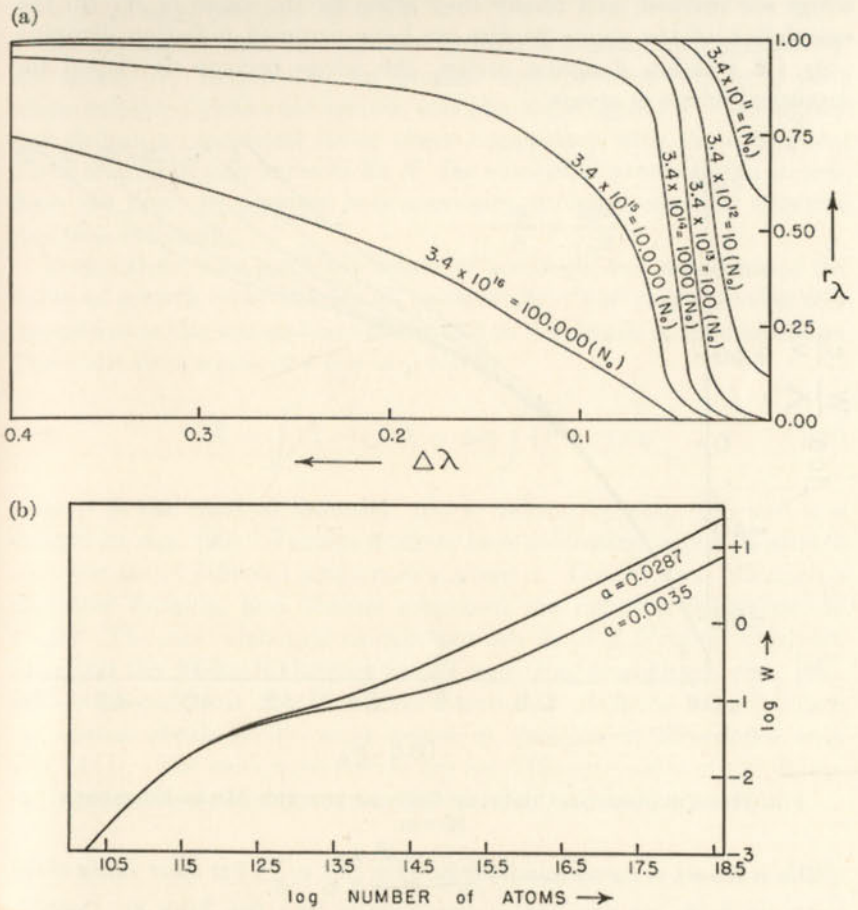

FIG. 10.—THE CURVE OF GROWTH FOR λ3933

(a) Theoretical profiles calculated for the Schuster-Schwarzschild model and pure radiation damping show how the shape of the line changes as the number of absorbing atoms increases. The number $N_0 = 3.4 \times 10^{11}$ is so chosen that the optical depth at the center of the line for N_0 atoms, X_0, will be 1. N denotes the number of atoms above the photosphere. The curves are calculated with $A = 1.66 \times 10^8$.

(b) From the integration of the profiles of Fig. 10(a) we obtain log W which we plot against log N, the number of atoms above the photosphere. Curves are given for $a = 0.0035$ and 0.0287 [cf. eqns. (44) and (48) of Chapter 8].

photosphere, the optical depth at the center of the line, which we call X_0, will be 1. When N is less than $100N_0$, the Doppler effect is dominant in fixing the line shape, and the line profile is bell-shaped. For a

time, W grows very slowly with N; then the damping wings begin to appear. At $1000N_0$ the line shows a combination of the bell-shaped Doppler profile and incipient "wings." Beyond $N = 10{,}000N_0$, the wings are marked, and finally they alone fix the value of W. In the calculation of the above profiles we have assumed radiation damping only. If collision damping occurs, the wings become developed for smaller numbers of atoms.

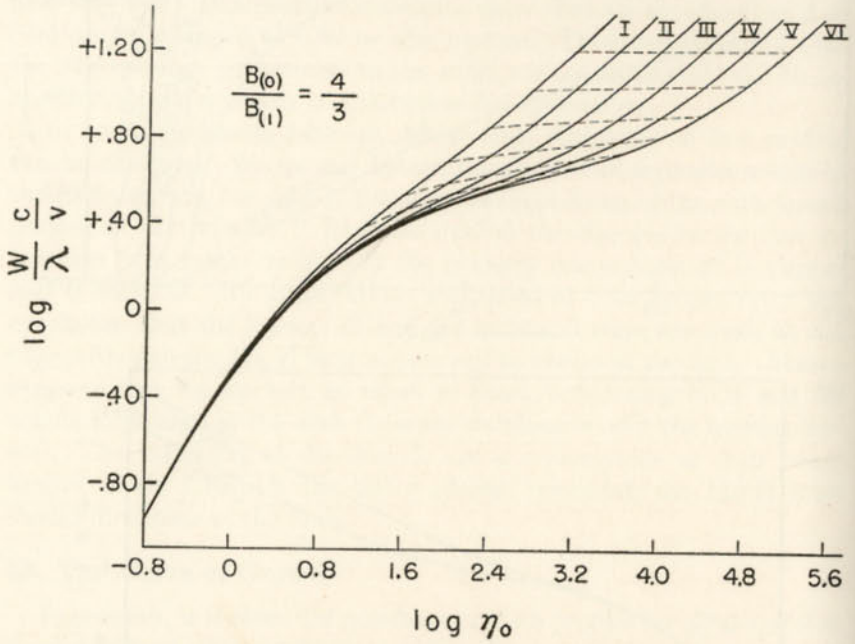

FIG. 11.—THEORETICAL CURVE OF GROWTH FOR THE MILNE-EDDINGTON MODEL

This is the set of curves calculated for $\frac{B_0}{B_1} = \frac{8}{3}\frac{n_\lambda}{x_0} = \frac{4}{3}$. For other values of the parameter B_0/B_1 one may employ corrections to $\log \eta$ (see Table 8). Curve I, $\log a = -1.0$; curve II, $\log a = -1.4$; curve III, $\log a = -1.8$; curve IV, $\log a = -2.2$; curve V, $\log a = -2.6$; curve VI, $\log a = -3.0$. (Courtesy, Marshal Wrubel, *Astrophysical Journal*, University of Chicago Press, **109**, 71, 1949.) Calculations for the Schuster-Schwarzschild model are also being carried out by Wrubel.

We could construct the relation between W and the number of atoms, i.e., the curve of growth, from a diagram such as Fig. 10a by measuring the areas under the curve and plotting the resultant $\log W$ against $\log Nf$. For example, we could calculate the profile of λ3933 by the method of Sec. 9 for different values of $\log N$, measure the area of the profile W, and plot it against the number of atoms. The results of such a calculation are shown in Fig. 10b where we have carried out computations for:

(1) pure radiation damping with $a = 0.0035$ and (2) collision plus radiation damping with $a = 0.0287$. Notice that for small numbers of atoms, W is proportional to N; later the curve flattens out and finally W varies as $\sqrt{N}$, or more precisely as $\sqrt{N\Gamma}$.

We emphasize that the curve of growth is a plot of W against Nf, not simply N. In practice, we measure the equivalent widths of lines whose relative f values are known, and plot them against f. This operation defines an empirical curve whose comparison with the theoretical curve of growth may serve to fix N, the number of atoms acting to produce the line. In practice it is necessary to know also the effective damping constant.

Fortunately, to a sufficient degree of accuracy, we can calculate the curve of growth once and for all analytically. The curve is relatively insensitive to the atmospheric model and to the details of the line shape. The equivalent width of a line is given by

$$W = \int (1 - r)\, d\lambda = \Delta\lambda_0 \int (1 - r)\, du \tag{142}$$

where r is the residual intensity, $\Delta\lambda_0$ is defined by eqn. (39) and u is defined by eqn. (29). Various workers have calculated curves of growth with the aid of different assumptions about r. Unsöld used Minnaert's empirical formula, and Menzel employed the Schuster-Schwarzschild model. The most elaborate calculations are those of Wrubel, which are based on the Milne-Eddington model and Chandrasekhar's eqn. (88). It is supposed that the Planckian function B depends linearly upon the optical depth at the wave length in question in accordance with eqn. (141). The calculated curves are for different values of the damping constant a, defined by eqns. (30) and (31) and the parameter

$$\frac{B_0}{B_1} = \frac{8}{3}\frac{n_\lambda}{x_0} \tag{143}$$

Cf. eqns. (141), (72), (76), (68), and (75). They are calculated for pure scattering and refer to the total flux from the star. Wrubel has also calculated theoretical curves for the radiation from the center of the disk [cf. eqn. (89)]. As ordinate one employs

$$\log \frac{W}{\lambda}\frac{c}{v} \tag{144}$$

where v is the most probable velocity of the atoms; and as abscissa the quantity, $\log \eta_0$, where

$$\eta_0 = \frac{N\alpha_0}{k} \tag{145}$$

Here α_0 is given by eqn. (33), k is the continuous absorption coefficient at the wave length in question, and N is the number of atoms per gram of stellar material capable of absorbing the line in question.

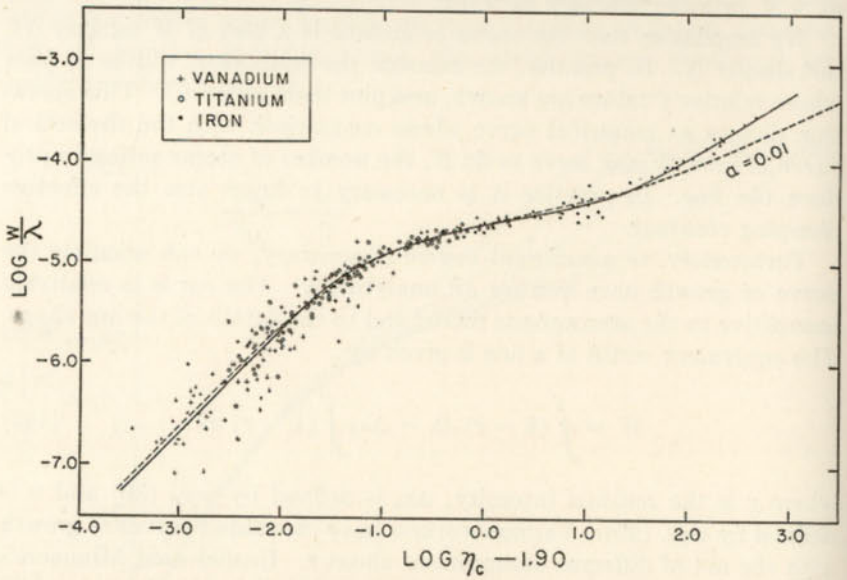

FIG. 12.—CURVE OF GROWTH FOR THE SUN

The empirical curve of growth for vanadium, titanium, and iron as derived from line intensity measures at the center of the disk is compared here with the theoretical curve calculated for the center of the disk. Ordinates are $\log \frac{W}{\lambda}$; abscissae are essentially $\log \eta_c - 1.90$. (Courtesy, Leo Goldberg and Keith Pierce.)

A different curve of growth is found for each damping constant and choice of B_0/B_1. Since B_0/B_1 varies along the spectrum and we normally combine lines measured over a considerable wave length range into a single curve of growth, it is expedient to use a single curve of growth for a fixed B_0/B_1 and to apply a correction $\Delta\eta_0$ to η_0, depending on the value of B_0/B_1 at the wave length in question.

To utilize the theoretical curve of growth we measure the equivalent widths of a group of lines whose f values are known.

From the spectral type we can usually estimate the temperature and electron pressure sufficiently close to obtain a good working value of v and k (see Ch. 7). Then for each line we may calculate $\log \eta_0/N$ and $\log \frac{Wc}{\lambda v}$, and plot our points on the theoretical curve by a horizontal shift.* The amount of horizontal shift will determine N. This quantity

* A vertical shift is sometimes necessary—this means that our choice of v, the kinetic velocity of the atoms, is in error. Some source of Doppler broadening in addition to purely thermal motions must enter. See Sec. 15.

will depend on the ionization equilibrium, the temperature, and the abundance of the element in question. In principle, from the curve of growth we should be able to determine the temperature of the atmosphere and the abundance of the constituent elements.

Example: Let us illustrate the curve of growth procedure by a discussion of spectral line intensities measured in the main sequence $B2.5$ star, γ Pegasi. The effective temperature is taken as 20,000°K (Table 12 of Ch. 7), and from a consideration of the model atmosphere that seems to represent the profiles of the hydrogen lines (Sec. 16) we may choose $\log P_e = 2.90$ at an optical depth of 0.6. The observed equivalent widths are derived from measures upon coudé plates taken at the Mount Wilson and McDonald Observatories, and Cassegrain spectrograph plates obtained at the Dominion Astrophysical Observatory.

As a typical example let us consider $2s^22p^23s - 2s^22p^23p$ transition array in O II. The strengths of the individual lines may be computed in terms of the parameter σ^2 as explained in Chapter 5.

Let $\bar{f}$ denote the weighted average f value for the entire transition array computed according to the rule (see p. 132):

$$\bar{f} = \frac{1}{\Sigma g_i} \Sigma\, g_i f(\alpha J; \alpha' J') = \frac{8\pi^2 mc}{3he^2} \frac{1}{\Sigma g_i} \Sigma \frac{S_1}{\lambda} \tag{146}$$

where S_1 is defined by eqn. (85) of Chapter 5, and Σg_i is the sum of the weights of all the levels in the $2s^22p^23s$ configuration. For a particular transition let us define a quantity

$$\mathbf{f}(\alpha J; \alpha' J') = \bar{f} \frac{S}{\Sigma S} \frac{s}{\Sigma s} = \frac{(2J'+1)}{\Sigma g_i} f(\alpha J; \alpha' J') \tag{147}$$

Here $S/\Sigma S$ is the strength of the multiplet in terms of the strength of the whole transition array. Notice that

$$N_{J'} f(\alpha J; \alpha' J') = N \mathbf{f}(\alpha J; \alpha' J') \tag{148}$$

where $N_{J'}$ is the number of atoms in the level J', $f(\alpha J; \alpha' J')$ is the true f value for the transition, and N is the number of atoms in the whole configuration; hence

$$\eta_0 = \frac{\pi e^2}{mc} \frac{c}{v\nu\sqrt{\pi}} \frac{N \mathbf{f}(\alpha J; \alpha' J')}{k} \tag{149}$$

In O II, $\bar{f}(3s - 3p) = 1.14$, $S/\Sigma S = 12/90$, and $s/\Sigma s = 0.14$ for $\lambda 4317.16$. Hence the $\mathbf{f}$ for this line is

$$\mathbf{f}(4317) = 1.14 \times \tfrac{12}{90} \times 0.14 = 0.0213$$

In the construction of the empirical curve of growth we would like to treat together all the lines of the $3s - 3p$ transition array. Different

terms, however, have different excitation potentials and consequently their populations will depend on the temperature. We allow for this effect by referring our calculations to the ^4P term (excitation potential = 22.90 volts). If $T = 20{,}000°\text{K}$, the corrections for the higher terms, computed from the expression, $\frac{5{,}040}{20{,}000}(\chi - 22.90)$, are as follows:

Term	Energy (wave numbers)	Energy (volts)	Boltzmann Correction
$3s(^3P)\ ^4P$	185,400	22.90	0
$\quad\ ^2P$	189,040	23.33	−0.11
$3s(^1D)\ ^2D$	206,972	25.55	−0.67

That is, we allow for the Boltzmann correction for the higher levels by treating them as though they had the same excitation potential as the ^4P level but smaller f values. For example, we add -0.11 to the f values of all lines arising from the ^2P level.

Table 7 lists the wave length, J', J, $\log \frac{S}{\Sigma S}$, $\log \frac{s}{\Sigma s}$, $\log \mathbf{f}$, and the Boltzmann correction. Next we compute for oxygen,

$$\alpha_0' = \frac{\pi e^2}{mc}\frac{c}{v\nu\sqrt{\pi}}\mathbf{f} = 1.31 \times 10^{-12}\left(\frac{\lambda}{4000}\right)\mathbf{f} \tag{150}$$

since $v = 4.55 \times 10^5$ cm/sec for this element. Here λ is expressed in Angstrom units.

It is necessary now to introduce the effective continuous absorption coefficient which we shall take as the sum of the contributions of true absorption corrected for negative absorption and electron scattering,

$$k_e = k' + \sigma \tag{151a}$$

(cf. Ch. 7, Sec. 4). Similarly the mean effective absorption coefficient is

$$\bar{k}_e = \bar{k}' + \sigma \tag{151b}$$

We may now compute

$$\frac{B_0}{B_1} = \frac{8}{3}\frac{k_e}{\bar{k}_e}\frac{(1 - e^{-u})}{u} \tag{152}$$

where u is defined in Problem 3 of Chapter 7. For each line it is now possible to compute

$$\log \frac{\eta_0}{N} = \log \frac{\alpha_0'}{k_e}$$

TABLE 7

SELECTED LINES IN $3s - 3p$ CONFIGURATION IN γ PEGASI

$3s - 3p$	J'	J	$\log \frac{S}{\Sigma S}$	$\log \frac{s}{\Sigma s}$	$\log f$	Boltz. Corr.	$\log \alpha_0'$	$-\log \frac{\eta_e}{N}$	W	$\log \frac{W}{\lambda}\frac{c}{v}$
3911.99	5/2	3/2	−1.18	−0.22	−1.29	−0.66	13.08	14.12	0.043	−0.14
3912.09	3/2	3/2		−1.18						
3945.05	1/2	3/2	−1.18	−0.95	−2.07	−0.11	13.95	14.46	0.037	−0.21
3954.37	1/2	1/2		−0.65	−1.77	−0.11	13.65	14.16	0.042	−0.15
3917.16	1/2	3/2	−0.88	−0.85	−1.68	0	13.53	14.04	0.054	−0.08
4325.77	1/2	1/2		−1.56	−2.38	0	14.21	14.74	0.028	−0.37
4345.57	3/2	1/2		−0.86	−1.68	0	13.51	14.06	0.037	−0.26
4349.44	5/2	5/2		−0.46	−1.28	0	13.11	13.65	0.066	00
4366.91	5/2	3/2		−0.82	−1.64	0	13.48	14.02	0.046	−0.16
4347.43	3/2	3/2	−0.95	−0.44	−1.33	−0.66	13.18	14.38	0.028	−0.37
4351.28	5/2	5/2		−0.25	−1.14	−0.66	12.99	14.98	0.050	−0.12
4714.89	3/2	5/2	−0.95	−0.22	−1.11	−0.11	12.95	13.63	0.077	+0.06
4416.97	1/2	3/2		−0.48	−1.37	−0.11	13.21	13.88	0.065	−0.01
4452.38	3/2	3/2		−1.18	−2.07	−0.11	13.90	14.58	0.036	−0.27
4590.98	5/2	7/2	−0.81	−0.24	−0.99	−0.66	12.81	14.10	0.058	−0.08
4596.19	3/2	5/2		−0.40	−1.15	−0.66	12.96	14.25	0.050	−0.14
4638.86	1/2	3/2	−0.65	−1.08	−1.67	0	13.49	14.13	0.067	−0.02
4641.83	3/2	5/2		−0.68	−1.27	0	13.08	13.72	0.082	+0.07
4650.85	1/2	1/2		−1.08	−1.67	0	13.49	14.13	0.060	−0.07
4661.65	3/2	3/2		−0.97	−1.56	0	13.39	14.03	0.061	−0.07
4676.25	5/2	5/2		−1.05	−1.64	0	13.45	14.17	0.057	−0.10

For the present illustrative example we shall suppose the lines are formed according to the mechanism of scattering, although the absorption mechanism may be better for $s - p$ and $p - d$ transitions. We shall employ Wrubel's curves of growth.

TABLE 8

CORRECTION TO LOG η TO REDUCE TO A SINGLE CURVE OF GROWTH $\left(\frac{B_0}{B_1} = \frac{4}{3}\right)$

Δ LOG η AS FUNCTION OF LOG $\frac{Wc}{\lambda v}$ AND $\frac{B_0}{B_1}$

$\frac{B_0}{B_1}$	Log $\frac{Wc}{\lambda v} = -1.0$	0.0	+1.0
0.4	+0.16	+0.22	+0.22
0.8	+0.07	+0.11	+0.11
1.2	+0.01	+0.02	+0.02
1.6	−0.03	−0.03	−0.03
2.0	−0.06	−0.07	−0.07
2.4	−0.09	−0.10	−0.10
2.8	−0.11	−0.12	−0.13
3.2	−0.13	−0.14	−0.14
3.6	−0.14	−0.17	−0.15

A more complete table is given by M. Wrubel, *Ap. J.* **109**, 66, 1949.

In order to use a single theoretical curve of growth for all the lines, let us choose the one given for $B_0/B_1 = 4/3$ and derive corrections $\Delta \log \eta$ to be applied to $\log \alpha'_0/k_e$ for B_0/B_1 values other than 4/3. The $\Delta \log \eta$ corrections (Table 8) depend on $\log \frac{Wc}{\lambda v}$ which is near 0.00 for most of the lines in this star so that a single correction curve may be used without fear of appreciable error. Then we introduce an η_c defined by

$$\log \eta_c = \log \alpha'_0 - \theta(\chi - \chi_0) + \log N + \Delta \log \eta - \log k_e \qquad (153)$$

as the abscissa of the curve of growth. The last two terms depend only on the wave length, whereas the first two must be computed for each line. We write:

$$\log \frac{\eta_c}{N} = \log \alpha'_0 + \Delta - \theta(\chi - \chi_0) \qquad (154)$$

where

$$\Delta = \Delta \log \eta - \log k_e$$

is given in the last column of Table 9. Column 9 of Table 7 gives $-\log \eta_c/N$ for each observed $3s - 3p$ line of O II, while the last two columns give the observed equivalent width W and $\log \frac{Wc}{\lambda v}$.

TABLE 9

CALCULATION OF $\Delta = \Delta$ LOG η − LOG k_e FOR CURVE OF GROWTH CALCULATIONS*

λ	x_0	Log $k_e(\lambda)$	B_0/B_1	$\Delta \log \eta$	Δ
3300	2.60	0.86	2.44	−0.10	−0.96
3500	2.45	0.91	2.92	−0.14	−1.05
<3650	2.35	0.95	3.32	−0.15	−1.10
>3650	2.35	0.35	0.85	+0.09	−0.26
3800	2.26	0.39	0.94	+0.07	−0.32
4000	2.14	0.44	1.10	+0.03	−0.41
4200	2.04	0.47	1.24	0.00	−0.47
4400	1.95	0.53	1.44	−0.02	−0.55
4600	1.86	0.57	1.63	−0.04	−0.61
4800	1.79	0.61	1.84	−0.06	−0.67

* The first column gives the wave length; the second column gives $x_0 = u(1 - e^{-u})^{-1}$ where $u = h\nu/kT_0$. Here $T_0 = 16{,}800°$K. The effective absorption coefficient k_e (col. 3) and its mean value, $\bar{k}_e = 2.75$ are calculated by the methods described in Chapter 7. B_0/B_1 (col. 5) is found from eqn. (152); Δ log η (col. 6) is interpolated from Table 8.

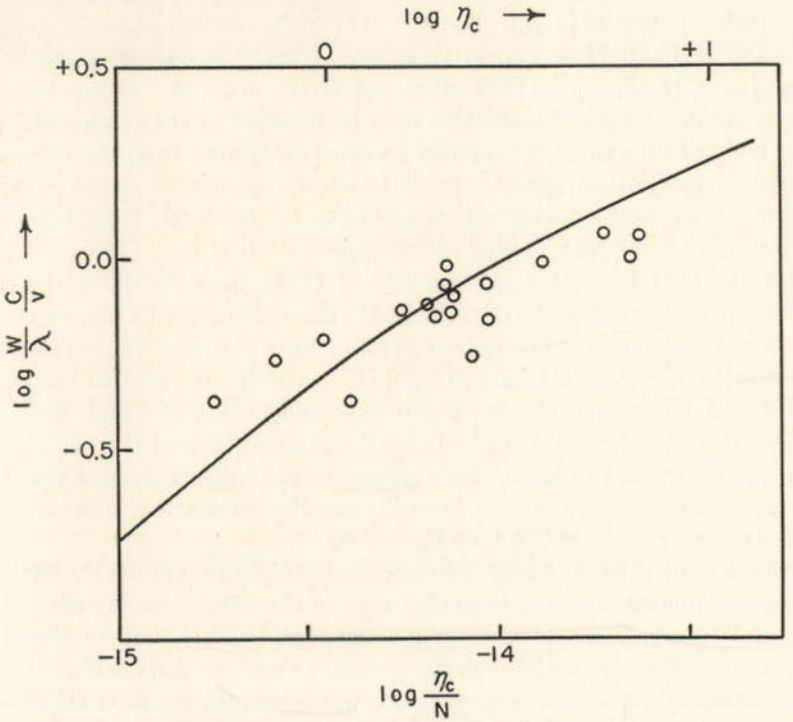

FIG. 13.—THE O II $3s - 3p$ TRANSITION IN γ PEGASI

We plot $\log \frac{Wc}{\lambda v}$ against $\log \frac{\eta_c}{N}$ (cf. Table 7) and fit the points to the theoretical curve of growth by a horizontal shift. Log η_c is indicated at the top; $\log \eta_c/N$ at the bottom.

We now plot $\log \frac{Wc}{\lambda\nu}$ against $\log \frac{\eta_e}{N}$ on transparent paper and fit the plot to the curve of growth by a horizontal displacement. In this way we find $\log N = 14.45$ for the number of O II atoms in the $2p^2 3s$ configuration per gram of stellar material.

If we denote by $N_{s,r}$ the number of atoms in the rth level of the sth stage of ionization, the combined Boltzmann and Saha equation, eqn. (14) of Chapter 4 may be written in the form

$$\log \frac{N_{s+1}}{N_{s,r}} = -\frac{5040}{T}(I_s - \chi_{s,r}) + \frac{5}{2}\log T + \log \frac{2B_{s+1}(\tau)}{g_{r,s}} - 0.48 - \log P_e \quad (155)$$

where I_s is the ionization potential of the atom in the sth stage of ionization, $B_{s+1}(T)$ is the partition function for the $(s+1)$ stage of ionization, $g_{r,s}$ is the statistical weight of the level or group of levels, s, whose excitation potential is $\chi_{s,r}$. For the O II $2p^2 3s$ configuration, $g_{r,s} = 30$, $B_{s+1}(T) = 10.20$, $(I - \chi_{r,s}) = 12.12$ ev. With $T = 20{,}000°$K, $\log N = \log N_{s,r} = 14.45$, eqn. (155) gives $\log N_{s+1}P_e = 21.49$. Other ions in their various stages of ionization may be handled in the same way. In the computation of α_0, we employ f values calculated from the tables of Bates and Miss Damgaard. Table 10 shows the results of the calculations. It gives the configuration and term to which the transitions are referred and the data needed for the application of eqn. (155). Notice that the O II lines give the number of O III ions multiplied by the electron pressure $N(\text{O III})P_e$; the Si III lines give $N(\text{Si IV})P_e$, etc.

Since silicon and sulfur appear in two stages of ionization, we can use the ratios of S IV/S III, and Si V/Si IV to check our assumed temperature and electron pressure. From the sulfur data we find that for $T = 20{,}000°$K we would need an electron pressure greater than 10^3 dynes to explain the above ratio, while silicon would suggest a lower electron pressure. For the purposes of our illustrative calculation, however, we shall retain $T = 20{,}000°$K; $\log P_e = 2.90$.

Finally we must allow for the distribution of atoms among the various stages of ionization. For example, most of the oxygen atoms are in the ground configuration of O II, while the high-level O II lines give the number of doubly-ionized oxygen atoms. From an application of the ionization equation we find that we must correct $\log N(\text{O III})P_e$ by the factor, $\log \frac{N(\text{O III}) + N(\text{O II})}{N(\text{O III})} = 0.85$, to get the total number of oxygen atoms multiplied by the electron pressure, viz., $\log N(\text{O})P_e$.

Successive columns of Table 11 give for each ion, $\log N_{s+1}P_e$, derived from the observed lines; $\delta \log N$, the correction necessary to reduce the

TABLE 10

ABUNDANCES OF THE IONS*

Ion	Configuration and Reference Term	$\log \frac{2B_{s+1}}{g_{r,s}}$	$I - \chi_{s,r}$	$\log N_{s,r}$	$\log N_{s+1}P_e$	
H I			3.38			
C II	$2s^2(^1S)3d^2D$	−0.53	6.30	13.45	21.60	
	$2s^2(^1S)3p^2P$	−0.31	8.02	14.05	21.98	
	$2s2p(^3P)3d^4F$	−0.98	6.67	13.05	20.64	21.09
	^4D	−0.83	6.57	13.07	20.86	
	^4P	−0.61	6.29	13.07	21.15	
	^2D	−0.53	6.34	12.60	20.74	
N II	$3s(^1P + ^3P)$	+0.02	11.09	14.09	21.58	
	$3p(^1P)$	+0.62	9.16	12.88	21.46	21.55
	$3d(^3P + ^3D + ^3F)$	−0.55	6.34	13.38	21.52	
O II	$2p^2(^3P)3d^2P$	−0.87	6.17	13.88	21.72	
	$2p^2(^3P)3p^4P$	−0.64	9.25	14.25	21.57	21.61
	$2p^2(^3P)3s^4P$	−0.17	12.12	14.45	21.49	
Mg II	3^2D	−0.70	6.14	13.77	21.79	21.95
	4^2P	−0.48	5.01	13.63	22.16	
Al III	4^2D	−0.70	7.86	12.52	20.11	
	4^2F	−0.85	7.63	12.65	20.15	20.07
	4^2P	−0.48	10.58	12.84	19.96	
Si III	4^3S	+0.15	14.39	14.06	20.86	20.83
	4^3F	−1.00	7.46	13.39	20.79	
Si IV	4^2S	0.00	21.00	12.29	17.26	17.45
	5^2D	−0.70	8.95	11.72	19.04	
P III	4^2S	0.00	15.48	12.49	18.9:	18.65
	3^2D	−0.70	15.60	12.98	18.62	
S II	$3p^24p^4D^0$	−0.60	7.42	13.65	21.45	
S III	$3p4s^3P^0$	0.00	17.23	13.35	19.27	19.37
	$3d^3D$	−0.70	16.66	14.10	19.47	
Cl II	$3p^34s^1D$	−0.43	7.77	12.95	20.83	20.75
	$4p^3P$	−0.91	7.43	13.05	20.5:	
A II	$3p^44s^2D$	−0.14	10.76	14.00	21.42	
	$3p^43d^4D$	−0.84	11.15	14.56	21.18	21.45
	$3p^44p^2D$	−0.61	7.82	14.26	21.84	

* *Astrophysical Journal* (University of Chicago Press) **109**, 262, 1949.

number of atoms in the ionization stage $(s + 1)$ to the total number of atoms of that element for $T = 20{,}000°\text{K}$, $\log P_e = 2.90$; $\log NP_e$, and finally the abundance relative to oxygen. Errors in the measured line intensities together with uncertainties in the theoretical f values limit the attainable accuracy. We need good theoretical calculations of the absolute strengths for the observable transition arrays. It is evident that deviations from LS coupling and configuration interaction must be taken into account.

TABLE 11

ABUNDANCES OF LIGHT ELEMENTS IN γ PEGASI*

Ion	Log $N_{s+1}P_e$	$\delta \log N$	Log NP_e	Relative Number of Atoms
C II	21.09	0.08	21.17	0.05
N II	21.55	0.26	21.81	0.23
O II	21.61	0.85	22.46	1.00
Mg II	21.95	0.00	21.95	0.31
Al III	20.07	0.43	20.50	0.011
Si III	20.83	0.58	21.41	0.09
Si IV	17.45	3.93	21.38	
P III	18.65	0.84	19.49	0.0011
S II	21.45	0.02	21.47	0.04
S III	19.37	1.32	20.69	
Cl II	20.75	0.01	20.76	0.02
A II	21.45	0.02	21.47	0.10

* *Astrophysical Journal* (University of Chicago Press), **109**, 262, 1949.

Another calculation (carried out with the aid of a model atmosphere that reproduced the profiles of the Balmer lines) and in which the variation of the line and continuous absorption coefficients with optical depth were taken into account gave the relative abundances of O, N, and C as 1.0, 0.2, and 0.12. These results show that the effects of stratification cannot be neglected. The best possible atmospheric models are required, together with improved observational data. The situation with respect to γ Pegasi† and a number of other O and B stars should be greatly improved with the analysis of carefully calibrated high dispersion coude spectrograms recently secured at the Mount Wilson Observatory.

14. Excitation Temperatures of Stellar Atmospheres

In Sec. 1 of Chapter 6 we mentioned that in addition to the effective temperature and color temperature of a star (which is really not a temperature at all but a parameter in a representation of the stellar energy distribution by Planck's formula), we could define an ionization temperature and an excitation temperature. The ionization temperature reproduces the observed ratio of atoms in successive stages of ionization, whereas the excitation temperature is defined by the distribution of atoms among excited levels. More precisely, the excitation temperature is the parameter employed when Boltzmann's formula is used to represent the distribution of atoms among the excited levels. If the stellar atmospheres were in local thermodynamic equilibrium, the effective ionization and excitation temperatures would closely agree.

† Some complications may be introduced in γ Pegasi by its radical velocity variability (~ 8 km/sec) which places it among the variables of the β Canis Majoris type.

We may find the excitation temperature of the sun with the aid of the solar curve of growth. In 1934, C. W. Allen obtained an empirical curve with the aid of measures made at Canberra. Menzel and Unsöld independently derived correct theoretical curves respectively for the Schuster-Schwarzschild model and for the empirical Minnaert formula for r_λ,

$$\frac{1}{1 - r_\lambda} = \frac{1}{1 - r_c} + \frac{1}{n_0 \alpha_\lambda}$$

where n_0 is the number of atoms "above the photosphere" and r_c is the central intensity.

Let N_a denote the total number of atoms in a given ionization stage and N_j the number in an excited level, j. We suppose that N_j/N_a can be expressed by Boltzmann's formula, eqn. (1) of Chapter 4, with some excitation temperature T. Consider two lines, λ and λ', that arise from levels of excitation potential χ_i and χ_j respectively, and whose relative f values are known. Knowing the equivalent width of each line, we can read from the curve of growth the corresponding η_i and η_j. From eqns, (32), (145), and Boltzmann's formula (writing η_{0j} as η_j etc.) we find

$$\log \eta_j - \log \eta_i = \log \frac{\lambda' k f' g'}{\lambda k' f g} - \frac{5040}{T}(\chi' - \chi) \qquad (156)$$

where the primed and unprimed symbols refer to quantities connected with levels j and i, respectively. The first term on the right-hand side may be calculated for each line since the absorption coefficients, k and k', the statistical weights, g and g', and the f's are known. The coefficient for $1/T$ is known, and since we have $\log \eta_j - \log \eta_i$ from the curve of growth we can find the temperature. In practice we usually employ a number of lines whose relative f values are known and for which the excitation potential of the lower level differs from one group to another. We group the lines according to χ and solve for T by least squares.

Table 12 summarizes the results of a number of these investigations. Possible Fe I may give a higher excitation temperature than Ti I, but the result is not conclusive. Substantial differences seem to arise when

account is taken of the variation of the absorption coefficient with wave length and the data are analyzed with the Milne-Eddington rather than with the Schuster-Schwarzschild model.

TABLE 12

THE EXCITATION TEMPERATURE OF THE SUN

Authority	Reference	Fe I	Ti I	V I
R. B. King	(1)		4400°K	
Menzel, Baker	(2)	4150 ± 50°K	4350 ± 200	
and Goldberg	(3)		4400	
K. O. Wright	(4)	4900 ± 125	4550 ± 125°	
R. B. King and K. O. Wright	(5)			5400 ± 200°K
Goldberg and Pierce	(6)	4770	4640 ± 290	
A. R. Sandage	(7)			5110° ± 190°K

(1) *Ap. J.* **87,** 40, 1938; laboratory *f* values and Unsöld's curve of growth.
(2) *Ap. J.* **87,** 81, 1938; theoretical *f* values and curve of growth based on Schuster-Schwarzschild model.
(3) *Ibid.*, *J*-file sum rule for Ti I.
(4) *Ap. J.* **99,** 249, 1944; laboratory *gf* values, curve of growth based on Schuster-Schwarzschild model. Wright found it impossible to represent the Fe I and Ti I data with the same excitation temperature.
(5) *Ap. J.* **106,** 224, 1947; laboratory *f* values by R. B. King, curve of growth based on Schuster-Schwarzschild model.
(6) Based on laboratory *f* values and Milne-Eddington curve of growth calculated for the center of the disk with k_λ variation taken into account. From lines with an excitation potential from 3–5 volts, the excitation temperature is 6000°K.
(7) *Ap. J.* **111,** 575, 1950; the effect of the temperature gradient in the solar atmospheres was investigated by constructing a theoretical curve of growth from line profiles calculated with the aid of Münch's model atmosphere.
More recently, A. R. Sandage and A. J. Hill (*Ap. J.* **113,** 525, 1951) have derived the excitation temperature from Cr I lines with laboratory *gf* values. They find T_{excit} = 3790°K, which is considerably lower than determinations from other elements.
Minnaert predicts that excitation temperatures determined by the usual methods from faint lines should vary between 5200°K and 6700°K according to the atomic levels compared.
For a summary of temperature determinations from molecules see J. Hunaerts, *Ann. d'Ap.* **10,** 237, 1947.

The excitation temperatures tend to fall below the effective temperatures in *F* and *A* stars as well as in the sun. For example, Sirius whose effective temperature is about 10,000°K, has an ionization temperature of about 8700°K, and an excitation temperature of 6000–7000°K. K. O. Wright's very careful discussion of the supergiant α Persei suggests that different elements have different excitation temperatures and that the ions show a lower temperature than do the neutral atoms. In supergiant atmospheres such stratification may be perhaps anticipated.

Molecular bands sometimes prove useful for excitation temperature determinations. Two methods are used: (a) a comparison of different vibration bands of the same band system; (b) a comparison of individual rotational lines of a given electronic vibration band.

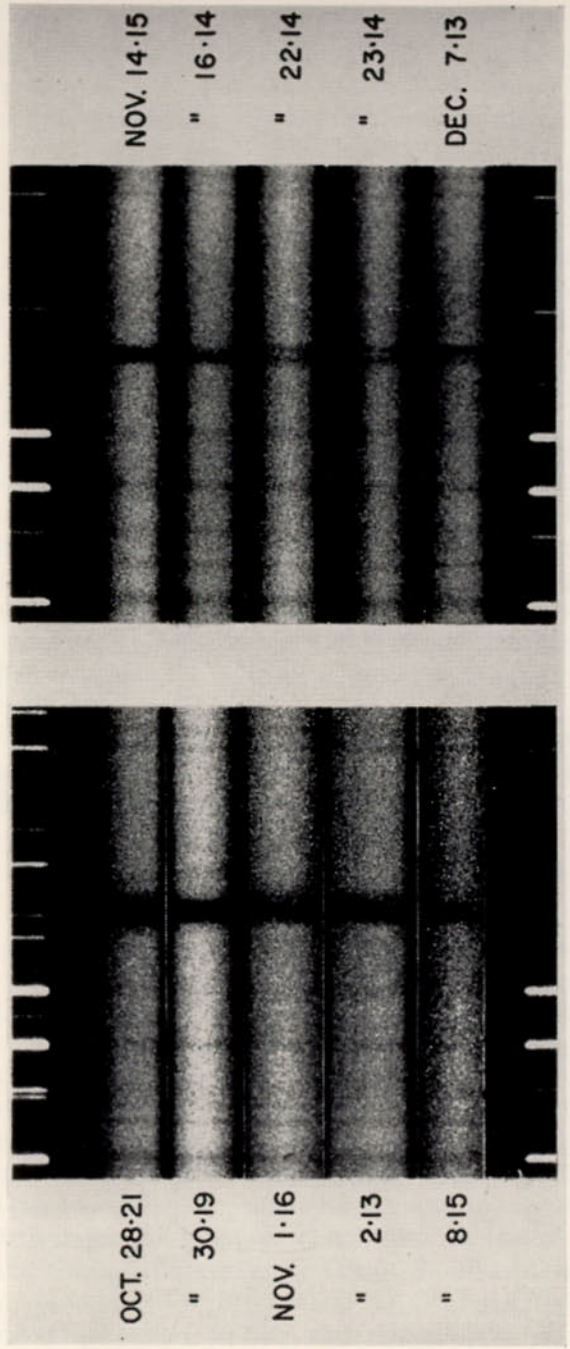

FIG. 14.—STRUCTURE IN THE CHROMOSPHERIC *K* LINE DURING THE EGRESS OF THE 1951 ECLIPSE OF 31 CYGNI

Shortly after the end of the geometrical eclipse the *K* line showed a broad bell-shaped profile which gradually narrowed until the line finally became resolved into two components whose total and relative intensities changed in an erratic fashion as the light from the *B* star passed through varying thicknesses of absorbing gases in the extended chromosphere of the *K*-type supergiant. (Courtesy, Andrew McKellar and Graham Odgers, Dominion Astrophysical Observatory, Victoria, B. C.)

With the dispersions ordinarily applied in stellar spectroscopy, the component lines of an individual band are not resolved and method (a) is the only one available. For bands of low intensity,

$$W_\nu(v'' - v') = N_0 \frac{\pi e^2}{mc} f(v'' - v') \frac{e^{-E''/kT}}{\sum e^{-E''/kT}} \tag{157}$$

where the energy of the low vibrational level $E(v'')$ is given by eqn. (22) of Chapter 2. The transition probability $f(v'' - v')$ has been calculated by Hutchisson for symmetric molecules such as C_2, and the formulae are still qualitatively applicable to molecules such as CN which are almost symmetrical. They are not valid, however, for molecules such as CH, TiO, ZrO, etc., in which the component atoms have appreciably different masses. McKellar and Buscombe determined temperatures of the carbon *R*-type stars from the relative intensities of C_2 and CN vibration bands of the same sequence. They employed both the Hutchisson theory and laboratory f values, and found temperatures in good accord with values inferred from the colors of these stars. The approximation that the band absorption is proportional to the number of absorbing molecules seems to be reasonably good for bands of moderate intensity for which McKellar estimates the equivalent widths of the individual lines to be about 0.1A.

Method (b) may be employed with high dispersion material such as is obtainable for the sun. If the bands are weak, the intensities of the individual rotational components will be

$$W_\nu(J) \sim N_0 \left(\frac{\pi e^2}{mc}\right) f(J) \frac{g(J) e^{-E(J)/kT}}{B(T)} \tag{158}$$

where $f(J)$, the f value for a line characterized by J, is known from theory, $E(J) = BJ(J + 1)$ is the energy of level J, $g(J) = 2J + 1$ is its statistical weight, and $B(T)$ is the partition function of the molecule $\Sigma g(J) e^{-E(J)/kT}$. Since B, F, and E are all known, measures of equivalent widths as a function of J will permit a determination of the excitation temperature. Physicists and chemists have employed this method to find the temperatures of arcs, flames, and glow discharges. In practice the method is applicable only when high dispersion data are available, e.g., in the case of the sun, where Birge found an excitation temperature of 4300°K from the intensity distribution in one of the solar λ3883 cyanogen bands. More recently (1940), L. Blitzer, from measures of 14 doublets in the (0–0) *R* branch of the CN band, found an excitation temperature of 4490 ± 100°K, while Miss Adam from a study of the C_2 Swan band found 4550°K. Roach obtained 4640 ± 550°K from the OH band.

J. Hunaerts determined the excitation temperature and the abundance of molecules of CN, CH, C_2, NH, and OH in the solar atmosphere from the equivalent widths of the lines of CN, CH, and C_2 and from the calibrated Rowland intensities of lines of NH and OH. He constructed curves of growth and analyzed the data with the Schuster-Schwarzschild model. The resultant excitation temperature, in the neighborhood of 4500°K, is in good accord with the value derived from the atomic lines.

15. Some Problems of the Curve of Growth—Turbulence

The curve of growth consists of three parts, the Doppler part wherein the equivalent width W is proportional to Nf, the flat portion where W increases slowly with Nf, and the damping part where W grows as $\sqrt{Nf\Gamma}$. For a star like the sun we adopt a most probable kinetic velocity, v, on the basis of its effective temperature, calculate $\log \frac{Wc}{\lambda v}$ and plot it against $\log \eta_0/N$. We then try to fit the empirical curve to the theoretical curve by a horizontal shift, a procedure that is usually satisfactory for main-sequence stars like the sun.

Struve and his co-workers found that the empirical curves derived for giants would not fit the theoretical curves unless one supposed that v was much larger than the effective temperature of the star would suggest. The curves of growth for 17 Leporis (T_e = 10,000°K), and ε Aurigae (T_e = 6500°K) resemble the theoretical curves, except that the values of v indicated would correspond to kinetic temperatures of 30,000,000°K and 2,000,000°K. Thus, either the kinetic temperature of the gas is unaccountably high or there is a large-scale motion of the gas; the latter effect is often called turbulence. The kinetic temperature v would be replaced by V defined by:

$$V^2 = \left(\frac{2kT}{M}\right) + \xi^2 \tag{159}$$

where ξ is interpreted as the turbulent velocity, the actual speed of large jets or masses of the gas. Struve found ξ to be 67 km/sec for 17 Leporis, and 20 km/sec for ε Aurigae. The line profiles lend further support to the idea that large bodies of gases in these stellar atmospheres are moving with speeds much greater than the thermal motions of the atoms themselves. The weak lines are broad and shallow. The strong lines, unlike those in dwarf stars, show no wings but are bell-shaped.

The spectrum of δ Canis Majoris presents difficulties of another type. From the conventional curve of growth, Miss Steel found a turbulent velocity of about 5 km/sec, while Struve points out that the profiles of the strong lines require a turbulent velocity of 30 km/sec. In the spectrum of η Aquilae, M. and B. Schwarzschild and W. S. Adams find a turbulent velocity of 4 km/sec from the curve of growth, whereas the line profiles give a turbulent velocity of 12.2 km/sec, if we interpret the broadening as arising from large scale gas motions and not from rotation. What are the reasons for these discrepancies? In stars such as 17 Leporis, the individual moving elements of gas are probably small compared with the mean free path of a light quantum, i.e., small compared with the depth of the photosphere. Hence masses of gas moving with different velocities absorb at different distances from the center of the line and a broadened profile and increased equivalent width results. On the other hand, in the atmosphere of a star such as the Cepheid, η Aquilae, Schwarzschild suggests that the linear dimensions of the turbulent elements exceed the depth of the effective photospheric layers. The profile is broadened but the equivalent width is not increased. The apparent increase of ξ with W in δ Canis Majoris remains puzzling, however.

Wrubel has recently discussed the influence of the turbulence spectrum upon line profiles and the curve of growth. A large variety of eddies occur simultaneously. The velocities characteristic of the small eddies (whose diameters are less than the thickness of the layers responsible for the absorption lines) will fix the turbulent velocity found from the curve of growth, whereas the line profile may reflect the velocities of larger masses in the atmosphere. Wrubel found that the difference between the turbulent velocities obtained from the curve of growth and those obtained from the line profiles suggested that much energy is stored in large eddies, that are of a size about 2.5 times the thickness of the layers responsible for the absorption lines. Possibly the turbulence is nonisotropic. From measures of the equivalent widths and central intensities of faint lines close to the limb, C. W. Allen concluded that there exists in the solar atmosphere a large-scale nonisotropic turbulence with a vertical velocity of about 1.7 km/sec and a horizontal velocity of about 2.8 km/sec.

Su Shu Huang and Struve have used the relation between equivalent widths and half-widths of absorption lines to derive turbulent velocities for both large and small eddies.*

As Struve emphasizes, the proper study of line intensities in stellar spectra should utilize, insofar as possible, the profiles of the lines as well as their total intensities. In this connection we may refer to the investigation by Spitzer, who studied the broad asymmetrical lines in certain M-type supergiants. In these stars the continuum cannot be located and we must work with the line shapes themselves, which would

* *Ap. J.* **112**, 410, 1952.

give values of V corresponding to enormous temperatures, but here again the concept of turbulence permits a rational explanation of the observations.

Supergiant atmospheres show complications other than turbulence. Thus, K. O. Wright found indications that in the atmosphere of α Persei, the lines of neutral metals, which seemed to show greater damping con-

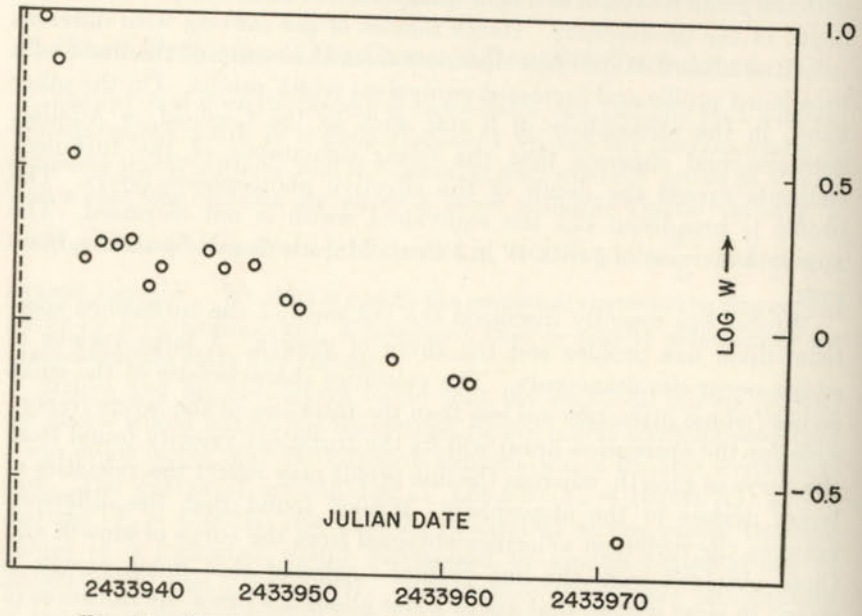

FIG. 15.—CHANGES IN INTENSITY OF THE CHROMOSPHERIC K LINE DURING THE EGRESS OF THE 1951 ECLIPSE OF 31 CYGNI

The logarithm of the equivalent width of the K line, as measured upon plates secured at the University of Michigan Observatory, is plotted against the Julian date. Note the rapid decline after the end of the geometrical eclipse (October 14, 1951) and the subsequent fluctuations. The K line became very weak about November 21 (J.D. 2433971) (compare Fig. 14) and subsequently became stronger before disappearing. The density of the absorbing gas is estimated to be comparable with that found in the lower strata of the solar corona.

stants and excitation temperatures than those of ionized metals, were formed in deeper layers than were the lines of the ionized metals.

Probably our best clues to the structure of supergiant atmospheres will come from studies of eclipsing systems such as ζ Aurigae or 31 Cygni, where a K supergiant eclipses a B-type companion, or VV Cephei where an M supergiant hides a much smaller F star. Olin Wilson finds that the density gradient in the atmosphere of ζ Aurigae is much less steep than the hypothesis of hydrostatic equilibrium would predict. In other words, the atmosphere of the giant K star cannot be in mechanical equilibrium

at its effective temperature. From curves of growth constructed for different levels of the atmosphere, Wilson finds some evidence for an increase of turbulence with height, but the increased turbulent velocities themselves do not suffice to support the distended atmosphere as McCrea had suggested long ago for the solar chromosphere. Evidently we must discard the picture of an atmosphere in static equilibrium and adopt in its stead some kind of a dynamical picture. The behavior of the chromospheric K line in the K-type component of 31 Cygni illustrates this point. As the B star emerges from eclipse, the wings of the K line produced in the chromosphere of the cool star rapidly weaken and the line shows a square profile corresponding to a turbulent velocity of about 20 km/sec. As the line further weakens it shows a structure consisting sometimes of a single line, at other times of a line and a companion of variable intensity and velocity displacement. The equivalent width of the main component varies irregularly. Probably the extended atmosphere of the giant star consists of a multitude of prominences in more or less rapid motion with respect to one another.

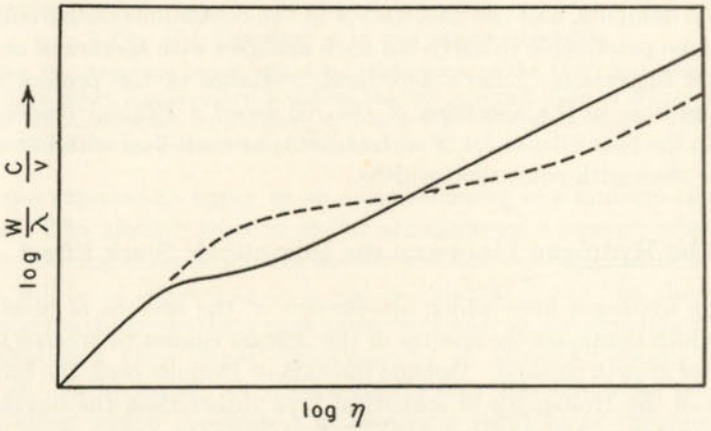

FIG. 16.—SCHEMATIC CURVES OF GROWTH FOR GIANTS AND DWARFS

In the (dashed) curve of growth for the giant, the flat portion is raised by turbulence but the damping constant is small. In the (solid) dwarf curve, turbulence is small but damping is large.

Generally, we expect the curves of growth for giants and dwarfs to differ as shown in Fig. 16. In the giants, turbulence often raises the flat portion, although the damping constant may remain comparable with the classical damping constant, γ, because of the low density. In dwarfs, on the other hand, the flat portion frequently corresponds to a kinetic temperature close to the effective temperature, while the damping portion requires a Γ much greater than γ.

The uncertainty in the damping constant introduces corresponding uncertainties in abundances derived from strong lines. Furthermore, in the best determined curves of growth there are small but significant departures from the theoretical curve.

L. Goldberg and K. Pierce and also K. O. Wright have found that the damping portion of the curve of growth rises more steeply than $\sqrt{N}$, as though Γ increased with the intensity of the line. Also, damping constants determined from lines arising from the high levels were systematically larger than those found from resonance and low level lines.

In the analysis of the later type stars, difficulties arise because of blends and uncertainty in locating the continuum. For the study of such spectra, Pannekoek and van Albada suggest that instead of estimating the blends of each line, one should calculate the theoretical intensities of all lines and then combine them to form synthetic blends. The intensity of each blend appears as a function of 6 parameters, the mean absorption coefficient, the temperature, the degree of ionization, the Doppler width (thermal motion plus turbulence), resonance plus collisional damping, and the uncertainty in the continuous background. It would be practicable to carry out such analyses with spectra of only the highest dispersion. Liller's and Lewis's studies of the profiles of the calcium lines in the spectrum of the *K*0 dwarf ε Eridani demonstrate that in the near ultraviolet of such objects one must deal with line shapes rather than with equivalent widths.

16. The Hydrogen Lines and the Interatomic Stark Effect

The hydrogen lines which are present in the spectra of most stars and which dominate the spectra of the *A* stars cannot be treated by the curve of growth method. Outside the narrow Doppler core, the broadening is of the Holtsmark or statistical type rather than the discrete-encounter type. Neighboring ions and electrons may produce strong momentary electric fields which disturb the hydrogenic energy levels and result in an increased absorption coefficient in the wings. These interatomic fields are distributed at random in direction and time and may fluctuate over a considerable range in a short time.

In 1913 Stark showed that when a field of the order of 10^5 volts/cm is applied to incandescent hydrogen, the Balmer lines split into a number of components. Lo Surdo, soon thereafter, observed the splitting of lines emitted in the cathode dark space of the discharge tube. The change in energy of a given level is expressible by an equation of the form

$$\delta T = aE + bE^2 + cE^3 + \cdots \tag{160}$$

If δT is measured in c.g.s. units and E in electrostatic units, the value of the first order Stark coefficient will be

$$a = \frac{3h^2}{8\pi^2 m\varepsilon} n(n_2 - n_1) \tag{161}$$

where n is the total quantum number and n_1 and n_2 may assume values from 0 to $n - 1$. If E is measured in kilovolts/cm, and λ in cms, the shift in wave length will be

$$\delta\lambda = 0.0643\lambda^2[n(n_2 - n_1) - n'(n_2' - n_1')]E \tag{162}$$

Notice that the number of components and the absolute value of the Stark splitting increases with higher members of the series.

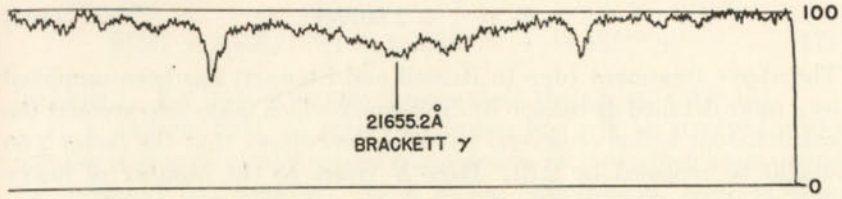

FIG. 17.—BRACKETT γ IN THE SOLAR SPECTRUM

Notice the extremely broad wings and shallowness of the (4–7) hydrogen transition. Stark effect is pronounced and since the line is formed close to the mechanism of local thermodynamic equilibrium, it has a high central intensity. (McMath-Hulbert Observatory, University of Michigan.)

These expressions apply to an atom radiating in a uniform constant field E. The electric fields in stellar atmospheres, however, arise from rapidly moving charges and are neither uniform nor constant with time. What will be of interest to us in the calculation of the line absorption coefficient is the probability that perturbations from surrounding charges will displace a given Stark component by an amount between $\delta\lambda$ and $\delta\lambda + d\lambda$. In hydrogen, we need consider only the first order or linear Stark effect which produces a symmetrical splitting of the line. We shall be particularly interested in the large shifts which determine the absorption in the wing. Within a sphere of radius R, let there be K charged particles. The probability of finding all K of these within a radius r is, of course,

$$\left[\frac{4\pi}{3} r^3 \Big/ \frac{4\pi}{3} R^3\right]^K$$

and the probability that no one of the K charged particles lies within the sphere of radius r is $[1 - (r/R)^3]^K$. Then the probability that at least one of the K particles falls within the sphere of radius r is

$$p = 1 - \left[1 - \left(\frac{r}{R}\right)^3\right]^K \sim 1 - \exp\left(-\frac{4\pi}{3} Nr^3\right)$$

where we have compared the expansions $(1 - x)^n$ and e^{-xn} and have noticed that

$$\tfrac{4}{3}\pi R^3 N = K$$

where N is the number of perturbing charges/cm^3. Hence the probability that at least one particle falls in the shell r to $r + dr$ is found by differentiation:

$$dp = e^{-y}\, dy \tag{163}$$

where

$$y = \left(\frac{r}{r_0}\right)^3 \quad \text{and} \quad \frac{4\pi}{3} r_0^3 N = 1 \tag{164}$$

determine the mean separation r_0 of the two perturbing particles. The "average" field corresponding to the distance r_0 will be

$$E_0 = \frac{\varepsilon}{r_0^2} = 2.60\varepsilon N^{2/3} \tag{165}$$

The above treatment (due to Russell and Stewart) has been amplified by a more detailed discussion by Holtsmark which takes into account the simultaneous action of several particles, and shows that the factor 2.60 should be replaced by 2.61. Here N refers to the number of heavy charges (ions); the contributions from the electrons to the observable line profile usually have been neglected.* We find

$$E_0 = 46.8\left(\frac{P_i}{T}\right)^{2/3} \tag{166}$$

where the ionic pressure P_i is expressed in dynes and E is given in electrostatic units. Under most circumstances the ionic pressure P_i will equal the electron pressure P_e.

A charged particle approaching a distance r from the atoms produces a displacement of the mth Stark component,

$$\Delta\nu = a_m E = \frac{C_m}{r^2} \tag{167}$$

* Outside of the Doppler cores of the lines, the chief cause of broadening is the statistical action of the ions: radiation damping can be neglected. The electrons, however, act according to the collision damping theory, since they move so rapidly. Hence the statistical, steady-field, Holtsmark theory cannot be applied to them. Our present theory of Stark broadening is inexact in that the action of the electrons is not taken into account. G. Odgers, *Ap. J.* **116**, 444, 1952, suggests that the electrons may contribute noticeably to the broadening of Hγ at large distances ($\sim$ 20A) from the line center and that the Holtsmark probability distribution overestimates the effects of large fields. From a comparison of the observed and computed profiles of Hγ in the late *O* stars, σ Orionis and 10 Lacertae, Ann Underhill, *ibid.*, p. 446, suggests that the theory tends to give too narrow profiles. Margaret K. Krogdahl finds that modifications of the Holtsmark theory are required for Hα, Hβ, and Lyman α. Happily a quantitative experimental check has been made by Jurgens who finds that the outer parts of the line profiles fit the Holtsmark theory very well indeed. The centers of the lines are broadened by other processes as theory predicts they should.

In particular a field E_0 will produce a shift

$$\Delta\nu_0 = \frac{C_m}{r_0^2} \tag{168}$$

where

$$\frac{\Delta\nu}{\Delta\nu_0} = \frac{\Delta\lambda}{\Delta\lambda_0} = \frac{r_0^2}{r^2} = \frac{E}{E_0} = \beta \tag{169}$$

Hence the statistical probability of a displacement $\Delta\lambda$ of a certain component is found from eqns. (163) and (169) to be

$$W(\beta) = \tfrac{3}{2}\beta^{-5/2} \exp\left(-\beta^{-3/2}\right) \tag{170}$$

or, more precisely, in accordance with the exact Holtsmark theory,

$$W(\beta) = 1.496\beta^{-5/2}(1 + 5.106\beta)^{-3/2} + 14.43\beta^{-3} + \cdots \tag{171}$$

for large β. For small β we may use the exact theory (cf. Table 13).

In a uniform field, E_0, every hydrogen line will be resolved into a number of symmetrically spaced components, each of which has a unique displacement $\Delta\lambda_0(n_1 n_2 n_1' n_2')$. In a stellar atmosphere, each of these components will be spread out into a broadened distribution about the static field position, $\lambda_0 + \Delta\lambda_0(n_1 n_2 n_1' n_2')$. The final absorption coefficient will be proportional to the properly weighted sum of the individual curves. Our chief interest is in the wings of the line, which at least for the Balmer series, are produced by momentary fields corresponding to β values much greater than 1. When we sum over the components of a Balmer line, we may write the asymptotic form of the absorption coefficient per atom as

$$\alpha(\Delta\lambda) = c_n E_0^{3/2} (\Delta\lambda)^{-5/2} = 321 c_n \frac{P_e}{T} (\Delta\lambda)^{-5/2} \tag{172}$$

where c_n has to be found by the theory of the Stark effect. We tabulate the c_n values for the first four Balmer lines from the work of Verweij, and the f values according to Menzel and Pekeris:

Line	Hα	Hβ	Hγ	Hδ
$c_n \times 10^{16}$	3.15	0.887	0.446	0.322
f	0.6408	0.1193	0.04467	0.02209

A somewhat superior formula may be obtained by including the next term in the asymptotic expansion. Recently, Miss Underhill has calculated the profile of $H\gamma$ in *O* stars, where she finds that the shape of the line is determined mostly by thermal Doppler effect, by radiation and

collision damping of the dispersion type, and by turbulence if any exists. Stark effect is dominant, however, for main-sequence stars cooler than 25,000°K.

TABLE 13

THE HOLTSMARK FUNCTION $W(\beta)$*

β	$W(\beta)$	β	$W(\beta)$	β	$W(\beta)$
0	0.00	2.0	0.339	6.0	0.024
0.5	0.095	2.5	0.257	8.0	0.0105
1.0	0.271	3.0	0.166	10.0	0.0055
1.5	0.364	4.0	0.080	15.0	0.0019

* From Verweij, *Pub. Astron. Inst. Amsterdam* No. 5.

The confluence of the lines near the limit of the Balmer series shows the influence of the Stark effect. The hydrogen lines gradually coalesce toward the higher series members and, for some maximum value of n, they will cease to be distinguishable from one another. The intermolecular Stark effect widens the lines until they overlap and cannot be resolved with any spectrograph. Between the last resolvable line whose quantum number is n_m and the series limit, the spectrum looks continuous. Inglis and Teller showed that n_m was related to the number of broadening charged particles per cm^3 by the relation

$$\log N = 23.26 - 7.5 \log n_m \tag{173}$$

For T less than $10^5/n_m$, N denotes the number of ions plus electrons, whereas for T greater than $10^5/n_m$, N denotes the number of ions only, since the electrons move too rapidly to contribute to the line broadening appreciably. Struve and Unsöld demonstrated the usefulness of this criterion in distinguishing giants and dwarfs. In the dwarf atmospheres, the electron and ion densities are much greater than in giant atmospheres, and therefore n_m is smaller.

Example: In the spectrum of 10 Lacertae, Struve has listed the Balmer lines up to $n = 14$. By eqn. (173) $\log N = 23.26 - 7.5 \times 1.15 = 14.63$. Since $T = 29{,}600°\text{K} > 10^5/n_m$ for this star, N here refers to the number of ions. This gives us an upper limit to the electron and ionic density as we cannot be sure that some kind of turbulence does not enter to widen the lines, and cause n_m to be smaller than it should be.

In the spectrum of χ Orionis, n_m is about 23. The temperature of this star is 20,400°K. Hence $\log N_e = \log N_i = 23.26 - 7.5 \times 1.36 = 13.06$, and the corresponding electron pressure, computed from $P_e = N_e kT$ is 32 dynes, much smaller than for a main-sequence star of the same spectral class.

With the aid of eqn. (172) we may compute the profile of a hydrogen line provided we know the variation of T, P_e, $\bar{k}$, and k_λ with optical depth. As Verweij, Miss Underhill, and others have pointed out, we cannot reproduce the observed profiles if we assume an atmosphere of constant density and temperature.

The line absorption coefficient per gram of stellar material will depend on the number of hydrogen atoms in the second level, $N_{0,2}$. From eqn. (14) of Chapter 4

$$\log \frac{N_1}{N_{0,2}} = -3.38\theta + 2.5 \log T - 1.08 - \log P_e \tag{174}$$

In a B-type star, the number of hydrogen ions N_1 will equal the number of hydrogen atoms, since hydrogen is nearly all ionized. For a numerical application let us consider Hδ and suppose that the number of hydrogen atoms per gram of stellar material is 4.19×10^{23}. When numerical values are introduced with the aid of eqns. (172) and (174), the absorption coefficient in the wing of Hδ will be

$$\log l_\lambda = \log N_{0,2}\alpha_\lambda + 2 \log P_e - 3.5 \log T + 3.38\theta - 2.5 \log \Delta\lambda - 10.72 \tag{175}$$

The variation of T, P_e and the continuous absorption coefficient k_λ will depend on the atmospheric model. As an illustration let us consider a star with a boundary temperature $T_0 = 16{,}800°\text{K}$ and calculate profiles for assumed $\log g = 3.50$, 3.80, and 4.10.* We calculate η and then use the methods of Sec. 9 to derive $r(\lambda)$. To fit the center of the profile, we may determine ε empirically, as has been done in Table 14 which compares the observed profiles of Hδ in γ Pegasi with one calculated by eqn. (88). Actually ε should be close to 1; the smaller empirical value implies that the boundary temperature is probably much lower than we have assumed. The agreement seems best for $\log g = 3.80$, although a slightly higher g and temperature seem possible.

A more rigorous treatment, which would be indicated for stars of higher temperature and lower surface gravity would require an analysis similar to that given by Miss Underhill for Hγ in the O stars.

Verweij employed Pannekoek's model atmospheres to make extensive calculations of Stark broadening. The calculated profiles are sensitive to surface gravity; a g value low enough to represent the cores of the lines gives a poor prediction for the wings. Out to about 5A from the line center in the A dwarfs, the Verweij theory predicts a wider core than is actually observed and the observed wings are broader than the

* *Ap. J.* **109**, 244, 1949. The atmospheric model given there in Table 7 for $\log g = 3.80$ has been substantiated by the calculations by Miss McDonald who finds an over-all variation in the flux $\mathfrak{F}$ of about 5 per cent in the range of optical depth 0.2 to 2.0.

calculated ones. Noncoherent scattering may account for some of the discrepancy.

The profiles of the Balmer lines in supergiant stars suggest absurdly low surface gravities as though the atmospheres of these stars are not in hydrostatic equilibrium.

TABLE 14

COMPARISON OF OBSERVED AND COMPUTED HYDROGEN LINE PROFILES IN γ PEGASI*

$\Delta\lambda$	Observed r	Computed r		
		Log g = 3.50	= 3.80	= 4.10
0	0.38	0.38	0.38	0.38
1	0.51	0.52	0.49	0.47
2	0.62	0.64	0.58	0.56
3	0.70	0.74	0.67	0.64
4	0.76	0.81	0.75	0.71
6	0.85	0.89	0.85	0.81
8	0.90	0.94	0.90	0.88
10	0.94	0.96	0.94	0.93

* *Astrophysical Journal* **109**, 244, 1949.

17. The Helium Lines in Stellar Spectra

Helium, as well as hydrogen, exhibits the Stark effect in stellar spectra. With fields of 15–25 kilovolts/cm, certain lines such as λ4713.3, λ4437.5, and λ3613.6 show the quadratic Stark effect. Collision damping by electrons produces the broadening, and we may apply the considerations of Sec. 4 of Chapter 8. With the aid of eqns. (9) and (11) and the collision parameter $\eta_0 = 0.64$ (appropriate for $n = 4$), we find

$$\Gamma = 38.8C^{2/3}V^{1/3}N_e \qquad (176)$$

where C is found from the quadratic Stark coefficient for the line. The ordinary curve of growth analysis then permits the determination of the number of atoms/gram acting to produce the line (see Table 15).

The behavior of the strong lines of the diffuse subordinate series $2^3P - n^3D$, $2^1P - n^1D$ is much more complicated. The fluctuating interatomic fields ($10^3 - 10^4$ volts/cm) cause a displacement of these lines to the red, the shift being small for early members of the series and large for the later members. The electric fields cause the appearance of lines forbidden by ordinary selection rules, e.g., $2p - 4f$, $2p - 5f$, etc., which fall to the violet of the diffuse series lines.

Many years ago Struve noticed that λ4471($2^3P - 4^3D$) was flanked by the forbidden line, λ4469.9($2^3P - 4^3F$), in the spectra of certain B

TABLE 15

HELIUM LINES IN γ PEGASI

Level	λ	W	Log Γ	a	Log N_r	Log $N(2^3P)$
2^3P	4713.3	0.255	10.19	0.064	15.99	15.99
2^1P	4437.5	0.123	10.91	0.32	15.56	16.11
2^1S	3613.6	0.059	11.46	0.92	15.01	15.88
					Mean =	16.00

Column (1) gives the lower level of the line listed in the second column. W denotes the equivalent width in angstroms. The fourth column gives log Γ computed from eqn. (176) and the fifth column gives a, defined in eqn. (31). Column 6 gives log N_r where N_r is the number of atoms in the lower level. In the last column these numbers are reduced to the number in the 2^3P level at 20,000°K by Boltzmann's equation. From the mean value of log $N(2^3P)$, eqn. (14) of Chapter 4 and the assumption that hydrogen is the most abundant gas in the atmosphere, we find a H/He ratio of about 25.

stars. This line appears in the laboratory discharge tube when the electron density is appreciable. Simultaneously the $p - d$ lines are broadened while others are unaffected. Since the stellar helium lines showed the same behavior, Struve concluded there was good evidence for an interatomic Stark effect arising from charged particles. Subsequent work by Goldberg, Foster and Douglas, Unsöld, Mrs. M. K. Krogdahl and Struve has confirmed this idea.

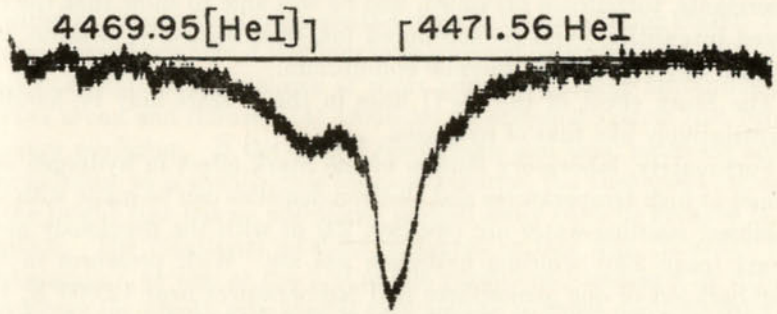

FIG. 18.—TRACING OF λ4471 IN γ PEGASI

Notice the forbidden λ4469.95 component in the violet wing of the $^3P - {}^3D$ transition. (Courtesy, McDonald Observatory.)

The laboratory experiments of J. S. Foster showed that with increasing electric field strength, the permitted λ4471($2^3P - 4^3D$) line shifts to the red, while λ4470 is displaced to the violet. The intensity of the latter grows with increasing field strength at the expense of λ4471, until at fields of 100 kev/cm it approaches equality with λ4471. For fields less than 15 kev/cm, the Stark effect is quadratic, whereas for fields

greater than 15 kev/cm the effect is linear. Thus, λ4471 displays "discrete" collisional broadening (quadratic Stark effect) plus Doppler broadening near the line core, and statistical Holtsmark broadening in the wings where the linear Stark effect prevails. The wave length of the stellar forbidden helium line λ4469.92 corresponds to a vanishingly small field strength when the line is produced in a static laboratory field. To match the observed stellar intensity, an appreciable static field would be required and this field would shift the line appreciably in position. In other words, the stellar line appears at the zero static-field position but with an intensity that corresponds to an appreciable static field strength. The answer seems to be that in an ionized gas where the electrostatic field comes from the ions and free electrons, its effect on the energy levels differs from that of a static laboratory field. In contradiction to what is observed in the laboratory, the space between λ4470 and λ4471 tends to be filled because of the broadening effects of collisions, as Struve pointed out in 1938.

Recently, Mrs. Krogdahl has given a quantum mechanical treatment of the collisional broadening of helium lines by proton encounters. She has shown that when the broadening is produced by the interatomic fields, a zero displacement of the λ4470 component is to be expected.

Some years ago, Goldberg discussed the behavior of the He I absorption lines in the *B* stars with the aid of the curve of growth. He assumed that in dwarfs, Stark effect broadened the lines whereas in the supergiants, turbulence prevailed, and he was able to show that the observed intensities could be accounted for, quantitatively, without any need for deviations from thermal equilibrium.

The Stark effect of the He II lines in the *O* stars may be handled quantitatively like that of hydrogen.

Fortunately, laboratory studies of the Stark effect in hydrogen and helium at high temperatures and electron densities can be made with the stabilized whirling-water arc (see Sec. 23) or with the previously mentioned (page 236) whirling hydrogen gas arc. With pressures in the neighborhood of one atmosphere and temperatures near 12,000°K, the electron density is in the neighborhood of 8×10^{16} electrons/cm^3 and the broadening produced by the interatomic fields is enormous. Only the first six or seven members of the Balmer series are visible, the higher members are smeared out. The spectrum recalls that of a white dwarf star, except that in the latter the broad hydrogen lines are observed in absorption. The experimenters employ the broadened profiles of Hα or Hβ to estimate the electron densities in the arc; from measures of the absolute line intensity they then derive the temperature by the Saha equation. G. Jürgens has made a quantitative test of the Holtsmark theory for the Stark broadening of lines from Hα to Hδ. W. Lochte-Holtgreven and W. Nissen examined the applicability of the Inglis-Teller equation (173). As long as n_m exceeds seven this equation gives the right order of magnitude although it seems to give too few electrons by a factor of about 2 at the densities they employed ($N_e \sim 10^{16}$). They suggest that the term 23.26 be replaced by 23.46.

Using a discharge tube filled with helium and with a small trace of hydrogen present, it has been possible to study quantitatively the broadening and shifting of helium lines as well as the appearance of forbidden components. The profiles and intensities of the hydrogen lines serve to fix the temperature and the electron density.

18. Stellar Rotation

The spectral lines in many early-type stars are broad and diffuse. For example, among the *A* stars the lines in α Aquilae or α Piscis Austrini are fuzzy compared with the lines in α Lyrae or α Canis Majoris. The reasons for believing these lines to be washed out by rapid axial rotation are: (1) The line widths are proportional to wave length which suggests a Doppler origin to the broadening, i.e., the observed line shape represents the superposition of line profiles from different parts of the disk of a spinning star. At longer wave lengths, the lines become wider and shallower and lines which are normally strong may even become practically invisible. Thus Shajn found the strong visual Fe II lines to be "washed out" in the spectrum of α Aquilae. (2) The relative intensities of lines in multiplets are the same as in nonrotating stars. This relation would not hold if the lines were widened by turbulence. (3) The lines in spectroscopic binaries of short period and large amplitude are always broad and diffuse. (4) Consider an eclipsing system just before primary minimum. If the orbital revolutions and axial rotations are in synchronism, as is usually true for close binaries, the uneclipsed segment of the bright star has an additional motion away from us because of its rotation. The rotational motions measured in this way (Rossiter and McLaughlin), as well as the line profile variations (discussed by Struve and Elvey for Algol), give speeds very similar to those deduced from an analysis of the broadened lines outside of eclipse.

The measured velocities usually range up to 250 or 300 km/sec, while speeds as high as 400 or 500 km/sec are found in stars such as ϕ Persei. The corresponding kinetic energy of rotation,

$$E = \tfrac{1}{2}K^2\omega^2M$$

where K is the radius of gyration, ω is the angular velocity, and M is the mass, is of the order of 10^{47} ergs. This quantity is comparable with the total amount of radiant energy stored within the star.

Main-sequence stars of spectral classes O, B, A, and early F show the largest rotations; the late F's rotate slowly, and in the G's rapid rotation occurs only in spectroscopic binaries. Supergiants of all types and normal giants of type F and later never show rapid rotations. The space velocities of the stars are not correlated with their rotational speeds; the axes appear distributed at random.

To deduce the rotational velocity from the broadened profile, Struve and Elvey supposed that the intrinsic profile radiated by a small area of the surface is essentially the same as that emitted by a nonrotating star of the same spectral class and luminosity. Each element of the surface radiates a profile $r_i(\lambda - \lambda_0)$ shifted by the Doppler effect from the undisplaced position by an amount $v\lambda/c$. The resultant profile,

$$r_\lambda = \int\int r\left(\lambda - \lambda_0 \pm \frac{v}{c}\lambda\right) dx\, dy$$

is obtained from an integration over the entire disk of the star. Now v is a function of x and y, and reaches its maximum, v_r, when $y = 0$ and x is the radius of the star. For a constant x, the component of the rotational velocity in the line of sight is constant. Hence it suffices to divide the apparent disk of the star into a number of vertical strips and sum over a set of displaced profiles, each multiplied by the area of the appropriate strip. For each trial rotational velocity a profile is constructed and compared with the observed profile. The excellent agreement between the observed and computed profiles strongly suggests that the diffuse lines in η Orionis, α Aquilae, α Virginis, α Piscis Austrini, and other such stars are broad because of rapid axial rotation. Carroll has shown that both the rotational velocity, v, and the true profile can be deduced from the measured profile since the rotationally distorted line retains certain features of the undisturbed profile.

Struve points out that the centrifugal force at the surfaces of certain of these spinning stars approaches that of gravity, a fact which supports the idea that the shells observed around some of the fastest rotating B stars arise from rotational instability. In accordance with theoretical expectations such shells are unstable and soon disintegrate. For example, that of γ Cassiopeiae disappeared after a few years. The shells around other stars, apparently not too different from that of γ Cassiopeiae, however, have lasted many years, e.g., *HD* 193182. Not all rapidly rotating stars show shells or bright lines, e.g., η Ursae Majoris, α Virginis, or α Aquilae show no signs of such appendages.

Among the B stars in the Pleiades there is a greater proportion of rapidly spinning objects than among B stars chosen at random. These

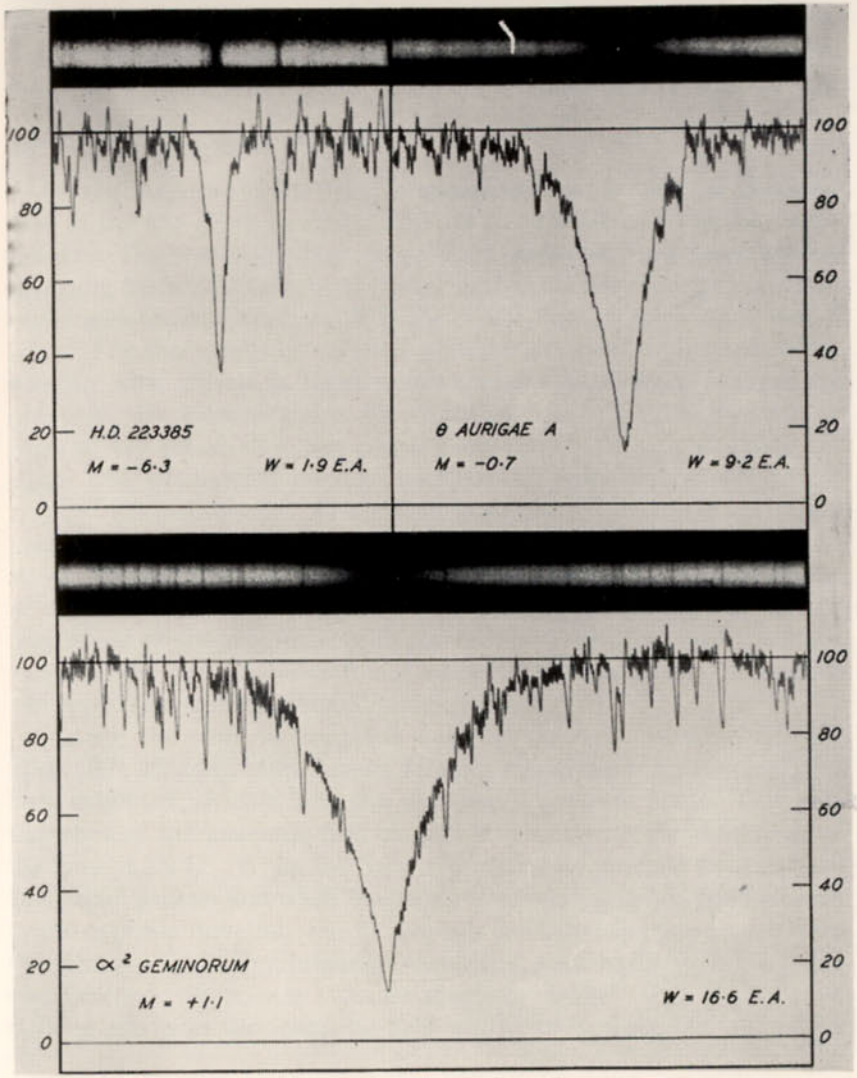

FIG. 19(a).—LUMINOSITY EFFECTS AT Hγ IN *A*-TYPE SPECTRA

Notice the weakness of the Hγ line in *HD* 223385, an *A*2 supergiant similar to α Cygni and its great strength in the dwarf, α^2 Geminorum. The microphotometer tracings show Hγ to be much wider in α^2 Geminorum than in θ Aurigae *A*, although the differences are not conspicuous to the eye.

stars are involved in nebulosity and Struve regards it as possible that the rotational speeds were built up from the infall of interstellar material. On the other hand, the stars themselves may have thrown off the material.

19. Stellar Magnetic Fields

Strong magnetic fields exist in sunspots, but the general magnetic field of the sun (such as exists) appears to be small and variable in intensity. The possibility that other stars, however, may have general magnetic fields could not be excluded, and H. W. Babcock guessed that one might observe appreciable fields in the rapidly spinning *A* and *F* stars. For this study he selected peculiar sharp-lined *A* stars, which possibly were objects in rapid rotation with axes directed towards the observer. He secured coude spectrograms with a double analyzer in front of the slit so that two parallel spectra of the star, analyzed for right- and left-handed circular polarization, respectively, are photographed simultaneously. If the field is similar to that of a uniformly magnetized sphere and the axis is pointed toward the observer, the observed spectral lines will tend to be split into two groups of components, of opposite circular polarization. The separation will depend on the magnitude of the magnetic field, the atomic transition, and the wave length of the line. Babcock found a field of 1500 gausses in 78 Virginis while a *K*0 control star showed no such effect.

Among the stars investigated was the spectrum variable *BD*–18° 3789 (*HD* 125248), *A*0*p*, where Morgan found that Eu II and Cr II lines exhibited periodic intensity changes in opposite phase. Observation showed the magnetic field to vary in phase with the intensities of the lines of Eu II. When the lines were strongest the field would attain 7000–8000 gausses and when they were weakest, it reached 6000 gausses in the opposite direction. A. J. Deutsch has listed the peculiar *A* stars that show periodic line intensity variations; very likely such stars will also be found to possess variable magnetic fields.* One of the most striking effects of the magnetic field will be to increase the equivalent

* Quite apart from the spectrum variations, these stars show abnormally narrow Ca II lines. The Si II lines, λ4128, λ4131 are often unusually strong. Morgan was able to divide these stars into subgroups with strong lines of various elements, e.g., Mn, Eu, Cr, and Sr. In α^2 Canum Venaticorum, Struve and Swings found the rare earth lines to show periodic changes in velocity as well as intensity. This star also shows a variable magnetic field. Deutsch found that the line width increases as the period decreases in the magnetic variables. Presumably the period of rotation is correlated with the period of magnetic variation. Lines of different elements may be intensified in different regions on the star and as the star rotates these regions are brought successively into view.

widths of many of the absorption lines, without any increase in the number of atoms in the photosphere. To understand this phenomenon let us consider, as an example, an iron line such as $\lambda 4325(^3F_2 - {}^3G_3^0)$. When viewed along the direction of the magnetic field, the line will be split into ten circularly polarized Zeeman components. The absorption coefficient of each one of these components will be washed out by the Doppler effect and instead of a half-width of about 0.03A, the over-all spread of the pattern will give the line an effective half-width of about 0.12A.

Therefore, the net absorption coefficient of the atom is spread over an appreciably greater range of wave length. The curve of growth for such a magnetically widened line will differ appreciably from that of the undisturbed line. The initial 45° rise will continue longer and the flat portion will set in at a higher value of the equivalent width. Hence the effect on the intensities will be greatest for lines that would normally fall on the flat portion of the curve of growth, since in the magnetic star such lines may fall in the region where W is proportional to N. The actual intensity of the line will depend on the magnetic field of the star, the number and separation of its Zeeman components as compared to its Doppler width, and the initial intensity.* For example, λ4205, Eu II, has 23 components spread over a range of nearly three times that of a normal Zeeman pattern. In a field of 8000 gausses, Babcock finds the equivalent width of this line to be changed by a factor of about eight. The huge intensity variations in stars such as *HD* 125248 probably arise at least in part from such magnetic intensification.

What is the origin of these fields? Babcock suggested that the observed Zeeman effect arose from the magnetic field of the whole star rather than from large spots, which on the sun at least tend to occur in pairs of opposite polarity. Hence the whole star must show a definite magnetic polarity, correlated perhaps with its sense of rotation. The variable fields are difficult to understand. M. Schwarzschild proposed an interpretation based on a system of standing hydrodynamical waves of magnetized material. Since the electrical conductivity of ionized gases is high, the magnetic field must be dragged along with the material in its motion (cf. Ch. 9). In this picture, there exists a permanent field of many thousands of gausses deep below the surface, overlying which is a zone of gas which screens the underlying layers and in which the field is variable. To obtain the observed magnetic amplitude, it is necessary to assume a velocity amplitude of the material of the order of

* In a magnetic star the curve of growth appropriate to each line would depend on its Zeeman pattern and the field. In the analysis of the spectrum of such a star it would appear most logical to select unblended lines whose Zeeman patterns are known and analyze them according to their individual curves of growth.

1 km/sec. This quantity is comparable with the velocities observed by Swings and Struve in the atmosphere of the magnetic variable α_2 Canum Venaticorum. The Schwarzschild theory looks promising, but the enormous permanent field required below the surface, perhaps as much as a million gausses, presents a difficult problem for the theory of stellar structure.

Cowling finds that a large internal magnetic field is not necessary to produce rapid oscillations. A satisfactory theory of magnetic stars has not yet been developed.

20. Absolute Magnitude Effects

Empirical studies first established the important fact that the spectra of the stars include important clues to their true luminosities. Miss Maury noticed that stars of the same Henry Draper spectral class often showed marked differences in line sharpness. From a study of the proper motions, Hertzsprung showed that the sharp-lined stars Miss Maury had indicated by "*c*" were intrinsically brighter than the broader lined objects indicated as "*b*" or "*a*."

Adams and Kohlschütter firmly established the spectroscopic differences between giants and dwarfs and laid the foundation for the determination of spectroscopic parallaxes. Subsequently, Adams and Joy and their colleagues determined the spectroscopic parallaxes of many hundreds of stars. As the spectroscopic data and trigonometric parallaxes improved, the accuracy increased until at the present time the probable error of a Mount Wilson spectroscopic parallax is about 0.4 magnitude. Lindblad and his colleagues made important contributions, especially in the use of low dispersion material and in the application of quantitative photometric methods. In recent years considerable work has been done on this problem by W. W. Morgan and J. Bidelman at Yerkes, P. C. Keenan at Yerkes and Perkins, J. Nassau and van Albada at Cleveland, the Vyssotskys at Virginia, Miss Hoffleit at Harvard, and others, chiefly as an aid to galactic structure studies.

The spectra of stars of the same spectral class and different absolute magnitudes differ in four characteristics: (1) Color effects or energy distribution; giants are redder than dwarfs of the same spectral class. (2) Sharpness of the lines, or "*c*" characteristics. (3) Intensities of lines not used in the determination of spectral class. (4) Intensities of bands such as CN. In early-type stars, the interstellar lines are also helpful. Colors alone might be employed if we could eliminate the effects of space reddening, while line sharpness is a qualitative rather than a quantitative criterion. With spectra of intermediate and high dispersion, criterion (3) is most important, while (4) can sometimes be used with very low dispersion spectra (see page 324).

In practice, the determination of the absolute magnitudes of stars of the same spectral class proceeds as follows: (1) From an intercomparison of stars of known absolute magnitude, lines are chosen that appear to vary with intrinsic stellar luminosity. (2) The intensity of each magnitude-sensitive line with respect to a neighboring nonvariable line is estimated. (3) From calibration curves derived from stars of known absolute magnitude, the ratio of the intensities of variable to nonvariable lines are converted to absolute magnitudes. In practice one employs a procedure similar to Argelander's method for variable stars. One estimates intensity differences on a step scale and reads the corresponding absolute magnitude from a calibration curve. The ratio of 4215 Sr II to 4250 Fe I is often employed as a luminosity criterion in classes *F* to *K*.

The establishment of absolute magnitude criteria in practical application depends somewhat on the type of instrument employed. The most suitable criteria may differ for various dispersions. The use of low dispersion limits the number of lines that can be employed but enables the observer to reach fainter stars. W. W. Morgan has demonstrated that good absolute magnitudes can be obtained with low-dispersion (110A/mm) spectra. The Morgan-Keenan-Kellman atlas suggests useful criteria that can be employed with plates of moderate to low dispersion.

On the theoretical side, the problem is to give a rational explanation of absolute magnitude effects in terms of surface gravity and temperature. Although many of the observed effects have been explained by theory, others have not been interpreted and calibrations must be carried out empirically. We do not yet know enough about stellar atmospheres to predict precisely the change in line intensity from a dwarf to a supergiant.

In the hotter stars, hydrogen furnishes useful absolute magnitude criteria; we have already mentioned how the number of observable Balmer lines makes possible the separation of dwarfs and supergiants. Theory predicts and observation confirms that in stars hotter than 10,000°K, the number of atoms above the photosphere capable of absorbing the Balmer lines will be the same in supergiants and dwarfs. The appearance of the hydrogen lines will differ markedly; in the dwarfs the earlier members will be broad, whereas in the supergiants they will be relatively sharp. Over a small range of spectral class, the equivalent widths of the Balmer lines longwards of λ3889 depends strongly on absolute magnitude.

In class *F* the first few Balmer lines show minor absolute magnitude effects, whereas in later classes the observed differences are not well understood. The Mount Wilson observers found that supergiant *K*'s may

be separated from giant *K*'s by the strengthened Balmer lines in the former. In fact, the Balmer lines appear to be much stronger than we would predict for the effective temperatures of these stars and thermodynamic equilibrium.

Other line ratios have frequently been employed as absolute magnitude criteria. In *M* stars perhaps the most important criterion is Ca I, λ4227 (cf. Fig. 7 of Ch. 4), which is the strongest line in the spectra of the dwarfs. In stars of increasing luminosity it progressively weakens until in the supergiants it is less intense than the absorption lines on either side.

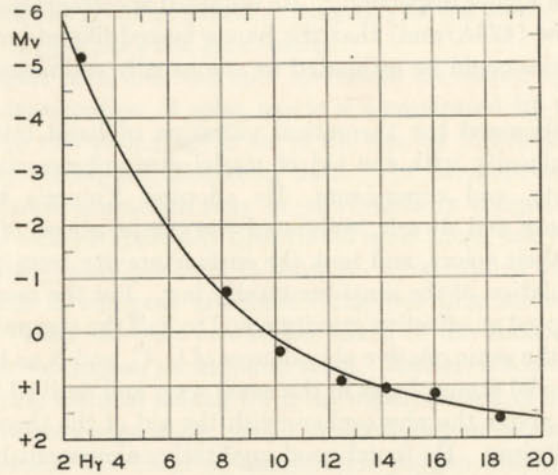

FIG. 19(b).—THE MEAN RELATION BETWEEN THE EQUIVALENT WIDTH OF $H\gamma$ IN ANGSTROM UNITS AND ABSOLUTE MAGNITUDES

(Courtesy, R. M. Petrie, Dominion Astrophysical Observatory, Victoria, B. C.)

We recall that for lines on the square-root portion of the curve of growth, i.e., lines for which the wings determine the total intensity, pressure broadening may play an important role since α_λ in the wings varies as $\sqrt{Nf\Gamma}$. In dwarfs the damping constant Γ, being essentially the collisional damping constant, is proportional to the density. Even if the number of atoms above the photosphere of a supergiant and a dwarf were the same, the vastly greater density of the dwarf atmosphere would so increase the damping constant in the wings of the line as to augment substantially the total intensity. In the sun the damping constant for resonance lines is of the order of ten times the classical value, and in *M* dwarfs it may be much greater. Lindblad found the λ4227 line in red dwarfs to be asymmetrically broadened, probably because of the formation of quasi-molecules such as are observed in sodium vapor.

Keenan and Nassau point out that by comparing the depth of the

λ4227 line with the intensity of the continuous spectrum on both sides of the line it is possible even with low dispersion spectrograms to separate not only giants from dwarfs, but also supergiants from giants.

Lindblad showed that with accurate spectrophotometry, the cyanogen band intensity is an excellent absolute magnitude criterion. He measured the intensity in terms of exposure ratios needed to give the cyanogen band and neighboring spectral regions the same blackening. With the cyanogen criterion one can employ dispersions so low that the atomic lines are invisible. In fact, Keenan showed that with good standard spectra the accuracy can be as great as that of methods requiring much higher dispersion.* He obtained spectrograms with a dispersion so low (425A/mm) that the bands looked like atomic lines and their intensities could be estimated as one usually estimates line intensities.

Keenan discussed the theoretical variation of band intensity with absolute luminosity with the aid of model atmospheres computed for dwarfs, giants, and supergiants. He adopted Kuiper's temperature scale for giants and dwarfs, estimated the temperatures of the supergiants from their colors, and took the surface gravity from the Russell-Moore formulation of the mass-luminosity law. For the more luminous stars, he adopted an effective gravity equal to half the computed gravity. He assumed the same relative abundances of O, C, and N as had Russell, calculated model atmospheres in the usual way, and derived the number of molecules above the photosphere with the aid of the theory of dissociative equilibrium. He found good qualitative agreement between the predictions of theory and the observations.

Keenan emphasizes that in separating giants and supergiants, it is necessary to have accurate spectral classes.

The *G*-band, a composite structure of molecular bands and atomic lines, is a useful criterion in class *M*. The break in the spectrum at λ4308 corresponding to the red end of the *G*-band becomes much more pronounced as the luminosity increases (Nassau and Keenan).

The theoretical interpretation of absolute magnitude effects will probably be approached best by the construction of synthetic spectra with the aid of *f* values and damping constants based to some extent at least on solar data and model atmospheres. Such an approach has been suggested by van Albada. Since most absolute magnitude work is done with low dispersion material, one must allow for the instrumental as well as the intrinsic blending of the lines. For a detailed discussion of absolute magnitude effects, the reader is referred to the basic papers of Adams

* In the supergiants, the maximum intensity of the cyanogen band occurs at type *G6*; in the giants near *K1*. In types later than *K1*, the band is weaker in supergiants than in giants.

and Joy and their collaborators, and of Lindblad and his colleagues, the Morgan-Keenan-Kellman Atlas, and subsequent articles by Keenan, Nassau, van Albada, and others.

21. Molecules in the Solar Atmosphere

A discussion of the Fraunhofer spectrum would be incomplete without a reference to the molecules in the solar atmosphere. We have mentioned molecules in connection with the problem of the dissociation equilibrium and the splitting of the spectral sequence and again in connection with the temperature determination of the solar atmosphere. H. D. Babcock has given an excellent summary of the results up to 1945, and we shall review his work here briefly.

Babcock used both disk and spot spectra in his search for molecular lines. The identification of solar bands is complicated by their superposition on the rich atomic spectrum of the sun, by blends among themselves, and by inadequate laboratory data. The band spectrum of even a single electronic transition may be bewilderingly complex. Furthermore, certain radicals (partially dissociated molecules), not yet observed in the laboratory, may be found in the sun. Unidentified molecular absorption bands in sunspots are more numerous than those which are recognized. Under the best conditions, much of the sunspot spectrum shows no true continuous background at all. Rather, it consists of many faint absorption features arising from the superposition of delicate lines too faint to be seen separately, which are probably molecular in origin.

The forbidden "*A*" band of atmospheric oxygen illustrates the dependence of the visibility of a band head upon the abundance of the responsible compound. With an air path of 100 km when the sun is low, the head of the band is sharply defined on the violet edge, but with an air path of only three meters, the absorption spectrum shows only two doublets in the *P* branch of the band, 40A to the red of the head. The lines of the *R* branch are weaker than those of the *P* branch and thus disappear first with decreasing abundance. Thus the absence of a given band head does not always mean the molecule in question is certainly absent. Many faint lines in the solar spectrum may be remnants of bands arising from the ground state of rare molecules or abundant molecules in excited levels.

Babcock calculates the relative number of molecules, *S*, above unit area of the photosphere by the method given by Russell and compares the results with the observations. Among the new molecules Babcock found in the sun is O_2, which is represented by bands involving transitions from the vibrational levels 18–21 to 0, 1, 2. The lower members of this band system, which must be very strong, all fall in the inaccessible ultraviolet. The compounds now identified in the sun are OH, NH, O_2, CH,

CN, CO, SiH, MgH, C_2, TiO, MgO, CaH, BH, ScO, AlO, ZrO, YO, MgF, SrF. It is of interest that the molecules give us our only clues to the existence of boron and the halogens in the sun. Other compounds, which are not observable in the sun, but which must be very abundant are H_2, NO, SiO, and N_2. Babcock believes that in the sunspots, lines arising from the high vibrational levels of NO and N_2 may become visible under favorable conditions. Lines of the pure vibration bands of CO have been observed with the aid of the lead-sulfide cell in the infrared solar spectrum.

It is of interest that H. D. Babcock found in the disk spectrum of the sun all of the 18 identified compounds that appear in the spots. There is evidence, however, that many compounds appear in spots that do not appear in the disk at all.

Roach developed a method for the determination of log Nf (where N is the number of molecules above the photosphere) for the molecules CN, C_2, CH, NH, and OH by the use of single resolved rotational lines. The determination of N itself, unfortunately, requires a knowledge of the absolute f values which are not yet known for most of the lines of interest. Lyddane, Rogers, and Roach estimated f values for CH, NH, and C_2 from the experimental values for OH and CN, and derived molecular abundances in the solar atmosphere with an estimated temperature of 5000°K. Hunaerts has employed more homogeneous observational data and the actual excitation temperatures of the molecules themselves to obtain abundance estimates. These results can be improved markedly by taking into account the stratification in the solar atmosphere. The CH and CN bands, for example, are found in different layers of the solar atmosphere. In this connection we should mention Gordon Newkirk's careful study of the CO vibration-rotation bands which not only assists in the determination of the carbon and oxygen abundances but also gives helpful clues to the structure of the uppermost portions of the solar photosphere.

22. The Abundances of the Elements as Derived from Astronomical Data

The quantitative determination of the chemical composition of the sun and stars has occupied the attention of a number of astronomers since the pioneer work of Henry Norris Russell a quarter of a century ago. The observational techniques and the theoretical interpretation of the data have gradually improved over the course of the years, and it is now possible to give a reasonable self-consistent picture of the abundances of the elements.

Abundances have been estimated in a large number of celestial objects, many of which appear to have abnormal compositions. Let us

first examine objects of supposedly "normal" composition, namely, the sun and certain early-type stars. The reason for including the early-type stars is that it seems to be possible to get information on certain light elements whose lines do not appear in the solar spectrum, e.g., neon, or which are represented by weak subordinate lines, e.g., oxygen or carbon.

TABLE 16

ABUNDANCES OF CHEMICAL ELEMENTS, DEDUCED FROM ASTROPHYSICAL DATA

Element	Log N	Element	Log N
H	13.27	Sr	4.37
H_2	5.85	Y	4.55
He	12.41	Zr	3.54
Li	2.57	Nb	3.51
Be	2.8	Mo	3.12
B	6.0	Ru	2.7
C	9.23	Rh	1.5
N	9.49	Pd	2.1
O	10.00	Ag	2.0
F	7.7:	Cd	3.2
Ne	10.04	In	1.0
Na	7.69	Sn	2.2
Mg	9.05	Sb	1.8
Al	7.67	Ba	4.02
Si	8.80	La	2.8
P	7.08	Ce	3.4
S	8.52	Pr	1.6
Cl	8.3	Nd	3.0
A	9.0:	Sm	2.5
K	6.39	Eu	2.4
Ca	7.72	Gd	2.1
Sc	4.42	Dy	2.6
Ti	6.05	Er	1.1
V	5.27	Tm	1.5
Cr	6.08	Yb	2.0
Mn	6.55	Lu	2.0
Fe	8.48	Hf	1.4
Co	6.14	Ta	1.0
Ni	7.44	W	1.2
Cu	5.77	Os	1.5
Zn	6.26	Ir	0.8
Ga	3.2	Pt	2.6
Ge	4.2	Hg	4.35
Rb	2.8	Pb	3.8

Table 16 was compiled from the following sources: Russell's pioneer investigation which embraced all elements whose lines could be identified in the solar spectrum still provides the only information for many of the heavier elements. Unsöld used the curve of growth method and

such f values as were available. Menzel and Goldberg employed a somewhat similar type of analysis using the same data. Minnaert deduced abundances from the intensities of the weak lines of a number of elements. This work has been extended recently by Claas who has analyzed the weak lines with the aid of a model solar atmosphere.

Turning to the stellar data, the writer has utilized Unsöld's results for τ Scorpii together with his own data for 10 Lacertae (which was analyzed by Unsöld's method), for eleven B stars treated with the aid of Wrubel's curves of growth, and for γ Pegasi which was studied both by the curve of growth and by the model atmosphere methods. These stars embrace a range in excitation temperature from 18,000°K to 30,000°K!

The agreement between the various determinations appears to be reasonably good for the more plentiful elements. Some scatter is found for hydrogen and helium. The B stars later than $B0$ tend to give very high hydrogen/oxygen ratios which are probably spurious. Keenan and Hynek find a hydrogen/oxygen ratio of about 1000. The ratio of hydrogen to the metals can be found for the solar atmosphere with some precision since the negative hydrogen ion contributes the continuous absorption. The abundance of lithium is taken from the work of Greenstein and Richardson whose determination is in good agreement with that by Claas. For beryllium and boron we rely on the old estimates by Russell. Numerous estimates exist for carbon, nitrogen, and oxygen, and all determinations will be substantially improved with better f values and model atmospheres for the sun and stars. The estimate of the abundance of fluorine is taken from the data of the gaseous nebulae and is to be regarded as highly uncertain. The abundance of neon is taken from the data for 10 Lacertae and τ Scorpii. Sodium, magnesium, aluminum, and silicon are well represented in the sun and stars, and our mean values should be reliable. An abundance determination of phosphorus is available only for γ Pegasi, as is true also for chlorine and argon. Sulfur is observed in a number of stars. The metals, from potassium to zinc, are well represented in the sun and for these and heavier metals we utilize exclusively the solar data. Determinations by Unsöld, by Menzel and Goldberg, by Minnaert, and by Claas are generally in good agreement, although Claas appears to derive an astonishingly high abundance for titanium. The measurement of absolute f values will be of great help for many of these elements. The chromium determination is by Sandage and Hill corrected for Estabrook's recent revision of the absolute f value for this metal. Since for Fe I the absolute f value determination by Kopfermann and Wessell is adopted, the abundance of iron is somewhat lower than that given by Unsöld, Minnaert, or Claas. For strontium, yttrium, zirconium, molybdenum, barium, mercury, and lead

we may utilize data by Unsöld or by Claas. For the other elements it is necessary to employ the estimates made by Russell many years ago.

Independent estimates of the abundances of elements such as C, N, and O may be made when the molecular line intensities of CO, CN, CH, etc., are analyzed in greater detail.

Table 17 gives for comparison the composition of a planetary nebula. The chief difficulty here is that the target areas for collisional excitations of the observed forbidden lines are unknown (all we can give are upper limits) and we must allow for the distribution of atoms among different stages of ionization. For any one element only a few stages of ionization are observed. Further complications are introduced by the nonuniform or filamentary structure of the nebulae. The gaseous nebulae appear to have about the same composition as the stars, as Bowen and Wyse pointed out some years ago.

TABLE 17

ESTIMATED ABUNDANCES OF ELEMENTS IN THE PLANETARY NEBULAE

Element	Log N	Element	Log N
H	13.11	F	6.6?
He	12.51	Ne	9.97
C	9.0	S	9.01
N	9.33	Cl	8.11
O	10.00	A	8.01

A point of considerable interest is whether stars of population Types I and II have the same composition. From a comparison of high velocity (Type II) and low velocity (Type I) F dwarfs, M. and B. Schwarzschild conclude that the abundance of carbon relative to the metals is about 2.5 times larger in the high velocity F dwarfs than in the low velocity dwarfs. Also the H/Fe ratio appears to be about twice as large in these stars of population II as in those of population I. J. W. Chamberlain and the writer found the H/Fe and H/Ca ratios to be of the order of 10 times larger in subdwarfs, which are Type II stars, than in normal (Type I) dwarfs. That is, the spectroscopic peculiarities of the Type II stars, the strengthening of the CH bands and the weakening of the CN bands and metal lines can be explained by a general reduction in the abundances of the heavy elements and a somewhat smaller reduction in the abundances of the elements of the oxygen group, relative to the abundances for the Type I stars. Schwarzschild, Spitzer, and Wildt suggested that these differences might be explained if we supposed that the Type II stars were formed from the initial gaseous medium, whereas

the Type I stars were formed later from denser interstellar clouds that were made up largely of grains which were richer in heavier elements. *

Many Type I stars as well as Type II objects appear to show abnormalities of composition. Greenstein's analysis of the *F* stars showed that the differences between the spectra of "metallic line" and "normal" *F* stars could be described as an abundance deficiency of elements which have a second ionization potential between 12 and 16 ev. Such differences are probably due to differences in atmospheric structure rather than real abundance differences. Rudkjobing suggests that the metallic stars could be interpreted as objects whose atmospheres are in radiative equilibrium whereas "normal" *F* stars are objects whose atmospheres are in convective equilibrium. The "rare-earth" *A* stars, which are usually spectrum variables may owe their strange spectroscopic properties to magnetic fields rather than to abnormalities in chemical composition.

Yet other stars such as *HD* 160641, studied by W. W. Morgan and W. P. Bidelman; *HD* 12448, studied by Popper; υ Sagittarii studied by Greenstein, and *HD* 30353, which was discussed by Bidelman, appear to be deficient in hydrogen, although helium is abundant. Likewise, the Wolf-Rayet stars appear to be deficient in hydrogen. They appear to fall into two sequences, a carbon-oxygen group and a nitrogen group, although at least one Wolf-Rayet star, *HD* 45166, appears to have a "normal" composition. Likewise, the late-type stars appear to fall into two families. In the *R* and *N* classes the carbon abundance seems to exceed that of oxygen. R Coronae Borealis, whose spectrum was analyzed by Berman, also is a star of the carbon group. In the *M* and *S* classes, oxygen is more abundant than carbon, but titanium is strong in class *M*, whereas zirconium is strong in class *S*. Merrill pointed out that the lines of relatively heavy elements tend to be favored in *S*-type spectra as compared with *M*-type spectra. Additional examples of abundance anomalies may be found in the literature.

23. Problems of the Fraunhofer Spectrum

We conclude this chapter with a list of some of the outstanding problems in the study of the dark-line spectra of the stars. First we enumerate some of the basic physical data required:

(1) Experimental relative and absolute *f* values of lines of many elements, particularly for transitions arising from high levels, are urgently needed.

(2) Further experimental studies of *f* values and dissociation constants of molecules are desired.

(3) Theoretical *f* values for transition arrays such as $3p - 3d$, $3d - 4f$, etc., in light elements will be very valuable. Not only should deviations from *LS* coupling be taken into account, as in the calculations of Garstang, but configuration interaction ought to be allowed for. Bates has shown how good approximations to the radial quantum integrals can be found for the lighter elements.

(4) Collisional damping constants are urgently needed for the important lines of abundant elements, not only for resonance transitions, but also for high level lines as well. Some of these damping constants could be determined experimentally; others might be amenable to theoretical treatment.

An important advance that may permit the determination of absolute *f* values and damping constants (at least for high-level lines of light elements in various stages of ionization) has been the development of the whirling-water arc. In this device an arc is struck between two carbon rods placed on the axis of a quartz tube 1/2 to 4 inches long and about 2 inches wide. Near the center of the tube a stream of water is injected tangentially in such a way as to form a whirling sheet of water over the inner surface of the tube. The stream of water shields the sides of the tube from the intense heat of the arc that dissociates and ionizes the water vapor near the center of the arc. The arc is struck along the bore formed by the whirling stream. With the arc cooled by a fast-flowing and whirling stream of water, currents of 1600 amperes may be drawn and temperatures measured from 10,000°K to 50,000°K. From the profiles and intensities of the hydrogen and oxygen lines produced in the tube, the temperature and electron density can be measured as a function of arc current and distance from the axis. The transition probabilities and damping constants of oxygen in various stages of ionization, for example, can be determined by comparing the lines with those of hydrogen. Other gases or soluble substances can be mixed with the stream of water so that *f* values for a variety of elements may be studied.*

The study of the solar atmosphere would be helped by the following observations:

(1) The study of line profile variations across the disk by photoelectric photometry or other methods of higher precision than photographic photometry.

* It appears that the ratio of hydrogen to the metals may vary from one group of Type II objects to another. Some high velocity stars differ relatively slightly from Type I objects in this respect. The subdwarfs may represent an extreme variety of Type II objects as perhaps do the members of globular clusters. As judged by the hydrogen lines and other criteria, the subdwarfs appear to be too early in spectral class for their colors. A similar effect is observed in the stars of globular clusters, where objects whose colors correspond to spectral class *K* have spectra that more nearly resemble those of stars of class *F*. An enhanced hydrogen to metal ratio appears to account for these anomalies.

* For an account of the experimental apparatus, see, e.g., H. Maecker, *Zeits. f. Phys.* **129,** 108, 1951; W. Lochte-Holtgreven, *Observatory* **72,** 142, 1952.

(2) The center-limb variations of weaker lines, especially near the edge of the disk.

(3) Photographs of the ultraviolet solar spectrum obtained from rockets fired above the ozone layer of the earth's atmosphere. A few such observations, covering the region occupied by the resonance lines of Fe II, Cr II, V II, Mg II, and other metals have been obtained. Blending is so serious that in order to interpret the spectrum it is necessary to construct synthetic spectra which are then compared with the tracings.

The Mg II pair at λ2800 is the strongest feature of the spectrum. When allowance is made for the greater opacity of the solar atmosphere in this region, the number of active atoms is found to be much greater than the number of Ca II atoms acting to produce the *H* and *K* lines. At no point do we observe the true continuum; only the bottoms and portions of the sides of strong absorption lines are seen. Spectra of higher resolution are needed to simplify the question of line identification and interpretation. Also, spectrograms covering the far ultraviolet and soft X-ray region are urgently needed.

Solar radiation at Ly α(λ1216*A*) and at other regions in the far ultraviolet has been measured by photon counters flown in aerobee rockets. Tousey finds that the intensity distribution in the ultraviolet falls far below that of a 6000°K black body and at λ2200A is less by a factor of 15. Friedman, Lichtman, Byram, and Chubb found intensities at λ1200A and at λ1500A to correspond to black bodies at 6000°K and 4500°K respectively, while the intensity at λ2050 corresponded to $T = 5000°\text{K} \pm 300°\text{K}$. From λ1180A to λ1300A, Ly α contributed essentially all of the solar radiation. A University of Colorado group photographed Ly α in emission superposed on a broad absorption line. The rocket was fired about 15 minutes after the end of a flare and while the bright plages were still prominent on the sun. The X rays, presumably produced in the corona, may have a broad energy distribution with a maximum near λ320A with an upper limit to the energy near 7A.

A fundamental problem is the interpretation of line intensities in the solar spectrum in terms of the structure (model) of the solar atmosphere, and the basic physical processes in the line and continuum. The treatment of individual line profiles is to be preferred to the statistical curve of growth procedure, which conceals much useful information that individual lines might disclose. If the lines are so weak that only their total intensities may be measured, one may group them according to excitation potential and calculate line profiles for each group with the aid of a model atmosphere. From the integration of these theoretical profiles one may then construct a curve of growth for each multiplet or

excitation group. In this way, the effects of stratification can be taken into account. In this connection we mention Minnaert's work on faint Fraunhofer lines and a recent analysis of the spectrum of γ Pegasi.

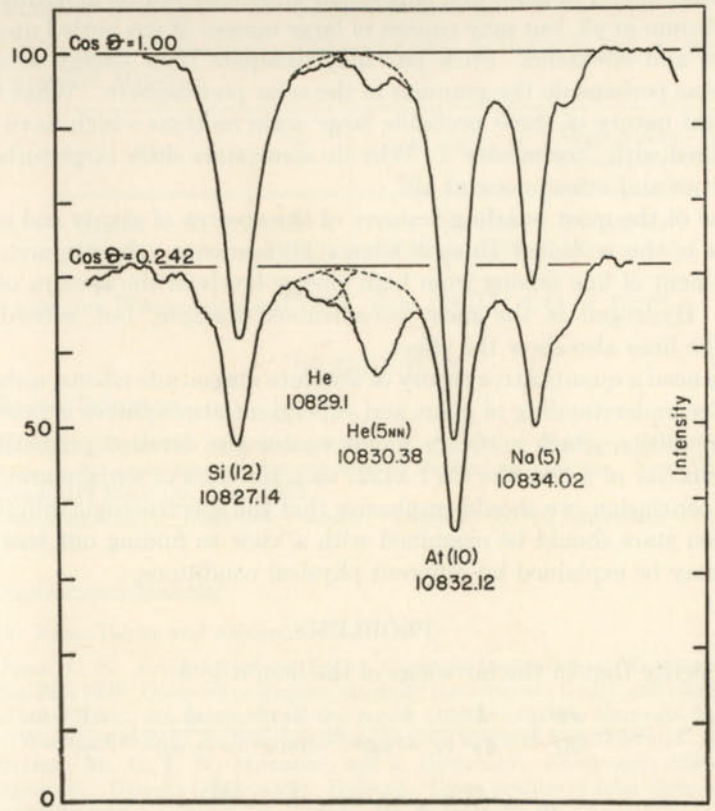

FIG. 20.—THE CENTER-LIMB VARIATION OF THE INFRARED HELIUM LINES

The $2^3S - 2^3P^0$ transition from the metastable 2^3S level appears weakly in absorption at the center of the disk ($\cos\theta = 1.00$), but strengthens toward the limb ($\cos\theta = 0.242$), because it is essentially of chromospheric origin. (McMath-Hulbert Observatory, University of Michigan.)

Furthermore, the basic theory of stellar line formation needs improvement. Fluorescence and noncoherent scattering must be taken into account whenever necessary. At the present time no adequate theory of central intensities is available. With reference to stars other than the sun, there is an urgent need for better data on the intensities of their dark-line spectra. The experiments of Hiltner and Code at the Yerkes Observatory indicate that it is possible to trace the spectrum of a bright star directly at the telescope with the aid of a photoelectric cell. Although the general features of the spectra of dwarf stars appear to be

understood, giants and supergiants provide many difficult questions since their atmospheres differ from those of main-sequence stars in a number of significant respects.* If ζ Aurigae or 31 Cygni are typical, the atmospheres of giant and supergiant stars may not be in hydrostatic equilibrium at all, but may consist of large masses of gas hurled upwards as jets and streamers. Such jets may dissipate their energy as shock waves as perhaps do the granules in the solar photosphere. What is the physical nature of these probable large scale motions which have been identified with "turbulence"? Why do some stars show large turbulent velocities and others none at all?

One of the most puzzling features of the spectra of giants and supergiants is the so-called Russell-Adams phenomenon: the apparent enhancement of line arising from high energy levels in the spectra of cool stars. Hydrogen is the most conspicuous example, but subordinate metallic lines also show the effect.

We need a quantitative theory of absolute magnitude effects, although a better understanding of giant and supergiant atmospheres is probably a prerequisite. Such a theory might enable the detailed prediction of the behavior of a line like Ca I λ4227 as a function of surface gravity.

In conclusion, we should emphasize that the spectroscopic differences between stars should be examined with a view to finding out how well they may be explained by different physical conditions.

PROBLEMS

1. Verify that in the far wings of the line, $u \geq 8$,

$$\alpha_\nu = \frac{\pi\varepsilon^2}{mc} f_{n'n} \frac{1}{4\pi^2} \frac{\Gamma}{(\nu - \nu_0)^2} = \frac{2\pi\varepsilon^4}{3m^2c^4} \frac{\nu_0^2}{(\nu - \nu_0)^2} f_{n'n} \frac{\Gamma}{\gamma_c}$$

and

$$\alpha_\lambda = 16.5 \times 10^{-26} f_{n'n} \frac{\Gamma}{\gamma_c} \frac{\lambda_0^2}{(\lambda - \lambda_0)^2}$$

2. If the infrared hydrogen lines are formed according to the mechanism of local thermal equilibrium, what would be the central intensity of Brackett γ, λ21655, in integrated sunlight? Assume the sun radiates like a black body, $T = 5750°\text{K}$ in this region.

3. For the sodium "D" lines, λ5889 and λ5896, $\rho = 4.6A$ ($T = 5700°\text{K}$). With $A = 6.8 \times 10^7$, calculate, α_0, $\Delta\lambda_0$, δ', and a for $\log P_g = 4.86$.

4. If $k_\lambda/\bar{k} = 0.76$, compute the residual intensity in λ5889, r_λ, for $\Delta\lambda = 0.10\text{A}, 0.20\text{A}, 0.4\text{A}, 0.6\text{A}, 1.00\text{A}$, and 1.20A, for $T = 5700°\text{K}$ and $\log P_g = 4.86$ by eqn. (88).

* Possibly the lines of neutral and ionized atoms arise from different layers so that they are really not comparable at all.

5. Assume the same model atmosphere as employed in Sec. 9, compute l/k, and the profile of λ5889, for $k/\bar{k} = 0.76$.

6. Solve eqn. (51) for l/k constant with the aid of the Eddington approximation and derive the source function $\mathcal{J}$.

7. Compare theoretical profiles of λ4227 in the atmosphere of a giant and a dwarf $M0$ star.

Star	T	$\log P_e$	$\log P_g$	Mass Above Photosphere
Giant.....	3400°K	−2.0	4.70	1.6 gm/cm²
Dwarf.....	3600°K	+0.30	5.70	1.0 gm/cm²

The van der Waals constant C [cf. eqn. (19)] is 4.44×10^{-32}.

REFERENCES

1. *General References*

Unsöld, A. *Physik der Sternatmosphären.* Berlin: Julius Springer, 1938.
Hynek, J. A., and Others. *Astrophysics, a Topical Symposium.* New York: McGraw-Hill Book Co., Inc., 1951.
Chandrasekhar, S. *Radiative Transfer.* London: Oxford University Press, 1950, chap. xii.

2. *Observational Material*

(a) Basic Tables and Atlases:

St. John, C. E. *Revised Rowland Table.* Carnegie Institution of Washington Publ. No. 396, 1928. Gives wave lengths, intensity (on arbitrary scale), and identification of solar lines. An extension to the region (λ6600–λ13490), Carnegie Institution of Washington Publ. No. 579, has been prepared by H. D. Babcock and C. E. Moore.
Minnaert, M., G. F. W. Mulders, and J. Houtgast. *Photometric Atlas of Solar Spectrum.* Utrecht Observatory, Holland. Gives profiles of solar lines on a true intensity scale.
Mohler, O. C., A. K. Pierce, R. R. McMath, and Leo Goldberg. *Photometric Atlas of the Infrared Solar Spectrum from λ8465 to λ25,242.* University of Michigan Observatory, 1951.
Hiltner, W. A., and R. Williams. *Photometric Atlas of Stellar Spectra.* University of Michigan, 1946.

(b) Fraunhofer Line Intensities: See, for example:

Allen, C. W. *Memoirs of Commonwealth Observatory,* Canberra, Australia, No. 5, 1, 2, 1934; No. 6, 1938; *Ap. J.* **88,** 125, 165, 1938 (λ8800–11,000); *M. N.* **96,** 842, 1936; **109,** 343, 1949 (weak lines).
Phillips, J. G. *Ap. J.* **96,** 61, 1942 (λ3530–3915).

(c) Calibration of Rowland Scale:

Menzel, D. H., L. Goldberg, and E. M. Cook. *Ap. J.* **91,** 320, 1940.
Roach, F. E., and J. G. Phillips. *Ap. J.* **96,** 71, 1942 (scale in ultraviolet).
Mulders, G. F. W. *Zeits. f. Ap.* **11,** 143, 1936.

See also C. W. Allen. *Op. cit.*, No. 5, p. 92.

(d) The Observational Determination of Line Profiles:

Shane, C. D. *Lick Obs. Bull.* **16,** 17, 1932; **19,** 119, 1942.
Redman, R. O. *M. N.* **95,** 290, 742, 1935.
Houtgast, J. Dissertation, Utrecht, 1944 (reviewed by Spitzer in *Ap. J.* **99,** 107, 1944).

3. *Line Broadening: Theory and Experiment*

For calculation of line absorption coefficient see:

Hjerting, F. *Ap. J.* **88,** 508, 1938.
Harris, D. L. *Ap. J.* **108,** 112, 1948.

For reviews of the theory of line broadening see:

Mitchell, A., and M. W. Zemansky. *Resonance Radiation and Excited Atoms.* Cambridge: Cambridge University Press, 1934, p. 322.
Unsöld, A. *Viertel. der Astr. Gesel., Leipzig* **78,** 213, 1943.

The application of empirical damping coefficients to the interpretation of solar line intensities is discussed, for example, by:

Allen, C. W. *M.N.* **100,** 4, 1940.

4. *Theory of Absorption Lines*

See, for example:

Eddington, A. S. *M.N.* **89,** 620, 1929.
Chandrasekhar, S. *Op. cit.*, chap. xii.
Strömgren, B. *Ap. J.* **86,** 1, 1937; *Zeits. f. Ap.* **10,** 237, 1935.

Applications of the theory of absorption-line formation have been given by, for example:

Harris, D. *Ap. J.* **109,** 53, 1949.
Tuberg, M. *Ap. J.* **103,** 145, 1946.

The method of weighting functions, which is important for weak lines is discussed by:

Unsöld, A., and W. Kurz. *Zeits. f. Ap.* **26,** 200, 1949.
Hunger, K. *Zeits. f. Ap.* **28,** 245, 1951.
Minnaert, M. *B.A.N.* **10,** 339, 399, 1948; **11,** 51, 1949.
Pecker, J. C. *B.A.N.* **11,** 43, 1949; *Ann. d'Ap.* **14,** 383, 1951.

For the theory of interlocking and central intensities see, for example:

Woolley, R. *M.N.* **94,** 631, 1934.
Dempster, R. *Ap. J.* **96,** 295, 1942.

Noncoherent scattering has been discussed by:

Woolley, R. *M.N.* **98,** 624, 1938.
Zanstra, H. *M.N.* **106,** 225, 1946.
Spitzer, L. *Ap. J.* **99,** 1, 1944.
Münch, G. *Ap. J.* **109,** 275, 1949.
Labs, D. *Zeits. f. Ap.* **28,** 150, 1951.
Savedoff, M., *Ap. J.* **115,** 509, 1952.

The polarization of λ4227 at the limb is discussed by:

Redman, R. O. *M.N.* **101,** 266, 1941; **103,** 329, 1943.
Zanstra, H. *M.N.* **101,** 250, 273, 1941.

Effect of electron scattering on spectral lines is discussed by:

Münch, G. *Ap. J.* **108,** 116, 1948.
Edmonds, Frank. *Ap. J.* **112,** 307, 1950.

For studies of center-limb variations in the line intensities see, for example:

Redman, R. O. *M.N.* **103,** 174, 1943; **96,** 488, 1936.
Adam, M. G. *M.N.* **98,** 112, 1938; **100,** 595, 1940.
Allen, C. W. *M.N.* **109,** 343, 1949.
Bruggencate, P., H. Gollnow, S. Günther, and W. Strohmeier. *Zeits. f. Ap.* **26,** 51, 1949 (Balmer lines).
Voigt, H. H. *Zeits. f. Ap.* **27,** 82, 1950 (Mg lines).

5. *Curve of Growth and Interpretation of Total Intensities*

(a) The theory is given by:

Unsöld, A. *Op. cit.*, p. 264.
Menzel, D. H. *Ap. J.* **84,** 462, 1936.
Wrubel, Marshall. *Ap. J.* **109,** 66, 1949; **111,** 157, 1950.

(b) Applications have been given by a large number of workers. A few examples are:

(1) *O*, *B*, and *A* Stars—

Unsöld, A. *Zeits. f. Ap.* **21,** 1, 1941.
Aller, L. H. *Ap. J.* **96,** 321, 1942; **104,** 347, 1946; **109,** 244, 1949.

(2) *F*, *G*, and *K* Stars—

Greenstein, J. L. *Ap. J.* **95,** 161, 1942; **107,** 151, 1948; **109,** 121, 1949.
Sandage, A. R., and A. J. Hill. *Ap. J.* **113,** 525, 1951, discuss the Cr I lines in the sun.
Claas, W. J. *Utrecht Researches* **12,** 1, 1951.
Wright, K. O. *Publ. Dom. Ap. Obs.* **8,** 1, 1948; 281, 1950; *Ap. J.* **99,** 249, 1944; *J.R.A.S.C.* **40,** 183, 1946; **41,** 49, 1947.
Unsöld, A. *Zeits. f. Ap.* **24,** 306, 1948.

(c) Turbulence is discussed by:

Struve, O., and C. T. Elvey. *Ap. J.* **79,** 409, 1934.
Huang, Su Shu. *Ap. J.* **112,** 399, 418, 1950.
Struve, O. *Ap. J.* **104,** 138, 1946.
Wrubel, M. *Ap. J.* **112,** 424, 1950.

(d) The analysis of the atmosphere of the giant star ζ Aurigae is given by:

Wilson, O. C. *Ap. J.* **107,** 126, 1948.

6. *Hydrogen and Helium Lines and the Stark Effect*

(a) For the theory of the Stark effect see:

Minkowski, R., *Geiger-Scheel Handbuch der Physik* **21,** 389, 1929.
White, H. E. *Introduction to Atomic Spectra.* New York: McGraw-Hill Book Co., Inc., 1934, Chap. 20.
Inglis, D. R., and E. Teller. *Ap. J.* **90,** 439, 1939.
Krogdahl, M. K. *Ap. J.* **102,** 64, 1945; **105,** 327, 1947; **110,** 355, 1949.

(b) The hydrogen lines in solar and stellar spectra are treated by:

VERWEIJ, S. *Publ. Astron. Instit. Amsterdam* **5**, 1936.
PANNEKOEK, A. *M.N.* **98**, 694, 1938.
VAN DIEN, E. *Ap. J.* **109**, 452, 1949.
DE JAGER, C. *Utrecht Researches*, **13**, 1, 1952.
UNDERHILL, A. *Publ. Dom. Ap. Obs.* **8**, 385, 1951.

(c) The helium lines have been discussed by:

STRUVE, O. *Ap. J.* **69**, 173; **70**, 85, 1929; *Obs.* **61**, 53, 1938.
ELVEY, C. T. *Ap. J.* **69**, 237, 1929.
GOLDBERG, L. *Ap. J.* **89**, 623, 1939.
UNSÖLD, A. *Zeits. f. Ap.* **23**, 75, 1944.

7. *Stellar Rotation*

A general account of the observations and their cosmogonic significance is given by:

STRUVE, O. *Pop. Astron.* **53**, 201, 259, 1945.

See also

SLETTEBAK, A. *Ap. J.* **110**, 498, 1949.
CHANDRASEKHAR, S., and G. MÜNCH. *Ap. J.* **111**, 142, 1950.

8. *Magnetic and Peculiar A Stars*

A survey of the peculiar *A* stars has been given by:

DEUTSCH, A. J. *Ap. J.* **105**, 283, 1947.

Observational studies and interpretations of the magnetic stars are described by:

BABCOCK, H. W. *Ap. J.* **105**, 105, 1947; **108**, 191, 1948; **110**, 126, 1949; **114**, 1, 1951; *P.A.S.P.* **59**, 112, 260, 1947; **60**, 245, 1948. *Nature* **166**, 249, 1950.
SCHWARZSCHILD, M. *Ann. d'Ap.* **12**, 148, 1949.
COWLING, T. G. *M.N.* **112**, 527, 1952.

9. *Absolute Magnitude Effects*

The earlier Mount Wilson work is summarized in the following papers by Adams and Joy and their collaborators:

Ap. J. **46**, 313, 1917; **53**, 13, 1921; **56**, 262, 1922; **64**, 225, 1926; **81**, 187, 1935.

A bibliography of the Swedish work is given by:

LINDBLAD, B. *Ap. J.* **104**, 325, 1946.

The modern classification is based on:

MORGAN, W. W., P. C. KEENAN, and E. KELLMAN. *An Atlas of Stellar Spectra.* Chicago: University of Chicago Press, 1943.

The use of molecular bands is discussed, for example, by:

KEENAN, P. C. *Ap. J.* **93**, 475, 1941.

10. *Molecules in Stellar Atmospheres*

(a) Solar Atmosphere

BABCOCK, H. D. *Ap. J.* **102**, 154, 1945.
ROACH, F. E. *Ap. J.* **89**, 99, 1939; *Phys. Rev.* **60**, 281, 1940 (abundance of CN, C_2, etc.).
HUNAERTS, J. *Ann. d'Ap.* **10**, 237, 1947.

(b) For temperature determination from bands, see

BIRGE, R. T. *Ap. J.* **55**, 273, 1922.
BLITZER, L. *Ap. J.* **91**, 421, 1940.
ADAM, M. G. *M.N.* **98**, 544, 1938.

(c) Center to limb variations in the CH and CN bands are described by:

PECKER, J. E., and R. PEYTURAUX. *Ann. d'Ap.* **10**, 90, 1948.

(d) Stellar Atmospheres

MCKELLAR, A., and W. BUSCOMBE. *Publ. Dom. Ap. Obs.* **7**, 361, 1948 (bands in *R* stars).
SETTERBERG, T. *Stockholm Ann.* **15**, 3, 1947 (CN and CH bands in late-type stars).

11. *Abundances of the Elements*

Summarizing accounts of the problem are given in

STRUVE, O. *Stellar Evolution.* Princeton: Princeton University Press, 1950.
Transactions of the Internat. Astron. Union, Vol. VII. Cambridge: Cambridge University Press, 1950, p. 457.
BROWN, HARRISON. *Rev. Mod. Phys.* **21**, 625, 1949.

References to detailed studies of individual stars are listed in Sec. (V-b). The classical papers include:

RUSSELL, H. N. *Ap. J.* **70**, 11, 1929.
STRÖMGREN, B. *Strömgren Festchrift.* Copenhagen: Ejnar Munksgaard Forlag, 1940, p. 258.
The latter paper describes the determination of the hydrogen to metal ratio.

Helium-rich stars are discussed by:

GREENSTEIN, J. L. *Ap. J.* **91**, 438, 1940 (υ Sagittarii).
POPPER, D. M. *P.A.S.P.* **59**, 320, 1947 (*HD* 124448).
BIDELMAN, W. P. *Ap. J.* **111**, 333, 1950 (*HD* 30353); **116**, 227, 1952. (*HD* 160641).

Some aspects of the problem of carbon abundance are discussed by

BIDELMAN, W. P. *Ap. J.* **112**, 219, 1950.
BIDELMAN, W. P., and P. C. KEENAN. *Ap. J.* **114**, 473, 1951.

A comparison of high- and low-velocity stars has been made by

SCHWARZSCHILD, M. and B. *Ap. J.* **112**, 248, 1950.
SCHWARZSCHILD, M., L. SPITZER, and R. WILDT. *Ap. J.* **114**, 398, 1951.
CHAMBERLAIN, J. W., and L. H. ALLER. *Ap. J.* **114**, 52, 1951.

CHAPTER 9

Solar Phenomena

1. Introduction

We begin our discussion with a review of what can be learned from direct photographs of the sun. The solar disk is not uniformly bright but shows a pronounced *limb darkening*. In Chapter 7 we showed how this darkening was a consequence of the temperature gradient in the solar atmosphere; the light from the limb reaches us from higher and cooler layers than the radiation emergent from the center of the disk.

Under conditions of good seeing we find that the bright surface or photosphere is resolved into small bright granules, which have been likened in appearance to rice grains, and which cover 50 to 60 per cent of the surface. The most striking features of all are the sunspots, refrigerated regions characterized by strong magnetic fields. Unlike the granules which occur everywhere on the solar surface they are confined to well-defined zones from 5° to 40° on either side of the equator. Near the limb we often observe in the sunspot zones large areas which are brighter than the surrounding photosphere. These are called faculae.

At times of solar eclipse, when the bright photosphere is hidden by the moon, we observe the outer envelopes that surround the sun, the chromosphere, a fiery-looking ring with numerous filamentary protuberances called prominences and the much fainter pearly corona which extends millions of miles from the sun. At times other than those of solar eclipse the prominences may be studied with a spectroscope with a widened slit, with the spectrohelioscope, or with the polarizing monochromator. The brighter portions of the inner corona can be studied under exceptionally fine atmospheric conditions with the coronagraph invented by Lyot.

The spectroheliograph, devised independently by Hale and Deslandres, enables one to photograph the disk of the sun in the light emitted in one of the dark lines of the Fraunhofer spectrum. For example, one may use the H and K lines of ionized calcium, the Hα line, the D_3 helium line, or any other sufficiently strong line. Spectroheliograms are usually obtained in the light of Hα or Ca II "K" and differ in appearance depending on the part of the line utilized. Near sunspot groups are large bright areas called "plages faculaires" by Deslandres. They are sometimes called bright flocculi. The faculae, observed in white light near

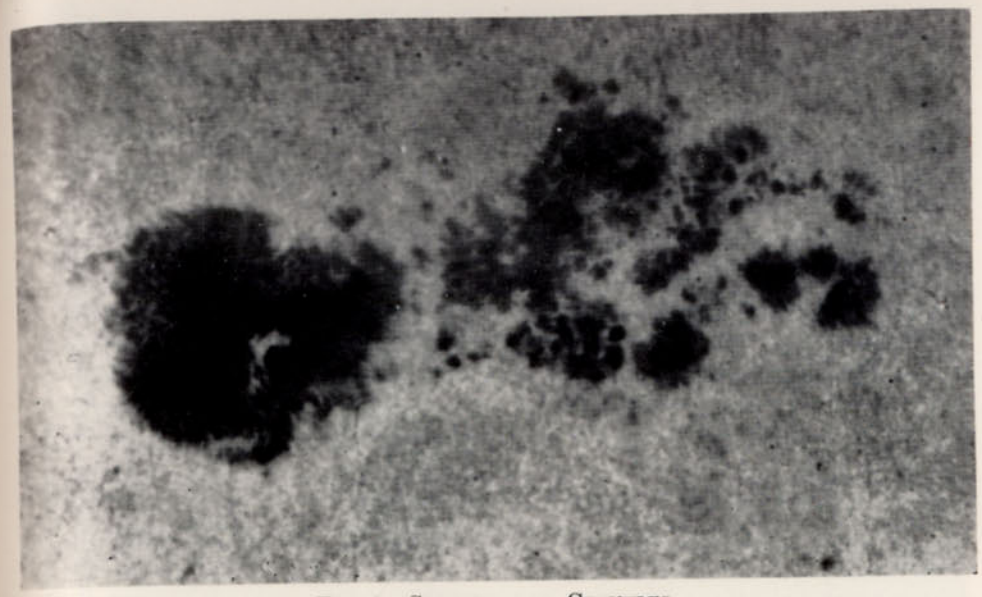

Fig. 1.—Sunspots and Granules

Photographed by Janssen June 22, 1885. (Courtesy, Meudon Observatory.)

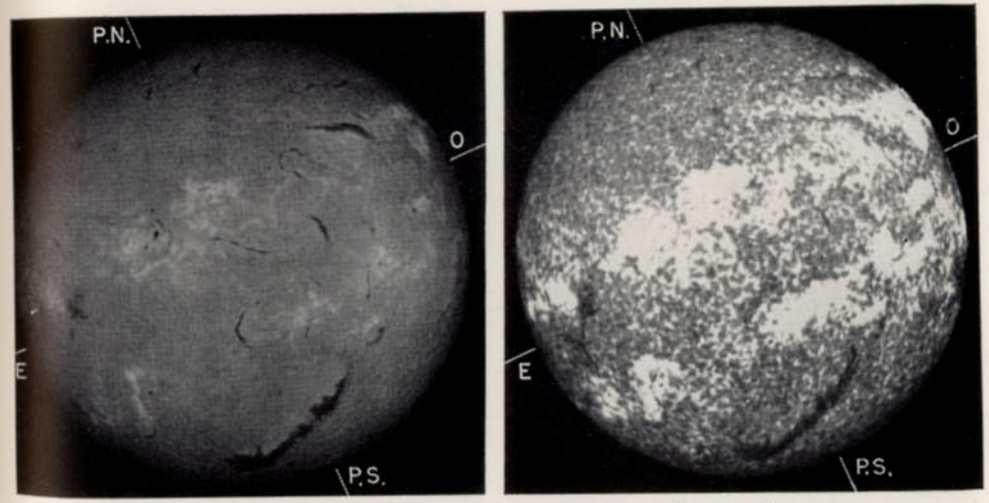

Fig. 2.—Spectroheliograms in Hydrogen and Ionized Calcium

Left: The monochromatic picture in the light of Hα shows the plages and prominences projected upon the disk as filaments.

Right: Notice that the plages in the light of the center of the K line are much more brilliant than in Hα. The fine structure of the background appears coarser.

October 5, 1947, $7^h\ 32^m$ G.C.T. (Courtesy, L. d'Azambuja, Meudon Observatory.)

Fig. 3.—The Great Sunspot Group Observed on Feb. 2, 1946
(Courtesy, Seth B. Nicholson and J. O. Hickox, Mount Wilson Observatory.)

the limb, coincide with the most intense portions of the plages.* Elsewhere on the disk are often seen large sinuous dark filaments or dark flocculi, prominences seen in projection (see Fig. 2).

2. Solar Rotation

Observations of sunspots and other phenomena establish that the sun does not rotate as a rigid body. The rotation period is shortest at the equator and increases towards the higher latitudes. The daily angular motion of solar rotation as determined from the motions of faculae, plages, sunspots, and filaments, and by radial velocity measures of Hα, λ4227, and the lower level lines is plotted against heliographic latitude in Fig. 4.

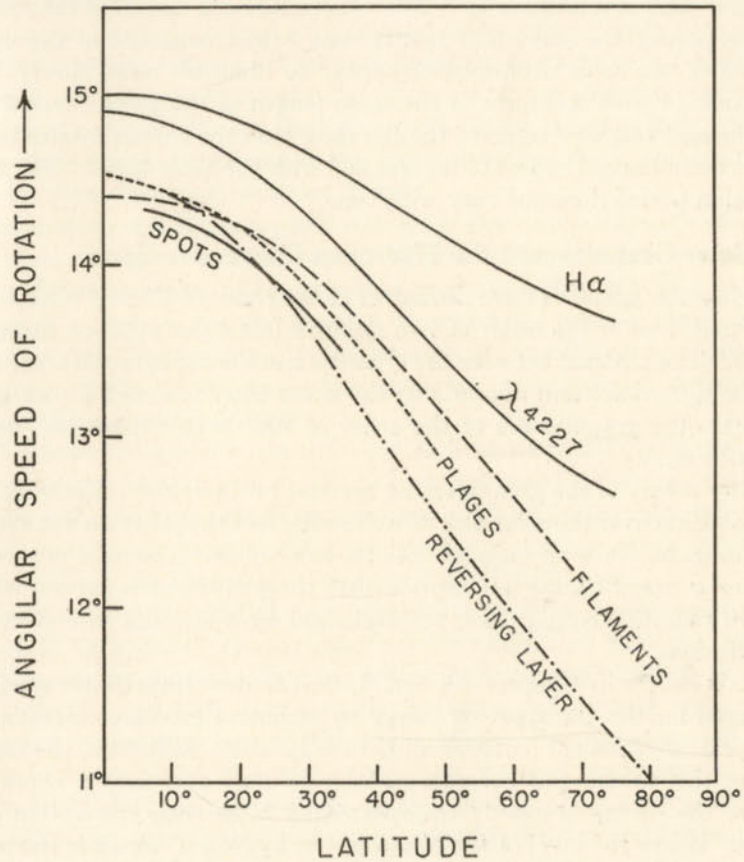

Fig. 4.—The Rotation of the Sun

* In the light of the center of the *K* line the plage is larger than the facula. Spectroheliograms taken a short distance away from the center of the line show "faculae" over the whole disk very similar to the white light form observed at the limb.

Measurements of the solar rotation from the position of spots on the disk were made many years ago by Scheiner, Carrington, Spoerer, Faye, and others. Chevalier and Maunder observed the rotation of the faculae, and Fox measured that of the flocculi from spectroheliograms obtained at Yerkes. The d'Azambujas have determined the solar rotation from the long-lived filaments. W. S. Adams, Duner, and others carried out extensive measures of the solar rotation from the Doppler shift in the Fraunhofer spectrum at the limb of the sun. If opposite limbs of the sun are observed, the lines are shifted to the violet on the approaching limb and to the red on the receding limb. Rotation measurements by the Doppler shift can be carried to latitudes as high as 75°; the solar rotation diminishes smoothly from a period of 24.6 days at the equator to 32.0 days at a latitude of +75°. The rotational speeds of the centers of the strong Hα and λ4227 (Ca I) lines (which originate in the upper layers of the solar atmosphere) appear to diminish more slowly with latitude. Lyot's measures of the wave length of the green coronal line on the east and west edges of the sun show that the corona rotates in the same direction as the rest of the sun and with the same speed. The solar rotation period does not vary with time.

3. Solar Granules and the Hydrogen Convective Zone

The solar granules have diameters of the order of 1″ to 2″ (Keenan), and half-lives of the order of two minutes (Grotrian and ten Bruggencate). The contrast between the granules and the background is greatest in the ultraviolet and depends on the wave length in such a way as to indicate the granules are of the order of 100° hotter than the "dark" interstices.

Any theory of the granules must account for their sizes, lifetimes, and distribution over the solar disk as well as the fact that they do not appear to change in size or appearance with the solar cycle. The most promising theory is based on the assumption that the photospheric layers, which are in radiative equilibrium, are underlaid by a stratum in convective equilibrium.

It is shown in Chapter 10, Sec. 5, that if the temperature gradient required for the transport of energy by radiative processes exceeds the temperature gradient corresponding to adiabatic equilibrium, the region where this occurs will become unstable and go over into a condition where the energy is mostly transported by large scale convection currents. Below the level of the photosphere, hydrogen, which is the most abundant element, becomes ionized and an unstable convection zone results.

Theoretical calculations by Unsöld and by Siedentopf show that the convection layer model gives a rational explanation of the sizes and

lifetimes of the granules and the differences in brightness between the granules and their background. The analysis is largely based on the old Prandtl concept of turbulence elements which, as we have discussed in Chapter 3, is somewhat inadequate.

The solar granules appear to offer an interesting application of the concept of the spectrum of turbulence. The direct measures of the mean random velocities lead to a value of 0.37 km/sec (Richardson and Schwarzschild). This value refers to granules of the order of 2″ or 1500 km diameter. From line profiles, C. W. Allen derived a turbulent velocity of 2.8 km/sec, at the limb and 1.7 km/sec at the center, however. The main contribution comes from elements of the size that have the highest velocity. Hence the turbulent velocity from line profiles corresponds to the maximum of the curve that relates turbulent velocity and element size. On the other hand, the turbulent velocity from the curve of growth, which Schwarzschild and Richardson adopt as 1.7 km/sec, refers to elements smaller than the thickness of the effective reversing layer that is responsible for the lines used in the curve of growth. Since these atmospheric layers are of the order of 80 km thick, the relevant element diameters may be about 20 km.

Richardson and Schwarzschild concluded that the turbulent elements of highest average velocity are about 150 km in diameter, i.e., about one tenth of the diameter of the observed granules and equivalent to the height of a layer in the photosphere by which the density would drop by a factor e. The value of 1.7 km/sec derived from the curve of growth falls beyond the maximum in the spectrum of turbulence, where the sizes of the elements are small.

The observed granules show a random brightness difference of 0.054 magnitudes at λ5800, corresponding to a temperature difference of 64°K. Apparently, the most contrasty features on the sun have not been resolved and the temperature differences may amount to as much as 400°K for elements at the maximum of the spectrum of turbulence.

From an analysis of the velocities of the granules by the statistical theory of turbulence, Frenkiel and Schwarzschild find that the turbulence spectrum does not decrease with increasing size (>2700 km) of the turbulent elements, but actually increases and appears to have a secondary maximum at 15,000 km.* Hence two separate driving mechanisms may be in action. One, the thermal instability of the strata just below the photosphere, gives small size turbulence elements. The other may correspond to very large eddies below the photosphere, or may represent large-scale, randomly excited, free oscillations in the outer layers of the sun.

* *Ap. J.* **116,** 422, 1952.

One further point merits attention. The convection zone cannot extend to the top of the photosphere since the limb-darkening measures (cf. Ch. 7) indicate that the uppermost strata are in radiative equilibrium. Keenan showed that if we suppose that convection sets in at an optical depth of about 2/3 we can secure good agreement with the observations.

4. Sunspots

Sunspots consist of a dark central area, or umbra, surrounded by a somewhat brighter section called the penumbra—characterized by filaments of granules radiating from the umbra. The sizes and shapes of the spots vary greatly, but the percentage of large to small spots is nearly constant with the phase of the cycle.

Usually, spots, of apparently common origin, appear in a group. A typical group appears as small spots, apparently formed from small pores between the granules, extending 3° or 4° in longitude. Two main spots develop, grow rapidly, and separate in longitude to a distance of 10° or more. The following spot attains a maximum size in three or four days, while the leader (which acquires the larger size) takes a week or nine days for its full development. Often smaller spots develop within the group. After attaining maximum size, a typical spot declines more slowly, taking weeks or even months. The following spot breaks up into several spots which shrink and disappear in a few days or weeks while the leader survives as a single spot which gradually fades away in a few weeks or months.

The largest spot group observed on the sun (January to May 1946) has been described by Nicholson and Hickox of Mount Wilson (see Fig. 3). It consisted of two large spots with complicated umbrae and a number of smaller spots. The group was so large that two days were required for the solar rotation to bring it into view. Both of the large spots were roughly oval in shape; the preceding spot was 62,000 miles long and 35,000 miles wide, and the following spot was 90,000 miles long and 60,000 miles wide. They were 40,000 miles apart; hence the total length of the group was nearly 200,000 miles. The total area of the group, six billion square miles, comprised 0.0054 of the sun's visible surface. When the group returned to the east limb on the next rotation its area had diminished but it had spread out to over 36° in longitude, or more than 220,000 miles. This great spot group made four transits across the disk, and was seen last on May 8 on the west limb, 99 days after it was first seen on January 29. The last remnant was a small stable spot, 10,000 miles in diameter.

Many years ago Hale noticed the vortical forms of gaseous filaments on Hα spectroheliograms, which suggested material flowing into the

spots. St. John's measurements of the displacements of the hydrogen lines confirmed the inward and downward motion of material, although he found no cyclonic motions. Moderately strong lines, of Rowland intensity 10 to 40, showed no shifts. On the other hand, Evershed's measures of lines of Rowland intensity -1, -2, or -3 indicated material flowing out of the spot tangent to the solar surface at rates up to 2 km/sec. Evershed and St. John studied stable spots, whereas Abetti found from short-lived spots that the gases responsible for the weak lines flowed outward along vortices opposite to the sense of the hydrogen vortices and with speeds of rotation of the order of 1 km/sec. How are these observations to be reconciled?

At the center of a strong line, e.g., $H\alpha$, we see to small optical depths, i.e., we observe radiation from great heights in the atmosphere. In a weak line, on the other hand, the radiation reaching us comes from much lower layers, i.e., from the photospheric levels. The centers of lines of intermediate strength represent radiation from intermediate layers. Hence the high- and low-level atoms appear to have oppositely directed vortical motions. The motions of the vortices on the Hα spectroheliograms appear to follow the sense of terrestrial cyclones in four fifths of all examples, i.e., the direction of rotation is clockwise in the southern hemisphere and counterclockwise in the northern hemisphere. This fact suggests the motions arise from Coriolis forces rather than from some other cause such as magnetic or electrical forces.

The temperature ratio of sunspot to photosphere follows from a comparison of their respective rates of emission of energy, the intensity distribution in their respective continua, and changes in line intensity from spot to photosphere.

Pettit and Nicholson compared the fluxes of spot and photosphere by means of a thermocouple. They found a flux ratio of 0.47 which would imply a spot temperature of about 4700°K. The true ratio may be actually smaller, because of scattered light from the photosphere, in which event an even lower temperature is implied.

The brightness of the umbra and penumbra varies from spot to spot. The larger spots have a tendency to be darker, but the size of the spot does not tell the whole story. Korn found the intensities of the umbrae to range from 0.05 to 0.85 that of the photosphere—corresponding to a temperature range from 3920°K to 5610°K. The intensities in the penumbra range from 0.52 to 0.82 that of the photosphere, implying a temperature range from 5210°K to 5580°K.

Finally, we may estimate the excitation and ionization temperature of a spot from a comparison of selected spectral lines in the spot and photosphere. The scattering of photospheric light into the spot image by the earth's atmosphere, the appearance of weak molecular lines in the

spot spectrum, and the splitting and polarization of lines in the magnetic field of the spot—all serve to complicate the problem. Miss Moore used eye estimates of intensities interpreted with the aid of the Rowland scale calibration. From a comparison of the same lines in spot and photosphere one can obtain $\delta\theta = \left(\frac{1}{T'} - \frac{1}{T}\right) \times 5040$. Here T is the excitation temperature of the photosphere, T' that of the spot. Miss

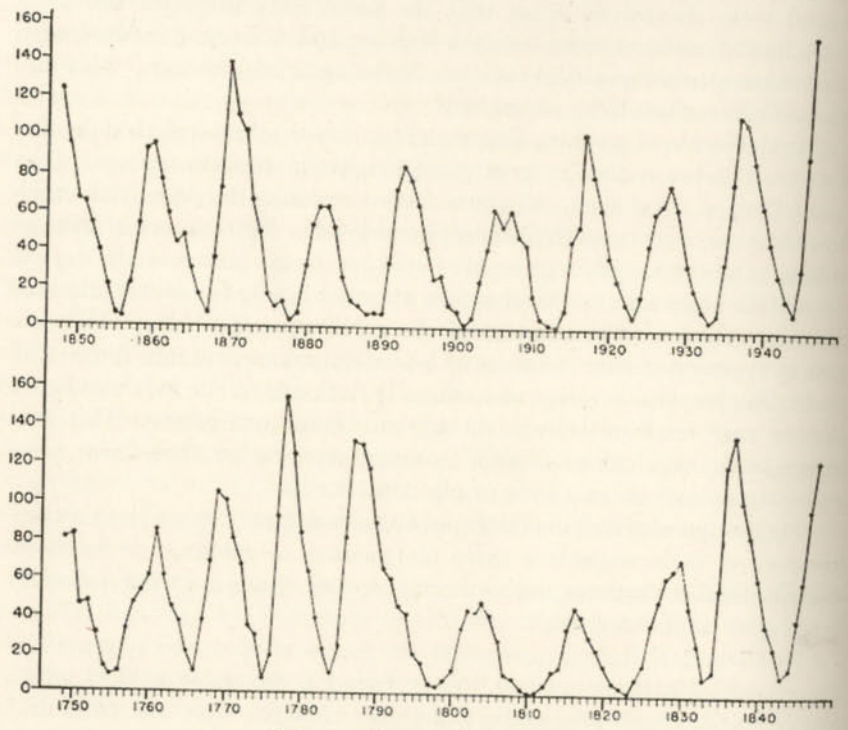

FIG. 5.—SUNSPOT NUMBERS

The most conspicuous feature of the solar cycle is the variation of the number of sunspots with a period of 11.5 years. Note the unequal heights of the various sunspot maxima. (Courtesy, D. H. Menzel, *Our Sun*, Cambridge: Harvard University Press, 1949.)

Moore found $\delta\theta = 0.19 \pm 0.01$. Similarly, the lines of neutral and ionized atoms, employed in connection with the Saha equation, give the electron pressure variation from spot to photosphere. Miss Moore found the ratio of the electron pressure in the spot to that in the photosphere to be 0.6 ± 0.1. If the ionization temperature is taken as equal to that of excitation, the spot temperature is 4720°K.

More recently, ten Bruggencate and von Klüber determined the excitation temperature of sun spots by a curve of growth method. They

employed iron and titanium lines and modified the curve of growth to allow for the influence of the Zeeman effect. Their investigations gave spot temperatures of the order of 3800°K to 3900°K, presumably because they studied large spots. They found 4.3 times as much neutral titanium above the spot as above the photosphere but only 0.67 as much Ti II. There are more atoms/cm² above the spot than above the photosphere because the opacity of the gases in the spot is lower. The electron pressure in the spot appeared to be about 4 per cent that of the photosphere.

A quantitative comparison of the spectra of spots and photosphere must take into account the fact that the Zeeman effect varies from line to line. Therefore the statistical treatment via the curve of growth is inadmissible. We should compare individual lines in spot and photosphere with due regard for their particular Zeeman patterns.

From a study of the λ5165 carbon band, Richardson found $\delta\theta = 0.17$ and spot and photosphere temperatures, 4500 ± 400°K and 5300 ± 400°K, respectively.

If the refrigeration of the spots is to be interpreted in terms of rising gases cooling by expansion, as Russell and others suggested many years ago, the spots should be considerably darker towards the limb than at the center of the disk. Observations by Richardson and by Wanders and Wormell show the darkening to the limb to be the same in the spots as in the photosphere; thus the temperature gradient follows the radiative equilibrium law, at least in the outer layers.

On the basis of a more detailed theoretical study, Thackeray has also concluded that there is no way of reconciling an adiabatic equilibrium in the spots with a radiative equilibrium in the photosphere.

5. Magnetic Fields of Sunspots

The vortical structure observed on Hα spectroheliograms suggested to Hale that it would be worth while to look for magnetic fields in the spots.* An observational test of this hypothesis could be made immediately. Some twelve years previously, Zeeman had shown that spectral lines radiated by atoms in a magnetic field were split into a number of components, polarized in a distinctive fashion.

With a high dispersion spectrograph and analyzers of polarized light, Nicol prisms, quarter-wave plates, etc., Hale was able to demonstrate that each spot possessed a magnetic field, and that these fields were large by terrestrial standards—of the order of 3000 to 4000 gausses. One may measure not only the magnitude but also the direction of the field. An outward-field direction would mean that a north-seeking or positive pole would be urged outwards. Hale denoted sunspot polarities

* Later work showed these vortices to be analogous to cyclones on the earth, i.e., purely hydrodynamical phenomena.

as R or V. For R polarity a particular polarized component of a line in a spot of positive polarity is displaced towards the red. With the same apparatus the same line component in a spot of negative polarity would be shifted toward the violet.

Hale and Nicholson classified spots in three groups, *unipolar*, *bipolar*, and *complex*. Unipolar spots are single spots or groups of spots with the same magnetic polarity. In their simplest form, bipolars consist of two spots of opposite polarity; the line joining them makes a small angle with the equator. The preceding spots of such pairs are of opposite polarity in the two hemispheres. For example, if the preceding spot in the northern hemisphere is positive (R or north-seeking), the preceding spot in the southern hemisphere will be negative. More often a bipolar group will consist of a stream of spots whose preceding and following members have opposite polarity. Direct telescopic observation cannot distinguish between spots of opposite polarity, although polarization tests in their spectra can tell them apart at once. In complex spot groups, spots of opposite polarity are mixed together. The bipolar appears to be the fundamental type.

Hale and Nicholson employed both the appearance of the bright calcium flocculi or plages and the magnetic polarities in their spot classification scheme:

(α) denotes unipolar spots for which the distribution of flocculi preceding and following the group is fairly symmetrical.

(αp) denotes unipolar spots in the preceding part of an elongated area of flocculi.

(αf) denotes unipolar spots in the following part of an elongated area of flocculi.

(β) denotes bipolar spots for which the preceding and following members, whether single or multiple, are approximately equal in area.

(βp) denotes bipolars for which the preceding member is the principal component of the group.

(βf) denotes bipolars in which the following member is the largest. The great sunspot group of January 29, 1946, in which the following member was the largest, was classified as βf.

($\beta\gamma$) denotes those groups that show bipolar characteristics but with no well-defined dividing line between groups of opposite polarity.

(γ) denotes complex spots.

Hale and Nicholson give numerous examples to show how the polarization criteria are to be employed to distinguish the character of spot groups.

The following table* gives the percentage and frequency of each spot group class for the interval from 1915 to 1924. The number given in the unclassified column is the percentage of all observed groups; the percentages in other columns are of groups actually classified.

Classification of Sunspot Groups

α	αp	αf	β	βp	βf	$\beta\gamma$	γ	Unclassified	
14	20	4	21	29	8	3	1	7	per cent of groups
284	409	80	423	592	159	61	17	149	total

Hale and Nicholson remark,† "The most striking fact brought out is the large preponderance of bipolar groups, and the tendency of unipolar groups, even when not lapsing intermittently into the bipolar state, to hover continually on its margin. A study of the daily history of the spots further emphasizes this tendency as it shows the frequent passage, back and forth, from one type to the other and the development from time to time of invisible spots in unipolar groups which never visibly attain the bipolar condition."

Of considerable importance is the relation between the solar cycle and the magnetic polarities of the spots. When a new cycle begins, the spots first appear in high latitudes (about $\pm 30°$). As the cycle advances, the number of spots increases and they appear closer and closer to the equator (see Fig. 6) until, as the cycle dies away, all are found in low latitudes. Before the old cycle dies away completely, a new cycle begins in a high latitude, with reversed polarity. If the preceding spot in a group of the dying cycle has R polarity, the preceding spot in a group of the new cycle in the same hemisphere will have V polarity. Since it requires 23 years for the status quo to be restored, we think of the complete solar cycle as requiring 2×11.5 years.

We shall summarize here some of the most important magnetic properties of the spots. The relation between the magnetic field H and the area of normal pairs is given by an equation of the form

$$H = a - b\frac{H_m}{A} \tag{1}$$

where $a = 3700$ gausses, and b is a constant which depends on the units in which the area A is measured. Thus, for large spots, the field does not depend closely on the area. The field is closely confined to the spot:

* *Ap. J.* **62**, 293, 1925. † *Ibid.*

it is largest at the center and becomes too small to detect at the edge of the penumbra. H_m is the maximum value of the spot field.

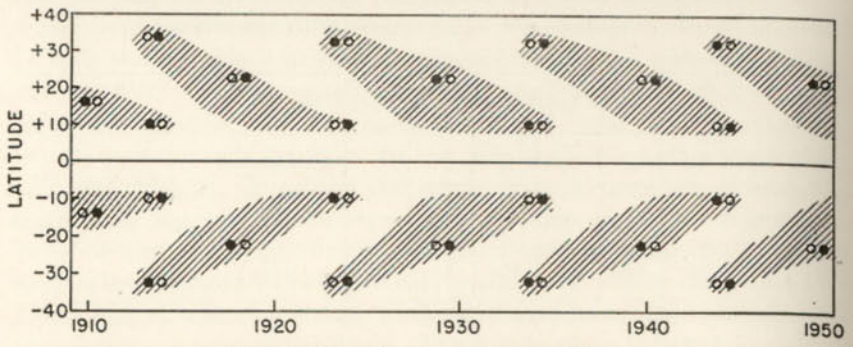

FIG. 6.—THE LAW OF SUNSPOT POLARITY

This diagram shows the approximate variation in latitude and polarities of sunspots observed at Mount Wilson from June, 1908 to January, 1950. The preceding spot is indicated on the right. Filled circles denote spots of north-seeking polarity; open circles denote those of south-seeking polarity. The cross-hatched area indicates roughly the distribution of the spots at any one time. Notice the decrease in the average latitude of the spots as the cycle advances (Spoerer's Law), and the reversal of polarity in each hemisphere at the end of each cycle.

Careful photometric measurements of the Zeeman components of the spot lines across the disk can be used to determine the inclination of the lines of force. Recent studies confirm the earlier results of Nicholson, who found that the angle θ between a normal drawn to the surface and the lines of force emerging from a spot could be closely represented by an equation of the form

$$\theta = \frac{\pi}{2}\left(\frac{r}{b}\right) \tag{2}$$

where b is the radius of the spot to the outer edge of the penumbra and r is the distance from the center. If H_0 is the field at the center the field strength in the spot can be represented fairly well by the formula

$$H = H_0\left(1 - \frac{r^2}{b^2}\right) \tag{3}$$

H. von Klüber made simultaneous observations of the magnetic field strength as a function of the distance across the spot and the intensity of the spot as measured upon calibrated direct photographs. He found the field to vary as the blackness of the spot. The most surprising result of this investigation was the detection of single spots in which the field reversed itself at the center, as though the two components of a bipolar spot were pushed together.

Statistical analyses of the Mount Wilson observations indicate that the field strengths of the spots appear to diminish from the center of the disk toward the limb. Although photospheric light scattered into the spot might account for some of this effect, the phenomenon appears to indicate a decrease of magnetic field strength with height in the atmosphere. From a comparison of lines of different intensity, R. B. King found a gradient of 2.5 gausses/km, J. Houtgast and A. van Sluiters found a gradient of 5.7 gausses/km, whereas from the divergence of the lines of force in the field Joy and Nicholson suggested 0.7 gausses/km. Possibly the field becomes attenuated faster than the spreading of the lines of force would indicate.

The area of a long-lived (60^d) spot increases rapidly at first, reaches its maximum in about ten days, and then gradually decreases. The magnetic field, on the other hand, reaches a maximum near 3000 gausses and remains roughly constant for about thirty days. Thereafter it declines, slowly at first and then more rapidly. Thus the total magnetic induction varies with the area. About a day would be required to establish the field, if it is produced by the darkening of the spot, which seems extremely doubtful.

The magnetic field in a spot does not remain strictly constant with time. Even quiet spots show variations of the order of 20 to 30 gausses an hour and in the course of several days variations of hundreds of gausses may occur. The variations do not seem to be more frequent or pronounced in magnitude when flares are observed in the spot group.

Following S. Chapman we may discuss the magnetic fluxes, dipole moments, and mechanical forces involved in spots. If we integrate the vertical components of the magnetic field $H\cos\theta$ over the area of a circular spot [cf. eqn. (3)], the emergent flux is found to be roughly

$$F = \tfrac{1}{3}\pi b^2 H_0 \tag{4}$$

which is related to the pole-strength m of the spot by

$$F = 2\pi m \tag{5}$$

For example, the spot *MW* 6618, September 21, 1939, had a field strength H_0 of 3600 gausses, a radius b of 28,000 km, and thus a magnetic flux of 3×10^{22} gausses cm^2.

The magnetic dipole moment M corresponding to a bar magnet of pole strength m and length d is $M = md$; e.g., the bipolar spot *MW* 6725 consisted of two spots each of radius b = 20,000 km, and of field strength, 3900 gausses, separated by 175,000 km. Hence the magnetic moment is

$$M = \left(\frac{F}{2\pi}\right) \times d = 5 \times 10^{16}\ \Gamma\ \text{km}^3 \tag{6}$$

or 600,000 times the dipole moment of the earth. The dipole moments of sunspots are usually nearly parallel to the equator, although the leading spot is often a little closer to the equator than the following spot.

If the lines of force of the components of a bipolar spot are joined together under the surface as Hale suggested, we may compare the spot pair with a horseshoe magnet. The flux from one spot simply flows into the other spot of the group. The magnetic flux from a unipolar spot must return to the solar surface somewhere in an unspotted region. The same phenomenon must also occur in bipolar and complex groups where the total north-seeking flux and south-seeking flux from recognized spots do not balance. The plages sometimes suggest where the missing magnetic flux returns to the sun. They precede the birth of a spot group and persist after it has vanished. Thus, they usually indicate that a particular unipolar spot is a remnant of a defunct bipolar group. As the sunspot group decays, the plages fade also and in the end they symmetrically surround the expiring remnant of the group. Hale and Nicholson found magnetic fields in the plages around a spot. They called such regions of appreciable magnetic flux, but no darkening, "invisible spots."

If we suppose that the magnetic fields of spots are produced by electrical currents flowing in circular paths about their axes, as in a solenoid, the total flow through the radial half plane passing through the axis of the magnet is $\frac{\bar{H}}{4\pi}$ e.m.u. $= \frac{10\bar{H}}{4\pi}$ amps per cm length along the axis. Thus if $\bar{H}$ is 3000 gausses, the current is 2400 amps per cm depth below the surface. The direction of current flow around the axis of the spot of north-seeking polarity is counterclockwise as seen from the earth.

The mechanical forces caused by these large magnetic fields must be considerable. The lines of force may be regarded as subject to stresses. If the field strength is H, these stresses consist of a tension $\frac{H^2}{8\pi}$ along the lines of force, and equal pressure p_{mag} normal to them. Alfvén supposed that the spot was maintained in equilibrium by a difference in gas pressure inside and outside the spot such that

$$p_s + p_{\text{mag}} = p_s + \frac{H^2}{8\pi} = p_0 \tag{7}$$

where p_0 is the gas pressure outside the spot and p_s is the gas pressure inside. The coolness of the spot and its sharp boundary present difficulty in any theory. How is such a refrigerated region to be maintained on the solar surface? Presumably radiation from the side would heat the spot material, p_s would increase, and $p_s + p_{\text{mag}}$ would exceed p_0.

The spot might then expand and additional material would be drawn up along the lines of magnetic force from great depths. If the spot is to be stable, these gases must be cooler when they arrive at the upper level than the material they replace. The adiabatic cooling of the rising gases must retard the warming of the spot. In view of the effect of the hydrogen convection zone it is likely that rising gases would be actually hotter. Cowling has argued that the base of the spot must be so deep that appreciable radiation would leak in from the side and the spot would have a fuzzy edge in contradiction with observation. This objection applies not merely to the Alfvén theory but to all present ideas on the origin of spots. The pressure difference between the spot and the surrounding material at the base apparently would require an inadmissibly large magnetic field.

Further, it is to be observed that two spots of opposite polarity in a bipolar group should attract one another. Following Chapman, consider two spots, each of pole strength $\frac{4 \times 10^{22}}{2\pi}$ Γ cm², and separated by 125,000 km. If we treat them as point poles the mutual attraction is $\left(\frac{4 \times 10^{22}}{2\pi}\right)^2 \frac{1}{(1.25 \times 10^{10})^2} = 2.6 \times 10^{23}$ dynes, or 260 million million tons. During the growth of a spot group, the two components tend to move apart against this strong magnetic attraction, apparently under the influence of powerful hydrodynamical forces. The magnetic energy stored in a sunspot is

$$\frac{1}{8\pi} \int H^2 \, dv \tag{8}$$

integrated over the entire volume of the spot. At the center, where the field is 3000 gausses, the energy/cm³ is 3.6×10^5 ergs, and since the energy radiated at the center of the spot is about 1.2×10^{10} ergs/cm², the radiation/sec is equal to the amount of magnetic energy contained at any one time in a layer a third of a kilometer thick.

From a study of large spots, Cowling showed that the magnetic field cannot grow and decay with the appearance of the spot, but must exist before the spot becomes visible and must persist after it disappears. Since a strong magnetic field is rarely observable in the absence of a visible spot, the field existing before and after the spot must be below visible layers, or different in form from that observed in a spot. Cowling calculated that about 300 years would be required for the electromagnetic decay of a sunspot field. Or, conversely, this is the time required for the field, if due to electric currents, to increase to its steady state value against the initial effects of self-induction. More recent work indicates that even longer times are required.

Cowling suggests that the growth and decay of the field is caused by the motion of gases which carry the magnetic field with them. Many years ago, Bjerknes suggested that lines of force run in a tube or vortex ring around the sun and just below its surface. When part of this field is convected to the surface a spot pair arises.

Alfvén suggested a theory of sunspots based on magneto-hydrodynamical waves which was amplified and extended by Walén. The magnetic fields are presumed to originate deep in the sun as vortex rings which move through the solar material. As these vortex rings intersect the surface of the sun, spots are produced. Cowling has shown that the present form of the theory probably cannot explain the origin of the spots. Unless the motions in the vortex rings are nearly parallel to the surface, the magneto-hydrodynamic waves suffer serious losses of energy as they rise through a stable region, but if they are horizontal they cannot produce spots. Although the exact mechanism of the Alfvén-Walén theory is open to question, there seems little doubt that the origin of sunspots must be sought in disturbances deep in the interior of the sun. To some extent, sunspots may be a consequence of the solar rotation but at the present time a satisfactory theory of their origin is not available.

In addition to the magnetic fields of the spots, one might anticipate a general solar magnetic field akin to that of the earth. Hale believed he found a field of about 25 gausses but subsequent measurements failed to confirm this result. G. Thiessen, working at the Hamburg Observatory with a highly sensitive photoelectric method, measured a field of the order of 1 or 2 gausses, with a probable error of about 0.5 gausses. More recently, von Klüber concluded there is no evidence for a general magnetic field but this result cannot be taken as final.

Cosmic ray analyses required that the sun have no field greater than about 10 gausses. Theoretical studies by Sweet suggest that the law of rotation of the sun cannot be reconciled with the existence of a general field.

The strongest argument for the existence of a general magnetic field, at least in the upper layers of the solar atmosphere, comes from the appearance of the corona, whose polar streamers at the time of sunspot minimum strongly recall the appearance of the lines of force around a magnetized sphere.

H. C. van de Hulst points out that the polar rays cannot be explained as ejected streams of material because the densities decrease too rapidly outwards. He suggests that they coincide with lines of magnetic force, and that the diffusion perpendicular to the magnetic field is negligible even if the field is low. Hence the form of the rays may give clues to the character of the magnetic field. This field may be variable with time; at the surface of the sun it seems to be intricate in structure.

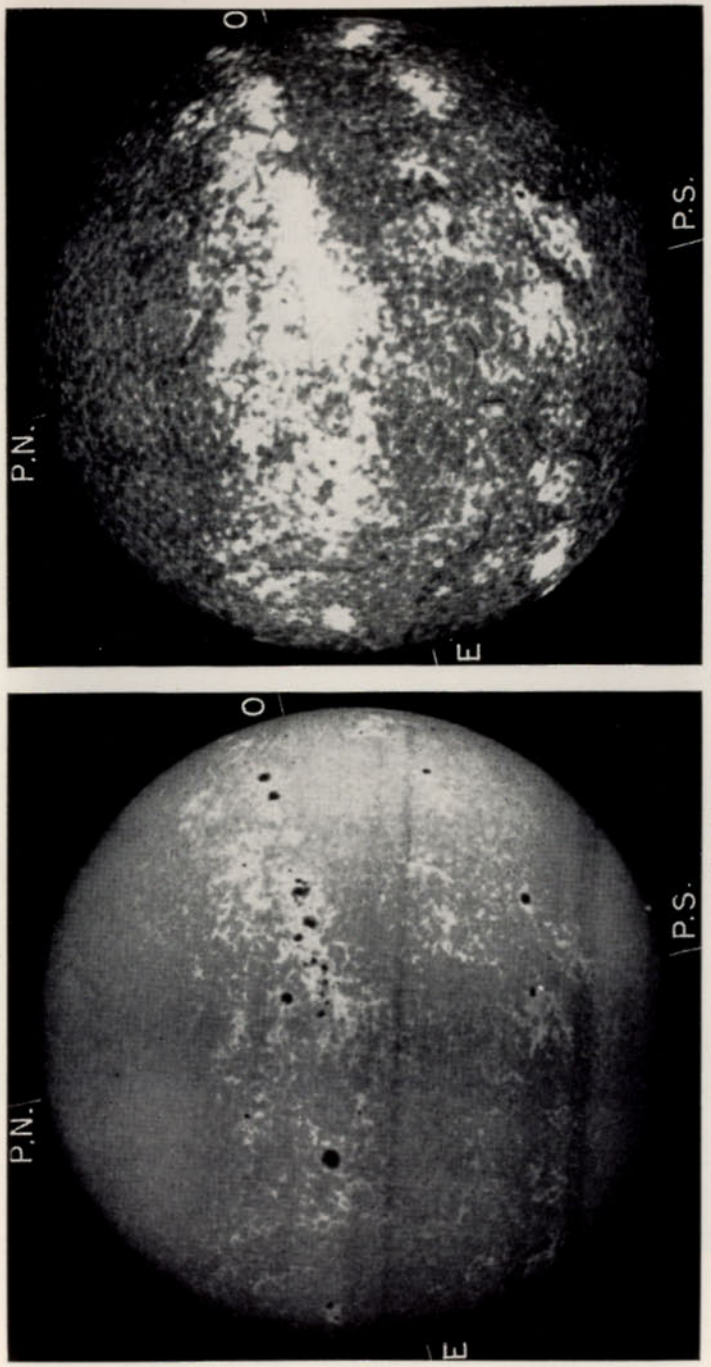

FIG. 7.—CALCIUM SPECTROHELIOGRAMS

Left: Solar image in the violet wing of the *K* line (K_{1V}). *Right:* Solar image in center of *K* line (K_3). August 14, 1947, $7^h\ 45^m$ G.C.T. (Courtesy, L. d'Azambuja, Meudon Observatory.)

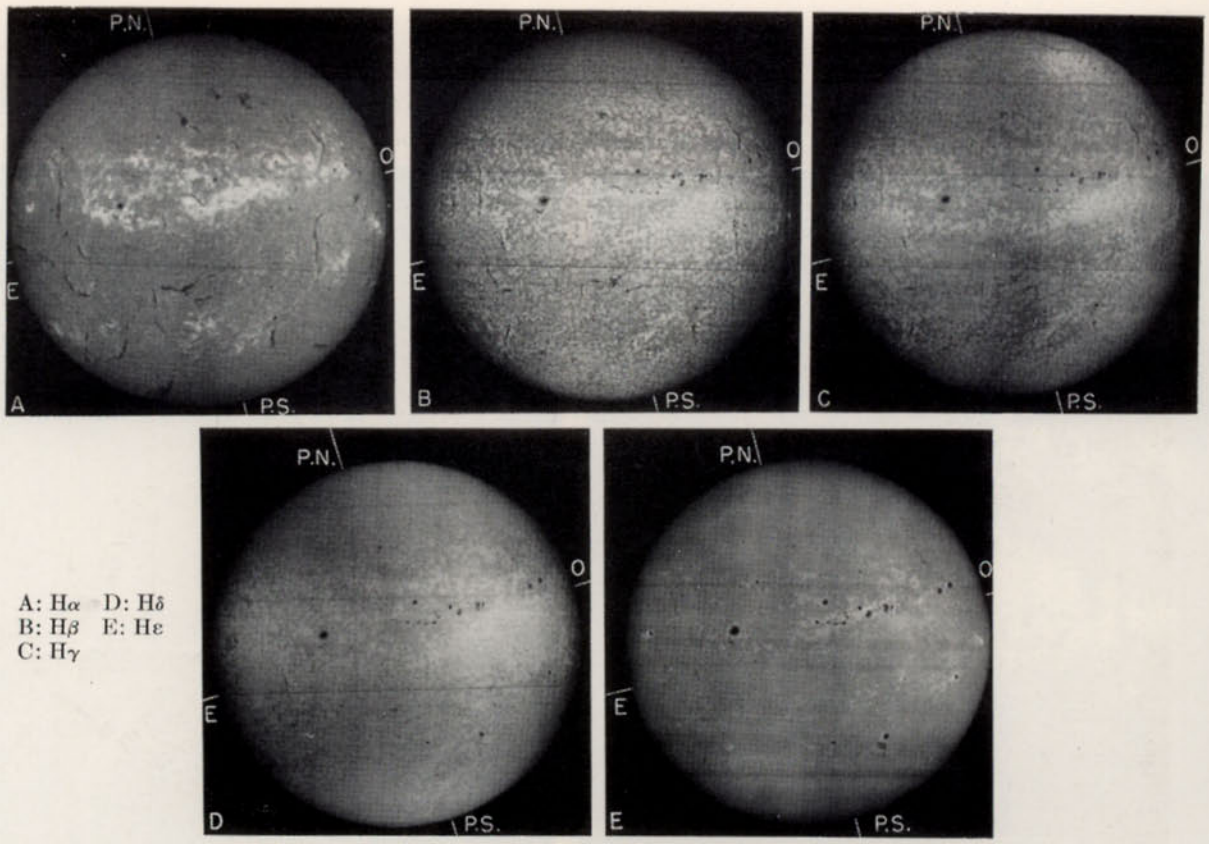

A: Hα D: Hδ
B: Hβ E: Hε
C: Hγ

FIG. 8.—HYDROGEN SPECTROHELIOGRAMS

Notice that the filaments and plages become less and less conspicuous from Hα to Hδ. Hε is submerged in the wing of the "*H*" (Ca II) line (compare Fig. 7 left for the *K* line wing, which is identical). The superposition of *H* (Ca II) and Hε which absorbs slightly over the plages causes a weakening of the plages in E. (*Courtesy, L. d'Azambuja, Meudon Observatory, August 14, 1947.*)

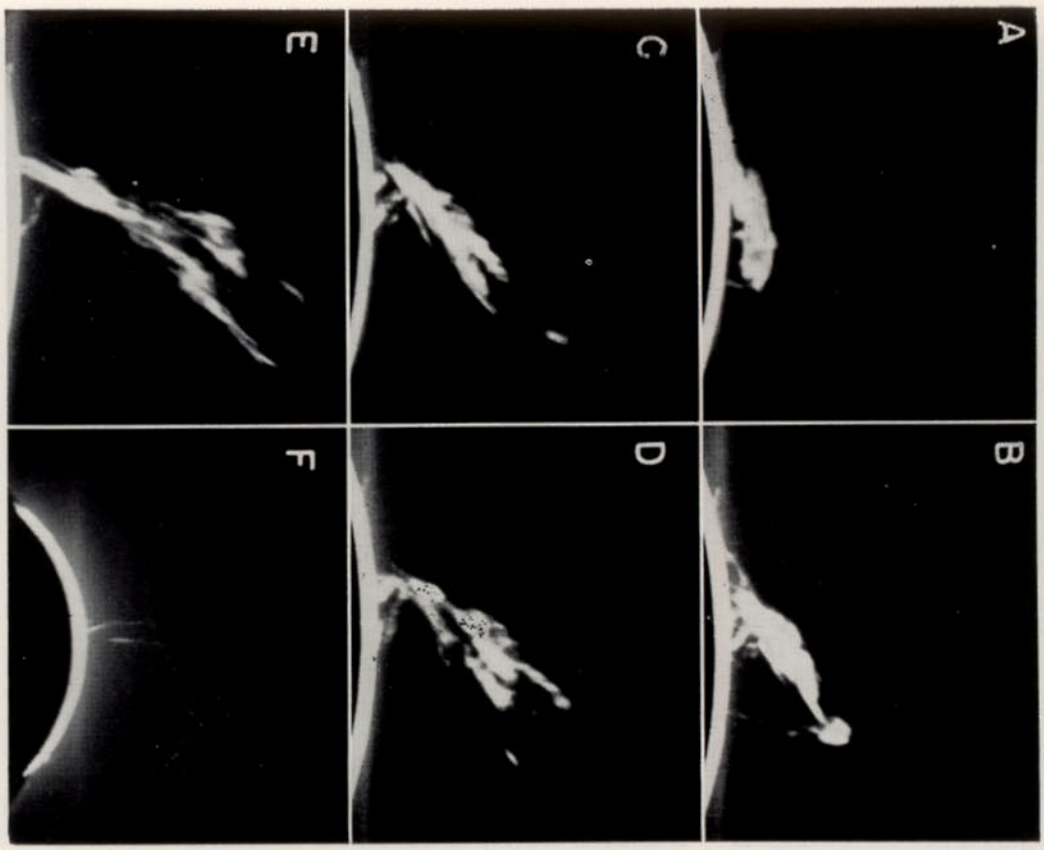

FIG. 9.—AN ERUPTIVE TYPE PROMINENCE

Prominence of September 17, 1937, photographed in the K_2 (Ca II) line. G.C.T. of exposures:

A: $14^h\ 50^m.69$ B: $14^h\ 55^m.84$ C: $15^h\ 06^m.13$
D: $15^h\ 09^m.11$ E: $15^h\ 14^m.31$ F: $16^h\ 06^m.7$

In F the prominence leaves the frame at 1,000,000 km above the sun. (McMath-Hulbert Observatory, University of Michigan.)

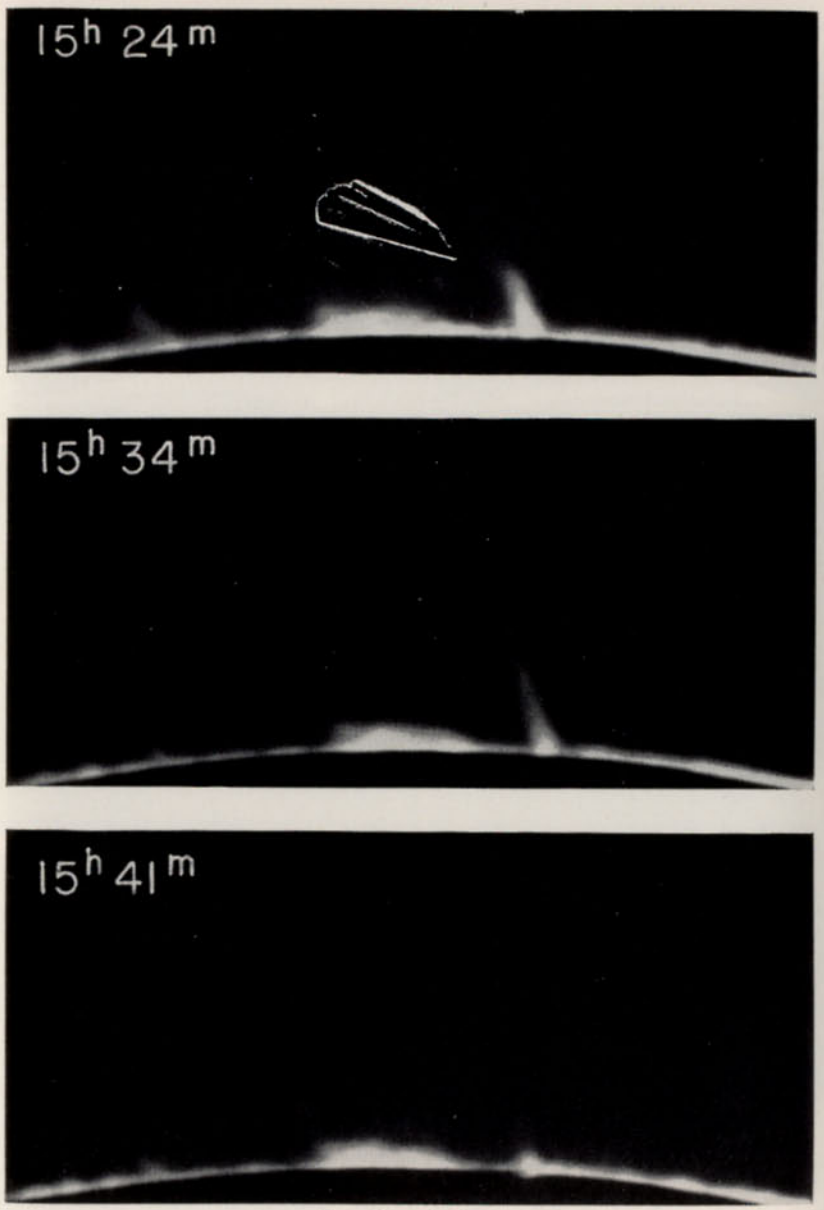

FIG. 10.—A SURGE

Photographed August 23, 1948, at the McMath-Hulbert Observatory.

Studies of magnetic fields in sunspots and elsewhere upon the solar disk have been aided by the greatly improved experimental techniques developed largely in Germany by G. Thiessen, H. von Klüber, W. Grotrian, and their colleagues.

The most powerful technique for the study of magnetic fields upon the solar surface, however, is that developed by H. W. and H. D. Babcock at the Mount Wilson Observatory. Their procedure involves the photoelectric measurement of minute Zeeman shifts in spectral lines formed in the fifth order of a grating that gives a dispersion of 11 mm/A and a resolution of 600,000. The entire disk of the sun can be scanned and fields down to about 1 gauss (the noise level in the photomultiplier tubes) can be measured.

The magnetic pattern of the sun includes a number of strong multipolar fields which persist from day to day with measurable fluctuations, as well as regions of smaller magnetic activity, some of which might be quite extensive. Areas with fields as strong as 30 gausses are measured near spot groups, incipient spots, and plages. Furthermore, following the disappearance of a visible sunspot, the field may last for several days. The Babcocks found persistent magnetic deflections in high latitudes. The field showed a fine structure but the predominant magnetic polarity is of opposite sign near the north and south poles of the sun. On some days at least, the sun appeared to have a badly distorted but real semblance of a dipole field. The magnetic effects are certainly so complex that extensive observations will be needed to establish their character.

6. Studies with the Spectroheliograph—Disk Phenomena

The amount of information obtainable from direct photographs of the solar disk is limited. One recognizes that faculous areas tend to be associated with sunspots and that they precede the development of spots and persist after the spots have disappeared.

Under conditions of good seeing, the faculae have been resolved into grains of about the same size as the photospheric granules. According to Waldmeier and P. ten Bruggencate, the facular grains have lifetimes of the order of two hours and exceed the brightness of the photospheric granules by 40 to 50 per cent.

Spectroheliograms show these faculae to coincide with the brighter portions of the plages and yield much more detail than direct photographs. The aspect of the spectroheliogram will depend on the line utilized and the part of the line. The strong Ca II "K" line has a central emission component called K_2 upon which is superposed a narrow absorption line K_3. Photographs taken in the light of the wings (K_1)

(see Fig. 7, left) show a mottled structure with bright plages around the sunspots. In the light of K_3, which corresponds to the highest level of the atmosphere (see Fig. 7, right), notice that the spots have disappeared, that the plages are prominent and that there appear long sinuous dark filaments. The latter, however, are seen better in Fig. 2. In K_2 the filaments disappear and in the outer part of the line K_1, the appearance of the spectroheliogram approaches that of a direct photograph.

Fig. 2 permits a comparison of a spectroheliogram taken at the center of the Hα line with a Ca II "K_3" image. Notice that the plages are less prominent in the hydrogen photograph, whereas the filaments are more pronounced and the spots are visible. The "fine structure" of the background in the hydrogen photograph appears more delicate; the individual grains are five or six times larger than the photospheric granules and appear dark on a bright background. Hydrogen spectroheliograms also often show a vortical structure around spots, which suggested to Hale that spots might contain magnetic fields. Spectroheliograms taken in the wings of the Hα line more nearly resemble K_1 spectroheliograms. Fig. 8 compares spectroheliograms taken in successive lines of the Balmer series. Notice the weakening of the plages and the increased prominence of the spots, toward the higher members of the series.

Spectroheliograms made in the light of Ca I λ4227, Na "D," Fe I, and other lines show many of the same features as the Ca II images, although the plages are of relatively lower intensity. Spectroheliograms taken in weak lines resemble those of hydrogen in that dark grains appear on a bright field but no vortical structure is evident.

Of great interest is the appearance of the disk in the light of the infrared helium line λ10,830 which arises from the metastable 2^3S level. A comparison of the He I and Hα photographs taken on the same date shows that the filaments are visible in absorption on both images, but that the plages appear dark in the helium image instead of bright as on the hydrogen images. On spectrograms, the He I line is visible only in the filaments and plages where it has a discontinuous appearance.

The structures observed in spectroheliograms are of two fundamental types, (1) those connected closely with the photosphere, granules, etc., (2) those originating in the high altitudes above the solar surface—the dark filaments, plages and bright flocculi which are connected with the prominences, whose properties we shall now study.

7. The Solar Prominences

Prominences are not distributed uniformly on the solar disk. They appear in two principal zones. The first group follows the sunspot zones. The second group is found in latitudes of about 45° at the start of the solar cycle, and migrates poleward. It reaches the pole near the maximum of solar activity and disappears soon thereafter. There seem to be appreciable differences between prominences associated throughout their lives with sunspots and other types.

Typical prominences are flat, wispy structures, 6000 to 12,000 km thick, 60,000 km high and 200,000 km long. They are usually observed on the limb with a spectrohelioscope, spectroheliograph, or polarizing monochromator. Still photographs fail to convey the complicated kinematics of much prominence motion; hence these objects are studied most effectively with the aid of motion pictures such as those first obtained at the McMath-Hulbert Observatory.

One can observe prominences not only in elevation at the limb, but also in plan as dark markings on the disk. The disk observations possess certain advantages over the observations at the limb. Certain types of prominences such as those associated with sunspots are low altitude objects which are visible at the limb only a day or so before the solar rotation carries them from view. Hence the disk appearance, where the prominences are seen in absorption against a bright chromospheric background, may give fuller and more continuous records. The greatest difficulty in the interpretation of the disk observations lies in the assignment of a particular disk prominence to the corresponding type observed at the limb. With the spectrohelioscope and with the Stone spectroheliograph of the McMath-Hulbert Observatory, rapid changes in development can be followed by the observer and if large vertical motions occur, the change in displacement of the line on the second slit can be pursued with the line shifter, or in the spectrum.

The earliest work, carried out by examination of the limb of the sun with a spectroscope and a widened slit, suggested two types of prominences. Objects in which a casual inspection revealed little activity were referred to as quiescent, those showing high velocities were called eruptive. More detailed studies, such as those by Pettit at Mount Wilson and by McMath and his co-workers at Michigan have shown this classification to be inadequate. Pettit employed the association of a prominence with a sunspot, its motion and structure, and whether it appeared to originate from the corona or from lower levels of the chromosphere in his classification scheme of six types: I Active, II Eruptive, III Sunspot, IV Tornado, V Quiescent, and VI Coronal. There are sometimes subgroups within each class, e.g., Pettit suggests nine subdivisions of the sunspot type.

Type I: Active prominences constitute the most frequent type and occur all over the sun's disk. Frequently, they develop from quiescent prominences and sometimes they evolve into the spectacular eruptive type. They show a mass of filaments connected with the photosphere, and these filaments often move along a curved path into a so-called

"center of attraction" at the base of the chromosphere. At times, a prominence appears to be literally pulled to shreds. Sometimes, prominences standing side by side are connected by streamers in which the material actually moves in both directions; these are the so-called interactive type.

Type II: Eruptive prominences often evolve from the active type and tend to favor the sunspot zones. Material moves into a center of attraction at an increasing pace, and as the activity mounts, the whole prominence may rise several hundred thousand kilometers before it is pulled into the center of attraction. It may even appear to leave the sun entirely, expanding as it rises and fading while in motion (see Fig. 9). During the whole course of development it continues to return streamers to the original centers of attraction. The record for height is held by the eruptive prominences observed by E. Pettit and J. O. Hickox on June 4, 1946, which reached a height of 1,703,000 km or 1.22 solar diameters.

Type III: Sunspot prominences often imitate the quiescent, active, and eruptive prominences found away from spots, and in addition display several characteristic types. Cinematographic records often reveal a high level of activity in the neighborhood of spots. Long wisps may appear in the region immediately above the spot, brighten, and descend to some center of attraction in or near the sunspot group. Rarely there appear graceful loop structures which seem correlated with high excitation in the overlying corona. There often appear the surges, which were recognized as a distinct type of prominence at the McMath-Hulbert Observatory. McMath and Pettit described them as small jets of material rising a few thousand kilometers, or as immense tongues of gas hurled outwards to a distance of a hundred thousand kilometers which suddenly retract or fade away. Sometimes the initial outburst breaks up and falls back in fragments. Their lifetimes range from about fifteen minutes to an hour, their velocities sometimes exceed 500 km/sec, and they protrude from the spot at all angles. They are sometimes observed to rise again and again from the same part of the spot. Upon spectroheliograms they often appear as sudden dark splotches in active spot regions. Surges bear a close relationship to solar flares.

Type IV: The rare Tornado prominences resemble cyclones or whirling waterspouts 5000 to 20,000 km in diameter and 25,000 to 100,000 km high. Pettit finds the helical motion suggested by their appearance to be confirmed by spectroscopic observations. They may evolve into eruptive or active prominences or simply disintegrate if the rotational velocity becomes sufficiently great.

Type V: Quiescent prominences include the longest lived of solar phenomena. They show a minimum of activity and motion and sometimes present a palisaded structure with closely packed filaments. McMath-Hulbert Observatory films show a great deal of turbulent internal motion. The thicknesses of quiescent prominences are of the order of 6000 km, their heights are about 40,000 km and their lengths are as great as 200,000 km. They often appear as dark sinuous filaments on the solar disk.

The d'Azambuja's observed them to form along meridians of solar longitude in active regions and then move poleward. As they move, they are drawn out of the meridians by solar rotation, and beyond 45° they are oriented along parallels of latitude. Equatorial filaments, seen on the limb, exhibit a maximum of structural detail while in higher latitudes such objects tend to resemble "haystacks," simply because of perspective.

Solar filaments may become active, disappear, and then reform in the same region after a few days. The average filament lasts four solar rotations, but some have been observed to survive as long as five years.

Type VI: Coronal prominences appear as long, slightly curved strips at great heights above the photosphere. They descend with speeds of the order of 100 to 200 km/sec more or less haphazardly into regions of attraction, which are possibly to be identified with sunspots.

The basis of the Pettit classification is essentially descriptive. The various subdivisions merge imperceptibly one into another and there are occasional objects that seemingly do not fit into any classification scheme at all.

Frequently, a single prominence will evolve from one class into another. The most obvious example is the development of a quiescent into an eruptive prominence.

In addition, there are the short chromospheric spikes or spicules, observed by W. O. Roberts at the Climax Solar Station of the University of Colorado and Harvard University. They are usually faint, short-lived (4 to 5 minutes) phenomena that attain heights of less than 8000 miles. They are most conspicuous near the poles of the sun. Roberts finds the velocities of these spicules along the solar radius to be of the order of 30 km/sec but these are possibly the faster moving, less typical ones. Certain characteristics are not unlike those of the granules: diameters of 1″ and 2″ and lifetimes of the order of 3 minutes. The velocity of outflow of material is much greater than in the granules.

The motions of prominences are best studied by moving pictures with a provision for determining the radial velocity. The streamers associated with sunspots seem to move along curved trajectories. On the other hand, Pettit concluded that eruptive prominences moved with constant velocities between sudden accelerations. Plots of height against time gave a series of straight-line segments. Other observers have not

been able to substantiate these findings. Certain of the straight-line portions of the published time-distance curves seem real, but the sharp corners may perhaps be regarded with skepticism. Pettit suggested that streamers and knots torn from active prominences also follow straight-line segments with a curved envelope but this conclusion is open to question. Measures of motion in three dimensions for a large number of prominences will be needed to settle this question.

The spectra of prominences supply important data; quiescent prominences tend to show D_3 (He I), H and K (Ca II), and the Balmer lines with weak lines of the metals, while those appearing over sunspots show strong lines of Fe II, Mg II, Na I, and He I. The differences are to be attributed to varying optical thicknesses and to excitation effects rather than to variations in chemical composition. Different elements appear to be well-mixed in prominences. Lyot's visual observations with the coronagraph and filters showed the prominence detail to be the same in different spectral regions. Flash spectrum images of different elements but the same arc length show similar structural details. If we compare prominence images of different intensity, we must allow for the effects of self-reversal whose importance Brück and Moss demonstrated from a comparison of the Hα and D_3 (He I) intensities. It may seem strange that gases as different as H, He, Ca, and Fe move together, since most of the effects we can think of that would cause motion would also act differently on the different elements. Evidently the gases tend to drag one another along in their motion. McCrea investigated this problem, employing the diffusion theory of Chapman and target areas for collisions derived from Ramsauer-type experiments. He found that if the density of a solar prominence is of the order of that of the lower chromosphere, $\sim 10^{10}$ atoms/cm^3, the elements would drag one another along even though the forces might act on just one of the elements. A much smaller density, however, would permit relatively large separations of different elements to occur if the forces responsible for prominence motion acted differently upon different elements. Actually, the thorough mixing of the chromospheric gases, in spite of the low density that appears to prevail in some places, suggests that the forces responsible for most prominence activity is non-selective as regards the elements involved. It seems unlikely that radiation pressure can play any important role in prominence motion, or equilibrium.

McMath has enumerated some facts an adequate prominence theory must explain: (1) The character of the motion and the fact that it can occur in all directions with respect to the sun. (2) No separation of gases. (3) Motions in streamers towards the chromosphere wherein sometimes several converge on one spot, and sometimes streamers from a given prominence show concurrent motion in random directions.

(4) When velocity changes occur, the new velocity either up or down is greater than the preceding velocity; accelerations are high and are observed at great heights. The downward motions from great heights are less than those of freely falling bodies. (5) Sometimes prominences appear to leave the sun while on other occasions bright clouds form in the inner corona from which streamers descend to the sun. (6) Relative frequencies of various prominence forms. (7) Occurrence of prominence activity in all solar latitudes. (8) Prominence activity is correlated with the sunspot cycle.

Although the Doppler displacements of the lines indicate an actual motion of the prominence material, we cannot be sure that all "motions" observed may not in part arise from a change in excitation and ionization in a previously existing medium. Much of the behavior of knots and streamers, the disintegration of prominences by shredding, and the ejection of prominences to coronal regions all suggest actual material motions. On the other hand, the condensations of streamers out of material in the coronal region and the fading and reappearance of filaments observed upon the disk, indicate that excitation conditions must play an important role.

8. Flares

Closely associated with active sunspot groups are the bright chromospheric eruptions or flares which appear sometimes in the order of minutes and fade in one hour or less. Waldmeier describes the outbursts not as eruptions of material, but simply as excitation effects.

The statistics of flares have been discussed by G. E. Hale, H. W. Newton, M. A. Ellison, M. Waldmeier, and by H. Dodson and R. Hedeman.

Flares cover a wide range of intensity and size. Some appear as tiny points of light on the solar disk whereas others such as the great flare of July, 1946, are described as being intensely brilliant. Some appear as long bright ropes, others appear as small bright spots whose arrangement suggests a certain chain-like nature. Although they occur most often in the region between spots or close to or over the penumbrae of spots, some have been observed extending directly over spot umbrae. Flares tend to occur repeatedly, not merely in the same region, but seemingly in exactly the same small portions of the solar disk. Some seem to follow, at least in part, channels already established by the dark filaments (prominences seen in projection on the disk). Although filaments sometimes disappear after the outbreak of a great flare, they sometimes seem to survive bright eruptions. The brightest flares are associated with complex spot groups and tend to occur when the group is growing most rapidly. They cover a larger area and tend to fade away more slowly

than the smaller outbursts. The total number is correlated with the sunspot number. Flare intensities are usually expressed on an arbitrary scale, although extensive quantitative measures have recently been made at the McMath-Hulbert Observatory by Helen Dodson and Ruth Hedeman.

Near the moment of peak intensity, high-velocity dark flocculi (darker than most filaments) are often observed. The work of M. A. Ellison, H. W. Newton, Orren C. Mohler, and Helen W. Dodson show these dark markings to be surges seen in projection upon the disk. (See Fig. 12.)

Richardson and Minkowski, C. W. Allen, and M. A. Ellison have described the spectra of flares. In a bright outburst, Hα develops bright, generally symmetrical emission wings soon after the onset of the flare. The emission wings fade away in a few minutes although the flare may persist longer. In the July, 1946, flare, bright Hα attained a width of 15A with a central intensity three times that of the continuum. Simultaneously, D_3 (He I) appeared in emission over the flare, although it remained in absorption over the nearby photosphere. The Si II, λ6347, λ6371, lines were reversed and the profiles of many iron and nickel lines were filled in. The continuous spectrum appeared to be brighter over a small area containing the flare.

In general, flare spectra resemble the flash spectrum. All the Fe II and the low excitation Fe I lines are strongly enhanced in flares. An increased intensity of the Fe II lines occurs in prominences and the "hot spots" of the solar chromosphere, but the low excitation Fe I lines are not intensified.

Not only are bright flares correlated with marked activity in the chromosphere, but they are also related to radio fadeouts and terrestrial magnetic disturbances. A bright flare is frequently followed by an immediate fadeout of short wave radio reception on the sunlit side of the earth. Magnetic storms sometimes occur one to two days later.

The sunspots, faculae, or plages, certain types of prominences and flares all appear to be closely related. The interpretation of these relations is one of the most difficult problems of astrophysics. Perhaps a significant clue is to be found in the magnetic fields of the spots. For example, the close similarity of the arcs and loops of certain sunspot type prominences with the directions of magnetic forces one would expect around spots, strongly suggests that magnetic forces determine at least in part the motions of ionized gases. It would appear worth while to examine more closely the magnetic character of sunspots and the behavior of gases in magnetic fields.

9. Electromagnetic Phenomena Associated with Sunspots

Solar electrodynamics constitutes one of the most difficult domains of astrophysics. One can set up Maxwell's equations and the equations

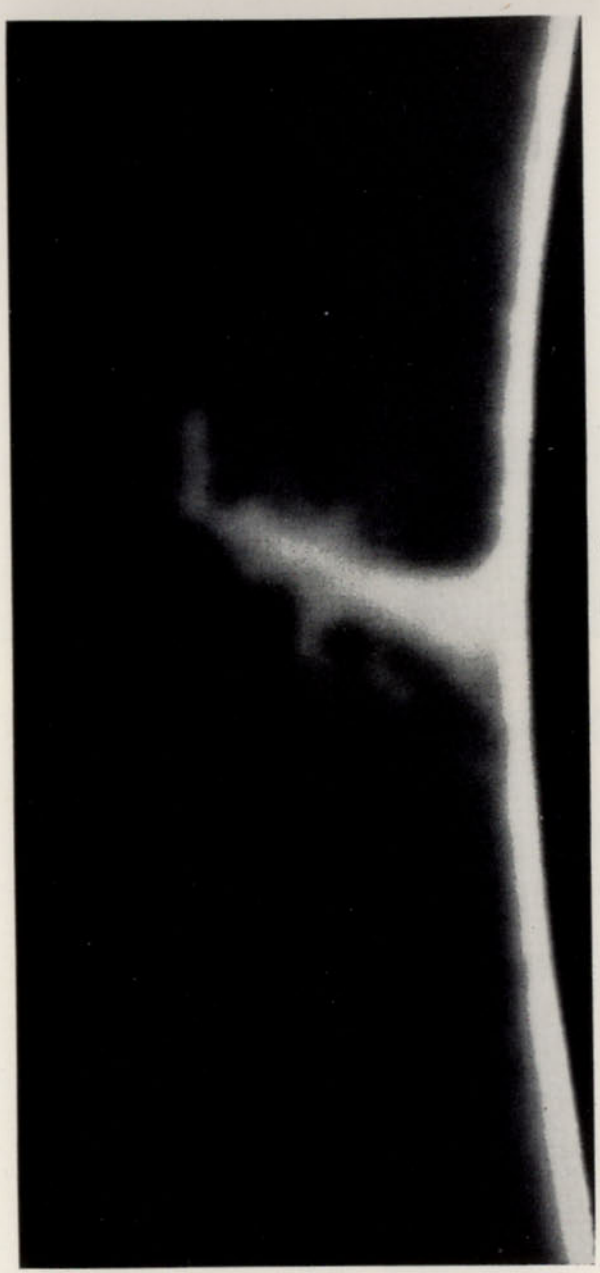

FIG. 11.—A TORNADO-TYPE PROMINENCE
August 21, 1948, $16^h\,28^m$ G.C.T., McMath-Hulbert Observatory.

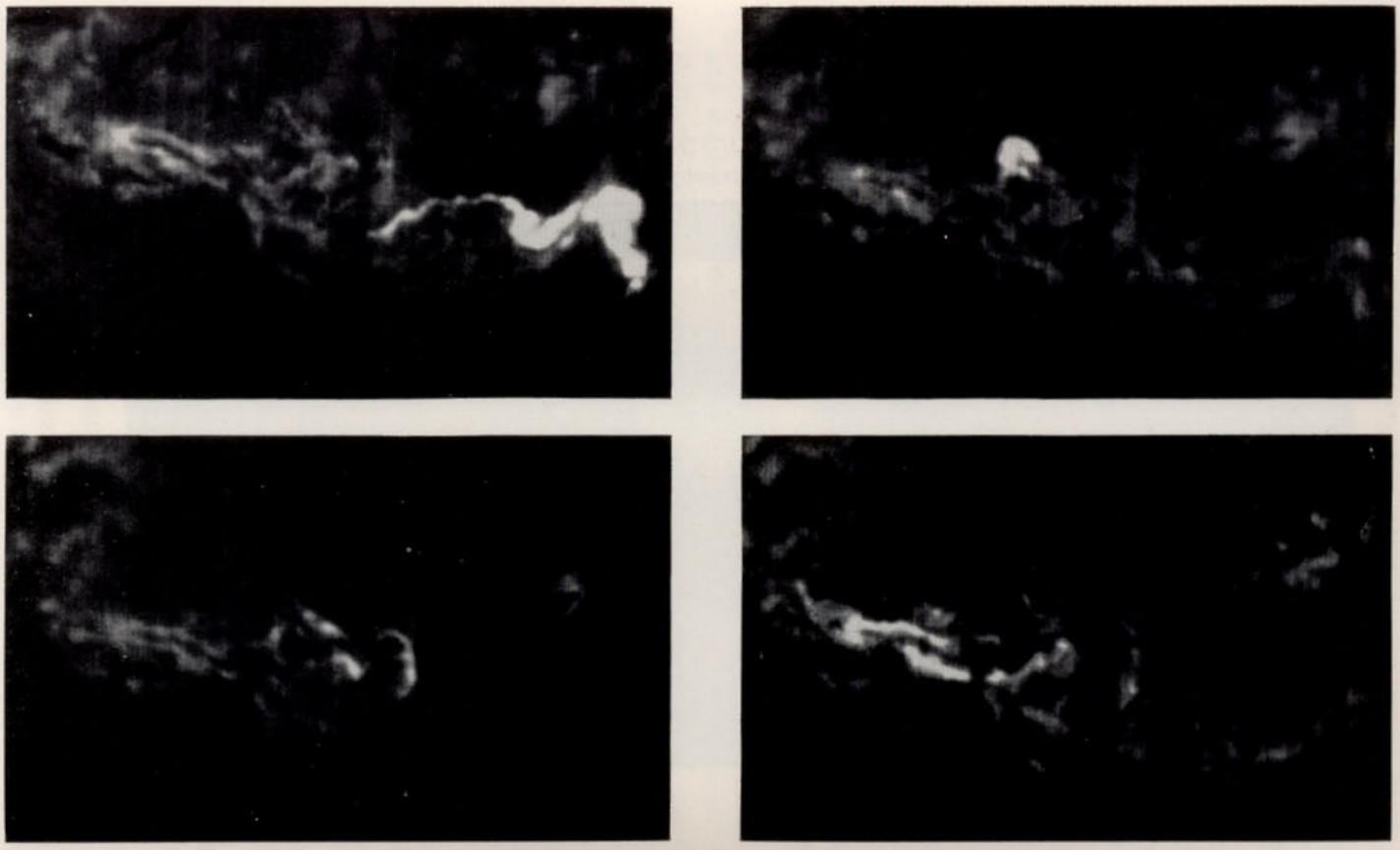

FIG. 12.—FOUR FLARES IN A LARGE ACTIVE SOLAR AREA

August 12, 1947, Hα spectroheliogram, McMath-Hulbert Observatory.

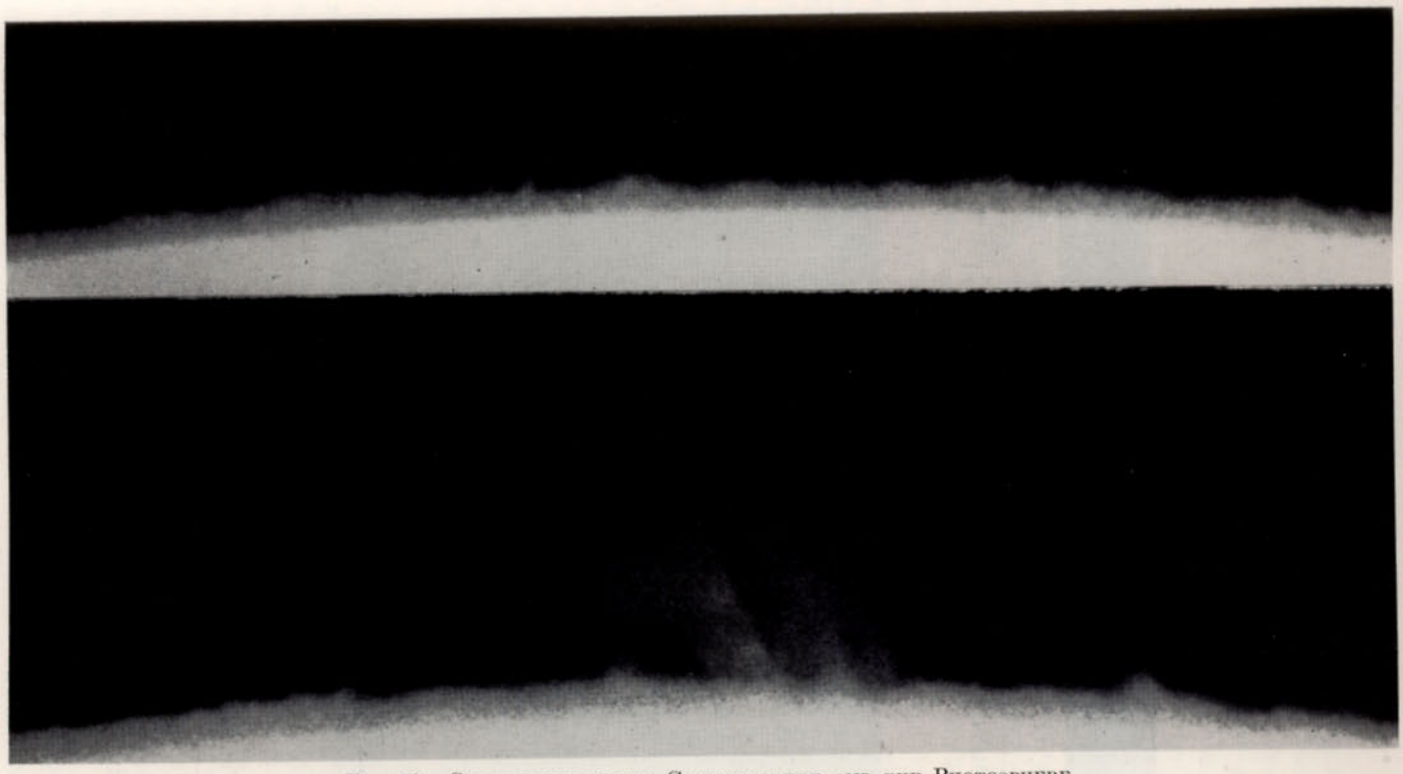

FIG. 13.—SEPARATION OF THE CHROMOSPHERE AND THE PHOTOSPHERE

This illustration, which shows the line of demarcation between the photosphere and the chromosphere, was taken from a motion picture film obtained by Bernard Lyot at the Pic du Midi in 1942 with a 0.38 meter refractor and a polarizing monochromatic filter of 1.5A band-pass centered on Hα. The upper strip shows an undisturbed portion of the chromosphere; the lower part shows a prominence rising above the chromosphere.

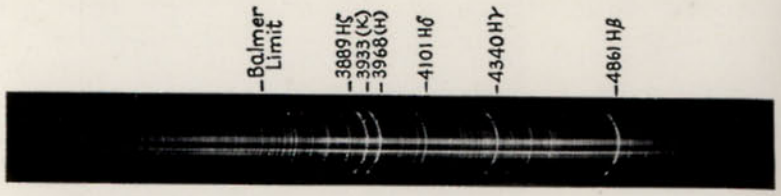

FIG. 14.—THE FLASH SPECTRUM PHOTOGRAPHED JUST BEFORE TOTALITY

(A spectrogram taken at the solar eclipse of August 30, 1932, Fryeburg, Maine, by D. H. Menzel of the Lick Observatory eclipse expedition.)

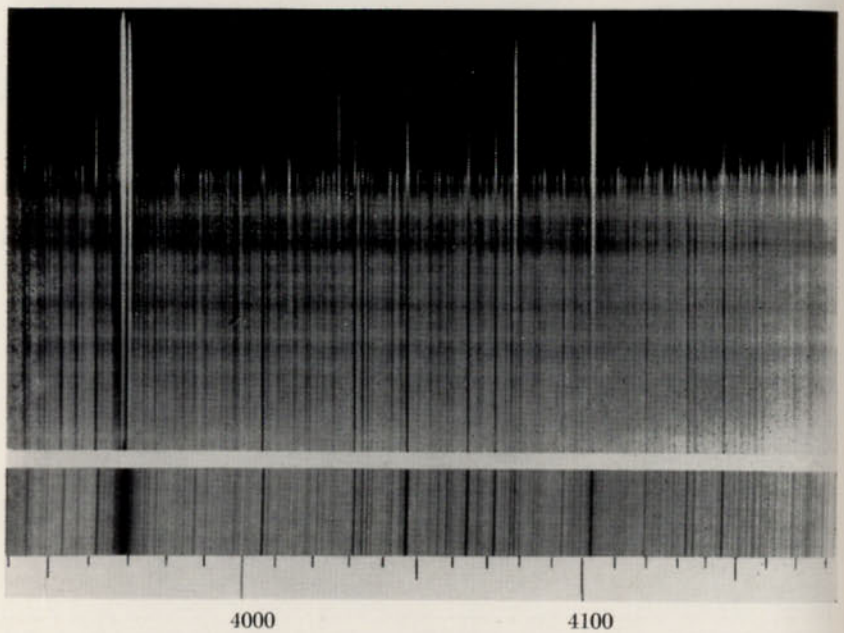

FIG. 15.—THE FLASH SPECTRUM PHOTOGRAPHED WITH THE MOVING-PLATE APPARATUS

(After W. W. Campbell; courtesy, Lick Observatory.)

of motion for charged particles in an anisotropic medium. The latter involve not only the macroscopic electric and magnetic fields, but also the microscopic forces arising from collisions, etc., and the loss of energy by radiation. There also exist the usual hydrodynamic effects which must be combined with the electromagnetic effects to yield a complete description of the motion. That is, the expression of the current flow has terms arising from body forces, pressures, etc., and from viscosity.

Rapid changes in magnetic fields induce electric fields. The induced electric field, although perpendicular to the varying magnetic field, is not necessarily always perpendicular to the total magnetic vector. At certain points the spot fields may cancel one another, but the induced electric field may remain, and if the conductivity is sufficient, an appreciable electric current may flow. Giovanelli suggested that under the influence of such electric fields free electrons may suddenly acquire enough energy to excite hydrogen and other atoms, thereby producing a flare. The complex character of the magnetic fields near spots renders quantitative discussion difficult. The actual changes in the fields may be of the order of several gausses/min, and if they are propagated as waves, the effects of such changes may become steadily more violent as the wave moves into regions of decreasing density, as Cowling has pointed out. A relatively moderate change at photospheric levels might produce fairly marked effects higher in the chromosphere, where a magnetic field cannot be measured directly. If a flare is due to a sudden change in a magnetic field, the effect will probably not be instantaneous but will be propagated along the lines of force with a velocity dependent on the densities involved. The fact that flares are not correlated with any undue magnetic activity speaks against the Giovanelli theory, however.

Among the attempts to explain the motion of a prominence we may mention those of David Evans and of Zanstra. Evans tried to account for prominence forms by the electrostatic diffusion of a charged cloud and the motions of ions in a magnetic field. By hydrodynamical experiments, Zanstra was able to reproduce certain features of solar prominences. Since prominences move, not through a vacuum but through a medium of apparently lower density, their motion should bear some resemblance to the streaming of one fluid through another (e.g., smoke through air). The prominence may be nearly in mechanical equilibrium with the surrounding chromospheric gases, it may be cooler and denser while the surrounding gases are hotter and more rarefied, but the gas kinetic pressures may be nearly equal.

The essential objection to all prominence theories so far proposed is that while they all give prominence-like forms, none has been able to predict the motions of any prominence from initial conditions. That is,

if we evaluate the space velocity of a moving prominence knot at an early stage in its history, all the theories fail completely to predict the subsequent motions. The attempts by Evans and others to derive prominence forms on the basis of various forces show that the shapes of prominences can be "explained" by a host of assumptions and postulated initial conditions, but we have yet to find which, if any, of these theories will prove useful.

Although the trajectories of spot prominences may be well enough defined by the magnetic field, the velocities are not explained. The general impression one obtains from the films is of material feeding into the neighborhood of the spot, either from the shredding of a nearby prominence or from some kind of condensation from the corona. The factors controlling the behavior of a prominence must range from nearly equilibrium conditions for filaments to catastrophic forces for eruptive prominences or surges. Radiation pressure from flares has been invoked to explain prominence motion, and it does seem that surges are often connected, in time at least, with flares. If the magnetic fields alone dominated their motions, the prominences should not only follow curved paths but should present smooth, orderly forms. The chaotic appearance of many of them is suggestive of turbulence. The ions of an ionized gas moving into a strong, inhomogeneous field would tend to follow the lines of force. Hence the gas would tend to be compressed laterally. Thus recombination may be facilitated and the prominence streamer would become visible.

Quantitative data on the prominences, save for some material on their motions, is lacking. A few line intensities have been measured but the data are often difficult to interpret. We would like to know something about the prominence masses involved. Perhaps densities might be estimated from the intensities of the Balmer lines, provided their emission arises primarily from recombination. It would be of interest to know how the densities within the prominences compare with those obtaining in the nearby chromosphere. Presumably, the prominences are both denser and cooler, but the actual differences will have to be established by observation. Quantitative measures of the monochromatic brightnesses of prominences, as well as of their motions, are urgently needed.

10. Observations of the Solar Chromosphere

Above the photosphere of the sun lies a thin envelope of relatively transparent gases which is called the chromosphere. It is distinctly separated from the photosphere and from the tenuous corona as well. (See Fig. 13.) Under conditions of excellent seeing, the solar chromosphere displays an intricate pattern of numerous tiny prominences, mostly 2″ to 7.5″ in length, in contact with the photosphere. The conventional prominences, described in Sec. 7, appear in the region of the corona.

The tiny prominences that compose the chromosphere proper, and to which Mohler refers as "jets," have an average height of 5.2″. Their average width of 1.8″ is closely comparable with the average width of a granule, 1.6″ (according to Keenan). These chromospheric jets are comparable in number with the granules with which they are presumably closely associated.

The best observations of the solar chromosphere are those obtained at the time of total solar eclipse. Weak as well as strong lines can be observed, and we can determine the distances to which the various radiations extend from the sun.

S. A. Mitchell employed essentially a slitless spectrograph. Just before totality, the dark-line spectrum of the photosphere vanishes, and the bright lines of the chromospheric spectrum appear. At this moment a spectrogram of the sun is taken; the narrow crescent of the sun serves as a slit and we obtain, in effect, a photograph of the chromospheric arc in each of the radiations it emits. (See Fig. 14.)

W. W. Campbell placed a screen in front of the photographic plate with a narrow slit parallel to the dispersion of the spectrograph so that only a short section of the central portions of the crescents fell on the plate. During the eclipse the photographic plate was moved uniformly at a constant rate in a direction perpendicular to the dispersion so that different portions of the flash spectrum were recorded on different portions of the plate. (See Fig. 15.) Campbell also secured "stationary-plate" spectrograms of the type obtained by S. A. Mitchell.

There is no difference between the stationary- and moving-plate arrangements so far as the optical parts are concerned. In each instrument the objective prism forms monochromatic images of the chromospheric crescent. The exposure with the moving-plate apparatus is started before the photosphere is completely covered so that the Fraunhofer spectrum is recorded on the lower part of the plate. The gradual transition from the dark-line spectrum of the photosphere to the bright-line spectrum of the chromosphere is well exhibited in Fig. 15.

Since the energy falling upon the plate is the integrated light from all levels above the surface of the moon, it makes no difference if the particular part of the moon's surface photographed with the moving-plate apparatus is a little low or a little high. On the other hand, the irregularities of the moon's surface produce difficulties in the interpretation of the chromospheric arcs observed in the fixed-plate method. A given "low-level" line will disappear and reappear due to the serrations of the

lunar surface. If a prominence happens to fall on the portion of the arc selected for observation by the moving-plate method, the observations might be difficult to interpret and the fixed-plate method then would have an advantage. On the other hand, the practical result obtained by the fixed-plate method depends on when the exposure is made. If it is a little late, the lines in the lower chromosphere are missed; if it is too early, the continuous spectrum spoils the observations.

Menzel's jumping-film method combines the advantages of flash spectrum photography as used by Mitchell with Campbell's moving-plate method. The spectrum is photographed as in Mitchell's method, but a series of exposures is taken, covering a range of heights.

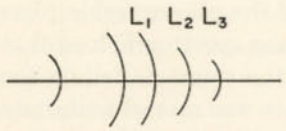

FIG. 16.—CHROMOSPHERIC ARCS

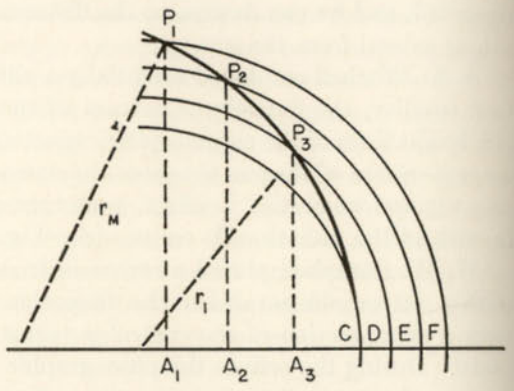

FIG. 17.—INTERPRETATION OF THE LENGTHS OF CHROMOSPHERIC ARCS

If both the moon and the sun were perfectly spherical, the lengths of the chromospheric arcs would determine accurately the heights to which the various line radiations could be traced above the photosphere. The heights follow from measurements of the lengths of the chords L_1L_1', L_2L_2', etc., from tip to tip. (See Fig. 16.) In practice, small corrections have to be made for the fact that the exposure takes a finite time.

In the idealized situation pictured, the observer obtains a plate when the limbs of the sun and moon are tangent as shown in Fig. 17, where r_1 denotes the solar radius, r_m that of the moon (as seen in projection), and the arcs DP_3, EP_2, FP_1 represent successively higher layers of the chromosphere. P_1, P_2, P_3 represent the points at which the lunar surface cuts off the chromospheric levels F, E, D, respectively. At P_3, for example, we observe the radiation from all radiating atoms above the level $CD = x$ (Fig. 18) and along the line of sight D_1D_1'. We must constantly keep this fact in mind in interpreting the chromospheric eclipse observations.

Suppose, for example, that P_2 corresponds to the tip of the chromospheric arc of line L_2 of height CE, and P_3 corresponds to the tip of L_3 of height CD. Measures of the half-chords P_2A_2, P_3A_3 and the known values of r_1 and r_m at the time of the eclipse enable one to calculate CE and CD in km. For example, the line of sight through P_3 may lie tangent to the layer of the chromosphere at the height of 1000 km, and the line of sight through P_2 may be tangent to the chromosphere at 2000 km. The tip of the spectral line corresponds to a definite intensity, which depends on the threshold sensitivity of the photographic plate, the transparency of the atmosphere and instrument, "seeing," etc. Under the given conditions of the observation, when the number of atoms along the line of sight reaches a certain value (or rather the emissivity of the column attains a certain critical value), the radiation will begin to record on the photograph. If L_2 and L_3 are two nearby lines in the spectrum (so that plate sensitivity, atmospheric transparency, etc., are the same for both), the amount of energy coming along the line of sight through P_2 will be the same as that along the line passing through P_3. We suppose that the amount of self-absorption in the tip of the arc L_2 is the same as that in the arc L_3. Furthermore, if the lines L_2 and L_3 belong to the same multiplet, so that the relative A values are known, there will be A_2/A_3 as many quanta emitted per second at a given point in L_2 as in L_3. Since the same number of quanta are required to produce the tip of L_2 and L_3, the number of atoms in the line of sight through the tip of L_2, $n(L_2)$ is related to $n(L_3)$ by $n(L_2)/n(L_3) = A_3/A_2$.

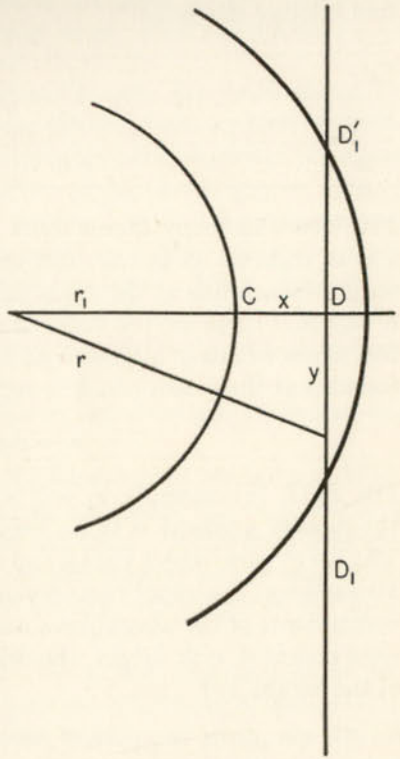

FIG. 18.—PLANE OF THE LINE OF SIGHT AND THE SOLAR RADIUS

The line of sight D_1DD_1' is tangent to the edge of the moon; r is the radius vector drawn to an arbitrary radiating volume along the line of sight.

If a line L_1 of the same multiplet is observed, then

$$\frac{n(L_1)}{n(L_2)} = \frac{A_2}{A_1} \quad \text{or} \quad \frac{n(L_1)}{n(L_3)} = \frac{A_3}{A_1} \tag{9}$$

S. A. Mitchell and Miss E. T. R. Williams employed this principle in their determination of the density gradient in the lower chromosphere. As an example, they give for a multiplet of five lines the following heights and relative strengths:*

Line	*a*	*b*	*c*	*d*	*e*
Observed height	1500	1200	800	800	600
$s/\Sigma s$	0.50	0.25	0.10	0.10	0.05

Five times as many atoms must emit this multiplet along the 800-km line of sight as along the 1500-km sight line, since the intensity is the same for each line at the tip of the arc. The density must vary in such a way that there are ten times as many atoms at 600 as at 1500 km and five times as many at 800 as at 1500 km. Mitchell and Miss Williams found that their data could be represented by a density law of the type

$$n \sim e^{-c_1 x} + De^{-c_2 x} \tag{10}$$

For Ti II, for example, $c_1 = 2 \times 10^{-8}$, $c_2 = 5 \times 10^{-8}$, $D = 60$. Thus the density gradient is to be regarded as the sum of two exponentials. The lower part, where the second term prevails, simulates an isothermal atmosphere; the upper part deviates considerably therefrom. If all the constituents of the atmosphere were evenly mixed, and the temperature were constant with height, the density, ρ, would be given as a function of the height by†

$$\rho = \rho_0 e^{-\frac{Mgx}{kT}} = \rho_0 e^{-ax} \tag{11}$$

The greater the value of kT/M, the lower the gradient. Here M is the mean atomic mass. In practical cases, $M = 1.66 \times 10^{-24}$ grams, i.e., the mass of the hydrogen atom. Hence at $T = 5000°$K, the theoretical gradient is $a = 6.68 \times 10^{-8}$. Mitchell and Miss Williams found the density gradients to be of the same order of magnitude for all the different metals, indicating that whatever mechanism was responsible for supporting the chromosphere, it must keep the elements well mixed.

From both the observational and theoretical point of view, the fundamental paper on the chromosphere is Menzel's discussion of the eclipse observations of Campbell. He calibrated relative line intensities in terms of line strengths given by atomic theory and determined the chromospheric density distribution from the height-intensity relation derived from moving-plate exposures. Menzel showed that the Fraunhofer lines

* *Ap. J.* **77**, 6, 1933.

† See, for example, E. H. Kennard, *Kinetic Theory of Gases* (New York: McGraw Hill Book Co., Inc., 1938), p. 76.

were formed almost entirely below the chromosphere in layers that produce both line and continuous absorption. From the base of the chromosphere to the bottom of the layers responsible for the Fraunhofer lines, the density increases by a factor of the order of 400. Hence the conventional use of the term "reversing layer" does not appear to be justified.

A comprehensive analysis of Mitchell's data has been given by R. Wildt who has taken into account the effects of atmospheric scintillation and the fact that during a single photographic exposure the moon covers, or uncovers, an appreciable fraction of the chromosphere. Hence light emitted at different levels is recorded with different exposure times. That is, the chromospheric crescents on a flash spectrogram are images obtained with varying effective exposures. Wildt studied the density gradients of H, He, and the metals and was able to derive the electron densities and the pressure of hydrogen in the solar atmosphere. Thus, at a height of 500 km above the limb of the sun, that is, above some point near the top of the photosphere, the density of hydrogen was found to be about 4×10^{15} atoms/cm^3.

The studies by Mitchell and Miss Williams, and of Menzel and Wildt all indicate that the metallic abundances are about the same as those found by Russell from the Fraunhofer spectrum. Wildt finds a hydrogen-to-metal ratio similar to that of the photosphere at the base of the chromosphere, but the ratio appears to increase with height in the upper layers.

An important fact brought out by the eclipse observations is that there exists a sharp demarcation line between the chromosphere and the photosphere. The chromospheric density gradient at levels, say 500 km above the well-defined limb of the sun, is much less steep than the density gradient in the photospheric layers. The observed sharpness of the limb of the sun is in agreement with the hypothesis that the negative hydrogen ion is responsible for the opacity and that the photospheric layers are in hydrostatic equilibrium. Were the chromospheric density gradient to persist into the photosphere, the edge of the solar disk would be noticeably fuzzy. (See Fig. 13.)

Both Campbell's and Mitchell's observations suffered from one common defect, the lack of photometric calibration, which would have permitted the reduction of the measured photographic densities on the plate to actual intensities. More recently, photometric measures have been included in flash spectrum studies, and progress along quantitative lines has become possible. As an example in point we may mention the observations of the flash spectrum obtained by the 1932 Lick Observatory expedition and discussed by Menzel and Cillié. Calibration exposures with a step wedge permitted photographic densities to be converted

to relative intensities. Since the spectrum of the solar limb, whose energy distribution is known, is also photographed on the same plate, the effects of atmospheric transparency, color sensitivity of the emulsion, etc., may be determined. Cillié and Menzel gave a careful theoretical analysis of their photometric data. They took into account the effects of self-reversal and showed how a curve-of-growth type of analysis may be applied to chromospheric emission lines in order to derive the true density gradient from the observed intensity gradient. The effect of self-reversal is particularly striking for the strong H and K lines but also appears in the hydrogen lines, as R. N. Thomas has shown.

We cannot use the method employed by Mitchell and Miss Williams to get the density gradient of hydrogen since we would have to compare lines arising not from the same upper level (or term) but from successively higher levels. The populations in these levels do not deviate from the values valid for thermodynamic equilibrium by the same amount. In fact, the deviations occur in such a way that the gradient found by Wildt is too low.

The logarithmic gradient $\frac{d \ln N}{dx}$ for neutral hydrogen at a height of about 1000 km above the limb is 1.54×10^{-8} cm^{-1} according to Cillié and Menzel, in good agreement with the value 1.62×10^{-8} cm^{-1} found by Pannekoek and Minnaert. R. N. Thomas, from a rediscussion of the Cillié-Menzel data in which he takes the effect of self-reversal into account, obtains a value of 1.68×10^{-8} cm^{-1}.

Helium exhibits an interesting behavior. The data of Cillié and Menzel, Pannekoek and Minnaert, as well as subsequent observations by E. J. Perepelkin and O. A. Melnikov, show that the intensities of the He I lines increase with height up to about 1000 km and then slowly decline. The λ4686 He II line, which is sometimes observed in regions of high excitation, falls off slowly in intensity with increasing distance from the limb.

11. The Electron Density and the Temperature of the Chromosphere

We may compute the electron density in the lower chromosphere from the Inglis-Teller formula [eqn. (173) of Ch. 8]. For example, Mitchell's plates showed Balmer lines up to $n = 37$. If most of the electrons of the chromosphere are supplied by hydrogen, as appears plausible because of the high abundance of this element, $N_i = N_e$, and we find $\log N_e = 11.49$ at a height of 500 km. Wildt has shown that the electron density of the upper chromosphere merges smoothly into that of the corona as evaluated by Baumbach. The intensity of the continuous spectrum at the head of the Balmer series gives yet another

estimate of N_e. If we employ Menzel and Cillié's measurements of the emission per unit volume per unit frequency interval at the base of the chromosphere, $E = 3.8 \times 10^{-16}$ ergs/cm^3/sec, in conjunction with eqn. (106) of Chapter 5, we find $N_e = 4 \times 10^{11}$ (which corresponds to about 0.6 dynes) for an electron temperature of 10,000°K. The electron pressure in the layers responsible for the Fraunhofer lines is of the order of 20 dynes.

The chromosphere deviates strongly from thermodynamic equilibrium so that it is not possible to specify a unique temperature that would characterize all physical processes occurring in these layers. Instead, one may define a temperature of the chromosphere in terms of any one of the following processes:

1. The distribution of electron velocities,
   (a) As measured from the Balmer continuum [cf. eqn. (107) of Ch. 5].
   (b) As measured from the profiles of emission lines.
   (c) As estimated from the intensity of radio waves.
2. Distribution of atoms among excited levels (Boltzmann formula).
3. Ionization equilibrium (Saha equation).

Cillié and Menzel measured the distribution of energies in the Balmer continuum. Their results lead to an electron temperature of 5000°K. Their method, however, is open to question. Lyot's observations suggest that the continuous spectrum of prominences arises largely from electron scattering.

The profiles of chromospheric emission lines broadened by Doppler motions (and possibly by turbulence as well) should provide a clue to the kinetic temperature. The intensity distribution in an emission line unaffected by self-reversal will be given by eqn. (21) of Chapter 3 if turbulence is not present. Measurement of the profile, $I(\lambda)$, will give the most probable velocity α and hence the kinetic temperature defined by eqn. (12) of Chapter 3. If turbulence is present and the motions can be represented by a random (Gaussian) distribution along the line of sight, α^2 in eqn. (21) of Chapter 3 will be replaced by V^2, defined by eqn. (159) of Chapter 8. If the turbulence much exceeds the thermal motions, equally intense lines of all elements should have nearly the same profiles. If α greatly exceeds the turbulent velocity ξ, the breadth of the line ought to decrease with increasing atomic weight.

R. O. Redman used eclipse observations of weak, sharp, chromospheric lines of hydrogen, helium, and a number of rare earths to estimate α. He found the line widths to depend on the atomic weight in such a way as to indicate that turbulence amounts to less than 1 km/sec and that the kinetic temperature is about 30,000°K. Wildt found the

density gradient of hydrogen to correspond to an atmosphere in hydrostatic equilibrium with a kinetic temperature of 35,000°K. He obtained the same gradient from a comparison of the electron density at the base of the chromosphere with the electron density at a height of 15,000 km as estimated by Baumbach from an interpretation of the continuous spectrum of the corona. The metallic gradients are steeper. Presumably, this is a consequence of increasing ionization with height in the solar atmosphere.

From his observations at the 1952 Khartoum eclipse, however, Redman finds that the kinetic temperature of the chromosphere cannot exceed 17,000°K, and the horizontal component of the turbulence cannot be greater than 2 km/sec.

The so-called excitation temperatures may be found from the relative populations of excited levels (cf. Sec. 14 of Ch. 8). Here we are concerned with emission lines rather than with absorption lines, however. Goldberg has computed the excitation temperature from the helium lines in the chromosphere. The effect of self-reversal upon the line intensities is negligible. The excitation temperature appears to increase with height in the chromosphere, the layers above 670 km giving $T = 4300°K$, the layers above 2300 km giving $T = 6700°K$. That is, the temperature gradient is reversed. The helium lines, e.g., λ4471, brighten steadily with increasing height above the photosphere, reach a maximum and then fade away at the highest levels. We shall see in Sec. 12 that the corona has an extremely high kinetic and excitation temperature. Hence it is plausible that, as the corona is approached, there is a steady rise in temperature.

The ionization equilibrium for the metals in the lower chromosphere is about what one would expect for an attenuated gas illuminated by a black body at 5000°K. Hydrogen and helium present quite a different problem. Application of the combined Boltzmann and Saha equations implies a temperature in the neighborhood of 10,000°K in order to explain the observed emission of hydrogen. Helium is observed in two stages of ionization. From the lines of neutral helium we may derive an estimate of the number of singly-ionized helium atoms, while from λ4686 of He II we estimate the number of doubly-ionized helium atoms (cf. Sec. 13 of Ch. 8). An ionization temperature of the order of 20,000°K seems necessary to interpret the observations. (See Problem 5.)

Further information of interest is obtained from an analysis of the relative intensities of successive members of the Balmer series (the Balmer decrement). The measures by Cillié and Menzel have been rediscussed by R. N. Thomas who has shown how the effects of self-absorption may be taken into account. He was able to obtain not only an estimate of the population in the upper levels, but also that in the second level.

Then, on the assumption that the solar chromosphere is in hydrostatic equilibrium, he was able to estimate the electron density gradient and the temperature gradient. The latter shows a positive value whose numerical magnitude is such that the rise of temperature to a million degrees in the corona (cf. Sec. 12) is understood. That is, the temperature gradient is of the order of 1° per 10 meters. The kinetic temperature is consistent with that found by Redman.

Finally, radio-frequency radiation from the sun (Sec. 16) provides important clues to the structure of the outer layers. The studies by John P. Hagen at the Naval Research Laboratory indicate that the kinetic temperature does not rise much above the photospheric value throughout most of the chromosphere. Then it rises rapidly as the corona itself is approached.

Summarizing the somewhat contradictory evidence on the temperature of the solar chromosphere, we enumerate first the evidence for a high temperature:

(a) Broadening of spectral lines (Redman).*
(b) Density gradients determined on the hypothesis of hydrostatic equilibrium (Mitchell, Wildt, Menzel, and Cillié).
(c) Ionization equilibrium of helium (see Problem 5).
(d) Balmer decrement (R. N. Thomas).

The evidence for a low temperature comes from:

(a) Intensity distribution in the Balmer continuum (Menzel and Cillié).
(b) Excitation temperatures of helium (Goldberg) and the metals (W. Petrie).
(c) Radio noise measurements (Hagen).
(d) Excitation of the ionosphere. Woolley has shown that if the temperature of the chromosphere were as high as 35,000°K, the level of ionization in the ionosphere would be much higher than is observed.

The radio data demand a low kinetic temperature throughout most of the chromosphere. Table 1 gives the variation of electron density and kinetic temperature in the chromosphere and corona consistent with our best present knowledge.

In any event it seems likely that the departures from thermodynamic equilibrium are so severe that a sharp distinction between the ionization temperature, excitation temperature, and electron temperature must be made. Wurm, as well as Hagen, suggested that the electron tempera-

* Unsöld has recently concluded, however, that Redman's data can be interpreted otherwise than in terms of a high kinetic temperature.

ture rises abruptly in the upper chromosphere, where the density falls off rapidly. The transition to the corona, which is characterized by a kinetic temperature of the order of a million degrees, takes place abruptly.

TABLE 1

THE ELECTRON DENSITY AND TEMPERATURE DISTRIBUTION IN THE CHROMOSPHERE AND INNER CORONA

Height in Kilometers	Number of Electrons per cm³	Temperature in °K
500	173,000 × 10⁶	5,070
1,000	135,000	5,130
2,000	85,200	5,240
4,000	36,300	5,750
6,000	15,100	6,140
10,000	2,540	8,320
14,000	620	28,800
20,000	368	180,000
28,000	263	840,000
35,000	230	840,000

The electron density is adopted from the work of Allen and van de Hulst for the corona, and the work of Wildt for the chromosphere. The temperature distribution in the corona is taken from Alfvén. The temperature distribution in the chromosphere is adopted so as to give a good fit with the radio data (after John P. Hagen, Naval Research Laboratory).

Hagen finds that the 8 mm radio wave observations made at the 1952 Khartoum eclipse cannot be fully represented by a uniform solar chromosphere with a monotonic rise in temperature upwards. The observations appear to be consistent with a model chromosphere of the type suggested by Giovanelli. In this picture the chromosphere is regarded as consisting of a network of high temperature (~20,000°K), and low temperature (~5000°K) radial columns.

12. The Appearance, Brightness, and Polarization of the Corona

The pearly outer envelope of the sun, the solar corona, is best observed at total eclipses. Its general appearance, as well as its detailed structure, shows a strong correlation with the solar activity. At sunspot minimum there is an extension of the corona in the equatorial direction; short spikes appear in the regions of both the north and south poles. At the maximum of the solar cycle, the polar spikes are missing and the corona has a more uniform appearance.

The activity in the underlying chromosphere and photosphere has a pronounced effect on the corona. Arches, fans, and fibrous filaments

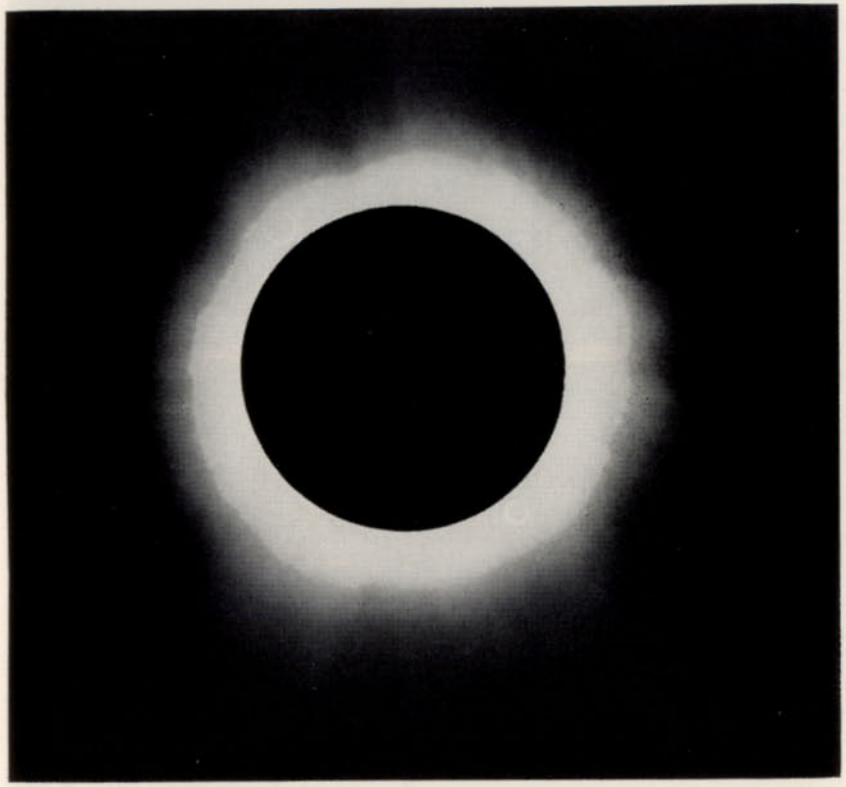

FIG. 19.—THE CORONA, AUGUST 30, 1905
(Courtesy, Lick Observatory.)

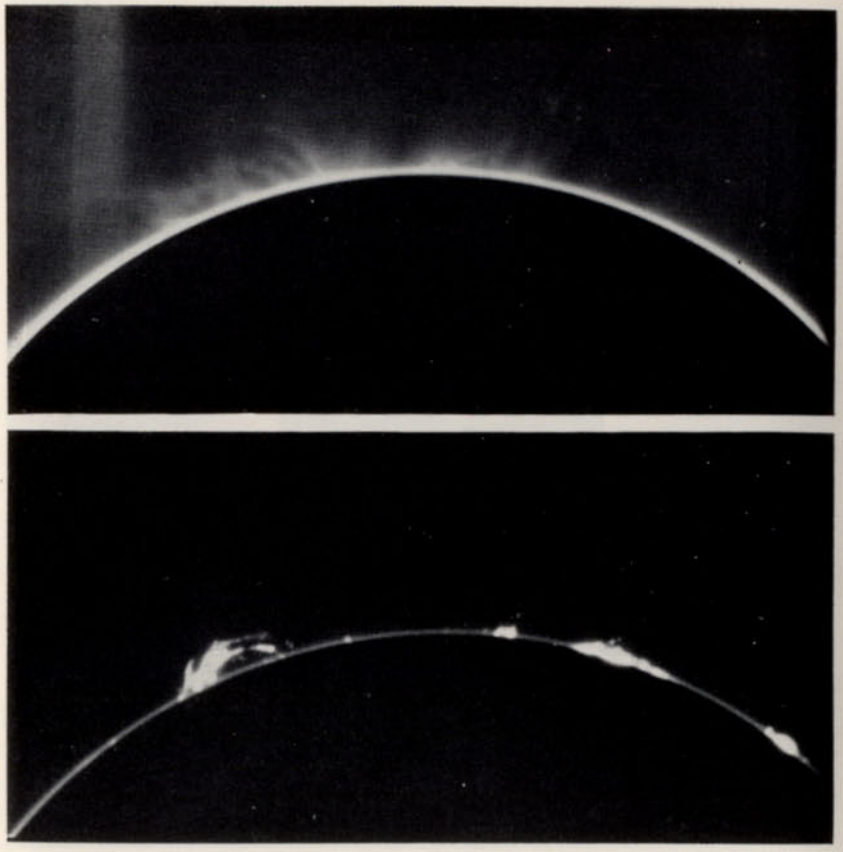

FIG. 20.—SIMULTANEOUS PHOTOGRAPHS OF THE INNER CORONA AND THE PROMINENCES

Top: The solar corona photographed with a coronagraph and polarizing monochromatic filter isolating the λ6379 line at the center of a band 3A wide. *Bottom:* The prominences photographed simultaneously in the light of Hα with the same apparatus. (Courtesy, B. Lyot.)

abound near regions of high excitation. Prominences often appear imprisoned on the interior of coronal arches, suggesting that the coronal and chromospheric phenomena are connected. Thus, coronal, as well as chromospheric, activity is strongly affected by apparent centers of attraction and excitation on the solar surface.

Unlike the prominences, the corona shows little large-scale motion. Lyot made simultaneous moving pictures of the coronal radiation on the one hand, and the prominences in the light of Hα on the other. Even when the film was speeded up 2400 times, the corona remained stationary; arches and jets appeared and faded continuously along invisible trajectories. That is, the corona modified its shape and appearance without perceptible motion. Waldmeier found local motion of the order of 5 km/sec over active sunspots and in one instance a Doppler shift in the λ5303 line corresponding to −150 km/sec.

The distribution of brightness in the corona as a function of distance from the sun has been studied by many observers. From a critical discussion of all observational data, Baumbach found that the mean photographic brightness of the corona averaged over all position angles may be expressed in the form

$$I(p) = 0.0532p^{-2.5} + 1.425p^{-7} + 2.565p^{-17} \qquad (12)$$

where the intensity of the center of the solar disk is taken as 10^6 and distances, p, are measured in units of the solar radius from the center of the sun.

The total light of the corona has been measured visually, photoelectrically, and by bolometric methods. Results differ from eclipse to eclipse and from observer to observer. Since the corona is much brighter in its innermost portions and varies in shape, form, and intensity with the solar cycle, and since the apparent size of the moon varies from eclipse to eclipse, some differences are to be expected. At the 1918 eclipse, Kunz and Stebbins found the total coronal brightness to be about half that of the full moon. Pettit and Nicholson obtained a bolometric brightness of 1.01×10^{-6} that of the sun or 0.47 that of the full moon.

The importance of polarization measurements of the corona was first emphasized in 1879 by Schuster who pointed out that such studies might give information on the size of the scattering particles. The observations are difficult and tend to be affected by scattered light. They do show the polarization to be independent of wave length, and that the electric vector of the light wave vibrates preferentially in the direction perpendicular to the radius drawn from the sun. Let us call the intensity of the plane-polarized component in this tangential direction I_t. The intensity of the component whose E vector vibrates along the

radius drawn to the sun will be I_R. Then the degree of polarization may be defined as

$$P = \frac{(I_t - I_R)}{I_0}, \quad \text{where } I_0 = I_t + I_R \tag{13}$$

On the assumption that the coronal light arises entirely from electron scattering, Baumbach calculated the degree of polarization as a function of the distance from the solar limb in units of solar radii. In Fig. 21 we compare his predictions with Öhman's polarization measurements. Notice that the observed polarization falls off rapidly with increasing distance from the sun. Evidently, some source other than pure electron scattering must be responsible for the light from the outer corona.

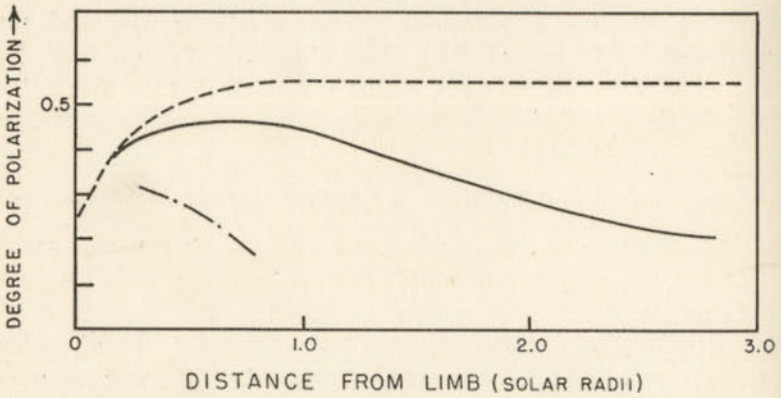

FIG. 21.—POLARIZATION IN THE CORONA

The dashed curve gives the theoretical degree of polarization on the assumption the coronal light comes entirely from electron scattering. The solid curve and dot-dashed curves give the measured polarization at the equator and at the pole, respectively. (After Y. Öhman, *Stockholm Observatory Annals* **15**, 2, 15, 1947.)

13. The Continuous Spectrum of the Corona and its Interpretation

Most of the coronal light arises from a strong continuous spectrum whose energy distribution is similar to that of the sun. Within the so-called inner corona, 5′ to 10′ of the limb, the spectrum of the corona is purely continuous. Beyond this point, in the so-called middle and outer corona, emission lines appear. Finally, in the outermost portion of the corona, the Fraunhofer absorption lines reappear. They are weaker than in the solar spectrum but of about the same width.

If the intense continuous spectrum of the inner corona arises primarily from electron scattering, as its faithful reproduction of the sun's color

would indicate, very large electronic velocities would be required to obliterate completely the dark-line Fraunhofer spectrum. The *H* and *K* lines of Ca II are almost completely washed out. The depression in the solar energy distribution caused by the crowding together of many strong dark lines beyond λ3800 is reproduced, however, in the coronal spectrum. No individual lines are present; all appear to be smoothed out by the swift motions of the scattering electrons. Grotrian estimated that a thermal width for the scattering electrons of the order of 60A would be required to produce the observed effects. Then [cf. eqn. (25) of Ch. 3] an electron temperature of the order of 300,000°K is implied.

The continuous spectrum of the middle and outer corona consists of two components: the *K* component which has no Fraunhofer lines and evidently arises from electron scattering, and the *F* component which is a pure reflection of the Fraunhofer spectrum. Grotrian suggested that the latter arose from scattering by small particles possibly related to those that cause the zodiacal light. The discussions by C. W. Allen and H. C. van de Hulst strongly favor this explanation. In fact, van de Hulst has subtracted the contribution of the "false corona" which contributes about 30 per cent of the total light and has shown that the true coronal light, due to electron scattering, may be represented by an expression of the form

$$I(p) = \frac{1.125}{p^7} + \frac{2.565}{p^{17}} \tag{14}$$

The ratio of the *F* and *K* components varies with position angle and perhaps from eclipse to eclipse. The streamers belong to the true corona which is stronger near the solar equator than the pole, while the false corona is circularly symmetrical at all distances from the sun.

From the coronal brightness distribution, eqn. (12), Baumbach calculated the emissivity $e(r)$ per unit volume per unit solid angle as a function of the distance from the center of the sun. Then, on the assumption that the luminosity arises from the scattering of the photospheric light by free electrons, he computed the electron density N_e as a function of r. We must modify his discussion so as to take account of the light of the true corona only. If

$$e(r) = A_1 r^{-a} + A_2 r^{-b} \tag{15}$$

we may write

$$I(p) = I_1(p) + I_2(p) = A_1 \int_{-\infty}^{+\infty} \frac{dy}{r^a} + A_2 \int_{-\infty}^{+\infty} \frac{dy}{r^b} \tag{16}$$

From the geometry of the problem (see Fig. 18, with $p = r_1 + x$)

$$r = \sqrt{p^2 + y^2}, \quad y = p \tan\theta, \quad r = p \sec\theta \tag{17}$$

Then*

$$I_1(p) = A_1 \int \frac{d(p \tan\theta)}{p^a \sec^a\theta} = \frac{2A_1}{p^{a-1}} \int_0^{\pi/2} \sec^{2-a}\theta \, d\theta = \sqrt{\pi} \frac{\Gamma\left(\frac{a-1}{2}\right)}{\Gamma\left(\frac{a}{2}\right)} \frac{A_1}{p^{a-1}} \quad (18)$$

with a similar expression for I_2. Here Γ denotes the gamma function. Thus if $I(p)$ is given in the form of eqn. (14), we may compute the emissivity with the aid of eqn. (18). With a millionth of the sun's brightness at the center of the disk as our unit of luminosity, and the solar radius as the unit of length, the emission function becomes

$$E(r) = \frac{j(r)}{4\pi} = \frac{1.15}{r^8} + \frac{4.157}{r^{18}} \quad (19)$$

For isotropic radiation the scattering coefficient per electron is 0.66×10^{-24}, and the corresponding scattering coefficient per unit length (solar radius) is

$$S = 0.66 \times 10^{-24} r_1 N_e = 4.60 \times 10^{-14} N_e \quad (20)$$

The total amount of scattered energy follows from an integration of the incident intensity over all directions:

$$j(r) = S \int_\Omega I \, d\omega = 4\pi S \bar{I} \quad (21)$$

where Ω is the solid angle subtended by the sun at the point r in the corona, and I is the intensity of sunlight. When $\bar{I}$ is computed, N_e may be found from $j(r)$.

Recently, van de Hulst has discussed the brightness, polarization, and electron density of the corona, in a more elaborate fashion, taking into account the fact that the density depends on the solar cycle and the latitude. He used Baumbach's work plus new photoelectric observations which show that the brightness at the maximum of the solar cycle is 1.8 times the brightness at minimum. Table 2 gives the electron density as a function of r for the equatorial and polar regions.

H. Alfvén and M. Waldmeier showed that if the inner corona was in hydrostatic equilibrium with a density gradient such as that implied by Baumbach's work, a temperature of the order of a million degrees would be required. Under these conditions, the actual heat loss of the corona would arise mainly from free-free transitions of electrons. Biermann and ten Bruggencate find the rate of heat loss of the whole corona to be 6×10^{25} ergs/sec, about a hundred times smaller than the observed

* See, for example, B. O. Peirce, *A Short Table of Integrals* (Boston: Ginn & Co., 1929), p. 62.

TABLE 2

THE ELECTRON DENSITIES IN THE SOLAR CORONA AT TIME OF SUNSPOT MINIMUM*

r Units of Solar Radius	N_e Equatorial Region	N_e Polar Region
1.00	227×10^6	174×10^6
1.03	178	127
1.06	132	87.2
1.1	90	53.2
1.2	39.8	16.3
1.3	21.2	5.98
1.5	8.3	1.41
1.7	4.00	0.542
2.0	1.58	0.196
2.6	0.374	0.040
3.0	0.176	0.017
4.0	0.050	0.004
5.0	0.025	
6.0	0.016	

* After H. C. van de Hulst, *B.A.N.* **11**, 135, 1950.

brightness. The observed coronal continuum is almost entirely scattered photospheric light and does not represent a loss of thermal energy from the corona.

14. The Line Spectrum of the Solar Corona

The identification of the emission lines in the solar corona marks an outstanding achievement of spectroscopy. The most conspicuous of these lines is the green λ5303 line discovered by Harkness in 1869. Other strong lines include the red radiations at λ6375 and λ6702, three lines in the infrared at λ7892, λ10,747, and λ10,798, and one in the ultraviolet at λ3388. Not all of these lines show the same intensity ratios in different parts of the corona. Lyot, who was able to photograph all of the stronger lines outside an eclipse, classified them in three groups on the basis of their behavior.

Unlike the forbidden lines in the nebulae, the coronal lines are fuzzy instead of sharp, with widths of the order of 0.8 to 1.0A, which become larger toward the red. Their radiation is unpolarized. Attempts to identify these lines proved unsuccessful for many years.

In 1939 Grotrian pointed out that the term separations, $^2P_{1/2} - {}^2P_{3/2}$, of the $3s^22p^5$ configuration of Fe X and that of $^3P_1 - {}^3P_2$ of the configuration $3s^23p^4$ of Fe XI, which had been measured by Edlén, corresponded to the frequencies of the red coronal lines, λ6374 and λ7892.

Edlén had also studied the spectra of Ca XII and Ca XIII and had noted that certain weak coronal lines coincided with the corresponding forbidden lines of these ions. The experimental basis for the identification of coronal lines is summarized in Table 3. The terms were computed from lines in the far ultraviolet, 90 to 150A. Hence the resultant prediction of the positions of the coronal lines could be subject to appreciable error. The important point, however, is that assuming the above identification to be correct, Edlén was able to work out the origins of the other coronal lines in a consistent fashion.

TABLE 3

THE EXPERIMENTAL BASIS FOR THE DIRECT IDENTIFICATION OF CORONAL LINES *

Laboratory Data			Corona	
Electron Configurations	Forbidden Transition	Separation as Obtained from Observed Laboratory Lines	Wave Number	Wave Length
Fe X $3s^23p^5$	$^2P_{1/2}-{}^2P_{3/2}$	15,687 cm^{-1}	15,683 cm^{-1}	6374.5 A
Fe XI $3s^23p^4$	$^3P_1-{}^3P_2$	12,673	12,668	7891.9
Ca XII $2s^22p^5$	$^2P_{1/2}-{}^2P_{3/2}$	30,028	30,039	3328
Ca XIII $2s^22p^4$	$^3P_1-{}^3P_2$	24,464	24,465	4086.3

* Courtesy, P. Swings, *Public. Astron. Soc. Pac.* **57**, 125, 1945.

Several important points are to be noted. Fe IX has a configuration $3s^23p^6\,{}^1S_0$ and hence can give no metastable levels. Fe VIII has a $3s^23p^63d$ configuration and therefore a $^2D_{3/2}$ and a $^2D_{5/2}$ level but the term separations of these levels are too small to give lines in the astronomically accessible region. The forbidden lines of Fe VII are observed in certain novae and peculiar stars, but definitely not in the corona. Hence we can look for the identification of the coronal lines among the $3s^23p - 3s^23p^5$ configurations of the iron group. Fe XII and Ne XIV are missing because the intensities of their lines that fall in observable parts of the spectrum are too low.

Edlén studied first the $3s^23p$ and $3s^23p^5$ configurations which give a ^2P term only. Laboratory investigations of isoelectronic sequences have shown that the splitting of this term accurately follows a relation known as the regular doublet law, viz.,

$$\nu(^3P_{3/2} - {}^3P_{1/2}) \sim (Z - \sigma)^4 \tag{22}$$

where Z is the atomic number and the screening factor σ is nearly constant. The identification of Fe XIV and Ni XVI by this method is illustrated in Table 4 of the isoelectronic sequence $3s^23p$ (Al I, Si II, etc.)

TABLE 4

GROUND TERM SPLITTINGS IN ISOELECTRONIC SEQUENCE $3s^23p$ *

Atomic No.	Ion	$^2P_{3/2} - {}^2P_{1/2}$ Term Separation cm^{-1}	$\sqrt[4]{\zeta}$	Difference
13	Al I	112.04	2.939	
				0.781
14	Si II	287.3	3.720	
				0.675
15	P III	559.6	4.395	
				0.622
16	S IV	950.2	5.017	
				0.599
17	Cl V	1,492	5.616	
				0.579
18	A VI	2,210	6.195	
				0.564
19	K VII	3,131	6.759	
				0.560
20	Ca VIII	4,305	7.319	
				0.552
21	Sc IX	5,759	7.871	
22	(Ti X)			
23	(V XI)			0.543
24	(Cr XII)			
25	(Mn XIII)			
26	Fe XIV	18,852.5*c*	10.588	
				0.538
27	(Co XV)	——	——	
28	Ni XVI	27,762*c*	11.664	

* P. Swings, "Edlén's Identification of the Coronal Lines," *Ap. J.* **98**, 119, 1943.

which is abstracted from the table by Edlén. The first two columns give the atomic number and the ion; the third column gives the term separation, $^2P_{3/2} - {}^2P_{1/2} = \Delta\tilde{\nu}$, in the wave number units, cm^{-1}, and the fourth column gives $\sqrt[4]{\zeta}$ where

$$\zeta = \tfrac{2}{3}\Delta\tilde{\nu} \tag{23}$$

Notice that the differences run very smoothly. If we assume that the green coronal line (whose wave number is 18,852 cm^{-1}) belongs to Fe XIV, the resultant mean value of the difference tabulated in the last column is quite consistent with the run of the table. The ions in parentheses are those whose term splittings have not been observed; *c* denotes an observed coronal line. Fe X and Ni XII can be identified in the same way from the $3s^23p^5$ isoelectronic sequence. The intensity ratios of the iron and nickel lines give further support to the suggested identifications.

For the $3s^23p^2$ and $3s^23p^4$ configurations, the extrapolation can be carried out by more complex but equally accurate methods. The results are shown schematically in Fig. 22. We find that Fe, Ni, and Ca contribute nearly all of the observed coronal lines. The next step is to examine the mechanism for the production of the coronal lines and see if the predicted intensities agree with the observed intensities after the known abundance ratio of Fe and Ni has been taken into account.

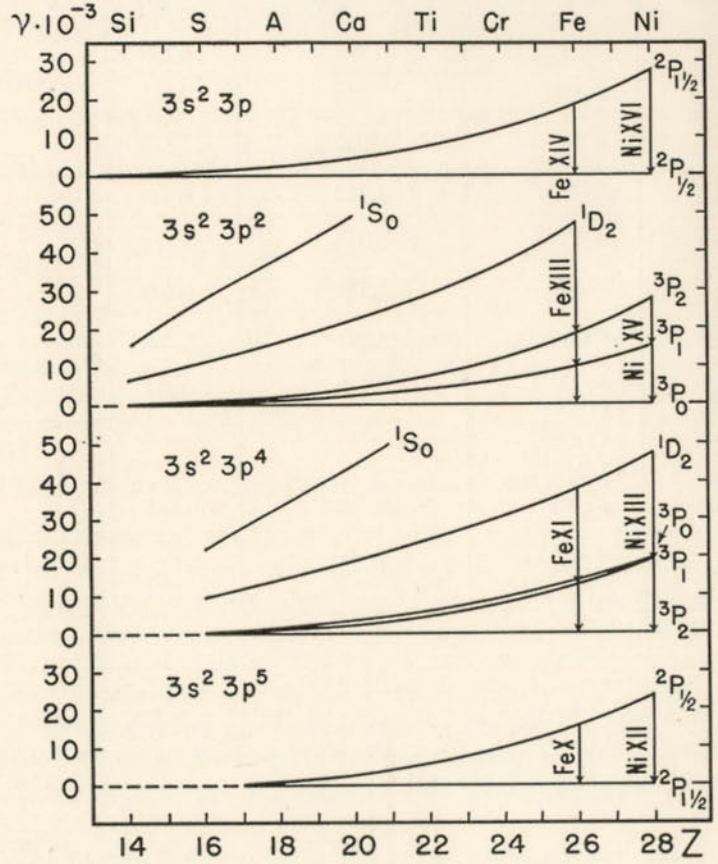

FIG. 22.—ISOELECTRONIC SEQUENCES INVOLVING THE CORONAL TRANSITIONS

(After B. Edlén; courtesy, *Astrophysical Journal*, University of Chicago Press, 98, 120, 1943.)

Edlén supposed that the coronal lines were produced by collisional excitation from the ground level, followed by a return to a lower level with the emission of a forbidden line. This is the mechanism responsible for the excitation of the forbidden lines in the planetary nebulae. Excitation by radiation also plays a role, but this process is probably

somewhat less important than collisional excitation. Edlén was able to account for the observed intensities of the coronal lines, not only qualitatively, but also semiquantitatively.

TABLE 5

CORONAL EMISSION LINES

Wave Length	Intensity in Sun		Intensity T Cor Bor	Identification	A_m	E.P. ev	I.P. ev
	Grotrian	Lyot					
3328.6	1.0			Ca XII	486	3.71	589
3388.0	16			Fe XIII	73.5	5.93	325
3454.1	2.3						
3601.0	2.1			Ni XVI	192	3.43	455
3642.9				Ni XIII	16.5	5.80	350
3800.4							
3986.1	0.7		6	Fe XI	9.08	4.66	261
4086.3	10			Ca XIII	319	3.02	655
4231.4	2.6			Ni XII	237	2.93	318
4359.4				A XIV	104	2.83	682
4567	1.1						
4586							
5116.03	4.3	2.2	14	Ni XIII	155	2.41	350
5302.86	100	100	100	Fe XIV	60.3	2.33	355
5534.6			59	A X	105	2.23	421
5694.42		1.2		Ca XV	95	2.18	814
6374.51	8.1	18	172	Fe X	69.3	1.94	233
6701.83	5.4	2		Ni XV	56.3	1.84	422
7069.62		2.2		Fe XV	38	31.7	390
7891.4		13		Fe XI	43.5	1.56	261
8024.21		0.5		Ni XV	20.2	3.38	422
10746.80		55		Fe XIII	14.0	1.15	325
10797.95		35		Fe XIII	9.5	2.29	325

Table 5 lists the emission lines observed in the corona. Successive columns give the wave length adopted from the work of S. A. Mitchell and of D. H. Menzel and W. Petrie, the intensity according to Grotrian and to Lyot, the intensity on Feb. 15, 1946, in the repeating nova T Corona Borealis as observed at Michigan, the identification, the transition probability, the excitation potential, and the ionization potential in ev. The ionization potential refers to the next lower ionization stage.

Edlén showed that other ionization stages of iron and nickel are not observed because the relevant transitions fall in an inaccessible part of the spectrum or the transition probabilities are too low. Highly ionized atoms of neighboring metals might be expected to appear, but if the chemical composition of the corona is the same as that of stellar atmospheres, the lines would be too weak to be observed against the strong background of the coronal continuum. Calcium and probably argon

are also present. No forbidden or permitted line of silicon, carbon, nitrogen, oxygen, or neon is possible in the corona under the conditions that presumably exist there.*

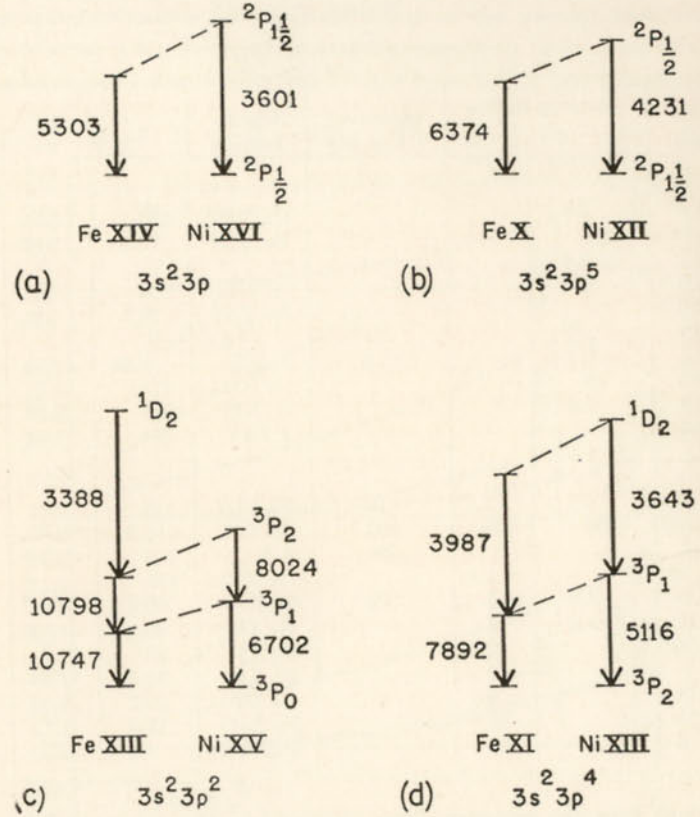

FIG. 23.—TRANSITION SCHEME FOR THE PRINCIPAL CORONAL LINES

(After B. Edlén. Courtesy, P. Swings, *Publications of Astronomical Society of the Pacific* **57**, 125, 1945.)

The great width of the coronal lines, the high level of ionization of Fe, Ca, and Ni, the washing out of the Fraunhofer spectrum by electron scattering, and the vast extent of the corona—all demand a temperature of the order of 500,000°K.

* A number of years ago, H. W. Babcock found the strong [Fe X] λ6374 coronal line extending into the region of the chromosphere. McMath, Goldberg, and Mohler have found this line as a fuzzy feature in absorption in the Fraunhofer spectrum with an equivalent width of the order of 0.01A, corresponding to about 10^{17} absorbing atoms. There does not seem to be enough Fe X in the corona to produce a line of this intensity; perhaps this material exists in quantity even in the chromosphere as Babcock's observation would suggest.

The absence of the recombination lines of abundant hydrogen is also indicative of a high temperature. Since the recombination rate at high temperatures varies as $T^{-3/2}$, at 500,000°K these lines would be 350 times weaker than at 10,000°K. Furthermore, they would be as wide as 7A and superposed on a strong continuum. An elementary calculation shows that these weak broad lines would show so little contrast with the continuum as to be invisible. Goldberg and Menzel find that Hα will be absent from the spectrum if $T_e^2 \gg 25N_e$. For $T_e = 300{,}000$°K and $N_e = 10^8$ we find that this inequality holds.

Lyot and Waldmeier's coronagraphic work shows that different coronal lines have different distributions. There are "red" regions of relatively low excitation where the λ6374 [Fe X] line is abnormally strong and "green" regions where the λ5303 [Fe XIV] line and other high excitation lines are strong. There is a positive correlation between the stronger chromospheric plages and the coronal maxima but the coronal line emission tends to be strongest in the spot regions. Here appears the λ5694 line, which Roberts finds to be at least occasionally associated with prominences of the sunspot type. It is normally about 0.05 as bright as λ5303 [Fe XIV] but Waldmeier once observed it to be three times as strong as λ5303 over an active spot group. Lyot found the line to show a different behavior from that of any other coronal line.

In some regions, Waldmeier found λ5303 to be unusually strong. He refers to these as "C regions." They appear to be related to terrestrial magnetic storms and aurorae, which seem to appear about 0.6 days after these areas cross the solar meridian, according to Waldmeier's observations.

15. Theories of Coronal Excitation

A satisfactory theory of the corona must not only account for the high degree of ionization observed, but also it must explain the simultaneous occurrence of four or more ionization stages of iron and nickel. It must account for the shape of the corona and the form of the streamers. Finally, it must explain why the excitation tends to be greater near disturbed areas such as sunspots.

Kiepenheuer has discussed the general form of the corona on the basis of various hypotheses about solar magnetic fields. The high excitation of the corona has been attributed to the kinetic energy of interstellar material accreted by the sun (Vand, Bondi, and Lyttleton), high speed particles accelerated by fluctuating magnetic fields in the neighborhood of spots (Kiepenheuer), illumination from small intensely heated areas on the solar surface (Menzel and Goldberg), dissipation of shock waves from solar granules (Biermann, Schwarzschild, and Schatzman). Critical assessment of these theories is difficult. Mechanisms such as

accretion or shock waves must be supplemented by other "local" phenomena to account for the high excitation near disturbed areas.

In the Schwarzschild theory, the energy of the corona is supplied by a stream of acoustical waves that originate in the turbulent motions of granules, transport mechanical energy through the photosphere and dissipate it as heat in the upper chromosphere and corona.

As the granules rise through the unstable layers, they are slowed down and part of the mechanical energy is dissipated in the form of compressional waves. Since their formation and dissipation takes place in a random way, the energy they transmit to the overlying strata may be partly in the form of acoustical waves which are simply superposed without phase or amplitude relation with one another. The waves move with a propagation velocity V which is almost identical with the velocity of sound. Since w is the mean material velocity in the waves, the energy density is ρw^2, and the noise flux is of the order of $\rho w^2 V/\text{cm}^2$. The exact numerical coefficient depends on the shape of the wave.

The kinetic energy of a granule of diameter d, density ρ, and velocity v is

$$E = \frac{1}{2}\rho\frac{\pi}{6}d^3v^2 \tag{24}$$

The granular velocities v are of the order of $\frac{1}{2}$ km/sec. With $\rho = 10^{-7}$ gm/cm^3 (corresponding to a point near the top of the convective layer), and $d = 10^8$ cm, the energy per granule will be about 6×10^{25} ergs. If, at any time, there are 10^6 granules on the surface of the sun and their lifetimes are 200 seconds each, the rate of energy transport will be

$$L_{\text{granules}} = \frac{NE}{t} = 3 \times 10^{29} \text{ ergs/sec} \tag{25}$$

If we take the velocity of the granule, $\frac{1}{2}$ km/sec, as equivalent to the material velocity of agitation, and note that the velocity of sound in an isothermal photospheric layer is

$$V = \sqrt{\frac{k}{M}T} \sim 7 \text{ km/sec} \tag{26}$$

where M is the mass of the average atom, the upper limit to the energy transport in the wave will be

$$F_{\max} = \rho\bar{w}^2 V = 1.7 \times 10^8 \text{ ergs/sec/cm}^2 \tag{27}$$

At any one instant, only a portion of the solar surface is covered by rising granules. Since the noise flux, $F = \rho\bar{w}^2 V$ is constant, a decrease in the density ρ will be accompanied by a rise in the velocity of agitation, w.

Not all of the energy carried by the granules is converted into sound energy. If only a tenth is so transformed, the amount of energy available for heating the chromosphere and corona will be about 3×10^{28} ergs. The total amount of radiation lost by the corona, principally as free-free and bound-free transitions is 10^{23} ergs/sec, while as much as 10^{27} ergs/sec may be radiated by the chromosphere. Hence the granular noise appears capable of supplying enough energy.

After a few "wave lengths," the acoustical waves degenerate into shock waves. Unlike an electromagnetic wave, whose velocity is governed solely by the properties of the medium through which it is passing, the amplitude of a compressional wave in a fluid will have an influence on its velocity. If the amplitude is large, the top will propagate with a greater speed than the base and the latter will tend to become distorted (see Fig. 24).

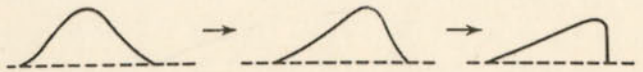

FIG. 24.—DEFORMATION OF A WAVE OF FINITE AMPLITUDE INTO A SHOCK WAVE

The crest of the wave moves faster than the velocity of sound, the wave becomes distorted, and finally evolves into a shock wave as the front face becomes vertical.

The number of wave lengths required for a sound wave to be transformed into a shock wave is of the order of V/w.*

The acoustical waves pass through the photospheric layers without appreciable dissipation of mechanical energy, since the material velocity w in an individual wave is much smaller than the sound velocity V. For example, in the photosphere, where $w = \frac{1}{2}$ km/sec and $V = 7$ km/sec, $w/V = 1/14$. In the chromospheric layers where the density has decreased by a factor of 100, w will have increased by a factor of 10, w/V will be 1/1.4, and the sound wave will be transformed to a shock wave.

A shock wave can be described as a surface of discontinuity moving in a fluid with a velocity U which is always greater than that of sound and is larger the greater the discontinuity in pressure and density. The material velocity w_1, the pressure p_1, and the density ρ_1 in front of the wave are related to the corresponding quantities w_2, p_2, ρ_2 behind the wave by means of the Hugoniot relation for the conservation of energy, and by the equation for the conservation of matter, and by the amount of momentum carried across the shock front.

* Small sounds do not evolve into shock waves because they are damped out by viscosity before they travel such a distance. In an explosion, on the other hand, P is much greater than P_0 (the initial pressure) and a shock wave appears at once and energy is quickly lost. Shock waves of velocity 6000 km/sec in tubes have been observed to fall appreciably in intensity in 2 meters.

The velocity and energy of a shock wave gradually decreases as it progresses. The discontinuity of P and ρ at the shock front is abrupt. As the wave passes through the gas, the latter experiences a nonreversible compression. Subsequently, it expands adiabatically, but the wave does not get back all the work done in the sudden compression; some of the latter is dissipated in heat.

We can calculate the amount of energy thus degraded if we suppose that the shape of the wake behind the front is always conserved. It is found that the greater the velocity of the material within the wave, the faster the dissipation of energy.

Schatzman has considered in some detail the transfer and dissipation of shock wave energy in the chromosphere. The compressional waves are transformed into shock waves within a few hundred kilometers. Because of the steep temperature gradients, V increases rapidly and the sound waves are refracted downwards through the chromosphere and dissipated into heat.* Shock waves cannot move through the corona where the mean free path of an atom is much greater than the size of the wave. Energy transport in this region is chiefly by conduction.

The shock wave mechanism seems to explain the observed temperature and density distributions in the chromosphere and corona. The sharp maximum of the temperature distribution in the lower corona arises from the effects of the bending of the sound waves by the steep gradient. If refraction were not present, the temperature maximum would be too far away from the photosphere.

Acoustical waves may explain the large turbulence observed in the atmospheres of the giant stars. Their low surface gravities permit the passage of progressive waves of long period, e.g., 10^4 seconds. The rate of energy dissipation is much slower than in the sun. From the condition of conservation of flux of mechanical energy, the equation of hydrostatic equilibrium, and the relation between opacity and absorption coefficient, it is possible to calculate the velocity of agitation of the material w at a chosen optical depth as a function of the mass, radius, and luminosity of the star. The values of w computed in this way are in good agreement with the observed values for stars like δ Canis Majoris, ε Aurigae, and η Aquilae. Stars of high surface gravity such as the sun

* The bending of the wave will depend on its period. If the period is as long as 200 seconds, the wave would simply be reflected by the steep density gradient and would never penetrate to the upper layers. For periods much shorter than 200 seconds, the velocity of propagation is almost independent of the frequency. Schatzman has suggested that waves with a quasi-period of the order of 15 seconds are required. If the period is known, we can compute the energy dissipation cm³/sec and determine what value of w is required to reproduce the observed energy output. At 1500 km we find a mean random velocity w of about 2 km/sec as compared with a maximum observed turbulent velocity of the order of 1 km/sec.

or 10 Lacertae cannot provide large turbulent velocities because of the strong dissipation of mechanical energy.

Although the general excitation of the corona may be explained by the hypothesis of granular noise, its behavior in the neighborhood of spots suggests that additional causes must act. It is possible that charged particles are accelerated to high speeds by varying magnetic fields. Alternatively, small areas may become intensely heated and produce an excess of radiation in the far ultraviolet capable of affecting the corona; these are the hot spots suggested by Menzel and Goldberg.

Allen finds that the accretion of the particles responsible for the zodiacal light as well as the sweeping up of interstellar material is much too small to supply the energy lost by the corona. The irregular nature of the temperature distribution as shown by the variation of λ5303 in space and time is difficult to understand if the source of energy is external to the sun. The complicated isophotic contour of this and other lines likewise makes it extremely doubtful that the corona is in hydrostatic equilibrium. On the contrary, these irregularities strongly suggest the influence of electromagnetic forces. A dynamical rather than a purely static model of the corona must be sought.

16. Radio-Frequency Radiation from the Sun

A new field of research was opened by the discovery of radio-frequency (r.f.) radiation. This solar noise may be divided into the following categories:

(a) Quiet thermal noise
(b) Steady sunspot noise
(c) Noise storms and bursts
(d) Outbursts
(e) Nonpolarized bursts

(a) *Quiet Thermal Noise*

Although the r.f. solar radiation shows a considerable fluctuation in intensity with time, at each frequency there exists a finite minimum solar noise flux that is related to the radiation from the sun's outer envelope. Fig. 25 shows the dependence of the intensity on the frequency. The r.f. flux is expressed in terms of the temperature a black body subtending the same diameter would have to have in order to emit the same amount of radiation. Notice that at low frequencies this temperature seems to be about a million degrees but that for frequencies greater than about 10^5 mc/sec, the "temperature" approaches 10,000°K.

The theoretical interpretation of this r.f. radiation from the quiet

sun in terms of thermal emission has been highly successful.* A radio wave of frequency ν will travel in an ionized medium as long as

$$\nu^2 > \frac{N_e e^2}{\pi m} \tag{28}$$

where N_e is the electron density. A wave whose frequency exceeds 10^5 megacycles could penetrate the chromosphere, $N_e < 10^{12}$, and its intensity should be correlated with the effective temperature of the sun, as is observed to be true. For wave lengths of the order of 5 meters, the critical electron density is of the order of $10^8/\text{cm}^3$. Such waves must originate in the corona; hence the high temperature of approximately $10^{6°}$K is understandable.

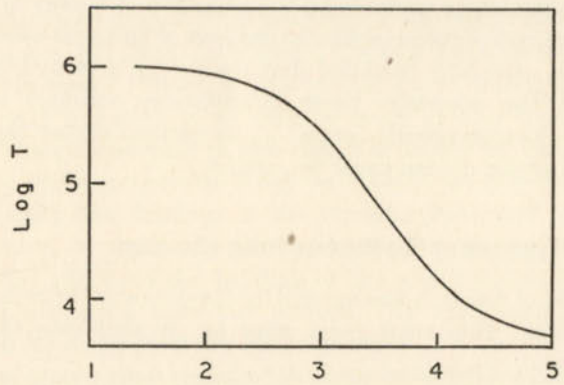

FIG. 25.—THE RELATION BETWEEN THE RADIO-FREQUENCY RADIATION FROM THE QUIET SUN (EXPRESSED IN TERMS OF THE LOGARITHM OF THE APPARENT TEMPERATURE) AND THE LOGARITHM OF THE FREQUENCY (MEGACYCLES/SEC)

(Adapted from a diagram by C. W. Allen—Seventh report of the Commission for the Study of the Relations Between Solar and Terrestrial Phenomena.)

From the wave length variation of the intensity of the radio-frequency radiation of the quiet sun, it is possible to determine the electron temperature of the chromosphere and corona, provided the electron densities in the corresponding layers are known. J. R. Hagen of the Naval Research Laboratory has discussed measurements of the monochromatic "temperature" T_λ of the sun at 0.85, 3.14, 10.6, and 50 cm. He assumed that the emission of radio waves takes place according to Kirchhoff's law. Hence the signal intensity I_λ at a given wave length will consist of contributions from different layers. Since the Rayleigh-Jeans law, eqn. (17)

* The radiation of the quiet sun can also be regarded as produced by free-free transitions. Equivalent formulae are obtained.

of Chapter 5, applies, the emission at any point is proportional to the temperature, and

$$I_\lambda \sim T_\lambda \sim \int k_\lambda \rho T_r e^{-\int k_\lambda \rho\, ds}\, ds \tag{29}$$

Here T_r is the electron temperature at a height r above the solar surface, while ds is the element of integration. The absorption coefficient for radio waves, k_λ, may be computed as a function of N_e, T, and λ with the aid of formulae given by Cowling. The integration is carried out over the relevant layers of the solar atmosphere. Hagen adopted N_e from the work of Wildt, Baumbach, and van de Hulst, and found the variation of T_r with height which would reproduce the observed radio-frequency intensities. His data give strong support to the idea that the kinetic temperature of the chromosphere is low and rises abruptly as the corona is approached. Similar studies have been carried out by Smerd and others.

With an apparatus of high resolution, or ideally from eclipse observations, it is possible to measure the brightening towards the limb, as a function of wave length. In this way we shall be able to find the variation of N_e as well as that of T_e. When data of high resolution and accuracy are available, these methods promise to be the most important for the determination of N_e and T_e in the solar envelope. To date it has not been possible to get a complete intensity curve $I(r)$ across the disk.* The best determined factor is the ratio of the center of the disk temperature T_0 to the apparent temperature of the whole visible disk. The observations agree well with the predictions of the theory of S. Smerd.

(*b*) *Steady Sunspot Noise*

In the higher frequencies ($\lambda < 10$ cm) there occurs in addition to the thermal noise a steady "hum" whose intensity depends on the size and number of sunspots. Near the sunspot maximum this hum may be comparable with the quiet thermal noise in the same wave lengths. The noise appears to be emitted from an area about ten times larger than the actual spot areas and sometimes lasts after the spot has disappeared. This sunspot "hum" is sometimes polarized. The effect of a magnetic field on an ionized gas is to doubly refract radio waves. The ordinary ray comes from deeper, the extraordinary ray from higher, layers in the solar atmosphere.

* For $\lambda < 60$ cm the radiation at the center of the disk comes from the photosphere. Towards the limb the radiation tends to come from the corona as the rays tend to come at grazing incidence. The apparent temperature of the limb is about 850,000°K. When $\lambda > 1$ meter, all radiation comes from the corona and the apparent temperature is high except toward the limb where the optical depth decreases because of refraction. The sun is large, fuzzy, and darkened to the limb.

(*c*) *Noise Storms and Bursts*

Radiation of meter wave length sometimes increases for hours or days and produces "noise storms" or enhanced radiation. Although this noise is associated with sunspots it differs from the steady sunspot hum in that it probably consists of many small bursts upon which are superposed large bursts with frequencies from 50 to 200 megacycles/sec with a lifetime of about 2 seconds. The burst radiation is incoherent, has a line spectrum, is circularly polarized, and is not correlated with disk phenomena. The intensity of the noise is connected with the central passage of sunspots and shows that the noise is emitted in a cone of total angle less than 40°.

(*d*) *Outbursts*

Outbursts also appear on meter wave lengths but last for times of the order of ten minutes and show a high, erratically varying intensity. They are closely associated with solar flares.

(*e*) *Isolated Nonpolarized Bursts*

Finally, isolated nonpolarized bursts with $\lambda \sim 10$ cms seem to come from sunspot areas.

The bursts and outbursts cannot be of thermal origin. They may originate from the oscillations of the positive and negative charges with respect to one another in an ionized gas or "plasma" (plasma oscillations). The period of oscillation is given by

$$T = \sqrt{\frac{\pi m}{N e^2}} \tag{30}$$

If a current of particles moves into an ionized gas, small oscillations may be amplified under certain conditions as Bohm and Gross showed. Giovanelli suggested that as the magnetic fields of sunspots grow, electric fields are induced that may accelerate electrons and produce oscillations. The emission of a plasma in the presence of a magnetic field is directed in space.

Outbursts are closely associated with intense flares. Payne Scott and A. G. Little found the source of this r.f. radiation to move with a speed of about 500 km/sec outward from the flare into the corona. That is, the outburst appears to be produced by a surge. The frequency of the radiation drifts is due, presumably, to the Doppler motion.

The theoretical work for the interpretation of the r.f. radiation from the disturbed sun is all of a preliminary character, and much remains to be done before the phenomena are completely explained.

17. Solar-Terrestrial Relationships

The influence of the sun on terrestrial affairs has attracted attention since the time of Herschel. Solar variations affect radio communications, magnetic compasses, and even power lines. An understanding of the effects of solar radiation upon the earth's atmosphere will make air travel safer, will improve radio communications and ultimately may solve questions of long-range weather forecasting. Space permits us to mention only a few of the highlights.

Correlations between solar activity on the one hand and the state of the ionosphere, terrestrial magnetism, and aurorae on the other are the best established. Radio fadeouts, disturbances of the earth's magnetic field, and bright auroral displays are commoner at times of greatest solar activity (sunspot maximum).

Much study has been devoted to the correlation of solar activity and ionospheric disturbances. The ionosphere consists of several layers of ionized gas, the *D*, *E*, and *F* layers, situated roughly at elevations of 70 to 100, 110 to 120, and 200 to 300 km above the surface of the earth. During the day, at small zenith distances of the sun, the *F*-layer is broken into two sublayers, the F_1 layer about 30 km thick at 220 km elevation, and the F_2 layer at 300 km and of 70 km thickness. The *E* and *F* layers are the most important for correlation studies. During the day the electron density in the *E* layers is about 1.5×10^5 electrons/cm^3, whereas in the *F* layers it ranges from 2.5×10^5 to 10^6 electrons/cm^3.

The highest frequency ν_c which is reflected from a given layer reveals the electron density in accordance with the relation

$$N_e = 1.24 \times 10^{-8} \nu_c^2 \tag{31}$$

The variation of N_e in the F_2 layer with the sunspot numbers has long been known. *E*, *F*, and F_2 layer ionization also shows a close correlation with the calcium flocculi figures. Stetson found the measured values of ν_c at night also to depend on the sunspot numbers as though the ionization of the layers were controlled by charged particles ejected by the sun.

The most striking correlations are those found between bright solar flares and S.I.D.'s (sudden ionospheric disturbances). Short radio waves cease to be reflected by the ionosphere, anomalous phase differences between the ground and reflected waves in other frequencies appear, and parasitics of atmospheric origin are reinforced. The radio fadeouts appear to be produced by the absorption in the *D* layer of ultraviolet radiation from the flare; they appear only on the sunward side of the earth. In addition there are often prolonged ionospheric disturbances so extensive as to affect the ionosphere over much of the earth, including

the night side. Bright aurorae and magnetic storms tend to occur at this time. Flares of moderate or weak intensity (importance 1 or 2) do not appear to be correlated with S.I.D.'s.

A study of terrestrial magnetism provides additional information.

It has long been known that a compass needle shows a small-scale wavering, which has been attributed to fluctuating magnetic fields arising from motions of ions in the upper atmosphere. First, there is a small diurnal motion of the needle presumably caused by the effect of sunlight on the upper regions of the atmosphere. Second, there is a constant wavering superposed on the diurnal motion. This wavering increases at the time of spring and fall equinoxes and tends to occur in bursts separated by a period of 27 days. Third, the needle sometimes shows rapid chaotic fluctuations characteristic of a "storm" that is often associated with radio fadeouts and bright flares. Studies of the correlation of geomagnetic activity with sunspots show that this activity tends to be heightened to a maximum about two days after the meridian passage of a very large spot group. The smaller the spot, the less definite the correlation, unless the group happens to contain important flares. The flares tend to be the important element in the correlation. The magnetic storms are generally related to flares near the center of the disk, but sometimes storms are associated with flares near the limb and may even be associated with coronal rather than with flare activity.

It has been suggested that at times of solar flares, corpuscular streams are ejected from the sun (perhaps by the pressure of Lyman radiation). These strike the earth on an average of 26 hours later and produce geomagnetic storms and bright aurorae that tend to last longer than the initial flare. Presumably, these are associated with the surges that are detected by the r.f. measurements. The closest relationship between ionospheric disturbances and magnetic storms and aurorae is found at high latitudes. Radar studies of the ionosphere indicate that at these times streams of ions move in the earth's upper atmosphere, in regions near the pole where the aurorae are observed.

Oliver Wulf and Seth B. Nicholson have suggested that ultraviolet light, rather than streams of particles, influences the magnetic fluctuations. Magnetic storms are produced by whirls and eddies of the charged gases of the upper atmosphere. The stability of these layers varies, and tempests may be triggered by the ultraviolet light from the sun more easily near the equinoxes when the layers are relatively unstable. In other words, the magnetic fluctuations are determined by the complex meteorology of the upper atmosphere which in turn is influenced by the sun.

A phenomenon of much interest is the increase of cosmic-ray intensity at the time of bright flares. The percentage increase is small and the prevailing opinion (April, 1952) is that the enhanced intensity is not due to the production of cosmic rays in disturbed areas of the sun but

to a change in the state of ionization (and magnetization) of the earth's upper atmosphere. The penetration of heavy charged particles is strongly influenced by the earth's field and if the latter is changed, the character of the cosmic ray spectrum observed at the earth's surface will likewise be modified.

The ionization level of the ionosphere, both in its quiet and in its disturbed condition, as well as its response to flares, etc., may provide some important clues to the solar radiation in spectral regions which cannot be observed directly. The results will depend on the mechanisms proposed for the ionization of the F and E layers, usually the photoionization of O and N, possibly by radiation beyond the Lyman limit from the upper chromosphere. The ionization in the E and D layer is harder to account for as the radiation must get through the F layer. X rays from the corona, photospheric radiation from $\lambda < 1300$A, and Lyman α from the chromosphere have been proposed, but no adequate theory has been established.

The high temperature of the corona implies some excess of far ultraviolet energy, but the actual amount of such energy must be very small, perhaps 10^{-7} that of the normal sun. The emission of high frequency energy and fast charged particles from disturbed areas of the sun seems well established and eventually more may be learned about the sun from a consideration of processes that occur in the upper atmosphere. At present, unfortunately, the detailed mechanisms which cause the ionospheric layers to behave as they do are not identified and the question must be left open.

Eclipse observations and study of the disturbed sun present some knotty problems. From the July 9, 1945, eclipse, Waldmeier concluded that the radiation responsible for the E layer was probably of coronal origin and associated with the λ5303 line, but the observations were not definitive. Bosson, Denisse, Gallet, and Seligman found a sharp fall in the electron density in F_2 when a spot group was covered. The Japanese observers found a correlation of the F_1 region with the occultation of active coronal regions.

From a study of the critical frequencies in the E, F_1, and F_2 layers and from the correlation of the ionization of the different ionospheric layers with spots, calcium flocculi, active coronal regions, etc., C. W. Allen concluded that the E layer is regulated by the flocculi and faculae while the F_1 and F_2 layers are associated with the lower corona. The augmented ionization of the D layer at the time of radio fadeouts is associated with flares, but the type of radiation responsible has not been identified. Lyman alpha emission has been suggested, but Ellison's observations show that phase anomalies in the reception of long wave lengths, at such times, persist after the Hα emission has disappeared. Perhaps radiation from other highly excited atoms play a role.

Variations in the far ultraviolet solar radiation may be inferred from effects on planets, comets, and the moon. W. Becker found brightness variations in Saturn and Uranus to be correlated by solar activity, while F. Link found the brightness of the lunar surface to be strongly affected by variations in the ultraviolet solar radiation as a consequence of fluorescence of the rocks. Variations in the brightness of comets may be produced by solar activity. The most striking example is the Schwassman-Wachmann comet, whose brightness is subject to sudden variations of the order of 5 magnitudes. N. Richter suggested that these variations were due to solar activity.

Finally, the data obtained by the Naval Research Laboratory from rockets fired above the earth's atmosphere reveal extreme ultraviolet radiation ($\lambda < 1300$A) and soft X rays.

The relation between solar activity and the weather has been the subject of an enormous number of investigations. Few correlations have been established. It does appear that the mean air temperature at the earth's surface (at least in the tropics) varies with the solar cycle in the sense of being lowest at maximum and highest at minimum. Curiously, C. G. Abbot found no real evidence for an $11\frac{1}{2}$ year periodicity in the solar constant, but several workers have suggested that the variations may be confined to the ultraviolet and have little effect on the total quantity of radiation. This presumably variable ultraviolet solar radiation may influence the ozone layer and the circulation of the upper atmosphere.

Long-period fluctuations in the circulation pattern of the lower atmosphere may depend on heat sources in the upper atmosphere. At present we have no reliable data on the variability of the direct solar heating of the upper atmosphere. Such data might help to solve some of the problems of atmospheric circulation and might even permit long-range weather forecasting. We must urge caution in drawing correlations between solar activity and the weather, however. The explosion of a volcano like Krakatoa, which filled the upper atmosphere with fine dust, may have far greater influence than the solar variability upon the temperature at the earth's surface.

PROBLEMS

1. Show that the total intensity in a bright line will be

$$I = B(T)(1 - e^{-\tau})$$

where I, the Planckian function $B(T)$, and the optical thickness of the radiating layer τ, all depend on the frequency. Assume thermodynamic equilibrium.

2. Calculate the curve of growth for the Ca II K line in emission in thermodynamic equilibrium at 10,000°K.

3. If the chromosphere is in hydrostatic equilibrium with $a = 0.9 \times 10^{-8}$ [cf. eqn. (11)] what is the required kinetic temperature?

4. The energy emitted/cm³/sec in the $n = 20$ to $n = 2$ transition in hydrogen at the base of the chromosphere is given by Menzel and Cillié as 2×10^{-4}. The Einstein coefficient A is 2160. If $N_e = 3.5 \times 10^{11}$, find the temperature from the combined Boltzmann and Saha equations.

5. Helium is observed in two stages of ionization. At the base of the chromosphere Menzel and Cillié find for the $2^3P - n^3D$ lines of He I:

λ	Terms	$I - \chi$	log A	log E
4026	5^3D	0.54	7.11	−4.49
3819	6^3D	0.37	6.86	−4.96
3705	7^3D	0.27	6.65	−5.44
3634	8^3D	0.21	6.47	−5.68

where E is the emission/cm³/sec, I is the ionization potential, A is the transition probability, and χ is the excitation potential. From these data calculate the number of He^+ ions/cm³, assuming, tentatively, $T = 10{,}000$°K and thermodynamic equilibrium. The amount of energy radiated per unit time and volume in λ4686 (4–3) of He II is given by log $E = -5.88$. Compute the number of doubly-ionized helium atoms, $N(He^{++})$ per cm³, and apply the ionization formula to the He^{++}/He^+ ratio to get an ionization temperature for helium.

6. Assume that in the inner corona, $N_e = 10^9$, $T = 500{,}000$°K. Calculate the relative intensity of the continuum arising from electron scattering and that at the center of Hα assuming it to arise entirely from recombination. Would the line be expected to appear in the outer corona where N_e = number of hydrogen ions = 10^7/cm³, and $T = 500{,}000$°K?

7. With the aid of the data of Table 2 compute the temperature distribution in the corona on the assumption it is in hydrostatic equilibrium.

8. Compare the amount of energy absorbed per gram of solar material per second at a point of optical depth 0.3 with that dissipated in an acoustical wave. Assume $w = 0.5$ km/sec, $\gamma = 5/3$.

REFERENCES

Out of the extensive literature on solar phenomena we shall select only a few representative papers. Additional bibliography will be found in the references cited.

1. *General*

MENZEL, D. H. *Our Sun.* Cambridge: Harvard University Press, 1949 (popular).

ABETTI, G. *The Sun.* New York: D. Van Nostrand Co., Inc., 1938 (a new Italian edition has been prepared).

WALDMEIER, M. *Sonne und Erde.* Zürich: Buchergilde Gutenberg, 1946.

HOYLE, F. *Some Recent Researches in Solar Physics.* London: Cambridge University Press, 1949.
UNSÖLD, A. *Physik der Sternatmosphären.* Berlin: Julius Springer, 1938.

2. *Granules*

For dimensions and photometry, see:

KEENAN, P. *Ap. J.* **88,** 360, 1938; **89,** 604, 1939.

An application of turbulence theory is given by:

SCHWARZSCHILD, M., and R. S. RICHARDSON. *Ap. J.* **111,** 351, 1950.

The basic theoretical treatment of granules is due to:

SIEDENTOPF, H. *A.N.* **247,** 297, 1933; **249,** 53, 1933; **255,** 157, 1935.

The theory of the hydrogen convective zone has been developed by Unsöld, *op. cit.*, and numerous other writers among whom we may mention:

RUDKJÖBING, M. *Zeits. f. Ap.* **21,** 254, 1942.
BIERMANN, L. *Zeits. f. Ap.* **21,** 320, 1942.

3. *Sunspots*

(a) Spectroscopic Studies:

MOORE, C. E. *Ap. J.* **75,** 222, 298, 1932.
TEN BRUGGENCATE, P., and H. VON KLÜBER. *Zeits. f. Ap.* **18,** 284, 1939; *Göttingen Veröff.* No. 78, 1944.

(b) Temperature Determinations:

PETTIT, E., and S. B. NICHOLSON. *Ap. J.* **71,** 153, 1930.
WANDERS, A. J. M. *Zeits. f. Ap.* **8,** 108, 1934.

(c) Magnetic Fields. The classical paper on the magnetic polarity law is:

HALE, G. E., and S. B. NICHOLSON. *Ap. J.* **62,** 270, 1925.

Measurements of magnetic fields on the solar surface by methods of high precision are discussed by:

VON KLÜBER, H. *Zeits. f. Ap.* **24,** 1, 121, 1947; **25,** 187, 1948; *M.N.* **111,** 2, 1951.
THIESSEN, G. *Zeits. f. Ap.* **26,** 16, 1949.
BABCOCK, H. W., and H. D. *Publ. Astron. Soc. Pac.* **64,** 282, 1952.

Variations in the magnetic fields of spots have been measured by:

BRUNNCKOW, K., and W. GROTRIAN. *Zeits. f. Ap.* **26,** 313, 1949.

Statistical studies of the Mount Wilson observations of sunspots, I and II (1938) have been made by:

COWLING, T. G. *M.N.* **106,** 218, 1946.
HOUTGAST, J., and A. VAN SLUITERS. *B.A.N.* **10,** 325, 1948.
GROTRIAN, W., and H. KÜNZEL. *Zeits. f. Ap.* **26,** 325, 1949; **28,** 28, 1950.

(d) Theoretical Studies:

ALFVÉN, H. *Cosmical Electrodynamics.* New York: Oxford University Press, 1950.
CHAPMAN, S. *M.N.* **103,** 117, 1943.
COWLING, T. G. *M.N.* **106,** 218, 446, 1947.

4. *Disk Phenomena*

Faculae (facular granules):

TEN BRUGGENCATE, P. *Zeits. f. Ap.* **19,** 59, 1939; **21,** 162, 1942.
WALDMEIER, M. *Helv. Phys. Acta* **13,** 14, 1939; *Zeits. f. Ap.* **26,** 147, 1949.

For an account of results obtained with the spectroheliograph, see:

D'AZAMBUJA, L., and M. *Ann. de Paris Obs.* (Meudon) **6,** No. 7, 1948.

5. *Prominences*

Classifications and descriptions:

PETTIT, E. *Ap. J.* **98,** 6, 1943; *P.A.S.P.* **53,** 289, 1941; **58,** 150, 1946.
MCMATH, R. *Publ. Mich. Obs.* **7,** 191, 1939.
NEWTON, H. W., and M. A. ELLISON. *M.N.* **102,** 2, 11, 1942.
ELLISON, M. A. *M.N.* **104,** 22, 1944.
DODSON, H. W., and R. R. MCMATH. *P.A.S.P.* **60,** 366, 1948 (filaments).
ROBERTS, W. O. *Ap. J.* **101,** 136, 1945 (spicules).
MOHLER, O. *M.N.* **111,** 630, 1951.

Motions:

PETTIT, E. *Ap. J.* **76,** 9, 1932.
WALDMEIER, M. *Zeits. f. Ap.* **15,** 299, 1938; **18,** 241, 1939; **21,** 130, 286, 1942.
PAN PUH. *Meudon Annals* **8,** No. 4, 1939.
MCMATH, R. *Publ. Mich. Obs.* **8,** 123, 1943.
HULME, H. R. *M.N.* **99,** 634, 1939.
DODSON, H. *M.N.* **108,** 383, 1948.

Perhaps the best idea of the motions of prominences is to be obtained from the moving pictures obtained at the McMath-Hulbert Observatory, at Climax, Colorado, and at the Pic du Midi by B. Lyot.

Spectra. The effects of self-reversal are discussed by:

THACKERAY, A. D., H. A. BRUCK, and W. MOSS. *M.N.* **103,** 258, 1943; **105,** 17, 282, 1945.
UNSÖLD, A. *Zeits. f. Ap.* **24,** 22, 1947, has given a quantitative analysis of the spectrum of a prominence. See also:
WALDMEIER, M. *Zeits. f. Ap.* **28,** 208, 1951.

6. *Flares*

(a) Spectra:

RICHARDSON, R. S., and R. MINKOWSKI. *Ap. J.* **89,** 347, 1939.
RICHARDSON, R. S. *Ap. J.* **90,** 368, 1939.
ALLEN, C. W. *M.N.* **100,** 635, 1940.

(b) General Properties and Statistics:

WALDMEIER, M. *Zeits. f. Ap.* **16,** 277, 1938; **20,** 46, 1940; *Astr. Zürich Mitt.*, No. 153, 1948.
DODSON, H., and R. HEDEMAN. *Ap. J.* **110,** 242, 1949, discuss the frequency and position of flares and their relation to sunspot groups.
ELLISON, M. A. *M.N.* **106,** 500, 1946; **109,** 1, 1949; *Observatory* **68,** 31, 1948.

Theoretical attempts to explain the origin of flares have been made by:

KIEPENHEUER, K. O. *Zeits. f. Ap.* **20,** 332, 1941.
GIOVANELLI, R. G. *Nature* **158,** 81, 1946; *M.N.* **107,** 338, 1947.

7. *Chromosphere*

(a) Basic Observational Data:

MITCHELL, S. A. *Ap. J.* **71,** 1, 1929; **72,** 146, 1930; **105,** 1, 1947.
MITCHELL, S. A., and E. T. R. WILLIAMS. *Ap. J.* **77,** 1, 1933.
MENZEL, D. H. *Publ. Lick Obs.* **17,** 1, 1931.
MENZEL, D. H., and G. G. CILLIÉ. *Harv. Circ.*, 410, 1935; *Ap. J.* **85,** 88, 1937.
PANNEKOEK, A., and M. MINNAERT. *Publ. Amsterdam Acad.* **13,** No. 5, 1928.
WILDT, R. *Ap. J.* **105,** 36, 1947.

(b) Temperature:

GOLDBERG, L. *Ap. J.* **90,** 673, 1939.
REDMAN, R. O. *M.N.* **102,** 141, 1942.
UNSÖLD, A. *Zeits. f. Naturforschung* **7,** 221, 1952.

Theoretical discussions of chromospheric support were given by:

MCCREA, W. H. *M.N.* **89,** 718, 1929; **95,** 509, 1935.

The theoretical problem of the chromosphere and the interpretation of eclipse observations is discussed by:

THOMAS, R. N. *Ap. J.* **108,** 130, 142, 1948; **109,** 480, 1949; **111,** 165, 1950; **112,** 337, 1950.; **115,** 551, 1952.
GIOVANELLI, R. G. *Austral. J. of Sci. Res.* **A, 1,** 275, 305, 360, 1948; *M.N.* **109,** 298, 1949.

8. *Corona*

(a) Observations:

LYOT, B. *C.R.* **202,** 1259, 1936; **203,** 1327, 1936; **206,** 648, 1938; *M.N.* **99,** 580, 1939; *Ann. d'Ap.* **7,** 31, 1944.
WALDMEIER, M. *Astr. Mitt. Zürich*, No. 146, 1945; No. 147, 1946; No. 149, 151, 1947; *Zeits. f. Ap.* **27,** 24, 42, 237, 1950; **28,** 262, 1951. Waldmeier's earlier papers are reviewed by ARMIN DEUTSCH. *Ap. J.* **101,** 117, 1945.
ÖHMAN, Y. *Stockholm Obs. Ann.* **15,** No. 2, 1947 (polarization).

The interpretation of the continuous spectrum and electron densities are discussed by:

GROTRIAN, W. *Zeits. f. Ap.* **2,** 106, 1931; **8,** 124, 1934.
BAUMBACH, S. *A.N.* **263,** 121, 1937.
ALLEN, C. W. *M.N.* **106,** 137, 1946.
VAN DE HULST, H. C. *Ap. J.* **105,** 471, 1947; *B.A.N.* **11,** 135, 150, 1950.

(b) Line Spectrum:

EDLÉN, B. *Zeits. f. Ap.* **22,** 30, 1942, reviewed by P. Swings in *Ap. J.* **98,** 116, 1943; *P.A.S.P.* **57,** 117, 1945.

(c) Theory:

KIEPENHEUER, K. O. *Zeits. f. Ap.* **10,** 260, 1935.
GOLDBERG, L., and D. H. MENZEL. *Harvard Obs. Monogr.* **7,** 279, 1948.
WOOLLEY, R., and S. GASCOIGNE. *M.N.* **106,** 113, 1946.
BONDI, H., F. HOYLE, and R. A. LYTTLETON. *M.N.* **107,** 184, 1947.
SCHWARZSCHILD, M. *Ap. J.* **107,** 1, 1948.
SCHATZMAN, E. *Ann. d'Ap.* **13,** 203, 1949.
SCHIRMER, HERBERT. *Zeits. f. Ap.* **27,** 132, 1950.

9. *Radio-Frequency Radiation from the Sun*

LOVELL, A. C. B. *Radio Astronomy.* London: Chapman & Hall, Ltd., 1952.
VAN DE HULST, H. C. *A Course in Radio Astronomy.* Leiden, 1951.
RYLE, M. *Reports on Progress in Physics* **13,** 184. London: Physical Society, 1950.
PAWSEY, J. L. *Proc. Instit. Elec. Engineers* **97,** Part III, No. 49, September, 1950.

An interpretation of the corona and the chromosphere with the aid of radio data has been given by:

HAGEN, J. P. *Ap. J.* **113,** 347, 1951.
SMERD, S. F. *Proc. Instit. Elec. Engineers* **97,** 447, 1950.

10. *Solar-Terrestrial Relationships*

The literature in this field is so extensive that it seems best to refer the reader to a few summarizing articles that contain extensive bibliographies of earlier papers.

Commission pour l'étude des Relations entre les phenomenes solaires et terrestres (7th report) Paris: Hemmerlé, Petit & Co., 1951.

Centennial Symposia. *Harvard Obs. Monogr.* **7,** 279–381, 1948.

For a discussion of the upper atmosphere and ionosphere, see:

BATES, D. R. *M.N.* **109,** 215, 1949 (review article).

A discussion of a possible excess of ultraviolet solar energy may be found in:

BATES, D. R., and M. J. SEATON. *Proc. Phys. Soc.* **B, 63,** 129, 1950.

The extreme complexity of the relation between flares, r.f. radiation and the ionosphere is illustrated by:

DODSON, HELEN, and L. OWREN. *Ap. J.* (in press), 1953.

INDEX OF NAMES

INDEX OF SUBJECTS

ASTRO

Astro Myths

✦

The Atmospheres of the Sun and Stars

KONALD